# Molecular Analyses of Malignant Pleural Mesothelioma

**Shir Kiong Lo**

National Heart and Lung Institute
Imperial College
Dovehouse Street
London SW3 6LY

A thesis submitted for MD (Res)
Faculty of Medicine, Imperial College London
2016

# Abstract

Malignant pleural mesothelioma (MPM) is an aggressive cancer that is strongly associated with asbestos exposure. Majority of patients with MPM present with advanced disease and the treatment paradigm mainly involves palliative chemotherapy and best supportive care. The current chemotherapy options are limited and ineffective hence there is an urgent need to improve patient outcomes. This requires better understanding of the genetic alterations driving MPM to improve diagnostic, prognostic and therapeutic strategies.

This research aims to gain further insights in the pathogenesis of MPM by exploring the tumour transcriptional and mutational profiles. We compared gene expression profiles of 25 MPM tumours and 5 non-malignant pleura. This revealed differentially expressed genes involved in cell migration, invasion, cell cycle and the immune system that contribute to the malignant phenotype of MPM. We then constructed MPM-associated co-expression networks using weighted gene correlation network analysis to identify clusters of highly correlated genes. These identified three distinct molecular subtypes of MPM associated with genes involved in WNT and TGF-ß signalling pathways. Our results also revealed genes involved in cell cycle control especially the mitotic phase correlated significantly with poor prognosis.

Through exome analysis of seven paired tumour/blood and 29 tumour samples, we identified frequent mutations in *BAP1* and *NF2*. Additionally, the mutational profile of MPM is enriched with genes encoding FAK, MAPK and WNT signalling pathways. We also found mutations in several novel genes involved in chromatin remodelling other than *BAP1* and *SETD2* that may contribute to dysregulation of gene expression in MPM.

In conclusion, MPM is a complex disease with heterogeneous molecular aberrations. By combining findings from both transcriptome and exome analyses, we identified alterations in genes involved in common signalling pathways such as FAK, WNT and MAPK. These may have important roles in driving MPM carcinogenesis with therapeutic implications and require further explorations.

# Abbreviations

| Abbreviations | Full name |
|---|---|
| **BAM** | Binary Alignment Map |
| **bp** | base pairs |
| **BRC** | Biomedical Research Centre |
| **BRU** | Biomedical Research Units |
| **CALBG** | Cancer and Leukaemia Group B |
| **CDK** | Cyclin Dependent Kinases |
| **cDNA** | complementary Deoxyribonucleic Acid |
| **CEA** | Carcinoembryonic Antigen |
| **CL4** | Claudin-4 |
| **COSMIC** | Catalogue of Somatic Mutations in Cancer |
| **CRL4** | Cullin4A-RING E3 ubiquitin Ligase |
| **cRNA** | complementary Ribonucleic Acid |
| **CSC** | Cancer Stem Cells |
| **CT** | Computed Tomography |
| **CTLA-4** | Cytotoxic T Lymphocyte Antigen-4 |
| **DM** | Data Mining |
| **DNA** | Deoxyribonucleic Acid |
| **DNMTi** | DNA Methyltransferase inhibitor |
| **dNTP** | deoxyribonucleotide triphosphate |
| **ECM** | Extracellular Matrix |
| **EGFR** | Epidermal Growth Factor Receptor |
| **EMA** | Epithelial Membrane Antigen |
| **EMT** | Epithelial-Mesenchymal Transition |
| **EORTC** | European Organisation for Research and Treatment of Cancer |
| **EPP** | Extra-Pleural Pneumonectomy |
| **ERK** | Extracellular-signal-Regulated Kinases |
| **ExAC** | Exome Aggregation Consortium |
| **FAK** | Focal Adhesion Kinase |
| **FC** | Fold Change |
| **FDR** | False Discovery Rate |
| **FFPE** | Formalin- Fixed, Paraffin-Embedded |
| **gm** | Grams |
| **GO** | Gene Ontology |
| **GS** | Gene Significance |
| **GWAS** | Genome-wide association study |
| **GWAS** | Genome-Wide Association Study |
| **H&E** | Haematoxylin and Eosin |
| **HA** | Hyaluronate |
| **HCA** | Hierarchical Clustering Algorithm |

| | |
|---|---|
| **HDACi** | Histone Deacetylase Inhibitors |
| **HGF** | Hepatocyte Growth Factor |
| **HMGB1** | High Molecular Group Binding Protein 1 |
| **IASLC** | International Association for the Study of Lung Cancer |
| **IGF1** | Insulin Growth Factor 1 |
| **IHC** | Immunohistochemistry |
| **IMIG** | International Mesothelioma Interest Group |
| **indels** | insertions/deletions |
| **IVT** | *in vitro* Transcription |
| **KEGG** | Kyoto Encyclopaedia of Genes and Genomes |
| **LCM** | Laser-Capture Micro-dissection |
| **LRP** | Lipoprotein-Related Protein |
| **MAPK** | Mitogen-Activated Protein Kinases |
| **MEMO** | Molecular Analyses of Malignant Pleural Mesothelioma |
| **MEs** | Module Eigengenes |
| **MET** | MET Proto-oncogene |
| **MHC** | Major Histocompatibility Complex |
| **miR** | micro RNA |
| **ml** | Millilitre |
| **MM** | Module Membership |
| **MPM** | Malignant Pleural Mesothelioma |
| **MSAC** | Mitotic Spindle and Assembly Checkpoint |
| **mTOR** | Mammalian Target of Rapamycin |
| **NER** | Nucleotide Excision Repair |
| **NF-κB** | Nuclear Factor Kappa-light-chain-enhancer of activated B cells |
| **ng** | Nanogram |
| **NGS** | Next Generation Sequencing |
| **NIHR** | National Institute for Health Research |
| **NK** | Natural Killer |
| **nt** | Nucleotides |
| **OCT** | Optimal Cutting Temperature |
| **OS** | Overall Survival |
| **PCA** | Principal Component Analysis |
| **PCR** | Polymerase Chain Reaction |
| **PD-1** | Programmed Death-1 |
| **PDP** | Podoplanin |
| **PEN** | Polyethylene Napthalate |
| **PFS** | Progression-Free Survival |
| **PI3K** | Phosphoinositide 3-Kinase |
| **PM** | Perfect Match |
| **PVCA** | Principal Variance Component Analysis |
| **RBH** | Royal Brompton and Harefield NHS Foundation Trust Hospital |
| **RIN** | RNA Integrity Number |
| **RMA** | Random Multiple Access |
| **RMH** | Royal Marsden NHS Foundation Trust Hospital |

| | |
|---|---|
| **RNA** | Ribonucleic Acid |
| **RTK** | Receptor Tyrosine Kinase |
| **RTS** | Review on Transcriptome Studies |
| **SGH** | St George's Hospital |
| **SHH** | Sonic Hedgehog |
| **siRNA** | small interfering RNA |
| **SMRP** | Soluble Mesothelin-Related Peptides |
| **SNP** | single Nucleotide Polymorphisms |
| **SNV** | Single Nucleotide Variants |
| **SV40** | Simian Virus 40 |
| **TGF-ß1** | Transforming Growth Factor Beta 1 |
| **TNF** | Tumour Necrosis Factor |
| **TOM** | Topological Overlap Matrix |
| **TSG** | Tumour Suppressor Gene |
| **TUCP** | Transcripts of Uncertain Coding Potential |
| **UK** | United Kingdom |
| **USA** | United States of America |
| **UV** | Ultraviolet |
| **VCF** | Varian Call Format |
| **WES** | Whole Exome Sequencing |
| **WGCNA** | Weighted Gene Co-expression Network Analysis |
| **WHO** | World Health Organisation |
| **WT1** | Wilms' Tumor-1 protein |
| **µg** | Microgram |
| **µl** | Microliter |
| **µm** | Micrometre |

# Acknowledgements

Firstly, I would like to express my sincere gratitude to both my supervisors, Professor Cookson and Dr Popat, for giving me this invaluable opportunity to conduct this research. I am extremely grateful for their guidance, motivation and patience.

My sincere thanks also go to Professor Moffatt and Professor Bowcock for their insightful advice and encouragement. I am also very grateful to the immense input from Professor Lathrop, Professor Nicholson, Dr Montero and their team.

I would also like to thank the Brunei Government and Lung Unit, Royal Marsden Hospital that funded me to study at the National Heart and Lung Institute, Imperial College. I would also like to acknowledge all the members of the Molecular Genetics & Genomics and Cancer Genomics group in particularly Liz, Hima, Saffron, Youming, Kenny and Spyros for their help and advice throughout my research.

Lastly, I would like to thank my family and friends who are always there for me.

# Declaration of Originality

I herewith certify that this dissertation is my original work and that all materials included which are not my own work have been acknowledged.

# Copyright Declaration

# Table of Contents

# List of Figures

# List of Tables

# Chapter 1 - Introduction

## 1.1 Background

Malignant mesothelioma is a neoplasm that originates from mesothelial cells lining the body cavities including the pleura, pericardium, peritoneum and tunica vaginalis. The pleura is the most commonly affected area and is known as malignant pleural mesothelioma (MPM) which is the focus of this thesis work. Asbestos is the main causative agent but other risk factors and genetic susceptibilities have been implicated. MPM is still considered a relatively rare type of cancer accounting for only 0.8% of cancer cases and 1.5% cancer deaths in the United Kingdom (UK)[1]. The long latency period between exposure and development of MPM has given rise to the increased incidence seen in many developed countries over the past two decades and the incidence continues to rise in many developing countries worldwide.

MPM is an aggressive cancer and is often diagnose at an advanced stage. Patients with MPM commonly present with dyspnoea, chest pain or pleural effusion. Initial assessments generally include a computed tomography (CT) scan, thoracentesis, pleural fluid cytology assessment, and pleural biopsy. The diagnosis of MPM remains challenging as it relies on an adequate tissue biopsy sample for histopathological analysis taking into considerations appropriate clinical, radiological and surgical findings.

MPM is categorised into three main histologic subtypes: epithelioid, sarcomatoid and biphasic MPM. Histologic subtype is a well-established prognostic factor in MPM. Epithelioid MPM confers significantly better prognosis compared to biphasic and sarcomatoid MPM. According to the International Association for the Study of Lung Cancer

(IASLC) and International Mesothelioma Interest Group (IMIG) studies the median survival for epithelioid, biphasic and sarcomatoid MPM are 19, 13 and 8 months respectively; and the median survival by stage of disease and after maximal cytoreductive surgery is also reported (Table 1.1)[2]. Two validated prognostic scoring systems developed by the Cancer and Leukaemia Group B (CALGB) and European Organisation for Research and Treatment of Cancer (EORTC) have been proposed for patients with MPM[3,4]. These groups examined the effects of various pre-treatment variables on survival in patients with MPM. Several variables were identified as important prognostic factors including age, performance status, histologic subtype, weight loss, haematologic and biochemistry parameters. Amongst these, poor performance status and non-epithelioid subtypes werereported by both groups to be associated with worse prognosis.

Chemotherapy is the standard of care for patients with MPM. A combination of pemetrexed (anti-folate) and cisplatin (platinum-compound) is an established frontline treatment with statistically significant improvement in overall survival by three months and quality of life over cisplatin alone as shown in a randomized phase III trial[5]. The response to chemotherapy remains short-lived and no other second-line treatments are licensed. However, a small subset of long–term responders can be identified. Surgery is not performed frequently as the majority of patients present with inoperable disease. For resectable disease, the optimal type of surgery is still unclear. A seminal feasibility clinical trial showed extra-pleural pneumonectomy (EPP) offers no benefit compared to no surgical intervention[6]. A prospective randomized trial (NCT02040272) has recently started recruiting in the UK and aims to answer the benefits of a less extensive surgery, extended pleurectomy decortication, versus no surgery. Adjuvant hemithoracic RT to improve loco regional control is no longer given as patient will require pneumonectomy while the benefit of prophylactic tract RT given to prevent tumour seeding at surgical instrumented site remains controversial as studies have shown conflicting result but is

still routinely given in some centres[7].

**Table 1.1. Median survival of patients with MPM according to disease stage (American Joint Committee on Cancer Cancer Staging Manual, 7th edition) and after surgery.**

| Stage | T | N | M | Median survival (months) (IMIG+IASLC) | |
|---|---|---|---|---|---|
| | | | | | With radical surgery |
| I | T1 | N0 | M0 | 20 | 30 |
| IA | T1a | N0 | M0 | | |
| IB | T1b | N0 | M0 | | |
| II | T2 | N0 | M0 | 19 | 22 |
| III | T1, T2 | N1 | M0 | 16 | 16 |
| | T1, T2 | N2 | M0 | | |
| | T3 | N0, 1, 2 | M0 | | |
| IV | T4 | Any N | M0 | 11 | 12 |
| | Any T | N3 | M0 | | |
| | Any T | Any N | M1 | | |

## 1.2 Mesothelial cells and the pleura

Mesothelial cells are derive from the mesoderm but are capable of expressing both epithelial and mesenchymal properties. They display mainly epithelial phenotypes and markers such as polygonal cell shape, cytokeratin intermediate filaments and basement membrane; and occasionally the presence of mesenchymal markers such as vimentin, desmin and alpha smooth muscle actin[8,9]. Simsir *et al*. have demonstrated mesothelial cells possess well-developed tight junctions, adherens junctions, gap junctions and desmosomes; and also

express predominantly N-cadherin in addition to E- and P- cadherins[10]. In response to insult, mesothelial cells begin to proliferate and regenerate. Several theories exist and suggest new mesothelial cells regenerate after injury from centripetal migration of cells at the wound edge and the origins of these regenerating mesothelial cells remain uncertain but free-floating cells from serosal fluid have been implicated[11]. Mesothelial cells are also capable of forming cells of different mesenchymal lineages through transdifferentiation from an epithelial to mesenchymal phenotype such as fibroblasts, endothelial and smooth muscle cells depending on the presence of different types of growth factors and cytokines[12]. These observations led to the speculation of the existence of cancer stem cells (CSC) in MPM. CSC share many characteristics of normal stem cells including self-renewal and multilineage differentiation. Aside from these, a CSC population has been hypothesised to play an essential role in tumour initiation, growth, recurrence, and treatment resistance[13–15]. Several studies aimed to identify CSC in MPM but results were not conclusive. Side population cells are considered to be potential CSC in various tumours and those with low or negative *CD105* were isolated from MPM and found to be tumorigenic[16]. Other studies claimed to have isolated floating stem cells from cultured peritoneal mesothelioma cells but lacked the usual stem cell markers such as *CD133, CD31* and *CD144*[17]. Yamazaki *et al* found MPM cell lines expressing *CD24* and *CD26* correlated with CSC properties[18]. Resistance to cancer therapy is another hallmark of CSC and Cortes-Derrick proposed chemoresistance to pemetrexed and cisplatin is associated with the expression of stem cell markers *CD133, Bmi-1, uPAR* and *ABCG2*[19]. Further characterization of CSC in MPM is warranted as it can lead to better understanding of the cells of origin, tumour progression and as potential therapeutic targets in MPM

Around 70% percent of malignant mesothelioma cases are pleural in origin and occur mainly on the parietal pleura instead of the visceral pleura[20,21]. The pleura is covered by a single layer of flattened mesothelial cells made up of squamous-like cells and cuboidal mesothelial cells.

The functions of mesothelium are to provide a protective barrier and to facilitate movement of the pleural surfaces during respiration through secretion of glycoproteins. Furthermore, they are involved in membrane transport, participate in inflammation and tissue repair process by secreting various immunomodulatory mediators such as cytokines, growth factors, nitric oxide, reactive nitrogen and oxygen species and also capable of changing cell adhesion molecule expression[22]. An *in vitro* study showed mesothelial cells produce a variety of extracellular matrix (ECM) molecules and regulate ECM turnover through the synthesis of matrix metalloproteinases and tissue inhibitors of metalloproteinases[23].

## 1.3 Epidemiology

Asbestos is a well-established causal factor for MPM. The World War II period saw the largest use of asbestos because of demand that accompanied industrialization. However, the rise in MPM cases did not occur immediately because of the long latency period between exposure and disease development. The long latency period explains the rising incidence of MPM worldwide despite asbestos being banned in many countries and the incidence is predicted to decline only sometime between year 2015 and 2030[24]. There is also a significant heterogeneity in incidence by country with industrialised countries having the highest incidence rate reflecting past use and production of asbestos[25]. Australia has the highest incidence in 2010 at 35 cases per million while incidence in the United States of America (USA) might have peaked and has been steadily declining since year 2000 due to the decline in asbestos use since 1960[26,27]. In the UK, the incidence rates have increased since late 1970s that correlated with the peak use of asbestos around early 1960s[1].

Data from the World Health Organisation (WHO) analysis of MPM from 1994-2008 reported an age-adjusted mortality rate of 4.9 per million with a mean age of death at 70 years and

observed large differences by sex with a male to female ratio of 3.6:1[28]. In 2011, there were 2,570 new cases recorded with a male to female ratio of 5.5:1; and 2,429 deaths from MPM recorded in 2012 in the UK. This is in keeping with the prediction that MPM mortality in Great Britain will peak at around 1,950-2,450 deaths per year between 2011-2015 and expected to decline rapidly thereafter[29].

In non-Western or developing countries the incidence is expected to peak at a later period due to later use of asbestos compared to Western countries. Many cases particularly in developing countries have been unreported leading to an underestimation of global incidence rate. Park *et al*. estimated 38,900 cases to have occurred between 1994-2008 in countries without reported mesothelioma based on cumulative data on incidence rate and asbestos use[30]. Similarly, inaccurate reporting of MPM deaths prior to the introduction of a uniform disease classification system may have contributed to the underestimated incidence rates globally[31].

Geographical areas and occupations associated with high exposure of asbestos correlated with higher incidence and deaths due to MPM. In the UK, areas of West Dunbartonshire and Barrow-in –Furness have the highest standardized mortality ratio and the occupations with the highest proportional mortality ratios are metal plate workers, vehicle body builders, plumbers, gas fitters and carpenters[32]. In addition, indirect non-occupational exposure to asbestos such as living in the vicinity of an industrial or natural source of asbestos areas or living with a person exposed to asbestos has accounted for 8.3% of all mesothelioma cases in Italy but has been estimated to account for approximately 30% of all cases in the USA[33]. Small clusters of mesothelioma have also occurred such as in the villages of Turkey possibly due to other environmental exposure such as erionite (an asbestos-like mineral) or transmission in an autosomal dominant manner as suggested by a six-generation extended pedigree analysis[34,35].

With the exception of the USA and possibly the UK, the observed incidence of this disease is just the tip of the iceberg especially in many developing countries. The increasing cases of this fatal disease worldwide and its limited treatment options highlighted the importance of research in understanding the disease biology in order to improve diagnosis, therapies and outcomes.

## 1.4 Risk factors

### 1.4.1 Asbestos

Asbestos is the most extensively investigated cause of MPM and it was not until 1947 when the first case of MPM with current diagnostic criteria was documented and published in the New England Journal of Medicine[36]. However, the first causal relationship between MPM and asbestos was reported by Wagner in 1956 whereby he documented 32 out of 33 MPM cases with asbestos exposure in the Kimberley area, South Africa[37].

There are two major groups of asbestos: serpentine and amphiboles. Chrysotile also known as white asbestos is the only serpentine and accounts for more than 90% of the asbestos used worldwide. Among the amphiboles, crocidolite, also known as blue asbestos, is considered to be the most oncogenic and found to confer increased risk by 500 fold compared to chrysotile[38]. The carcinogenicity of chrysotile remains controversial and its contribution to malignant mesothelioma was thought to be attributed to contamination with amphiboles while other studies found chrysotile do not accumulate in the lungs as they could be partially digested compared to amphibole asbestos which are resistant to cellular enzymes[39]. However, studies on lung fibre contents in patients with MPM have found increased odd ratios not only for amphiboles fibres but also chrysotile fibres alone[40]. Aside from solubility, the

carcinogenicity of asbestos fibres also depends on its diameter and length. The biologically active or inhalable asbestos fibres are those with a diameter of less than 3 micrometres and a length between 5 and 100 micrometres[41]. Only 20% of all asbestos fibres fall into this category including crocidolite that have the capacity to penetrate and irritate the pleura to induce disease including pleural plaques, asbestosis or malignant mesothelioma[42]. In general, the majority of patients are exposed to both types of asbestos and the WHO has concluded that all types of asbestos are in fact oncogenic[43].

Around 80% of MPM are related to asbestos but the remaining 20% of cases have no documented asbestos exposure suggesting other etiologic factors including genetic susceptibility in certain individuals[44]. Even in cases where asbestos exposure was not known lung content examination from a study revealed significant asbestos fibres count were present in these cases suggesting potential unrecognized exposure[45]. The lifetime risk of developing MPM after asbestos exposure ranges from 4 to 10% and majority of exposed individuals develop other asbestos-related lung disease such as pulmonary fibrosis, pleural plaques, recurrent effusions and lung cancer[46]. The risk of lung cancer in asbestos-exposed individuals is further increased by cigarette smoking that is prevalent in this group of individuals and the risk persists for up to 40 years even after smoking cessation compared to asbestos workers who never smoke[47]. In contrast, smoking alone does not increase the risk of MPM in a case-control study[48]. Either way, smoking cessation may be the only way to reduce the risk of lung cancer in previously asbestos-exposed workers.

The mean latency period between asbestos exposure to the time of MPM diagnosis is around 32 years after initial exposure and only 1% of the cases had a latent period of less than 15 years while no cases was identified in those with less than 10 years of exposure[49]. More recent studies have revised and reported the mean latency period to be between 42.8 to 48.5

years[50,51]. There is no definite explanation for this long latent period but one could postulate that cells exposed to asbestos acquire multiple molecular aberrations over the years and eventually transform. The findings by Hilliard *et al*. showed the latency period is inversely correlated with intensity of exposure and found the latency period for intermittent and continuous exposure to be 42 years versus 49.5 years respectively[51]. A pooled analysis of 8 cohort studies found the median latency period to be 38.4 years and women tended to have a longer latency period compared to men[52]. The number of female cases not known to be directly exposed to asbestos tends to be lower compared to those with known occupational exposure. Indirect exposure to asbestos could be a result from proximity to asbestos factories, close contact with asbestos workers with fibres found in their clothing, asbestos in old buildings or electrical apparatus. In addition, the study observed the median duration of exposure was 3.75 years and the risk of developing pleural MPM increased up to 45 years after first exposure. A population-based case control study on asbestos-exposed males estimated a dose-response relationship with logistic regression method and found the effect of total duration of asbestos exposure decreased when age at first exposure and time since last exposure increased[53].

Studies based on history of asbestos exposure invariably suffer from inaccurate estimation of exposure while studies based on lung content analyses might offer more precise risk estimation. The risk of asbestos-induced MPM was found to be dose-dependent in animal models[54]. However, the effect appears to be different in humans as shown in a lung content analysis study which found higher levels of exposure to asbestos is more likely to cause asbestosis instead of MPM and the latter is more likely to occur with smaller amount of exposure to crocidolite compared to chrysotile[55].

The mechanisms of asbestos-induced malignant changes in mesothelial cells are multifaceted.

Firstly, long and thin asbestos fibres including crocidolite can directly penetrate and deposit in the pleura to initiate asbestos-related disease including MPM[42]. Secondly, asbestos fibres are capable of disrupting mitotic spindles during mitosis resulting in aneuploidy and other chromosomal abnormalities leading to cell transformation[56]. Thirdly, asbestos fibres generate a chronic inflammatory process by generating extracellular high molecular group binding protein 1 (HMGB1) following phagocytosis of asbestos fibres by macrophages and human mesothelial cells. HMGB1 leads to secretion of tumour necrosis factor (TNF)-alpha that promotes cell survival and resistance to asbestos-induced cytotoxicity through activation of nuclear factor kappa-light-chain-enhancer of activated B cells (NF-κB)[57]. Furthermore, HMGB1 releases reactive oxygen and nitrogen species thereby inducing DNA damage, strand breaks and G to T transversions[58]. Asbestos fibres are capable of inducing autophosphorylation of mitogen-activated protein kinases (MAPK) and extracellular-signal-regulated kinases (ERK) 1 and 2[59]. The MAPK/ERK cascade is also activated by asbestos-induced autophosphorylation of epidermal growth factor receptor (*EGFR*).

### 1.4.2 Other risk factors including genetic susceptibility

Around 20% of MPM cases are not associated with asbestos exposure suggesting other etiologic factors or genetic susceptibility. A number of other non-asbestos related agents are implicated in the development of MPM. Erionite, a naturally occurring fibrous zeolite compound is strongly associated with MPM after high incidence of MPM was reported in villages of Cappadocia, Turkey and found extensive use of erionite in the houses of MPM cases. Intrapleural injections of erionite in animal models resulted in MPM in >90% of cases[60]. However, some households were spared despite the presence of erionite in the home buildings and analysis of a six generation extended pedigree in Turkey suggested a possibility of genetic susceptibility through autosomal dominant transmission[35]. This was challenged by

another study that found the risk of MPM was due to indoor exposure to erionite and familial clustering might be coincidental or erionite might be contributing to MPM in genetically susceptible individuals[61].

Multiwalled carbon nanotubes, products of nanotechnology, have also been implicated in MPM development due to their morphological resemblance to asbestos fibres including needle-like shape, high durability and propensity to migrate to the pleural when inhaled. Thin and high crystallinity carbon nanotubes have been shown to pierce the mesothelial cell membrane and induce cytotoxicity *in vitro* and initiate inflammation with subsequent transformation *in vivo* in mesothelial cells[62]. The same study observed frequent homozygous deletion of *CDKN2A/2B* that is often inactivated in MPM. There is no evidence reported to date regarding human exposure to carbon nanotubes and development of MPM.

Simian virus 40 (SV40) is a polyomavirus with double-stranded DNA of monkey origin and the most likely route of transmission to human was through SV40 contaminated polio vaccines between 1955-1963[63]. SV40 has been identified in several tumours including MPM. SV40 exerts its oncogenic effects via an antisense mechanism that suppresses late viral gene expression allowing cells to survive the infection and the high levels of wild type p53 in human mesothelial cells allow SV40 to persist in an episomal state with expression of large T antigen (Tag)[64]. SV40 Tag binds to and inactivates tumour suppressors p53, pRb and other proteins leading to activation of insulin-like growth factor 1 (*IGF 1*) pathway including *AKT* activation leading to cell survival and proliferation[65]. In addition, Tag is able to transactivate *MET* and *ERK* pathways through production of hepatocyte growth factor (*HGF*) and upregulation of *Notch-1* respectively [66,67].

Intrapleural inoculation of SV40 in hamsters resulted in the development of MPM[68]. This led

to the identification of SV40 sequences by polymerase chain reaction (PCR) in 60% of human mesotheliomas specimens and was later confirmed in a multi-centre study in the USA[69,70]. However other groups outside of the USA did not detect SV40 in MPM suggesting possible geographical variations in the use of previously SV40-contaminated polio vaccine or differences in detection methods[71,72]. Lopez-Rios *et al* also showed that most of their initial positive results of SV40 in 60% of MPM were due to plasmid PCR amplification rather than that of SV40[73]. To date, it is still not entirely clear the causal role of SV40 in MPM due to the conflicting laboratories results and the overall incidence of MPM is not consistent with the millions of previously SV40-contaminated polio vaccines.

*In vitro* studies have demonstrated that SV40 can transform human mesothelial cells but asbestos acts synergistically as strong co-carcinogen in increasing the rate of malignant transformation[64,74]. These suggest SV40 contribution to MPM development as a co-factor and potentially could be a marker to identify asbestos exposed individuals who may be at high risk of developing MPM.

Ionising radiation is a well-recognized carcinogen and a potential risk factor for the development of MPM. This has been reported in patients receiving therapeutic radiation for cancer such as Wilms' tumour or lymphoma and in patients who had previously received radiographic contrast medium Thorotrast[75,76]. The causal association was further supported by development of MPM in rat models injected with radioactive material and a review on epidemiological studies found statistical significant increase in MPM risk especially with Thorotrast and radiation therapy[77,78]. Although there is no definite causal link between radiation and MPM but a possible causal association is evident from the case reports and the plausible oncogenic actions of radiation.

Polymorphisms in several metabolic genes involved in oxidation processes are implicated in conferring an increased risk of MPM. Previous study found genetic polymorphisms in two metabolic genes *GTSM1* and *NAT2* associated with an increased risk of asbestos-induced MPM development and the risk is 7-fold higher in the presence of both polymorphisms[79]. Another case-control study identified increased risk of MPM is associated with polymorphisms in *mEH*, combination of *mEH* and *NAT2*, *mEH* and *GTSM1*; and *NAT2* and *GTSM1* in the presence of asbestos exposure[80]. However, the studies involved small number of cases and these genes have not been reported again in MPM to draw any significant associations.

Genome-wide association study (GWAS) was carried out in an Italian sample involving 407 MPM cases and 389 controls with a replication Australian study involving 428 MPM cases and 1289 controls to identify genetic risk factors in the development of MPM[81,82]. These did not identify any single marker that reached the genome-wide significance threshold and there was no replication between the two studies. These could be explained by the small sample size as MPM is still a relatively rare cancer and sample heterogeneity. However, five chromosomal regions (3q26.2, 4q32.1, 7p22.2, 14q11.2, 15q14) from the Australian study showed significant associations with the top single nucleotide polymorphisms (SNP) from the Italian study especially in the region of a cell adhesion protein, *SDK1*. This gene has recently been identified through exome data mining to be associated with asbestos exposure[83]. Thus, *SDK1* may be an important candidate gene in asbestos-induced disease such as MPM.

In recent years, germline mutations in *BAP1* have been reported in families with a high incidence of MPM[84,85]. Meta-analysis of seven unrelated families found the majority of these cases arise in individuals or families with other cancers known as *BAP1* cancer syndrome that includes atypical melanocytic tumours, uveal melanoma, cutaneous melanomas, renal cell

carcinomas and possibly other cancers that have not yet to be classified as part of the syndrome[85]. The prevalence of germline *BAP1* mutation is extremely low in sporadic MPM and estimated to be between 0-2 %[86–88]. Sneddon *et al* also did not identify any history of *BAP1*-associated cancers in sporadic *BAP-1* mutant MPM cases suggesting germline *BAP1* mutation and familial *BAP1* cancer syndrome is not a common occurrence[87]. As such, routine genetic screening for germline *BAP1* mutation is not applicable but could be considered for patients with MPM and family history of other *BAP1*-associated cancer.

## 1.5 Diagnostic biomarkers

Most MPM are readily identified or suspected on routine haematoxylin-eosin (H&E) staining where they exhibit three histologic subtypes that are broadly categorized in to epithelioid, sarcomatoid or mixed (biphasic) based on cell morphology. A definitive histopathological diagnosis of MPM requires immunohistochemistry (IHC) workup. The IMIG recommends the use of at least 2 mesothelial and 2 carcinoma antibodies depending on the differential diagnoses considered[89]. The differential diagnoses for epithelioid MPM includes adenocarcinomas; for sarcomatoid MPM includes sarcomas and other spindle cell neoplasms; and for mixed MPM includes mixed or biphasic tumours such as synovial sarcoma and metastatic pleomorphic carcinoma of lung.

The most established positive mesothelioma markers include calretinin, epithelial membrane antigen (EMA), cytokeratin 5/6 (CK5/6), podoplanin (PDP) and Wilms' tumor-1 protein (WT1). As for carcinoma markers, carcinoembryonic antigen (CEA), claudin-4 (CL4), Ber-EP4 and p63 are useful panels. Initial positive staining for EMA and calretinin together with negative staining for CEA and Ber-EP4 support the diagnosis of MPM and exclude adenocarcinoma. Any equivocal results will require further MPM antibodies such as PDP and

WT-1. PDP is able to differentiate epithelioid MPM from adenocarcinomas but can also be expressed in squamous carcinoma. WT1 is a useful MPM diagnostic marker and able to differentiate lung adenocarcinoma but not breast adenocarcinoma hence their use may be limited to male patients. D2-40 and calretinin are positive markers most consistently expressed in sarcomatoid MPM. In the setting of other suspected cancers, the use of specific antibodies such as thyroid transcription factor 1 positivity confirms pulmonary origin of an adenocarcinoma. Amongst the negative markers for MPM, CL*4* is the most specific while EpCAM may show focal positivity and CEA expression is very rare in MPM. The diagnosis of benign reactive mesothelial proliferation requires loss of immunoreactivity to EMA and positive immunoreactivity to desmin.

The diagnosis of MPM based on cytological analysis of pleural fluid is non-invasive and has lower morbidity rate. Recent evidence has indicated cytopathological diagnosis of MPM can be reliable with 100% positive predictive value if carried out in conjunction with other ancillary techniques such as IHC, molecular biology, electron microscopy and analysis of soluble biomarkers but has lower sensitivity compared to histopathological diagnosis that remains as the gold-standard diagnostic tool[90].

Several biomarkers in serum, plasma or pleural effusion have been established as potential diagnostic markers in MPM but none can be used solely due to low sensitivity or still requiring further validation in larger studies. Soluble mesothelin-related peptides (SMRP) are elevated in the serum of patients with MPM with a specificity of 95% and sensitivity of 83% compared to controls[91]. Multivariate analyses showed the sensitivity ranged from 20-70% and level of SMRP correlate significantly with age, low BMI, smoking history, cumulative asbestos exposure and detection of disease recurrence or progression[92]. However, the potential use of SMRP are limited to epithelioid or biphasic MPM as they are not elevated in

sarcomatoid MPM, a subtype that remains a diagnostic challenge. Osteopontin, an extracellular cell adhesion protein, has low specificity as a plasma diagnostic marker but in contrast to SMRP it may be elevated in sarcomatoid MPM[93]. Both sensitivity and specificity are increased by combining both SMRP and plasma osteopontin for diagnostic accuracy but require further validation[94]. High level of hyaluronate (HA) is secreted into the effusion of MPM but high levels are detected in only 50-60% of MPM effusions[95]. Combining SMRP and HA biomarkers with a two-step model to predict MPM showed high specificity but no improvement in sensitivity[96]. Another study identified elevated levels of serum fibulin 3, an extracellular glycoprotein, has a sensitivity of 96.7% and specificity of 95.5% in distinguishing patients with MPM from those with exposure to asbestos but without the disease[97]. Levels are also significantly higher in pleural effusion due to MPM and together with plasma level may be helpful to differentiate effusion due to MPM or other benign lesions. However, this could not be validated in a subsequent study that found SMRP to be a better serum diagnostic marker compared to fibulin 3[98]. In conclusion, SMRP remains the best available biomarker that may be clinically useful to distinguish MPM from other diseases.

## 1.6 Molecular changes in MPM

### 1.6.1 Chromosomal alterations

Chromosomal alterations in MPM have been studied on cell cultures and primary tumours with comparative genomic hybridization array, SNP array and representative oligonucleotide microarray analysis[99–105]. All studies reported loss of chromosomal regions 1p, 3p, 9p and 22q. The genes at some of the deleted loci have been identified including 9p21.3 that encodes *CDKN2A* and 22q12 that encod*es NF2*. The frequent loss of region 3p21 involves tumour suppressor gene (TSG) *RASSF1A* (3p21.3) that is inactivated by allelic loss or methylation.

More recently, somatic *BAP1* (3p21.1) mutations in MPM have been identified and together with loss of chromosome 3p21 lead to biallelic inactivation of *BAP1*[106]. Other frequent losses are in the region of 4q, 13q and 14q. Gains of chromosomal regions are less common and include regions 1q, 5p, 7p, 8q, and 17q. Whole genome sequencing of one primary MPM tumour with matched normal tissue using sequencing-by-synthesis and pyrosequencing also revealed more large scale genomic alterations, particularly deoxyribonucleic acid (DNA) rearrangements involving chromosomes 8, 17 and 21, than point mutations[107]. The study reported one large deletion involving *DPP10* at 2q12.3–2q14.2 but loss of this region was not detected by earlier studies involving MPM cell lines or tumours. Clearly more samples are needed as this study only focused on single tumour genome and the depth of sequencing might be biased towards discovery of rearrangement-type mutations.

### 1.6.2 DNA methylation

DNA methylation of clusters of CpG dinucleotides ("CpG islands") in the promoter regions of genes leads to transcriptional silencing. This epigenetic modification plays a major role in carcinogenesis through inactivation of tumour suppressor and other growth regulatory genes[108]. Global epigenetic analysis of MPM has shown differences in methylation profile when compared to normal pleural or other tumours suggesting the presence of aberrant CpG island methylation that is specific and may be involved in the carcinogenesis of MPM. The first methylation study on MPM was carried out on 158 MPM and 18 normal pleural samples. DNA methylation profile was able to differentiate between MPM and non-malignant pleura and was a significant predictor of shorter survival[109]. Another study compared the methylation profile between MPM and lung adenocarcinomas and found 11% of heterozygously deleted genes were affected by DNA methylation and/or trimethylated histone H3 lysine 27 in MPM[110]. Amongst these genes, *TMEM30B, KAZALD1* and *MAPK13* were specifically

methylated in MPM and may be useful as differential diagnostic markers. In the same study, a subset of patients with low frequency of DNA methylation had longer survival. Other genes that have prognostic implications include hypermethylation of *LZTS1, SLC6A20, TMS1*, *HIC-1* or combination of *RARbeta* with either *RASSF1A* or *DARK* that have been associated with shorter survival[111–113]. Other authors have studied the methylation status in MPM with a more directed approach by analysing specific pathway genes. These identified hypermethylation of cell cycle genes (*APC, CCND2, CDKN2A, CDKN2B, HPPBP1* and *RASSF1*) was significantly associated with higher asbestos burden[114]. Kohno *et al* found WNT pathway is deregulated in MPM via epigenetic silencing and found promoter methylation of *WIF-1* and *SFRP1, 2* and *4*, are common events in MPM[115]. Epigenetic silencing of *miR-34b/c*, a direct transcriptional target of *TP53*, by methylation is a crucial event in MPM and forced expression of miR-34b/c led to significant antitumor effect[116].

In light of these aberrant epigenetic findings in MPM, several histone deacetylase inhibitors (HDACi) have been tested. The largest of the studies was a phase III trial that tested vorinostat but did not show any survival benefit compared to best supportive care in patients who relapsed after first-line systemic chemotherapy[117]. A more promising result was achieved with valproate, an HDACi, given with doxorubicin that yielded a response rate of 16% in a small phase II study. This was further supported by *in vitro* study that showed tumour growth suppression when combined with standard of care chemotherapy regime, pemetrexed plus cisplatin[118].

### 1.6.3 Mirco RNA

Micro RNA (miR) are involved in regulating gene expression at the post transcriptional level and half of known miR are located in cancer-associated genomic regions or in fragile sites,

regions of loss of heterozygosity, minimal amplicons or common breakpoints involving TSG, oncogenes and genes in specific signalling pathways[119]. In a study investigating the prognostic role of miR in surgically treated patients with MPM, only miR-29c* had significant different expression with higher levels correlating with longer time to progression and survival[120]. miR-31 is frequently lost in MPM due to its chromosomal location at 9p21. A study showed loss of miR-31 in MPM cell lines is associated with more aggressive phenotype and reintroduction of this miR led to inhibition of cell cycle progression[121]. Several groups have identified specific miR that may be of diagnostic value in MPM. Seven miR (miR-141, miR-200a, miR-200b, miR-200c, miR-203, miR-205, and miR-429) areshown to be downregulated in MPM irrespective of the histologic subtype. Upregulation of miR-484, miR-320, hsa-let-7a, and miR-125a-5p are able to discriminate MPM from benign asbestos-related disease while differential expression of three miR (miR-193, miR-200c, and miR-192) are able to distinguish MPM from lung adenocarcinoma[122,123]. Further miR profiling studies and validation of the findings are required to establish their roles in MPM carcinogenesis.

### 1.6.4 Gene expression profiling

Microarray-based transcriptomic studies have led to the identification of deregulated gene expression changes relevant to the biology of MPM. Earlier studies on cell lines found gene expression changes related to mesothelial cell transformation are involved in DNA repair, cell adhesion, cell migration, macromolecule stability and cell cycle[124,125]. Altered gene expression patterns in asbestos-induced tumours in rats found up-regulation of *c-myc, Fra-1* and *EGFR* at different stages of carcinogenesis and genes involved in integrin-linked signal transduction and extracellular matrix (ECM)[126].

Studies analysing gene expression in MPM cells (including cell lines) versus non-malignant

mesothelial cells have limited sample size with the largest number of tumour samples being 53 and utilized different microarray platforms across studies[127–134]. Collectively, these studies showed deregulated genes in MPM are associated with cell cycle, cell proliferation, apoptosis, DNA damage repair, cell adhesion, cell migration, invasion and cytoskeletal support pathways. Genes driving the different phases of cell cycle including checkpoints have been reported by more than two independent studies. The more recent study by Suraokar *et al* with the largest sample size to date revealed mitotic spindle and assembly checkpoint (MSAC) as the most significantly altered pathway followed by cytoskeleton/spindle microtubules network[134]. Eighteen up-regulated MSAC pathway component genes were able to classify the tumours into three molecular subgroups of potential therapeutic implications. Reynies *et al* analysed the expression profile from 38 MPM cultures as well as the mutation status of genes frequently mutated in MPM[135]. This resulted in a three-gene signature (*PPL, UPK3B* and *TFP1*) that defined two subgroups that partly correlated with histologic subtype. *BAP1* mutations are frequently detected in subgroup C1 made up of epithelioid subtype and epithelial-mesenchymal transition (EMT) pathway is preferentially upregulated in subgroup C2 that included sarcomatoid MPM characterised by mesenchymal phenotype. At present, molecular classification cannot replace classical histological classification in the clinical settings.

Melaiu *et al* performed an extensive literature review on transcriptome studies (RTS) in MPM combined with data mining (DM)[136]. A total of 397 significant genes were shared between RTS and DM that are significantly involved in pathways associated with focal adhesion, MAPK signalling, p53 signalling, ECM-receptor interaction, regulation of actin cytoskeleton, cytokine-cytokine receptor interaction, neurotrophin signalling and cell adhesion molecules. Notably, genes encoding for matrix components, various cell adhesion molecules such as integrins, cytokines, growth factors and growth factor receptors are over-represented in four

of the pathways. This suggests cell-cell and cell-matrix interactions in the tumour microenvironment appear to be an important biological mechanism in MPM. The same group also identified 119 genes from RTS alone that were differentially expressed in at least two studies and investigated with reverse transcriptase-quantitative PCR in 15 MPM and 20 non-MPM tissue samples. Fifty-nine out of the 119 genes were found to be significantly deregulated and are associated with cell cycle, focal adhesion, ECM-receptor interaction, DNA replication and metabolic pathways[137]. Of these, nine genes (*ACSL1*, *CCNO*, *CFB*, *PDGFRB*, *SULF1*, *TACC1*, *THBS2*, *TIMP3*, *XPOT*) were significantly deregulated in both MPM cell lines and 12 genes (*ASS1*, *CCNB1*, *CDH11*, *COL1A1*, *CXADR*, *EIF4G1*, *GALNT7*, *ITGA4*, *KRT5*, *PTGIS*, *RAN*, *SOD1*) in at least one MPM cell line.

Several groups have generated list of gene classifier from microarray gene expression analysis to improve prognostic assessments. Pass *et al* profiled 21 MPM tumour tissues from pre-surgical patients and constructed a 27-gene classifier that predicted long- and short-term survivors post surgery[138]. Lopez-Rios *et al* identified higher expression levels of Aurora kinases A and B, genes related to cell cycle and mitosis, correlated with shorter survival and generated a 29-gene classifier predictive of 1 year survival[139]. A 22-gene list of prognostic genes was published by Gordon *et al* and validated gene expression ratios of four of the genes (*KIAA0977, GDIA1, L6, CTHBP*) that could predict treatment-related outcomes irrespective of histologic subtypes[140]. In a subsequent study the same group came up with another prognostic classifier with a 7-gene list and the expression ratios of four (*CD9, KIAA1199,THDB, DLG5*) of the genes were validated to predict 1 year survival[141]. Another study undertaken by Glinsky *et al* used 11-gene signature of the polycomb group *BMI-1*-driven pathway in several cancer types including MPM that was able to predict therapy failure and short survival[142]. There is a lack of concordance between all these studies with few overlapping genes. Three genes were reproducible individually between two studies: *BTG2*

has anti-proliferative function and involved in G1/S transition, *SELENBP1* may play a role in ubiquitination-de-ubiquitination-mediated protein degradation and *CFI* is involved in the complement cascade.

### 1.6.5 Gene mutations and associated pathways

High-throughput sequencing of DNA such as whole exome sequencing (WES) represents another technology that allows a comprehensive characterisation of somatic mutations in protein-coding exons in different cancer types. This has led to better understanding of cancer biology with advances in cancer diagnosis and treatment resulting in improved clinical outcomes.

Alifrangis *et al* presented an abstract on WES and copy number analysis of 19 MPM cell lines and 6 MPM early passage lines[143]. Interestingly, they reported absence of mutations in oncogenes but MPM cell lines harboured mutations in several TSG including *NF2* and detected mutations in histone modifying genes such as *MLL2* and *SETD2*. However, no mutation in *BAP1* was reported. They also performed high-throughput screening across 48 therapeutic compounds and identified phosphoinositide 3-kinase (PI3K)/mammalian target of rapamycin (mTOR) inhibition as the critical pathway to be targeted despite an absence of mutations in PI3K-related genes.

Recently, Guo *et al* performed WES on DNA of 22 MPM frozen tissues collected prior to surgery and matched blood samples[144]. This study presented the first unbiased overview of the molecular landscape in MPM. Other studies have used a more directed approach by sequencing genes in specific pathways, known cancer genes and genes with actionable mutations[145–148]. Guo *et al* identified somatic *BAP1* mutations and copy number alterations in

41% of cases. Another study by Lo *et al* analysed 52 known cancer genes with targeted sequencing on DNA from 123 formalin- fixed, paraffin-embedded (FFPE) MPM tissues. They identified genetic variations in *BAP1* in 58% of cases that significantly correlated with loss of nuclear *BAP1* staining. The frequent mutations in *BAP1* from these two studies further confirmed previous findings of somatic mutations in *BAP1* between 22-61% of MPM cases[84,106,149]. These mutations result in truncated *BAP1* protein that inhibits nucleus localisation and aberrant deubiquitinase activity.

*BAP1* is a TSG involved in various biologic processes including chromatin dynamics, DNA damage response and regulation of the cell cycle and growth. Studies on xenograft models showed transfection of *BAP1* into a *BAP1*-null cell line decreased proliferation while knockout of *BAP1* in adult mice led to myeloid transformation[150,151]. The mechanisms of how loss of *BAP1* lead to cell transformation is not well understood. It is known that *BAP1* encodes a nuclear ubiquitin C-terminal hydrolase and has been shown to deubiquitinate several proteins including *HCF-1* to modulate expression of genes bound by transcription factors *E2F* and *YY1*[152]. *BAP1* together with human orthologues of additional sex combs (*ASXL1/ASXL2*) form the Polycomb repressive deubiquitinase complex and deubiquitinate histone H2A implicated in gene silencing[153]. *BAP1* also interacts with members of the Fox transcription factors (*FOXK1/FOXK2*) that are implicated in cell cycle regulation and proliferation. Recent studies revealed repression of *FOXK2* target genes by *BAP1* but in the absence of *BAP1* upregulation of *FOXK2* target genes is possible only in the presence of Ring1B-BMI1 complex, an E3 ubiquitin ligase for histone H2A[154]. Sacco *et al* has shown in their recent work that *BAP1* differentially regulates the expression of class 1 histone deactylase expression with downregulation and upregulation of *HDAC2* and *HDAC1* respectively in MPM cell lines with genetic *BAP1* inactivation[155]. This may have therapeutic implication with HDAC inhibitor for patients with *BAP1* mutation. *BAP1* loss is associated

with more aggressive phenotype and high metastatic potential in uveal melanoma but this has not been shown in MPM or associated with any distinct phenotypes except higher smoking rates[156].

Both studies by Guo *et al* and Lo *et al* also reported frequent *NF2* mutations located at 22q12 in about 50% of cases consistent with previous studies on cell lines and primary MPM tumours[144,146,157]. *NF2* inactivation also occurs as a result of small, large and homozygous deletions of chromosome 22 or possibly through aberrant splicing leading to altered transcripts in tumours that do not harbour mutations or deletions[158]. These result in loss of Merlin, a component of the Hippo signalling pathway, and subsequent transcriptional upregulation of *YAP1*, that is negatively regulated by Merlin through phosphorylation and sequestration under physiological state, thus leading to inhibition of cell-cycle arrest and apoptosis[159]. In addition, in *vitro* study demonstrated loss of Merlin increased motility and invasiveness of MPM cells through increased phosphorylation of focal adhesion kinase (FAK)[160]. Interestingly, a recent study revealed common mechanism between *NF2* and *BAP1*[161]. The study identified cullin4A-RING E3 ubiquitin ligase (CRL4) as the major binding partner of wild type *NF2* to inhibit CRL4-mediated ubiquitination of histones and other target proteins. Thus loss of *NF2*, leads to activation of CRL4 activity including promoting cell proliferation.

Other than *NF2*, *LATS2* is another component of the Hippo pathway that is inactivated by deletions or mutations in 22% of MPM cell lines and primary tumours[162]. A recent study by Miyanaga *et al* analysed the Hippo pathway genes with RNA and targeted exon sequencing[145]. They identified not only mutations in *NF2* but also *LATS2, RASSF1*, and a gene fusion involving *LATS2-PSEN1*. These data indicate aberrant signalling via the Hippo pathway is an important event in MPM carcinogenesis.

Copy number analysis by Guo *et al* found the commonest focal deletion (45%) encompassed the 9p21 region consistent with a previous study[163]. Deletion of *CDKN2A* leads to loss of $p14^{ARF}$ and $p16^{INK4A}$ that result in degradation of p53 through activation of *MDM2* and inactivation of pRB through activation of *CDK4* respectively. Therefore, genetic defects in $p14^{ARF}$ and $p16^{INK4A}$ lead to deregulated cell cycle control. These alterations are also demonstrated in asbestos-induced MPM in mice and in multiwalled carbon nanotubes-induced MPM as described by Nagai *et al*[62]. Combined knockout of *INK4A* and *ARF* in mice models play a key contributor and displayed accelerated asbestos-induced MPM compared to single gene knockout[164].

Despite the absence of mutations in oncogenes, integrative pathway analysis of the somatic mutations and copy number alterations identified frequent genetic alterations in MAPK, WNT, cell cycle, p53/DNA repair and PI3K-AKT pathways [144,146]. MAPK signalling cascade is multilevel and occurs in a specific manner with subsequent phosphorylation of cytosolic substrates and translocation to the nucleus to activate transcription factors including c-myc and STATs. *In vitro* studies have demonstrated activation of MAPK signalling as a result of asbestos exposure via *EGFR*-induced ERK activation and via p38 activation that induced a chronic immune response[59,165]. Cell line studies revealed the invasiveness of MPM cells is linked to phosphorylation of p38 leading to *TGFβ 1*-stimulated production of *MMP2*[166]. *In vivo* activation of MAPK in MPM is also evident from analysing phosphorylated proteins by IHC and Western blot but did not differentiate MPM from reactive mesothelial cells thereby questioning its significance in MPM carcinogenesis[167]. But another study found significant ERK phosphorylation by IHC in MPM when compared to normal lung tissues and well differentiated lung cancer that may be prognostic[168]. More recently, an *in vitro* study showed MAPK genes might have different roles in different MPM subtypes and found *ERK2* to be critical in the transformation and homeostasis of epithelioid MPM[169]. Thus, MAPK pathway

requires further investigations as it is important for cell survival and is deregulated in MPM as shown by both exome sequencing and gene expression data.

Both canonical and non-canonical WNT signalling pathways are involved in determining cell fate, cell polarity, cell proliferation and cell death. In the presence of WNT ligands, WNT/ β catenin canonical pathway is activated through formation of a protein complex involving *Fz, LRP5/6* and *Dvl* leading to *LRP6* phosphorylation and activation of Axin complex that inhibits degradation of β catenin. Thus β catenin translocates to the nucleus to interact with *TCF/LEF* leading to β catenin- dependent WNT-responsive gene activation[170].

Overexpression of *Dvl* and cytosolic β catenin has been demonstrated in MPM compared to controls and inhibition of *Dvl* leads to significant antitumor effects both *in vivo* and *in vitro*[171]. Gene expression analysis of WNT pathway genes using a WNT-specific microarrays showed up-regulation of numerous WNT genes (*WNT1*, *WNT2*, *WNT5*) and WNT-related genes (*MYC*, *CCND1*, *JUN*); and down-regulation of WNT antagonists (*DKK1*, *SFRP2*, and *SFRP4*) in MPM[172]. The same study also found *WNT2* is frequently upregulated and inhibition of *WNT2* by siRNA or monoclonal antibody resulted in programmed cell death in MPM cells. Further characterization of WNT pathway in MPM has utilized RT-PCR and real time RT-PCR that confirmed frequent overexpression of *WNT3, WNT5A, FZD2, 4, 6* and *LEF1*; and downregulation of *WNT4, FZD3, SFRP4, APC* and axin2[173]. The authors also demonstrated that *WNT3A* stimulated MPM cell proliferation and targeting β catenin could modulate and sensitise MPM cells to cytotoxic drugs. Several antagonists of WNT signalling (*WIF-1, SFRP1, SFRP2*) are also downregulated in MPM due to promoter hypermethylation as shown by Kohno *et al*[115]. These results suggest deregulation of the WNT pathway is active and relevant in MPM development thus providing means of therapeutic targets and mode of drug resistance.

The PI3K/AKT/mTOR pathway is a major pathway regulating cell cycle, cell growth, migration, invasion and apoptosis in many cancers. *AKT* activation plays a central role in this pathway that is present in MPM cell lines[174,175]. Phosphorylated *AKT* is present in 88% of MPM by IHC but not shown to be prognostic[176]. *PTEN* is a central negative regulator of *AKT* and cell line study by Suzuki *et al* reported *PTEN* homozygous deletion in MPM contributed to *AKT* activation[175]. Loss of *PTEN* expression by IHC was observed in 62% of MPM cases and significantly correlated with shorter survival independent of histologic subtypes[177]. A recent study exploring PTEN-PI3K pathway and downstream proteins in MPM by IHC showed nuclear *PTEN* loss in only 23% of cases but confirmed overexpression of other genes in the pathway including *mTOR, AKT, MAPK* and *FOXO3A*[178]. Low protein expression of p36, downstream effector of the pathway, correlated significantly with longer progression-free and overall survival. Apart from loss of *PTEN, AKT* is activated by receptor tyrosine kinase (RTK) *EGFR, MET* and *AXL*. A cell-line study showed dual targeting of PI3K/mTOR pathway with BEZ235 resulted in greater decreased cell viability and similar results are achieved with combined RTK inhibition compared to single RTK inhibition[179]. Infrequent mutation in *PIK3CA*, the activated p110α catalytic subunit that is essential in translocating AKT onto the plasma membrane, was identified by Lo *et al*. Thus, PI3K/AKT pathway is active in MPM and represents a critical pathway to be targeted consistent with the findings by Alifrangis *et al*[143,146].

Aberrant cell cycle regulation has been described above and contributes to impaired response to DNA damage. DNA repair pathway plays an important role in maintaining genome stability and defects in repair process (due to altered gene expression or SNPs) leads to carcinogenesis and act synergistically with asbestos while adequate repair leads to chemo-and radiotherapy resistance. Roe *et al* showed up-regulation of three base-excision repair genes (*PCNA, FEN1* and *UNG2*) in MPM that represent the major repair system for DNA damage

caused by oxidative stress[133]. The same study also found upregulation of p44 involved in nucleotide-excision repair. A case control study revealed association of *XRCC1* and *ERCC1* SNPs with MPM in a population exposed to high asbestos level. This suggests increased susceptibility to DNA damage favours asbestos-induced carcinogenicity[180]. In addition, polymorphism in *ERCC1* may contribute to cisplatin-resistance. There is little evidence on defect in mismatch-repair system in MPM except upregulation of *MSH6* expression. Genes involved in homologous recombinant repair of double-strand breaks are also upregulated in MPM including *RAD50, RAD54L, RAD21* and *BRCA2*[133]. A cell line study also confirmed overexpression of *BRCA1/2* that contributes to treatment resistance but sensitivity to cisplatin could be restored when *BRCA2* level was lowered with *ERK2* inhbitors[181]. Genes involved in non-homologous end joining repair are also implicated in MPM and include upregulation of *XRCC4* expression, *Ku80* expression and a point mutation in *Ku70* that leads to impair dimerization with *Ku80*[125,133,182].

## 1.7 Conclusions

There is no doubt that progress has been made in the past few years that provided broad insights into the mechanisms of MPM carcinogenesis but improvement in clinical outcome of patients has not been translated. In addition, there are many aspects in MPM carcinogenesis thatstill remain unclear and unknown. Transcriptome studies have provided invaluable biological mechanisms relevant in MPM carcinogenesis. The lack of reproducible genes between microarray studies could possibly be due to experimental or biology variability such as different microarray platforms, analytical tools, small sample size, contamination of tumour tissues with admixture of non-malignant or stromal tissues. Application of exome sequencing in MPM is still lacking behind compared to other tumours and these are limited by similar reasons as described thus limiting a precise delineation of the molecular landscape

in MPM. Current sequencing studies have revealed lack of any "driver'" genes in MPM possibly as a result of large-scale chromosomal loss in MPM and the observed marked heterogeneity in mutation profile between tumours.

Nevertheless, recent findings have been consistent amongst studies with frequent inactivating mutations in *BAP1*, *NF2* and *CDKN2A* and some of the critical genes or pathways have started to emerge as common events in MPM including cell-cell, cell-matrix, Hippo, WNT, PI3K/AKT, MAPK and cell cycle/DNA repair pathways. However, more research are still required in MPM to look for novel biomarkers and therapeutic targets that can eventually lead to clinical benefits. Larger sample size study may be challenging in MPM but the establishment of tissue repositories including the UK Mesobank will aim to provide accessible tissue samples for research. In the interim, small but well-designed studies are still invaluable and by combining datasets from different studies using meta-analysis could lead to identification of more robust and significant genes or pathways for further validation.

In this research, I hope to improve our understanding in the pathogenesis of MPM by examining the gene expression and mutational profiles to identify novel candidate genes and pathways. This research was performed on an independent cohort of MPM tissues and we utilised different data analytical tools compared to published studies for both gene expression and exome sequencing data. The weighted gene co-expression network analysis was used for functional interpretation of differentially expressed genes and this method has not been implemented in MPM study. In terms of whole exome data, candidate variants were selected using different filtering algorithm and criteria.

## 1.8 Hypothesis

I hypothesise that there are important molecular aberrations responsible in driving MPM carcinogenesis.

## 1.9 Aims

To identify and validate candidate molecular alterations and pathways in MPM through gene expression profiling and whole exome sequencing.

To correlate these findings with clinical phenotypes for the identification of potential diagnostic, prognostic and therapeutic biomarkers.

# Chapter 2 - Materials and Methods

## 2.1 Materials

**Table 2.1. Material and Suppliers**

| Material | Supplier |
|---|---|
| 100-bp DNA ladder | New England Biolabs, Herts, UK |
| 1X Tris-Borate-EDTA buffer | Sigma-Aldrich, Dorset, UK |
| Affymetrix® Human Gene 2.1 ST Array Plate | Affymetrix, California, USA |
| Agarose | Sigma-Aldrich, Dorset, UK |
| Ambion® WT Expression Kit | Life Technologies, California, USA |
| BiOstic® FFPE Tissue DNA Isolation Kit | MO Bio Laboratories, California, USA |
| Chloroform-isoamyl alcohol | Sigma-Aldrich, Dorset, UK |
| Deionised distilled water | MilliQ, Hertfordshire, UK |
| Ethanol | Fisher Scientitfic, Loughborough, UK |
| GelRed | Biotium, California, USA |
| GeneChip® hybridisation, wash and stain kit | Affymetrix, California, USA |
| GeneChip® WT Terminal Labeling Kit | Affymetrix, California, USA |
| HotStarTaq *Plus* Master Mix Kit | Qiagen, Crawley, UK |
| Hyclone™ Water | Fisher Scientific, Loughborough, UK |
| Isopropanol | Sigma-Aldrich, Dorset, UK |
| Membrane Slide 0.17 PEN | Carl Zeiss, Cambridgeshire, UK |
| Optimal Cutting Temperature compound | Fisher Scientific, Loughborough, UK |
| Phase Lock Gel | 5 Prime, USA |
| Phenol | Sigma-Aldrich, Dorset, UK |
| Proteinase K | Qiagen, Crawley, UK |
| Qiagen RNeasy® fibrous midi kit | Qiagen, Crawley, UK |
| Quant-iT™ PicoGreen® dsDNA Assay Kit | Life Technologies, California, USA |
| Revised Primers-SYBR Fast Universal kit | D-Mark Biosciences, Toronto, Canada |
| RNA 6000 Nano LabChip kit | Agilent Technologies, California, USA |
| Sample AdhesiveCap 500 clear (D) | Carl Zeiss, Cambridgeshire, UK |
| Sodium Dodecyl Sulphate (SDS) | Sigma-Aldrich, Dorset, UK |
| SureSelect$^{XT}$ Human All Exon V4 | Agilent Technologies, California, USA |
| SureSelect$^{XT}$ reagent kit | Agilent Technologies, California, USA |
| TissueRuptor | Qiagen, Crawley, UK |
| TissueRuptor | Qiagen, Crawley, UK |
| TissueRuptor disposable probe | Qiagen, Crawley, UK |
| Tris-HCl | Qiagen, Crawley, UK |
| Wizard® Genomic DNA Purification Kit | Promega, Southampton, UK |
| Xylene | ReAgent, Cheshire, UK |

## 2.2 Methods

### 2.2.1 Tissue and clinical data collection

Tissue samples were identified from three institutions (1) the Royal Brompton and Harefield NHS Foundation Trust Hospital (RBH), (2) St George's Hospital (SGH) and (3) the Royal Marsden NHS Foundation Trust Hospital (RMH). The use of tissues from RBH was approved by the Respiratory Biomedical Research Units (BRU) Heads of Consortia under the ethical approval given to the BRU Advanced Lung Disease Biobank and the Brompton and Harefield NHS Trust Diagnostic Tissue Bank. A study protocol, Molecular Analyses of Malignant Pleural Mesothelioma (MEMO) (Appendix 2.1), was written by me and co-supervised by the study's primary investigator, Dr Popat. This was approved by research ethics committees and local research and development department for the use of tissues from SGH and RMH.

Funding for this project to cover the costs for sample procurement and reagents was successfully secured from RBH Respiratory BRU Pump-Priming project and RMH Biomedical Research Centre (BRC); both awarded under National Institute for Health Research (NIHR).

Tissue samples identified included frozen tumour tissues stored with or without ribonucleic acid (RNA) *later* and non-malignant frozen pleural tissues stored with or without RNA *later* from RBH. Tissues identified for use under the MEMO study included tumour formalin fixed, paraffin-embedded (FFPE) blocks. In addition, frozen tumour tissues with matched peripheral blood were contributed from an existing study, EQUALITY (an Imperial College London (ICL)-sponsored, prospective study on thoracic cancers undergoing biopsy at SGH (REC reference: 10/H0808/53). Written informed consents for use of tissue +/- blood for research

were available for all participants whose samples were used.

A clinical database was created to store patients' demographic and clinical details collected through retrospective review of case notes and electronic patient records. The data was anonymised in a link-coded manner and entered into a password protected excel worksheet. The following data if available were collected for all patients:

- date of birth
- gender
- date of diagnosis
- histological subtype
- date of death or last follow up
- history of previous cancer or family history of cancer in first degree relatives
- smoking history and asbestos exposure
- treatment details including types of treatments received, date when treatment was commenced and completed, treatment response and date of disease progression.

### 2.2.2 Tissue preparation and quality assessment

#### *2.2.2.1 Microtomy*

Frozen tissue samples were embedded in Optimal Cutting Temperature (OCT) compound followed by cutting five micrometre (µm) sections on a microtome-cryostat. A maximum of two sections per sample were obtained and mounted onto a glass slide for haematoxylin and eosin (H&E) staining. The remaining frozen tissues were immediately stored back in -80 degrees Celsius (°C) freezer after removing as much OCT compound as possible.

Sections from FFPE samples were prepared using a rotary microtome to cut a maximum of two sections of five µm thickness which were mounted onto a glass slide for H&E staining. After histologic assessment, a further five sections were prepared for nuclei acid extractions. In selected FFPE samples for micro-dissection, a further 5-10 sections were prepared and mounted onto a polyethylene napthalate (PEN)-membrane slide.

#### *2.2.2.2 Haematoxylin and Eosin staining*

H&E staining on the sections was performed according to routine histologic protocol[183]. Briefly, the oxidation product of haematoxylin, haematin, stained the nuclei blue and eosin stained the other structures red. Over-staining with eosin was washed out in running water before fixing with xylene.

#### *2.2.2.3 Pathological review*

Sections stained with H&E were examined with a brightfield microscope by me in addition to two certified histopathologists (Professor Nicholson and Dr Montero-Fernandez, RBH) for histopathological verification and tumour abundance assessment. Tumour samples with a minimum arbitrary tumour abundance threshold of 30% viable-appearing tumour cells were taken forward for genomic nuclei acid extractions. Non-malignant areas from selected FFPE samples were identified and marked for micro-dissection to obtain matched normal tissue representative of germline genome.

#### *2.2.2.4 Laser-capture micro-dissection*

Laser-capture micro-dissection (LCM) on FFPE sections was carried out using the PALM

Microbeam (Carl Zeiss, Cambridgeshire, UK) instrument at UCL Cancer Institute and Wolfson Institute for Biomedical Research Centre. Each sections from the selected FFPE samples for micro-dissection were mounted onto individual PEN-membrane slide which was highly absorptive in the UV (ultraviolet)-A range to facilitate laser cutting. To improve laser cutting efficiency, residual paraffin was removed from each section before micro-dissection. The de-paraffination procedure involved immersing membrane slide in xylene for five minutes repeated twice followed by graduated ethanol washes using 100% ethanol for one minute, 96% ethanol for one minute and 70% ethanol for one minute. The deparaffinised membrane slides were left to dry in room temperature prior to micro-dissection. The areas for micro-dissection in each section were visualised via microscopy (Figure 2.1) and targeted for non-contact LCM with each UV laser pulse (Figure 2.2 & 2.3). The dissected non-tumour areas from each section were catapulted and pooled into a 500 microlitre (µl) tube with adhesive cap for each FFPE sample. The micro-dissected areas ranged from 50 to 100 $\mu m^2$ per dissection and each sample had around 300 to 600 micro-dissections pooled together.

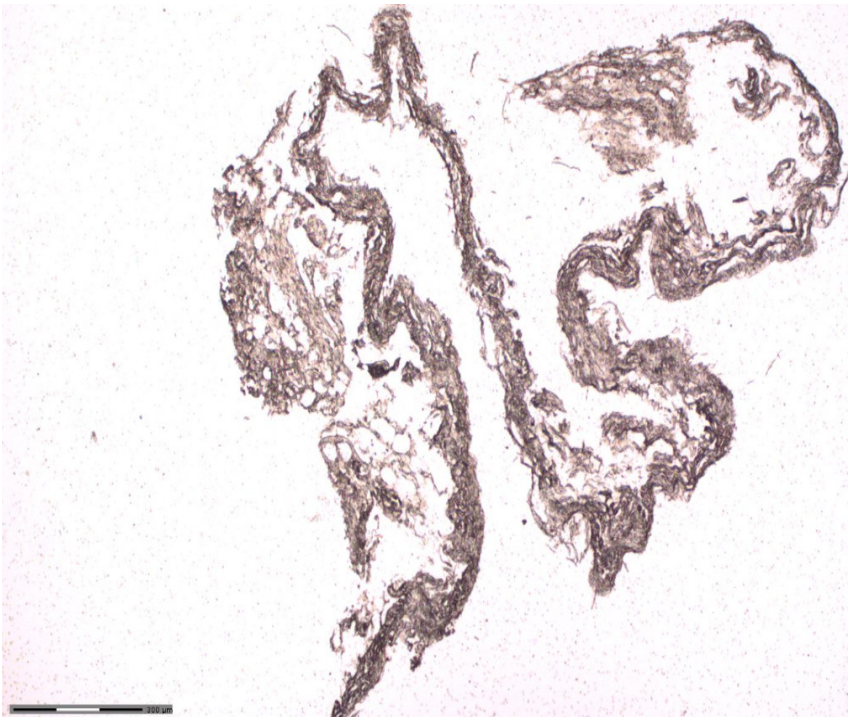

**Figure 2.1. Non-tumour areas identified and visualised via microscopy.**

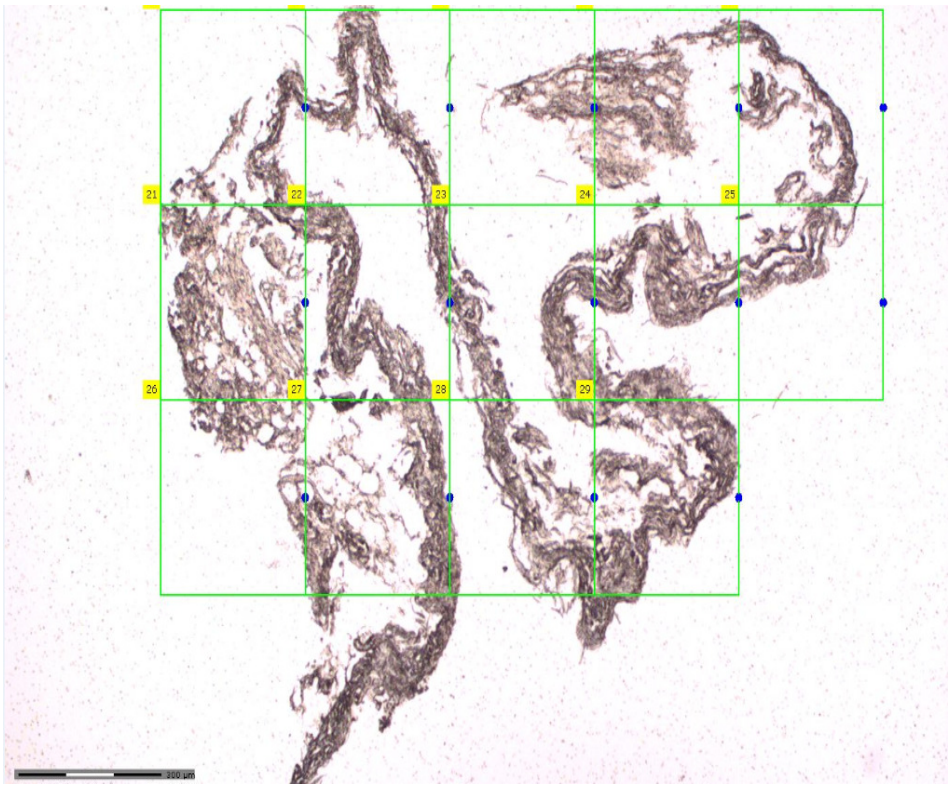


**Figure 2.2. Areas for micro-dissection are marked as shown.**

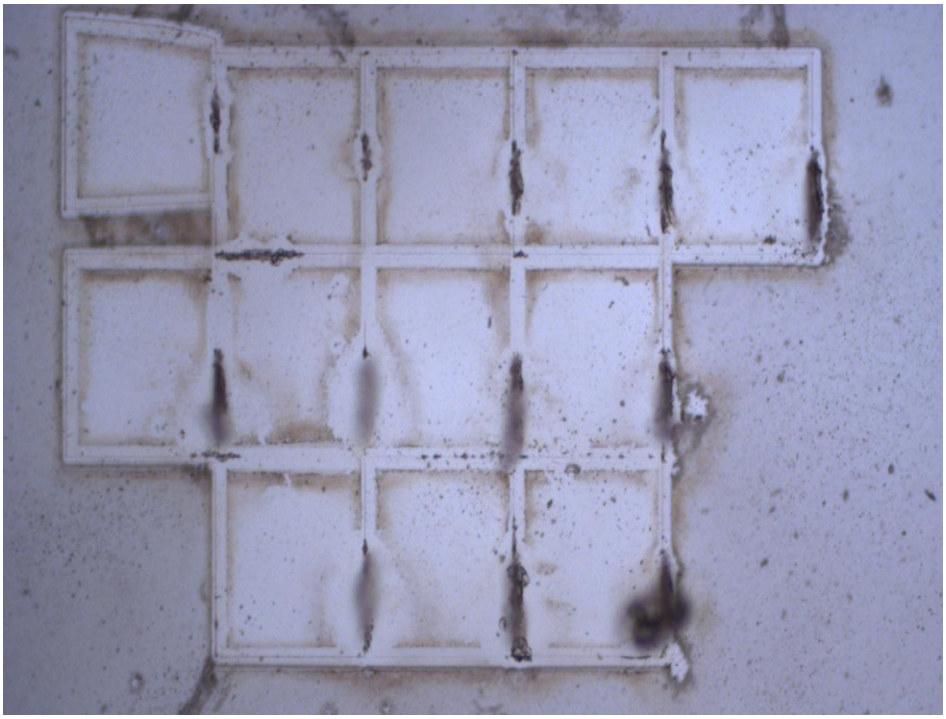

**Figure 2.3. Dissected sections are catapulted and captured into an adhesive cap tube.**

### 2.2.3 RNA isolation

#### *2.2.3.1 Frozen tissues*

Total RNA was isolated from frozen tumour and non-malignant pleural tissues with Qiagen RNeasy® fibrous midi kit (Qiagen, Crawley, UK) as per manufacturer's instructions. Each piece of tissue was submerged in two millilitres (ml) of Buffer RLT (guanidine thiocyanate and beta mercaptoethanol) and ruptured using a TissueRuptor disposable probe and the TissueRuptor (Qiagen, Crawley, UK) for just under a minute. Four ml of RNAse free water and 65 µl of Proteinase K were added to aid protein digestion and inactivate nucleases followed by incubation in a waterbath at 55°C for 90 minutes. The resulting lysate was centrifuged at 3273 x g for 10 minutes to pellet the cell debris and the supernatant was transferred into a new tube containing three ml of 100% ethanol for RNA precipitation. Three

ml of the mixture were transferred at a time to the Midi spin column containing a silica resin membrane to bind the RNA. The spin column was centrifuged at 3273 x g (Beckman Coulter Allegra® X-12R centrifuge) for five minutes and the flow-through was discarded. This step was repeated until all the mixture was transferred. The spin column was then washed by adding two ml of Buffer RW1 (Guanidine Thiocyanante and ethanol) to remove biomolecules (proteins, fatty acids, carbohydrates) and centrifuged for five minutes at 3270 x g. Contaminating deoxyribonucleic acid (DNA) was eliminated by incubation with 160 µl of DNase I (140 µl RDD Buffer and 20 µl DNase I) for 15 minutes at room temperature. The column was incubated with two ml of RW1 buffer at room temperature for two minutes and then centrifuged at 3270 x g for five minutes. This was followed by adding two and a half ml of RPE buffer to remove traces of salt then centrifugation at 3270 x g for five minutes. The bound RNA was eluted from the column by adding 150 µl RNase-free water. The elute was collected from the column following centrifugation at 3270 x g for three minutes and re-applied to the column to repeat the incubation and centrifugation steps once more. The RNA was stored at –80°C until further use.

#### *2.2.3.2 RNA quantification and purity analysis*

RNA yield and purity were measured using the Thermo Scientific NanoDropTM 1000 Spectrophotometer (NanoDrop Technologies, Thermo Fisher Scientific, Delaware, USA). This records the RNA concentration and the A260/280 ratio. The purity of RNA is determined by absorbance at 260 and 280nm with A260/280 ratio of 1.9 to 2.1 being ideal. A lower value may indicate the presence of other contaminants such as protein or phenol.

*2.2.3.3 RNA quality analysis*

The quality of RNA was assessed using one µl of RNA samples, the RNA 6000 Nano Assay™ kit and the Agilent 2100 Bioanalyser™. The gel-dye mix was prepared as per manufacturer's instructions. The appropriate well on the RNA chip was loaded with nine µl of the gel–dye mix and pressure applied to the well via a one ml syringe on a chip priming station. The ladder well and all sample wells were then loaded with five µl of the RNA 6000 Nano marker. The RNA samples and one µl of RNA ladder were denatured at 70 °C for two minutes and then loaded to the appropriate wells. The mixture in the wells was mixed by vortexing for one minute at 2400 rates per minute prior to bioanalyser assessment. The integrity of total RNA was assessed using the 2100 Agilent bioanalyser to determine RNA size, quality and quantity by electrophoresis. A software in the bioanalyser classifies total RNA by generating a RNA Integrity Number (RIN) score from one to 10. A score of one indicates degraded RNA and a score of 10 indicates highly intact RNA. A ratio of 28s to 18s ribosomal subunits of 1.9-2.1 also indicates little or no RNA degradation. Figure 2.4 shows two RNA samples with high RIN score.

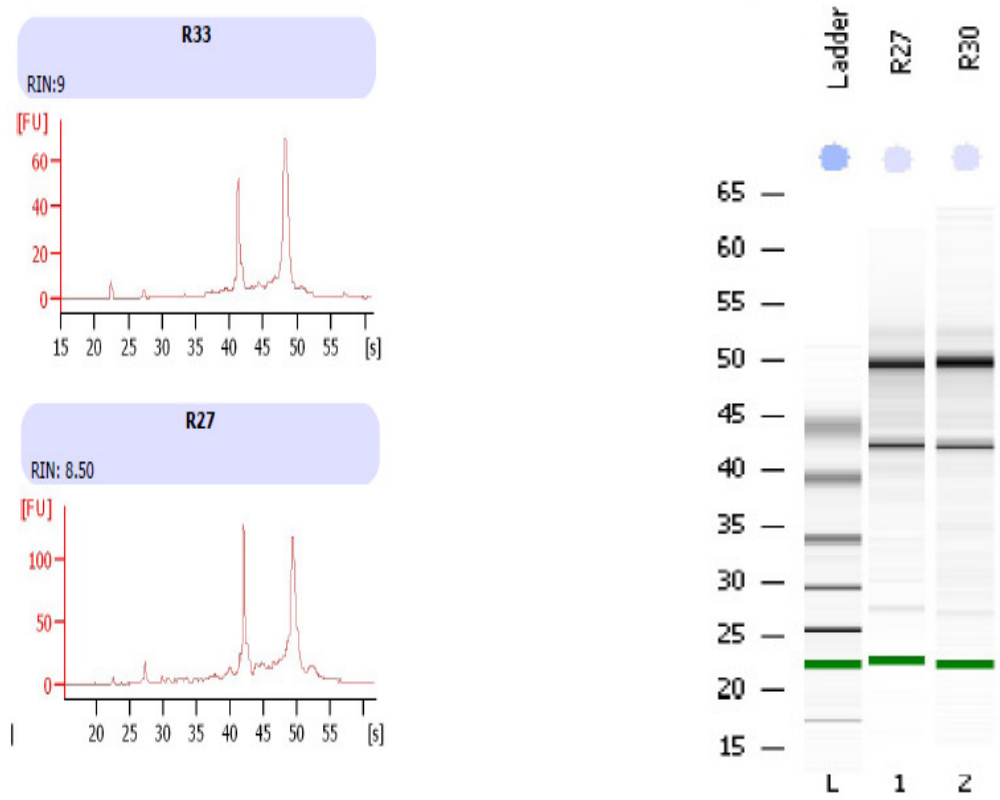


**Figure 2.4. Electrophoretic traces generated on Bioanalyser for RNA samples. This figure shows traces from two cases showing high quality RNA with distinct 18S and 28S rRNA peaks (on the left) and the corresponding gel electrophoresis showing discreet bands of high molecular weight RNA.**

### 2.2.4 Gene Expression Profiling

RNA samples from tumour and unmatched non-malignant pleural tissues (control) with A260/280 ratio of ≥ 1.8 and RIN of ≥ 6.0 were labelled and hybridised in two batches on Affymetrix® Human Gene 2.1 ST Array Plate. The Human Gene 2.1 ST Array Plate covers > 33,500 coding transcripts, > 11,000 long intergenic non-coding transcripts and > 25,000 RefSeq (Entrez) gene counts. The array provides high coverage of the transcribed genome based on data sourced from RefSeq (release51), Ensemble (release 65), lncRNA DB and Broad Institute, Human Body Map lincRNAs and TUCP (transcripts of uncertain coding potential) catalogue. The array contains a median of 21 probes per transcript and 25 bases in

length for each unique probe measuring a median of 525 bases per transcript.

The following subsections describe the process of generating amplified sense-strand complementary DNA (cDNA) using the Ambion® WT Expression Kit (Life Technologies, California, USA) ready for fragmentation and labelling using Affymetrix GeneChip® WT Terminal Labeling Kit (Affymetrix, California, USA) before hybridization onto Affymetrix® Human Gene 2.1 ST Array Plate (Affymetrix, California, USA). All steps were carried out following the manufacturers' protocols. The starting total RNA quantity was 200 nanogram (ng) for tumour and 100 ng for control samples. The Affymetrix® GeneChip® Poly-A RNA control kit (Affymetrix, California, USA) was used to prepare Poly-A RNA control dilutions for 100 ng and 200 ng of total RNA used. The controls were amplified and labelled together with the total RNA samples to monitor the efficiency of the labelling process during the entire experiments.

#### *2.2.4.1 cRNA Amplification*

The synthesis and purification of amplified antisense complementary RNA (cRNA) involved a two days' process. The first day involved synthesis of first strand cDNA. A master mix containing one µl of first-strand enzyme mix (oligo (T7) primer) and four µl of first-strand buffer mix per reaction was prepared. Five µl of the master mix was added to total RNA made up in three µl nuclease-free water mixed with two µl of diluted Poly-A RNA control. The reaction was incubated for one hour at 25 °C then one hour at 42 °C followed by a final incubation for at least two minutes at four °C in a Pettier Thermal Cycler–PTC225 DNA Engine Tetrad (MJ Research).

The synthesis of second-strand cDNA was generated by the addition of second-strand master

mix containing five µl of second-strand enzyme mix (DNA polymerase and RNase H) mixed with 12.5 µl of second-strand buffer mix and re-suspended in nuclease-free water to achieve a final total volume of 50µl. The samples were then incubated in the thermal cycler for one hour at 16 °C then 10 minutes at 65 °C followed by a final incubation for at least two minutes at four °C. Antisense cRNA was synthesized by *in vitro* transcription (IVT) using 30 µl of the IVT master mix containing 6 µl of IVT enzyme mix (T7 RNA polymerase) mixed with 24 µl of IVT buffer mix added to each sample. This was left to incubate in the thermal cycler for 16 hours at 40 °C.

The second day involved purification of cRNA by removal of contaminants and unincorporated nucleotides. This was carried out by isopropanol precipitation using nucleic acid binding beads. A master mix containing 10 µl of nuclei acid binding beads and 50 µl of nuclei acid binding buffer concentrate for each reaction was prepared. This was added to cRNA together with 60 µl of 100% isopropanol and transferred onto a U-bottom plate. The plate was gently shaken on a Lab-Line Titer Plate Shaker for two minutes. The plate was then placed on a magnetic stand to capture the magnetic beads and the supernatant was discarded. The beads were washed twice using 100 µl of nuclei acid wash solution. The purified cRNA was then eluted from the nucleic acid binding beads by adding 35 µl of preheated elution solution. The concentrations and quality of cRNA were analysed using the NanoDrop-1000 spectrophotometer and RNA 6000 Nano Assay™ kit with the Agilent 2100 Bioanalyser™. An electropherogram of a good cRNA synthesis consisted of a smear of products between 50 and 4500 nucleotides (nt) long as shown in Figure 2.5.

B

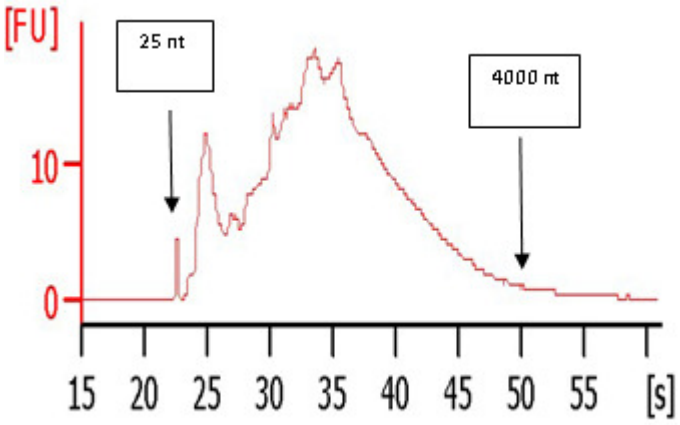


**Figure 2.5. Bioanalyser Electropherogram (A) and Gel Image (B) of cRNA. Based on the data from an RNA size reference ladder, the fluorescence of 25 nt is between 20 and 25 seconds and 4000 nt is detected at 50 seconds as marked. [FU], fluorescence unit; [S], second.**

*2.2.4.2 cDNA Amplification*

The synthesis of sense-strand cDNA involved reverse transcription of cRNA using random primers. Ten µg of purified cRNA was prepared and made up to a volume of 22 µl with nuclease-free water. On ice, two µl of random primers were added to each sample followed by denaturing of cRNA in the thermal cycler for five minutes at 70 °C, five minutes at 25 °C and two minutes at four °C. After the incubation, the second cycle master mix was prepared using eight µl of 2$^{nd}$-Cycle Buffer Mix and eight µl of 2$^{nd}$-Cycle Enzyme Mix for each reaction. Sixteen µl of the master mix was added to each sample followed by incubation in the thermal cycler for 10 minutes at 25 °C, then 90 minutes at 42 °C and two minutes at four °C. This was followed by the addition of two µl of RNase H to degrade cRNA template leaving only single-stranded cDNA and left to incubate in the thermal cycler for 45 minutes at 37 °C, five minutes at 95 °C and two minutes at four °C.

The purification of cDNA involved ethanol precipitation using nucleic acid binding beads. A

master mix containing 10 µl of nuclei acid binding beads and 50 µl of nuclei acid binding buffer concentrate for each reaction was prepared. This was added to cDNA together with 120 µl of 100% ethanol and transferred onto a U-bottom plate. The plate was gently shaken on a Lab-Line Titer Plate Shaker for two minutes. The magnetic beads were captured with the use of magnetic stand and discarding the supernatant. The beads were washed twice using 100 µl of nuclei acid wash solution. The cDNA was eluted from the nucleic acid binding beads by the addition of 30 µl of pre-heated elution solution. The concentrations and quality of purified cDNA were analysed using the NanoDrop-1000 spectrophotometer and RNA 6000 Nano Assay™ kit with the Agilent 2100 Bioanalyser™. The median cDNA profile size should be around 400 nt. The figure below, Figure 2.6, shows an example of a cDNA profile.

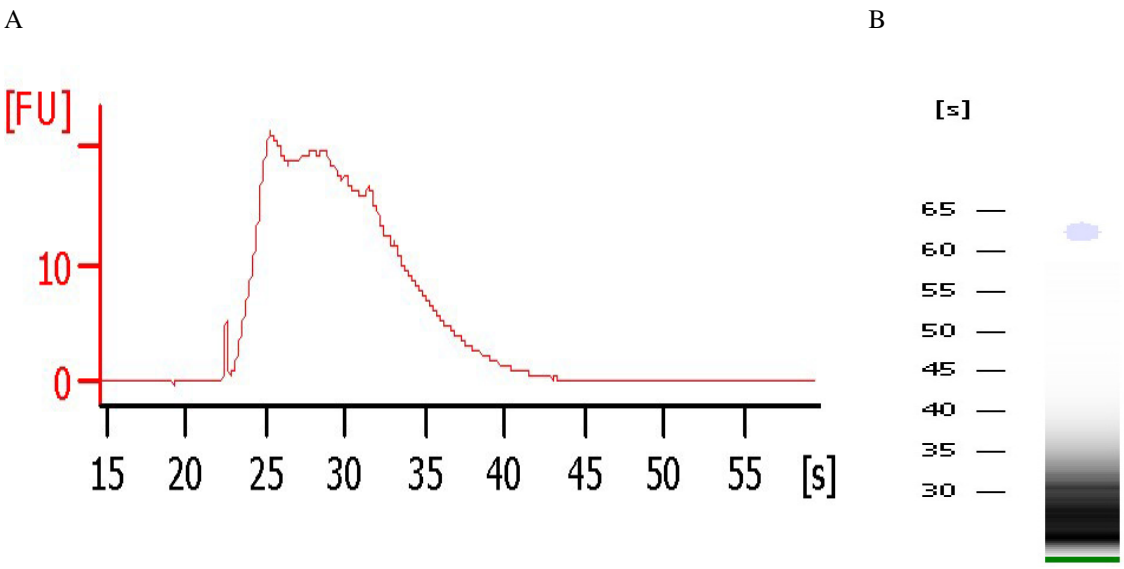


**Figure 2.6. Bioanalyser Electropherogram (A) and Gel Image (B) of cDNA. [FU], fluorescence unit; [S], second.**

### *2.2.4.3 Fragmentation, Labelling and Hybridization*

The process of cDNA fragmentation, labelling and hybridisation was all carried out on the same day. The Affymetrix GeneChip® WT Terminal Labeling Kit (Affymetrix, California,

USA) was used for cDNA fragmentation and labelling. The fragmentation step involved using five and a half µg of single-stranded cDNA made up to a total volume of 31.2 µl with nuclease-free water. The fragmentation master mix was prepared with 10 µl of RNase-free water, 4.8 µl of 10X cDNA fragmentation buffer, one µl of UDG (10 U/µl) and one µl of APE 1 (1,000 U/µl) for each reaction. This mixture was added to each sample and left to incubate in the thermal cycler for 60 minutes at 37 °C, two minutes at 93 °C and two minutes at four °C. The quality of fragmented cDNA was analysed using RNA 6000 Nano Assay™ kit with the Agilent 2100 Bioanalyser™. For successful fragmentation, the expected range in peak size of the fragmented samples should be approximately 40 to 70 nt. Figure 2.7 shows an example of a successful cDNA fragmentation.

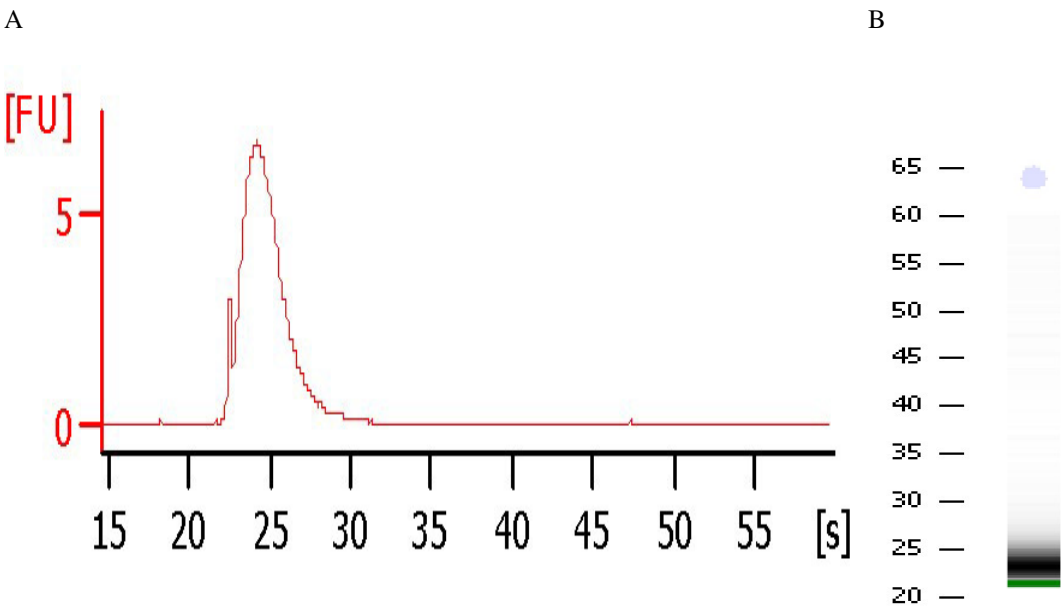


**Figure 2.7. Bioanalyser Electropherogram (A) and Gel Image (B) of fragmented ss cDNA. [FU], fluorescence unit; [S], second.**

The labelling master mix was prepared using 12 µl of five X TdT buffer, two µl of TdT and one µl of DNA labelling reagent for each reaction. This was added to 45 µl of fragmented single-stranded cDNA samples followed by incubation in the thermal cycler for 60 minutes at

37 °C, 10 minutes at 70 °C and four °C for at least two minutes.

The hybridisation step involved the use of the GeneChip® hybridisation, wash and stain kit (Affymetrix, California, USA). The 20X eukaryotic hybridisation controls (*bioB, bioC, bioD, cre*) were denatured at 65 °C for five minutes on a heating block. Hybridization cocktail was prepared and consisted of 1.2 µl of control Oligonucleotide B2, six µl of denatured 20X eukaryotic hybridisation controls, 24 µl of 5X WT Hyb Add 1 and eight µl of 15X W Hyb Add 4 for each array/sample. This cocktail mix was added to 32.8 µl of the fragmented and labelled cDNA. The cocktail was denatured in the thermal cycler for five minutes at 95 °C followed by 45 °C for five minutes and centrifuged for one minute at 5000 rpm at room temperature.

The GeneTitan™ Multi-Channel Instrument was used to process the array plate from target hybridisation to data generation using a combination of a hybridisation oven, fluidics processing and imaging device. Prior to hybridisation process, the setup of the GeneTitan™ Instrument involved deionising stain trays and lids, filling up the trays with the recommended buffer, filling up the bottles for washing and emptying the bottle for rinsing. This was followed by loading 90 µl of the centrifuged supernatant hybridisation mix into the appropriate well of the Affymetrix® Human Gene 2.1 ST Array Plate. The hybridisation process and scanning of the array plate took approximately 16 hours on the GeneTitan™ Instrument.

#### *2.2.4.4 Pre-processing of raw microarray data*

Raw microarray data from Affymetrix was generated with the extension CEL format. The CEL file contained the raw probe data from measured probe intensities in the hybridised

microarray. Data analysis was carried with R studio software and the relevant packages.

The preprocessing steps of Affymetrix probe-level expression data consisted of quality assessment, background adjustment, normalization, and summarization at the probe set level as a measure of the expression level of corresponding messenger RNA (mRNA). The assessment of raw data quality was performed using arrayQualityMetrics (version 3.2)[184]. This package produces a comprehensive report in a specified directory and an HTML page. The report contains a metadata table about the quality of the arrays and for outlier detection. The quality assessment is based on comparison between arrays, array intensity distributions and individual array quality.

After removing outlier arrays, the apt-probeset-summarize programme (Affymetrix Power Tools) was used for background correction, normalisation and summarising probe data from CEL files. Probe intensities was adjusted for background intensities (none or nonspecific hybridisation and fluorescent artefacts) to give a more accurate measure of spot intensity. Normalisation was performed to correct for differences in probe intensities between samples based on the assumption that the distribution of intensities was constant and taking into account housekeeping genes and spike in controls. The random multiple access (RMA) procedure was used for both background adjustment using only perfect match (PM) probe intensities and for probe-level data normalisation with quantile normalisation method[185,186]. This was followed by median polish procedure to summarise the PM intensities. Expression values of each probe set were calculated by using the rmasummary function that summarised the probe set intensity summaries on a logarithm of 2 scale. Transcripts with expression level that were below the median expression value in all samples were identified and removed.

Next, the variability of experimental effects was quantified using principal variance

component analysis (PVCA) (version 1.10 R package) method[187]. Variables from the phenotype file were specified and included for PVCA analysis to identify the prominent sources of variability. This method involves principal component analysis to reduce data dimension while retaining the maximum variability of the data, and variance components analysis to fit a mixed linear model to each principal components using a number of factors as random variables. The proportion of total variance was estimated by standardising the corresponding eigenvalues as weights.

#### *2.2.4.5 Differential Gene expression analysis*

After pre-processing and filtering steps, the gene expression data was analysed using unsupervised 2-dimensional hierarchical clustering algorithm to assess clustering of samples. Differentially expressed genes were identified by applying parametric tests to rank genes with respect to the resulting probability (p)-value using the limma package (version 3.2)[188]. First, a design matrix representing the gene expression data and the contrast matrix representing the coefficients of the design matrix that modelled the contrasts of difference between the tumours and controls were specified. A linear model was used to model the data set and the contrast matrix allowed the fitted coefficients to be compared and to generate moderate t-statistics using the empirical Bayes method. The raw p-values were adjusted for multiple testing using the Benjamini & Hochberg method to control for expected false discovery rate (FDR)[189].Transcript clusters were then annotated using HuGene-2_0-st-v1 Transcript Cluster Annotations (Affymetrix, California, USA). Genes with an adjusted p-value of $\leq 0.01$ and fold change (FC) in the level of expression of $\geq$ two were selected and analysed using WebGestalt Gene Set Analysis ToolKit to identify enriched Gene Ontology (GO) terms and Kyoto Encyclopaedia of Genes and Genomes (KEGG) pathways[190].

*2.2.4.6 Weighted gene co-expression network analysis*

The weighted gene co-expression network analysis (WGCNA, version 1.49) was used to construct MPM-associated gene co-expression networks and identification of potential hub genes (genes with high connectivity) contributing to MPM carcinogenesis[191]. Differentially expressed genes with an adjusted p-value of $\leq 0.05$ were selected together with clinicopathological variables for WGCNA analysis.

Firstly, gene expression profiles were converted into connection weights using a Pearson correlation to relate every pairwise gene-gene relationship. These were then transformed into an adjacency matrix by using a soft thresholding power β. A power β of nine was chosen based on the network exhibiting approximate scale-free topology criteria and high connectivity. The adjacency was then transformed into a network distance measure known as the topological overlap matrix (TOM) to allow identification of genes that form highly integrated clusters of co-expressed genes (modules). Modules containing genes with high topological overlap were identified by (1) calculating the corresponding TOM dissimilarity measures (TOM-1), (2) hierarchical clustering analysis to produce a clustering dendrogram of genes based on TOM dissimilarity, (3) dynamic tree-cut algorithm to calculate the module eigengenes and clustering them based on a height cut of 0.25 corresponding to a correlation of 0.75.

Next, the module eigengenes (MEs) were computed by retaining the first principal component following principal components analysis of the $\log_2$ expression data for each module. MEs represent a summary measure for the overall co-expression network in that module. The MEs were then tested for association with clinicopathological variables adjusted for age and gender using the linear regression model. The resulting p-values were adjusted for multiple testing by

Benjamini & Hochberg method. For each gene, an intramodular connectivity ($k_{me}$) was calculated that measured its connectivity with respect to other genes in a particular module. Module membership (MM) of a gene was derived from Pearson's correlation coefficient between the expression profile of that particular gene and the MEs.

The biological significance of a gene to a clinical variable known as gene significance (GS) was calculated for each gene. The linear regression model was used to regress the clinicopathological variables and individual gene expression profile adjusted for age and gender. The GS measure was defined as minus the logarithm of the resulting adjusted p-value. To assess associations with survival data, Cox proportional hazards model was used to regress survival time on individual gene expression profile adjusted for age and gender. The hazard ratio was computed with the corresponding p-value for each genes and the prognostic GS of a gene was defined as minus the logarithm of the p-value. The ModuleEnrichment function was used to generate bar plot, 95% confidence interval of the mean and a Kruskal Wallis p-value to identify modules enriched with genes associated with survival. Spearman's correlation was used to relate the GS and $k_{me}$ or MM that allowed us to identify potential hub genes that have high GS for the clinical variable of interest and high connectivity within the module.

The network from WGCNA analysis was visualised through Cytoscape Software 3.0.1[192]. Reactome Cytoscape Plugin was used for functional enrichment analysis for GO terms and associated pathways. CyTargetLinker from Cytoscape was used to generate biological networks with regulatory and drug-target interactions. Regulatory data was extracted from homosapiens Regulatory Interaction Networks, Cytoscape.

### 2.2.5 DNA isolation

#### *2.2.5.1 Frozen tissues*

Total genomic DNA was isolated from frozen tumour tissues containing 30% or more viable-appearing tumour cells using the phenol-chloroform method. Each piece of tissue was ruptured in 2710 µl re-suspension buffer (0.075M NaCl, 0.024M EDTA pH 8, deionised distilled water) and 271µl 10% SDS using a TissueRuptor disposable probe and the TissueRuptor (Qiagen, Crawley, UK) for approximately one minute. This was followed by adding 22µl of Proteinase K to aid protein digestion and the resulting lysate was left to incubate overnight in a water bath at 37°C.

On the following day, three ml of the clear lysate was transferred to a pre-spun light phase lock gel tube containing an equal volume of buffered phenol solution, mixed thoroughly and centrifuged for 10 minutes at 2000 x g (Beckman Coulter Allegra® X-12R centrifuge) to yield a lower organic protein-containing phase and an upper nuclei acid containing aqueous phase. Next, three ml of phenol:chloroform:isoamyl solution (25:24:1) were added and centrifuged for 10 minutes at 2000 x g. In order to partition the remaining lipids, three ml of chloroform:isoamyl (24:1) were added and centrifuged for 10 minutes at 2000 x g. The aqueous phase was decanted into a new tube containing 300µl Sodium Acetate and six ml of 100% ethanol for precipitation and cooled for 90 minutes at -20°C. DNA pellet was separated from the supernatant by centrifugation at 1800 x g and at four °C for one hour. The supernatant was removed and the pellet was left to dry at room temperature for 20 - 30 minutes to remove traces of ethanol. Finally, DNA was re-suspended in 250µl 10mM Tris-HCL (Qiagen, Crawley, UK) and stored overnight at four °C. DNA was assessed for quality and yield the next day and the remaining samples were stored at -80°C until further use.

*2.2.5.2 Blood*

DNA isolation from whole blood samples identified from EQUALITY study was carried out using Wizard ® Genomic DNA Purification Kit (Promega, Southampton, UK) following the manufacturer's instructions. Blood sample was transferred into a 50 ml centrifuge tube containing 30 ml of Cell Lysis solution for red blood cells lysis. These were mixed thoroughly by inverting the tube several times. The mixture was incubated at room temperature for 30 minutes on a rocker set at medium speed. This was followed by centrifugation at 2000 x g for 10 minutes at room temperature. The supernatant was discarded leaving behind the white blood cells pellet with approximately 1.4ml of residual liquid. The white blood cells were re-suspended by vortexing the tube vigorously followed by the addition of 10ml of Nuclei Lysis solution to lyse the white blood cells. The mixture was incubated in a water bath at 37°C for two hours. The cellular proteins were removed by salt-precipitation method involving the addition of 3.3 ml of Protein Precipitation Solution and centrifugation at 2000 x g at room temperature for 10 minutes. This resulted in a lower protein-containing phase and an upper genomic DNA-containing phase. The supernatant was transferred to a fresh tube containing 10 ml of isopropanol to concentrate and desalt the genomic DNA. By gently inverting the tube, DNA was visible as thread like strands and DNA pellet was obtained by centrifugation the mixture at 2000x g for two minutes at room temperature. After discarding the supernatant, 10 ml of 70% ethanol was added to wash the DNA pellet followed by centrifugation at 2000 x g for 2minutes. The ethanol was discarded and DNA pellet was left to air dry for 10 minutes. Finally, the DNA was re-suspended in 800 µl of rehydration solution and left to incubate for few days at four °C before assessing the quality and yield.

#### *2.2.5.3 FFPE*

DNA was isolated from five micro-dissected FFPE sections of five µm thickness using the BiOstic® FFPE Tissue DNA Isolation Kit (MO Bio Laboratories, California, and USA). This was carried out by collaborators at McGill University and Genome Quebec Innovation Centre, Canada. Briefly, paraffin wax from samples was melted away using an optimised wax melting buffer without the use of organic solvent, xylene, and the addition of proteinase K to aid tissue digestion. This was followed by a 90°C heating step to remove cross-linking in DNA. The sample was then mixed with a salt binding buffer and 100% ethanol for binding to silica filters. Impurities were washed from the column and pure DNA was eluted in a low salt buffer.

#### *2.2.5.4 DNA quantification and purity analysis*

DNA yield and purity were assessed using the Thermo Scientific NanoDropTM 1000 Spectrophotometer (NanoDrop Technologies, Thermo Fisher Scientific, Delaware, USA). This records the DNA concentration and the A260/280 ratio. DNA concentration is determined by absorbance at 260 nm, the peak for DNA, and the modified Beer Lambert equation (a reading of 1.0 at 260 nm corresponded to 50 µg/ml of double-stranded DNA). Purity is estimated by the ratio of absorbance at 260 and 280 nm. The absorbance at 260 nm measures not only double-stranded DNA but also single-stranded DNA and other contaminants such as proteins and extraction buffers. A ratio around 1.8 indicates good quality DNA. Lower values indicate protein contamination and higher values of 2.1 or more indicate RNA contamination.

DNA quantification was also performed by fluorometry using Quant-iT™ PicoGreen®

dsDNA Assay Kit (Life Technologies, California, USA). This was carried out by collaborators at McGill University and Genome Quebec Innovation Centre, Canada, on DNA isolated from frozen samples sent for whole exome sequencing and from micro-dissected FFPE sections. PicoGreen® quantified double-stranded DNA with high sensitivity. The fluorescent dye exhibits an emission peak at 530 nm and fluorescent enhancement is exceptionally high when bound specifically to double-stranded DNA.

### 2.2.6 Whole exome sequencing

Whole exome sequencing of genomic DNA was carried out by collaborators at McGill University and Genome Quebec Innovation Centre, Canada, with Illumina HiSeq platform. This platform utilises sequencing by synthesis technology to generate exome data[193]. The technology enables detection of single bases when added to DNA strands using fluorescent reversible terminator deoxyribonucleotides. The images of fluorescent terminator are captured as deoxyribonucleotide triphosphate (dNTP) is added, and then cleave so that the next base could be added and imaged. The presence of four reversible terminator-bound dNTPs minimises incorporation bias present during each sequencing cycle.

Libraries were generated robotically using SureSelect$^{XT}$ reagent kit (Agilent Technologies, California, USA) following the SureSelect$^{XT}$ Target Enrichment System for Illumina Paired-End Multiplex Sequencing protocol. Briefly, three μg of concentrated and purified genomic DNA was fragmented to around 200 base pairs (bp) using the Covaris instrument. After end-repair and A-tailing, sequencing adapters were ligated onto the DNA fragments followed by PCR amplification of the adaptor-ligated library. After purification with AMPure XP beads, the adapter-ligated DNA libraries were concentrated for hybridisation using SureSelect$^{XT}$ Human All Exon V4 baits (Agilent Technologies, California, USA). The captured product was

amplified with indexing primers by PCR and purified with AMPure XP beads. The concentration of the sequencing libraries was quantified using the Quant-iT™ PicoGreen® dsDNA Assay Kit (Life Technologies, California, USA) and the Kapa Illumina GA with Revised Primers-SYBR Fast Universal kit (D-Mark). Average size fragment was determined using a LaChip GX (PerkinElmer) instrument. Each captured library was loaded on the Illumina HiSeq2000 for sequencing according to standard protocols

#### *2.2.6.1 Data processing and quality control*

Raw image files were processed with Illumina base calling software 1.7 for base calling using default parameters and the sequences of each library were generated as 90 bp paired-end reads. The target regions were sequenced to 100-160X mean coverage in each sample. These were trimmed from the 3'end to give a base quality score of at least 30 as encoded in phred 33. Sequencing adapters were clipped off to generate all reads with a length of at least 50 bp.

The reads were then mapped to the reference human genome (UCSC hg19) using Burrows–Wheeler aligner[194]. A single global Binary Alignment Map (BAM) file for each tumour and normal samples was generated using the Picard software[195]. Data quality control was processed with GATK software as suggested by the Broad Institute and these include realignment of short insertions and deletions (indels), recalculation of the realigned read mate coordinates, marking of read duplicates and base quality recalibration to generate a more accurate quality score based on covariates such as reported quality score, position within the read accounting for the preceding and current nucleotide.

*2.2.6.2 Variant analysis*

GATK Unified Genotyper variant discovery tool was used for calling variants from the processed BAM files[196] . This was followed by variant score recalibration for single nucleotide variants (SNVs) and indels separately to generate variant call format (VCF) files for SNVs and indels respectively. The VCF files were annotated using ANNOVAR[197] to obtain gene-based (e.g. functional consequences on genes), region-based (e.g. conserved regions) and filter-based annotations (e.g. 1000 Genomes Project, dbSNP) for each variant.

In order to identify candidate SNVs and indels, the annotated files were subjected to a series of filtering steps. Somatic variants were identified after removing variants present in the matched normal samples. Common single nucleotide polymorphisms (SNPs) present in dbSNP138, 1000 Genomes Project and NHLBI GO Exome Sequencing Project 6500 were filtered out. The functional significance of each variant was assessed using Polyphen-2 (genetics.bwh.harvard.edu/pph2/), SIFT (sift.jcvi.org/) and MutationTaster (www.mutationtaster.org/) programs, which score variants by the predicted effect on protein functions. Variants with non-deleterious or non-damaging functional consequences were removed.

Potential driver mutations were identified from one of the following criteria:

- somatic non-synonymous SNV predicted to alter protein function by one of the three algorithms: Polyphen-2 (genetics.bwh.harvard.edu/pph2/), SIFT (sift.jcvi.org/) and MutationTaster (mutationtaster.org/)

- recurrent somatic mutations that cluster in a specific domain of the gene (mutation

hotspots) or recurrent somatic mutations distributed along a gene

- genes implicated in other types of malignancy

Pathways enrichment of somatic mutations (nonsense, damaging or deleterious missense, splicing mutations and indels) were analysed with NetworkAnalyst tool whereby genes from our exome data were used as priory and mapped to a manually curated protein-protein interaction database to construct non-random networks[198].

*2.2.6.3 Polymerase chain reaction and Sanger sequencing*

Candidate point mutations or indels identified from whole exome sequencing were chosen for confirmation by amplifying the region of interest using polymerase chain reaction (PCR) followed by DNA sequencing with chain-terminating inhibitors method, Sanger sequencing. This method is based on the incorporation of 2',3'dideoxynucleotides (ddNTP's) by DNA polymerase at the 3' end of the growing chain during in vitro DNA replication. Chain elongation is terminated selectively at A, C, G or T due to the lack of 3'-hydoxyl group[199].

First, the genomic sequence of the candidate variants was obtained from UCSC Genome Browser (UCSC Genome Bioinformatics). PCR primers of at least 200 bases long were designed using the Primer3web (version 4.0.0) or ExonPrimer (http://ihg.gsf.de/ihg/ExonPrimer.html) programme and checked for sequence specificity with In-Silico PCR (UCSC Genome Bioinformatics). A working solution of 10 micro-molar (µM) for each primer pair was prepared using five µl of 50 µM stock solution of the forward primer and five µl of 50 µM stock solution of the reverse primer in 15 µl of Hyclone ™ molecular biology grade water (Fisher Scientific, Loughborough, UK). The primer pairs were initially tested on one µl of control DNA (10ng/µl). Next, DNA from tumour +/- normal (10ng/µl)

samples with the candidate mutations was subjected to PCR using the specific primer pairs.

Each 20 µl of the PCR reactions consisted of 10 µl of the HotStarTaq *Plus* Master Mix (HotStarTaq *Plus* DNA polymerase, PCR Buffer with 3mM $MgCl_2$ and 400 µM of each dNT, HotStarTaq *Plus* Master Mix Kit, Qiagen, Crawley, UK), eight µl of RNase-Free Water (HotStarTaq *Plus* Master Mix Kit, Qiagen, Crawley, UK), one µl of tumour+/-normal DNA (10ng/ µl) and one µl of the primer pair working solution.

PCR was carried out using Pettier Thermal Cycler–PTC225 DNA Engine Tetrad (MJ Research). The PCR cycling conditions were optimised and consisted of an initial activation of HotStarTaq *Plus* DNA polymerase at 95°C incubation step for five minutes followed by 35 cycles of denaturing at 95°C for 15 seconds, annealing at 56 °C for 30 seconds, extension at 72 °C for 30 seconds and a final hold at 4 °C.

Gels were prepared using two grams (gm) of 2 % agarose (Sigma-Aldrich, Dorset, UK) in 100 ml of 1X Tris-Borate-EDTA buffer (Sigma-Aldrich, Dorset, UK) and dissolved in a microwave. One µl of GelRed™ (Biotium, California, USA) was then added to the gel solution. The solution was poured into a gel-casting tray with comb inserted and allowed to set at room temperature for 30 minutes. A 100-bp DNA ladder (New England Biolabs, Herts, UK) was used as the molecular size marker and samples were loaded into individual wells and electrophoresed in 1X Tris-Borate-EDTA buffer at 100 voltages for 45 minutes. The agarose gel was then inspected under ultraviolet light (FirstLight UV illuminator, Ultra Violet Products Inc., BioDoc-It ™ imaging system) to visualize the bands of the amplicons.

The amplicons were subjected to Sanger sequencing provided by Eurofins Genomic. The results were available in SEQ file and analysed using SEQUENCHER (Gene Codes

Corporation) that allowed editing, trimming and quality checks of the sequences to detect the mutation of interest.

# Chapter 3 - Global Gene Expression Profiling of Malignant Pleural Mesothelioma

## 3.1 Introduction

Gene expression profiling using high-throughput array-based technologies allows simultaneous analysis of many genes from multiple samples. Studying the altered expression of genes, including oncogenes and tumour suppressor genes, and correlations with cellular and physiological state would lead to better understanding of cancer biology. Cancers including malignant pleural mesothelioma (MPM) are classified primarily based on histopathological features of the tumour but similar morphological subtypes show clinical heterogeneity in terms of prognosis and response to therapies. Global gene expression profiling allows identification of new subtypes based on gene signatures to improve class classification, prognosis and response to treatment prediction[200]. This is particularly important in clinical setting as it could potentially lead to personalised therapies based on the molecular signatures of the cancer such as in breast cancer and diffuse large B-cell lymphoma[201,202].

Till date numerous microarray studies on gene expression in MPM have been conducted and reviewed by Melaiu *et al*[136]. These studies were carried out on cell lines and on human MPM tissues to improve diagnosis, histological classification and identification of predictive biomarkers for this fatal disease. These have identified deregulated oncogenes, tumour suppressor genes and other genes of prognostic value. However, these biomarkers have not proven to be of clinical value as majority of them have not been reproducible between various studies. These could be due to several reasons including relatively small sample size, contamination of tumour samples with normal stromal cells that prevents precise delineation

of deregulated genes, use of different microarray platforms and inconsistent statistical methodologies. Nevertheless, data from further microarray studies could be still be useful in identifying novel biomarkers and could be integrated with existing data to increase statistical power for meta-analysis.

The first objective of this chapter is to identify genes that are deregulated in MPM compared to non-malignant pleura (controls) and their associated enriched pathways. Secondly, we applied weighted gene co-expression network analysis (WGCNA), a 'guilt-by-association'-based method which has not been performed in MPM gene expression studies, to detect clusters of genes that are coexpressed or coregulated (modules) independent of the clinical phenotypes across the MPM cases[203]. This methodology has been applied successfully in cancer research and has led to the identification of several molecular targets including *ASPM* gene in glioblastoma[204]. Genes that are coexpressed may share similar biological process and provide further biological information about the genes that are differentially expressed between MPM and controls. The identified modules are then tested for association with clinical phenotypes including histological subtypes and survival outcome. The pathways and networks of these clusters will be interrogated to reveal their roles in the pathogenesis of MPM.

## 3.2 Materials and methods

### 3.2.1 Tissues acquisition

Tissues used for total ribonucleic acid (RNA) extractions were provided by Biomedical Research Units (BRU) Advanced Lung Disease Biobank and the Brompton and Harefield NHS Trust Diagnostic Tissue Bank. The use of these tissues had been ethically approved and

written informed consents from patients were verified. A total of 26 MPM and 10 control frozen tissues stored with or without RNA *later* were identified. Tissues not stored in RNA *later* were subjected to pathological review using newly prepared haematoxylin and eosin (H&E) stained sections to confirm diagnosis and tumour abundance (Chapter 2 section 2.2.2.2 and 2.2.2.3). For all other tissues, histopathological reports were checked and verified. Tissues used as controls were taken from patients who underwent surgical procedures for pneumothorax and the histology was non-malignant reactive pleura.

### 3.2.2 RNA isolation, quantification and quality assessments

Total RNA was extracted from the collected tissues using Qiagen RNeasy® fibrous midi kit (Qiagen, Crawley, UK) as described in Chapter 2 section 2.2.3.1. RNA concentration and yield were quantified with Thermo Scientific NanoDropTM 1000 Spectrophotometer (NanoDrop Technologies, Thermo Fisher Scientific, Delaware, USA). The quality of RNA was assessed with RNA 6000 Nano Assay™ kit and the Agilent 2100 Bioanalyser™ (Agilent Technologies, California, USA) (Chapter 2 section 2.2.3.3). A RNA Integrity Number (RIN) score was generated to assess the quality of each RNA samples.

### 3.2.3 Gene expression profiling

Section 2.2.4 in Chapter 2 described in detail the process of gene expression profiling carried out with Affymetrix® Human Gene 2.1 ST Array Plate (Affymetrix, California, USA). Briefly, this involved generating amplified sense-strand complementary deoxyribonucleic acid (cDNA) with the Ambion® WT Expression Kit (Life Technologies, California, USA) for fragmentation and labelling processes using Affymetrix GeneChip® WT Terminal Labeling Kit (Affymetrix, California, USA). The sense-strand cDNA was then hybridised onto

Affymetrix® Human Gene 2.1 ST Array Plate (Affymetrix, California, USA) and processed with GeneTitan™ Multi-Channel Instrument.

### 3.2.4 Data pre-processing and analysis

The quality assessment of raw probe level intensity data was carried out with Expression Console (EC) software (Affymetrix, California, USA) and arrayQualityMetrics (version 3.2) as described in Chapter 2 section 2.2.4.4 The preprocessing steps included background adjustment, normalisation, and summarisation at the probeset level as a measure of the expression level of corresponding mRNA with the apt-probeset-summarize programme (Affymetrix Power Tools).

Differentially expressed probesets with a false discovery rate (FDR) of 1% and fold change (FC) in expression level of $\geq 2$ in MPM compared to controls were identified using the empirical Bayes method (Chapter 2 section 2.2.4.5). The genes were interrogated for gene ontology (GO) terms and Kyoto Encyclopaedia of Genes and Genomes (KEGG) pathways enrichment using WebGestalt Gene Set Analysis ToolKit[205]. We then applied weighted gene co-expression network analysis (WGCNA version 1.49) on the differentially expressed probesets with a FDR of 5% to identify clusters of co-expressed genes (modules) based on topological overlap matrix (TOM) dissimilarity measure (Chapter 2 section 2.2.4.6). The associations between modules and clinical variables including survival time were assessed using linear regression model adjusted for gender and age.

## 3.3 Results

Total RNA was extracted from 26 MPM and 10 non-malignant pleural tissues (controls). The

mean RNA yield and RIN were 74.4 µg and 8.2 respectively for MPM, and 47.7 µg and 7.6 respectively for controls. The table (Table 3.1) below shows the results of the total RNA yield and RIN obtained.

**Table 3.1. Total RNA results. Control samples denoted by C, Epithelioid MPM by E, Biphasic MPM by B, Sarcomatoid MPM by S.**

| Sample ID | Histology | Cx (ng/ul) | Yield (µg) | RINS |
|---|---|---|---|---|
| C2 | C | 117.8 | 17.7 | 8.8 |
| C3 | C | 37.6 | 5.6 | 7.2 |
| C4 | C | 146.9 | 22.0 | 7.1 |
| C5 | C | 1081.3 | 162.2 | 7.9 |
| C8 | C | 862.2 | 129.3 | 6.8 |
| C10R | C | 376.3 | 56.4 | 7 |
| C11 | C | 34.5 | 5.2 | 6.5 |
| C12R | C | 43.9 | 6.6 | 8.4 |
| C13 | C | 72.1 | 10.8 | 8.6 |
| C14 | C | 406.4 | 61.0 | 7.4 |
| M1 | E | 1802.2 | 270.3 | 9.2 |
| M2 | B | 1461.2 | 219.2 | 6.4 |
| M3 | E | 1234 | 185.1 | 9.2 |
| M4 | E | 1163.1 | 174.5 | 8.5 |
| M5 | E | 784.3 | 117.6 | 8 |
| M6 | B | 551.8 | 82.8 | 8.7 |
| M7 | E | 550.8 | 82.6 | 8.5 |
| M8 | E | 497.8 | 74.7 | 9.3 |
| M9 | E | 465 | 69.8 | 7.9 |
| M10 | E | 429.1 | 64.4 | 8.9 |
| M11 | E | 378 | 56.7 | 6.6 |
| M12 | B | 368.9 | 55.3 | 9 |
| M13 | E | 356.2 | 53.4 | 8.2 |
| M14 | E | 343.5 | 51.5 | 8.5 |
| M15 | E | 310.7 | 46.6 | 9.1 |
| M16 | E | 291.7 | 43.8 | 7.6 |
| M17 | E | 287.9 | 43.2 | 8.2 |
| M18 | E | 269.5 | 40.4 | 8.8 |
| M19 | S | 261.8 | 39.3 | 7.1 |
| M20 | E | 219.5 | 32.9 | 7.7 |
| M21 | B | 208.7 | 31.3 | 9.1 |
| M22 | E | 168.9 | 25.3 | 8.1 |
| M23R | E | 154.9 | 23.2 | 7.6 |
| M24 | B | 132.6 | 19.9 | 7.1 |
| M25 | E | 106.3 | 16.0 | 7.8 |
| M26 | E | 93.8 | 14.1 | 7.7 |

### 3.3.1 Quality assessment and microarray preprocessing steps

The Expression Console software (Affymetrix, California, USA) was used to monitor assay data quality by assessing control probes such as target prep or hybridisation controls. Each array contains probe sets for Poly-A RNA controls from *B. subtilis* genes (*lys, phe, thr and dap*) that are absent in eukaryotic samples. The Poly-A RNA controls were spiked in to total RNA samples and evaluated like internal control genes to monitor the labelling process during the entire experiments. The signals should be present for all of the Poly-A controls with ascending values in the order of *lys, phe, thr* and *dap* as shown in Figure 3.1.

The hybridisation controls (*BioB, BioC, BioD* and *Cre*) were mixed in to the hybridisation cocktail after target preparation. This allows evaluation of hybridisation efficiency independent of the prior target preparation steps. *Bio B* (red) should be present at least 70% of the time and the signals for the others should be in the ascending order of *Bio C* (blue), *Bio D* (green) and *cre* (pink) as shown in Figure 3.2.

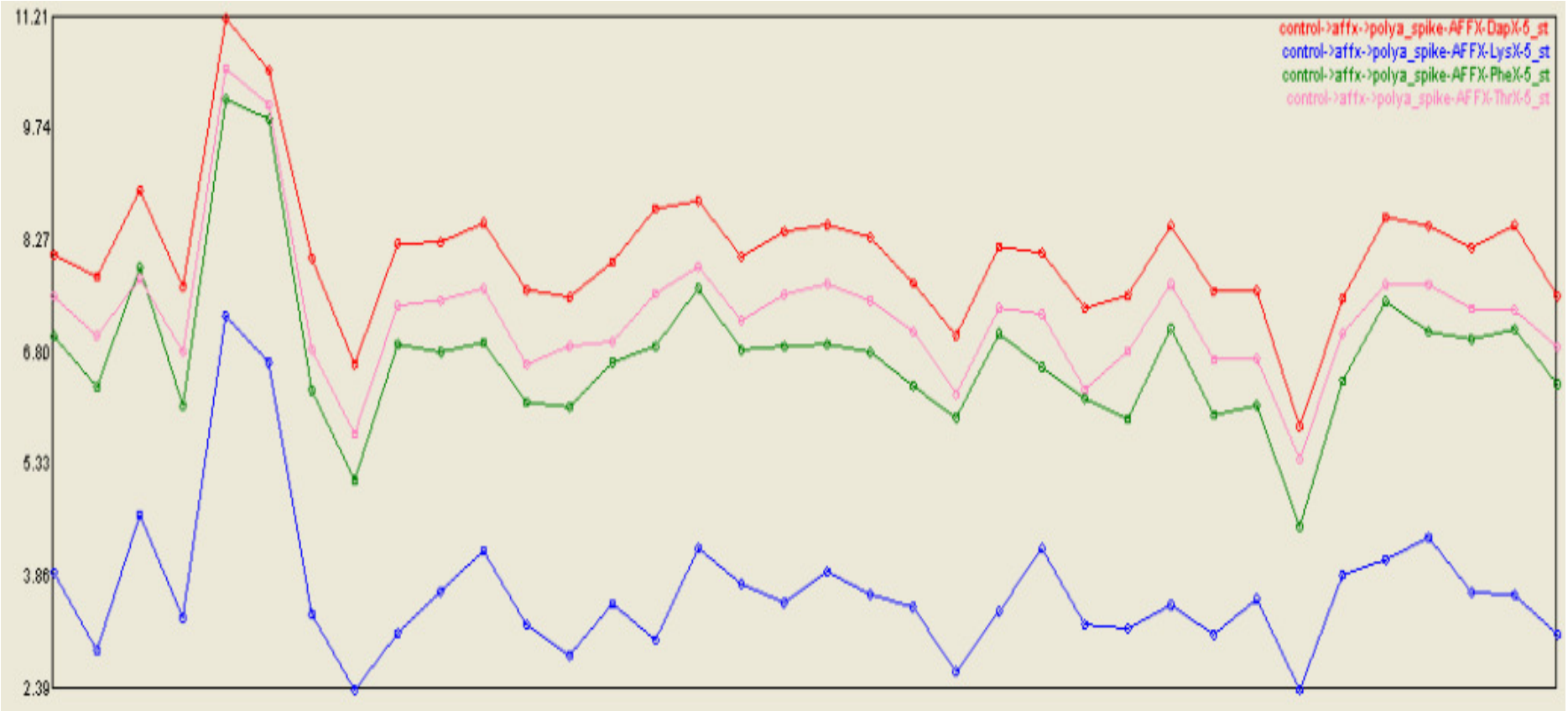


**Figure 3.1. Signal values for Poly-A controls. Each sample is represented by a dot on the line and signal value for each polyA spike control is shown on y-axis. The graph shows the presence of signals for all Poly-A controls with ascending values in the order of *lys*, *phe*, *thr* and *dap*.**

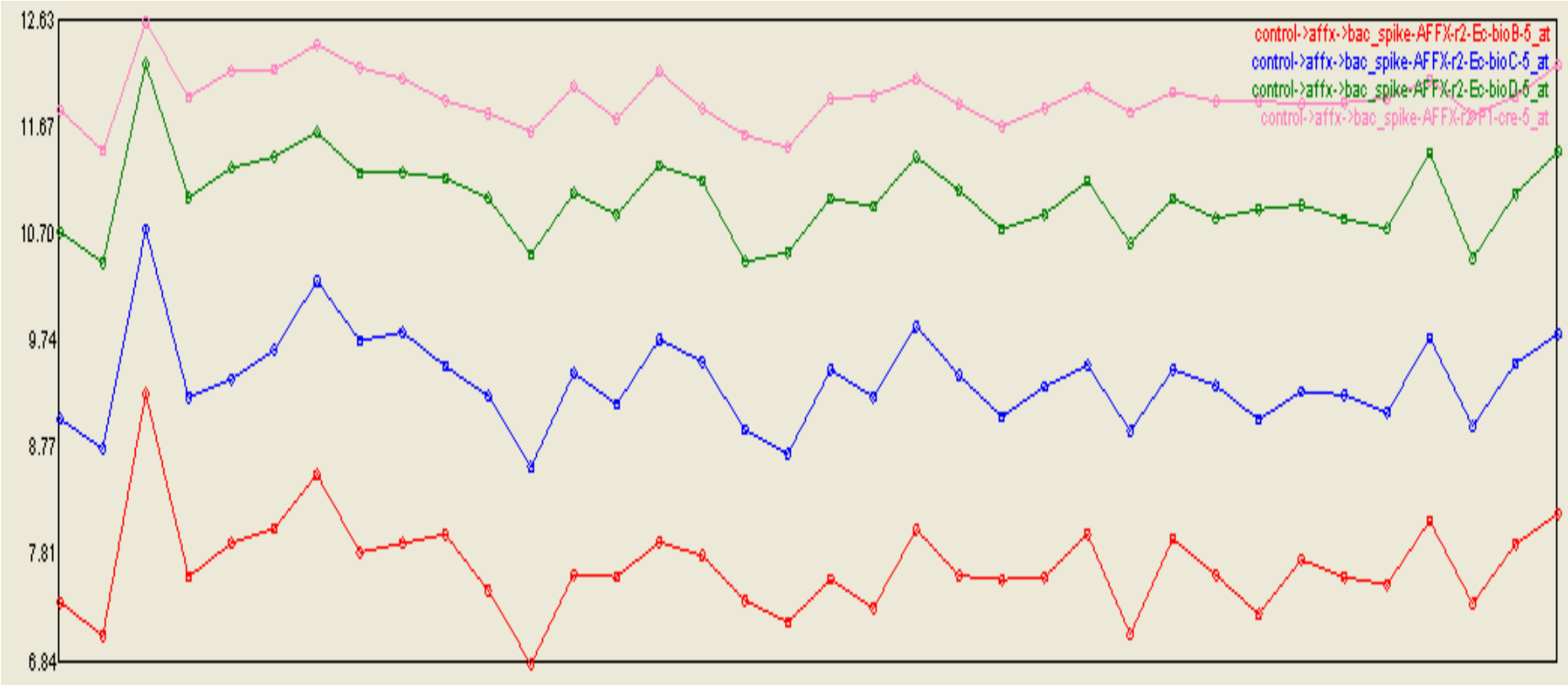


**Figure 3.2. Signal values for hybridization controls. Each sample is represented by a dot on the line and signal value for each bacterial spike control is shown on y-axis. The signals for the controls are in ascending order from *Bio C* (blue) to *Bio D* (green) to *cre* (pink) while *Bio B* (red) is present at least 70% of the time.**

Microarray data quality was assessed with arrayQualityMetrics (version 3.2). Homogeneity of probe intensity levels between arrays was assessed and compared with boxplot and density plot. The raw data was transformed to a logarithm of 2 scale with the upper and lower quartile represented on either end of the box and the median was represented as the line in the middle of the box as shown in Figure 3.3. The intensity distributions were visualised using a density plots showing similar shapes and ranges for each array as shown in Figure 3.4. Outlier arrays were detected based on Kolmogorov-Smirnov statistic $K_a$ computed between each array's distribution and of the pooled data. The results did not indicate the distributions in any of the 36 arrays were drastically different from each other.

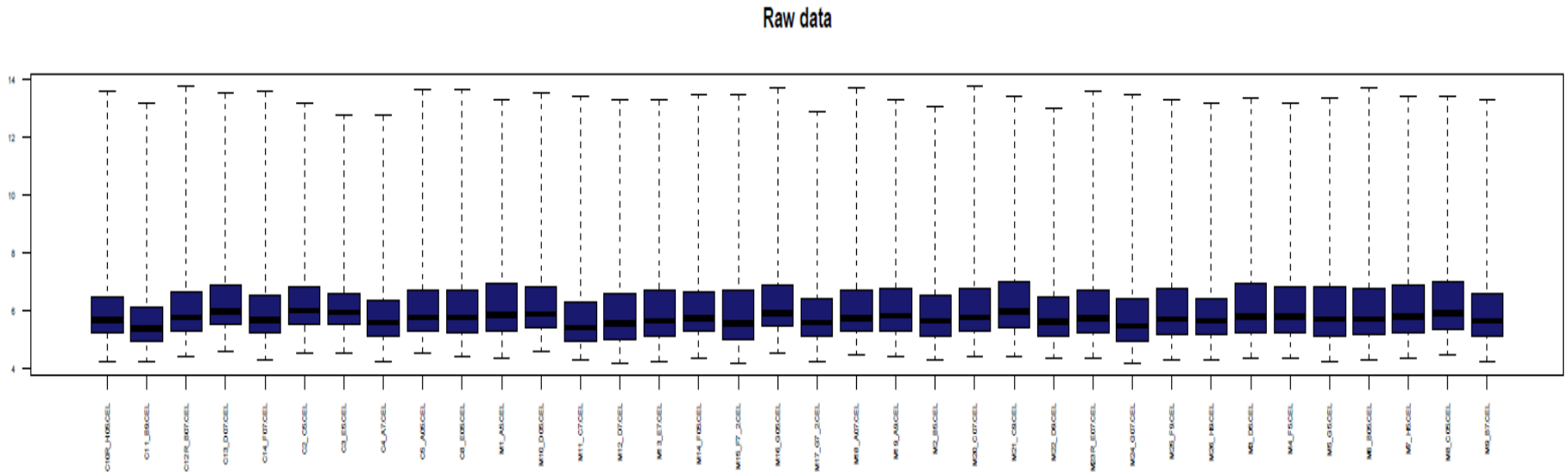


**Figure 3.3. Boxplots of raw signal intensity (logarithm of 2 scale on y-axis) distributions of each array (x-axis). The distributions of raw perfect match probes log-intensities are not expected to be identical prior to normalisation step as shown.**

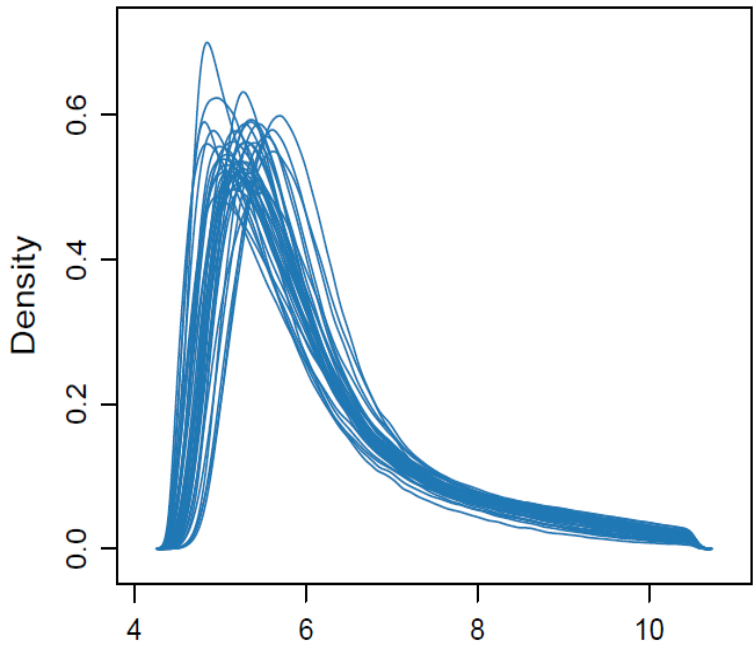


**Figure 3.4. Density (x-axis) plots of log-intensity (y-axis) distributions. This figure shows the density plot of each array superimposed on a single graph as shown for better comparison between arrays and identification of arrays with different distribution.**

Distance ($d_{ab}$) between two arrays ($a$ and $b$) was computed according to the formula $d_{ab}$ = mean | $M_{ai}$ where $M_{ai}$ was the value of the $i$-th probe on array $a$. These were represented in a heatmap (Figure 3.5) and outliers were detected if the sum of distances to all other arrays was exceptionally large. The results showed array 2 and 7 (marked with an asterisk *) were flagged as outlier samples.

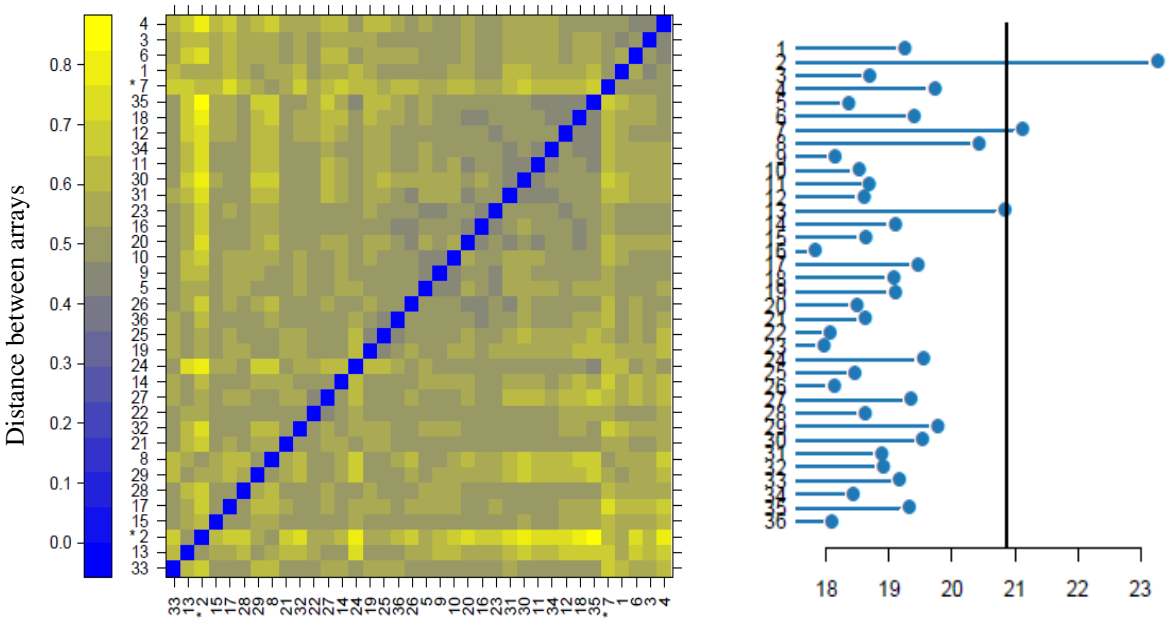


**Figure 3.5. Colour heatmap of distances between arrays. The distance between arrays is denoted by different colour scheme as shown on the bar chart on the left. Array 2 and 7 with large distances to other arrays are identifed as outliers as shown above.**

MA plots allow the identification of intensity-dependent biases by plotting the log-ratio intensity of one array compared to a reference "pseudo" array. The plot shows the logarithm of the relative expression between the two arrays (M) on the Yaxis against the average log-intensity of both arrays (A) on the X axis. Outliers are detected based on Hoeffding's statistics *Da* computed on the joint distribution of A and M for each array. The M values should centre on zero indicating no dependency between the intensities and the log-ratio. Figure 3.6 shows 4 arrays with the highest *Da* on the top panel and four arrays with the lowest *Da* on the bottom panel. No arrays were detected with a *Da* of more than 0.15 that would have otherwise been flagged as outliers.

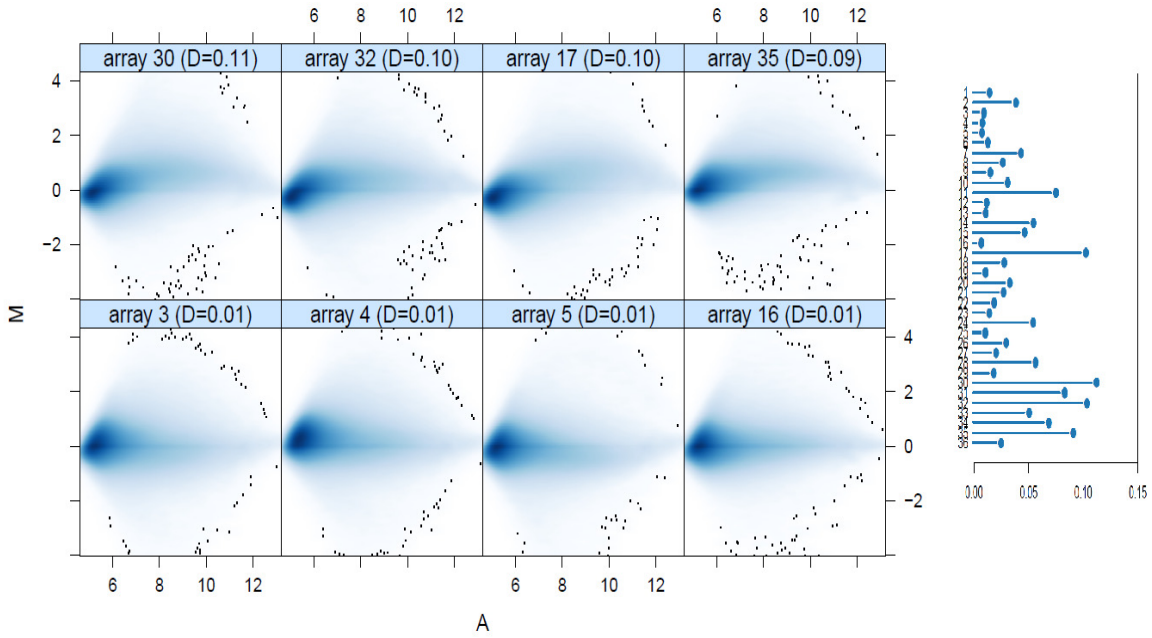


**Figure 3.6. MA plots of arrays. This shows the logarithm of the relative expression between the two arrays (M) on the y-axis against the average log-intensity of both arrays (A) on the x-axis. The arrays with the highest (top panel) and lowest (bottom panel) *Da* are displayed in this figure.**

In summary, two arrays from control samples C3 and C11 were identified as outliers by arrayQualityMetrics and were removed. The remaining 34 arrays were subjected to background adjustment, normalisation and summarisation using random multiple access (RMA) procedure. Figure 3.7 displays the boxplots of RMA treated data showing no deviation indicating the raw intensities were corrected by normalisation.

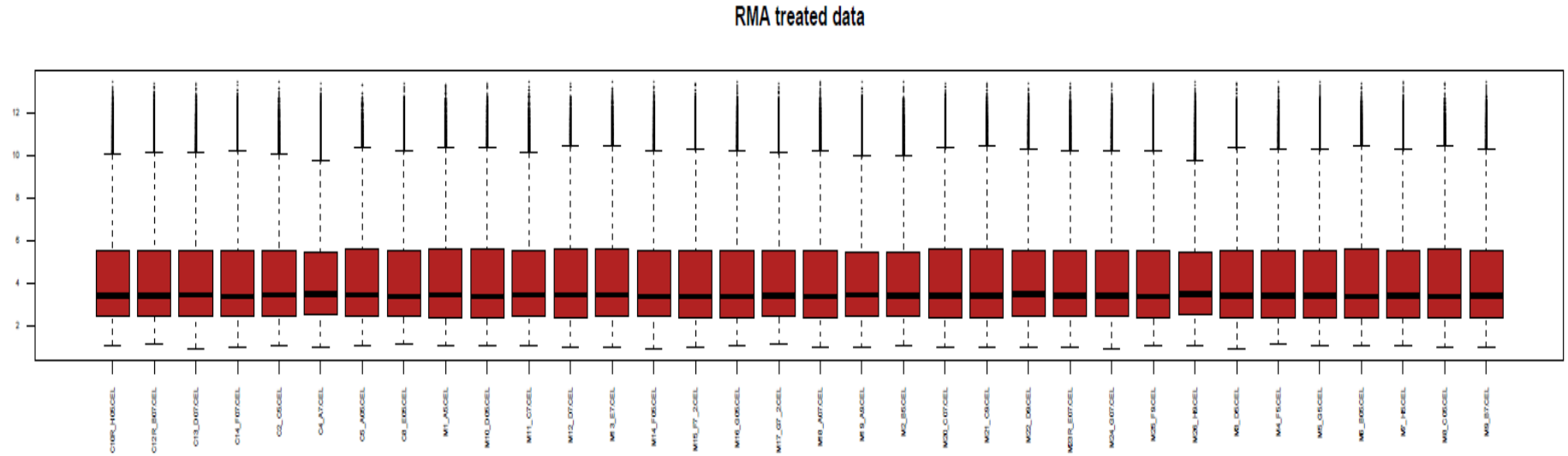


**Figure 3.7. Boxplots for quantile normalized data. Normalisation processed with RMA and the figure displays the logarithm of 2 scale of intensities on the y-axis and distribution of each array on the x-axis. After normalisation, the arrays have comparable median expression levels as shown in the figure.**

After the pre-processing steps, probe sets with expression levels below the median across all samples were removed from the dataset. This reduced the probe sets from 53,617 to 38,139.

The principal variance component analysis (PVCA, version 1.10) analysis identified age as the most prominent source of variability accounting for 10% of the total variance in the data as shown in Figure 3.8. The experiments were done in two batches and PVCA revealed that this explained 2.5% (denoted by GT in Figure 3.8) of the overall variation in the RMA treated data.

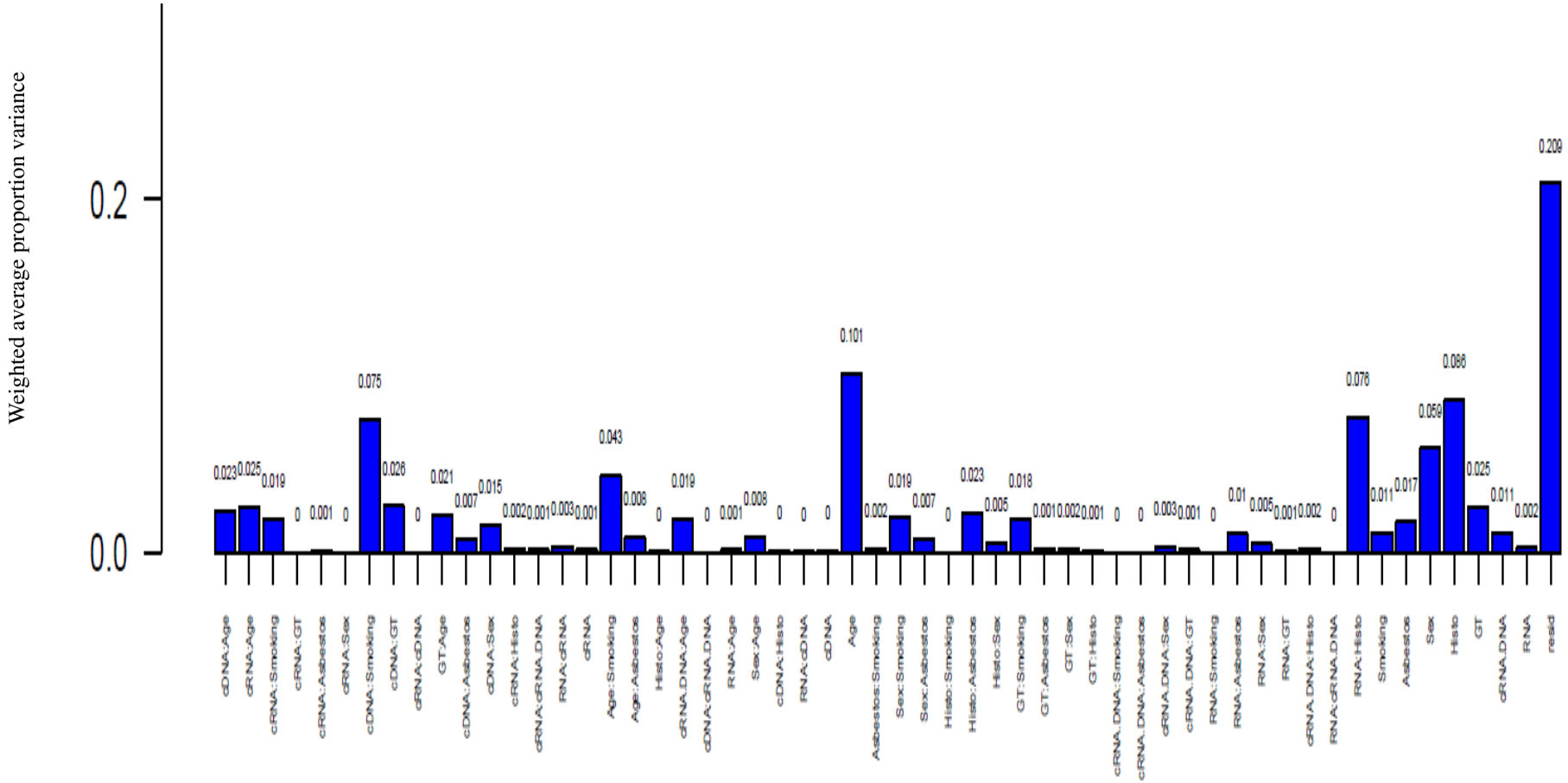


**Figure 3.8. Batch effects analysis. Bar chart showing the proportion of variance (y-axis) from each possible factor (x-axis) as estimated by PVCA.**

In order to reduce variation due to age, three control samples (C10, C12 and C13) with much younger age compared to the others were removed. Sarcomatoid subtype was only represented by tumour sample M19 and was removed from subsequent analyses. This reduced the variance due to age from 10.1% to 1.7% and for tissue subtypes from 8.6% to 4.6%.

### 3.3.2 Differential gene expression

The expression data from a total of 25 tumour samples and five control samples were analysed for differential gene expression. The table below (Table 3.2) shows the clinical profiles for the 30 samples.

**Table 3.2. Demographics and clinical data for 25 tumours and 5 control samples. E= epithelioid, B= biphasic.**

| Clinical variables | Tumour | Control |
|---|---|---|
| **Age** | 55-82 (median 67) | 51-78 (median 68) |
| **Gender** | 20 Males: 5 Females | 5 Males |
| **Histology** | 20 E-MPM<br>5 B-MPM | 5 Non-malignant reactive pleura |
| **Asbestos exposure**<br><br>**Yes**<br>**No**<br>**Not known** | <br><br>21<br>3<br>1 | <br><br>3<br>2<br>0 |
| **Smoking history**<br><br>**Ever smoked**<br>**Never smoked**<br>**Not known** | <br><br>13<br>10<br>2 | <br><br>4<br>1<br>0 |

Prior to testing for differential gene expression, clustering of the samples was assessed with unsupervised two dimensional hierarchical clustering algorithm (HCA) (Figure 3.9) and principal component analysis (PCA) (Figure 3.10). Both HCA and PCA successfully segregated the tumours from the controls and demonstrated molecular homogeneity shared amongst the tumour samples. Thus, subsequent statistical analysis to test for differentially expressed genes was carried out without splitting the tumour samples into their respective subtypes.

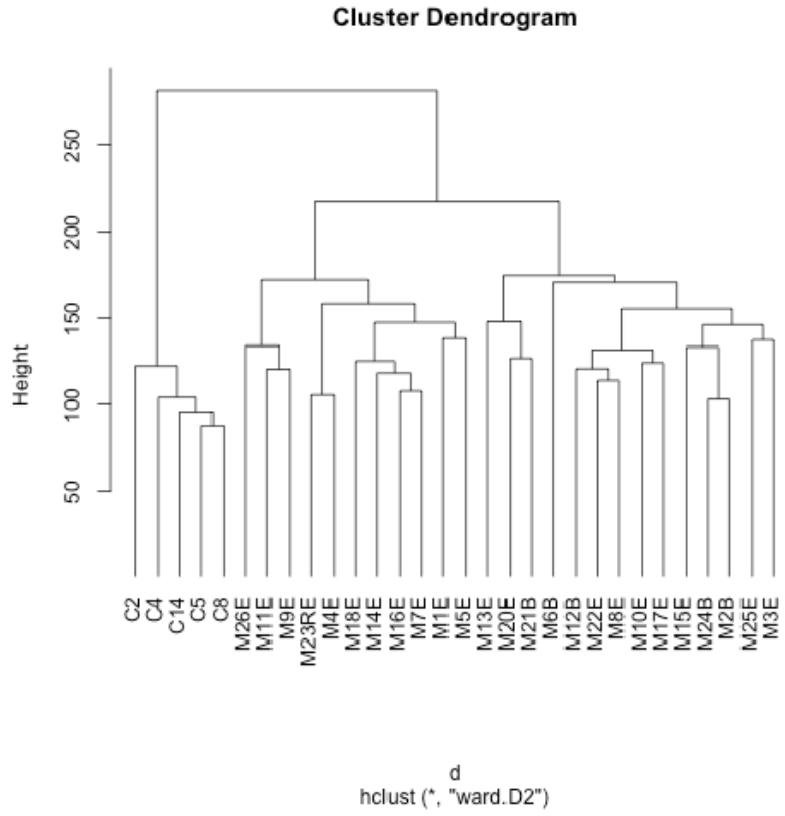


**Figure 3.9. Unsupervised hierarchical cluster analysis of the final 30 samples. The analysis shows clear separation of tumour from control samples. Control samples are denoted by letter C## and tumour samples denoted by letter M##E for E-MPM and M##B for B-MPM.**

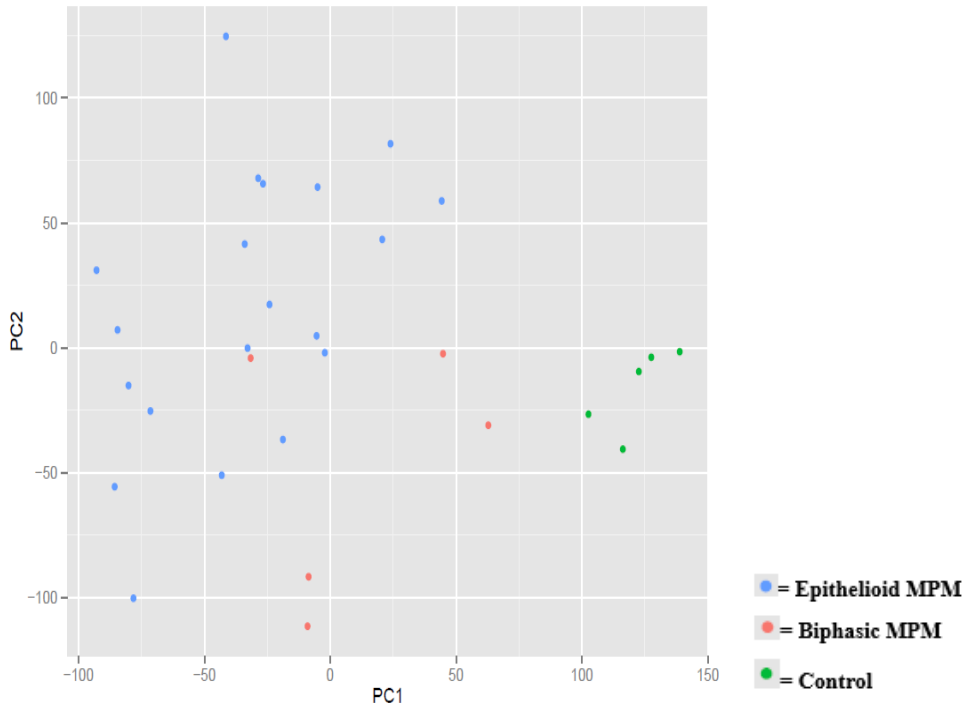


**Figure 3.10. Scatter plot for the first two principal components (PC)of the full dataset. Each sample is represented by a dot on the plot and control samples in green appear to cluster together.**

We applied the empirical Bayes method (as described in section 2.2.4.5) to detect differentially expressed genes between tumour and control samples (Appendix 3.1). The analysis identified 643 genes (651 probesets) with an adjusted p-value of $\leq 0.01$ and absolute FC in the level of expression of $\geq 2$.

### *3.3.2.1 Upregulated genes*

A total of 291 differentially expressed genes were upregulated in tumours compared to controls with an absolute FC level ranging from 2.00-87.61 (Appendix 3.1). Table 3.3 shows the top 20 upregulated genes with the highest FC in the level of expression. Twelve of these are transmembrane genes involved in cell-cell communications, transmembrane signalling,

ions transport and maintenance of cell structure.

**Table 3.3. Top 20 statistically validated differentially expressed genes with the highest fold change (FC) in the level of expression.**

| Gene symbols | Gene.names | Gene.ID | adj.P.Val | FC |
|---|---|---|---|---|
| *ITLN1* | intelectin 1 (galactofuranose binding) | 55600 | 0.000467 | 87.43 |
| *UPK1B* | uroplakin 1B | 7348 | 6.16E-05 | 64.45 |
| *UPK3B* | uroplakin 3B | 80761 | 1.39E-05 | 47.50 |
| *CALB2* | calbindin 2 | 794 | 5.17E-05 | 41.36 |
| *LRRN4* | leucine rich repeat neuronal 4 | 164312 | 4.83E-05 | 40.22 |
| *BNC1* | basonuclin 1 | 646 | 1.18E-07 | 39.67 |
| *PLLP* | Plasmolipin | 51090 | 2.45E-05 | 35.02 |
| *CTSE* | cathepsin E | 1510 | 0.000194 | 32.45 |
| *LRP2* | low density lipoprotein receptor-related protein 2 | 4036 | 0.001847 | 30.48 |
| *FLRT3* | fibronectin leucine rich transmembrane protein 3 | 23767 | 0.000103 | 23.43 |
| *SLPI* | secretory leukocyte peptidase inhibitor | 6590 | 0.000456 | 21.41 |
| *CDH1* | cadherin 1, type 1, E-cadherin (epithelial) | 999 | 0.000864 | 20.39 |
| *CACNG4* | calcium channel, voltage-dependent, gamma subunit 4 | 27092 | 0.00031 | 20.25 |
| *MMP24* | matrix metallopeptidase 24 (membrane-inserted) | 10893 | 5.68E-05 | 18.64 |
| *KRT5* | keratin 5 | 3852 | 1.55E-05 | 18.51 |
| *ANXA3* | annexin A3 | 306 | 3.57E-05 | 17.63 |
| *MUC16* | mucin 16, cell surface associated | 94025 | 0.001016 | 17.39 |
| *C19orf33* | chromosome 19 open reading frame 33 | 64073 | 1.41E-05 | 17.03 |
| *HNRNPA1P 33* | heterogeneous nuclear ribonucleoprotein A1 pseudogene 33 | 728643 | 0.000153 | 16.00 |
| *MAL2* | mal, T-cell differentiation protein 2 (gene/pseudogene) | 114569 | 0.000295 | 15.56 |

Next, we focused on the top five upregulated genes: *ITLN1, UPK1B, UPK3B, CALB2* and *LRRN4*. *ITLN1* is a galactose-binding lectin expressed mainly in small intestine, renal collecting tubule cells and some mesothelial cells. Studies have shown over-expression of *ITLN1* by immunohistochemistry (IHC) in 80% of epithelioid MPM but rarely in biphasic or sarcomatoid MPM; and no expression was seen in reactive mesothelial cells or lung adenocarcinomas[206,207]. Tsuji *et al* also detected higher concentrations of *ITLN1* in pleural effusions of MPM compared to lung adenocarcinomas[207]. The exact role of *ITLN1* in tumorigenesis is not fully understood. Human mesothelial cells exposed to crocidolite asbestos and transfected with simian virus 40 resulted in over-expression of *ITLN1*[208]. Another study using immortalised human mesothelial cell line showed induction of *ITLN1* resulted in marked increase in cell growth, invasiveness and chromosomal aberrations with translocation events[209]. These suggest involvement of *ITLN1* in MPM tumorigenesis might be an early event and could be a potential diagnostic biomarker for MPM.

*CALB2* is a member of the EF-hand family of calcium binding proteins that encodes calretinin, a validated IHC marker for diagnosing MPM. The protein is detected in virtually all mesothelioma of epithelioid and biphasic subtypes but only in less than 10% of lung adenocarcinomas[210]. The involvement of *CALB2* in tumorigenesis has not been well studied. However, calretinin has been shown to interact with cytoskeletal elements and cell proliferation in colon cancer cells[211]. The role of *CALB2* in MPM has been investigated by one study and found elevated calretinin levels strongly correlated with increased resistance of mesothelial cells to asbestos cytotoxicity *in vitro*. In addition, this protective effect could be inhibited with phosphoinositide 3-kinase (PI3K) inhibitor[212]. This suggests *CALB2* might contribute to MPM carcinogenesis possibly through up-regulation of PI3K signalling resulting in increased cell survival from asbestos cytotoxicity.

*UPK1B* and *UPK3B* are transmembrane proteins that are specific for urothelial lineage. Previous study found over-expression of both uroplakins in epithelioid compared to sarcomatoid MPM[139]. Another transcriptomic microarray study identified *UPK3B* as one of the three predictive genes that was able to distinguish the different molecular subtypes of MPM[135]. In addition, *UPK3B* and *LRRN4* have recently been identified as novel mesothelial lineage markers and both showed heterogeneous expression in epithelioid mesothelioma cell lines[213]. *LRRN4* is a leucine rich repeat neuronal protein and has not been implicated in cancer but shown to be dysregulated in response to lung injury raising a possible role in inflammation[214]. Little is known about these three genes and in view of their significant upregulation in our study, further studies are required to elucidate their roles in MPM pathogenesis.

It is also worth noting *BNC1*, the most statistically significant upregulated gene in our data and has not been described in MPM. *BNC1* was first discovered in keratinocytes and found to be associated with proliferation, cell-adhesion, intracellular transport and ion-channels. Studies found opposing roles of *BNC1* in tumorigenesis depending on cell types; reduced expression in renal cell carcinoma cell lines conferred survival advantage but elevated expression in breast cancer was associated with tumour invasiveness and its expression was positively regulated by p63 in squamous carcinoma[215–217]. Recent evidence identified further oncogenic role of *BNC1* in epithelial dedifferentiation through modulation of transforming growth factor beta 1 (TGF-ß1) responsive genes including epithelial-mesenchymal transition (EMT)-related transcription factors[218]. TGF-ß production can be stimulated by MPM and interacts with Hippo pathway to promote tumour growth[219]. Furthermore, EMT process has been described in MPM suggesting potential role for *BNC1* in promoting this process and tumour growth in MPM[220].

To gain further biological insights, we interrogated the list of differentially expressed upregulated genes for enriched GO terms and KEGG pathways as described in Chapter 2 section 2.2.4.5. The analysis identified cell junction organisation as the top over-represented GO terms (Table 3.4) and the genes are enriched in cancer pathways, Hedgehog signalling, cell cycle and pathways involved with cell junction organisation (Table 3.5).

**Table 3.4. Top enriched GO terms for upregulated genes.**

| GO category | Category name | GO ID | No of genes | adj.P value |
|---|---|---|---|---|
| biological process | cell junction organisation | GO:0034330 | 19 | 1.29E-06 |
| biological process | cell junction assembly | GO:0034329 | 16 | 2.59E-05 |
| cellular component | cell junction | GO:0030054 | 32 | 3.77E-05 |

**Table 3.5. KEGG pathway analysis of upregulated genes.**

| PathwayName | Genes | adj.P value |
|---|---|---|
| Pathways in cancer | *FGF9, WNT9A, NKX3-1, ITGA3, CDH1, SKP2, CKS1B, BMP4, WNT3, MET, RAC3, LAMC2, EGFR, WNT2B, FGF18, ARNT2, LAMA5* | 0.0005 |
| Adherens junction | *PTPRF, MET, CDH1, RAC3, EGFR, BAIAP2, SSX2IP* | 0.0027 |
| ECM-receptor interaction | *HMMR, ITGB4, ITGA3, AGRN, LAMC2, LAMA5, SDC4* | 0.004 |
| Regulation of actin cytoskeleton | *FGF9, SSH3, ITGA3, FGF18, EZR, ITGB4, PFN2, RAC3, PAK4, BAIAP2, EGFR* | 0.004 |
| Cell cycle | *MCM4, MAD2L1, CDC6, MCM2, CCNB1, CCNB2, SFN, SKP2* | 0.0065 |
| Hedgehog signalling pathway | *BMP4, WNT9A, WNT3, LRP2, WNT2B* | 0.0162 |
| Cell adhesion molecules (CAMs) | *PTPRF, CDH4, CDH3, F11R, CLDN15, CDH1, SDC4* | 0.0228 |
| Axon guidance | *EFNA5, SEMA3C, EFNA1, MET, PAK4, RAC3, PLXNB1* | 0.0228 |
| Focal adhesion | *ITGA3, MET, ITGB4, RAC3, LAMA5, LAMC2, PAK4, EGFR* | 0.0461 |

The upregulated genes implicated in cancer pathways include proto-oncogenes (*EGFR, MET, RAC3*), potential tumour suppressor gene (*NKX3-1*), genes associated with proliferation (*FGF9, FGF18*), cell cycle/survival genes (*SKP2, CKS1B, ARNT2, RAC3*), cell-cell interactions (*CDH1*), extracellular matrix (ECM) interactions and cytoskeletal remodelling (*ITGA3, LAMA5, LAMC2, BMP4, RAC3* and components of WNT).

Eight of the upregulated genes are associated with cell cycle pathway of which *CCNB1, CCNB2, CDC6 and MAD2L1* are regulators of cell cycle check points and have been described in MPM[134,221,222]. *CCNB1* is involved in G2/M transition of the cell cycle by interacting with *CDC2* to form mitosis-promoting factor kinase complex. Both *CCNB1* and *MAD2L1* regulate mitotic spindle checkpoint and chromosome segregation; and overexpression of these genes are linked to chromosomal instability[223,224]. *CDC6* regulates G1/S transition of the cell cycle and is needed for the loading of DNA replicative helicase minichromosome maintenance proteins (including *MCM2* and *MCM4*) onto the origins of replication. *CDC6* over-expression promotes persistent DNA replication and may confer resistance to accumulation of DNA damage and cell entry into senescence[225]. Over-expression or amplification of *SKP2* has been detected in a variety of cancers. *SKP2* has not been described in MPM but abnormalities in chromosome 5p that encodes for *SKP2* (5p13) was overrepresented in MPM cell lines and cultures[226]. *CKS1B* is a member of the cyclin-dependent kinases (CDK) that regulates mitosis and together with *SKP2* form the $SCF^{SKP2\_CKS1}$ ubiquitin ligase complex that regulates proteasome degradation of $p27^{Kip1}$ (CDK inhibitor), *FOXO1* and *RASSF1A* thereby abolishing their tumour suppressor functions including cell cycle arrest and death[227–229].

Both enrichment analyses identified overrepresentation of genes involved in cell junction organisation including adherens junction, actin cytoskeleton, ECM-receptor interactions and

axon guidance. Integrins are α/ß heterodimeric transmembrane receptors that promote cell-ECM interactions by binding to a wide variety of ECM proteins including the laminin family. Upon ligand binding, they cluster on cell surface area termed as focal adhesion site. This forms an important connection between ECM and actin cytoskeleton; and is an important mediator of focal adhesion kinase (FAK) activation by promoting its recruitment, phosphorylation and formation of FAK-Src complex. Phosphorylated FAK also forms a complex with *GRB2* that binds to *SOS* to activate *RAS* and downstream MAPK and PI3K/Akt pathways[230].

We identified overexpression of two integrin receptors: *ITGA3* and *ITGB4*; and two laminin members: *LAMA5* and *LAMC2* that have been shown to promote cell invasion. *ITGA3* forms an integrin complex (α3β1) with the beta-1 subunit and is a major receptor for laminin-5. Silencing of *ITGA3* expression using RNAi reduced adhesion, spreading and proliferation of 4T1 murine cancer cell *in vivo*[231]. Functional *in vitro* study showed the interaction of α3β1 and laminin-5 promoted cell growth via activation of MAPK pathway[232]. Upregulation of *ITGB4* was observed in invasive xenograft pancreatic cancer model and knockdown of *ITGB4* reduced cancer cells migration and invasion[233]. *LAMC2,* γ2 chain of laminin-5, exerts its oncogenic role via the EGF-like repeats in domain III that allows interaction with *EGFR*. *In vitro* study using breast cancer cell line demonstrated the binding of *LAMC2* to *EGFR* increased *MMP2* expression and enhanced cell migration[234]. *LAMA5* is a subunit of laminin-10, -11 and -15 that also binds to α3β1integrin. Study using *LAMA5* knockout mouse model and RNAi demonstrated involvement of *LAMA5* in cell survival and epithelial cells differentiation via activation of PI3K/Akt[235].

Axonal guidance molecules include the Slit, Netrin, Eph/erin and Semaphorin families act as repulsive or attractive force to guide axonal growth and migration[236]. Aberrant expression of

these molecules and their associated partners is linked with the initiation and progression of cancers and recent study found several genes associated with axon guidance were mutated in pancreatic cancer[237]. Recent data also suggested FAK as the main effector of Eph-ephrin and Semaphorin signalling pathways[238,239]. Two ephrin ligands (*EFNA1* and *EFNA5*) are identified in our study. *EFNA1* is overexpressed in HCC and promoted proliferation in *EFNA1*-deficient cell line[240]. Furthermore, gene expression analysis revealed *EFNA1* induced overexpression of genes associated with cell cycle, angiogenesis and invasion[241]. The role of *EFNA5* in tumorigenesis was demonstrated by increased invasion, anchorage-independent growth and morphogenetic changes in *EFNA5*-expressing murine fibroblasts[242]. Of the semaphorin members, we identified upregulation of *SEMA3C* and *PLXNB1*, receptor for *SEMA4D* that have also been shown to be involved in cancer progression and vascularity[243,244]. These studies showed tumour growth and micro vessel density examined *in vivo* were reduced after *SEMA3C* silencing while inactivation of *PLXNB1* in *HER2* overexpressing breast cancer reduced invasiveness and number of metastases.

Actin reorganization is another important element contributing to cell motility. Overexpression of *EZR*, a membrane cytoskeleton linker, promotes cell motility and survival through PI3/Akt pathway[245,246]. *EZR* has been shown to trigger activation of FAK through phosphorylation of FAK at Tyr-397 independently of cell-matrix adhesion[247]. The downstream effectors of FAK signalling include the small GTPases of the Rho family that regulate dynamic reorganization of the actin cytoskeleton. *RAC3*, one of the Rho GTPases, is implicated in reorganising the actin cytoskeleton through formation of lamellipodia necessary for cell dissemination but also activation of extracellular-signal-regulated kinases (ERK) / nuclear factor kappa-light-chain-enhancer of activated B cells (NF-kB) leading to increase cell survival and proliferation[248]. *PAK4*, one of the PAK serine/threonine kinases that are important effectors of Rho family GTPases, together with *CDC42* induced actin

polymerisation and formation of filipodia[249]. *In vitro* study showed *PAK4* is required for Ras driven anchorage-independent cell transformation[250]. Taking all these data together, FAK and mitogen-activated protein kinases (MAPK) signalling pathways may be important mediators of MPM cells migration and invasion.

Five genes (*LRP2, BMP4, WNT9A, WNT3, WNT2B*) are involved in Hedgehog and WNT signalling pathways. The hedgehog pathway involves ligand binding to *PTCH1/2* that relieves the repression of *SMO* and activates signal transduction to SUFU-GLI complexes leading to activation of *GLI* transcription factors. *LRP2*, a member of the *LDL* receptor gene family, has recently been identified as a binding protein for sonic hedgehog and controls internalisation, cellular trafficking of sonic hedgehog-patched 1 complexes. A mice model study showed overexpression of *LRP2* is critical for hedgehog signalling and lack of *LRP2* resulted in failure to respond to sonic hedgehog despite functional expression of *PTCH1* and *SMO*[251].

Aberrant WNT signalling is active in malignant mesothelioma and targeting WNT signals using siRNA or antibodies against *WNT1* or *2* and dominant-negative *Dvl* led to suppression of mesothelioma cells growth *in vitro*[171,173,252,253]. Two WNT ligands, *WNT2B* and *WNT3*, identified in our study have been reported by Fox *et al* to be upregulated in MPM. Both genes are involved in positive regulation of WNT canonical pathway through binding with frizzled receptors to activate *Dvl* that inhibits phosphorylation of *GSK-3β* thereby reducing the binding affinities of *AXIN1* and *APC* for *CTNNB1* that promotes its degradation. Unphosphorylated *CTNNB1* translocate into the nucleus and displaces Groucho/TLE from TCF/LEF binding sites to activate transcription of genes involved in several biological process such as cell growth and proliferation (c-myc, cyclin D) and cell invasion/migration (*MMP7, UPAR, SLUG, LAMA5).*

The involvement of WNT and hedgehog signalling pathways in MPM is further supported by overexpression of *BMP4* in our study. The expression of *BMP4* is regulated and can be induced by both pathways[254,255]. *BMP4*, a member of the TGF-ß superfamily, has opposing roles in cancer pathogenesis. This was reviewed and majority of studies demonstrated suppression of cell growth *in vivo* and *in vitro* by *BMP4* but is capable of initiating morphological changes and EMT process[256]. In MPM, *BMP4* has been shown to be overexpressed in a molecular subtype associated with genes involved in ECM components suggesting an invasion role in MPM[130].

#### *3.3.2.2 Downregulated genes*

A total of 352 differentially expressed genes were downregulated in tumours compared to controls (Appendix 3.1). The absolute FC in expression level for downregulated genes was much smaller (ranged from 2.00-7.65) compared to upregulated genes. *MMRN1*, a novel gene in MPM has the highest FC in expression level amongst the downregulated genes. *MMRN1* is a soluble protein found in platelets and in the endothelium of blood vessels that has been shown to function as an adhesive ligand promoting platelet adhesion at sites of vascular injury[257]. *In vitro* study showed *MMRN1* adhesion to cellular receptors enhanced its formation of large, branching ECM fibres[258]. In addition, proteomic analysis identified direct interaction of *MMRN1* with tumour suppressor, *CDKN2A*[259]. This raises the possibility that downregulation of *MMRN1* might contribute to MPM tumorigenesis through tumour-driven vascular permeability, destabilisation of ECM and possibly cell-cycle progression.

*MYH11*, another top downregulated genes, encodes for a major contractile protein, smooth muscle myosin heavy chain 11, that utilises the energy of ATP hydrolysis to move actin filaments and produce muscle force. Recent evidence indicated the potential roles of *MYH11*

in tumorigenesis including cell migration, adhesion and control of cell shape, as well as in cell-signalling pathways such as interaction with Rho and the pro-apoptotic protein Bmf (BCL2-modifying factor)[260–262]. In addition, *MYH11* is underexpressed in breast cancer cell lines compared to hybrids and in microsatellite stable hereditary nonpolyposis colorectal cancer[263,264]. Low expression of *MYH11* by IHC correlated with poorer survival in patients with colorectal cancer[265]. *MYH11* has not been reported in MPM and it is possible that it contributes to MPM carcinogenesis through modulation of cell adhesions and migrations.

Enrichment analysis identified regulation of immune system as the top overrepresented GO terms (Table 3.6). This consists of 78 genes involved in several functions including T cell activation (*BCL11A, CD28, IKZF1, DOCK2, IRF4, PTPN22, PTPRC, RHOH, THEMIS*), B cell activation (*BCL11A, BANK1, CD40LG, CD40, IKZF1, CXCR5, PLCG2, PTPRC*), cell adhesion and recognition molecules and cytokine-cytokine receptor interactions. The top enriched KEGG pathways include cell adhesion, immune deficiency and cytokine-cytokine receptor interactions (Table 3.7).

**Table 3.6. Top enriched GO terms for downregulated genes.**

| GO category | Category name | GO ID | No of genes | adj.P value |
|---|---|---|---|---|
| biological process | immune system process | GO:0002376 | 78 | 2.26E-11 |
| biological process | regulation of immune system process | GO:0002682 | 50 | 4.69E-11 |
| biological process | cell adhesion | GO:0007155 | 51 | 2.81E-10 |

**Table 3.7. KEGG pathway analysis of downregulated genes.**

| PathwayName | EntrezGene | adj.P val |
|---|---|---|
| Cell adhesion molecules (CAMs) | *PTPRC,CD99, CD40LG, CDH5, PTPRM, SELE, CD40, ICAM2, CD28, ESAM, SELL, CD34* | 0.0004 |
| Primary immunodeficiency | *PTPRC, CD40, JAK3, CD40LG, CD19, CIITA* | 0.0007 |
| Cytokine-cytokine receptor interaction | *CSF2RB, IL12RB2, CCR6, CXCR5, CD40LG, IL6, LEP, IL2RA, CD40, NGFR, IL21R, IL3RA, PDGFRB* | 0.0009 |

The cell adhesion genes that are associated with recruitment of immune cells included *SELE, SELL, CD34, CD99, ICAM2* and *ESAM*. Downregulation of these genes might suggest impaired infiltration of immune cells to the tumour microenvironment in mediating effective anti-tumour immune response.

Downregulation of *SELE* results in interrupted attachment of T cells to the tumour vasculature. Treatment with imiquimod, a TLR7 agonist, is associated with induction of *SELE* on tumour vasculature, increased infiltration of CD8+ T cells, inhibition of tumour associated Treg cells and tumour regression[266]. TLR7 agonist has been tested in murine MPM model and resulted in induction of CD8+ T-cell, type I IFN anti-tumour responses and primary tumour growth retardation[267]. The authors also showed the combinations of TLR7 agonist and agonistic anti-CD40 antibody to mimic CD4+ T-cell assistance led to higher systemic immune response and inhibition of growth in not only the primary tumour but also distant metastatic lesion[268].

*SELL* and *CD34* are known to promote tethering and rolling of immune cells on the endothelia[269]. Downregulation of *SELL* in knockout mouse model resulted in improper

adhesion and migration of lymphocytes that might represent another immune escape mechanism[270]. *CD34*-/- animal models exhibited increased tumour growth at later stage of cancer development and are associated with impaired homing of mast cells[271]. *CD99* is a cell surface glycoprotein expressed on both leucocytes and endothelial cell contacts allowing its participation in transendothelial migration of monocytes and lymphocytes to sites of inflammation[272]. Loss of *CD99* and lower protein level in tumour stromal are associated with poor prognosis in several tumour types including lung cancer[273].

*ICAM2* stimulates the migration and cytotoxicity of natural killer (NK) cells upon binding to leucocyte adhesion LFA-1 protein[274]. In cancer cells, *ICAM2*-transfection enhanced adhesion, activation of NK cells and reduction in metastasis[275]. *ESAM*, a member of the immunoglobulin superfamily is expressed on endothelial tight junctions and is involved in maintaining the integrity of endothelial cells. Targeted deletion of *ESAM* in knockdown mouse models reduced tumour angiogenesis and growth but conversely disruption in vascular permeability might modulate transendothelial migration of cells including tumour and immune-related cells[276,277].

Apart from immune cells recruitment, activation of lymphocytes is also crucial in initiating anti-tumour process. Several genes involved in this process are downregulated in our study. *CD40* belongs to the superfamily of TNF receptors and are expressed on endothelial cells and antigen-presenting cells such as B cells, macrophages and dendritic cells. *CD40* together with its ligand *CD40L* are important for clonal B cell expansion, differentiation and germinal centre formation. The role of *CD40*-activated B cells in anti-tumour immunity has been reviewed[278]. *In vitro* and *in vivo* studies showed signalling via *CD40* activates host antigen-presenting cells to evoke an effective cytotoxic T cell response; and direct tumour cytotoxicity was observed upon *CD40L* ligation on *CD40* expressing tumours. In MPM, enhancing *CD40*

activation with agonist anti-*CD40* antibody injected into mice model resulted in tumour regression but unexpectedly with no increase in CD8+ tumour-specific T cells; and instead promoted follicular B-cell activity suggesting the role of memory B cells in recognizing auto-antigens on MPM cells[279].

The role of *PTPRC* (*CD45)* in modulating the immune system has been reviewed[280]. *CD45* is a key regulator of T-cell and B-cell receptors signalling through dephosphorylation of the negative regulatory *Src* family kinases *Lck* and *Lyn* respectively. *CD19* is critical for mounting an optimal immune response through antigen-independent development and immunoglobulin-induced activation of B cells[281]. In addition, *CD19* deficient mice exhibited impaired response to transmembrane signals and T-cell dependent humoral responses.

*JAK3* activating mutation and over-expression are associated with several haematopoietic and solid malignancies but also has a key role in T cell development and regulation of immune system[282]. Previous studies demonstrated the involvement of *COX* in MPM pathogenesis and observed significant production of *PGE2* by asbestos from alveolar macrophages that inhibits mesothelial cell-mediated cytotoxicity[283]. Another study found *PGE2* inhibited upregulation of *JAK3* in naïve T cells and downregulated *JAK3* expression in primed T cells resulting in inhibition of T cell proliferation through impaired activation of *STAT5* and decreased induction of c-myc and c-Jun[284].

Downregulation of several cytokines and its receptors identified in our study (Table 3.7) such as IL*2RA, IL3RA, IL21R,* might also contribute to impaired anti-tumour immunity. *IL2* is an important growth factor for lymphocytes and *IL2RA* has a key function in mediating its effect by forming a complex with *IL2, IL2R* $\beta$ and $\gamma c$[285]. *In vitro study* showed *IL2RA* expression is suppressed by cancer derived immunosuppressive factor thereby markedly suppressing T cell

proliferation[286]. As such, it is plausible that the function and expansion of cytotoxic T lymphocytes can be inhibited due to the repressed expression of *IL2RA*. Downregulation of *IL3RA*, a subunit of the receptor for *IL3*, might contribute to reduction in infiltration of immune cells through impaired *IL-3* signalling as demonstrated in murine tumour model resulted whereby *IL3* overexpression resulted in slower tumour growth due to increased immunogenicity and host-cell infiltration by macrophages[287]. *IL-21R* is the receptor for *IL21* cytokine that exerts its antitumour effect by promoting both T cell-mediated and NK cell-mediated cytotoxicity. *IL-21*-primed CD8+ T cells have characteristics of memory T cells and exerts its anti-tumour effects not only by inducing CD8+T cells but also NK cells and able to suppress the expression of *FOXP3* and expansion of regulatory T cell[288,289].

Tumour cells can also acquire defects in antigen processing and presentation that facilitate evasion from the adaptive immune system. Effective T-cell priming requires co-stimulatory receptors on naïve T-cells and the most important of which is *CD28* that is normally expressed in 95% of CD4+T cells and approximately 50% of CD8+T cells. Interactions of *CD28* and its ligands are crucial in the regulation of adaptive cellular immunity. Down-regulation of *CD28* leads to decreased binding with its ligands B7 on antigen presenting cells thereby impairing antigen/MHC complex presentation[290,291]. *CIITA* is a major transcriptor of major histocompatibility complex (MHC) class II genes and downregulation of *CIITA* results in impaired antigen presentation. Results from melanoma cell line study demonstrated greater anti-tumour responses in a dose-dependent manner with exosomes from *CIITA*-transduced tumour cells compared to exosomes from parental tumour cells[292]. This represents another novel strategy to genetically modified tumour cells to express MHC class II gene products.

### 3.3.3 Weighted gene co-expression network analysis

We selected 3,227 probesets (3,092 genes) with a FDR of 5% from the list of differentially expressed genes (Appendix 3.1) for WGCNA as described in Chapter 2 section 2.2.4.6 to construct MPM-associated co-expression network and identify modules of highly connected genes.

A soft-thresholding power (β) of 9 (Figure 3.11) to which co-expression similarity was raised to calculate adjacency was chosen to construct the weighted gene network. At this β level, the scale free topology fit was approximately satisfied with a R^2 threshold of 0.95. By increasing the R^2 value further would lead to networks with low connectivity.

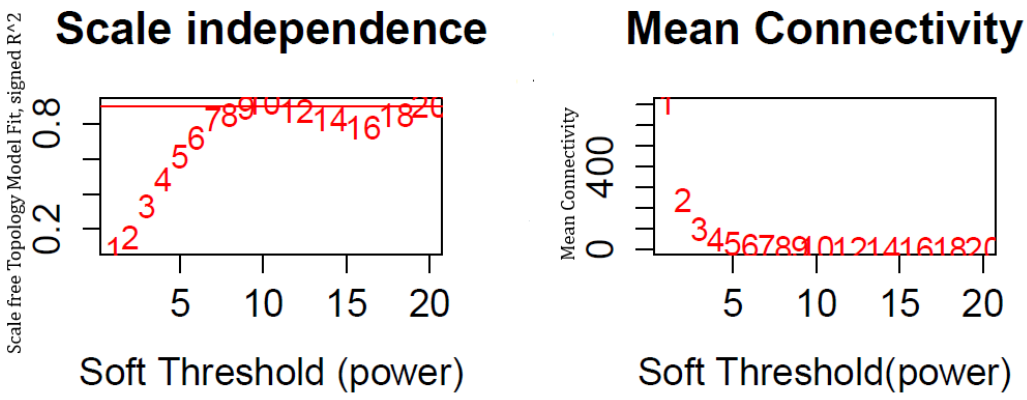


**Figure 3.11. Analysis of network topology for various soft-thresholding powers. The left panel showed the scale-free fit (y-axis) as a function of the soft-thresholding power (x-axis). The right panel showed the mean connectivity (y-axis) as a function of the soft-thresholding power (x-axis).**

A total of 14 modules (Figure 3.12) were detected with module sizes ranging from 51 to 605 genes (Table 3.8). The grey module contained genes that do not share similar co-expression with other genes in the network and therefore was not included in the dendrogram. A heatmap

is generated to visualise the weighted network as shown in Figure 3.13.

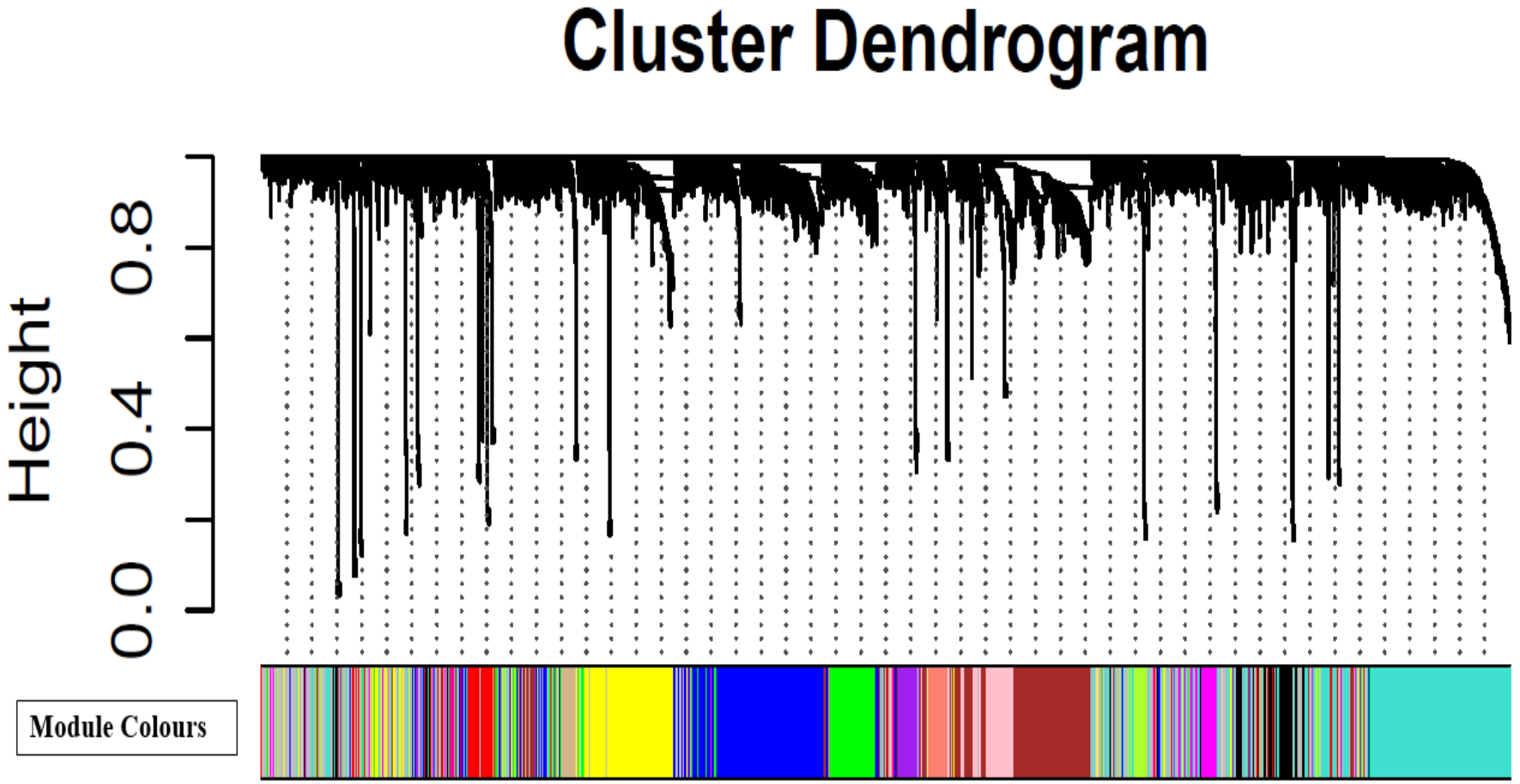


**Figure 3.12. Clustering dendrogram of genes, with dissimilarity based on topological overlap, together with assigned module colours.**

**Table 3.8. Modules and corresponding number of genes (modSize).**

| Module | No of genes in module (modSize) |
|---|---|
| Black | 129 |
| Blue | 436 |
| Brown | 353 |
| Green | 177 |
| Green-yellow | 74 |
| Grey | 500 |
| Magenta | 90 |
| Pink | 113 |
| Purple | 76 |
| Red | 119 |
| Salmon | 51 |
| Tan | 64 |
| Turquoise | 605 |
| Yellow | 305 |

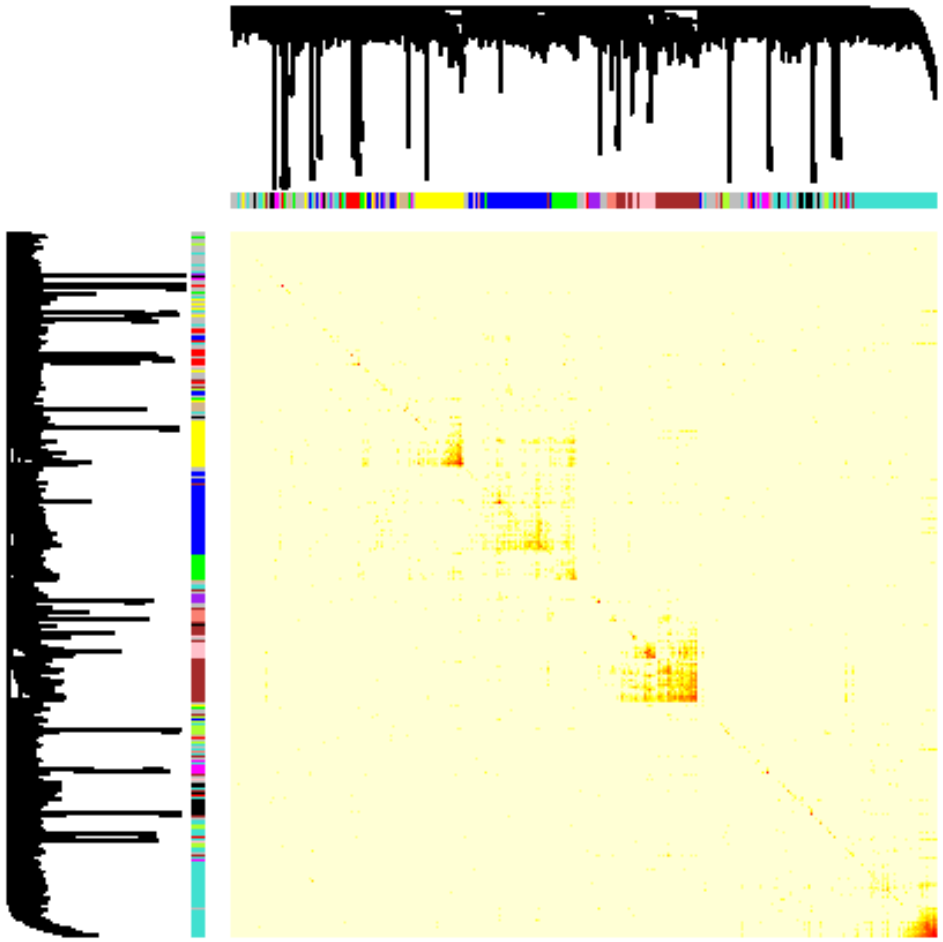

**Figure 3.13. Topological Overlap Matrix. This is depicted by the heatmap with light colour denoting low overlap and darker colour denoting higher overlap. Modules are denoted by the blocks of darker colours along the diagonal. Left and top panels show the gene dendrogram and module assignment.**

The proportion of variance explained by the first three principal components for each module are summarised in Table 3.9. On average, the first principal component, also known as module eigengenes (MEs), explained approximately 44% of the total variance for each associated module.

**Table 3.9. Proportion of variance explained by the first 3 principal components (PC) for each module.**

| MEs | PC 1 | PC 2 | PC 3 |
|---|---|---|---|
| MEblack | 40.19% | 7.65% | 5.66% |
| MEblue | 44.65% | 7.17% | 5.13% |
| MEbrown | 45.98% | 7.05% | 4.69% |
| MEgreen | 48.18% | 6.09% | 5.76% |
| MEyellow | 42.40% | 7.69% | 6.07% |
| MEmagenta | 39.89% | 7.04% | 5.61% |
| MEpink | 50.89% | 7.48% | 4.56% |
| MEpurple | 42.28% | 10.02% | 5.47% |
| MEred | 39.45% | 7.51% | 6.25% |
| MEsalmon | 50.71% | 7.48% | 5.87% |
| MEtan | 44.47% | 7.17% | 5.66% |
| MEturquoise | 37.27% | 8.13% | 5.41% |
| MEyellow | 41.20% | 8.01% | 4.92% |

The MEs in each module were tested for association with histological subtypes, smoking status and asbestos exposure using linear regression model adjusted for age and gender (as described in Chapter 2 section 2.2.4.6). The analysis found statistically significant association between the blue module (436 genes) with histological subtypes (adjusted p-value= 0.003). None of the MEs were significantly associated with either smoking status or asbestos

exposure. GO analysis (Table 3.10) revealed the blue module was enriched in genes involved in biological processes of cell junction organisation.

**Table 3.10. Top enriched GO terms for blue module associated with histological subtypes.**

| GO category | Category name | GO ID | No of genes | adj.P value |
|---|---|---|---|---|
| biological process | cell junction organization | GO:0034330 | 18 | 0.0137 |
| biological process | tight junction assembly | GO:0070830 | 8 | 0.0137 |
| biological process | morphogenesis of embryonic epithelium | GO:0016331 | 14 | 0.0197 |

In order to identify genes in the blue module with high connectivity and strong association with histological subtypes, the module membership (MM) for each gene in the blue module and gene significance (GS) of each gene associated with histological subtypes were calculated as described in Chapter 2 section 2.2.4.6. Figure 3.14 shows a statistically significant positive correlation between GS for histological subtypes and MM of genes in the blue module indicating that genes with high connectivity are also significantly associated with histological subtypes. An arbitrary GS value of ≥ 1.0 and MM value of ≥ 0.7 were chosen to identify hub genes with strongest connectivity and link with histological subtypes. This resulted in 31 hub genes (Table 3.11) and a visualisation of this network with Cytoscape Software 3.0.1 is shown in Figure 3.15.

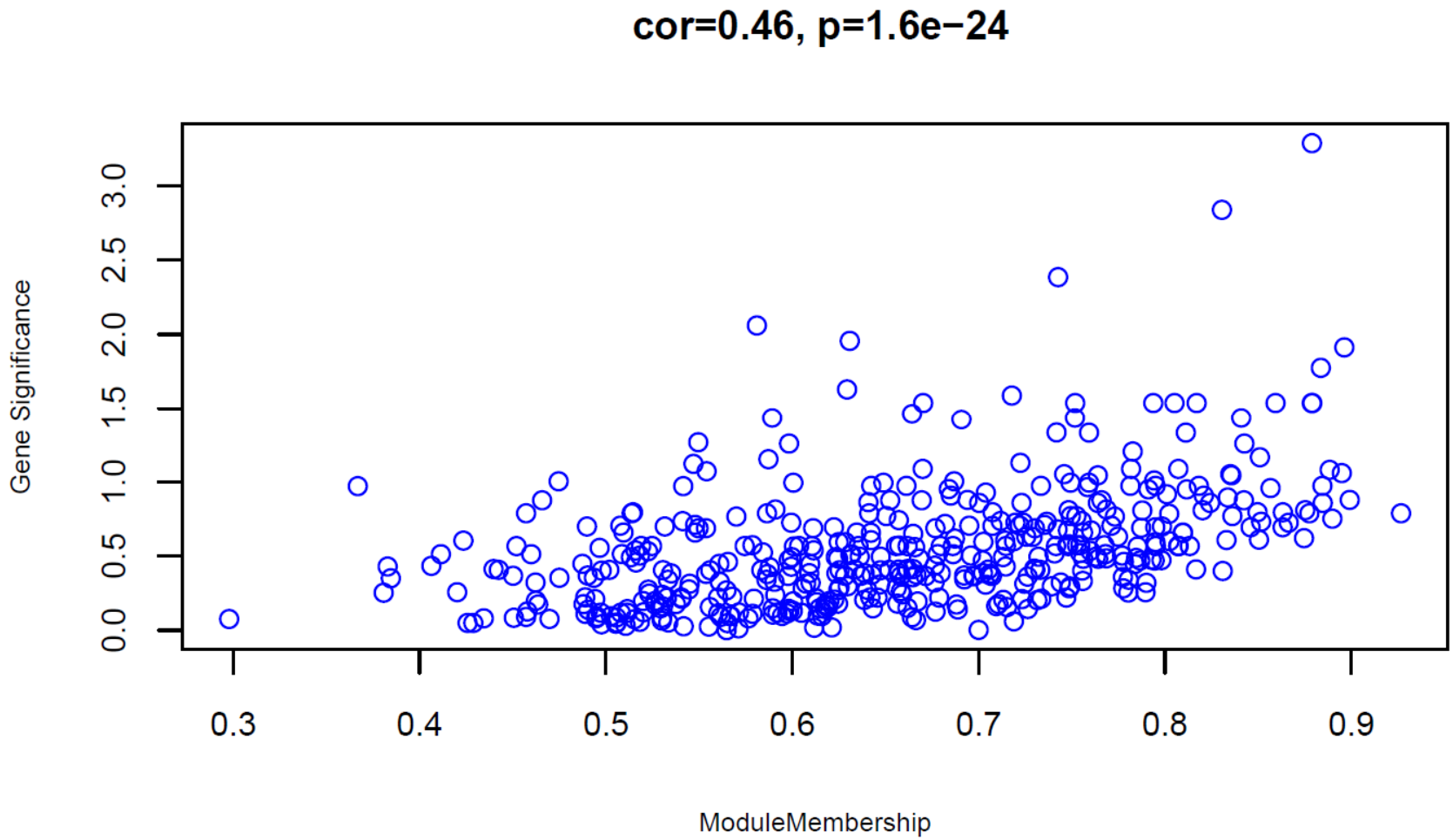


**Figure 3.14. A scatterplot for gene significance (GS) for histological subtypes versus module membership (MM) in the blue module demonstrating positive correlation.**

**Table 3.11. Top hub genes in the blue module. These hub genes are defined by an absolute Module membership (MM) ≥ 0.7and gene significance (GS) ≥ 1.0 with corresponding fold change (FC) and adjusted p value from differential gene expression analysis.**

| Gene | GS | MM | FC | adj. p value |
|---|---|---|---|---|
| *CARNS1* | 1.91 | 0.9 | 5.02 | 0.002105113 |
| *PLLP* | 1.08 | 0.89 | 35.08 | 2.44908E-05 |
| *PTPRF* | 1.06 | 0.89 | 5.33 | 1.58227E-05 |
| *PRR15* | 3.29 | 0.88 | 12.25 | 0.000197445 |
| *KLK11* | 1.78 | 0.88 | 5.84 | 0.000218948 |
| *LRRN4* | 1.54 | 0.88 | 40.30 | 4.83018E-05 |
| *CCDC64* | 1.54 | 0.88 | 4.70 | 0.013362278 |
| *BNC1* | 1.54 | 0.86 | 39.62 | 1.17508E-07 |
| *LRRC1* | 1.43 | 0.84 | 6.51 | 0.001049806 |
| *PDZD2* | 1.26 | 0.84 | 6.65 | 0.001794995 |
| *REC8* | 1.05 | 0.84 | 4.93 | 0.000545429 |
| *KLHL31* | 1.04 | 0.84 | 5.34 | 0.002498679 |
| *UPK3B* | 1.54 | 0.82 | 47.56 | 1.3889E-05 |
| *C19orf33* | 1.54 | 0.81 | 17.09 | 1.41006E-05 |
| *TM4SF1* | 1.33 | 0.81 | 2.73 | 0.01108929 |
| *SELENBP1* | 1.54 | 0.79 | 2.47 | 0.0421346 |
| *MMP24* | 1.01 | 0.79 | 18.66 | 5.68068E-05 |
| *CMTM8* | 1.21 | 0.78 | 4.76 | 4.12692E-06 |
| *TMEM151A* | 1.33 | 0.76 | 5.03 | 0.002740044 |
| *HOOK1* | 1.54 | 0.75 | 2.63 | 0.048263673 |
| *KLK10* | 1.43 | 0.75 | 2.78 | 0.02259675 |
| *IGSF9* | 2.39 | 0.74 | 4.45 | 0.001196221 |
| *CYSTM1* | 1.33 | 0.74 | 1.78 | 0.04086658 |
| *SLPI* | 1.59 | 0.72 | 21.47 | 0.000456269 |
| *MIR181A1HG* | 1.13 | -0.72 | 1.75 | 0.038039179 |
| *RASGRP3* | 1.05 | -0.75 | 2.26 | 0.000429178 |
| *GLRX* | 1.04 | -0.76 | 1.75 | 0.038329462 |
| *ADAM19* | 1.09 | -0.78 | 2.96 | 0.01631073 |
| *IMPDH1* | 1.09 | -0.81 | 1.73 | 0.029372633 |
| *ADAMTS6* | 2.84 | -0.83 | 3.40 | 0.028963716 |
| *ANXA6* | 1.17 | -0.85 | 1.99 | 0.01202954 |

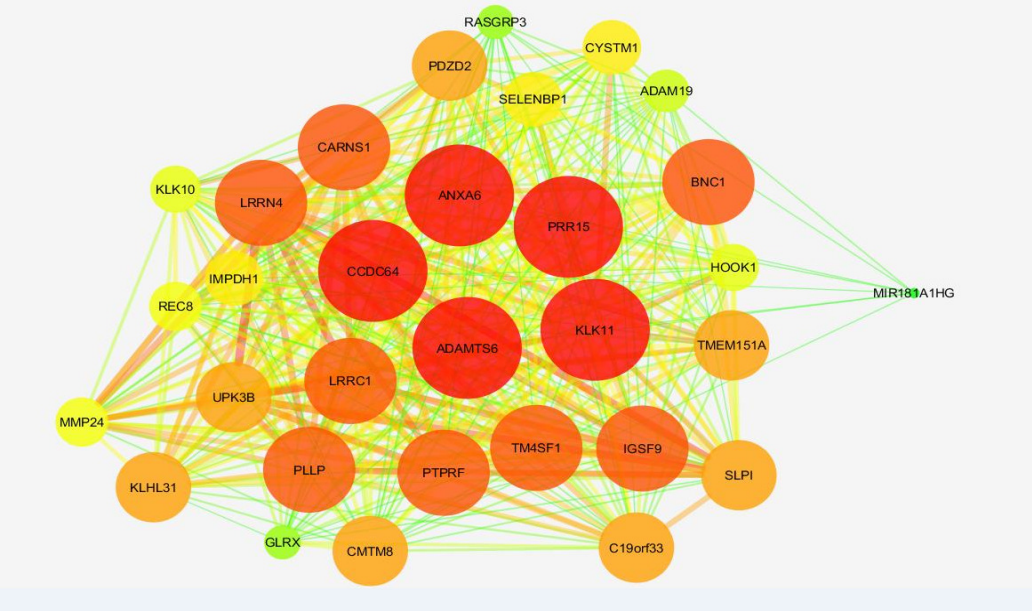


**Figure 3.15. Cytoscape visualisation of the top hub genes in blue module with high connectivity and gene significance (GS). Nodes with high degree of intramodular connectivity appear larger and darker in colour. Strong connections between nodes are represented by darker and wider edges.**

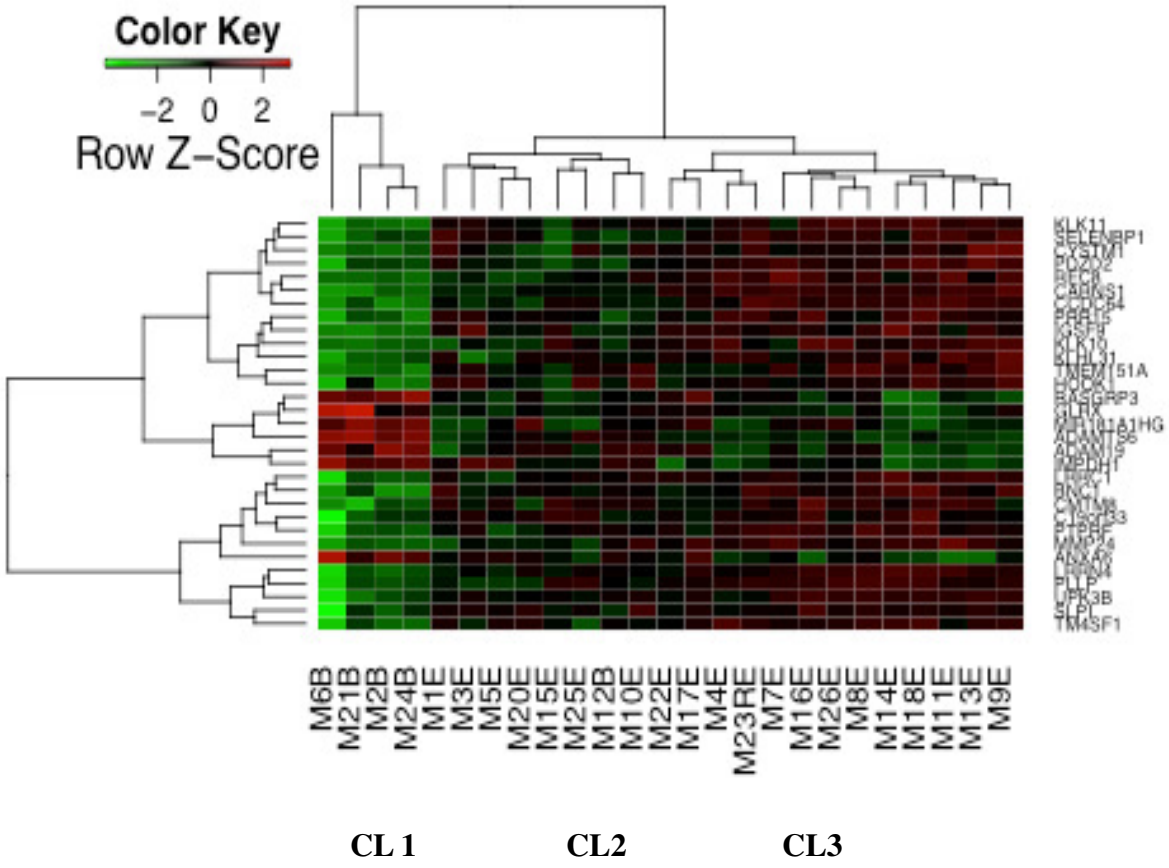


**Figure 3.16. Hierarchical cluster analysis of the expression level of the hub genes. The analysis identified 3 clusters (CL) of MPM cases (M) with epithelioid denoted by E and biphasic by B. Columns correspond to MPM cases and rows correspond to 31 hub genes associated with subtype classifications.**

Using the expression profiles of the 31 hub genes we reclassified the tumours into three molecular subtypes. Cluster 1 consisted of four out of the five biphasic MPM, cluster 2 included one biphasic MPM and 4 epithelioid MPM; and the remaining epithelioid MPM are grouped together in cluster 3 (Figure 3.16). Amongst these hub genes, *CARNS1* has the strongest connectivity and *PRR15* is the gene most significantly associated with histological subtypes (Table11).

*CARNS1* is a member of the ATP-grasp family of ATPases and catalyses the formation of

carnosine and harmocarnosine present mainly in skeletal muscle and the central nervous system respectively. Little is known about the role of carnosine in cancer but has been suggested to have a protective effect against oxidative stress[293]. Recent evidence demonstrated potential tumour suppressive function of *CARNS1* by inhibiting the proliferation of malignant glioma cells *in vitro* and reducing growth *in vivo* in a NIH3T3-HER2/neu mouse model[294,295]. Another study demonstrated *CARNS1* as a Mapsin-dependent tumour suppressor in claudin-low breast carcinoma[296]. The expression of Mapsin, a tumour suppressor gene, is regulated by transcription factors or epigenetic modifiers and is expressed at higher levels in epithelial cells and downregulated in mesenchymal cells. *In vivo* induction of Mapsin not only significantly upregulated *CARNS1* but was able to revert aggressive claudin-low breast carcinomas towards a more differentiated 'epithelial-like phenotype'. Interestingly, claudins are not frequently expressed in MPM; and their expression by IHC are lower in sarcomatoid and biphasic MPM compared to epithelioid MPM[297]. The differential expression of *CARNS1* across the 3 clusters in our study suggests possible downregulation of tumour suppressor Mapsin in the biphasic tumours (CL1).

*PRR15* encodes a protein of unknown function and its expression is restricted to post mitotic epithelial cells in mouse model and the pattern of expression is similar to negative cell cycle regulators suggesting a role in regulating cell proliferation[298]. *PRR15* expression by in situ hybridisation was studied in mouse and human gastrointestinal tumours. The study found *PRR15* was detected in tumours harbouring *APC* mutations suggesting its involvement in defective WNT signalling[299]. Thus the higher expression of *PRR15* in CL1 compared to CL3 suggests this pathway may be more active in epithelioid than biphasic subtypes.

The expression level of seven hub genes is higher in CL1 as depicted in the heatmap in Figure 3.16. These include *ADAMTS6, ADAM19, ANXA6* and *RASGRP3* that are involved in ECM

degradation and cell invasion; *IMPDH1* and *GLRX* are involved in cell proliferation while the role of *MIR181A1HG* is unknown but has been shown to be highly expressed in acute promyelocytic leukaemia[300]. Amongst these genes, *ANXA6* has the strongest connectivity and *ADAMTS6* is the gene most significantly associated with histological subtypes (Table 3.11).

*ANXA6* is a member of the annexin family of calcium-dependent phospholipid binding proteins. Study in breast cancer tumours demonstrated downregulation of *ANXA6* in tumour compared to normal breast tissue correlated with enhanced tumour cell proliferation mainly due to increased cytosolic calcium in cells expressing low level of *ANXA6*[301]. On the contrary, the study showed depletion of *ANXA6* in invasive breast cancer cell line reduced tumour cell invasion/migration that might be attributed to the inhibition of FAK and PI3kinase/Akt pathway activation. The role of *ANXA6* in promoting cell invasion/migration is further supported by increased NF-Kß activity and *MMP-13* expression that promotes ECM degradation in *ANXA6*-overexpressing chondrocytes[302]. Taking all these together, downregulation of *ANXA6* in cancer cells promotes cell proliferation while upregulation gives rise to a more invasive phenotype corresponding to the biphasic tumours in CL1 in Figure 3.16. *ADAMTS6* is a newly described ADAMTS (a disintegrin and metalloprotease with thrombospondin motifs) family members but its exact function is not well understood. However, there is evidence suggesting its role in compromising ECM structure from a retinal pigment epithelium derived cell line study[303].

It is also worth noting *ADAM 19* and *IMPDH1*. *ADAM19* is an endopeptidase that degrades ECM to promote invasion and is also capable of releasing several growth factors and cytokines including tumour necrosis factor (TNF)-alpha and TNF-alpha-related activation-induced cytokine. It is upregulated in several malignancies and correlated with tumour invasiveness in primary brain tumour[304]. Cell line study identified *ADAM19* as a downstream

target of TGF-ß pathway whereby stimulation of ovarian cancer cells with TGF-ß1 resulted in binding of *SMAD4* to *ADAM19* gene promoter sites accompanied by an increase in *ADAM19* mRNA levels[305]. *IMPDH1* together with *IMPDH2* are involved in the rate-limiting step for GTP and dGTP biosynthesis. *IMPDH* is implicated in cell proliferation and inhibition of *IMPDH* reduced guanine nucleotide pools thereby interrupting DNA synthesis and cell cycle progression by arresting cells in G1[306]. *IMPDH* is a recognised target for anticancer and immunosuppressive drugs and therefore potentially could be an attractive target in biphasic MPM tumours[307].

Next, we investigated the role of epithelial-mesenchymal transition (EMT) across the subtypes based on the findings of higher expression of genes associated with invasion, degradation of ECM and TGF-ß signalling in CL1. The boxplots below (Figure 3.17) display the differences in expression level of EMT markers (*CDH1, SNAI1, SNAI2, ZEB1, ZEB2, TWIST1*) across the 3 clusters. The results showed the mesenchymal transcriptional regulators are consistently more overexpressed in biphasic MPM tumours in CL1 with lower expression of epithelial marker, *CDH1*. The differences across the 3 clusters are statistically significant for *SNAI1, SNAI2, ZEB2, TWIST1 and CDH1*. Although not statistically significant, expression of *ZEB1* also showed an upward trend from CL3 to CL1.

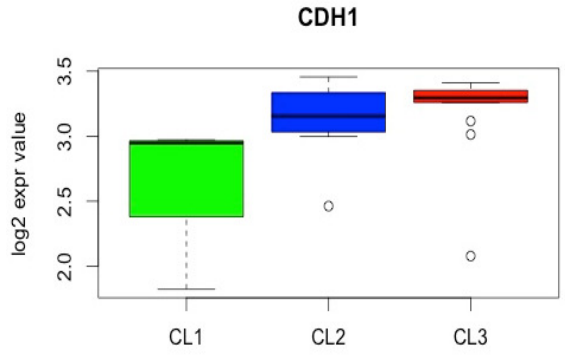


$p = 0.022$

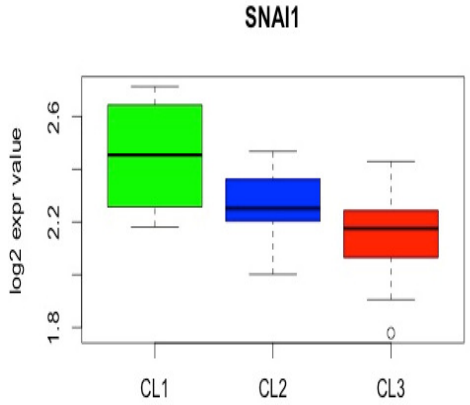


$p = 0.048$

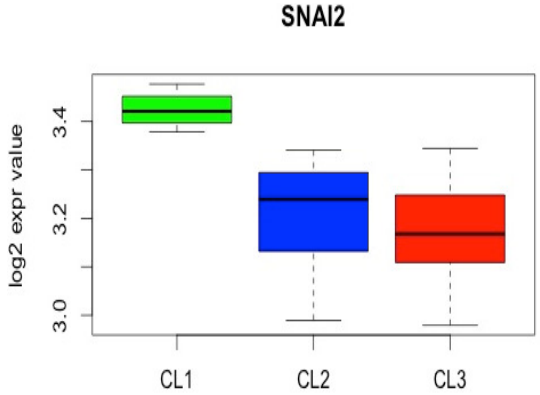


$p = 0.006$

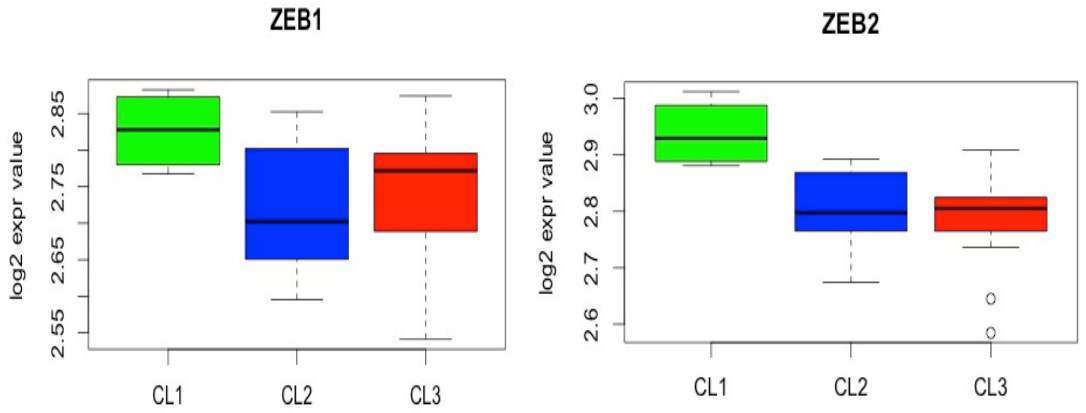


$p = 0.193$




$p = 0.015$

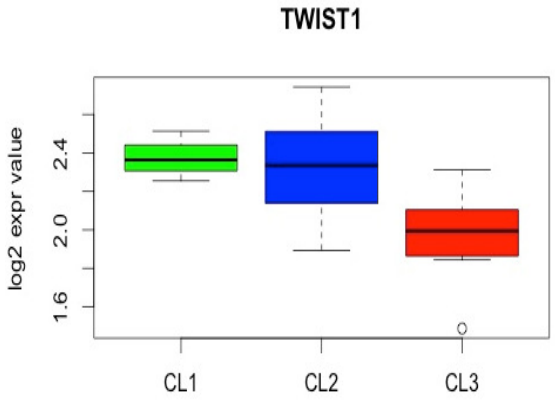


$p = 0.003$

**Figure 3.17. EMT markers. Boxplots for epithelial marker (*CDH1*) and mesenchymal markers (*SNAI1, SNAI2, ZEB1, ZEB2* and *TWIST1*) with the corresponding p-value computed from ANOVA.**

Survival data were available for each of the 25 tumour cases. Using Cox proportional hazards model to regress survival time on individual gene expression profile (adjusted for age and gender), a GS for survival was defined as minus logarithm of the hazard ratio probability value (described in Chapter 2 section 2.2.4.6). The diagram below (Figure 3.18) shows the turquoise module (605 genes) is significantly enriched with genes associated with survival time.

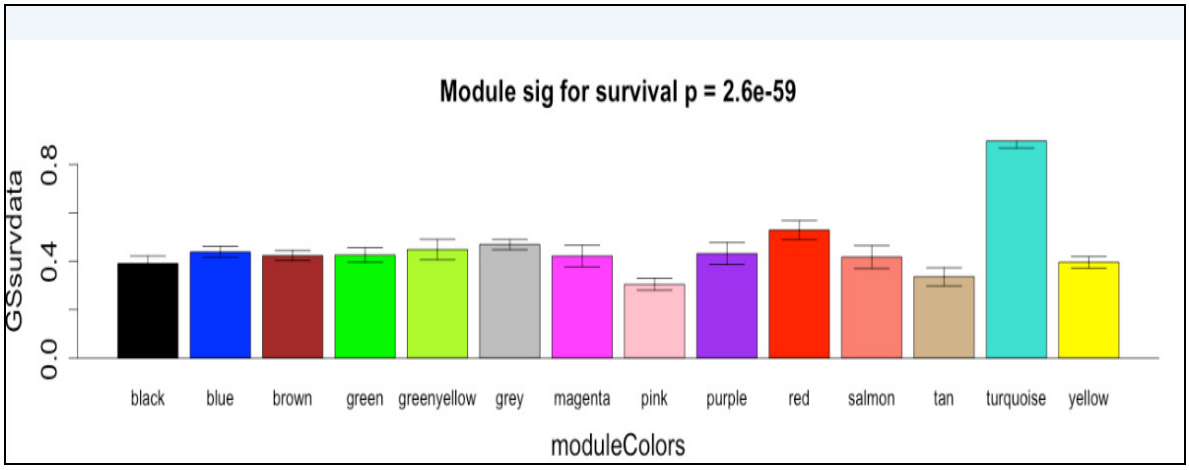


**Figure 3.18. Modules associated with survival time. Bar plots for each module (x-axis) and the corresponding gene significance (GS) for survival time (y-axis). The analysis shows turquoise module has the highest mean value of GS for survival time with a Kruskal Wallis p-value of 2.6e-59.**

Enrichment analysis revealed cell cycle process as the top over-represented GO terms for the turquoise model (Table 3.12).

**Table 3.12. Top enriched GO terms for turquoise module associated with survival time.**

| GO category | Category name | GO ID | No of genes | adj.P value |
|---|---|---|---|---|
| biological process | cell cycle process | GO:0022402 | 112 | 1.24E-22 |
| biological process | cell cycle | GO:0007049 | 126 | 7.93E-22 |
| biological process | cell cycle phase | GO:0022403 | 37 | 1.41E-20 |

A statistically significant positive correlation is observed between GS for survival time and MM for genes in the turquoise module (Figure 3.19) indicating genes with high connectivity are also strongly linked with survival time. Twenty-five hub genes associated with survival time in the turquoise module are identified using an arbitrary GS value of ≥ 2.0 and MM value of ≥ 0.7 (Table 3.13). The interactive network amongst the hub genes is displayed using Cytoscape Software 3.0.1 as shown in Figure 3.20.

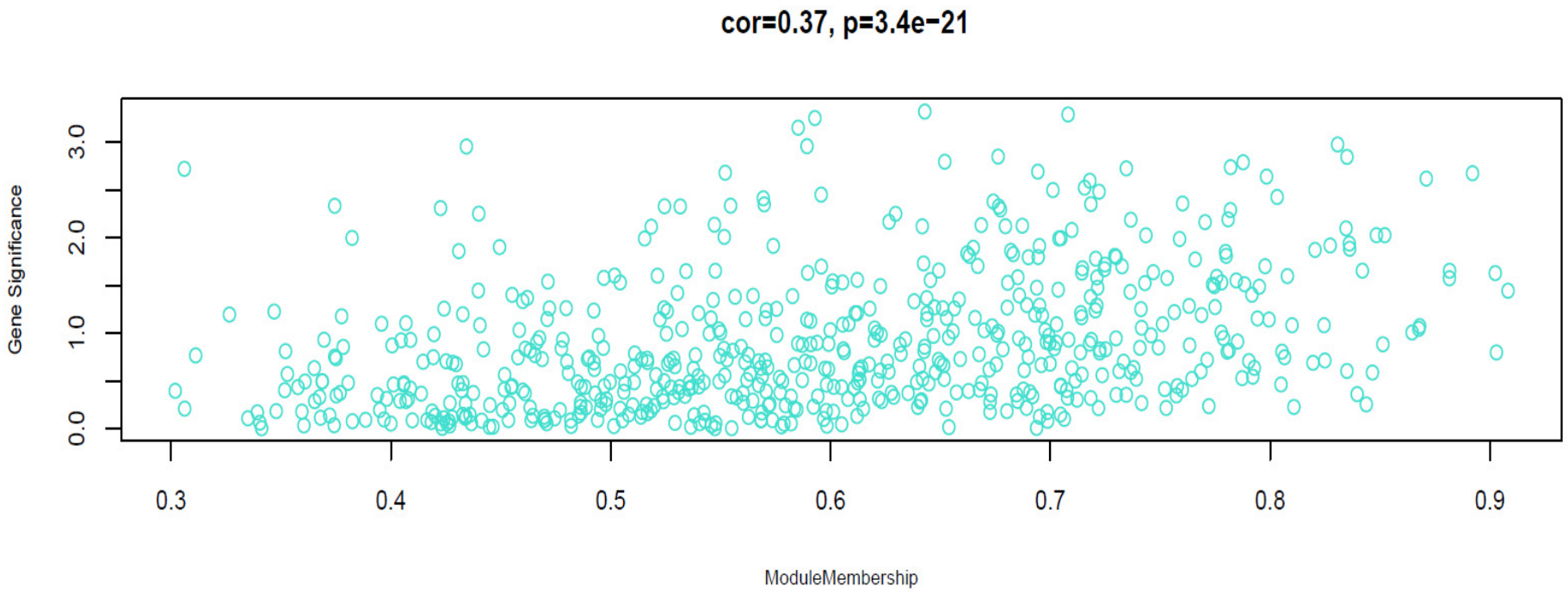


**Figure 3.19. A scatterplot of GS for survival time versus MM in the turquoise module showing a statistically significant correlation between GS and MM in this module.**

**Table 3.13. Top hub genes in the turquoise module. These hub genes are defined by absolute MM ≥0.7 and GS ≥ 2.0 with corresponding FC and adjusted p value identified from differential gene expression analysis.**

| Gene | GS survival | MM turquoise | FC | adj.p value |
|---|---|---|---|---|
| *PDRG1* | 2.67 | 0.89 | 1.62 | 0.01065877 |
| *E2F1* | 2.62 | 0.87 | 2.06 | 0.043738806 |
| *TIMM50* | 2.03 | 0.85 | 1.56 | 0.017060413 |
| *PSMD8* | 2.03 | 0.85 | 1.34 | 0.041059079 |
| *MCM7* | 2.85 | 0.83 | 1.87 | 0.008922121 |
| *GSG2* | 2.1 | 0.83 | 2.04 | 0.042485814 |
| *PXMP4* | 2.97 | 0.83 | 1.53 | 0.043561541 |
| *MOCS3* | 2.43 | 0.8 | 1.93 | 0.014510297 |
| *NSDHL* | 2.64 | 0.8 | 1.80 | 0.00287891 |
| *SGOL1* | 2.79 | 0.79 | 2.98 | 0.020787539 |
| *CCT4* | 2.74 | 0.78 | 1.59 | 0.006244544 |
| *CDCA8* | 2.29 | 0.78 | 2.72 | 0.017160609 |
| *CENPH* | 2.19 | 0.78 | 1.70 | 0.026323983 |
| *CCT5* | 2.16 | 0.77 | 1.44 | 0.035352582 |
| *PBK* | 2.36 | 0.76 | 3.41 | 0.002567779 |
| *CDC20* | 2.02 | 0.74 | 2.69 | 0.036215521 |
| *NR2C2AP* | 2.19 | 0.74 | 2.07 | 0.014312739 |
| *DAGLA* | 2.72 | 0.73 | 2.00 | 0.004631814 |
| *TPX2* | 2.48 | 0.72 | 3.25 | 0.012000329 |
| *BUB1* | 2.35 | 0.72 | 2.55 | 0.041013206 |
| *SKA3* | 2.6 | 0.72 | 2.46 | 0.046605563 |
| *POLD2* | 2.52 | 0.72 | 1.59 | 0.031978027 |
| *MRPS17* | 2.08 | 0.71 | 1.50 | 0.032925202 |
| *RFC3* | 3.29 | 0.71 | 1.51 | 0.047574394 |
| *CKAP2L* | 2.5 | 0.7 | 2.89 | 0.013096869 |

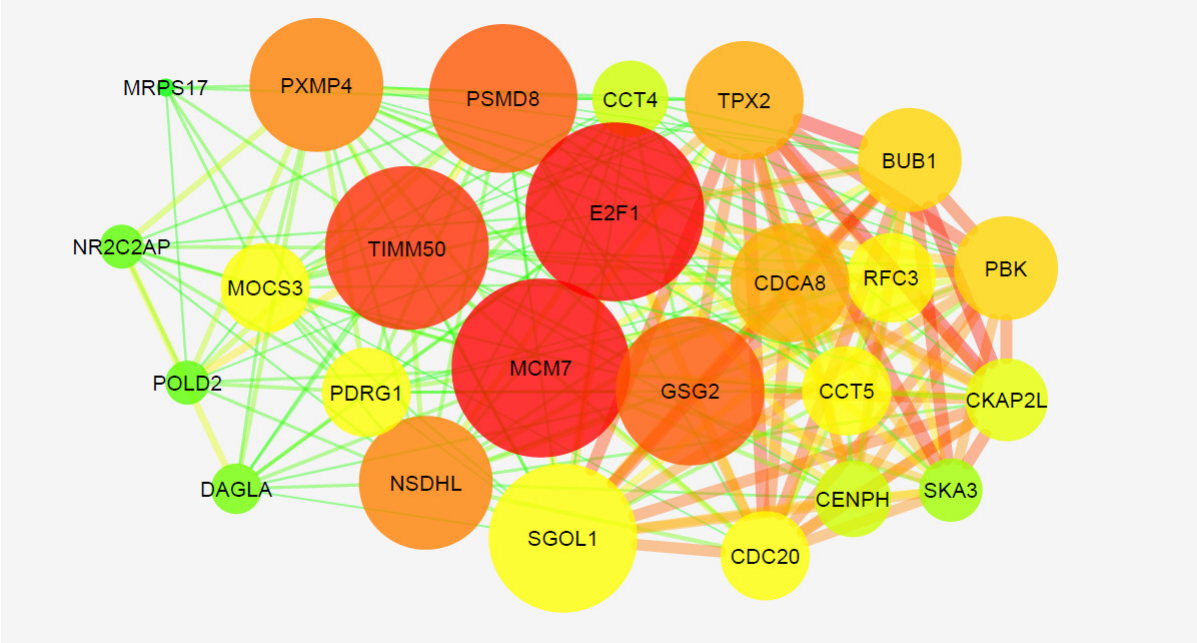


**Figure 3.20. Cytoscape visualisation of the top hub genes in turquoise module with high connectivity and gene significance (GS). Nodes with high degree of intramodular connectivity appear larger and darker in colour. Strong connections between nodes are represented by darker and wider edges.**

The hub genes associated with survival time are enriched in pathways involved in regulation of the cell cycle, in particularly the mitotic phase (Table 3.14). The hub genes are also involved in *PLK1* and Aurora B signalling pathways that have several important functions in the mitotic phase of the cell cycle such as regulation of centrosome maturation, spindle assembly, mitotic exit and cytokinesis.

**Table 3.14. Top pathways enriched by 25 hub genes associated with survival time.**

| Pathway | FDR | Nodes |
|---|---|---|
| Mitotic Metaphase and Anaphase | <1.000e-03 | *CDCA8,BUB1,PSMD8,SGOL1,CDC20,CENPH* |
| PLK1 signalling events | <5.000e-04 | *BUB1,SGOL1,TPX2,CDC20* |
| Mitotic Prometaphase | 3.33E-04 | *CDCA8,BUB1,SGOL1,CDC20,CENPH* |
| Synthesis of DNA | 2.75E-03 | *MCM7,PSMD8,RFC3,POLD2* |
| DNA replication | 3.00E-03 | *MCM7,RFC3,POLD2* |
| Aurora B signalling | 3.67E-03 | *CDCA8,BUB1,SGOL1* |
| Cell Cycle Checkpoints | 3.57E-03 | *MCM7,PSMD8,CDC20,RFC3* |
| S Phase | 3.63E-03 | *MCM7,PSMD8,RFC3,POLD2* |
| Cell cycle | 3.33E-03 | *E2F1,MCM7,BUB1,CDC20* |
| Regulation of DNA replication | 1.49E-02 | *E2F1,MCM7,PSMD8* |
| M/G1 Transition | 1.62E-02 | *E2F1,MCM7,PSMD8* |
| Mismatch repair | 2.78E-02 | *RFC3,POLD2* |

The expression profiles of the 25 hub genes stratified the tumours into three clusters (Figure 3.21) with different prognostic outcomes as shown in the Kaplan-Meier survival plots in Figure 3.22.

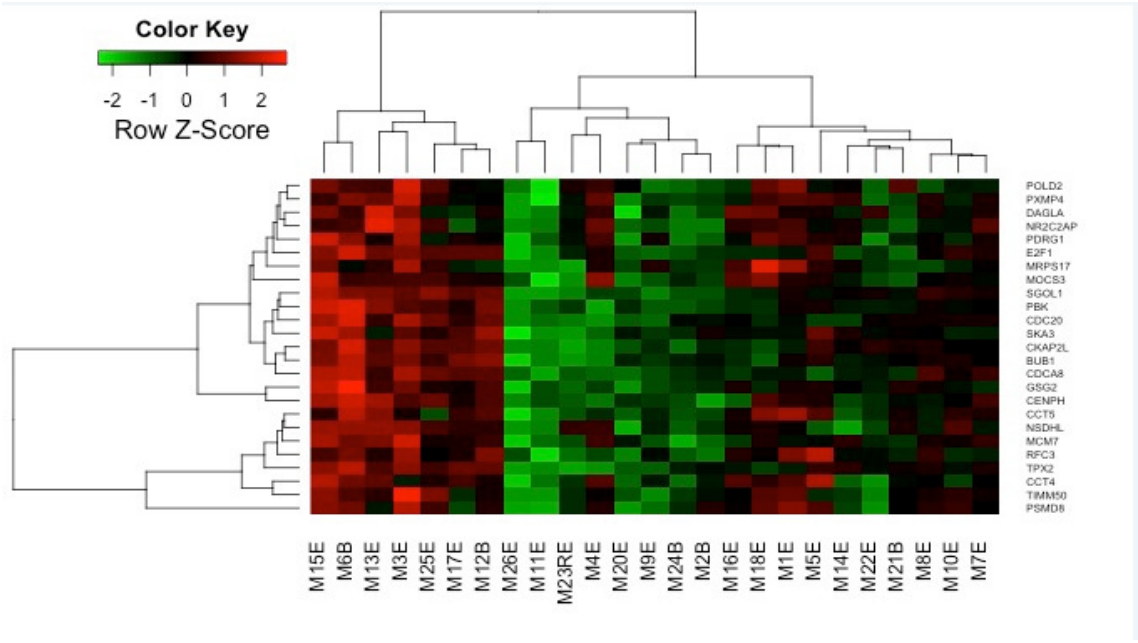


**Figure 3.21. Hierarchical cluster analysis of the expression level of the hub genes associated with survival time. The analysis identified 3 clusters (CL) of MPM cases. Rows correspond to 25 hub genes associated with survival time and columns correspond to MPM cases (M).**

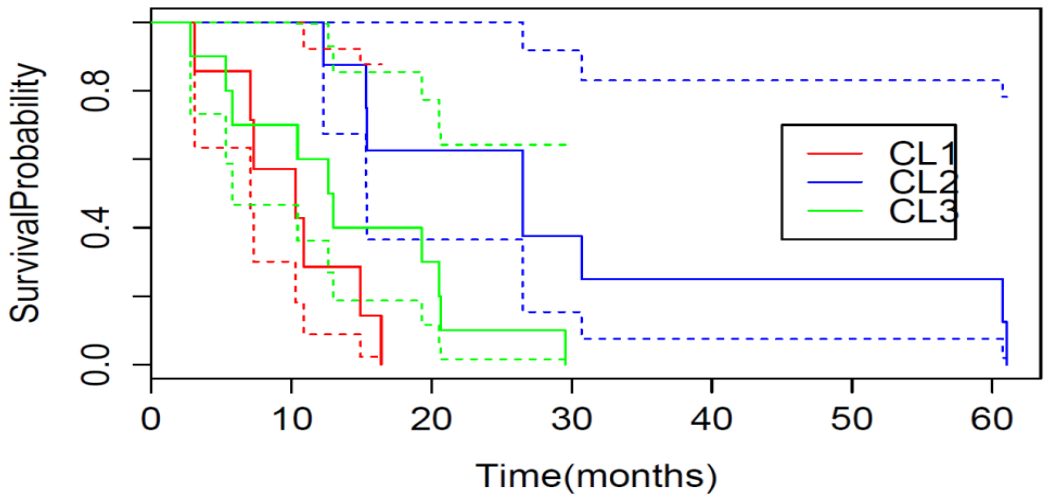


**Chisq= 13.5 on 2 degrees of freedom, p= 0.001**

**Figure 3.22. Kaplan-Meier overall survival plot for cluster (CL) 1, 2 and 3. This demonstrates CL1 has the worst prognosis while CL2 has the best prognosis.**

The top three genes with the highest intra-modular connectivity are *PDRG1*, *E2F1* and *TIMM50* (Table 3.13). *PDRG1* may have a role in DNA damage response and study found its mRNA level is up and downregulated by ultraviolet radiation and *p53* respectively[308]. In addition, knockdown of *PDRG1* in colon cancer cell suppressed tumour cell growth and *PDRG1*-associated proteins are involved in apoptosis and cell cycle demonstrating its participation in cell growth regulation.

The expression of *E2F1*, a pivotal transcription factor involve in cell cycle, DNA synthesis, repair, proliferation and apoptosis, has been shown to be positively correlated with cancer cell proliferation[309]. The role of *E2F1* in MPM has been previously studied that demonstrated knock down of *E2FI* using small interfering RNA (siRNA) in MPM cell lines and in xenograft models treated with arsenic trioxide (ATO) significantly inhibited cell viability and proliferation[310].

*TIMM50* facilitates transfer of proteins to the inner mitochondrial membrane required for normal mitochondrial function. *TIMM50* plays an active role in modulating growth and development while knockdown of *TIMM50* by siRNA increased the sensitivity of human cell lines to apoptosis by stimulating the release of mitochondrial apoptotic proteins that activate the caspase-dependent and –independent cell death pathways[311].

Seven of the hub genes associated with survival time (*CDCA8, BUB1, PSMD8, SGOL1, CDC20, CENPH, TPX2*) are related to mitotic spindle assembly checkpoint (MSAC). Overexpression of *BUB1* has been previously described in MPM and is identified as one of the 11 genes in the prognostic classifier list associated with poor prognosis[142]. This serine/threonine protein kinase is a key component in mitotic checkpoint that regulates APC/C activity through recruitment of MAD1-MAD2 and inhibits APC/C activity by forming

a complex with other proteins to bind and phosphorylate an E3 ubiquitin ligase *CDC20* that regulates separation of chromosomes for degradation at specific mitotic stages[312]. *BUB1* also interacts with another novel gene in MPM, *SGOL1*, a protein-coding gene that maintains chromosome cohesion during mitosis[313]. This in turn allows *SGOL1* to recruit a protein phosphatase, PP2, that retains cohesin at centromeres by counteracting PLK1 kinase activity to protect sister chromatids from early separation and maintain chromosomal stability. Several spliced variants of *SGOL1* have been identified and their overexpression resulted in aberrant chromosome alignment and resistance to taxane chemotherapy[314,315]. Overexpression of *CDCA8*, a new component required for chromatin-induced microtubule stabilization and spindle formation is phosphorylated by *AURKB* and inhibition of *CDCA8* resulted in growth suppression of lung cancer cell *in vitro*[316].

Four other genes (*MCM7, PSMD8, RFC3, POLD2*) are related to DNA synthesis/replication. *PSMD8* is a 26S proteasome involved in activation of cyclin dependent kinase, *CDC28*, and shown to be upregulated in breast cancer[317]. Overexpression of *MCM7* in body cavity fluid of patients with mesothelioma correlated positively with Ki-67 and *TOP2A* (also identified in the turquoise module with MM=0.69 and GS 2.12); and together are able to distinguish reactive mesothelial cells from malignant mesothelioma cells[318].

Both *POLD2* and *RFC3* are involved in DNA repair. *POLD2* is a subunit of the DNA polymerase delta complex whose expression is negatively regulated by tumour suppressor, *PTEN*. *POLD2* is known to be involved in ovarian carcinogenesis and is associated with poor survival in gliomas[319,320.] *RFC3* is a novel gene in MPM and has the highest GS value associated with survival time. *RFC3* is a potential oncogene whose expression is upregulated by cancer promoter genes, *MYCN* and *SHH*; and downregulated by tumour suppressors *TP53* and *CDKN2A* of which the latter is frequently lost in MPM[321–324.] In addition, *E2F1* is able to

promote *RFC3* expression by binding to the *RFC3* gene promoter region[325].

## 3.4 Discussions

MPM is a highly aggressive tumour with poor prognosis and limited treatment options. MPM is categorized into three broad histological subtypes (epithelioid, sarcomatoid and biphasic) according to the presence and relative amount of epithelioid and spindle cell components. Histological subtype is one of the main prognostic factors in MPM but this is not always the case[326]. Gene expression profiling has successfully reclassified tumours into different subtypes and prognostic groups with more precision[327]. This is based on molecular signatures identified from gene expression variations that correlate with cellular and physiological state of the disease.

Our global gene expression profiling study of MPM compared to non-malignant pleura revealed diverse molecular events that may contribute to the phenotype of this disease. Our data identified aberrant expression of genes involved in biological functions such as cell junction organization including cell morphology, movement and interactions with ECM, cell cycle process, and immune system regulation. The top five differentially expressed genes (*ITLN1, UPK1B, UPK3B, CALB2* and *LRRN4*) with the highest absolute FC in expression level in our study are notable as potential diagnostic biomarkers (except *CALB2* which is an established validated IHC marker for the diagnosis of MPM) and their roles in the pathogenesis of MPM require further studies.

Uncontrolled cell growth and proliferation due to aberrant cell cycle regulation is one of the hallmarks of cancer. The *CDKN2A* locus that encodes $p16^{INK4A}$ and $p14^{ARF}$ (components of pRb and p53 cell cycle regulatory pathways); and *CDKN2B* are frequently deleted in MPM

leading to uncontrolled cell cycle progression[328]. Our study further supports the role of cell cycle genes in MPM progression and maintenance. We identified genes associated with cell cycle checkpoint, MSAC, and tumours with high expression of MSAC genes could potentially be targeted with nontaxane molecular inhibitor, epithilone B, as shown by Suraokar *et al*[134].

Cell junctions comprise of adhesive protein complexes that provide contact and signalling between neighbouring cells or between cell and the ECM thereby regulating cell morphology, adhesions and mobility. Abnormal expression of genes involved in these processes is implicated in tumorigenesis including malignant transformation, migration/invasion and metastasis[329]. We observed FAK, a cytoplasmic tyrosine kinase and a multifunctional regulator of cell signalling within the tumour microenvironment, is at the intersection of many of the genes and pathways associated with cell morphology, adhesions and migration. In addition, several upregulated growth factors and/or their receptors identified in our study including *EGFR, FGF9, FGF18, MET* and *HMMR* are capable of activating FAK. The amino-terminal domain of FAK interacts with intracellular domain of *EGFR* and is an important signalling integrator for *EGF-EGFR* mediated cell migration[330]. The fibroblast growth factors are also implicated in phosphorylation of FAK at Ser-910[331]. *MET* has also been shown to have direct interaction with FAK independently of its ligand *HGF*[332]. Hyaluronan, a glycosaminoglycan of the ECM, binds to its receptor *HMMR* and are able to induce epithelial cell lines to undergo transformation to mesenchymal-like phenotype and activation of PI3K/Akt pathway via FAK[333].

In addition, we identified genes involved in Hedgehog and WNT signalling pathways. Deregulated Hedgehog signalling is active in MPM with significant increase in expression of *GL1*, sonic hedgehog and human hedgehog interacting protein detected by q-PCR and *in situ*

hybridisation in tumour samples[334]. *LRP2* an important regulator of Hedgehog signalling is one of the top 20 up-regulated genes (adj. p value= 0.002, FC= 30.48) in our study. Aberrant WNT signalling is active in MPM and targeting WNT signals using siRNA or antibodies against *WNT1* or *2* and dominant-negative *Dvl* led to suppression of mesothelioma cells growth *in vitro*[171,173,252,253]. Our findings further support the involvement of these two pathways in MPM carcinogenesis that may have potential therapeutic implications.

Interestingly, recent studies have identified interactions between both Hedgehog and WNT pathways with FAK signalling. *In vitro* study on hepatoma cell line showed Sonic hedgehog mediated cell migration and invasion by regulating FAK/AKT signalling pathways. Enhancing Hedgehog signalling by rSHH-N led to increased phosphorylation of AKT and FAK while Hedgehog signalling inhibitor resulted in decreased AKT and FAK activities[335]. On the contrary, FAK appears to act upstream of WNT signalling as demonstrated in MCF-7 breast cancer cell line whereby suppression of FAK led to reduced *WNT3/3A* expression levels[336].

As described, many of the genes and pathways identified are linked to FAK signalling. However, *PTK2* that encodes FAK was not identified as one of the differentially expressed genes in our data. The Cancer Genome Atlas showed high messenger RNA (mRNA) levels of FAK in several cancer types and activation of FAK identified with antibody recognition of the FAK Y397 auto-phosphorylation site correlated with tumour progression[337]. Other study observed increased FAK activity is associated with *PTK2* amplification or copy number gain but does not always correlate with FAK mRNA expression and mRNA level does not always translate into FAK protein level[338]. In MPM, *NF2* that encodes Merlin is frequently inactivated and Merlin is required to inhibit tumour growth and cell contact through reduction of several signalling pathways including FAK-Src[339]. Merlin negative MPM cell lines depend

on cell-ECM induced FAK signalling and are particularly sensitive to FAK inhibitor *in vivo* and *in vitro*[340]. Taking all these together, our data suggest the role of FAK in MPM require further exploration and in fact FAK inhibitors have already been tested in patients with MPM showing positive results[341].

Our analysis revealed 78 out of 352 downregulated genes are associated with immune system regulation suggesting contribution of dysfunctional immune system to the transformation and progression of this disease. The interaction of cancer and the immune system is complex and involves the interactions between tumour immunogenicity, cooperation of all known effectors in both innate and adaptive immunity that regulates host's immune response and capabilities of cancer cells to evade the immune system[342].

MPM is considered weakly immunogenic but a case report of spontaneous tumour regression provided evidence for anti-tumour response mounted by modulation of the immune system[343]. Subsequently, studies showed the presence of tumour-infiltrating CD8+ T cells in MPM tumours is associated with better prognosis in patients undergoing surgery and higher CD8+ T cells is also associated with reduced metastases in patients with MPM receiving chemotherapy[344,345]. Our data demonstrated downregulation of several immune-related genes that might result in impaired anti-tumour immune response. These genes are involved in recruitment, activation and expansion of immune cells including CD8+ T cells and genes involved in antigen processing and presenting. Modulating the immune system with recombinant viral proteins, vaccines or antibody and dendritic-cell based applications is an appealing approach in targeting tumours including MPM. This strategy involves inducing antigen-specific immune response to activate cytotoxicity and eventually generate immunological memory to ensure long-term remission. In fact, preclinical data and clinical studies in MPM have shown promising cytotoxic result with antibodies against immune check

point receptors such as cytotoxic T lymphocyte antigen-4 and programmed cell death protein-1[346–348]. In addition, other immune-related genes (*SELE, CD40* and *CIITA*) that could potentially be modulated with immunotherapy have also been identified from our study.

WGCNA allows the identification of groups of genes (modules) that are co-expressed independent of phenotypes and share similar biological process. This methodology has successfully revealed molecular targets including *ASPM* gene in glioblastoma and networks associated with survival in breast cancer[204,349]. We used WGCNA to assess the data set containing 3092 differentially expressed genes with an adjusted p-value of $\leq 0.05$. This identified 14 modules of which the blue module (436 genes) and the turquoise module (605 genes) are significantly associated with histological subtypes and survival time respectively. We then chose the hub genes (genes with high connectivity in the respective module as measured by MM and high significance for the respective clinical trait as measured by GS) with an arbitrary cut off values of MM and GS to stratify histological subtypes and prognosis.

We identified 31 hub genes in the blue module of which 26 have a FC in expression level of $\geq 2$. Seven (*PLLP, PRR15, LRRN4, BNC1, UPK3B, MMP24, C19orf33*) out of these 26 genes are in the top 20 differentially expressed genes with the highest FC in expression level. These hub genes are able to distinguish 4 out of the 5 biphasic tumours from the epithelioid subtypes. One of the biphasic tumour is grouped with 8 epithelioid subtypes in CL2 and the remaining 12 epithelioid subtypes are grouped in CL3. *CARNS1* has the highest connectivity in the module and is associated with tumour suppressor Mapsin. Its differential expression across the three clusters suggests a tumour suppressive function of Mapsin in the pathogenesis of the different MPM subtypes. Interestingly, a recent study revealed the role of Mapsin in modulating the immune system towards tumour elimination by depleting cancer cells of the stemness and regulating the HDAC1-dependent cytokine expression profile to reduce immune

suppression[1]. Thus, Mapsin- based therapies may have an important therapeutic implication in MPM.

*PRR15* has the highest GS value associated with histological subtypes and its up- and down-regulation are associated with TGF-ß and WNT signalling respectively. Based on the differential expression of *PRR15* in the 3 molecular subtypes, we hypothesised these two pathways may be preferentially activated across the different subtypes which could explain the more aggressive and invasive phenotype of biphasic tumours in CL1 compared to epithelioid tumours in CL3. In addition, the expression of *ADAM19*, one of the hub genes that is a downstream effector of TGF-ß, is higher in CL1. This further supports our assumption that TGF-ß might be the preferential pathway in CL1. We interrogated the other genes in the blue module and identified an additional 9 genes (*TGFB2, WNT9A, WNT7B, WNT2B, CDH1, INADL, PARD6B, MPP5* and *PRKCI)* that are associated with these two pathways.

TGF-ß is a recognised stimulator of EMT process that was first observed in cell culture and subsequently several *in vitro* studies demonstrated similar findings[350–352]. TGF-ß-induced EMT occurs not only via Smad-dependent pathway but also via activation of MAPK pathway and small GTPases of the Rho family to regulate transcription of regulators of EMT and cell proliferation[353–355]. The involvement of EMT process is further supported by the overexpression of other hub genes: *ANXA6, ADAMTS6* and *RASGRP3*; that are involved in ECM degradation. The process of physiological EMT involves a defined sequence of events for the conversion of epithelial tissue into a mesenchymal phenotype but this coordination is lost and occurs in a haphazard manner in cancer. Cancer cells undergo EMT to promote migration and invasion involving the transcriptional downregulation of genes that maintain epithelial apical-basolateral polarity, cytoskeletal organisation, cell-cell contact (tight junctions, adherens junctions and desmosomes); and upregulation of genes associated with

ECM-remodelling, mesenchymal cytoskeleton and cell migration. We examined the expression profiles of mesenchymal markers *SNAI1, SNAI2, TWIST, ZEB1* and *ZEB2*. These genes have been shown to be the main regulators of EMT that induce epigenetic silencing of *CDH1* by binding to its promoter region[356–359]. The expression of *SNAI1, SNAI2, TWIST and ZEB2* are consistently higher in CL1 and the differences in expression level are statistically different across the three clusters. We demonstrated EMT process might have an important role in governing the morphological differences across the subtypes and these observations are in keeping with a published study in MPM[360].

We identified 25 hub genes in the turquoise module that are significantly associated with survival time. Further interrogation into these genes revealed their significant association with cell-cycle process. Aberrant cell cycle regulation is a common oncogenic event in many tumour types including MPM. These hub genes are able to categorise the tumours into three prognostic groups. *PDGR1* has the highest connectivity with other genes in the turquoise module. This gene has not been reported in MPM and is implicated in defective DNA repair pathway. This is particularly relevant in MPM as 80% of MPM is attributed to asbestos that is capable of inducing DNA damage. *Lam et al* demonstrated the expression level of *E2F1*, one of the top hub genes associated with survival time, together with *SKP2* could be downregulated by ATO. Thus, further studies are warranted to investigate the clinical use of ATO in MPM.

Seven of the 25 prognostic hub genes are also associated with MSAC and 5 of these (*CDCA8, PSMD8, SGOL1, CDC20, CENPH*) have not been reported in MPM. Similar findings on deregulation of MSAC pathway were also reported by Crispi *et al* and Suraokar *et* al[134,222]. These further support the importance of MSAC genes in the pathogenesis of MPM.

Four prognostic hub genes (*BUB1, SGOL1, TPX2* and *CDCA8*) are associated with Aurora kinase signalling that could have therapeutic implications. It is worth noting that the prognostic role of *BUB1* in MPM is further supported by 2 other published studies and is included in the 11 prognostic classifier gene list by Glinski *et al*[142,222]. *In vitro* study showed promising activity of aurora kinase inhibitor in inhibiting MPM cell growth and trials have been set up testing several commercially available aurora kinase inhibitors in MPM[361].

There are few limitations identified from our study. Firstly, our sample size might not be the largest to date and this is mainly due to the low incidence of MPM compared to other solid tumours and the small tissue size obtained for diagnostic purpose results in inadequate surplus tissues for research. The latter can also affect the quality and yield of RNA obtained. In addition, majority of the frozen tumour samples used in our study were not stored in RNAlater that might affect the integrity of RNA. This explains the reason for the need to use higher RNA quantity for the tumour samples compared to controls in generating cDNA.

Gene expression microarray experiments can be affected by a number of non-biological variables that can have an impact on the results[362]. These variables are termed batch effects and include differences such as reagents lot, the time, place and technicians carrying out the experiments. Of the batch effects identified in our study, the number of array plates used accounted for 2.5% of the variance in the RMA treated data. Lastly, treatment data for the majority of the tumour cases were not available and therefore the survival time could be confounded by treatments received along the course of the disease.

In conclusion, our study identified simultaneous aberrant expression in genes involved in cell migration, invasion, cell cycle and the immune system that support the malignant phenotype of this disease. To our knowledge, WGCNA methodology has not been applied in MPM

transcriptome data. Through this approach, we identified hub genes that are able to stratify tumours into three distinct molecular subtypes and prognostic groups. Our analyses identified several pathways including FAK (and its downstream pathways including MAPK and PI3K), TGF-ß, Hedgehog, WNT, MSAC and Aurora kinase that might contribute to the pathogenesis of MPM and these should be evaluated further for potential therapeutic targets.

# Chapter 4 - Whole Exome Sequencing of Malignant Pleural Mesothelioma

## 4.1 Introduction

Approximately 85% of human diseases occur as a result of mutations in the protein coding regions of the genome. Therefore, selective sequencing of protein coding regions, the exome, allows identification of mutations relevant to the disease. Whole exome sequencing provides higher sequence coverage, manageable output data, lower costs and higher sensitivity to detect mutations with low allele frequencies compared with whole-genome sequencing. These benefits generally outweigh the limitations of exome sequencing, which rely on an initial hybridization step and therefore can lead to exome "dropout" and failure to capture anything not included in the original exome probe library.

In recent years, whole exome sequencing has successfully revealed the molecular landscape in a variety of cancer types[363]. This has provided key understanding in the biological mechanisms relevant to the disease with improvement in personalised medicine to inform treatment choices, early diagnosis and other potential therapeutic discovery.

Little is known about the full genetic landscape of malignant pleural mesothelioma (MPM) but previous studies have consistently identified several genetic alterations in MPM. These include frequent losses of chromosome arms 1p, 3p, 9p and 22q; gains in chromosome 1q, 5p, 7p, 8q, and 17q; and inactivation of *CDKN2A, NF2* and *BAP1*[106,364]. The use of next-generation sequencing in MPM is rare compared to other tumour types. Thus far, whole genome sequencing of a single MPM tumour and matched normal tissue has been reported

and uncovered chromosomal rearrangement events as the dominant type of molecular aberrations[107]. These included 15 rearrangements that disrupted 17 genes and one of these resulted in a large deletion in *DPP10* of which its expression was associated with significantly better survival compared to patients whose tumours lacked *DPP10* expression. Two other groups have carried out whole exome sequencing with MPM cell lines and identified molecular aberrations in genes associated with mammalian SWI/SNF chromatin remodelling complexes and histone modifiers[143,365]. The first comprehensive overview of the molecular landscape in MPM was revealed by Guo *et al* who performed whole exome sequencing together with copy number alteration analysis on 22 MPM frozen tissues and matched blood samples[144]. They confirmed frequent genetic alterations in previously described genes including *CDKN2A, NF2*, *BAP1* and a novel gene, *CUL1*. To explore further the molecular alterations underlying MPM, we performed whole exome sequencing on a discovery cohort consisted of seven matched pairs of MPM frozen tissues and whole blood; and a validation cohort of 29 MPM frozen tissues without matched normal counterparts.

## 4.2 Materials and Methods

### 4.2.1 Tissues acquisition and preparation

A total of eight frozen tumour tissues and matched blood samples (discovery cohort) were identified from EQUALITY study, an Imperial College London-sponsored, prospective study on thoracic cancers undergoing biopsy at St George's Hospital (REC reference: 10/H0808/53). A further 29 frozen tumour tissues without matched blood samples (validation cohort) were provided by National Institute for Health Research-Biomedical Research Units (NIHR-BRU) Advanced Lung Disease Biobank and Royal Brompton and Harefield (RBH) NHS Trust Diagnostic Tissue Bank. Tissues were collected during diagnostic procedure prior

to any anti-cancer treatment. In addition, 13 formalin fixed, paraffin-embedded (FFPE) tumour blocks from the validation cohort were identified and selected to undergo laser microdissection (LCM) (Chapter 2 section 2.2.2.4) or microtomy section (Chapter 2 section 2.2.2.1) to isolate adjacent non-tumour cells for matched normal DNA.

Tumour frozen tissues and FFPE were sectioned, stained with routine haematoxylin and eosin, and reviewed by two certified pathologists to verify tumour histology, abundance and to identify adjacent non-tumour areas in the FFPE sections (Chapter 2 section 2.2.2.2 and 2.2.2.3). Tumour tissues with a minimum arbitrary threshold of 30% viable-appearing malignant cells were selected for genomic deoxyribonucleic acid (DNA) isolation.

### 4.2.2 DNA isolation plus quantity and quality assessments

Total genomic DNA was isolated from frozen tumour tissues using the phenol-chloroform method as described in Chapter 2 section 2.2.5.1. Briefly, equal volume of phenol-chloroform was added in a stepwise manner to an aqueous solution of homogenised tissue. By mixing the two phases and separating them by centrifugation yielded the lower organic phase and the upper DNA-containing aqueous phase. DNA was then precipitated with 100% ethanol and the pellet was isolated by centrifugation.

DNA isolation from whole blood samples was carried out with Wizard ® Genomic DNA Purification Kit (Promega, London, UK) following the manufacturer's instructions (Chapter 2 section 2.2.5.2). Briefly, red blood cells were lysed followed by lysis of white blood cells and their nuclei. The cellular proteins were removed by salt-precipitation method that resulted in a lower protein-containing phase and an upper DNA-containing phase. DNA was precipitated with isopropanol and pellet was obtained by centrifugation. DNA from non-tumour FFPE

sections was isolated with BiOstic® FFPE Tissue DNA Isolation Kit (MO Bio Laboratories, California, USA) as described in Chapter 2 section 2.2.5.3.

DNA yield and purity were assessed using the Thermo Scientific NanoDropTM 1000 Spectrophotometer (NanoDrop Technologies) and Quant-iT™ PicoGreen® dsDNA Assay Kit (Life Technologies, California, USA).

### 4.2.3 Whole exome sequencing

Genomic DNA from tumour and blood samples were fragmented and hybridised as per SureSelect$^{XT}$ Target Enrichment System for Illumina Paired-End Multiplex Sequencing protocol (Chapter 2 section 2.2.6). The captured libraries were sequenced on Illumina HiSeq2000 according to the standard protocol.

### 4.2.4 Data processing and quality control

Read alignment and data quality control were processed with GATK software from the Broad Institute. Variant calling was carried out with GATK Unified Genotyper variant discovery tool[196]. The variants were annotated with ANNOVAR to obtain gene-based (e.g. functional consequences on genes), region-based (e.g. conserved regions) and filter-based annotations (e.g. 1000 Genomes Project, dbSNP) for each variant.

### 4.2.5 Candidate somatic variants

After removing germline variants, the annotated file was subjected to a series of filtering steps to identify candidate somatic variants. Single nucleotide variants (SNV) and

insertions/deletions (indels) with a quality score of <50 or present in either dbSNP138, 1000 Genomes Project or NHLBI GO Exome Sequencing Project were filtered out. Potential driver mutations were identified from one of the following criteria:

- somatic non-synonymous SNV predicted to alter protein function by one of the three algorithms: Polyphen-2 (genetics.bwh.harvard.edu/pph2/), SIFT (sift.jcvi.org/) and MutationTaster (mutationtaster.org/)

- recurrent somatic mutations that cluster in a specific domain of the gene (mutation hotspots) or recurrent somatic mutations distributed along a gene

- genes implicated in other types of malignancy

### 4.2.6 Pathway analysis

Somatic mutations (nonsense, damaging or deleterious missense, splicing mutations and indels) were analysed for pathway enrichment with NetworkAnalyst tool whereby genes from our exome data were used as priory and mapped to a manually curated protein-protein interaction database to construct non-random networks[198].

### 4.2.7 Validation of candidate mutations

Specific primers were designed with Primer3web (version 4.0.0) or ExonPrimer (http://ihg.gsf.de/ihg/ExonPrimer.html) to amplify candidate SNV or indels using polymerase chain reaction (PCR) with HotStarTaq *Plus* Master Mix kit (Qiagen, Crawley, UK) followed by Sanger sequencing (Chapter 2 section 2.2.6.3).

## 4.3 Results

### 4.3.1 Cases demographic and clinical characteristics

Genomic DNA was isolated from a total of 37 frozen tumour tissues with and without matched blood samples (discovery cohort = 8 matched pairs of tumour tissues and blood, validation cohort = 29 frozen tissues) and whole exome was sequenced successfully for all but one (MESOEQ15) from discovery cohort. Table 4.1 summarises the cases and tumour characteristics. The majority of the cases were of male gender and 35% of the cases were above 70 years of age. About 70% of cases had a documented exposure to asbestos and 62% of cases had ever smoked. Stage of disease was not or poorly recorded and was unreliable in this dataset hence it was not included. Epithelioid MPM was the predominant subtype and no sarcomatoid MPM was identified from both cohorts. The mean tumour abundance was lower in the discovery cohort compared to the validation cohort and a total of 17 tumour samples (see Table 4.2 and 4.3) had less than the minimum 60% tumour abundance requirement according to the International Cancer Genome Consortium guidelines[366]. Treatment data were not available for majority of the cases as further oncological management was undertaken by the referring hospitals after completing the diagnostic procedures.

**Table 4.1. Baseline demographics and clinical characteristics of discovery and validation cohorts. CT=chemotherapy, RT=radiotherapy.**

| Characteristics | Discovery cohort (n=7) | Validation cohort (n=29) |
|---|---|---|
| **Age, years** | | |
| Median | 68 | 67 |
| Range | 60-80 | 52-82 |
| ≤ 70 | 5 (71%) | 18 (62%) |
| > 70 | 2 (29%) | 11 (38%) |
| **Sex** | | |
| Male | 5 (71%) | 23 (79%) |
| Female | 2 (29%) | 6 (21%) |
| **Smoking** | | |
| Ever smoked | 6 (86%) | 17 (59%) |
| Never smoked | 0 | 9 (31%) |
| Not known | 1 (14%) | 3 (10%) |
| **Asbestos exposure** | | |
| Yes | 4 (57%) | 22 (76%) |
| No | 2 (29%) | 6 (21%) |
| Not known | 1 (14%) | 1 (3%) |
| **Histological subtypes** | | |
| Epithelioid MPM | 6 (86%) | 21 (72%) |
| Biphasic MPM | 1 (14%) | 8 (28%) |
| Sarcomatoid MPM | 0 | 0 |
| **Tumour abundance (%)** | | |
| Mean | 50 | 65 |
| Range | 30-80 | 30-95 |
| **Treatment** | | |
| CT | | 4 (14%) |
| RT | | 2 (7%) |
| CT+RT | | 3 (10%) |
| None | | 4 (14%) |
| Not known | 7 (100%) | 16 (55%) |

### 4.3.2 DNA results

From the discovery cohort, the median DNA yield from tumour and matched blood was 67.1 micrograms (µg) (ranged from 12.7-273.1 µg) and 79.4 µg (ranged from 35.3-111.7 µg) respectively (Table 4.2).

**Table 4.2. Total DNA results of discovery cohort. Tumour samples denoted by MESOEQ##TF and matched blood samples denoted by MESOEQ##BL. DNA concentration (Cx) in ng/µl and 260/280 ratio quantified by Thermo Scientific NanoDropTM 1000 Spectrophotometer (NanoDrop Technologies). NA= not applicable.**

| Sample ID | Tumour % | Cx (ng/µl) | volume (µl) | Yield(µg) | 260/280 |
|---|---|---|---|---|---|
| MESOEQ13TF | 30 | 496.2 | 250 | 124.1 | 1.9 |
| MESOEQ21TF | 70 | 268.3 | 250 | 67.1 | 1.9 |
| MESOEQ22TF | 30 | 50.6 | 250 | 12.7 | 1.8 |
| MESOEQ30TF | 30 | 172.3 | 250 | 43.1 | 2.0 |
| MESOEQ36TF | 80 | 1092.4 | 250 | 273.1 | 2.0 |
| MESOEQ38TF | 50 | 631.7 | 250 | 157.9 | 1.9 |
| MESOEQ40TF | 70 | 174.7 | 250 | 43.7 | 2.0 |
| MESOEQ13BL | NA | 44.1 | 800 | 35.3 | 2.1 |
| MESOEQ21BL | NA | 52.2 | 800 | 41.8 | 1.9 |
| MESOEQ22BL | NA | 52.3 | 800 | 41.8 | 2.0 |
| MESOEQ30BL | NA | 129.9 | 800 | 104.0 | 1.9 |
| MESOEQ36BL | NA | 101.0 | 800 | 80.8 | 1.9 |
| MESOEQ38BL | NA | 99.2 | 800 | 79.4 | 1.9 |
| MESOEQ40BL | NA | 139.6 | 800 | 111.7 | 1.9 |

The median DNA yield was 100 µg (ranged from 14.7-562.5 µg) in the validation cohort (Table 4.3).

**Table 4.3. Total DNA results of validation cohort. Tumour samples denoted by MESOD##. DNA concentration (Cx) in ng/µl and 260/280 ratio quantified by Thermo Scientific NanoDropTM 1000 Spectrophotometer (NanoDrop Technologies).**

| Sample ID | Tumour % | Cx (ng/µl) | Yield(µg) | 260/280 |
|---|---|---|---|---|
| MESOD1 | 30 | 58.7 | 14.7 | 1.6 |
| MESOD2 | 30 | 61.6 | 15.4 | 1.6 |
| MESOD3 | 55 | 77.9 | 19.5 | 1.6 |
| MESOD5 | 80 | 108.6 | 27.1 | 1.7 |
| MESOD6 | 30 | 133.1 | 33.3 | 1.9 |
| MESOD8 | 40 | 166.8 | 41.7 | 1.8 |
| MESOD10 | 90 | 215.6 | 53.9 | 1.9 |
| MESOD12 | 95 | 238.9 | 59.7 | 1.9 |
| MESOD13 | 50 | 270.9 | 67.7 | 1.9 |
| MESOD14 | 80 | 281.2 | 70.3 | 1.7 |
| MESOD15 | 40 | 336.3 | 84.1 | 1.9 |
| MESOD16 | 95 | 348.4 | 87.1 | 1.9 |
| MESOD17 | 70 | 388.4 | 97.1 | 1.9 |
| MESOD18 | 90 | 389.4 | 97.3 | 1.9 |
| MESOD19 | 70 | 402.9 | 100.7 | 2.0 |
| MESOD21 | 30 | 419.2 | 104.8 | 1.9 |
| MESOD22 | 90 | 443.8 | 111.0 | 2.0 |
| MESOD24 | 50 | 483.9 | 121.0 | 1.9 |
| MESOD25 | 95 | 533.5 | 133.4 | 1.9 |
| MESOD26 | 70 | 596.9 | 149.2 | 1.9 |
| MESOD27 | 70 | 602.0 | 150.5 | 2.0 |
| MESOD28 | 35 | 624.2 | 156.1 | 1.9 |
| MESOD29 | 80 | 927.9 | 232.0 | 1.9 |
| MESOD30 | 40 | 1134.1 | 283.5 | 2.0 |
| MESOD31 | 90 | 1196.6 | 299.2 | 2.0 |
| MESOD32 | 90 | 1422.7 | 355.7 | 1.9 |
| MESOD33 | 40 | 1794.1 | 448.5 | 2.0 |
| MESOD34 | 80 | 2250.0 | 562.5 | 1.9 |
| MESOD35 | 90 | 479.5 | 119.9 | 2.0 |

In an attempt to obtain matched normal for the validation set, LCM and microtomy section of adjacent non-malignant areas were carried out on eight and five FFPE tumour blocks respectively. The DNA yield was virtually zero for the LCM samples while the DNA yield from two of the samples sectioned with microtome was critically low (Table 4.4). The DNA from the remaining three sectioned samples was not taken forward for whole exome sequencing.

**Table 4.4. Total DNA results of matched normal from validation cohort. DNA concentration (Cx) in ng/µl quantified by Quant-iT™ PicoGreen® dsDNA Assay Kit (Life Technologies, California, USA).**

| Sample ID | Cx (ng/µl) | volume (µl) | Yield (µg) |
|---|---|---|---|
| MESOD35N | -0.03 | 16 | nil |
| MESOD30N | -0.03 | 16 | nil |
| MESOD19N | 0.02 | 16 | 0.3 |
| MESOD14N | 0.38 | 16 | 6.1 |
| MESOD2N | 0.01 | 16 | 0.2 |
| MESOD32N | 0.30 | 16 | 4.9 |
| MESOD6N | -0.05 | 16 | nil |
| MESOD29N | -0.06 | 16 | nil |
| MESOD24N | 2.07 | 40 | 82.8 |
| MESOD28N | 5.17 | 40 | 206.9 |
| MESOD33N | 5.10 | 40 | 204.1 |
| MESOD3N | 2.37 | 40 | 94.7 |
| MESOD6N | 4.25 | 40 | 170.1 |

### 4.3.3 Overview of somatic mutations in discovery cohort

The exomes were successfully sequenced for all 7 matched pairs of tumour and blood DNA except MESOEQ15. An average of 3.5Gb sequencing data were generated for each sample with a mean coverage of 164X for tumour and 106X for normal (blood) (Table 4.5 and Appendix 4.1). On average, 98.5% of the bases sequenced achieved 10X coverage.

**Table 4.5. Total number of bases sequenced and mean coverage results.**

| Case ID | Tumour bases sequenced | Normal bases sequenced | Mean tumour exome coverage | Mean normal exome coverage |
|---|---|---|---|---|
| MESOEQ13 | 5.10E+07 | 5.10E+07 | 214.9 | 78.3 |
| MESOEQ21 | 5.10E+07 | 5.10E+07 | 188.8 | 83.4 |
| MESOEQ22 | 5.10E+07 | 5.10E+07 | 139.6 | 101.0 |
| MESOEQ30 | 5.09E+07 | 5.09E+07 | 105.1 | 144.9 |
| MESOEQ36 | 5.10E+07 | 5.10E+07 | 114.2 | 143.0 |
| MESOEQ38 | 5.10E+07 | 5.10E+07 | 162.2 | 82.2 |
| MESOEQ40 | 5.09E+07 | 5.09E+07 | 224.4 | 106.6 |

After filtering, we identified a total of 1,226 somatic mutations in 1,074 genes of potential biological significance distributed predominantly in the protein coding (97.7%) and to a lesser extent in the splice site (2.3%) regions. These included 334 synonymous mutations, 765 missense mutations, 84 nonsense mutations including 83 stop-gain and 1 stop-loss mutation, 28 splice site mutations and 15 insertions/deletions including 12 indels causing frameshift mutations and 3 indels that did not alter reading frame. A median of 78 somatic mutations in exonic/splice site regions per tumour sample was observed with MESOEQ38 harbouring small numbers of somatic mutations and MESOEQ22 having a higher rate of somatic

mutations compared to the rest (Table 4.6). The observed ratio of non-synonymous to synonymous change was 2.5 with 88.3% of the SNV occurring at G:C base pairs. The observed somatic mutation spectrum in the seven tumour samples showed G:C>A:T as the predominant transition and transversion was dominated by G:C > T:A as noted in other cancers such as non-small cell and small cell lung cancers[367,368].

**Table 4.6. Distribution of somatic mutations across each sample.**

| Mutation types | MESOEQ 13 | MESOEQ 21 | MESOEQ 22 | MESOEQ 30 | MESOEQ 36 | MESOEQ 38 | MESOEQ 40 |
|---|---|---|---|---|---|---|---|
| Silent | 26 | 19 | 210 | 59 | 19 | 9 | 51 |
| nonsense | 3 | 0 | 69 | 11 | 1 | 0 | 3 |
| missense | 31 | 55 | 509 | 123 | 18 | 16 | 91 |
| splicing | 2 | 3 | 16 | 4 | 1 | 1 | 4 |
| indels | 0 | 1 | 1 | 9 | 1 | 0 | 3 |
| Total | 62 | 78 | 805 | 206 | 40 | 26 | 152 |

After removing non-silent mutations, a total of 892 somatic mutations across 821 genes were identified. A median of 69 non-synonymous mutations per tumour sample was observed. These are much lower compared to solid tumours with known mutagens such as lung cancer and melanoma where 200 missense mutations per tumour have been observed[369]. We used three functional prediction algorithms to evaluate missense mutations for the identification of potential driver mutations. Of the 765 missense mutations, functional impact could not be predicted for 22 variants using all three algorithms possibly due to non-availability of suitable transcripts. The remaining 743 missense variants, 208 (28.0%) missense mutations were predicted by all three algorithms, 205 (27.5%) were predicted by two out of the three algorithms and 185 (24.9%) were predicted by one out of the three algorithms to be at least

probably damaging or deleterious (Appendix 4.2).

### 4.3.4 Overview of mutations in validation cohort

In the validation cohort of 29 tumour samples, each sample was sequenced at a mean coverage of 149X and an average of 98.9% bases were covered at 10X. After filtering, a total of 4,684 mutations were identified comprising of 1,253 synonymous mutations, 2,764 missense mutations, 110 nonsense mutations and 553 indels or substitution of which 305 indels and substitution altered the reading frame. By excluding non-silent mutations, there were a total of 3,431 mutations distributed across 2,764 genes.

### 4.3.5 Candidate genes

Candidate genes were selected based on any one of these criteria: (a) nonsense, splicing, indels and missense mutations with protein alteration predicted to be probably damaging or deleterious by one of the three functional algorithms (b) overlapping variants present in one or more tumour sample in discovery cohort and validation cohort (c) genes reported to be associated with cancers. We selected several variants and confirmed the presence of the mutations with Sanger sequencing (Appendix 4.3).

We found the mucin family genes, in particularly *MUC4* and *MUC12,* frequently mutated in more than 70% of the tumours in both cohorts. These results should be interpreted with caution since the mucin genes encode for extremely large proteins and the statistical tests in variant calling have not taken into account larger target size. Thus, these variants are likely to be false positives.

Other mucin genes that were less frequently mutated included *MUC5B* and *MUC16* in 14% of

all tumours. The somatic status was determined in two out of nine *MUC5B* variants and four out of six *MUC16* variants The role of *MUC5B* in cancer has not been studied extensively but results from breast cancer cell lines demonstrated its capability in promoting tumour proliferation and invasion[370]. Interestingly, *MUC16* is known to bind to mesothelin, frequently overexpressed in epithelioid MPM and promotes MPM cell invasion by inducing *MMP-9*[371]. However, it is not known how mutations in *MUC16* might alter *MSLN-MUC16* molecular interaction contributing to carcinogenesis.

*SAFB2*, scaffold attachment factor B2, and its paralog *SAFB1* act as transcriptional repressor regulating genes involved in apoptosis and the immune system[372]. Four mutations were noted in *SAFB2* and of these a somatic non-synonymous mutation resulting in T950P protein change occurred in 61% of all tumours. It is uncommon for a hotspot mutation to occur at such high frequency and further interrogation revealed the variant is present in Exome Aggregation Consortium (ExAC) data set with an allele frequency of 0.007. This is unlikely to be a disease-causing variant as it would imply the incidence of MPM to be 1 in 142. Two other recurrent mutated genes in the discovery cohort include *SRCAP* and *SHANK3* but these are considered not significant in MPM as the variants are also present in ExAC database.

Two other novel genes not described previously as mutated in MPM are *AIDA* and *SPDYE6.* Somatic mutations in *AIDA,* an Axin-interacting protein, are present in two tumours and also mutated in an additional tumour in the validation cohort accounting for 8.3% of all tumours. *SPDYE6,* one of the speedy/RINGO family members E, mutations were also observed in 8.3% of all tumours. A somatic missense mutation resulting in protein change p.R337H occurred in two tumours and an additional mutation (p.R305C) was present in one tumour in the validation set. The speedy/RINGO family members E have been shown to activate cyclin dependent kinases *CDK1*, *CDK2* and *CDK5* but their interactions resulted in slow G2-M

transition of the cell cycle[373].

Next, we compared non-silent mutations present in discovery cohort to genes from the Catalogue of Somatic Mutations in Cancer (COSMIC) database and genes implicated in cancer as reported by Vogelstein et al and Leiserson et al[369,374].These revealed somatic mutations in 40 genes implicated in human cancers across the tumours in discovery cohort except MESOEQ21 and MESOEQ38 (Appendix 4.4). The majority of the mutations occurred in not more than one tumour except mutations in *NF2* and *XPC* present in two out of seven tumours. Twelve of these genes were also mutated in the validation cohort including *BAP1* and *NF2* (Appendix 4.5).

*BAP1* mutations occurred in 25% of all tumour samples combined (one from discovery cohort and eight from validation cohort). Eleven variants of different mutation types (Table 4.7) were distributed across *BAP1* with the majority occurring in the ubiquitin carboxy-terminal hydrolase and nuclear localisation signal domains that might result in loss of *BAP1* ubiquitinase activity (Figure 4.1). Tumour MESOEQ22 and MESOD25 each harboured two *BAP1* mutations. We were not able to determine the somatic status of these mutations except for a stop codon (p.E373X) in MESOEQ22 that also harboured a germline *BAP1* mutation (p.R227C). Three variants were confirmed with Sanger sequencing including the germline mutation in MESOEQ22. Interestingly, C/G to T/A transition in exon 16 that results in a stop codon (p.Q684X) in MESOD18 has been reported as a germline mutation in a family with individuals diagnosed with MPM and skin cancers[84]. Germline *BAP1* mutation has been identified to predispose individuals to a hereditary cancer syndrome including MPM, uveal melanoma, cutaneous melanoma, and renal cell carcinoma[85]. There was a strong family history of cancers in MESOD18 with individuals diagnosed with MPM, lung and oesophageal cancer while there was only one family individual with head and neck cancer for

MESOEQ22. The phenotype of *BAP1* cancer syndrome is still not fully characterised and it is not known if the family history of cancers in these two cases represent part of the syndrome.

**Table 4.7. *BAP1* mutations in both discovery and validation cohort. E= epithelioid MPM, B= biphasic MPM.**

| Samples ID | Mutation types | Protein change | Somatic / Germline | Validation: Sanger sequencing | Subtype |
|---|---|---|---|---|---|
| MESOEQ22 | nonsynonymous | p.R227C | germline | yes | E |
| MESOEQ22 | stopgain | p.E373X | somatic | no | E |
| MESOD27 | frameshift deletion | p.56_62del, | unknown | not done | E |
| MESOD22 | frameshift deletion | p.R114fs, | unknown | not done | E |
| MESOD17 | frameshift deletion | p.558_560del, | unknown | not done | E |
| MESOD14 | frameshift deletion | p.162_162del, | unknown | not done | B |
| MESOD10 | frameshift deletion | p.146_147del, | unknown | not done | E |
| MESOD25 | frameshift insertion | p.K658fs, | unknown | not done | B |
| MESOD25 | nonframeshift deletion | p.659_659del, | unknown | not done | B |
| MESOD13 | nonsynonymous | p.H141P, | unknown | yes | E |
| MESOD18 | stopgain | p.Q684X, | reported germline | yes | E |

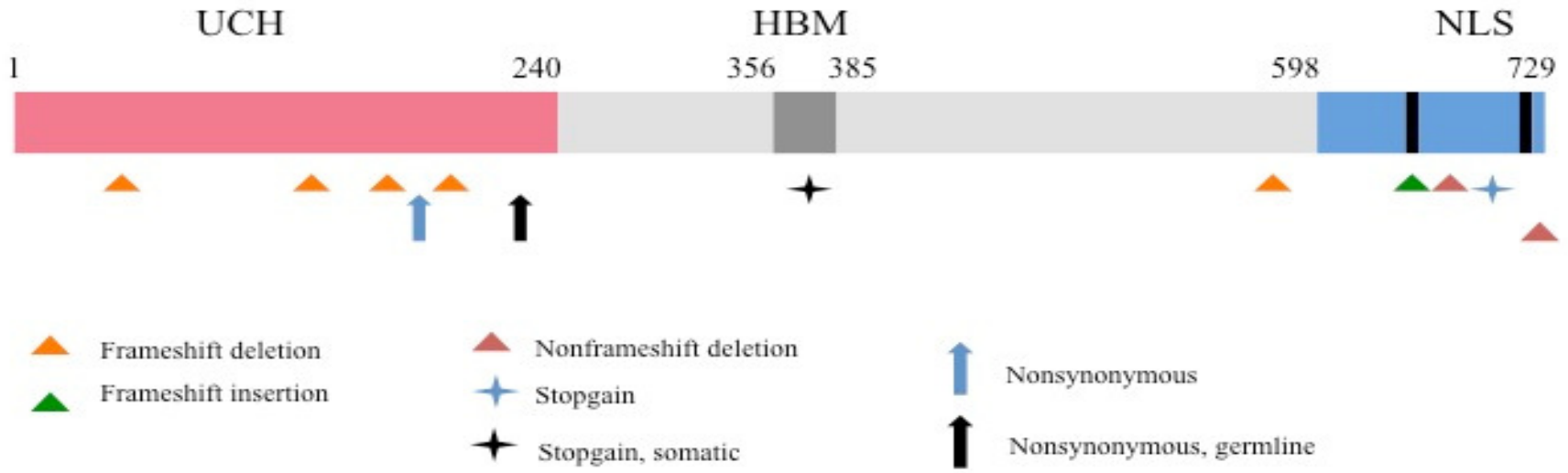


**Figure 4.1. Types and relative positions of *BAP1* mutations identified. UCH= ubiquitin carboxy-terminal hydrolase, HBM= HCF1-binding domain, NLS= nuclear localization signal**

The baseline clinical characteristics of patients with and without *BAP1* mutations are displayed in Table 4.8. Data on smoking history and asbestos exposure were not available in four and two patients respectively. The relationship between *BAP1* mutation status and clinical characteristics was assessed using Fisher's exact test. We did not identify any significant association between *BAP1* mutation with age (p=0.438), gender (p=1.0), histological subtype (p=1.0), asbestos exposure (p=1.0), smoking status (p=0.17) and personal and family history of malignancy (p=1.0).

**Table 4.8. Baseline clinical characteristics of patients with and without *BAP1* mutations**

| **Clinical characteristics** | ***BAP1* mutant (N=9)** | ***BAP1* wild-type (N=27)** |
|---|---|---|
| Median age | 66 | 68 |
| Age≤70 | 7 (78%) | 16 (59%) |
| Age≥71 | 2 (22%) | 11 (41%) |
| Male | 7 (78%) | 21 (78%) |
| Female | 2 (22%) | 6 (22%) |
| Epithelioid | 7 (78%) | 20 (74%) |
| Biphasic | 2 (22%) | 7 (26%) |
| Asbestos exposure | 7 (78%) | 19 (70%) |
| Ever smoked | 4 (44%) | 19 (70%) |
| Personal history of cancer | 0 (0%) | 2 (7%) |
| Family history of MPM | 1 (11%) | 1 (4%) |
| Family history of cancer | 3 (33%) | 9 (33%) |

Survival wasdefined as time from date of diagnosis to time of death and these data were available for all patients except three with no follow-up data. Overall survival (OS) was

estimated using the Kaplan-Meier method and one patient was censored at the time of the last available follow-up. There was no significant difference in OS associated with *BAP1* mutation status (HR= 0.806, 95%CI 0.35-1.85, p=0.325) (Figure 4.2). The median survival for patients with *BAP1* mutant tumours was 13.8 months (95%C1 5.8-NA) and for those with *BAP1* wild-type tumours was 12.3 months (95%CI 9.3-26.8).

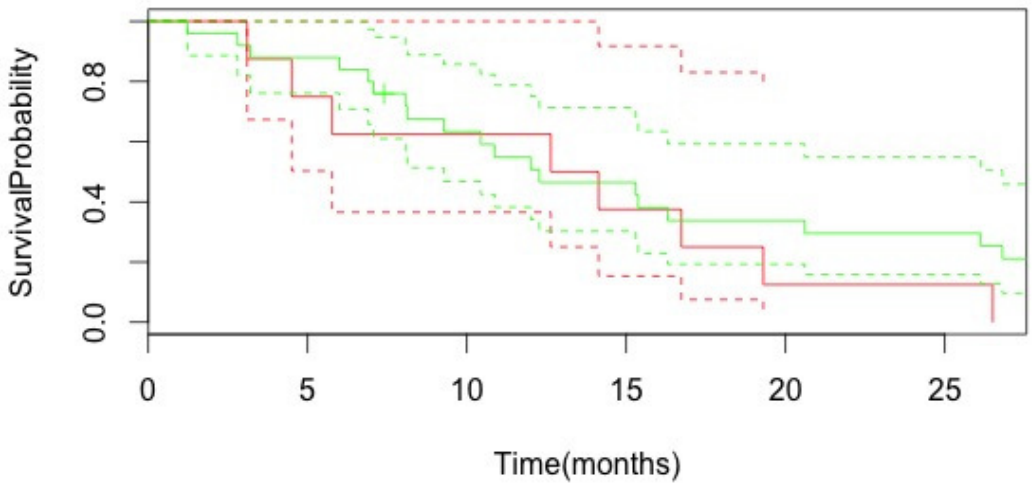


**Figure 4.2. Kaplan-Meier survival curves for patients with *BAP1* mutations (red line) and *BAP1* wild-type (green line). The hazard ratio = 0.806 (95% CI 0.35-1.85, p=0.325).**

We also observed frequent *NF2* mutations with six variants identified (Table 4.9). *NF2* mutations occurred in 16.7% (6 out of 36 tumours) of all tumour samples. The somatic status was confirmed for two variants, a non-frameshift deletion and a splice site mutation. Two mutations that resulted in protein change p.R221X and p.76_76del were validated with Sanger sequencing. One of the mutations of unknown somatic status that resulted in a stop codon (p.R221X) is a pathogenic single nucleotide polymorphism (SNP) (rs74315496) previously reported in a patient with neurofibromatosis 2[375]. This potentially suggests a common pathway between MPM and neurofibromatosis 2 that may be of interest.

**Table 4.9. *NF2* mutations in both discovery and validation cohort. E= epithelioid MPM, B= biphasic MPM.**

| Samples ID | Mutation types | Protein change | Somatic / Germline | Validation: Sanger sequencing | Subtype |
|---|---|---|---|---|---|
| MESOEQ40 | nonframeshift deletion | p.76_76del, | somatic | yes | E |
| MESOEQ13 | splicing | | somatic | not done | B |
| MESOD16 | frameshift deletion | p.A354fs, | unknown | not done | E |
| MESOD12 | frameshift deletion | p.F35fs, | unknown | not done | B |
| MESOD30 | frameshift insertion | p.P129fs, | unknown | not done | E |
| MESOD14 | stopgain SNV | p.R221X, | unknown | yes | B |

*XPC* mutations occurred in two out of the seven tumours in the discovery set but none in the validation set. *XPC* plays a key role in nucleotide excision repair (NER), in particularly global genome-NER by recognising and eliminating helix distorting lesions. Asbestos generates extracellular high molecular group binding protein 1 (HMGB1) that releases reactive oxygen and nitrogen species leading to DNA damage and strand breaks[58]. Defective *XPC* function results in carcinogenesis as demonstrated in homozygous mutant mice model and thus may play a role in asbestos-induced malignancy such as MPM[376]. In addition, polymorphisms in *XPC* confer sensitivity to platinum compound which is the main chemotherapy agent in MPM[377]. However, it has not been possible to test for this association due to insufficient treatment data in our study.

Other genes implicated in cancer that were mutated in both cohorts include *AR, FOXK1, GATA3, GNA11, NAB2, NOTCH1, RNF213, SETD2* and *USP6* (Appendix 4.5). *USP6* is implicated in aneurysmal bone cyst tumour that exerts its oncogenic effect through

juxtaposition of its coding sequence with several partner genes. Three non-synonymous mutations in *USP6* were identified and 26 tumours in the validation set harboured two of the variants. Two of the variants are present in ExAC database with allele frequency of around 25% and hence are highly unlikely to be pathognomonic of MPM.

*AR* regulates androgen-dependent signalling network and this pathway has not been reported to play a role in MPM. *AR* expression assessed by IHC was positive in 65% of peritoneal mesothelioma cases but absent in 100% of pleural MPM[378,379]. Mutations in *AR* have not been described in MPM and currently there is insufficient evidence to suggest its role in MPM carcinogenesis. The high frequency (61% of all tumours) of mutations observed in our study need to be interpreted with caution as these might represent false-positive findings.

The forkhead transcription factor, *FOXK1,* was mutated in 44% of our MPM cases. This gene resides in chromosome region 7p22.2 that was replicated in two genome-wide association studies identifying genetic predisposition to MPM[81,82]. Interestingly, *FOXK1* has been shown to interact with *BAP1* that is frequently mutated in MPM[380].

Our study observed the presence of *NOTCH1* mutations in 29% of tumours. One of the two variants that resulted in a c. 580A>C was present in nine tumours in the validation set and reported in COSMIC database. Activating *NOTCH1* mutations are implicated in acute lymphoblastic T-cell leukaemia and the highly conserved Notch signalling is deregulated in several cancers including MPM[381]. A study demonstrated *NOTCH1* activation was required for simian virus 40-induced mesothelial cell transformation while its inhibition led to cell growth arrest[67]. In addition, *NOTCH1* activation promoted MPM cell survival via downregulation of *PTEN* and Akt phosphorylation[382]. The role of *NOTCH1* in MPM carcinogenesis and as a potential actionable target requires further exploration.

*RNF213*, a specialised type of zinc finger, was mutated in 8.3% of our MPM cases. It has been identified as a translocation partner with *ALK* in anaplastic large cell lymphoma[383]. The gene function is not well understood but has probable E3 ubiquitin ligase activity and involvement in angiogenesis[384]. It is not known if *RNF213* may have any interactions with *BAP1*, a frequently altered gene in MPM with similar function.

*GATA3* is the master regulator of luminal epithelial cell differentiation and possibly has a tumour suppressive effect. *GATA3* is mutated in approximately 10% of breast cancer and in 5.5% of MPM from our data[385]. Interestingly, the study by Hattori et al also assessed the expression of *GATA3* by immunohistochemistry (IHC) and found positivity in only 2.4% of MPM but a different study observed positivity in 58% of epithelioid and sarcomatoid MPM[379].

*GNA11,* one of the guanine-nucleotide binding proteins involved in transmembrane signalling, is frequently mutated in uveal melanoma and tumours with coexisting *BAP1* loss have higher propensity for metastasis and activation of mitogen-activated protein kinase (MAPK) pathway[386,387]. Two tumours from our study harboured mutations in *GNA11* but both had no mutations in *BAP1*. This might suggest the interactions between *GNA11* and *BAP1* may not apply in MPM. However, whole exome sequencing will not identify other alterations in *BAP1* such as loss in copy number or whole gene deletion.

*NAB2* was mutated in 5.5% of MPM in our data and its implication in carcinogenesis is not known but a gene fusion involving the repressor domain of *NAB2* replaced with a carboxy-terminal transactivation domain from *STAT6*, is a molecular hallmark of solitary fibrous tumour[388].

*SETD2* is a histone H3 lysine 36 methyltransferase and both somatic and germline variants have been described in MPM[143,365]. Depletion of *SETD2* has been shown in renal cell cancer to result in genome instability through impaired DNA repair, nucleosome reassembly and suppression of replication stress[389].

### 4.3.6 Altered pathways

Integrative network analysis of somatic missense, nonsense and splice site mutations revealed pathway involving focal adhesion as significantly altered (adj. p value=6.61E-16). Fourteen genes from our dataset (*COL2A1, COL1A2, PIK3CB, PARVB, LAMA5 8, DOCK1 2, SHC2, KDR, BCAR1, TNXB, FLNB, VEGFB, ITGA9 1, ACTN1*) were implicated in this pathway in a total of 11 tumours (two in discovery and nine in validation cohort). Interestingly 13 of these genes were mutated exclusively in MESOEQ22 that harboured germline mutation in *BAP1*. The interactions between the focal adhesion genes and *BAP1* are displayed in Figure 4.3 created with NetworkAnalyst[198]. However, this exclusivity is not obvious in the validation cohort as only *ITGA9* and *LAMA5* were identified in *BAP1* mutated tumours.

Cell cycle pathway was also significantly altered (adj. p= 2.48E-15) involving five genes (*CDC14A, CDC25A, DBF4, PRKDC, SKP1*) mutated in only two tumours in the discovery cohort.

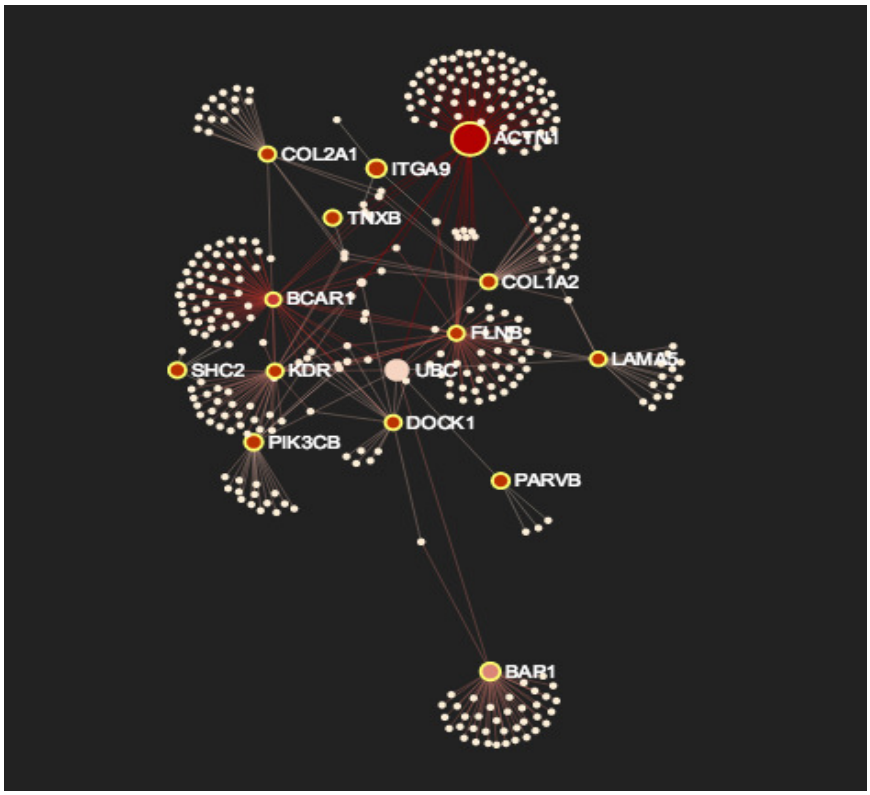


**Figure 4.3. Network visualization of genes involved in focal adhesion pathway and their interactions with *BAP1*. The network was created with NetworkAnalyst showing protein-protein interactions between the genes identified from WES data (highlighted with an outer yellow ring)..**

Eleven genes from our data (*ATF4, CACNA1B, CACNA1A, FLNB, HSPA8, MAP4K1, MAPK13, PLAG2G6, RPS6KA6, STK4, RASGRP4, SMYD3*) were implicated in MAPK pathway (adj. p=2.88E-14). They were present in four tumours from the discovery cohort while four tumours in the validation cohort also harboured mutations in *CACNA1A, CACNA1B, SMYD3* and *HSPA8*.

In addition, the WNT pathway was also significantly deregulated (adj. p=1.08E-05) involving three genes (*FZD2, TBL1XR1* and *CHD8)*. We also observed mutations in *LRP2* that might be related to WNT pathway. These alterations were observed in two tumours in the discovery

cohort while five tumours in the validation cohort had mutations in *FZD2* and *LRP2*.

Further enrichment analysis identified somatic mutations in 13 genes involved in chromatin modification. Except for *SETD2*, these genes have not been described as being mutated in MPM. Interestingly, these genes were only observed in tumours without *BAP1* mutation (Figure 4.4). Four genes (*JMJD1C, SETD2, ASH1L* and *SMYD3*) were also mutated in the validation set and exclusively in *BAP1* wild-type tumours except *ASH1L.*

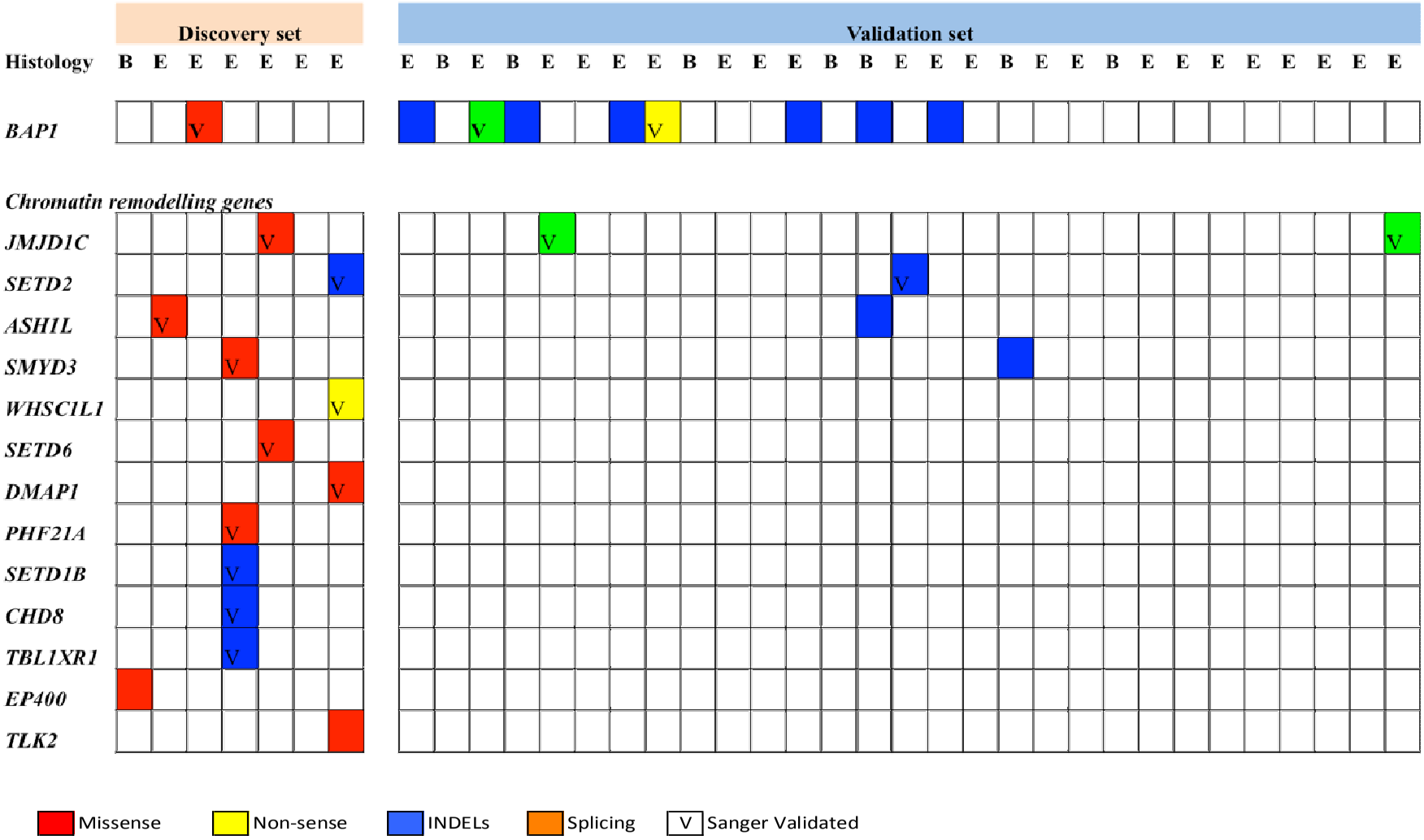


Figure 4.4. List of chromatin remodelling genes (rows) identified from our study and samples (column) harbouring the mutations.

## 4.4 Discussions

This whole exome sequencing study analysed the somatic mutations of seven MPM tumours and matched blood samples with GATK UnifiedGenotyper algorithm. This has similar sensitivity in identifying high allelic fraction SNVs compared to other popular algorithms such as Mutect[390].

Our results detected a total of 1,226 somatic mutations in 1,074 genes in at least one tumour sample from the discovery cohort. We also demonstrated MPM tumours harbour mutational burden (median nonsynonymous mutations per tumour was 69) comparable to other tumour types such as oesophageal squamous cancer, Non-Hodgkin lymphoma, colorectal cancer and head and neck cancer as depicted by Vogelstein et al (Figure 4.5)[369]. However, the mutational load was lower compared to tumours with known potent mutagens such as cigarette smoking and lung cancer; and ultraviolet light and melanoma. This is somewhat surprising since asbestos is a well-known mutagen and remains the main risk factor for developing MPM[37]. On the other hand, the mutational analyses in the other tumours reported by Vogelstein et al were done with whole genome sequencing data instead of whole exome. It would be interesting to compare the mutational burden between the exomes and genomes in MPM to see if this accounts for our unexpected finding.

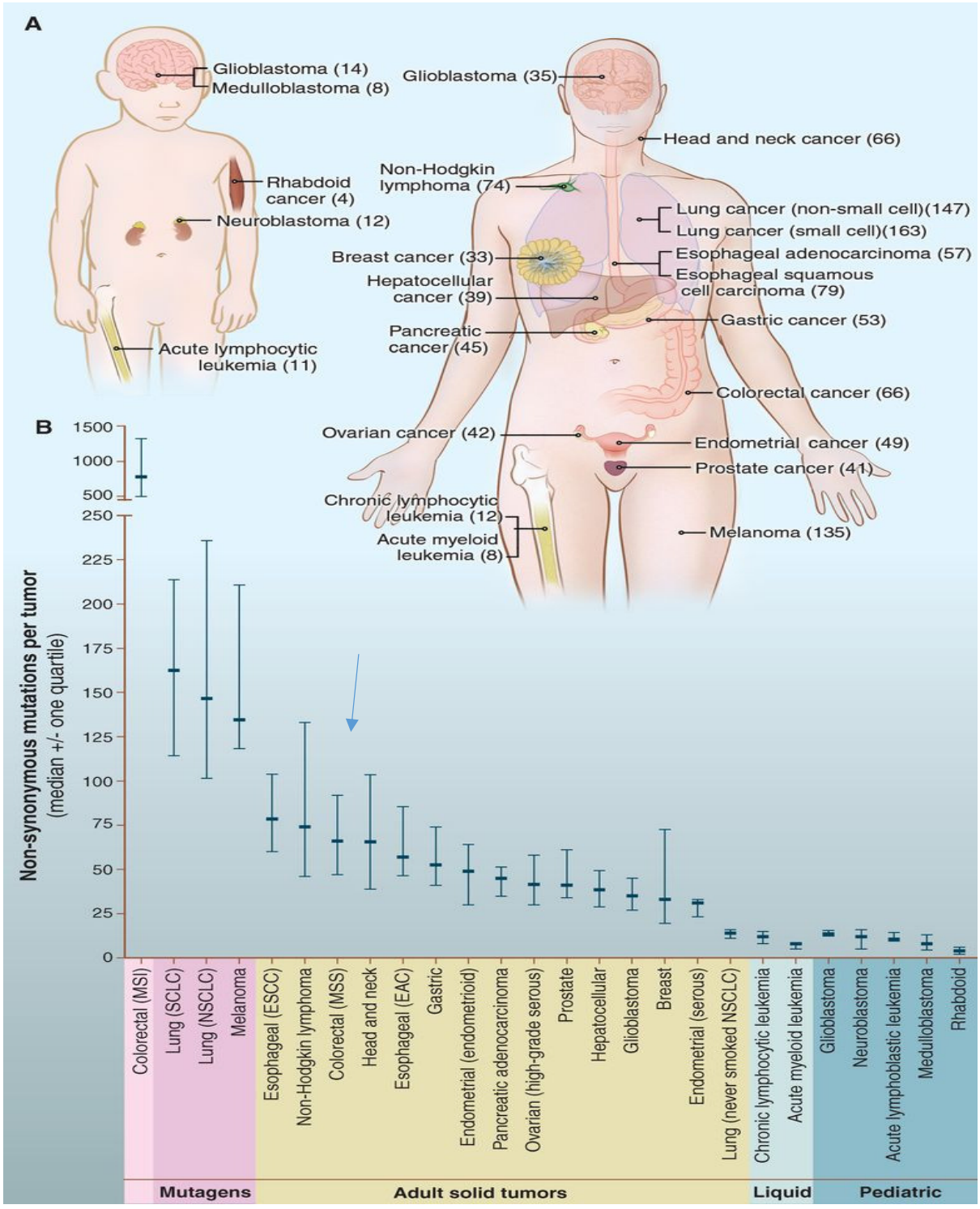


**Figure 4.5. Number of somatic mutations in representative human cancers detected by genome-wide sequencing studies (adapted from Vogelstein et al). The estimated position of MPMis depicted by the blue arrow.**

We found *BAP1* and *NF2* are frequently altered in MPM. In addition, we have also identified multiple mutated genes that have not been previously described in MPM that might provide new genetic insights into the carcinogenesis of MPM.

*BAP1* is a deubiquitinating enzyme and a tumour suppressor gene implicated in various biologic processes including chromatin dynamics, DNA damage response and regulation of cell cycle and growth. *BAP1* is increasingly recognised as an important gene that is frequently mutated and lost in cancers especially uveal melanoma, clear cell renal carcinoma and MPM. Recently, a pancancer sequencing study identified mutations in *BAP1* as one of the seven genes associated with detrimental survival outcome[391]. We found *BAP1* was mutated in 25% of tumours across both discovery and validation cohorts consistent with previous reports[106]. There were two germline and one somatic mutations while the somatic status for the remaining eight variants in the validation cohort was not known. Previous studies identified somatic *BAP1* mutation was associated with age, E-MPM subtype and smoking[106,149,156]. We did not detect any significant associations of *BAP1* mutation status with the predefined clinical characteristics including survival. This might be due to small sample size that limits the detection of any significant associations. Interestingly, we also identified mutations in *FOXK1*, a *BAP1* interacting partner. *FOXK1* regulates cell cycle progression but has been found to co-precipitate with *BAP1* and together with *HCF-1, ASXL1* and/or *ASXL2, OGT* and/or *FOXK2* form a *BAP1* complex that might have potential roles in regulating *BAP1* function[380].

We also identified six genetic alterations involving *NF2* that encodes for Merlin, the key regulator of Hippo signalling pathway. Around 40-50% of MPM are reported to exhibit homozygous disruption of the *NF2* by mutation and/or deletion resulting in lack of expression of functional Merlin protein[158]. Interestingly, we identified and confirmed a novel gene,

*INADL,* missense mutation in the discovery cohort and a nonframeshift insertion in the validation cohort. *INADL* forms a stable tight junction protein complex with Angiomotin and Pals1 that associate with Merlin in regulating mitogenic signalling[392]. Thus, deregulated form of *INADL* might imply failure of Merlin to bind properly to the complex and this requires further exploration. The loss of Merlin leads to dysfunctional Hippo pathway and subsequent increased in YAP/PDZ-binding motif activity capable of inducing oncogenic transformation due to the activation of transcription factors including transcription enhancers activation domain (TEAD) family members. This in turn up-regulates the expression of several growth promoting factors, including genes involved in survival and cell cycle such as c-myc and survivin respectively[393]. An *in vitro* study demonstrated that loss of Merlin increased the motility and invasiveness of MPM cells through increased phosphorylation of focal adhesion kinase (FAK)[160].

FAK is a non-receptor cytosolic protein tyrosine kinase with a central catalytic domain flanked by large N- and C-terminal domains that indirectly localizes at contact points of cells with extracellular matrix through interactions with integrin-associated proteins[394]. It has important roles in regulating cell survival, motility, metastasis, invasion and angiogenesis[395–398]. The importance of FAK signalling and as a potential therapeutic target in MPM was further supported by significant deregulation of focal adhesion pathway from our exome data. In addition, we also identified upregulated genes and associated pathways involving cell morphology, adhesions and migration from our gene expression study (Chapter 3) that are linked to FAK signalling.

A study using *in vitro* and xenograft models demonstrated MPM cells with low Merlin expression had increased sensitivity to FAK inhibitor. Targeting FAK has also been shown to inhibit self-renewal of cancer stem cells (CSC) that are linked to metastases and recurrence[340].

This led to the evaluation of FAK inhibitors in MPM in the clinical setting including GSK compound, GSK2256098, in patients with relapsed disease and the result was encouraging with improvement in median progression-free survival (PFS) of 4.5 months compared to historical control of 1.5 months[341]. There was also increased activity seen in a subset of patients with Merlin negative MPM achieving a median PFS of 6 months. However, the Verastem FAK inhibitor defactinib (VS6063) demonstrated no efficacy over placebo in a randomized trial in the first-line maintenance setting for MPM in both the intent-to-treat population and in patients with low Merlin expressing tumours[399]. It is currently unclear whether this was related to trial design, a drug related-issue or a true finding that FAK may not be a key driver despite the preclinical evidence.

MAPK and WNT are the other two pathways that were also significantly altered in our data that further support the findings by Guo et al[144]. MAPK activation is important for cell survival and apoptotic events. Significant protein phosphorylation of the MAPK cascade in MPM has been shown in previous studies[168]. Both *in vivo* and *in vitro* studies have also demonstrated activation of extracellular-signal-regulated kinases (ERK) and p38 in MPM cells exposed to asbestos[59,165]. Our study did not identify any known oncogenes such as *KRAS* and *BRAF* in this pathway but we found somatic mutations in 11 genes encoding the MAPK cascade. Mutations in *CACNA1A, CACNA1B, HSPA8* and *SMYD3* were also present in the validation cohort. Both *CACNA1A* and *CACNA1B* belong to voltage-gated calcium channel family that regulates the balance between extracellular and intracellular calcium levels that are crucial in regulating many signalling processes including cell cycle, proliferation and migration. Studies have shown calcium influx through the voltage-gated calcium channels can have direct and indirect effect on MAPK signalling[400]. A meta-analysis of microarray datasets revealed overexpression of *CACNA1A* in most cancers and correlated with poor survival in lung and ovarian cancers suggesting possible involvement in the onset and progression of

certain malignancies[401]. The role of *CACNA1B* in cancer is less well understood but the same study found it is significantly overexpressed in breast cancer. *HSPA8* belongs to heat shock protein 70 family and knockdown with RNA interference in tumour cells revealed anti-proliferative property[402]. *SMYD3*, a histone methyltransferase, plays a key role in regulating oncogenic Ras signalling through methylation of *MAP3K2* at lysine 260 and is a potential drug target[403].

The importance of MAPK signalling in MPM is further supported by the findings from our gene expression profiling study of 25 MPM tumours (Chapter 3). Several genes involved in MAPK pathway including *EGFR, MET, PAK4, RAC3, LAMA5, LAMC2, ITGA3* and *ITGB4* were significantly over-expressed in MPM. Figure 4.6 displays the interactions of the mutated and over-expressed genes with other components in the MAPK pathway.


**Figure 4.6. MAPK signalling pathway. The network was created with NetworkAnalyst showing protein-protein interactions between the genes identified from WES and gene expression data (highlighted with an outer yellow ring) with components encoding MAPK pathway**

The highly conserved WNT family of secreted proteins and downstream effectors are crucial for cell-cell communication events including cell fate determination, migration, polarity, neural patterning, and organogenesis during embryonic development and maintenance of stem cells. Thus perturbations in WNT signalling are important for cancer initiation and progression including cell survival, proliferation, invasion and metastases. These are frequently observed in cancers including MPM and studies have demonstrated accumulation of *CTNNB1* protein level, deregulated expression of several WNT ligands, frizzled receptors

(receptor for WNT proteins), *APC* and *AXIN2* in MPM[173,404]. Targeting components of WNT pathway such as siRNA knockdown of dishevelled proteins downstream of WNT have resulted in suppression of MPM cell growth[405]. We identified somatic mutations in *FZD2*, *TBL1XR1, CDH8, LRP2* and *AIDA* that are implicated in WNT pathway. *AIDA*, *FZD2* and *LRP2* mutations were also present in the validation cohort. *AIDA* has a potential tumour suppressor role identified to block Axin-mediated JNK activation by disrupting Axin homodimerization and subsequent inactivation of non-canonical WNT pathway[406]. *FZD2* has been shown to be overexpressed in late stage mesenchymal-type cancer cell lines and tumours[407]. Both *in vivo* and *in vitro* studies have identified a novel non-canonical WNT pathway driven by *FZD2* that drives the epithelial-mesenchymal transition process and is associated with metastasis and poor survival outcome. Targeting *FZD2* in xenograft model has shown promising inhibition of tumour growth and metastasis making it a potential therapeutic target in MPM. *LRP2* is a member of the lipoprotein-related protein (LRP) family but only *LRP5* and *LRP6* are LRP-family WNT-associated receptors. *LRP2* encodes megalin that is involved in intracellular transporter of sonic hedgehog (SHH)[408]. Deregulation in hedgehog signalling is implicated in various cancers and plays a key role in proliferation and differentiation. Studies have also demonstrated an interaction between SHH and WNT signalling in tumours to coordinate and regulate cell cycle progression[409]. This suggests *LRP2* may have an indirect role in WNT signalling.

Deregulated expression of genes involved in WNT signalling was one of the main findings from our gene expression study in MPM (Chapter 3). Our findings revealed significant over-expression of WNT ligands *WNT2B, WNT3, WNT9A* and transforming growth factor β member, *BMP4* in MPM compared to non-malignant pleural. A visual representation of the interactions between the mutated and over-expressed genes involved in WNT signalling is shown in Figure 4.7. Taking all together, our data supports previous findings that WNT

signalling is active in MPM and may offer new avenues for intervention and development of therapeutic targets.

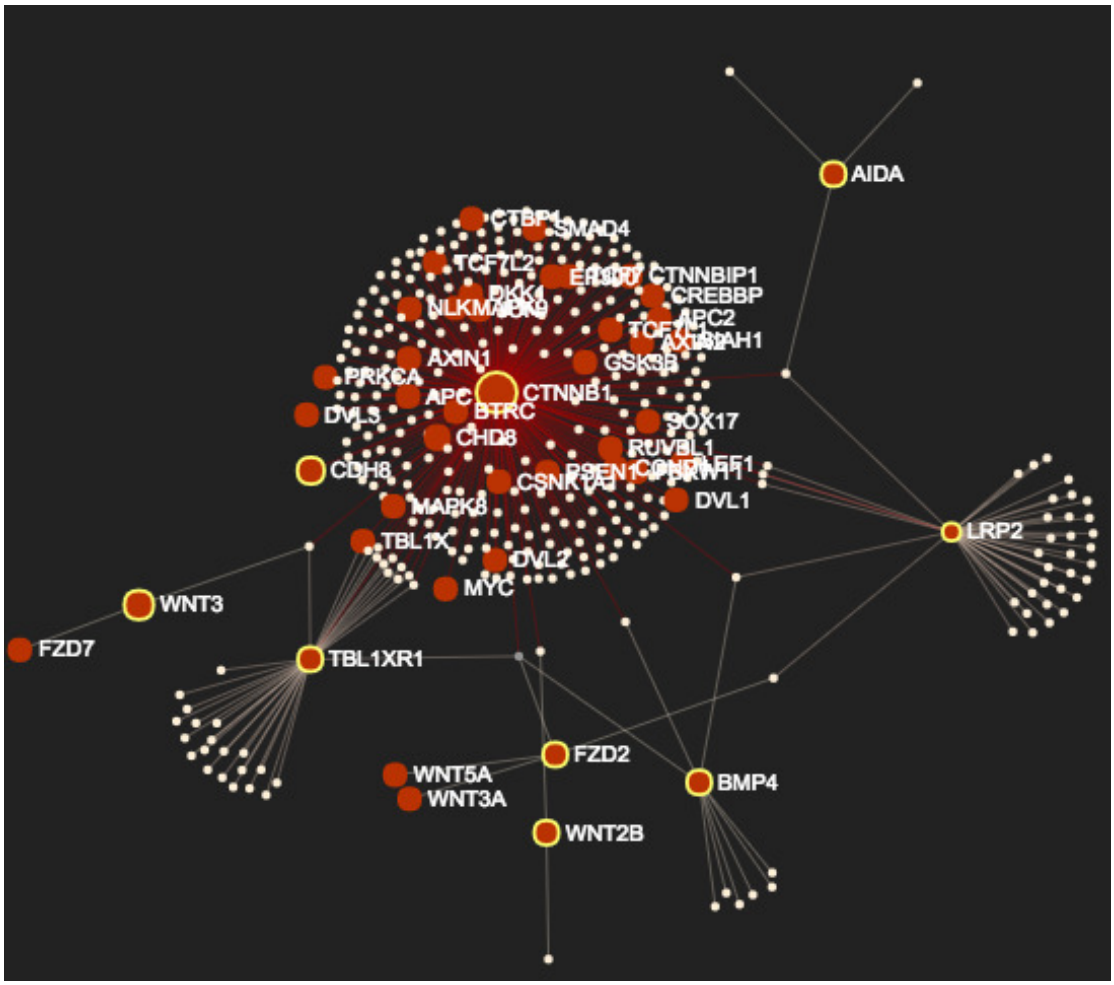


**Figure 4.7. WNT signalling pathway. The network was created with NetworkAnalyst showing protein-protein interactions between the genes identified from WES and gene expression data (highlighted with an outer yellow ring) with components encoding WNT pathway.**

Chromatin is important in regulating gene transcription and maintaining genome stability. Recent next generation sequencing studies in cancer have revealed molecular alterations in genes encoding chromatin regulatory factors and enzymes that result in disruption of chromatin remodelling.

Our study identified somatic mutations in 13 genes participating in chromatin regulation that could be associated with MPM carcinogenic events through alterations in gene transcriptions. Five of these genes (*SETD1B, SETD2, SETD6, SMYD3, WHSCIL1* and *ASH1L)* encode histone lysine methyltransferase enzymes and were mutated in a total of 7 out of 36 tumours. Histone lysine methyltransferases play a key role in regulating chromatin processes including transcription and DNA repair[410]. Lysine methylation occurs mainly within the tails of histone H3 and H4 resulting in transcriptional activity or repression depending on the target residues[411]. Its deregulation has emerged as a common factor in cancer pathogenesis.

*SETD2* is located close to 3p21 locus that also encodes *BAP1* and this region is frequently lost in several tumour types including MPM[99]. Thus a combination of loss of copy number in this region and *SETD2* mutation might potentially lead to its loss of function. Depletion of *SETD2* has been shown in renal cell cancer resulting in genome instability through impaired DNA repair, nucleosome reassembly and suppression of replication stress[389]. *SETD6* mediates monomethylation of the p65 subunit of Nuclear Factor Kappa-light-chain-enhancer of activated B cells (NF-κB) resulting in inhibition of NF-κB mediated inflammatory responses[412]. NF-κB is critical in the pathogenesis of MPM and the pathway is activated via asbestos-induced release of HMGB1 and TNF-α[57]. Thus dysfunctional *SETD6* might represent another mechanism for the activation of NF-κB pathway in MPM. The oncogenic role of *SMYD3* has been reported in several cancers and is implicated in MAPK signalling as described above[413]. *In vitro* study demonstrated the activity of *SMYD3* could be reduced with BCI-121, a small molecule inhibitor, resulting in cell growth inhibition[414]. This may be of therapeutic importance especially in a small subset of MPM tumours harbouring *SMYD3* mutations. Overexpression of *WHSC1L1* has been demonstrated in several cancer types and contributes to carcinogenesis by affecting the expression of cell cycle genes that promotes mitosis[415]. Its expression is low in normal tissues thus could be a potential therapeutic target

in various cancer types including MPM. The oncogenic role of *ASH1L* is not well understood but has been shown to be able to suppress *IL-6* production by facilitating the ubiquitin-enzyme A20 through histone modification at Tnfaip3 promoter[416]. *IL-6* is a key mediator in MPM cell proliferation and confers resistant to chemotherapy thus deregulated *ASH1L* may have a role in MPM carcinogenesis.

The importance of epigenetic alterations in MPM from our study was supported by previous studies that showed differential methylation profile in MPM compared to normal pleural and may be prognostic[109,113]. In addition, asbestos contributes to MPM carcinogenesis by altering the epigenome through hypermethylation of several cell cycle genes[114]. These have led to the use of histone deactylase inhibitors (HDACi) and methyltransferase inhibitors (DNMTi) in patients with MPM including vorinostat that was trialled in the largest phase III clinical trial in MPM[117]. However this did not translate into an overall survival benefit and it may be a combination of both HDACi and DNMTi that may provide therapeutic benefits as demonstrated by an *in vivo* study[417].

Comparing our study to the recent sequencing studies by Guo *et al* and Lo *et al*, one of the main differences is that the tumour tissues in both reported studies were obtained from patients who had been treated with chemotherapy (40% in Guo *et al* and 100% in Lo *et al*)[144,146]. Thus the chemotherapy effect on the genome may have contributed to the mutations detected and may not truly reflect the mutational landscape of MPM. On the contrary, the main limitations of our study include smaller sample size of tumour/normal pairs and lower tumour cellularity. These may limit the power to detect SNV that may be pathogenic but occurring at a very low frequency. The International Cancer Genome Consortium has set out guidelines in collecting high quality tumour samples for next generation sequencing studies and one of the recommendations is a minimum of 80% tumour cellularity[366]. However, less stringent criteria may apply to certain tumour types whereby obtaining adequate tissues may

be challenging such as MPM due to its lower incidence compared to other solid cancers. In terms of data analysis, we utilised UnifiedGenotyper for variant calling and currently there is no gold standard algorithm or tool. This tool is comparable to the recently introduced Mutect but lacks sensitivity in detecting allele sites with low fraction. Another potential limitation of our study is using Sanger sequencing as the method of choice to validate variants. Sanger sequencing is considered the gold standard for mutation detection and is highly sensitive for the detection of point mutations, splice site mutations, and small insertions and deletions. However, one of its drawbacks is having a lower sensitivity in detecting variants with an allele frequency of less than 20%. Despite the identification of candidate variants and genes in our study, the lack of matched normal in the validation cohort meant the somatic status of some of these variants could not be verified.

In conclusion, the findings of our study are in keeping with published reports including absence of known oncogenes, frequent mutations in *BAP1, NF2* and alterations in MAPK and WNT pathways. However, we identified several genes encoding these two pathways that have not been previously reported in MPM and may potentially be targetable. Other findings that contribute further insights into MPM carcinogenesis include significantly altered focal adhesion signalling pathway that is clinically relevant given the positive results from clinical trials with FAK inhibitor in patients with MPM. In addition, we identified genes other than *BAP1* that are involved in chromatin remodelling indicating the potential roles of epigenetic events in MPM carcinogenesis.

# Chapter 5 - Summary and future work

## 5.1 General conclusions

The genetic landscape of malignant pleural mesothelioma (MPM) is still far from being fully characterised but increasing research efforts have been invested to provide better understanding and insights into this complex disease. To date, the recurrent findings from published works have been dominated mainly by the following:

1. Chromosomal alterations including deletions (1p, 3p, 4q, 6q, 9p, 13q, 14q, and 22q) and gains (1q, 5p, 7p, 8q, and 17q) of specific chromosomal regions[364].

2. Frequent molecular aberrations involving *CDKN2A, NF2* and *BAP1*[106,157,163].

This thesis work aimed to identify molecular alterations in MPM by studying the expression and mutational profiles. In Chapter 3, we studied the gene expression profile of 25 MPM tumours and 5 non-malignant pleural. We identified 643 differentially expressed genes with a Benjamin Hochberg corrected p-value of $\leq 0.01$ and absolute fold change in the level of expression of $\geq 2$. Next, we constructed MPM-associated co-expression network and identify modules of highly connected genes with weighted gene co-expression network analysis (WGCNA) tool[203]. The major findings from this chapter were:

1. Significant deregulated expression of genes involved in cell migration, invasion, cell cycle and the immune system that contribute to the malignant phenotype of MPM.

2. Focal adhesion kinase (FAK) signalling appears to be a common denominator in many of the upregulated genes and pathways identified.

3. Genes involved in WNT and transforming growth factor beta (TGF-ß) signalling pathways that are linked with epithelial mesenchymal transition (EMT) process are associated with molecular subtype classification.

4. Genes involved in cell cycle process are associated with poor survival prognosis.

In Chapter 4, the exomes of seven tumour-normal pairs were successfully sequenced and revealed 1, 226 somatic mutations distributed in 1,074 genes. In addition, the exome data from 29 tumours were available. The major findings from this study were:

1. Absence of mutations in known oncogenes

2. Frequent mutations in *BAP1* and *NF2* consistent with published data.

3. Significant alterations in FAK, mitogen-activated protein kinases (MAPK) and WNT signalling pathways of which many of the genes encoding these pathways are novel in MPM.

4. Mutations in genes involved in chromatin remodelling other than *BAP1* modulating epigenetic events that may contribute to disturbance in global gene expression in MPM.

5. Low frequency of recurrent mutational events might suggest heterogeneity in mutation profile between tumours.

6. Identification of potential targetable mutations and pathways that might have therapeutic importance for patients with MPM.

This research has not only confirmed findings from previous works but also provided new information about the molecular landscape of MPM. From our study, the molecular alterations in MPM may be better defined by activation of common signalling pathways instead of a defined set of genes or mutations. These are evident from the identification of significant alterations in FAK and WNT signalling pathways at both deoxyribonucleic acid (DNA) and ribonucleic acid (RNA) levels. Aberrant activation of FAK promotes cancer through complex signalling networks involving cell survival, proliferation, migration, invasion, EMT, angiogenesis and cancer stem cell activities. Our findings highlighted the importance of this pathway in MPM carcinogenesis and in fact targeting FAK *in vitro* and in tumour xenograft models demonstrated good cytotoxicity effect especially in MPM tumours with low expression of merlin[418]. In addition to FAK, we also identified significant alteration in WNT pathway with mutations and deregulated expression of novel components. This pathway regulates various processes involved in cancer progression, including tumour initiation, tumour growth, cell senescence, cell death, differentiation and metastasis. Targeting this pathway has been challenging mainly due to lack of specific targets, potential redundancy of pathway components and cross talks with other oncogenic pathways. Interestingly, recent studies have shown that FAK and WNT pathways are interconnected to promote tumorigenesis. This was demonstrated in an *APC* deleted model of colorectal cancer whereby the FAK/PYK2 axis is required for the activation of the WNT pathway and in breast cancer, the inhibition of FAK *in vivo* and *in vitro* led to decreased self-renewal capacity and reduced levels of *WNT3A* and *CTNNB1*[419,420]. Thus, our findings support the relevance of these two pathways that may have a dynamic and complex interactions in promoting MPM carcinogenesis that require further research.

In light of the exciting era of cancer immunotherapy, it is worth noting the identification of significantly altered expression of genes associated with the immune system from our study.

The discovery of immune checkpoint receptors such as cytotoxic T lymphocyte antigen-4 (CTLA-4) and programmed death-1 (PD-1) responsible for inactivating the immune system in cancers have gained immense interest. Blocking immune checkpoints have shown significant improvement in clinical outcomes in several cancer types including melanoma and non-small cell lung cancer[421,422]. In MPM, preclinical data and clinical studies with anti-CTLA4 and anti-PD-1 antibodies have already shown promising results[346–348]. Studies have also examined the expression of PD-L1 (ligand of PD-1) by immunohistochemistry in MPM and found overexpression of PD-L1 in tumours ranging between 20-90% especially in sarcomatoid subtype and is associated with poorer survival[423,424].We identified downregulation of 78 genes involved in immune functions including T cell, B cell activation, cell adhesion and cytokine-cytokine receptor interactions. Interestingly, *CD28* is one of the underexpressed genes and CTLA-4 induces T-cell inactivation by competing with *CD28* for B7 ligands *CD80* and *CD86* expressed on antigen presenting cells. Taking all these together, defective antitumor immunity is evident in MPM and further research is needed to improve our understanding in the role of the immune system in MPM carcinogenesis that may unravel new therapeutic targets.

Genomic intra- and intertumoral heterogeneity are recognised features in cancers. Previous transcriptomic study in MPM revealed distinctive genomic profiles in growth factors involved in differentiation, metabolism, and regulation of apoptosis that determined MPM differentiation[425]. Our study also revealed differences in gene expression between subtypes and heterogeneous mutational profiles between each tumour. However, the full molecular profile may be under-represented due to single sampling from each tumour being studied. Through multiregional sequencing of a tumour, other studies have revealed tumours evolve through different branches with subclones that harbour distinct genomic profiles that can lead to tumour recurrence, metastasis and present challenges to precision medicine[426,427]. This approach has not been explored in MPM and could potentially reveal a more comprehensive

genomic profile and identify dominant signalling pathways and biological processes with actionable mutated genes.

The advent of next generation sequencing methods (NGS) including targeted, whole genome or whole transcriptome sequencing coupled with bioinformatics-based data analysis offer unparalleled high-throughput approach in studying cancer genomics. We utilised microarray-based and whole exome sequencing approaches to examine the gene expression and mutational profiles in MPM respectively. These may have their limitations in comparison to other methods.

Microarray-based technology allows a comprehensive simultaneous characterisation of the expression of thousands of genes in a given cell at a given time point. On the other hand, RNA sequencing allows a more comprehensive characterisation of tumour transcriptome and correlation with structural and copy number alterations, insertions, deletions and single nucleotide mutations. In comparison to microarray-based approach, RNA sequencing allows rapid and higher sensitivity in the detection of not only known but also discovering novel transcripts, global transcriptomic alterations with absolute instead of relative value and post-transcriptional changes on a larger scale[428]. The data can also be mined to detect alternative splice variants, fusion transcripts and microRNAs as demonstrated in different cancer types[429–431]. Despite the unprecedented offers of RNA sequencing, microarray-based approach is still commonly preferred mainly due to its lower cost and is a less complex dataset to analyse. RNA sequencing is fairly new in MPM and to date there is only one published study on transcriptome sequencing involving four MPM tumours[182]. This study revealed a different mutational profile in each tumour and found novel mutations in thousands of expressed genes of which *XRCC6*, *PDZK1IP1*, *ACTR1A*, and *AVEN* could be associated with MPM carcinogenesis.

One of the limitations of exome sequencing is that it covers only the protein-coding regions (1% of the genome). Whole genome sequencing provides an unbiased interrogation of both the coding and non-coding regions of the genome. Although little is known about the pathogenic significance of the non-coding regions, emerging evidence have revealed their roles in diseases including cancer such as a single nucleotide polymorphism in the 5' untranslated region of *RAD51* as a modifier of breast cancer risk in *BRCA1* and *BRCA2* mutation carriers[432]. In addition, whole genome allows detection of larger genomic alterations including structural variants, loss of heterozygosity and copy number that may be difficult to detect with exome data. This was demonstrated in a study that sequenced both the genome and exome of myeloma specimens and found half of the protein-coding mutations occurred in chromosomal translocations that were missed by exome sequencing[433]. Recently, the whole genome of 10 MPM tumours were sequenced and identified novel mutations in genes associated with integrin-linked kinase pathway and clinical correlation revealed molecular differences between gender and histology subtypes involving *BAP1, TP53, MYH9* and *RHOA* that may be involved in MPM carcinogenesis[434]. However, no significant mutations in non-protein coding regions or large structural variants such as translocations were reported.

Aside from NGS methods, DNA methylation and proteomic profiling are two other approaches that can reveal important epigenetic and functional events respectively driving the disease process. As such, a combined methodological approach comprising mutational, transcriptomic, methylation and proteomics data may eventually reveal the full molecular landscape of MPM. Recently, Bueno *et al* published a comprehensive genomic analysis of 216 MPM tumours (the largest sample size to date) with RNA, whole exome and targeted exome sequencing[435]. Using RNA sequencing data, they identified four molecular subtypes (sarcomatoid, epithelioid, biphasic-epithelioid and biphasic-sarcomatoid) of MPM. As sarcomatoid MPM was not represented in our samples, we were able to stratify the tumours

into three molecular subtypes (biphasic in CL1, epithelioid in CL3 and biphasic-epithelioid in CL2 as described in Chapter 3) with WGCNA of our gene expression data. The study also identified 10 significantly mutated genes and pathway alterations in Hippo, mammalian target of rapamycin, histone methylation, RNA helicase and p53 signalling. Of these, mutations in *NF2, BAP1* and *SETD2* together with aberrations in chromatin remodelling were also identified in our exome findings (Chapter 4).

Nevertheless, unravelling the full molecular alterations in MPM remains a challenging research task and collaborative efforts are paramount to ensure this goal is achieved. Both the International Cancer Genome Consortium and The Cancer Genome Atlas are compiling omics data from all types of cancers including mesothelioma in order to improve our understanding of the molecular mechanisms driving cancer. As part of our continuous research effort in MPM, the section below describes our ongoing work and future directions in this project.

## 5.2 Ongoing and future work

As mentioned, one of the main limitations from our study was the small sample size that makes it difficult to allow identification of recurrent events occurring at low frequency or assessing significant correlation with clinical features. Hence, we aimed to obtain more samples to allow detection of significant mutations. In addition, sarcomatoid subtype was not represented in our study to allow expression or mutational characterisation. Therefore, in addition to the sequenced 7 matched tumour-normal pairs from our study, our group had extracted genomic DNA from a further 14 paired tumour tissues acquired from the MesobanK tissue repository and the exomes have been successfully sequenced. Both datasets will be merged in due course and reanalysed to define significantly mutated genes with the recently introduced MutSigCV algorithm[436]. This approach will remove a high number of artefactual

findings and allow identification of genes relevant to MPM. Along with this, copy number alterations that are indicative of chromosomal instability will also be analysed. There will also be plans to perform whole transcriptome shotgun sequencing contingent on the availability of adequate tumour samples. This will not only allow further evaluation of gene expression and single nucleotide variants (SNV) discovery but also post-transcriptional SNV and fusion gene detections.

Candidate variants will then be confirmed with Sanger sequencing. The frequency of candidate variants will be determined in an independent set of tumours with targeted capture sequencing that enables robust detection of clinically informative genes from formalin fixed, paraffin-embedded (FFPE) tumour DNA[437]. FFPE tissues remain the standard material for analysis in the clinical settings. The preservation of tissue morphology in FFPE enables the isolation and analysis of relatively enriched tumour material space. Furthermore, the ease and low cost involved in storage is an advantage compared to frozen tissues. The protein expression of candidate variants will also be examined by either immunohistochemistry or fluorescence *in situ* hybridisations methods.

In preparation for this, we have acquired 307 MPM FFPE blocks as the follow up cohort. These were identified from the Royal Brompton and Harefield NHS Trust (RBHT) Diagnostic Tissue Bank and St George's Hospital (SGH) under an ethically approved study, Molecular Epidemiology of Malignant Mesothelioma (MEMO) (see Chapter 2). These were sectioned, stained with routine haematoxylin and eosin, and reviewed by two certified pathologists to verify tumour histology and abundance as described in Chapter 2 section 2.2.2.2 and 2.2.2.3. FFPE sections were prepared on a total of 122 and 185 tumour FFPE tissues from RBHT and SGH respectively with 30% or more viable-appearing malignant cells. Genomic DNA had been successfully isolated as described in Chapter 2 section 2.2.5.3. Tumour tissue

microarrays will be prepared from the FFPE blocks to examine the protein expression of candidate variants.

The baseline clinical characteristics of the follow up cases were summarised in Table 5.1. Majority of the cases were of male gender and epithelioid MPM was the predominant subtype.

**Table 5.1. Cases demographic and clinical characteristics.**

| Characteristics | Follow up cohort n= 307 |
|---|---|
| **Age, years** | |
| Median | 71 |
| Range | 45-91 |
| ≤ 70 | 153 (49.8%) |
| > 70 | 154 (50.2%) |
| **Sex** | |
| Male | 242 (78.8%) |
| Female | 65 (21.2%) |
| **Histological subtypes** | |
| Epithelioid MPM | 214 (69.7) |
| Biphasic MPM | 60 (19.5) |
| Sarcomatoid MPM | 33 (10.7) |

Survival data was also available for 302 cases and patients who were alive at last follow up were censored. A total of 287 events were observed. The median overall survival (OS) for all cases was 10.2 months (95% CI 8.3- 12.1) (Figure 5.1). Univariate survival analysis by histological subtypes (Figure 5.2) showed OS was significantly longer in epithelioid MPM (median OS 13.1 months, 95% CI 11.3- 15.0) than biphasic MPM (median OS 7.2 months, 95% CI 4.6-9.8) and sarcomatoid MPM (median OS 5.1 months, 95% CI 3.3-6.9) after a

median follow-up time of 12.9 months, 5.9 months and 5.1 months respectively (Figure 5.2). The hazard ratio was 1.73 (95% CI 1.3-2.3) for biphasic MPM and 2.99 (95% CI 2.0-4.4) for sarcomatoid MPM. Multivariate survival analyses showed age and gender was not significant in the final model.

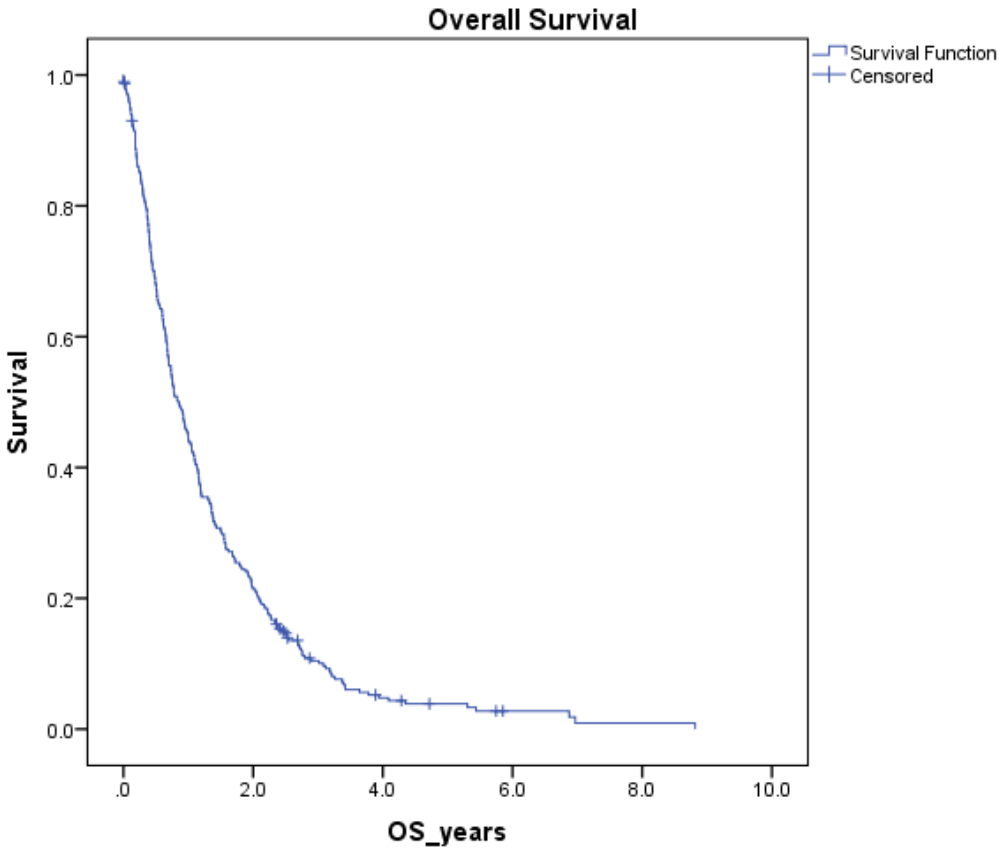


**Figure 5.1. Kaplan-Meier curve for OS in all 302 cases.**

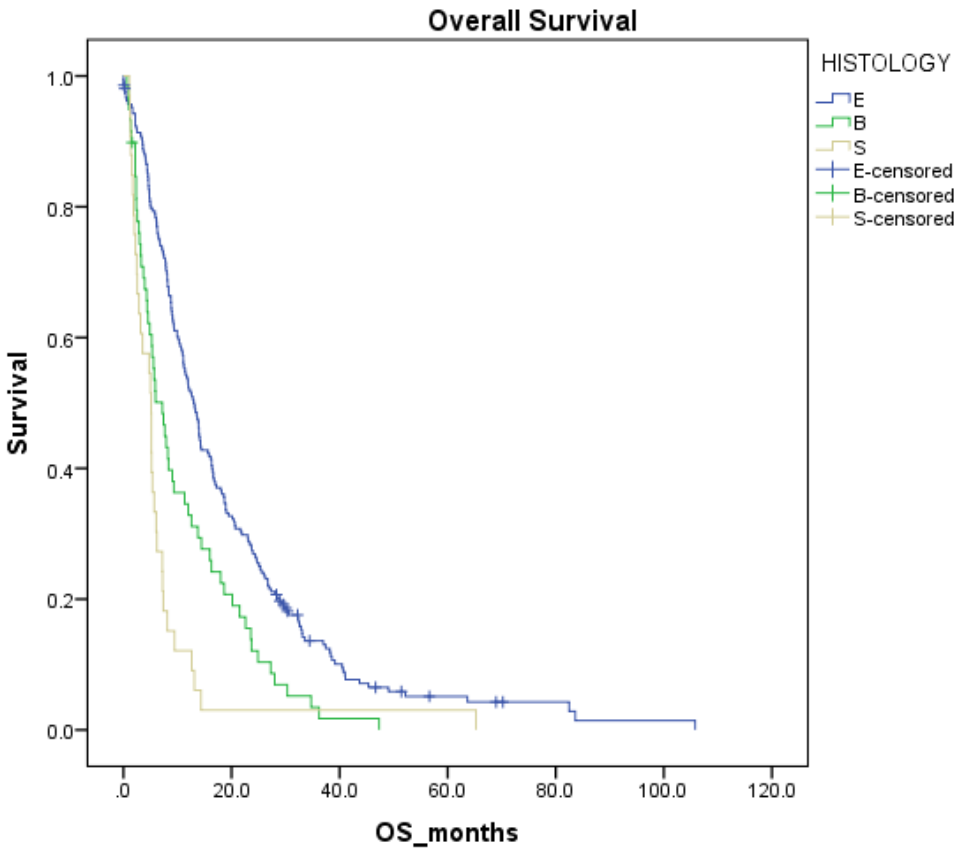


**Figure 5.2. Kaplan Meier curves for OS by histological subtypes. Log rank p value < 0.0001. E= epithelioid, B= biphasic, S= sarcomatoid.**

The data generated will be analysed for the following:

1. Identification of targetable variants and signalling pathways for subsequent functional assays.

2. Correlation with clinical data to allow patient stratification and identification of diagnostic and prognostic biomarkers.

Lastly, we hope the knowledge generated by this research project will have great potential in providing further insights into the molecular mechanisms involved in MPM carcinogenesis.

Future directions of our work are not limited to those described above and we hope this project will serve as a platform for further collaborative work with other investigators in an effort to improve the clinical outcomes of patients with this deadly disease.

# Bibliography


1. Cancer Research UK.

2. Rusch, V. W. *et al.* Initial analysis of the international association for the study of lung cancer mesothelioma database. *J. Thorac. Oncol.* **7,** 1631–1639 (2012).

3. Herndon, J. E. *et al.* Factors predictive of survival among 337 patients with mesothelioma treated between 1984 and 1994 by the Cancer and Leukemia Group B. *Chest* **113,** 723–731 (1998).

4. Fennell, D. A. *et al.* Statistical validation of the EORTC prognostic model for malignant pleural mesothelioma based on three consecutive phase II trials. *J. Clin. Oncol.* **23,** 184–189 (2005).

5. Vogelzang, N. J. *et al.* Phase III study of pemetrexed in combination with cisplatin versus cisplatin alone in patients with malignant pleural mesothelioma. *J. Clin. Oncol.* **21,** 2636–2644 (2003).

6. Treasure, T. *et al.* Extra-pleural pneumonectomy versus no extra-pleural pneumonectomy for patients with malignant pleural mesothelioma: clinical outcomes of the Mesothelioma and Radical Surgery (MARS) randomised feasibility study. *Lancet. Oncol.* **12,** 763–72 (2011).

7. Rusch, V. W. *et al.* A phase II trial of surgical resection and adjuvant high-dose hemithoracic radiation for malignant pleural mesothelioma. *J. Thorac. Cardiovasc. Surg.* **122,** 788–795 (2001).

8. Czernobilsky, B., Moll, R., Levy, R. & Franke, W. W. Co-expression of cytokeratin and vimentin filaments in mesothelial, granulosa and rete ovarii cells of the human ovary. *Eur. J. Cell Biol.* **37,** 175–190 (1985).

9. Afify, A. M., Al-Khafaji, B. M., Paulino, A. F. G. & Davila, R. M. Diagnostic use of muscle markers in the cytologic evaluation of serous fluids. *Appl. Immunohistochem. Mol. Morphol.* **10,** 178–182 (2002).

10. Simsir, A., Fetsch, P., Mehta, D., Zakowski, M. & Abati, A. E-cadherin, N-cadherin, and calretinin in pleural effusions: the good, the bad, the worthless. *Diagn. Cytopathol.* **20,** 125–130 (1999).

11. Ryan, G. B., Grobéty, J. & Majno, G. Mesothelial injury and recovery. *Am. J. Pathol.* **71,** 93–112 (1973).

12. Pérez-Pomares, J. M. & Muñoz-Chápuli, R. Epithelial-mesenchymal transitions: a mesodermal cell strategy for evolutive innovation in Metazoans. *Anat. Rec.* **268,** 343–351 (2002).

13. Cho, R. W. & Clarke, M. F. Recent advances in cancer stem cells. *Curr. Opin. Genet. Dev.* **18,** 48–53 (2008).

14. Wang, J. C. Y. & Dick, J. E. Cancer stem cells: lessons from leukemia. *Trends Cell Biol.* **15,** 494–501 (2005).

15. Al-Hajj, M., Wicha, M. S., Benito-Hernandez, A., Morrison, S. J. & Clarke, M. F. Prospective identification of tumorigenic breast cancer cells. *Proc. Natl. Acad. Sci. U. S. A.* **100,** 3983–3988 (2003).

16. Frei, C. *et al.* Pleural mesothelioma side populations have a precursor phenotype. *Carcinogenesis* **32,** 1324–1332 (2011).

17. Varghese, S., Whipple, R., Martin, S. S. & Alexander, H. R. Multipotent cancer stem cells derived from human malignant peritoneal mesothelioma promote tumorigenesis. *PLoS One* **7,** e52825 (2012).

18. Yamazaki, H. *et al.* Characterization of cancer stem cell properties of CD24 and CD26-positive human malignant mesothelioma cells. *Biochem. Biophys. Res. Commun.* **419,** 529–536 (2012).

19. Cortes-Dericks, L., Carboni, G. L., Schmid, R. A. & Karoubi, G. Putative cancer stem cells in malignant pleural mesothelioma show resistance to cisplatin and pemetrexed. *Int. J. Oncol.* **37,** 437–444 (2010).

20. Boutin, C. & Rey, F. Thoracoscopy in pleural malignant mesothelioma: a prospective study of 188 consecutive patients. Part 1: Diagnosis. *Cancer* **72,** 389–393 (1993).

21. Suzuki, Y. Pathology of human malignant mesothelioma--preliminary analysis of 1,517 mesothelioma cases. *Ind. Health* **39,** 183–185 (2001).

22. Pelin, K., Hirvonen, A. & Linnainmaa, K. Expression of cell adhesion molecules and connexins in gap junctional intercellular communication deficient human mesothelioma tumour cell lines and communication competent primary mesothelial cells. *Carcinogenesis* **15,** 2673–2675 (1994).

23. Marshall, B. C. *et al.* Metalloproteinases and tissue inhibitor of metalloproteinases in mesothelial cells. Cellular differentiation influences expression. *J. Clin. Invest.* **91,** 1792–1799 (1993).

24. Craighead, J. E. Epidemiology of mesothelioma and historical background. *Recent results cancer Res. Fortschritte der Krebsforsch. Progrès dans les Rech. sur le cancer* **189,** 13–25 (2011).

25. Britton, M. The epidemiology of mesothelioma. *Semin. Oncol.* **29,** 18–25 (2002).

26. Musk, A. W. & de Klerk, N. H. Epidemiology of malignant mesothelioma in Australia. *Lung Cancer* **45 Suppl 1,** S21–3 (2004).

27. Weill, H., Hughes, J. & Churg, A. Changing trends in US mesothelioma incidence. *Occup. Environ. Med.* **62,** 270 (2005).

28. Delgermaa, V. *et al.* Global mesothelioma deaths reported to the World Health Organization between 1994 and 2008. *Bull. World Health Organ.* **89,** 716–24, 724A–724C (2011).

29. Hodgson, J. T., McElvenny, D. M., Darnton, A. J., Price, M. J. & Peto, J. The expected burden of mesothelioma mortality in Great Britain from 2002 to 2050. *Br. J. Cancer* **92,** 587–593 (2005).

30. Park, E.-K. *et al.* Global magnitude of reported and unreported mesothelioma. *Environ. Health Perspect.* **119,** 514–518 (2011).

31. Camidge, D. R., Stockton, D. L. & Bain, M. Factors affecting the mesothelioma detection rate within national and international epidemiological studies: insights from Scottish linked cancer registry-mortality data. *Br. J. Cancer* **95,** 649–652 (2006).

32. McElvenny, D. M., Darnton, A. J., Price, M. J. & Hodgson, J. T. Mesothelioma mortality in Great Britain from 1968 to 2001. *Occup. Med. (Lond).* **55,** 79–87 (2005).

33. Mirabelli, D. *et al.* Non-occupational exposure to asbestos and malignant mesothelioma in the Italian National Registry of Mesotheliomas. *Occup. Environ. Med.* **67,** 792–794 (2010).

34. Metintas, S., Metintas, M., Ucgun, I. & Oner, U. Malignant mesothelioma due to environmental exposure to asbestos: follow-up of a Turkish cohort living in a rural area. *Chest* **122,** 2224–9 (2002).

35. Roushdy-Hammady, I., Siegel, J., Emri, S., Testa, J. R. & Carbone, M. Genetic-susceptibility factor and malignant mesothelioma in the Cappadocian region of Turkey. *Lancet (London, England)* **357,** 444–445 (2001).

36. Case 33111. *N. Engl. J. Med.* **236,** 407–412 (1947).

37. WAGNER, J. C., SLEGGS, C. A. & MARCHAND, P. Diffuse pleural mesothelioma and asbestos exposure in the North Western Cape Province. *Br. J. Ind. Med.* **17,** 260–271 (1960).

38. Hodgson, J. T. & Darnton, A. The quantitative risks of mesothelioma and lung cancer in relation to asbestos exposure. *Ann. Occup. Hyg.* **44,** 565–601 (2000).

39. Mossman, B. T. & Churg, A. Mechanisms in the pathogenesis of asbestosis and silicosis. *Am. J. Respir. Crit. Care Med.* **157,** 1666–1680 (1998).

40. McDonald, J. C. Epidemiology of malignant mesothelioma--an outline. *Ann. Occup. Hyg.* **54,** 851–857 (2010).

41. Neumann, V., Löseke, S. & Tannapfel, A. Mesothelioma and analysis of tissue fiber content. *Recent results cancer Res. Fortschritte der Krebsforsch. Progrès dans les Rech. sur le cancer* **189,** 79–95 (2011).

42. Sebastien, P., Janson, X., Gaudichet, A., Hirsch, A. & Bignon, J. Asbestos retention in human respiratory tissues: comparative measurements in lung parenchyma and in parietal pleura. *IARC Sci. Publ.* 237–246 (1980). at <http://www.ncbi.nlm.nih.gov/pubmed/7239642>

43. *World Health Organisation (WHO). Elimination of asbestos-related diseases. Geneva: WHO, 2006*. at

<http://apps.who.int/iris/bitstream/10665/69479/1/WHO_SDE_OEH_06.03_eng.pdf>

44. Leigh, J. & Driscoll, T. Malignant mesothelioma in Australia, 1945-2002. *Int. J. Occup. Environ. Health* **9,** 206–217

45. McDonald, J. C. & McDonald, A. D. The epidemiology of mesothelioma in historical context. *Eur. Respir. J.* **9,** 1932–1942 (1996).

46. Sluis-Cremer, G. K. Asbestos disease at low exposures after long residence times. *Ann. N. Y. Acad. Sci.* **643,** 182–193 (1991).

47. Frost, G., Darnton, A. & Harding, A.-H. The effect of smoking on the risk of lung cancer mortality for asbestos workers in Great Britain (1971-2005). *Ann. Occup. Hyg.* **55,** 239–247 (2011).

48. Muscat, J. E. & Wynder, E. L. Cigarette smoking, asbestos exposure, and malignant mesothelioma. *Cancer Res.* **51,** 2263–2267 (1991).

49. Lanphear, B. P. & Buncher, C. R. Latent period for malignant mesothelioma of occupational origin. *J. Occup. Med.* **34,** 718–721 (1992).

50. Hyland, R. A., Ware, S., Johnson, A. R. & Yates, D. H. Incidence trends and gender differences in malignant mesothelioma in New South Wales, Australia. *Scand. J. Work. Environ. Health* **33,** 286–292 (2007).

51. Hilliard, A. K., Lovett, J. K. & McGavin, C. R. The rise and fall in incidence of malignant mesothelioma from a British Naval Dockyard, 1979-1999. *Occup. Med. (Lond).* **53,** 209–212 (2003).

52. Reid, A. *et al.* Mesothelioma risk after 40 years since first exposure to asbestos: a pooled analysis. *Thorax* **69,** 843–850 (2014).

53. Lacourt, A. *et al.* Temporal patterns of occupational asbestos exposure and risk of pleural mesothelioma. *Eur. Respir. J.* **39,** 1304–1312 (2012).

54. Smith, W. E. & Hubert, D. D. The intrapleural route as a means for estimating carcinogenicity. 92–101

55. Gibbs, A. R. & Pooley, F. D. Analysis and interpretation of inorganic mineral particles in 'lung' tissues. *Thorax* **51,** 327–334 (1996).

56. Ault, J. G. *et al.* Behavior of crocidolite asbestos during mitosis in living vertebrate lung epithelial cells. *Cancer Res.* **55,** 792–798 (1995).

57. Yang, H. *et al.* Programmed necrosis induced by asbestos in human mesothelial cells causes high-mobility group box 1 protein release and resultant inflammation. *Proc. Natl. Acad. Sci. U. S. A.* **107,** 12611–12616 (2010).

58. Kamp, D. W., Israbian, V. A., Preusen, S. E., Zhang, C. X. & Weitzman, S. A. Asbestos causes DNA strand breaks in cultured pulmonary epithelial cells: role of iron-catalyzed free radicals. *Am. J. Physiol.* **268,** L471–80 (1995).

59. Zanella, C. L., Posada, J., Tritton, T. R. & Mossman, B. T. Asbestos causes stimulation of the extracellular signal-regulated kinase 1 mitogen-activated protein kinase cascade after phosphorylation of the epidermal growth factor receptor. *Cancer Res.* **56,** 5334–5338 (1996).

60. Carthew, P., Hill, R. J., Edwards, R. E. & Lee, P. N. Intrapleural administration of fibres induces mesothelioma in rats in the same relative order of hazard as occurs in man after exposure. *Hum. Exp. Toxicol.* **11,** 530–534 (1992).

61. Metintas, M., Hillerdal, G., Metintas, S. & Dumortier, P. Endemic malignant mesothelioma: exposure to erionite is more important than genetic factors. *Arch. Environ. Occup. Health* **65,** 86–93

62. Nagai, H. *et al.* Diameter and rigidity of multiwalled carbon nanotubes are critical factors in mesothelial injury and carcinogenesis. *Proc. Natl. Acad. Sci. U. S. A.* **108,** E1330–8 (2011).

63. Cutrone, R. *et al.* Some oral poliovirus vaccines were contaminated with infectious SV40 after 1961. *Cancer Res.* **65,** 10273–10279 (2005).

64. Bocchetta, M. *et al.* Human mesothelial cells are unusually susceptible to simian virus 40-mediated transformation and asbestos cocarcinogenicity. *Proc. Natl. Acad. Sci. U. S. A.* **97,** 10214–10219 (2000).

65. Bocchetta, M. & Carbone, M. in (eds. Pass, H. I., Vogelzang, N. J. & Carbone, M.) 34–59 (Springer New York, 2005). doi:10.1007/0-387-28274-2_3

66. Cacciotti, P. *et al.* SV40 replication in human mesothelial cells induces HGF/Met receptor activation: a model for viral-related carcinogenesis of human malignant mesothelioma. *Proc. Natl. Acad. Sci. U. S. A.* **98,** 12032–12037 (2001).

67. Bocchetta, M., Miele, L., Pass, H. I. & Carbone, M. Notch-1 induction, a novel activity of SV40 required for growth of SV40-transformed human mesothelial cells. *Oncogene* **22,** 81–89 (2003).

68. Cicala, C., Pompetti, F. & Carbone, M. SV40 induces mesotheliomas in hamsters. *Am. J. Pathol.* **142,** 1524–1533 (1993).

69. Carbone, M. *et al.* Simian virus 40-like DNA sequences in human pleural mesothelioma. *Oncogene* **9,** 1781–1790 (1994).

70. Testa, J. R. *et al.* A multi-institutional study confirms the presence and expression of simian virus 40 in human malignant mesotheliomas. *Cancer Res.* **58,** 4505–4509 (1998).

71. Mayall, F., Barratt, K. & Shanks, J. The detection of Simian virus 40 in mesotheliomas from New Zealand and England using real time FRET probe PCR protocols. *J. Clin. Pathol.* **56,** 728–730 (2003).

72. Hirvonen, A. *et al.* Simian virus 40 (SV40)-like DNA sequences not detectable in finnish mesothelioma patients not exposed to SV40-contaminated polio vaccines. *Mol. Carcinog.* **26,** 93–99 (1999).

73. López-Ríos, F., Illei, P. B., Rusch, V. & Ladanyi, M. Evidence against a role for SV40 infection in human mesotheliomas and high risk of false-positive PCR results owing to presence of SV40 sequences in common laboratory plasmids. *Lancet (London, England)* **364,** 1157–1166

74. Kroczynska, B. *et al.* Crocidolite asbestos and SV40 are cocarcinogens in human mesothelial cells and in causing mesothelioma in hamsters. *Proc. Natl. Acad. Sci. U. S. A.* **103,** 14128–14133 (2006).

75. Huncharek, M. Non-asbestos related diffuse malignant mesothelioma. *Tumori* **88,** 1–9

76. Chirieac, L. R. *et al.* Clinicopathologic characteristics of malignant mesotheliomas arising in patients with a history of radiation for Hodgkin and non-Hodgkin lymphoma. *J. Clin. Oncol.* **31,** 4544–4549 (2013).

77. Sanders, C. L. & Jackson, T. A. Induction of mesotheliomas and sarcomas from 'hot spots' of 239 PuO 2 activity. *Health Phys.* **22,** 755–759 (1972).

78. Goodman, J. E., Nascarella, M. A. & Valberg, P. A. Ionizing radiation: a risk factor for mesothelioma. *Cancer Causes Control* **20,** 1237–1254 (2009).

79. Hirvonen, A. *et al.* Inherited GSTM1 and NAT2 defects as concurrent risk modifiers in asbestos-related human malignant mesothelioma. *Cancer Res.* **55,** 2981–2983 (1995).

80. Neri, M. *et al.* Pleural malignant mesothelioma, genetic susceptibility and asbestos exposure. *Mutat. Res.* **592,** 36–44 (2005).

81. Cadby, G. *et al.* A genome-wide association study for malignant mesothelioma risk. *Lung Cancer* **82,** 1–8 (2013).

82. Matullo, G. *et al.* Genetic variants associated with increased risk of malignant pleural mesothelioma: a genome-wide association study. *PLoS One* **8,** e61253 (2013).

83. Mäki-Nevala, S. *et al.* Driver Gene and Novel Mutations in Asbestos-Exposed Lung Adenocarcinoma and Malignant Mesothelioma Detected by Exome Sequencing. *Lung* (2015). doi:10.1007/s00408-015-9814-7

84. Testa, J. R. *et al.* Germline BAP1 mutations predispose to malignant mesothelioma. *Nat. Genet.* **43,** 1022–1025 (2011).

85. Carbone, M. *et al.* BAP1 cancer syndrome: malignant mesothelioma, uveal and cutaneous melanoma, and MBAITs. *J. Transl. Med.* **10,** 179 (2012).

86. Rusch, A. *et al.* Prevalence of BRCA-1 associated protein 1 germline mutation in sporadic malignant pleural mesothelioma cases. *Lung Cancer* **87,** 77–79 (2015).

87. Sneddon, S. *et al.* Absence of germline mutations in BAP1 in sporadic cases of malignant mesothelioma. *Gene* **563,** 103–105 (2015).

88. Betti, M. *et al.* Inference on germline BAP1 mutations and asbestos exposure from the analysis of familial and sporadic mesothelioma in a high-risk area. *Genes. Chromosomes Cancer* **54,** 51–62 (2015).

89. Hjerpe, A. *et al.* Guidelines for cytopathologic diagnosis of epithelioid and mixed type malignant mesothelioma. Complementary statement from the International Mesothelioma Interest Group, also endorsed by the International Academy of Cytology and the Papanicolaou Society o. *Cytojournal* **12,** 26 (2015).

90. Segal, A. *et al.* A diagnosis of malignant pleural mesothelioma can be made by effusion cytology: results of a 20 year audit. *Pathology* **45,** 44–48 (2013).

91. Robinson, B. W. S. *et al.* Mesothelin-family proteins and diagnosis of mesothelioma. *Lancet (London, England)* **362,** 1612–1616 (2003).

92. Hollevoet, K. *et al.* Serum mesothelin for diagnosing malignant pleural mesothelioma: an individual patient data meta-analysis. *J. Clin. Oncol.* **30,** 1541–1549 (2012).

93. Pass, H. I. *et al.* Asbestos exposure, pleural mesothelioma, and serum osteopontin levels. *N. Engl. J. Med.* **353,** 1564–1573 (2005).

94. Cristaudo, A. *et al.* Combined serum mesothelin and plasma osteopontin measurements in malignant pleural mesothelioma. *J. Thorac. Oncol.* **6,** 1587–1593 (2011).

95. Thylén, A., Hjerpe, A. & Martensson, G. Hyaluronan content in pleural fluid as a prognostic factor in patients with malignant pleural mesothelioma. *Cancer* **92,** 1224–1230 (2001).

96. Mundt, F. *et al.* Hyaluronan and N-ERC/mesothelin as key biomarkers in a specific two-step model to predict pleural malignant mesothelioma. *PLoS One* **8,** e72030 (2013).

97. Pass, H. I. *et al.* Fibulin-3 as a blood and effusion biomarker for pleural mesothelioma. *N. Engl. J. Med.* **367,** 1417–1427 (2012).

98. Creaney, J. *et al.* Comparison of fibulin-3 and mesothelin as markers in malignant mesothelioma. *Thorax* **69,** 895–902 (2014).

99. Krismann, M., Müller, K.-M., Jaworska, M. & Johnen, G. Molecular cytogenetic differences between histological subtypes of malignant mesotheliomas: DNA cytometry and comparative genomic hybridization of 90 cases. *J. Pathol.* **197,** 363–371 (2002).

100. Lindholm, P. M. *et al.* Gene copy number analysis in malignant pleural mesothelioma using oligonucleotide array CGH. *Cytogenet. Genome Res.* **119,** 46–52 (2007).

101. Taniguchi, T. *et al.* Genomic profiling of malignant pleural mesothelioma with array-based comparative genomic hybridization shows frequent non-random chromosomal alteration regions including JUN amplification on 1p32. *Cancer Sci.* **98,** 438–446 (2007).

102. Ivanov, S. V *et al.* Genomic events associated with progression of pleural malignant mesothelioma. *Int. J. Cancer* **124,** 589–599 (2009).

103. Cheung, M. *et al.* The promyelocytic leukemia zinc-finger gene, PLZF, is frequently downregulated in malignant mesothelioma cells and contributes to cell survival.

*Oncogene* **29,** 1633–1640 (2010).

104. Christensen, B. C. *et al.* Integrated profiling reveals a global correlation between epigenetic and genetic alterations in mesothelioma. *Cancer Res.* **70,** 5686–5694 (2010).

105. Jean, D. *et al.* Syntenic relationships between genomic profiles of fiber-induced murine and human malignant mesothelioma. *Am. J. Pathol.* **178,** 881–894 (2011).

106. Bott, M. *et al.* The nuclear deubiquitinase BAP1 is commonly inactivated by somatic mutations and 3p21.1 losses in malignant pleural mesothelioma. *Nat. Genet.* **43,** 668–672 (2011).

107. Bueno, R. *et al.* Second generation sequencing of the mesothelioma tumor genome. *PLoS One* **5,** e10612 (2010).

108. Esteller, M. Aberrant DNA methylation as a cancer-inducing mechanism. *Annu. Rev. Pharmacol. Toxicol.* **45,** 629–656 (2005).

109. Christensen, B. C. *et al.* Epigenetic profiles distinguish pleural mesothelioma from normal pleura and predict lung asbestos burden and clinical outcome. *Cancer Res.* **69,** 227–234 (2009).

110. Goto, Y. *et al.* Epigenetic profiles distinguish malignant pleural mesothelioma from lung adenocarcinoma. *Cancer Res.* **69,** 9073–9082 (2009).

111. Tsou, J. A. *et al.* DNA methylation profile of 28 potential marker loci in malignant mesothelioma. *Lung Cancer* **58,** 220–230 (2007).

112. Suzuki, M. *et al.* Aberrant methylation profile of human malignant mesotheliomas and its relationship to SV40 infection. *Oncogene* **24,** 1302–1308 (2005).

113. Fischer, J. R. *et al.* Promoter methylation of RASSF1A, RARbeta and DAPK predict poor prognosis of patients with malignant mesothelioma. *Lung Cancer* **54,** 109–116 (2006).

114. Christensen, B. C. *et al.* Asbestos exposure predicts cell cycle control gene promoter methylation in pleural mesothelioma. *Carcinogenesis* **29,** 1555–1559 (2008).

115. Kohno, H. *et al.* Aberrant promoter methylation of WIF-1 and SFRP1, 2, 4 genes in mesothelioma. *Oncol. Rep.* **24,** 423–431 (2010).

116. Kubo, T. *et al.* Epigenetic silencing of microRNA-34b/c plays an important role in the pathogenesis of malignant pleural mesothelioma. *Clin. Cancer Res.* **17,** 4965–4974 (2011).

117. Krug, L. M. *et al.* Vorinostat in patients with advanced malignant pleural mesothelioma who have progressed on previous chemotherapy (VANTAGE-014): a phase 3, double-blind, randomised, placebo-controlled trial. *Lancet. Oncol.* **16,** 447–456 (2015).

118. Vandermeers, F. *et al.* Valproate, in combination with pemetrexed and cisplatin, provides additional efficacy to the treatment of malignant mesothelioma. *Clin. Cancer Res.* **15,** 2818–2828 (2009).

119. Calin, G. A. *et al.* Human microRNA genes are frequently located at fragile sites and genomic regions involved in cancers. *Proc. Natl. Acad. Sci. U. S. A.* **101,** 2999–3004 (2004).

120. Pass, H. I. *et al.* hsa-miR-29c* is linked to the prognosis of malignant pleural mesothelioma. *Cancer Res.* **70,** 1916–1924 (2010).

121. Ivanov, S. V *et al.* Pro-tumorigenic Effects of miR-31 Loss in Mesothelioma. *J. Biol. Chem.* **285,** 22809–22817 (2010).

122. Ak, G. *et al.* MicroRNA and mRNA features of malignant pleural mesothelioma and benign asbestos-related pleural effusion. *Biomed Res. Int.* **2015,** 635748 (2015).

123. Benjamin, H. *et al.* A diagnostic assay based on microRNA expression accurately identifies malignant pleural mesothelioma. *J. Mol. Diagn.* **12,** 771–779 (2010).

124. Rihn, B. H. *et al.* Differential gene expression in mesothelioma. *FEBS Lett.* **480,** 95–100 (2000).

125. Kettunen, E. *et al.* Gene expression profiling of malignant mesothelioma cell lines: cDNA array study. *Int. J. Cancer* **91,** 492–496 (2001).

126. Sandhu, H., Dehnen, W., Roller, M., Abel, J. & Unfried, K. mRNA expression patterns in different stages of asbestos-induced carcinogenesis in rats. *Carcinogenesis* **21,** 1023–1029 (2000).

127. Singhal, S. *et al.* Gene expression profiling of malignant mesothelioma. *Clin. Cancer Res.* **9,** 3080–3097 (2003).

128. Hoang, C. D. *et al.* Gene expression profiling identifies matriptase overexpression in malignant mesothelioma. *Chest* **125,** 1843–1852 (2004).

129. Mohr, S. *et al.* Microdissection, mRNA amplification and microarray: a study of pleural mesothelial and malignant mesothelioma cells. *Biochimie* **86,** 13–19 (2004).

130. Gordon, G. J. *et al.* Identification of novel candidate oncogenes and tumor suppressors in malignant pleural mesothelioma using large-scale transcriptional profiling. *Am. J. Pathol.* **166,** 1827–40 (2005).

131. Crispi, S. *et al.* Global gene expression profiling of human pleural mesotheliomas: identification of matrix metalloproteinase 14 (MMP-14) as potential tumour target. *PLoS One* **4,** e7016 (2009).

132. Røe, O. D. *et al.* Genome-wide profile of pleural mesothelioma versus parietal and visceral pleura: the emerging gene portrait of the mesothelioma phenotype. *PLoS One* **4,** e6554 (2009).

133. Røe, O. D. *et al.* Malignant pleural mesothelioma: genome-wide expression patterns reflecting general resistance mechanisms and a proposal of novel targets. *Lung Cancer* **67,** 57–68 (2010).

134. Suraokar, M. B. *et al.* Expression profiling stratifies mesothelioma tumors and signifies

deregulation of spindle checkpoint pathway and microtubule network with therapeutic implications. *Ann. Oncol.* **25,** 1184–92 (2014).

135. de Reyniès, A. *et al.* Molecular classification of malignant pleural mesothelioma: identification of a poor prognosis subgroup linked to the epithelial-to-mesenchymal transition. *Clin. Cancer Res.* **20,** 1323–34 (2014).

136. Melaiu, O. *et al.* A review of transcriptome studies combined with data mining reveals novel potential markers of malignant pleural mesothelioma. *Mutat. Res.* **750,** 132–140

137. Melaiu, O. *et al.* Expression status of candidate genes in mesothelioma tissues and cell lines. *Mutat. Res.* **771,** 6–12 (2015).

138. Pass, H. I. *et al.* Gene expression profiles predict survival and progression of pleural mesothelioma. *Clin. Cancer Res.* **10,** 849–859 (2004).

139. López-Ríos, F. *et al.* Global gene expression profiling of pleural mesotheliomas: overexpression of aurora kinases and P16/CDKN2A deletion as prognostic factors and critical evaluation of microarray-based prognostic prediction. *Cancer Res.* **66,** 2970–9 (2006).

140. Gordon, G. J. *et al.* Translation of microarray data into clinically relevant cancer diagnostic tests using gene expression ratios in lung cancer and mesothelioma. *Cancer Res.* **62,** 4963–4967 (2002).

141. Gordon, G. J. *et al.* Validation of genomics-based prognostic tests in malignant pleural mesothelioma. *Clin. Cancer Res.* **11,** 4406–4414 (2005).

142. Glinsky, G. V, Berezovska, O. & Glinskii, A. B. Microarray analysis identifies a death-from-cancer signature predicting therapy failure in patients with multiple types of cancer. *J. Clin. Invest.* **115,** 1503–21 (2005).

143. Alifrangis, C. et al. Genomic characterization and high-throughput therapeutic screening of malignant mesothelioma to reveal novel tumor dependencies. | 2013 ASCO Annual Meeting | Abstracts | Meeting Library. at <http://meetinglibrary.asco.org/content/110569-132>

144. Guo, G. *et al.* Whole-exome sequencing reveals frequent genetic alterations in BAP1, NF2, CDKN2A, and CUL1 in malignant pleural mesothelioma. *Cancer Res.* **75,** 264–269 (2015).

145. Miyanaga, A. *et al.* Hippo pathway gene mutations in malignant mesothelioma: revealed by RNA and targeted exon sequencing. *J. Thorac. Oncol.* **10,** 844–851 (2015).

146. Lo Iacono, M. *et al.* Targeted next-generation sequencing of cancer genes in advanced stage malignant pleural mesothelioma: a retrospective study. *J. Thorac. Oncol.* **10,** 492–499 (2015).

147. Shukuya, T. *et al.* Identification of actionable mutations in malignant pleural mesothelioma. *Lung Cancer* **86,** 35–40 (2014).

148. Lim, C. B. *et al.* Mutational analysis of hedgehog signaling pathway genes in human

malignant mesothelioma. *PLoS One* **8,** e66685 (2013).

149. Yoshikawa, Y. *et al.* Frequent inactivation of the BAP1 gene in epithelioid-type malignant mesothelioma. *Cancer Sci.* **103,** 868–874 (2012).

150. Ventii, K. H. *et al.* BRCA1-associated protein-1 is a tumor suppressor that requires deubiquitinating activity and nuclear localization. *Cancer Res.* **68,** 6953–6962 (2008).

151. Dey, A. *et al.* Loss of the tumor suppressor BAP1 causes myeloid transformation. *Science* **337,** 1541–1546 (2012).

152. Misaghi, S. *et al.* Association of C-terminal ubiquitin hydrolase BRCA1-associated protein 1 with cell cycle regulator host cell factor 1. *Mol. Cell. Biol.* **29,** 2181–2192 (2009).

153. Scheuermann, J. C. *et al.* Histone H2A deubiquitinase activity of the Polycomb repressive complex PR-DUB. *Nature* **465,** 243–247 (2010).

154. Okino, Y., Machida, Y., Frankland-Searby, S. & Machida, Y. J. BRCA1-associated protein 1 (BAP1) deubiquitinase antagonizes the ubiquitin-mediated activation of FoxK2 target genes. *J. Biol. Chem.* **290,** 1580–1591 (2015).

155. Sacco, J. J. *et al.* Loss of the deubiquitylase BAP1 alters class I histone deacetylase expression and sensitivity of mesothelioma cells to HDAC inhibitors. *Oncotarget* **6,** 13757–13771 (2015).

156. Zauderer, M. G. *et al.* Clinical characteristics of patients with malignant pleural mesothelioma harboring somatic BAP1 mutations. *J. Thorac. Oncol.* **8,** 1430–1433 (2013).

157. Bianchi, A. B. *et al.* High frequency of inactivating mutations in the neurofibromatosis type 2 gene (NF2) in primary malignant mesotheliomas. *Proc. Natl. Acad. Sci. U. S. A.* **92,** 10854–10858 (1995).

158. Sekido, Y. *et al.* Neurofibromatosis type 2 (NF2) gene is somatically mutated in mesothelioma but not in lung cancer. *Cancer Res.* **55,** 1227–1231 (1995).

159. Yokoyama, T. *et al.* YAP1 is involved in mesothelioma development and negatively regulated by Merlin through phosphorylation. *Carcinogenesis* **29,** 2139–2146 (2008).

160. Poulikakos, P. I. *et al.* Re-expression of the tumor suppressor NF2/merlin inhibits invasiveness in mesothelioma cells and negatively regulates FAK. *Oncogene* **25,** 5960–5968 (2006).

161. Li, W. *et al.* Merlin/NF2 suppresses tumorigenesis by inhibiting the E3 ubiquitin ligase CRL4(DCAF1) in the nucleus. *Cell* **140,** 477–490 (2010).

162. Murakami, H. *et al.* LATS2 is a tumor suppressor gene of malignant mesothelioma. *Cancer Res.* **71,** 873–883 (2011).

163. Xio, S. *et al.* Codeletion of p15 and p16 in primary malignant mesothelioma. *Oncogene* **11,** 511–515 (1995).

164. Altomare, D. A. *et al.* Losses of both products of the Cdkn2a/Arf locus contribute to asbestos-induced mesothelioma development and cooperate to accelerate tumorigenesis. *PLoS One* **6,** e18828 (2011).

165. Swain, W. A., O'Byrne, K. J. & Faux, S. P. Activation of p38 MAP kinase by asbestos in rat mesothelial cells is mediated by oxidative stress. *Am. J. Physiol. Lung Cell. Mol. Physiol.* **286,** L859–65 (2004).

166. Zhong, J. *et al.* ERK1/2 and p38 MAP kinase control MMP-2, MT1-MMP, and TIMP action and affect cell migration: a comparison between mesothelioma and mesothelial cells. *J. Cell. Physiol.* **207,** 540–552 (2006).

167. Vintman, L., Nielsen, S., Berner, A., Reich, R. & Davidson, B. Mitogen-activated protein kinase expression and activation does not differentiate benign from malignant mesothelial cells. *Cancer* **103,** 2427–2433 (2005).

168. de Melo, M., Gerbase, M. W., Curran, J. & Pache, J.-C. Phosphorylated extracellular signal-regulated kinases are significantly increased in malignant mesothelioma. *J. Histochem. Cytochem.* **54,** 855–861 (2006).

169. Shukla, A. *et al.* ERK2 is essential for the growth of human epithelioid malignant mesotheliomas. *Int. J. Cancer* **129,** 1075–1086 (2011).

170. MacDonald, B. T., Tamai, K. & He, X. Wnt/beta-catenin signaling: components, mechanisms, and diseases. *Dev. Cell* **17,** 9–26 (2009).

171. Uematsu, K. *et al.* Wnt pathway activation in mesothelioma: evidence of Dishevelled overexpression and transcriptional activity of beta-catenin. *Cancer Res.* **63,** 4547–51 (2003).

172. Mazieres, J. *et al.* Wnt2 as a new therapeutic target in malignant pleural mesothelioma. *Int. J. Cancer* **117,** 326–332 (2005).

173. Fox, S. A. *et al.* Expression profile and function of Wnt signaling mechanisms in malignant mesothelioma cells. *Biochem. Biophys. Res. Commun.* **440,** 82–7 (2013).

174. Ramos-Nino, M. E. *et al.* Human mesothelioma cells exhibit tumor cell-specific differences in phosphatidylinositol 3-kinase/AKT activity that predict the efficacy of Onconase. *Mol. Cancer Ther.* **4,** 835–842 (2005).

175. Suzuki, Y. *et al.* Activation of the PI3K-AKT pathway in human malignant mesothelioma cells. *Mol. Med. Rep.* **2,** 181–188

176. Watzka, S. B. *et al.* Integrin-linked kinase, phosphorylated AKT and the prognosis of malignant pleural mesothelioma. *Eur. J. Cardiothorac. Surg.* **39,** 180–184 (2011).

177. Opitz, I. *et al.* PTEN expression is a strong predictor of survival in mesothelioma patients. *Eur. J. Cardiothorac. Surg.* **33,** 502–506 (2008).

178. Cedrés, S. *et al.* Exploratory analysis of activation of PTEN-PI3K pathway and downstream proteins in malignant pleural mesothelioma (MPM). *Lung Cancer* **77,** 192–198 (2012).

179. Zhou, S. *et al.* Multipoint targeting of the PI3K/mTOR pathway in mesothelioma. *Br. J. Cancer* **110,** 2479–2488 (2014).

180. Betti, M. *et al.* XRCC1 and ERCC1 variants modify malignant mesothelioma risk: a case-control study. *Mutat. Res.* **708,** 11–20 (2011).

181. Shukla, A. *et al.* Blocking of ERK1 and ERK2 sensitizes human mesothelioma cells to doxorubicin. *Mol. Cancer* **9,** 314 (2010).

182. Sugarbaker, D. J. *et al.* Transcriptome sequencing of malignant pleural mesothelioma tumors. *Proc. Natl. Acad. Sci. U. S. A.* **105,** 3521–3526 (2008).

183. John D. Bancroft, M. G. D. *Theory and Practice of Histological Techniques*. at <http://www.amazon.co.uk/Theory-Practice-Histological-Techniques-Bancroft/dp/0443064350>

184. Kauffmann, A., Gentleman, R. & Huber, W. arrayQualityMetrics--a bioconductor package for quality assessment of microarray data. *Bioinformatics* **25,** 415–6 (2009).

185. Irizarry, R. A. *et al.* Exploration, normalization, and summaries of high density oligonucleotide array probe level data. *Biostatistics* **4,** 249–64 (2003).

186. Bolstad, B. M., Irizarry, R. A., Astrand, M. & Speed, T. P. A comparison of normalization methods for high density oligonucleotide array data based on variance and bias. *Bioinformatics* **19,** 185–93 (2003).

187. Pierre R. Bushel, J. L. Estimating batch effect in Microarray data with Principal Variance Component Analysis (PVCA) method. at <http://docplayer.net/241890-Estimating-batch-effect-in-microarray-data-with-principal-variance-component-analysis-pvca-method.html>

188. Smyth, G. K. Linear models and empirical bayes methods for assessing differential expression in microarray experiments. *Stat. Appl. Genet. Mol. Biol.* **3,** Article3 (2004).

189. Yoav Benjamini and Yosef Hochberg. Controlling the False Discovery Rate: A Practical and Powerful Approach to Multiple Testing. at <http://www.jstor.org/stable/2346101?seq=1#page_scan_tab_contents>

190. Zhang, B., Kirov, S. & Snoddy, J. WebGestalt: an integrated system for exploring gene sets in various biological contexts. *Nucleic Acids Res.* **33,** W741–8 (2005).

191. Langfelder, P. & Horvath, S. WGCNA: an R package for weighted correlation network analysis. *BMC Bioinformatics* **9,** 559 (2008).

192. Bindea, G., Galon, J. & Mlecnik, B. CluePedia Cytoscape plugin: pathway insights using integrated experimental and in silico data. *Bioinformatics* **29,** 661–3 (2013).

193. Bentley, D. R. *et al.* Accurate whole human genome sequencing using reversible terminator chemistry. *Nature* **456,** 53–9 (2008).

194. Li, H. & Durbin, R. Fast and accurate short read alignment with Burrows-Wheeler transform. *Bioinformatics* **25,** 1754–60 (2009).

195. Picard tools. Picard Tools. at <http://broadinstitute.github.io/picard/>

196. DePristo, M. A. *et al.* A framework for variation discovery and genotyping using next-generation DNA sequencing data. *Nat. Genet.* **43,** 491–8 (2011).

197. Wang, K., Li, M. & Hakonarson, H. ANNOVAR: functional annotation of genetic variants from high-throughput sequencing data. *Nucleic Acids Res.* **38,** e164 (2010).

198. Xia, J., Benner, M. J. & Hancock, R. E. W. NetworkAnalyst--integrative approaches for protein-protein interaction network analysis and visual exploration. *Nucleic Acids Res.* **42,** W167–74 (2014).

199. Sanger, F., Nicklen, S. & Coulson, A. R. DNA sequencing with chain-terminating inhibitors. *Proc. Natl. Acad. Sci. U. S. A.* **74,** 5463–7 (1977).

200. Golub, T. R. *et al.* Molecular classification of cancer: class discovery and class prediction by gene expression monitoring. *Science* **286,** 531–7 (1999).

201. Perou, C. M. *et al.* Molecular portraits of human breast tumours. *Nature* **406,** 747–52 (2000).

202. Alizadeh, A. A. *et al.* Distinct types of diffuse large B-cell lymphoma identified by gene expression profiling. *Nature* **403,** 503–11 (2000).

203. Langfelder, P. & Horvath, S. WGCNA: an R package for weighted correlation network analysis. *BMC Bioinformatics* **9,** 559 (2008).

204. Horvath, S. *et al.* Analysis of oncogenic signaling networks in glioblastoma identifies ASPM as a molecular target. *Proc. Natl. Acad. Sci. U. S. A.* **103,** 17402–7 (2006).

205. Wang, J., Duncan, D., Shi, Z. & Zhang, B. WEB-based GEne SeT AnaLysis Toolkit (WebGestalt): update 2013. *Nucleic Acids Res.* **41,** W77–83 (2013).

206. Washimi, K. *et al.* Specific expression of human intelectin-1 in malignant pleural mesothelioma and gastrointestinal goblet cells. *PLoS One* **7,** e39889 (2012).

207. Tsuji, S. *et al.* Secretion of intelectin-1 from malignant pleural mesothelioma into pleural effusion. *Br. J. Cancer* **103,** 517–23 (2010).

208. Wali, A. *et al.* Identification of intelectin overexpression in malignant pleural mesothelioma by serial analysis of gene expression (SAGE). *Lung Cancer* **48,** 19–29 (2005).

209. Wali, A. *et al.* Intelectin overexpression causes chromosomal aberrations in immortalized human mesothelial cells. *Cancer Res.* **66,** 600–c– (2006).

210. Ordóñez, N. G. The immunohistochemical diagnosis of mesothelioma: a comparative study of epithelioid mesothelioma and lung adenocarcinoma. *Am. J. Surg. Pathol.* **27,** 1031–51 (2003).

211. Gander, J. C., Gotzos, V., Fellay, B. & Schwaller, B. Inhibition of the proliferative cycle and apoptotic events in WiDr cells after down-regulation of the calcium-binding

protein calretinin using antisense oligodeoxynucleotides. *Exp. Cell Res.* **225,** 399–410 (1996).

212. Blum, W. & Schwaller, B. Calretinin is essential for mesothelioma cell growth/survival in vitro: a potential new target for malignant mesothelioma therapy? *Int. J. cancer* **133,** 2077–2088 (2013).

213. Kanamori-Katayama, M. *et al.* LRRN4 and UPK3B are markers of primary mesothelial cells. *PLoS One* **6,** e25391 (2011).

214. Simon, B. A. *et al.* Microarray analysis of regional cellular responses to local mechanical stress in acute lung injury. *Am. J. Physiol. Lung Cell. Mol. Physiol.* **291,** L851–61 (2006).

215. Morris, M. R. *et al.* Identification of candidate tumour suppressor genes frequently methylated in renal cell carcinoma. *Oncogene* **29,** 2104–17 (2010).

216. Guo, L. *et al.* Selection of brain metastasis-initiating breast cancer cells determined by growth on hard agar. *Am. J. Pathol.* **178,** 2357–66 (2011).

217. Boldrup, L., Coates, P. J., Laurell, G. & Nylander, K. p63 Transcriptionally regulates BNC1, a Pol I and Pol II transcription factor that regulates ribosomal biogenesis and epithelial differentiation. *Eur. J. Cancer* **48,** 1401–6 (2012).

218. Feuerborn, A., Mathow, D., Srivastava, P. K., Gretz, N. & Gröne, H.-J. Basonuclin-1 modulates epithelial plasticity and TGF-β1-induced loss of epithelial cell integrity. *Oncogene* **34,** 1185–95 (2015).

219. Fujii, M. *et al.* TGF-β synergizes with defects in the Hippo pathway to stimulate human malignant mesothelioma growth. *J. Exp. Med.* **209,** 479–94 (2012).

220. Casarsa, C. *et al.* Epithelial-to-mesenchymal transition, cell polarity and stemness-associated features in malignant pleural mesothelioma. *Cancer Lett.* **302,** 136–43 (2011).

221. Romagnoli, S. *et al.* Identification of potential therapeutic targets in malignant mesothelioma using cell-cycle gene expression analysis. *Am. J. Pathol.* **174,** 762–70 (2009).

222. Crispi, S. *et al.* Global gene expression profiling of human pleural mesotheliomas: identification of matrix metalloproteinase 14 (MMP-14) as potential tumour target. *PLoS One* **4,** e7016 (2009).

223. Cahill, D. P. *et al.* Mutations of mitotic checkpoint genes in human cancers. *Nature* **392,** 300–3 (1998).

224. Scintu, M. *et al.* Genomic instability and increased expression of BUB1B and MAD2L1 genes in ductal breast carcinoma. *Cancer Lett.* **254,** 298–307 (2007).

225. Bartkova, J. *et al.* Oncogene-induced senescence is part of the tumorigenesis barrier imposed by DNA damage checkpoints. *Nature* **444,** 633–7 (2006).

226. Pelin-Enlund, K. *et al.* Asbestos-related malignant mesothelioma: growth, cytology, tumorigenicity and consistent chromosome findings in cell lines from five patients. *Carcinogenesis* **11,** 673–81 (1990).

227. Cardozo, T. & Pagano, M. The SCF ubiquitin ligase: insights into a molecular machine. *Nat. Rev. Mol. Cell Biol.* **5,** 739–51 (2004).

228. Huang, H. *et al.* Skp2 inhibits FOXO1 in tumor suppression through ubiquitin-mediated degradation. *Proc. Natl. Acad. Sci. U. S. A.* **102,** 1649–54 (2005).

229. Song, M. S. *et al.* Skp2 regulates the antiproliferative function of the tumor suppressor RASSF1A via ubiquitin-mediated degradation at the G1-S transition. *Oncogene* **27,** 3176–3185 (2007).

230. Yano, H. *et al.* Roles played by a subset of integrin signaling molecules in cadherin-based cell-cell adhesion. *J. Cell Biol.* **166,** 283–95 (2004).

231. Zhou, B. *et al.* Integrin α3β1 can function to promote spontaneous metastasis and lung colonization of invasive breast carcinoma. *Mol. Cancer Res.* **12,** 143–54 (2014).

232. Gonzales, M. *et al.* A cell signal pathway involving laminin-5, alpha3beta1 integrin, and mitogen-activated protein kinase can regulate epithelial cell proliferation. *Mol. Biol. Cell* **10,** 259–70 (1999).

233. Masugi, Y. *et al.* Upregulation of integrin β4 promotes epithelial-mesenchymal transition and is a novel prognostic marker in pancreatic ductal adenocarcinoma. *Lab. Invest.* **95,** 308–19 (2015).

234. Schenk, S. *et al.* Binding to EGF receptor of a laminin-5 EGF-like fragment liberated during MMP-dependent mammary gland involution. *J. Cell Biol.* **161,** 197–209 (2003).

235. Ritié, L. *et al.* Abnormal Wnt and PI3Kinase signaling in the malformed intestine of lama5 deficient mice. *PLoS One* **7,** e37710 (2012).

236. Dickson, B. J. Molecular mechanisms of axon guidance. *Science* **298,** 1959–64 (2002).

237. Biankin, A. V *et al.* Pancreatic cancer genomes reveal aberrations in axon guidance pathway genes. *Nature* **491,** 399–405 (2012).

238. Parri, M. *et al.* EphrinA1 activates a Src/focal adhesion kinase-mediated motility response leading to rho-dependent actino/myosin contractility. *J. Biol. Chem.* **282,** 19619–28 (2007).

239. Ng, T. *et al.* Class 3 semaphorin mediates dendrite growth in adult newborn neurons through Cdk5/FAK pathway. *PLoS One* **8,** e65572 (2013).

240. Cui, X.-D. *et al.* EFNA1 ligand and its receptor EphA2: potential biomarkers for hepatocellular carcinoma. *Int. J. cancer* **126,** 940–949 (2010).

241. Iida, H. *et al.* Ephrin-A1 expression contributes to the malignant characteristics of {alpha}-fetoprotein producing hepatocellular carcinoma. *Gut* **54,** 843–51 (2005).

242. Campbell, T. N., Attwell, S., Arcellana-Panlilio, M. & Robbins, S. M. Ephrin A5 expression promotes invasion and transformation of murine fibroblasts. *Biochem. Biophys. Res. Commun.* **350,** 623–8 (2006).

243. Miyato, H., Tsuno, N. H. & Kitayama, J. Semaphorin 3C is involved in the progression of gastric cancer. *Cancer Sci.* **103,** 1961–6 (2012).

244. Worzfeld, T. *et al.* ErbB-2 signals through Plexin-B1 to promote breast cancer metastasis. *J. Clin. Invest.* **122,** 1296–305 (2012).

245. Crepaldi, T., Gautreau, A., Comoglio, P. M., Louvard, D. & Arpin, M. Ezrin is an effector of hepatocyte growth factor-mediated migration and morphogenesis in epithelial cells. *J. Cell Biol.* **138,** 423–34 (1997).

246. Gautreau, A., Poullet, P., Louvard, D. & Arpin, M. Ezrin, a plasma membrane-microfilament linker, signals cell survival through the phosphatidylinositol 3-kinase/Akt pathway. *Proc. Natl. Acad. Sci.* **96,** 7300–7305 (1999).

247. Poullet, P. *et al.* Ezrin interacts with focal adhesion kinase and induces its activation independently of cell-matrix adhesion. *J. Biol. Chem.* **276,** 37686–91 (2001).

248. Gest, C. *et al.* Rac3 induces a molecular pathway triggering breast cancer cell aggressiveness: differences in MDA-MB-231 and MCF-7 breast cancer cell lines. *BMC Cancer* **13,** 63 (2013).

249. Abo, A. *et al.* PAK4, a novel effector for Cdc42Hs, is implicated in the reorganization of the actin cytoskeleton and in the formation of filopodia. *EMBO J.* **17,** 6527–40 (1998).

250. Callow, M. G. *et al.* Requirement for PAK4 in the anchorage-independent growth of human cancer cell lines. *J. Biol. Chem.* **277,** 550–8 (2002).

251. Christ, A. *et al.* LRP2 is an auxiliary SHH receptor required to condition the forebrain ventral midline for inductive signals. *Dev. Cell* **22,** 268–78 (2012).

252. You, L. *et al.* Inhibition of Wnt-1 signaling induces apoptosis in beta-catenin-deficient mesothelioma cells. *Cancer Res.* **64,** 3474–8 (2004).

253. He, B. *et al.* A monoclonal antibody against Wnt-1 induces apoptosis in human cancer cells. *Neoplasia* **6,** 7–14

254. Roberts, D. J. *et al.* Sonic hedgehog is an endodermal signal inducing Bmp-4 and Hox genes during induction and regionalization of the chick hindgut. *Development* **121,** 3163–74 (1995).

255. Dai, J. *et al.* Prostate cancer induces bone metastasis through Wnt-induced bone morphogenetic protein-dependent and independent mechanisms. *Cancer Res.* **68,** 5785–94 (2008).

256. Kallioniemi, A. Bone morphogenetic protein 4-a fascinating regulator of cancer cell behavior. *Cancer Genet.* **205,** 267–77 (2012).

257. Tasneem, S. *et al.* Platelet adhesion to multimerin 1 in vitro: influences of platelet membrane receptors, von Willebrand factor and shear. *J. Thromb. Haemost.* **7,** 685–92 (2009).

258. Jeimy, S. B., Tasneem, S., Cramer, E. M. & Hayward, C. P. M. Multimerin 1. *Platelets* **19,** 83–95 (2008).

259. Souza-Rodrígues, E. *et al.* Proteomic analysis of p16ink4a-binding proteins. *Proteomics* **7,** 4102–11 (2007).

260. Mira Krendel, M. S. M. Myosins: Tails (and Heads) of Functional Diversity. at <http://bio.fsu.edu/~moerland/5334.pdf>

261. Post, P. L., Bokoch, G. M. & Mooseker, M. S. Human myosin-IXb is a mechanochemically active motor and a GAP for rho. *J. Cell Sci.* **111 ( Pt 7,** 941–50 (1998).

262. Puthalakath, H. *et al.* Bmf: a proapoptotic BH3-only protein regulated by interaction with the myosin V actin motor complex, activated by anoikis. *Science* **293,** 1829–32 (2001).

263. Seitz, S. *et al.* Genetic background of different cancer cell lines influences the gene set involved in chromosome 8 mediated breast tumor suppression. *Genes. Chromosomes Cancer* **45,** 612–27 (2006).

264. Lee, W.-S. *et al.* Identification of differentially expressed genes in microsatellite stable HNPCC and sporadic colon cancer. *J. Surg. Res.* **144,** 29–35 (2008).

265. Wang, R.-J. *et al.* Down-regulated MYH11 Expression Correlates with Poor Prognosis in Stage II and III Colorectal Cancer. *Asian Pacific J. Cancer Prev.* **15,** 7223–7228 (2014).

266. Clark, R. A. *et al.* Human squamous cell carcinomas evade the immune response by down-regulation of vascular E-selectin and recruitment of regulatory T cells. *J. Exp. Med.* **205,** 2221–34 (2008).

267. Broomfield, S. A. *et al.* Locally administered TLR7 agonists drive systemic antitumor immune responses that are enhanced by anti-CD40 immunotherapy. *J. Immunol.* **182,** 5217–24 (2009).

268. Currie, A. J. *et al.* Targeting the effector site with IFN-alphabeta-inducing TLR ligands reactivates tumor-resident CD8 T cell responses to eradicate established solid tumors. *J. Immunol.* **180,** 1535–44 (2008).

269. Butcher, E. C. & Picker, L. J. Lymphocyte homing and homeostasis. *Science* **272,** 60–6 (1996).

270. Galkina, E. *et al.* L-Selectin Shedding Does Not Regulate Constitutive T Cell Trafficking but Controls the Migration Pathways of Antigen-activated T Lymphocytes. *J. Exp. Med.* **198,** 1323–1335 (2003).

271. Maltby, S. *et al.* Opposing roles for CD34 in B16 melanoma tumor growth alter early

stage vasculature and late stage immune cell infiltration. *PLoS One* **6,** e18160 (2011).

272. Bixel, G. *et al.* Mouse CD99 participates in T-cell recruitment into inflamed skin. *Blood* **104,** 3205–13 (2004).

273. Edlund, K. *et al.* CD99 is a novel prognostic stromal marker in non-small cell lung cancer. *Int. J. Cancer* **131,** 2264–73 (2012).

274. Carpenito, C., Pyszniak, A. M. & Takei, F. ICAM-2 provides a costimulatory signal for T cell stimulation by allogeneic class II MHC. *Scand. J. Immunol.* **45,** 248–54 (1997).

275. Tanaka, H. *et al.* ICAM-2 gene therapy for peritoneal dissemination of scirrhous gastric carcinoma. *Clin. Cancer Res.* **10,** 4885–92 (2004).

276. Cangara, H. M. *et al.* Role of endothelial cell-selective adhesion molecule in hematogeneous metastasis. *Microvasc. Res.* **80,** 133–41 (2010).

277. Wegmann, F. *et al.* ESAM supports neutrophil extravasation, activation of Rho, and VEGF-induced vascular permeability. *J. Exp. Med.* **203,** 1671–7 (2006).

278. Vonderheide, R. H. Prospect of targeting the CD40 pathway for cancer therapy. *Clin. Cancer Res.* **13,** 1083–8 (2007).

279. Jackaman, C., Cornwall, S., Graham, P. T. & Nelson, D. J. CD40-activated B cells contribute to mesothelioma tumor regression. *Immunol. Cell Biol.* **89,** 255–67 (2011).

280. Saunders, A. E. & Johnson, P. Modulation of immune cell signalling by the leukocyte common tyrosine phosphatase, CD45. *Cell. Signal.* **22,** 339–48 (2010).

281. Poe, J. C., Minard-Colin, V., Kountikov, E. I., Haas, K. M. & Tedder, T. F. A c-Myc and surface CD19 signaling amplification loop promotes B cell lymphoma development and progression in mice. *J. Immunol.* **189,** 2318–25 (2012).

282. Rochman, Y., Spolski, R. & Leonard, W. J. New insights into the regulation of T cells by gamma(c) family cytokines. *Nat. Rev. Immunol.* **9,** 480–90 (2009).

283. Bissonnette, E., Carré, B., Dubois, C. & Rola-Pleszczynski, M. Inhibition of alveolar macrophage cytotoxicity by asbestos: possible role of prostaglandins. *J. Leukoc. Biol.* **47,** 129–34 (1990).

284. Kolenko, V. *et al.* Downregulation of JAK3 protein levels in T lymphocytes by prostaglandin E2 and other cyclic adenosine monophosphate-elevating agents: impact on interleukin-2 receptor signaling pathway. *Blood* **93,** 2308–18 (1999).

285. Lowenthal, J. W., Zubler, R. H., Nabholz, M. & MacDonald, H. R. Similarities between interleukin-2 receptor number and affinity on activated B and T lymphocytes. *Nature* **315,** 669–672 (1985).

286. Ebert, E. C., Roberts, A. I., Devereux, D. & Nagase, H. Selective immunosuppressive action of a factor produced by colon cancer cells. *Cancer Res.* **50,** 6158–61 (1990).

287. Wu, Y. Z. *et al.* Mechanisms mediating the effects of IL-3 gene expression on tumor

growth. *J. Leukoc. Biol.* **68,** 890–6 (2000).

288. Hinrichs, C. S. *et al.* IL-2 and IL-21 confer opposing differentiation programs to CD8+ T cells for adoptive immunotherapy. *Blood* **111,** 5326–33 (2008).

289. Santegoets, S. J., Turksma, A. W., Powell Jr, D. J., Hooijberg, E. & de Gruijl, T. D. IL-21 in cancer immunotherapy: At the right place at the right time. *Oncoimmunology* **2,** e24522 (2013).

290. Ceeraz, S., Nowak, E. C. & Noelle, R. J. B7 family checkpoint regulators in immune regulation and disease. *Trends Immunol.* **34,** 556–63 (2013).

291. Tsukishiro, T., Donnenberg, A. D. & Whiteside, T. L. Rapid turnover of the CD8(+)CD28(-) T-cell subset of effector cells in the circulation of patients with head and neck cancer. *Cancer Immunol. Immunother.* **52,** 599–607 (2003).

292. Lee, Y. S., Kim, S. H., Cho, J. A. & Kim, C. W. Introduction of the CIITA gene into tumor cells produces exosomes with enhanced anti-tumor effects. *Exp Mol Med* **43,** 281–290 (2011).

293. Hipkiss, A. R. Could carnosine or related structures suppress Alzheimer's disease? *J. Alzheimers. Dis.* **11,** 229–40 (2007).

294. Renner, C. *et al.* Carnosine inhibits ATP production in cells from malignant glioma. *Neurol. Res.* **32,** 101–5 (2010).

295. Renner, C. *et al.* Carnosine retards tumor growth in vivo in an NIH3T3-HER2/neu mouse model. *Mol. Cancer* **9,** 2 (2010).

296. Beltran, A. S. *et al.* Suppression of breast tumor growth and metastasis by an engineered transcription factor. *PLoS One* **6,** e24595 (2011).

297. Soini, Y., Kinnula, V., Kahlos, K. & Pääkkö, P. Claudins in differential diagnosis between mesothelioma and metastatic adenocarcinoma of the pleura. *J. Clin. Pathol.* **59,** 250–4 (2006).

298. Meunier, D., Peters, T., Lüttges, A., Curfs, J. & Fundele, R. Preferential expression of the G90 gene in post-mitotic cells during mouse embryonic development. *Anat. Embryol. (Berl).* **207,** 109–17 (2003).

299. Meunier, D. *et al.* Expression analysis of proline rich 15 (Prr15) in mouse and human gastrointestinal tumors. *Mol. Carcinog.* **50,** 8–15 (2011).

300. Lammer, F. *et al.* Next Generation RNA Sequencing of Acute Promyelocytic Leukemia (APL) Identifies Novel Long Non Coding RNAs Including New Variants of MIR181A1HG That Are Differentially Expressed during Myeloid Differentiation. *Blood* **124,** 1031 (2014).

301. Sakwe, A. M., Koumangoye, R., Guillory, B. & Ochieng, J. Annexin A6 contributes to the invasiveness of breast carcinoma cells by influencing the organization and localization of functional focal adhesions. *Exp. Cell Res.* **317,** 823–37 (2011).

302. Campbell, K. A. *et al.* Annexin A6 interacts with p65 and stimulates NF-κB activity and catabolic events in articular chondrocytes. *Arthritis Rheum.* **65,** 3120–9 (2013).

303. Bevitt, D. J. *et al.* Expression of ADAMTS metalloproteinases in the retinal pigment epithelium derived cell line ARPE-19: transcriptional regulation by TNFα. *Biochim. Biophys. Acta - Gene Struct. Expr.* **1626,** 83–91 (2003).

304. Wildeboer, D., Naus, S., Amy Sang, Q.-X., Bartsch, J. W. & Pagenstecher, A. Metalloproteinase disintegrins ADAM8 and ADAM19 are highly regulated in human primary brain tumors and their expression levels and activities are associated with invasiveness. *J. Neuropathol. Exp. Neurol.* **65,** 516–27 (2006).

305. Chan, M. W. *et al.* Aberrant transforming growth factor beta1 signaling and SMAD4 nuclear translocation confer epigenetic repression of ADAM19 in ovarian cancer. *Neoplasia* **10,** 908–19 (2008).

306. Laliberté, J., Yee, A., Xiong, Y. & Mitchell, B. S. Effects of guanine nucleotide depletion on cell cycle progression in human T lymphocytes. *Blood* **91,** 2896–904 (1998).

307. Shu, Q. & Nair, V. Inosine monophosphate dehydrogenase (IMPDH) as a target in drug discovery. *Med. Res. Rev.* **28,** 219–32 (2008).

308. Luo, X., Huang, Y. & Sheikh, M. S. Cloning and characterization of a novel gene PDRG that is differentially regulated by p53 and ultraviolet radiation. *Oncogene* **22,** 7247–57 (2003).

309. Zacharatos, P. *et al.* Distinct expression patterns of the transcription factor E2F-1 in relation to tumour growth parameters in common human carcinomas. *J. Pathol.* **203,** 744–53 (2004).

310. Lam, S.-K., Li, Y.-Y., Zheng, C.-Y. & Ho, J. C.-M. Downregulation of thymidylate synthase and E2F1 by arsenic trioxide in mesothelioma. *Int. J. Oncol.* **46,** 113–22 (2015).

311. Guo, Y. *et al.* Tim50, a component of the mitochondrial translocator, regulates mitochondrial integrity and cell death. *J. Biol. Chem.* **279,** 24813–25 (2004).

312. Peters, J.-M. The anaphase promoting complex/cyclosome: a machine designed to destroy. *Nat. Rev. Mol. Cell Biol.* **7,** 644–656 (2006).

313. Kawashima, S. A., Yamagishi, Y., Honda, T., Ishiguro, K. & Watanabe, Y. Phosphorylation of H2A by Bub1 prevents chromosomal instability through localizing shugoshin. *Science* **327,** 172–7 (2010).

314. Kahyo, T. *et al.* A novel tumor-derived SGOL1 variant causes abnormal mitosis and unstable chromatid cohesion. *Oncogene* **30,** 4453–63 (2011).

315. Matsuura, S. *et al.* SGOL1 variant B induces abnormal mitosis and resistance to taxane in non-small cell lung cancers. *Sci. Rep.* **3,** (2013).

316. Hayama, S. *et al.* Phosphorylation and activation of cell division cycle associated 8 by

aurora kinase B plays a significant role in human lung carcinogenesis. *Cancer Res.* **67,** 4113–22 (2007).

317. Deng, S. *et al.* Over-expression of genes and proteins of ubiquitin specific peptidases (USPs) and proteasome subunits (PSs) in breast cancer tissue observed by the methods of RFDD-PCR and proteomics. *Breast Cancer Res. Treat.* **104,** 21–30 (2007).

318. Kimura, F. *et al.* Differential diagnosis of reactive mesothelial cells and malignant mesothelioma cells using the cell proliferation markers minichromosome maintenance protein 7, geminin, topoisomerase II alpha and Ki-67. *Acta Cytol.* **57,** 384–90 (2013).

319. Landen, C. N., Birrer, M. J. & Sood, A. K. Early events in the pathogenesis of epithelial ovarian cancer. *J. Clin. Oncol.* **26,** 995–1005 (2008).

320. Bredel, M. *et al.* A network model of a cooperative genetic landscape in brain tumors. *JAMA* **302,** 261–75 (2009).

321. Mac, S. M., D'Cunha, C. A. & Farnham, P. J. Direct recruitment of N-myc to target gene promoters. *Mol. Carcinog.* **29,** 76–86 (2000).

322. Oliver, T. G. *et al.* Transcriptional profiling of the Sonic hedgehog response: a critical role for N-myc in proliferation of neuronal precursors. *Proc. Natl. Acad. Sci. U. S. A.* **100,** 7331–6 (2003).

323. Spurgers, K. B. *et al.* Identification of cell cycle regulatory genes as principal targets of p53-mediated transcriptional repression. *J. Biol. Chem.* **281,** 25134–42 (2006).

324. Vernell, R., Helin, K. & Müller, H. Identification of target genes of the p16INK4A-pRB-E2F pathway. *J. Biol. Chem.* **278,** 46124–37 (2003).

325. Ren, B. *et al.* E2F integrates cell cycle progression with DNA repair, replication, and G(2)/M checkpoints. *Genes Dev.* **16,** 245–56 (2002).

326. Arrossi, A. V, Lin, E., Rice, D. & Moran, C. A. Histologic assessment and prognostic factors of malignant pleural mesothelioma treated with extrapleural pneumonectomy. *Am. J. Clin. Pathol.* **130,** 754–64 (2008).

327. Weigelt, B. *et al.* Molecular portraits and 70-gene prognosis signature are preserved throughout the metastatic process of breast cancer. *Cancer Res.* **65,** 9155–8 (2005).

328. Sekido, Y. Genomic abnormalities and signal transduction dysregulation in malignant mesothelioma cells. *Cancer Sci.* **101,** 1–6 (2010).

329. Morris, M. A., Young, L. S. & Dawson, C. W. DNA tumour viruses promote tumour cell invasion and metastasis by deregulating the normal processes of cell adhesion and motility. *Eur. J. Cell Biol.* **87,** 677–97 (2008).

330. Hauck, C. R. *et al.* Inhibition of focal adhesion kinase expression or activity disrupts epidermal growth factor-stimulated signaling promoting the migration of invasive human carcinoma cells. *Cancer Res.* **61,** 7079–90 (2001).

331. Hunger-Glaser, I., Fan, R. S., Perez-Salazar, E. & Rozengurt, E. PDGF and FGF induce

focal adhesion kinase (FAK) phosphorylation at Ser-910: dissociation from Tyr-397 phosphorylation and requirement for ERK activation. *J. Cell. Physiol.* **200,** 213–22 (2004).

332. Garcia, S. *et al.* Overexpression of c-Met and of the transducers PI3K, FAK and JAK in breast carcinomas correlates with shorter survival and neoangiogenesis. *Int. J. Oncol.* **31,** 49–58 (2007).

333. Zoltan-Jones, A., Huang, L., Ghatak, S. & Toole, B. P. Elevated hyaluronan production induces mesenchymal and transformed properties in epithelial cells. *J. Biol. Chem.* **278,** 45801–10 (2003).

334. Shi, Y. *et al.* Role of hedgehog signaling in malignant pleural mesothelioma. *Clin. Cancer Res.* **18,** 4646–56 (2012).

335. Chen, J.-S. *et al.* Sonic hedgehog signaling pathway induces cell migration and invasion through focal adhesion kinase/AKT signaling-mediated activation of matrix metalloproteinase (MMP)-2 and MMP-9 in liver cancer. *Carcinogenesis* **34,** 10–9 (2013).

336. Fonar, Y. *et al.* Focal adhesion kinase protein regulates Wnt3a gene expression to control cell fate specification in the developing neural plate. *Mol. Biol. Cell* **22,** 2409–21 (2011).

337. Zhao, J. & Guan, J.-L. Signal transduction by focal adhesion kinase in cancer. *Cancer Metastasis Rev.* **28,** 35–49 (2009).

338. Canel, M. *et al.* Overexpression of focal adhesion kinase in head and neck squamous cell carcinoma is independent of fak gene copy number. *Clin. Cancer Res.* **12,** 3272–9 (2006).

339. Li, W., Cooper, J., Karajannis, M. A. & Giancotti, F. G. Merlin: a tumour suppressor with functions at the cell cortex and in the nucleus. *EMBO Rep.* **13,** 204–15 (2012).

340. Shapiro, I. M. *et al.* Merlin deficiency predicts FAK inhibitor sensitivity: a synthetic lethal relationship. *Sci. Transl. Med.* **6,** 237ra68 (2014).

341. Soria, J. C. *et al.* 610 Loss of the Tumor Suppressor Merlin as a Potential Predictive Biomarker of Clinical Activity for the Oral, Focal Adhesion Kinase (FAK) Inhibitor GSK2256098 in Pts with Recurrent Mesothelioma. *Eur. J. Cancer* **48,** 188 (2016).

342. Dranoff, G. Cytokines in cancer pathogenesis and cancer therapy. *Nat. Rev. Cancer* **4,** 11–22 (2004).

343. Robinson, B. W., Robinson, C. & Lake, R. A. Localised spontaneous regression in mesothelioma -- possible immunological mechanism. *Lung Cancer* **32,** 197–201 (2001).

344. Anraku, M. *et al.* Impact of tumor-infiltrating T cells on survival in patients with malignant pleural mesothelioma. *J. Thorac. Cardiovasc. Surg.* **135,** 823–9 (2008).

345. Yamada, N. *et al.* CD8+ tumor-infiltrating lymphocytes predict favorable prognosis in

malignant pleural mesothelioma after resection. *Cancer Immunol. Immunother.* **59,** 1543–9 (2010).

346. Wu, L., Yun, Z., Tagawa, T., Rey-McIntyre, K. & de Perrot, M. CTLA-4 blockade expands infiltrating T cells and inhibits cancer cell repopulation during the intervals of chemotherapy in murine mesothelioma. *Mol. Cancer Ther.* **11,** 1809–1819 (2012).

347. Calabrò, L. *et al.* Tremelimumab for patients with chemotherapy-resistant advanced malignant mesothelioma: an open-label, single-arm, phase 2 trial. *Lancet. Oncol.* **14,** 1104–1111 (2013).

348. Alley, E. W. *et al.* Abstract CT103: Clinical safety and efficacy of pembrolizumab (MK-3475) in patients with malignant pleural mesothelioma: Preliminary results from KEYNOTE-028. *Cancer Res.* **75,** CT103–CT103 (2015).

349. Clarke, C. *et al.* Correlating transcriptional networks to breast cancer survival: a large-scale coexpression analysis. *Carcinogenesis* **34,** 2300–8 (2013).

350. Moses, H. L. TGF-beta regulation of epithelial cell proliferation. *Mol. Reprod. Dev.* **32,** 179–84 (1992).

351. Miettinen, P. J., Ebner, R., Lopez, A. R. & Derynck, R. TGF-beta induced transdifferentiation of mammary epithelial cells to mesenchymal cells: involvement of type I receptors. *J. Cell Biol.* **127,** 2021–36 (1994).

352. Piek, E., Moustakas, A., Kurisaki, A., Heldin, C. H. & ten Dijke, P. TGF-(beta) type I receptor/ALK-5 and Smad proteins mediate epithelial to mesenchymal transdifferentiation in NMuMG breast epithelial cells. *J. Cell Sci.* **112 ( Pt 2,** 4557–68 (1999).

353. Valcourt, U., Kowanetz, M., Niimi, H., Heldin, C.-H. & Moustakas, A. TGF-beta and the Smad signaling pathway support transcriptomic reprogramming during epithelial-mesenchymal cell transition. *Mol. Biol. Cell* **16,** 1987–2002 (2005).

354. Bhowmick, N. A., Zent, R., Ghiassi, M., McDonnell, M. & Moses, H. L. Integrin beta 1 signaling is necessary for transforming growth factor-beta activation of p38MAPK and epithelial plasticity. *J. Biol. Chem.* **276,** 46707–13 (2001).

355. Bhowmick, N. A. *et al.* Transforming growth factor-beta1 mediates epithelial to mesenchymal transdifferentiation through a RhoA-dependent mechanism. *Mol. Biol. Cell* **12,** 27–36 (2001).

356. Nieto, M. A. The snail superfamily of zinc-finger transcription factors. *Nat. Rev. Mol. Cell Biol.* **3,** 155–66 (2002).

357. Yang, J. *et al.* Twist, a master regulator of morphogenesis, plays an essential role in tumor metastasis. *Cell* **117,** 927–39 (2004).

358. Medici, D., Hay, E. D. & Olsen, B. R. Snail and Slug promote epithelial-mesenchymal transition through beta-catenin-T-cell factor-4-dependent expression of transforming growth factor-beta3. *Mol. Biol. Cell* **19,** 4875–87 (2008).

359. Pardali, K. & Moustakas, A. Actions of TGF-beta as tumor suppressor and pro-metastatic factor in human cancer. *Biochim. Biophys. Acta* **1775,** 21–62 (2007).

360. Fassina, A. *et al.* Epithelial-mesenchymal transition in malignant mesothelioma. *Mod. Pathol.* **25,** 86–99 (2012).

361. Crispi, S. *et al.* Antiproliferative effect of Aurora kinase targeting in mesothelioma. *Lung Cancer* **70,** 271–9 (2010).

362. Lander, E. S. Array of hope. *Nat. Genet.* **21,** 3–4 (1999).

363. Garraway, L. A. & Lander, E. S. Lessons from the cancer genome. *Cell* **153,** 17–37 (2013).

364. Jean, D., Daubriac, J., Le Pimpec-Barthes, F., Galateau-Salle, F. & Jaurand, M.-C. Molecular changes in mesothelioma with an impact on prognosis and treatment. *Arch. Pathol. Lab. Med.* **136,** 277–293 (2012).

365. Yoshikawa, Y. *et al.* Biallelic germline and somatic mutations in malignant mesothelioma: Multiple mutations in transcription regulators including mSWI/SNF genes. *Int. J. Cancer* **136,** n/a–n/a (2014).

366. E.6 Quality Standards of Samples. at <https://icgc.org/icgc/goals-structure-policies-guidelines/e6-quality-standards-of-samples>

367. Lee, W. *et al.* The mutation spectrum revealed by paired genome sequences from a lung cancer patient. *Nature* **465,** 473–477 (2010).

368. Pleasance, E. D. *et al.* A small-cell lung cancer genome with complex signatures of tobacco exposure. *Nature* **463,** 184–190 (2010).

369. Vogelstein, B. *et al.* Cancer genome landscapes. *Science* **339,** 1546–1558 (2013).

370. Valque, H., Gouyer, V., Gottrand, F. & Desseyn, J.-L. MUC5B leads to aggressive behavior of breast cancer MCF7 cells. *PLoS One* **7,** e46699 (2012).

371. Servais, E. L. *et al.* Mesothelin overexpression promotes mesothelioma cell invasion and MMP-9 secretion in an orthotopic mouse model and in epithelioid pleural mesothelioma patients. *Clin. Cancer Res.* **18,** 2478–2489 (2012).

372. Hammerich-Hille, S. *et al.* SAFB1 mediates repression of immune regulators and apoptotic genes in breast cancer cells. *J. Biol. Chem.* **285,** 3608–3616 (2010).

373. Dinarina, A. *et al.* Negative regulation of cell-cycle progression by RINGO/Speedy E. *Biochem. J.* **410,** 535–542 (2008).

374. Leiserson, M. D. M. *et al.* Pan-cancer network analysis identifies combinations of rare somatic mutations across pathways and protein complexes. *Nat. Genet.* **47,** 106–114 (2014).

375. MacCollin, M. *et al.* Mutational analysis of patients with neurofibromatosis 2. *Am. J. Hum. Genet.* **55,** 314–320 (1994).

376. Friedberg, E. C. *et al.* Defective nucleotide excision repair in xpc mutant mice and its association with cancer predisposition. *Mutat. Res.* **459,** 99–108 (2000).

377. Zhu, X.-L. *et al.* XPC Lys939Gln polymorphism is associated with the decreased response to platinum based chemotherapy in advanced non-small-cell lung cancer. *Chin. Med. J. (Engl).* **123,** 3427–3432 (2010).

378. Chua, T. C. *et al.* Differential expression of Ki-67 and sex steroid hormone receptors between genders in peritoneal mesothelioma. *Pathol. Oncol. Res.* **15,** 671–678 (2009).

379. Hattori, Y., Yoshida, A., Yoshida, M., Takahashi, M. & Tsuta, K. Evaluation of androgen receptor and GATA binding protein 3 as immunohistochemical markers in the diagnosis of metastatic breast carcinoma to the lung. *Pathol. Int.* **65,** 286–292 (2015).

380. Yu, H. *et al.* The ubiquitin carboxyl hydrolase BAP1 forms a ternary complex with YY1 and HCF-1 and is a critical regulator of gene expression. *Mol. Cell. Biol.* **30,** 5071–5085 (2010).

381. Weng, A. P. *et al.* Activating mutations of NOTCH1 in human T cell acute lymphoblastic leukemia. *Science* **306,** 269–271 (2004).

382. Graziani, I. *et al.* Opposite effects of Notch-1 and Notch-2 on mesothelioma cell survival under hypoxia are exerted through the Akt pathway. *Cancer Res.* **68,** 9678–9685 (2008).

383. Cools, J. *et al.* Identification of novel fusion partners of ALK, the anaplastic lymphoma kinase, in anaplastic large-cell lymphoma and inflammatory myofibroblastic tumor. *Genes. Chromosomes Cancer* **34,** 354–362 (2002).

384. Liu, W. *et al.* Identification of RNF213 as a susceptibility gene for moyamoya disease and its possible role in vascular development. *PLoS One* **6,** e22542 (2011).

385. Jiang, Y.-Z., Yu, K.-D., Zuo, W.-J., Peng, W.-T. & Shao, Z.-M. GATA3 mutations define a unique subtype of luminal-like breast cancer with improved survival. *Cancer* **120,** 1329–1337 (2014).

386. Van Raamsdonk, C. D. *et al.* Mutations in GNA11 in uveal melanoma. *N. Engl. J. Med.* **363,** 2191–2199 (2010).

387. Harbour, J. W. *et al.* Frequent mutation of BAP1 in metastasizing uveal melanomas. *Science* **330,** 1410–1413 (2010).

388. Doyle, L. A., Vivero, M., Fletcher, C. D., Mertens, F. & Hornick, J. L. Nuclear expression of STAT6 distinguishes solitary fibrous tumor from histologic mimics. *Mod. Pathol.* **27,** 390–395 (2014).

389. Kanu, N. *et al.* SETD2 loss-of-function promotes renal cancer branched evolution through replication stress and impaired DNA repair. *Oncogene* **34,** 5699–5708 (2015).

390. Xu, H., DiCarlo, J., Satya, R. V., Peng, Q. & Wang, Y. Comparison of somatic mutation calling methods in amplicon and whole exome sequence data. *BMC Genomics* **15,** 244 (2014).

391. Kandoth, C. *et al.* Mutational landscape and significance across 12 major cancer types. *Nature* **502,** 333–339 (2013).

392. Yi, C. *et al.* A tight junction-associated Merlin-angiomotin complex mediates Merlin's regulation of mitogenic signaling and tumor suppressive functions. *Cancer Cell* **19,** 527–540 (2011).

393. Zhao, B. *et al.* TEAD mediates YAP-dependent gene induction and growth control. *Genes Dev.* **22,** 1962–1971 (2008).

394. Caron-Lormier, G. & Berry, H. Amplification and oscillations in the FAK/Src kinase system during integrin signaling. *J. Theor. Biol.* **232,** 235–248 (2005).

395. Sonoda, Y. *et al.* Anti-apoptotic role of focal adhesion kinase (FAK). Induction of inhibitor-of-apoptosis proteins and apoptosis suppression by the overexpression of FAK in a human leukemic cell line, HL-60. *J. Biol. Chem.* **275,** 16309–16315 (2000).

396. Tilghman, R. W. *et al.* Focal adhesion kinase is required for the spatial organization of the leading edge in migrating cells. *J. Cell Sci.* **118,** 2613–2623 (2005).

397. Benlimame, N. *et al.* FAK signaling is critical for ErbB-2/ErbB-3 receptor cooperation for oncogenic transformation and invasion. *J. Cell Biol.* **171,** 505–516 (2005).

398. Peng, X. *et al.* Overexpression of focal adhesion kinase in vascular endothelial cells promotes angiogenesis in transgenic mice. *Cardiovasc. Res.* **64,** 421–430 (2004).

399. News Release - Novel Drugs Targeting Cancer Stem Cells. (2010). at <http://phx.corporate-ir.net/phoenix.zhtml?c=250749&p=irol-newsArticle&ID=2090793>

400. White, C. D. & Sacks, D. B. Regulation of MAP kinase signaling by calcium. *Methods Mol. Biol.* **661,** 151–165 (2010).

401. Wang, C.-Y., Lai, M.-D., Phan, N. N., Sun, Z. & Lin, Y.-C. Meta-Analysis of Public Microarray Datasets Reveals Voltage-Gated Calcium Gene Signatures in Clinical Cancer Patients. *PLoS One* **10,** e0125766 (2015).

402. Rohde, M. *et al.* Members of the heat-shock protein 70 family promote cancer cell growth by distinct mechanisms. *Genes Dev.* **19,** 570–582 (2005).

403. Mazur, P. K. *et al.* SMYD3 links lysine methylation of MAP3K2 to Ras-driven cancer. *Nature* **510,** 283–287 (2014).

404. Abutaily, A. S., Collins, J. E. & Roche, W. R. Cadherins, catenins and APC in pleural malignant mesothelioma. *J. Pathol.* **201,** 355–362 (2003).

405. Uematsu, K. *et al.* Targeting the Wnt signaling pathway with dishevelled and cisplatin synergistically suppresses mesothelioma cell growth. *Anticancer Res.* **27,** 4239–4242

406. Rui, Y. *et al.* A beta-catenin-independent dorsalization pathway activated by Axin/JNK signaling and antagonized by aida. *Dev. Cell* **13,** 268–282 (2007).

407. Gujral, T. S. *et al.* A Noncanonical Frizzled2 Pathway Regulates Epithelial-Mesenchymal Transition and Metastasis. *Cell* **159,** 844–856 (2014).

408. Morales, C. R. *et al.* Epithelial trafficking of Sonic hedgehog by megalin. *J. Histochem. Cytochem.* **54,** 1115–1127 (2006).

409. Akiyoshi, T. *et al.* Gli1, downregulated in colorectal cancers, inhibits proliferation of colon cancer cells involving Wnt signalling activation. *Gut* **55,** 991–999 (2006).

410. Kouzarides, T. Chromatin modifications and their function. *Cell* **128,** 693–705 (2007).

411. Barski, A. *et al.* High-resolution profiling of histone methylations in the human genome. *Cell* **129,** 823–837 (2007).

412. Levy, D. *et al.* Lysine methylation of the NF-κB subunit RelA by SETD6 couples activity of the histone methyltransferase GLP at chromatin to tonic repression of NF-κB signaling. *Nat. Immunol.* **12,** 29–36 (2011).

413. Hamamoto, R. *et al.* Enhanced SMYD3 expression is essential for the growth of breast cancer cells. *Cancer Sci.* **97,** 113–118 (2006).

414. Peserico, A. *et al.* A SMYD3 Small-Molecule Inhibitor Impairing Cancer Cell Growth. *J. Cell. Physiol.* **230,** 2447–2460 (2015).

415. Kang, D. *et al.* The histone methyltransferase Wolf-Hirschhorn syndrome candidate 1-like 1 (WHSC1L1) is involved in human carcinogenesis. *Genes. Chromosomes Cancer* **52,** 126–139 (2013).

416. Xia, M. *et al.* Histone methyltransferase Ash1l suppresses interleukin-6 production and inflammatory autoimmune diseases by inducing the ubiquitin-editing enzyme A20. *Immunity* **39,** 470–481 (2013).

417. Leclercq, S. *et al.* A 5-aza-2'-deoxycytidine/valproate combination induces cytotoxic T-cell response against mesothelioma. *Eur. Respir. J.* **38,** 1105–1116 (2011).

418. Shapiro, I. M. *et al.* Merlin Deficiency Predicts FAK Inhibitor Sensitivity: A Synthetic Lethal Relationship. *Sci. Transl. Med.* **6 ,** 237ra68–237ra68 (2014).

419. Gao, C. *et al.* FAK/PYK2 promotes the Wnt/β-catenin pathway and intestinal tumorigenesis by phosphorylating GSK3β. *Elife* **4,** (2015).

420. Williams, K. E., Bundred, N. J., Landberg, G., Clarke, R. B. & Farnie, G. Focal adhesion kinase and Wnt signaling regulate human ductal carcinoma in situ stem cell activity and response to radiotherapy. *Stem Cells* **33,** 327–341 (2015).

421. Mahoney, K. M., Freeman, G. J. & McDermott, D. F. The Next Immune-Checkpoint Inhibitors: PD-1/PD-L1 Blockade in Melanoma. *Clin. Ther.* **37,** 764–82 (2015).

422. Brahmer, J. *et al.* Nivolumab versus Docetaxel in Advanced Squamous-Cell Non-Small-Cell Lung Cancer. *N. Engl. J. Med.* **373,** 123–135 (2015).

423. Cedrés, S. *et al.* Analysis of expression of programmed cell death 1 ligand 1 (PD-L1)

in malignant pleural mesothelioma (MPM). *PLoS One* **10,** e0121071 (2015).

424. Mansfield, A. S. *et al.* B7-H1 expression in malignant pleural mesothelioma is associated with sarcomatoid histology and poor prognosis. *J. Thorac. Oncol.* **9,** 1036–1040 (2014).

425. Sun, X. *et al.* Molecular characterization of tumour heterogeneity and malignant mesothelioma cell differentiation by gene profiling. *J. Pathol.* **207,** 91–101 (2005).

426. Gerlinger, M. *et al.* Genomic architecture and evolution of clear cell renal cell carcinomas defined by multiregion sequencing. *Nat. Genet.* **46,** 225–233 (2014).

427. Fisher, R., Pusztai, L. & Swanton, C. Cancer heterogeneity: implications for targeted therapeutics. *Br. J. Cancer* **108,** 479–485 (2013).

428. Marioni, J. C., Mason, C. E., Mane, S. M., Stephens, M. & Gilad, Y. RNA-seq: an assessment of technical reproducibility and comparison with gene expression arrays. *Genome Res.* **18,** 1509–1517 (2008).

429. Sultan, M. *et al.* A global view of gene activity and alternative splicing by deep sequencing of the human transcriptome. *Science* **321,** 956–960 (2008).

430. Maher, C. A. *et al.* Transcriptome sequencing to detect gene fusions in cancer. *Nature* **458,** 97–101 (2009).

431. Wyman, S. K. *et al.* Repertoire of microRNAs in epithelial ovarian cancer as determined by next generation sequencing of small RNA cDNA libraries. *PLoS One* **4,** e5311 (2009).

432. Antoniou, A. C. *et al.* RAD51 135G-->C modifies breast cancer risk among BRCA2 mutation carriers: results from a combined analysis of 19 studies. *Am. J. Hum. Genet.* **81,** 1186–1200 (2007).

433. Chapman, M. a *et al.* Initial genome sequencing and analysis of multiple myeloma. *Nature* **471,** 467–472 (2011).

434. De Rienzo, A. *et al.* Gender-Specific Molecular and Clinical Features Underlie Malignant Pleural Mesothelioma. *Cancer Res.* **76,** 319–328 (2016).

435. Bueno, R. *et al.* Comprehensive genomic analysis of malignant pleural mesothelioma identifies recurrent mutations, gene fusions and splicing alterations. *Nat. Genet.* (2016). doi:10.1038/ng.3520

436. Lawrence, M. S. *et al.* Mutational heterogeneity in cancer and the search for new cancer-associated genes. *Nature* **499,** 214–8 (2013).

437. Wong, S. Q. *et al.* Targeted-capture massively-parallel sequencing enables robust detection of clinically informative mutations from formalin-fixed tumours. *Sci. Rep.* **3,** 3494 (2013).

# Appendices

**Appendix 2.1 - MEMO CCR4020 Protocol**

# Molecular Epidemiology of Malignant MesOthelioma: MEMO

Chief Investigator: Dr Sanjay Popat

Study Co-ordinator Alison Norton

**Study Sponsor-Royal Marsden NHS Foundation Trust**

The Royal Marsden NHS Foundation Trust, Fulham Road, London SW3 6JJ

**Version:** 2.0; **Date:** 03/06/2014;

**Funder:** Royal Marsden Hospital Lung Unit

**Study coordinating centre:** Royal Marsden Hospital

# Protocol Signature Page

Study title: MEMO- Molecular Epidemiology of Malignant MesOthelioma

Protocol version: 2.0

Version date: 03/06/2014

Approved by Chief Investigator

Dr Sanjay Popat BSc MBBS MRCP PhD

Date:

By signing the above, the investigator agrees to adhere to the protocol as outlined and that this study will be conducted in accordance with the principles outlined in the NHS Research Governance Framework for Health and Social Care. It will be conducted in compliance with the protocol, the Data Protection Act, and other regulatory requirements as appropriate.

# Study Management Group

Dr Sanjay Popat

Dr Tim Benepal

Dr Mary O'Brien

Dr Jaishree Bhosle

Dr Brendan Tinwell

Dr Andrew Wotherspoon

Prof Andrew Nicholson

Prof William Cookson

Prof Miriam Moffatt

# Study Coordination Centre

For queries, please contact the coordinator:


| | |
|---|---|
| Study Coordinator: | Alison Norton |
| Address: | Royal Marsden Hospital, Sutton, SM2 5PT |
| Tel: | 020 8642 6011 x3276 |

# Clinical Queries

Clinical queries should be directed to the study coordinator who will direct the query to the appropriate person.

# Sponsor

The Royal Marsden NHS Foundation Trust is the main research sponsor for this study. For further information regarding the sponsorship conditions, please contact the Research and Development Manager at:

Clinical Research & Development Office
DM20, Royal Marsden Hospital
Sutton SM2 5PT
Tel: 020 8661 3909

# Funder

This study is funded by the Royal Marsden Hospital Lung Unit

This protocol describes the "MEMO" study and provides information about study design and management. Every care was taken in its drafting, but corrections or amendments may be necessary. These will be circulated to investigators in the study. Problems relating to this study should be referred, in the first instance, to the Chief Investigator.

This study will adhere to the principles outlined in the NHS Research Governance Framework for Health and Social Care. It will be conducted in compliance with the protocol, the Data Protection Act, the principles of Good Clinical Practice (GCP), and other regulatory requirements as appropriate.

# Investigators and Contacts

| | |
|---|---|
| Chief Investigator | Dr Sanjay Popat<br>Royal Marsden Hospital<br>London SW3 6JJ<br>Tel: 020 7808 2132 Fax: 020 7808 2688 |
| Study Sponsor | Royal Marsden Hospital |
| Study Coordinator | Ms Alison Norton<br>Royal Marsden Hospital<br>Sutton, SM2 5PT |
| Co-investigator | Dr Tim Benepal<br>St George's Hospital<br>London, SW17 0QT<br>Tel: 020 8672 1255 |
| Co-investigator | Dr Mary O'Brien<br>Royal Marsden Hospital<br>London SW3 6JJ<br>Tel: 020 7352 8171 |
| Co-investigator | Dr Jaishree Bhosle<br>Royal Marsden Hospital<br>London SW3 6JJ<br>Tel: 020 7352 8171 |
| Co-investigator | Dr Shir Kiong Lu<br>Royal Marsden Hospital<br>London, SW3 6JJ<br>Tel: 02073528171 |
| Co-investigator | Dr Brendan Tinwell<br>Dept Pathology<br>St George's Hospital<br>London, SW17 0QT |

| | |
|---|---|
| Co-investigator | Dr Andrew Wotherspoon<br>Dept Histopathology<br>Royal Marsden Hospital<br>London SW3 6JJ |
| Co-investigator | Prof Andrew Nicholson<br>Dept Histology<br>Royal Brompton Hospital<br>London SW6 6NP |
| Co-investigator | Prof Bill Cookson<br>National Heart and Lung Institute<br>Imperial College London<br>London SW3 6LY |
| Co-investigator | Prof Miriam Moffatt<br>National Heart and Lung Institute<br>Imperial College London<br>London SW3 6LY |

# Protocol Amendment Page and Study Administration

| | |
|---|---|
| Protocol reference: | |
| Version number and Date: | Version 2.0;03/6/2014 |
| Effective Date: | |
| Review Date: | |
| Superseded Version Number and Date (if applicable) | Version1.1; 18/6/2013 |

| Revision Chronology | Effective Date | Reason for Change |
|---|---|---|
| | | |
| | | |
| | | |
| | | |

# List of Abbreviations

| | |
|---|---|
| BAP 1 | BRCA1 associated protein 1 |
| CTGF | Connective tissue growth factor |
| EGFR | Epidermal growth factor receptor |
| FAK | Focal adhesion kinase |
| FFPE | Formalin-fixed paraffin-embedded |
| HDAC | Histone deacetylase |
| ICL | Imperial College London |
| IGFR | Insulin-like growth factor receptor |
| IHC | Immunohistochemistry |
| IP | Intellectual property |
| MM | Malignant mesothelioma |
| MTA | Material transfer agreement |
| mTORC1 | mammalian target of rapamycin complex 1 |
| NCRI | National Cancer Research Institute |
| PI3K | Phosphoinositide 3-kinase |
| RBH | Royal Brompton Hospital |
| RMH | Royal Marsden Hospital |
| SGH | St George's Hospital |
| TGF-B | Tissue growth factor beta |
| TMA | Tissue microarray |
| TS | Thymidylate synthase |
| Yap 1 | Yes-associated protein 1 |

# Study Synopsis

| | |
|---|---|
| **Title** | MEMO |
| **Short Title** | Molecular Epidemiology of Malignant Mesothelioma |
| **Study Design** | A retrospective study investigating the molecular epidemiology of patients with malignant mesothelioma |
| **Study Objectives** | 1. An exploratory retrospective study to document molecular abnormalities in tumour biopsies of patients with malignant mesothelioma seen at the Royal Marsden Hospital or St George's Hospital and their associations with clinical outcomes<br>2. To act as a validation dataset for molecular aberrations identified from whole genome analysis of mesothelioma |
| **Inclusion Criteria** | 1. Patients with a confirmed pathological diagnosis of malignant mesothelioma (any primary site) and availability of archival tissues<br>2. Patients seen at the Royal Marsden Hospital or St George's Hospital between 2000 to 2009<br>3. Age ≥18 years; |
| **Exclusion Criteria** | 1. Patients for whom a tissue diagnosis of confirmed mesothelioma has not been made |

# 1. Background and Rationale

## 1.1 General background

Outcomes from malignant mesothelioma (MM) are generally poor, with few long-term survivors and a 5-year survival of around 5%. Whilst this is in part due to presentation of patients with advanced/locally advanced disease, other significant factors include lack of effective therapies, and a poor understanding of the biology of these tumours, especially in the UK.

This lack of research into thoracic tumours when compared to other tumour types was highlighted in an National Cancer Research Institute (NCRI) framework review (1). This identified a need for research into thoracic tumours including MM

Our study into the underlying biological processes of MM aims to address these deficiencies, with a view to exploring molecular aberrations in patients with mesothelioma, and to generate a validation dataset for which findings of ongoing whole genome/transcriptome analyses at Imperial College London (ICL) can be validated.

## 1.2 Malignant Mesothelioma

MM is an uncommon but almost universally fatal malignant cancer of mesothelial cells, principally affecting the pleura and peritoneum. Exposure to asbestos is the primary causative environmental carcinogen, and a long latency is observed, with a median of 50 years (2). Although the disease is traditionally considered rare, due to this long latency incidence has

been rising rapidly, and has risen 12-fold from 1968-2001 in the UK. Deaths from MM have risen rapidly from 153 in 1968 to 1,848 in 2001, and the disease currently accounts for approximately 2,000 new cases in the UK per year, (3). However, incidence continues to rise rapidly, and epidemiological modelling predicts a peak between 2011-15.

Prognosis from MM is usually poor and early diagnosis is unusual. Even in those fit for chemotherapy, median survival is approximately 1 year in unselected cases (4). Despite this, a number of active chemotherapy regimens have shown efficacy in improving survival (5;6), and importantly, in palliating symptoms (7-9). Moreover, radical and debulking surgery or multimodality therapy (10), has potential to play a role in improving survival and palliation (10;11), in selected patients.

Given the poor understanding of carcinogenic pathways involved in MM development, there is a need to validate and identify new targets for therapy. In the case of systemic therapy, platinum-based pemetrexed doublet therapy has become an international standard (4), but despite this, clinical and radiological responses are only seen in the minority of cases. Discovery of markers with prognostic and predictive utility are therefore urgently required to better target the limited therapies available, and a number of such biomarkers have been proposed.

# 2.0 Biomarkers and Molecular Epidemiology

Whilst MM is an increasingly common disease in many countries, the molecular epidemiology and biomarkers of outcome have been poorly investigated. However, the limited studies of MM biology have demonstrated a number of cytogenetic abnormalities, including losses at chromosome 1p, 3p, 9p, and 6q, 13q, and 15q. Loss of an entire copy of chromosome 4 or 22 is also often observed. Recurrent areas of deletion include chromosome 9p21 (which includes the loci *CDKN2A/ARF* and *CDKN2B*) and 22q12 (including *NF2*), with functional studies showing that re-introduction of the encoded protein at these loci results in a regression of the malignant phenotype (12;13). Moreover a heterozygous (+/-) *NF2* knockout mouse demonstrates an accelerated rate of MM development when exposed to asbestos (14). Studies have also suggested that *NF2* somatic mutations are common and activate integrin-dependent mammalian target of rapamycin complex 1 (mTORC1) signalling (15;16). *NF2* encodes a membrane-cytoskeleton-associated protein, merlin that regulates cell growth via the Hippo signalling pathway to inhibit the transcriptional and oncogenic function of yes-associated protein 1 (Yap 1) (17;18). Everolimus, an mTOR inhibitor, is currently being trialled in MM patients and loss of NF2 is being investigated as a potential biomarker to predict drug sensitivity. mTOR inhibition results in compensatory activation of other signalling pathways such as MET, insulin growth factor receptor (IGFR) and epidermal growth factor receptor (EGFR) with activation of downstream AKT pathways, and so it is likely that combination therapy will be required. Recent data also suggest a role for *NF2* loss and functional interaction between Hippo and tissue growth factor beta (TGF-B) pathways, and imply connective tissue growth factor (CTGF) over-expression as transforming (19).

A number of signalling pathways may be involved in mediating the malignancy phenotype, including phosphoinositide 3-kinase (PI3K) signalling through either aberrant AKT activity (20), or through MEK/Fra1 (21). However, clearly identified mechanisms of carcinogenesis in MM remain unclear, with significant heterogeneity in findings from tumours.

The role of focal adhesion kinase (FAK) in promoting cell migration and invasion has been suggested in several cancer types including MM. *NF2* loss induces FAK phosphorylation which enables it to interact with Src and the p85 subunit of PI3K (22). These data provide the rationale for testing FAK, Src kinase, and PI3K inhibitors.

Finally, BRCA-1 associated protein 1 (BAP1) regulates cell proliferation through histone modifications and somatic mutations are common in MM (23). It occurs mainly in epithelioid sub-type MM and germline BAP1 mutation is associated with increased risk of MM. Histone deacetylase (HDAC) inhibitor, vorinostat has been tested in MM and demonstrated no survival advantages but molecular subset analysis of this trial has not been performed.

Standard systemic therapy for MM is based on a combination of platinum and pemetrexed chemotherapy. Despite this, however, response rates remain low, with many patients not benefitting from such therapy. A number of molecular phenotypes have been investigated for patients with MM. The biological and clinical significance of many of these features, however, remains uncertain. Further investigation of MM, correlating molecular phenotype with clinical outcome remains key to understanding the biological processes underlying tumourigeneis and therapeutic sensitivity.

Pemetrexed is a cytotoxic anti-folate and actions as a selective thymidylate synthase (TS) inhibitor. It has been hypothesised in the basis of cell line data to be most active in tumour

types with inherent low TS expression (adenocarcinoma) and poorly active in those with high TS expression (small cell lung cancer) (24). The role of TS expression in MM has been poorly characterized, as well as its inter-relationship with other prognostic or predictive markers e.g. proliferation index, with some studies suggesting that TS expression level correlates with outcome from pemetrexed-based chemotherapy, and others not (25;26).

# 3.0 Study Objectives/Endpoint

## 3.1 Objectives

1. To retrospectively explore and document molecular abnormalities in tumour biopsies of patients with MM seen at the Royal Marsden Hospital (RMH) or St George's Hospital (SGH) and their associations with clinical outcomes

2. To act as a validation dataset for molecular aberrations identified from whole genome analysis of MM

## 3.2 Endpoints

1. To document and estimate the frequencies of different molecular abnormalities identified in tumour specimens of MM

2. To correlate the molecular abnormalities with clinical outcomes such as survival and response to chemotherapy to generate potential biomarkers for patients with MM

# 4.0 Eligibility

## 4.1 Inclusion Criteria

1. Patients with a confirmed pathological diagnosis of MM (any primary site) and availability of archival tissues

2. Patients seen at the RMH or SGH between 2000 to 2009

3. Age ≥18 years

## 4.2 Exclusion Criteria

1. Patients for whom a tissue diagnosis of confirmed MM has not been made

# 5.0 Study Design and Procedures

## 5.1 Patient Identification

Patients will be identified from those seen at the RMH or SGH with a pathological diagnosis of MM. Patient records will be cross-referenced with the inclusion/exclusion criteria to identify potentially eligible patients. In the first instance, patients will be identified if having undergone surgical thoracoscopy or other diagnostic procedures at the RMH or SGH.

## 5.2 Consent

No patients will be involved in this study. All specimens used from patients are formalin-fixed paraffin embedded (FFPE) material surplus to clinical requirements, and will be used in a linked-coded manner. There will be no study specific consent form.

## 5.3 Sample and Clinical Data Collection

Patients meeting the inclusion / exclusion criteria with FFPE material will be identified. Patient demographics and outcomes will be collected from the case notes at the RMH and SGH, using a common template. A common clinical data dataset without patient identifiers will be held at the RMH.

Tumour and normal (reactive pleural fibrosis) FFPE materials will be collected from both institutions then transferred and stored at the pathology laboratory at RMH Biomedical Research Centre (BRC). Material transfer agreements (MTA) will be sought and put in place

between (a) tissue-providing centres and the RMH and (b) collaborators, if different from tissue-providing centres, and the RMH.

Central pathological review will be performed on the FFPE tumour materials to confirm the diagnosis and tumour abundance. FFPE analyses including tissue microarray (TMA) formation will be performed with collaborators at ICL/Royal Brompton Hospital (RBH), where the chief investigator holds an academic position. The clinical dataset will be forwarded to ICL/RBH if required, to facilitate exploratory analyses. Immunohistochemistry (IHC) will be carried out at the laboratory at ICL/RBH/RMH. Surplus FFPE materials will otherwise be returned to the RMH and SGH upon completion of analyses.

## 5.4 Planned Laboratory Analyses

Samples will be used for investigation into MM carcinogenesis, and molecular variants influencing drug therapy.

Laboratory analyses will involve primarily IHC or CISH and other techniques (including molecular methods e.g. sequencing) to meet the ends of this study. Contingent on numbers of blocks obtained, samples will be classified into epithelioid and non-epithelioid subtypes, and into patients treated with systemic therapy or not. FFPE material may be used for formation into TMA, or single section analyses.

IHC or CISH, if appropriate, on tumours will be performed at a number of markers contingent on the literature. This may involve Ki67, TS, *NF2*, YAP, FAK and BAP1. Other potential biomarkers may be assessed contingent on the field. Appropriate IHC scoring systems will be used contingent on type of marker analysed and will range from semi-quantitative 0-+++ or a

quantitative H-score. Clinical covariates including survival and response to chemotherapy will be assessed contingent on marker status.

FFPE material will be primarily used as a validation dataset to estimate the frequencies and to examine the distribution of novel carcinogenic markers identified from whole genome sequencing/expression profiling analyses occurring with ICL and other external collaborators, and may also be used for exploratory analyses.

# 6.0 Regulatory Issues

## 6.1 Ethics Approval

The Chief Investigator will have been granted Ethics Committee approval for this study, and will take responsibility for the conduct of the study. The study will be conducted in accordance with the NHS Research Governance Framework for Health and Social Care, the Data Protection Act, and other regulatory requirements as appropriate.

The tissue used in this research will be surplus archived samples obtained as part of diagnosis or treatment. Consent for use of tissue will not be required for patients diagnosed before 1st September 2006 according to the Human Tissue Act regulations and Medical Research Council guidelines. For patients diagnosed after 1st September 2006 and alive, samples will be used only if patients provided written consent on the generic institution consent form. Due to the poor prognosis of mesothelioma, majority of patients enrolled in this study will have died and samples from deceased patients may be analysed without giving generic institution consent and we do not intend to seek consent from relatives of deceased patients. In addition, the results from the research will not affect patient's clinical outcomes/interests and we will not be looking for germline mutations that could affect patient's family.

## 6.2 Confidentiality

The Chief Investigator will preserve the confidentiality of participants taking part in the study as per the Data Protection Act. All molecular analyses will be performed on linked-coded

(anonymized) samples.

## 6.3 Indemnity, Sponsorship, and Funding

The RMH NHS Foundation Trust will act as the main sponsor for this study. This study is part funded by the RMH Lung Unit. Further grant support for this study will be applied for, as appropriate.

## 6.4 Study Management, Audits and Inspections

The overall monitoring of the study will be performed by the study management group. Investigators will also meet regularly to discuss study progress.

The study may be subject to inspection and audit by the sponsor and other regulatory bodies to ensure adherence to appropriate guidelines and laws.

## 6.5 Intellectual Property

Biological specimens will be treated as "gift" from patients, and will not be used for commercial exploitation. It is recognised that intellectual property (IP) may arise from the results of laboratory analyses. This will be addressed by a contract-specified material-transfer-agreement (MTA) for the protocol between the RMH, SGH and ICL/RBH as required.

## 6.6 Study Management

The day-to-day management of the study will be co-ordinated by the study management

group and collaborators at the National Heart and Lung Institute, ICL.

# 7.0 Statistical Considerations

## 7.1 Study Power

This is an exploratory study and the plan is to include all cases that meet the inclusion/exclusion criteria and this has been estimated to be around 300. The expected rates of abnormality in the ICL cohort are expected to be between 30-50%. 95% confidence limits have been calculated to determine the lower and upper confidence limits expected for our cohort with 300 patients.

| Alpha | % Abnormal in ICL Cohort | 95% Confidence interval Width | Lower | Upper |
|---|---|---|---|---|
| 0.95 | 30 | 5.2 | 24.8 | 35.2 |
| 0.95 | 35 | 5.4 | 29.6 | 40.4 |
| 0.95 | 40 | 5.5 | 34.5 | 45.5 |
| 0.95 | 45 | 5.6 | 39.4 | 50.6 |
| 0.95 | 50 | 5.7 | 44.3 | 55.7 |

## 7.2 Data Analysis

Cases will be divided into groups according to their marker status and the proportion of cases with individual marker or a combination will be given with 95% confidence intervals. This grouping will be correlated with outcome measures using standard statistical methods. Time-

to-endpoint analyses, overall survival defined as from time of diagnosis to time of death will be measured and examined by the Kaplan-Meier method for groups with and without the markers and groups compared by the logrank test for univariable tests, and using Cox's proportional hazards for known clinical factors. For each different markers of interest, the response rates to chemotherapy will be compared between groups with and without the markers and examined using the $X^2$ test. Other statistical analyses will be invoked as appropriate (e.g. K-means clustering for microarray data).

# 8.0 Results Dissemination and Publication Policy

The results of this study will be disseminated by presentation at academic meetings and publication in peer-reviewed journals. Investigators will be asked to contribute to co-authorship of any publications arising from this study.

# 9.0 References


(1) NRCI strategic planning group on lung cancer. Lung Cancer Research in the UK. 1-56. 1-10-2006. London, National Cancer Research Institute. Ref Type: Report

(2) Bianchi C, Giarelli L, Grandi G, Brollo A, Ramani L, Zuch C. Latency periods in asbestos-related mesothelioma of the pleura. Eur J Cancer Prev 1997; 6(2):162-166.

(3) Cancer Research UK. CancerStats Monograph 2004. London: Cancer Research UK; 2004.

(4) Vogelzang NJ, Rusthoven JJ, Symanowski J, Denham C, Kaukel E, Ruffie P et al. Phase III Study of Pemetrexed in Combination With Cisplatin Versus Cisplatin Alone in Patients With Malignant Pleural Mesothelioma. J Clin Oncol 2003; 21(14):2636-2644.

(5) Vogelzang NJ, Rusthoven JJ, Symanowski J, Denham C, Kaukel E, Ruffie P et al. Phase III Study of Pemetrexed in Combination With Cisplatin Versus Cisplatin Alone in Patients With Malignant Pleural Mesothelioma. J Clin Oncol 2003; 21(14):2636-2644.

(6) van Meerbeeck JP, Gaafar R, Manegold C, Van Klaveren RJ, Van Marck EA, Vincent M et al. Randomized Phase III Study of Cisplatin With or Without Raltitrexed in Patients With Malignant Pleural Mesothelioma: An Intergroup Study of the European Organisation for Research and Treatment of Cancer Lung Cancer Group and the National Cancer Institute of Canada. J Clin Oncol 2005; 23(28):6881-6889.

(7) Bottomley A, Gaafa R, Manegold C, Burgers S, Coens C, Legrand C et al. Short-Term Treatment-Related Symptoms and Quality of Life: Results From an International Randomized Phase III Study of Cisplatin With or Without Raltitrexed in Patients With Malignant Pleural Mesothelioma: An EORTC Lung-Cancer Group and National Cancer Institute, Canada, Intergroup Study. J Clin Oncol 2006; 24(9):1435-1442.

(8) Andreopoulou E, Ross PJ, O'Brien MER, Ford HER, Priest K, Eisen T et al. The palliative benefits of MVP (mitomycin C, vinblastine and cisplatin) chemotherapy in patients with malignant mesothelioma. Ann Oncol 2004; 15(9):1406-1412.

(9) Steele JP, Shamash J, Evans MT, Gower NH, Tischkowitz MD, Rudd RM. Phase II study of vinorelbine in patients with malignant pleural mesothelioma. J Clin Oncol 2000; 18(23):3912-3917.

(10) Weder W, Stahel RA, Bernhard J, Bodis S, Vogt P, Ballabeni P et al. Multicenter trial of neo-adjuvant chemotherapy followed by extrapleural pneumonectomy in malignant pleural mesothelioma. Ann Oncol 2007; 18(7):1196-1202.

(11) Aelony Y, Yao JF. Prolonged survival after talc poudrage for malignant pleural mesothelioma: case series. Respirology 2005; 10(5):649-655.

(12) Frizelle SP, Grim J, Zhou J, Gupta P, Curiel DT, Geradts J et al. Re-expression of p16INK4a in mesothelioma cells results in cell cycle arrest, cell death, tumor suppression and tumor regression. Oncogene 1998; 16(24):3087-3095.

(13) Poulikakos PI, Xiao GH, Gallagher R, Jablonski S, Jhanwar SC, Testa JR. Re-expression of the tumor suppressor NF2/merlin inhibits invasiveness in mesothelioma cells and negatively regulates FAK. Oncogene 2006; 25(44):5960-5968.

(14) Altomare DA, Vaslet CA, Skele KL, De Rienzo A, Devarajan K, Jhanwar SC et al. A mouse model recapitulating molecular features of human mesothelioma. Cancer Res 2005; 65(18):8090-8095.

(15) Thurneysen C, Opitz I, Kurtz S, Weder W, Stahel RA, Felley-Bosco E. Functional inactivation of NF2/merlin in human mesothelioma. Lung Cancer 2009; 64(2):140-147.

(16) Lopez-Lago MA, Okada T, Murillo MM, Socci N, Giancotti FG. Loss of the tumor suppressor gene NF2, encoding merlin, constitutively activates integrin-dependent mTORC1 signalling. Mol Cell Biol 2009; 29(15):4235-4249.

(17) Mizuno T, Murakami H, Fujii M, Ishiguro F, Tanaka I, Kondo Y et al. YAP induces malignant mesothelioma cell proliferation by upregulating transcription of cell cycle-promoting genes. Oncogene 2012.

(18) Sekido Y. Inactivation of Merlin in malignant mesothelioma cells and the Hippo signalling cascade dysregulation. Pathol Int 2011; 61(6):331-344.

(19) Fujii M, Toyoda T, Nakanishi H, Yatabe Y, Sato A, Matsudaira Y et al. TGF-beta synergizes with defects in the Hippo pathway to stimulate human malignant mesothelioma growth. J Exp Med 2012; 209(3):479-494.

(20) Altomare DA, You H, Xiao GH, Ramos-Nino ME, Skele KL, De Rienzo A et al. Human and mouse mesotheliomas exhibit elevated AKT/PKB activity, which can be targeted pharmacologically to inhibit tumor cell growth. Oncogene 2005; 24(40):6080-6089.

(21) Ramos-Nino ME, Blumen SR, Sabo-Attwood T, Pass H, Carbone M, Testa JR et al. HGF mediates cell proliferation of human mesothelioma cells through a PI3K/MEK5/Fra-1 pathway. Am J Respir Cell Mol Biol 2008; 38(2):209-217.

(22) Poulikakos PI, Xiao GH, Gallagher R, Jablonski S, Jhanwar SC, Testa JR. Re-expression of the tumor suppressor NF2/merlin inhibits invasiveness in mesothelioma cells and negatively regulates FAK. Oncogene 2006; 25(44):5960-5968.

(23) Bott M, Brevet M, Taylor BS, Shimizu S, Ito T, Wang L et al. The nuclear deubiquitinase BAP1 is commonly inactivated by somatic mutations and 3p21.1 losses

in malignant pleural mesothelioma. Nat Genet 2011; 43(7):668-672.

(24) Takezawa K, Okamoto I, Okamoto W, Takeda M, Sakai K, Tsukioka S et al. Thymidylate synthase as a determinant of pemetrexed sensitivity in non-small cell lung cancer. Br J Cancer 2011; 104(10):1594-1601.

(25) Kao SC, Lee K, Klebe S, Henderson D, McCaughan B, Vardy J et al. Excision Repair Cross Complementation Group 1 and Thymidylate Synthase Expression in Patients With Mesothelioma. Clin Lung Cancer 2012.

(26) Righi L, Papotti MG, Ceppi P, Bille A, Bacillo E, Molinaro L et al. Thymidylate synthase but not excision repair cross-complementation group 1 tumor expression predicts outcome in patients with malignant pleural mesothelioma treated with pemetrexed-based chemotherapy. J Clin Oncol 2010; 28(9):1534-1539.

## Appendix 3.1 - List of Differentially Expressed Genes

| probesets | Gene.symbols | logFC | AveExpr | adj.P.Val |
|---|---|---|---|---|
| 16761012 | A2M | -0.79 | 9.95 | 0.005028618 |
| 16908316 | AAMP | 0.52 | 6.08 | 0.029999525 |
| 16823109 | ABCA3 | 1.79 | 6.58 | 0.004665936 |
| 16839294 | ABR | 0.52 | 7.78 | 0.01350639 |
| 16843728 | ACACA | 0.83 | 7.31 | 0.004319194 |
| 16876440 | ACP1 | 0.47 | 7.23 | 0.008999768 |
| 16716350 | ACTA2 | -1.25 | 6.01 | 0.032396736 |
| 16881594 | ACTG2 | -0.64 | 2.38 | 0.024462218 |
| 16886308 | ACVR2A | -0.85 | 6.05 | 0.016955195 |
| 16751381 | ACVRL1 | -1.48 | 4.90 | 0.002719692 |
| 17045806 | ADCY1 | -0.92 | 4.34 | 0.0177897 |
| 16958201 | ADCY5 | -0.56 | 4.03 | 0.031777783 |
| 17044905 | ADCYAP1R1 | -0.68 | 3.16 | 0.014441129 |
| 16706238 | ADK | -0.60 | 8.19 | 0.029803028 |
| 16709245 | ADRA2A | -1.75 | 5.73 | 0.011077896 |
| 16727702 | ADRBK1 | -0.48 | 7.28 | 0.040390831 |
| 16928428 | ADRBK2 | -0.75 | 7.06 | 0.000661477 |
| 16917183 | JAG1 | -0.87 | 8.40 | 0.008138164 |
| 16700385 | AGT | -0.93 | 4.93 | 0.001049806 |
| 16738400 | APLNR | -1.55 | 6.78 | 0.014616204 |
| 16918496 | AHCY | 1.04 | 7.68 | 0.001431864 |
| 17030643 | AIF1 | -0.53 | 8.01 | 0.044388831 |
| 17006683 | AIF1 | -0.52 | 7.66 | 0.038484879 |
| 17027817 | AIF1 | -0.52 | 7.66 | 0.038484879 |
| 17038140 | AIF1 | -0.52 | 7.66 | 0.038484879 |
| 17040735 | AIF1 | -0.52 | 7.66 | 0.038484879 |
| 17035441 | AIF1 | -0.55 | 8.01 | 0.030724616 |
| 17011302 | AIM1 | -1.52 | 6.46 | 0.001094005 |
| 16872352 | AKT2 | 0.29 | 5.77 | 0.030939687 |
| 16757160 | ALDH2 | 1.01 | 8.85 | 0.015439261 |
| 16727976 | ALDH3B1 | 1.23 | 6.98 | 0.002550094 |
| 16763182 | ABCD2 | -1.74 | 3.82 | 0.000739182 |
| 16817790 | ALDOA | 0.56 | 7.11 | 0.001811295 |
| 16704375 | ALOX5 | -0.73 | 7.11 | 0.032508512 |
| 16830220 | ALOX12P2 | 2.63 | 6.11 | 0.001690497 |
| 17080082 | ANGPT1 | -1.56 | 4.65 | 0.000653427 |
| 17074259 | ANGPT2 | -1.91 | 6.95 | 0.000510132 |
| 16969911 | ANK2 | -1.63 | 5.79 | 0.000275103 |
| 16972912 | SLC25A4 | 0.89 | 6.41 | 0.038950581 |
| 17106574 | SLC25A5 | 0.73 | 8.19 | 0.006157436 |
| 16968213 | ANXA3 | 4.14 | 8.11 | 3.57E-05 |
| 16881069 | ANXA4 | 0.90 | 9.27 | 0.00326115 |
| 17001800 | ANXA6 | -0.99 | 9.25 | 0.01202954 |
| 17056701 | AOAH | -0.91 | 7.42 | 0.027275532 |
| 16863124 | APOC1 | 1.24 | 6.89 | 0.032242602 |
| 17101368 | SHROOM2 | 1.21 | 4.13 | 0.000716615 |
| 16834621 | ARL4D | 1.45 | 7.03 | 0.011018364 |
| 17109078 | ARHGAP6 | -1.03 | 4.74 | 0.000212944 |
| 16761843 | ARHGDIB | -0.91 | 5.10 | 0.00130173 |
| 16966214 | RHOH | -1.65 | 4.10 | 0.000530151 |
| 16997519 | ARSB | -0.74 | 5.59 | 0.009767157 |
| 16858687 | ASNA1 | 0.61 | 9.08 | 0.02412805 |

| | | | | |
|---|---|---|---|---|
| 17090296 | ASS1 | 1.02 | 9.13 | 0.011824105 |
| 16890490 | ATIC | 0.65 | 8.69 | 0.007531991 |
| 16673525 | ATP1B1 | 0.84 | 8.19 | 0.009117949 |
| 16830621 | ATP1B2 | -0.67 | 5.98 | 0.030146833 |
| 16839887 | ATP2A3 | -1.51 | 6.02 | 0.00074238 |
| 16854928 | ATP5A1 | 0.62 | 8.73 | 0.030551116 |
| 16999379 | ALDH7A1 | 0.49 | 5.87 | 0.04676989 |
| 16766260 | ATP5B | 0.54 | 10.68 | 0.005028198 |
| 16924537 | ATP5J | 0.58 | 5.11 | 0.013898501 |
| 16663792 | ATP6V0B | 0.52 | 5.73 | 0.005667457 |
| 16925293 | ATP5O | 0.49 | 6.08 | 0.034913704 |
| 16766946 | AVPR1A | -1.14 | 5.76 | 0.01384768 |
| 16727462 | BBS1 | 0.59 | 6.40 | 0.006821203 |
| 16802771 | BBS4 | 1.18 | 7.40 | 0.000154278 |
| 16874082 | BCAT2 | 0.86 | 5.93 | 0.001361864 |
| 16855673 | BCL2 | -0.78 | 6.76 | 0.034910126 |
| 16815918 | TNFRSF17 | -1.08 | 3.09 | 0.021821543 |
| 16856216 | HCN2 | 1.06 | 4.22 | 0.010861211 |
| 16788036 | BDKRB1 | 1.52 | 4.51 | 0.04496503 |
| 16749759 | BICD1 | -0.81 | 6.11 | 0.021198014 |
| 17011279 | PRDM1 | -1.20 | 6.27 | 0.00228695 |
| 17065750 | BLK | -1.01 | 4.27 | 0.015558878 |
| 16732037 | CXCR5 | -1.41 | 3.72 | 0.001690497 |
| 16812746 | BNC1 | 5.31 | 7.88 | 1.18E-07 |
| 16793129 | BMP4 | 1.76 | 7.32 | 0.000356926 |
| 17101698 | BMX | -1.56 | 2.97 | 3.70E-06 |
| 16856203 | BSG | 0.96 | 9.97 | 0.000227676 |
| 16775364 | KLF5 | 1.26 | 6.44 | 0.000563279 |
| 17112735 | BTK | -0.99 | 5.75 | 0.008999768 |
| 16901755 | BUB1 | 1.35 | 5.47 | 0.041013206 |
| 17008544 | BYSL | 0.73 | 5.57 | 0.0073213 |
| 17070653 | OSGIN2 | 0.90 | 5.94 | 0.031386654 |
| 16726707 | MRPL49 | 0.49 | 5.72 | 0.0338111 |
| 16739117 | TMEM258 | 0.51 | 5.32 | 0.008537511 |
| 16725670 | DAGLA | 1.00 | 5.77 | 0.004631814 |
| 16926445 | PTTG1IP | 0.52 | 9.83 | 0.023532536 |
| 17084723 | CA9 | 3.18 | 6.88 | 0.00150143 |
| 16874012 | CA11 | 1.29 | 6.66 | 0.038051871 |
| 16746728 | CACNA1C | -0.92 | 6.06 | 0.046787896 |
| 17059195 | CACNA2D1 | -1.47 | 7.00 | 0.006229481 |
| 16903771 | CACNB4 | -1.62 | 4.91 | 0.000366196 |
| 16878137 | CAD | 0.76 | 7.30 | 0.001978684 |
| 16820849 | CALB2 | 5.37 | 9.34 | 5.17E-05 |
| 16987945 | CAMK4 | -0.89 | 4.63 | 0.015779003 |
| 16993397 | CANX | 0.39 | 10.61 | 0.016439345 |
| 16861380 | CAPNS1 | 0.54 | 10.15 | 0.017597773 |
| 17113362 | CAPN6 | 3.04 | 7.55 | 0.007464485 |
| 16743874 | CASP5 | -1.09 | 3.88 | 0.00412635 |
| 16978959 | CASP6 | 0.94 | 4.92 | 0.036283776 |
| 16956983 | CBLB | -0.73 | 8.13 | 0.009225792 |
| 16922477 | CBR1 | 0.69 | 5.63 | 0.004470175 |
| 16985599 | CCNB1 | 2.00 | 5.67 | 0.001909284 |
| 16991839 | CCNG1 | 0.59 | 8.16 | 0.010317365 |
| 16669169 | CD2 | -1.08 | 5.46 | 0.04086658 |
| 16745016 | CD3D | -1.25 | 6.18 | 0.015439261 |
| 16731806 | CD3G | -1.16 | 4.69 | 0.016955195 |
| 16725468 | CD5 | -0.93 | 5.97 | 0.025936826 |
| 16817489 | CD19 | -2.02 | 4.61 | 0.000799686 |

| | | | | |
|---|---|---|---|---|
| 16725252 | MS4A1 | -2.93 | 6.27 | 0.01631073 |
| 16747261 | CD27 | -1.38 | 6.15 | 0.018376056 |
| 16889807 | CD28 | -1.66 | 5.31 | 0.000235992 |
| 17097653 | TNFSF8 | -1.09 | 6.59 | 0.013350291 |
| 16864675 | CD33 | -0.60 | 6.29 | 0.040623853 |
| 16874890 | SIGLEC6 | -0.69 | 3.58 | 0.040415958 |
| 16698801 | CD34 | -1.16 | 8.86 | 0.007922723 |
| 17047795 | CD36 | -1.96 | 4.23 | 0.002700734 |
| 16772144 | SCARB1 | 0.77 | 6.99 | 0.008444942 |
| 16864059 | CD37 | -1.14 | 7.45 | 0.010039892 |
| 16707791 | ENTPD1 | -1.29 | 4.56 | 6.16E-05 |
| 17100304 | ENTPD2 | 1.21 | 4.77 | 0.022818513 |
| 16914449 | CD40 | -1.02 | 5.48 | 0.003837347 |
| 17107329 | CD40LG | -1.38 | 3.46 | 0.001832257 |
| 16723653 | CD44 | -1.61 | 6.43 | 0.001105987 |
| 16695437 | CD48 | -1.04 | 7.02 | 0.015913143 |
| 16668582 | CD53 | -0.81 | 9.50 | 0.015880796 |
| 16761201 | CD69 | -1.53 | 6.49 | 0.027924641 |
| 17093694 | CD72 | -0.75 | 5.24 | 0.01869106 |
| 16862604 | CD79A | -2.36 | 7.01 | 0.01732704 |
| 16847719 | CD79B | -1.50 | 4.83 | 0.002113366 |
| 16720392 | CD151 | 0.42 | 8.10 | 0.033546474 |
| 16705159 | CDK1 | 1.21 | 5.03 | 0.041773458 |
| 16834056 | CDC6 | 1.59 | 5.74 | 0.002569923 |
| 16663514 | CDC20 | 1.43 | 5.78 | 0.036215521 |
| 16856187 | CDC34 | 0.57 | 7.36 | 0.04212478 |
| 16820486 | CDH1 | 4.35 | 8.05 | 0.000864133 |
| 16820463 | CDH3 | 3.51 | 7.83 | 0.001349107 |
| 16915541 | CDH4 | 1.72 | 5.68 | 0.000873906 |
| 16819794 | CDH5 | -1.58 | 7.68 | 0.005959278 |
| 16821377 | CDH13 | -1.95 | 6.56 | 0.02292966 |
| 16766683 | CDK4 | 0.49 | 8.54 | 0.041307561 |
| 17064360 | CDK5 | 0.89 | 6.60 | 0.007909082 |
| 16985637 | CDK7 | 0.75 | 6.49 | 0.008127261 |
| 16968468 | CDS1 | 1.23 | 4.82 | 0.02004605 |
| 16661149 | CD52 | -1.07 | 5.74 | 0.017875017 |
| 16677425 | CENPF | 1.47 | 5.99 | 0.019355126 |
| 17115077 | CETN2 | 0.81 | 7.53 | 0.000181676 |
| 16743111 | CTSC | -0.66 | 9.11 | 0.033266217 |
| 16779024 | RCBTB2 | -0.60 | 6.44 | 0.01805536 |
| 16795664 | FOXN3 | -0.65 | 6.65 | 0.006923742 |
| 16905292 | CHN1 | -0.97 | 5.69 | 0.041734024 |
| 16700806 | LYST | -1.14 | 7.04 | 0.000335481 |
| 16796998 | CKB | 1.58 | 5.20 | 0.00955707 |
| 16671503 | CKS1B | 1.15 | 6.06 | 0.000154278 |
| 17086634 | CKS2 | 1.62 | 8.28 | 0.0045247 |
| 16948738 | AP2M1 | 0.72 | 8.43 | 0.0003748 |
| 17049692 | AP1S1 | 0.68 | 6.06 | 0.015461148 |
| 16872248 | CLC | -1.45 | 3.34 | 0.002961292 |
| 16825333 | CLN3 | 0.81 | 7.12 | 0.006532925 |
| 16791419 | CMA1 | -1.77 | 3.58 | 5.17E-05 |
| 16938707 | CCR4 | -0.90 | 4.28 | 0.009693681 |
| 17014651 | CCR6 | -1.35 | 3.33 | 0.000380492 |
| 16844381 | CCR7 | -1.83 | 6.22 | 0.005187186 |
| 16769690 | CMKLR1 | -0.94 | 7.43 | 0.002795866 |
| 16858496 | CNN1 | -2.29 | 6.88 | 0.010462986 |
| 16683460 | CNR2 | -0.55 | 3.30 | 0.006380246 |
| 17048473 | COL1A2 | -1.20 | 10.84 | 0.012224831 |

| | | | | |
|---|---|---|---|---|
| 16780929 | COL4A1 | -1.51 | 7.90 | 0.010144377 |
| 16776431 | COL4A2 | -1.16 | 8.17 | 0.028313587 |
| 17090957 | COL5A1 | -1.16 | 7.80 | 0.038095053 |
| 16906352 | COL5A2 | -1.68 | 7.24 | 0.019713579 |
| 16909828 | COL6A3 | -1.01 | 9.81 | 0.03424377 |
| 17087430 | COL15A1 | -2.04 | 7.41 | 0.00712053 |
| 16684461 | COL16A1 | -1.16 | 5.82 | 0.02390527 |
| 17010042 | COL19A1 | -1.71 | 3.09 | 0.000197445 |
| 16870453 | COMP | -2.60 | 7.65 | 0.020009556 |
| 16821614 | COX4I1 | 0.40 | 11.15 | 0.038094073 |
| 16883205 | COX5B | 0.61 | 4.76 | 0.002597144 |
| 17008088 | COX6A1 | 0.57 | 11.45 | 0.005840512 |
| 16861118 | COX6B1 | 0.75 | 7.69 | 0.001175595 |
| 17105010 | COX7B | 0.64 | 6.23 | 0.015739185 |
| 16986983 | COX7C | 0.57 | 4.93 | 0.007628544 |
| 16832768 | CPD | -0.64 | 8.08 | 0.030688059 |
| 16664852 | CPT2 | 0.57 | 6.33 | 0.02891434 |
| 16676819 | CR1 | -1.74 | 6.05 | 0.029299821 |
| 16676795 | CR2 | -2.46 | 3.70 | 0.003800106 |
| 16789743 | CRIP1 | 1.22 | 7.18 | 0.018572209 |
| 16724194 | CRY2 | -0.48 | 5.79 | 0.030324898 |
| 16766001 | CS | 0.44 | 7.30 | 0.040847974 |
| 16914671 | CSE1L | 0.68 | 9.58 | 0.006205785 |
| 16929677 | CSF2RB | -1.10 | 5.75 | 0.000883381 |
| 16986913 | VCAN | -1.20 | 10.38 | 0.038867549 |
| 16838887 | SLC25A10 | 1.27 | 5.98 | 0.004528308 |
| 16915015 | CSTF1 | 0.56 | 6.66 | 0.006229481 |
| 16889819 | CTLA4 | -1.24 | 3.59 | 0.019792018 |
| 16989750 | CTNNA1 | 0.44 | 7.77 | 0.005792415 |
| 16676547 | CTSE | 5.02 | 8.05 | 0.000193974 |
| 16791427 | CTSG | -1.61 | 3.52 | 0.000107648 |
| 17096285 | CTSV | 1.33 | 3.76 | 0.007881553 |
| 16920762 | CTSZ | -0.81 | 8.75 | 0.009569715 |
| 17049729 | CUX1 | 0.59 | 7.36 | 0.032981961 |
| 17102538 | CYBB | -0.63 | 10.35 | 0.035280185 |
| 17073565 | CYC1 | 0.83 | 8.11 | 0.007017806 |
| 16818842 | CYLD | -0.69 | 7.83 | 0.003851986 |
| 16707541 | CYP26A1 | 1.38 | 4.29 | 0.041638363 |
| 16779701 | DACH1 | -1.02 | 4.26 | 0.001837551 |
| 16940705 | DAG1 | 0.77 | 6.67 | 0.010678171 |
| 16752244 | DGKA | -0.77 | 6.36 | 0.038292709 |
| 16962407 | DGKG | -0.65 | 3.74 | 0.003439455 |
| 16874005 | DBP | 0.86 | 6.69 | 0.029093717 |
| 16823087 | ECI1 | 1.10 | 7.80 | 0.000999387 |
| 16836896 | ACE | -0.96 | 5.23 | 0.004631814 |
| 16738963 | DDB1 | 0.41 | 8.32 | 0.00814217 |
| 16701975 | AKR1C1 | -0.84 | 2.71 | 0.01373974 |
| 16766578 | DDIT3 | 0.73 | 4.16 | 0.0168028 |
| 16682842 | DDOST | 0.61 | 7.83 | 0.002680938 |
| 17055910 | DFNA5 | 1.12 | 6.31 | 0.033104806 |
| 16741501 | DHCR7 | 1.77 | 6.99 | 3.69E-06 |
| 16687618 | DHCR24 | 2.68 | 8.98 | 4.22E-06 |
| 16935669 | CYB5R3 | -0.61 | 7.71 | 0.014636766 |
| 16827679 | NQO1 | 2.25 | 8.40 | 0.000615713 |
| 17105284 | DIAPH2 | -0.45 | 8.02 | 0.014903543 |
| 16825779 | 37135 | -1.05 | 6.04 | 0.011329237 |
| 16731169 | DLAT | 0.54 | 6.95 | 0.017591588 |
| 16742879 | DLG2 | -1.43 | 3.93 | 0.000869046 |

| | | | | |
|---|---|---|---|---|
| 16835656 | DLX4 | 0.56 | 4.32 | 0.029564449 |
| 16714998 | DNA2 | 0.69 | 5.26 | 0.042727556 |
| 17115571 | DNASE1L1 | 0.45 | 7.29 | 0.044561067 |
| 16712244 | TRDMT1 | -0.93 | 4.15 | 0.002719692 |
| 16992122 | DOCK2 | -1.06 | 7.84 | 0.002388825 |
| 16696120 | DPT | -2.50 | 8.07 | 0.004787552 |
| 16925341 | RCAN1 | -0.88 | 4.45 | 0.007464485 |
| 16851768 | DSG2 | 1.65 | 7.68 | 0.014931101 |
| 17004612 | DSP | 2.44 | 8.17 | 0.014728149 |
| 16757391 | DTX1 | -0.85 | 4.52 | 0.008999768 |
| 17095899 | ECM2 | -1.24 | 7.89 | 0.040983724 |
| 16709128 | DUSP5 | -1.19 | 5.72 | 0.042518128 |
| 16840550 | DVL2 | 0.51 | 5.83 | 0.042544944 |
| 16948712 | DVL3 | 0.52 | 7.90 | 0.045255361 |
| 16918445 | E2F1 | 1.04 | 5.75 | 0.043738806 |
| 16894539 | E2F6 | 0.66 | 5.24 | 0.01480654 |
| 17002278 | EBF1 | -1.80 | 6.25 | 0.001451103 |
| 16682989 | ECE1 | -0.89 | 7.15 | 0.014739525 |
| 16861887 | ECH1 | 0.75 | 7.25 | 0.042992262 |
| 16667760 | S1PR1 | -1.62 | 6.83 | 0.000520867 |
| 16921258 | EEF1A2 | 2.63 | 6.02 | 0.001958832 |
| 16671642 | EFNA1 | 1.60 | 5.75 | 0.003541398 |
| 16856538 | EFNA2 | 0.77 | 4.27 | 0.015547851 |
| 16998682 | EFNA5 | 2.25 | 7.71 | 0.000165075 |
| 16830653 | EFNB3 | 1.30 | 5.20 | 0.011077896 |
| 16668170 | CELSR2 | 1.30 | 5.90 | 0.001431864 |
| 17046135 | EGFR | 1.63 | 8.52 | 0.002500349 |
| 16682098 | EPHA2 | 0.81 | 7.97 | 0.011018364 |
| 17067963 | EIF4EBP1 | 0.97 | 7.93 | 0.0421346 |
| 16675924 | ELF3 | 0.92 | 4.16 | 0.03234765 |
| 17110481 | ELK1 | 0.62 | 7.31 | 0.00879171 |
| 16755339 | ELK3 | -0.88 | 7.30 | 0.006606747 |
| 16709739 | EMX2 | -0.96 | 3.96 | 0.014607798 |
| 17098594 | ENG | -1.13 | 8.78 | 0.001844689 |
| 16969766 | ENPEP | -1.28 | 5.63 | 0.013889215 |
| 16930534 | EP300 | -0.38 | 8.42 | 0.030396125 |
| 16879721 | EPAS1 | -0.90 | 9.33 | 0.007097819 |
| 17023551 | EPB41L2 | -0.57 | 8.35 | 0.036472257 |
| 17066446 | DMTN | 0.73 | 5.14 | 0.025292216 |
| 17098027 | STOM | -0.89 | 8.99 | 0.000459515 |
| 17052690 | EPHB6 | 2.00 | 6.12 | 0.013179829 |
| 16687028 | EPS15 | -0.56 | 8.24 | 0.015558878 |
| 16925602 | ERG | -0.97 | 6.45 | 0.035499302 |
| 17013809 | ESR1 | -0.64 | 3.77 | 0.010876802 |
| 16745997 | ETS1 | -1.11 | 8.04 | 0.003232985 |
| 16748407 | ETV6 | -0.59 | 8.36 | 0.011724275 |
| 16961331 | MECOM | -1.38 | 3.86 | 0.000246254 |
| 16849047 | EVPL | 0.92 | 5.61 | 0.031794929 |
| 16928761 | EWSR1 | -0.44 | 6.97 | 0.008101502 |
| 17078134 | EYA1 | -0.79 | 3.11 | 0.010224618 |
| 16986417 | F2RL1 | 1.47 | 4.55 | 0.01051819 |
| 17115729 | F8 | -0.89 | 6.11 | 0.015121652 |
| 16776798 | F10 | -0.70 | 3.58 | 0.011294995 |
| 17015331 | F13A1 | -1.65 | 9.42 | 0.000907558 |
| 17078592 | FABP4 | -2.30 | 6.26 | 0.046135766 |
| 16736722 | FANCF | 1.04 | 5.91 | 0.007335327 |
| 16850107 | FASN | 0.90 | 7.37 | 0.033301454 |
| 16808793 | FBN1 | -1.14 | 9.67 | 0.022734863 |

| | | | | |
|---|---|---|---|---|
| 16897834 | EFEMP1 | 0.62 | 11.77 | 0.008265301 |
| 16725172 | MS4A2 | -1.01 | 3.21 | 0.002849275 |
| 16867975 | FCER2 | -1.31 | 3.85 | 0.012588067 |
| 17099707 | FCN1 | -1.58 | 5.31 | 0.005455767 |
| 16855477 | FECH | 0.52 | 6.80 | 0.049019216 |
| 16725735 | FEN1 | 0.92 | 5.38 | 0.009933077 |
| 16773086 | FGF9 | 3.43 | 6.91 | 0.000146244 |
| 16780754 | FGF14 | -1.11 | 3.34 | 0.021609667 |
| 16746808 | FKBP4 | 0.59 | 7.30 | 0.033279228 |
| 17004198 | FOXF2 | 1.49 | 5.05 | 0.009933077 |
| 17091928 | FOXD4 | 0.87 | 4.99 | 0.006244544 |
| 16760048 | FOXM1 | 1.22 | 5.80 | 0.040039322 |
| 16778392 | FOXO1 | -1.01 | 6.49 | 0.001977587 |
| 17011450 | FOXO3 | -0.98 | 6.36 | 0.010973189 |
| 16733377 | FLI1 | -0.90 | 6.98 | 0.001343249 |
| 17051286 | FLNC | 1.04 | 9.25 | 0.03559341 |
| 16777715 | FLT1 | -0.89 | 6.49 | 0.015461148 |
| 17003958 | FLT4 | -1.27 | 4.85 | 0.02412805 |
| 16675638 | NR5A2 | -1.43 | 4.25 | 0.000897471 |
| 16739208 | FTH1 | -1.03 | 7.76 | 0.013388643 |
| 16785483 | FUT8 | -0.84 | 6.86 | 0.018958874 |
| 16995601 | FYB | -0.88 | 8.92 | 0.006690857 |
| 17016697 | GABBR1 | -0.86 | 6.78 | 0.011824105 |
| 17028593 | GABBR1 | -0.87 | 7.21 | 0.010876802 |
| 17026529 | GABBR1 | -0.90 | 7.04 | 0.010685173 |
| 17031378 | GABBR1 | -0.92 | 7.42 | 0.00995933 |
| 17033830 | GABBR1 | -0.90 | 6.89 | 0.009663603 |
| 17036121 | GABBR1 | -0.91 | 7.19 | 0.009447187 |
| 17038872 | GABBR1 | -0.91 | 7.19 | 0.009447187 |
| 16795508 | GALC | -0.50 | 5.57 | 0.034910126 |
| 16683397 | GALE | 1.27 | 4.95 | 0.002026515 |
| 16925194 | GART | 0.60 | 6.43 | 0.028472331 |
| 16958844 | GATA2 | -0.74 | 3.75 | 0.00326115 |
| 16689354 | GBP2 | -0.74 | 7.52 | 0.047823906 |
| 16689352 | GBP2 | -0.86 | 6.46 | 0.03238455 |
| 16713877 | GDF10 | -0.51 | 3.42 | 0.027312731 |
| 17079210 | GEM | -2.19 | 5.74 | 8.59E-05 |
| 16814895 | GFER | 0.73 | 5.56 | 0.001977587 |
| 17075248 | GFRA2 | -1.72 | 3.73 | 6.42E-06 |
| 16662329 | GJA4 | -0.85 | 5.30 | 0.030464325 |
| 16885153 | GLI2 | 1.18 | 6.93 | 0.02522701 |
| 16998293 | GLRX | -0.81 | 5.32 | 0.038329462 |
| 16716239 | GLUD1 | -0.86 | 5.88 | 0.003512006 |
| 17015033 | GMDS | -0.47 | 5.73 | 0.020787539 |
| 17054614 | GNA12 | -0.51 | 6.12 | 0.025386404 |
| 16856896 | GNA15 | -0.66 | 5.82 | 0.035788812 |
| 16940988 | GNAI2 | -0.45 | 5.17 | 0.040611238 |
| 16927874 | GNAZ | 0.60 | 5.50 | 0.041068624 |
| 16717359 | GOT1 | 0.73 | 7.87 | 0.023409439 |
| 16661314 | SFN | 2.52 | 5.90 | 0.007880507 |
| 16860709 | GPI | 0.68 | 9.89 | 0.0108719 |
| 16845219 | CCR10 | -0.39 | 3.05 | 0.048764761 |
| 16873352 | GPR4 | -1.25 | 4.69 | 0.003669752 |
| 16943181 | GPR15 | -0.68 | 2.65 | 0.018616123 |
| 16780585 | GPR18 | -1.05 | 4.86 | 0.012696086 |
| 17105069 | LPAR4 | -1.11 | 4.16 | 0.031676711 |
| 16930486 | MCHR1 | -0.82 | 3.89 | 0.001944711 |
| 16942625 | GPR27 | 0.90 | 4.34 | 0.025386404 |

| | | | | |
|---|---|---|---|---|
| 17062491 | GPR37 | 3.13 | 6.01 | 0.000841666 |
| 16991208 | GPX3 | -0.85 | 2.56 | 0.013961095 |
| 16991192 | GPX3 | -1.07 | 5.72 | 0.012002805 |
| 16833876 | GRB7 | 2.03 | 5.20 | 0.001398413 |
| 17106688 | GRIA3 | -0.96 | 3.21 | 0.000874966 |
| 16937094 | GRM7 | -0.60 | 3.23 | 0.007472363 |
| 17076063 | GSR | 0.60 | 9.14 | 0.03084029 |
| 16727919 | GSTP1 | 0.46 | 7.34 | 0.043440666 |
| 16879923 | MSH6 | 0.53 | 7.09 | 0.012795273 |
| 16825210 | GTF3C1 | 0.48 | 8.08 | 0.046769142 |
| 16895772 | GTF3C2 | 0.42 | 7.40 | 0.015630552 |
| 16971712 | GUCY1A3 | -1.30 | 7.11 | 0.012588067 |
| 16971737 | GUCY1B3 | -1.31 | 6.71 | 0.008753493 |
| 16980245 | GYPE | -1.17 | 4.50 | 0.001052997 |
| 16856195 | GZMM | -0.76 | 4.14 | 0.041307561 |
| 16745236 | H2AFX | 0.85 | 7.65 | 0.038527446 |
| 16978334 | H2AFZ | 0.43 | 5.92 | 0.046598957 |
| 17005573 | HIST1H2BD | 1.64 | 4.30 | 0.004162135 |
| 17111251 | HSD17B10 | 0.64 | 6.81 | 0.020357132 |
| 16874935 | HAS1 | 2.63 | 6.70 | 0.012366834 |
| 16734840 | HBB | -0.70 | 3.03 | 0.017773573 |
| 16912472 | HCK | -0.76 | 7.43 | 0.023367556 |
| 16957986 | HCLS1 | -0.84 | 7.27 | 0.017686424 |
| 16809075 | HDC | -1.07 | 2.79 | 0.000181676 |
| 16694742 | HDGF | 0.54 | 5.24 | 0.001837551 |
| 16752061 | NCKAP1L | -0.74 | 7.84 | 0.017773573 |
| 16811437 | HEXA | 0.46 | 8.03 | 0.040049302 |
| 16707493 | HHEX | -0.95 | 4.51 | 0.000146108 |
| 16785058 | HIF1A | -0.70 | 9.85 | 0.019587498 |
| 16785083 | HIF1A | -1.71 | 5.20 | 0.000522176 |
| 16999572 | HINT1 | 0.64 | 6.31 | 0.009488344 |
| 17024335 | HIVEP2 | -0.81 | 7.95 | 0.038051871 |
| 17003124 | HK3 | -0.82 | 4.20 | 0.029647519 |
| 17037290 | HLA-DMB | -0.50 | 6.90 | 0.046164473 |
| 17007352 | HLA-DPB1 | -0.54 | 8.05 | 0.03949699 |
| 17031219 | HLA-DPB1 | -0.54 | 8.05 | 0.03949699 |
| 17041318 | HLA-DPB1 | -0.54 | 8.05 | 0.03949699 |
| 16677723 | HLX | -0.52 | 4.85 | 0.048213306 |
| 17107753 | HMGB3 | 0.52 | 4.29 | 0.037187959 |
| 16991859 | HMMR | 1.39 | 5.34 | 0.007934112 |
| 16886105 | HNMT | -0.82 | 7.51 | 0.03559341 |
| 16872052 | HNRNPL | 0.34 | 9.84 | 0.037233519 |
| 17049366 | AGFG2 | 1.11 | 6.83 | 0.035136085 |
| 16821398 | HSBP1 | 0.67 | 7.84 | 0.010366891 |
| 17073759 | HSF1 | 0.56 | 6.57 | 0.017667263 |
| 16819994 | HSF4 | 0.69 | 5.67 | 0.043397402 |
| 16989146 | HSPA4 | 0.49 | 7.96 | 0.019182147 |
| 17000485 | HSPA9 | 0.53 | 9.48 | 0.022323152 |
| 16691414 | IGSF3 | 1.42 | 5.54 | 0.004044647 |
| 16968675 | HSP90AB3P | 0.63 | 5.73 | 0.040390831 |
| 16906962 | HSPD1 | 0.88 | 8.02 | 0.001689175 |
| 16683105 | HSPG2 | -0.78 | 9.37 | 0.014343097 |
| 16879958 | FOXN2 | -0.60 | 7.36 | 0.017854783 |
| 16778938 | HTR2A | -2.54 | 4.67 | 0.001844689 |
| 17097661 | TNC | -2.77 | 8.44 | 0.002244491 |
| 16847760 | ICAM2 | -1.26 | 6.12 | 0.001240458 |
| 16868679 | ICAM3 | -0.82 | 6.21 | 0.019633776 |
| 16821621 | IRF8 | -0.73 | 7.70 | 0.04882767 |

| | | | | |
|---|---|---|---|---|
| 16837689 | ICT1 | 0.58 | 8.35 | 0.035303656 |
| 16769250 | IGF1 | -2.10 | 8.75 | 0.002639629 |
| 16976211 | IGFBP7 | -0.84 | 10.40 | 0.024462218 |
| 16797603 | IGHG1 | -2.08 | 4.51 | 0.032254679 |
| 16797358 | IGHG2 | -0.89 | 6.30 | 0.033584759 |
| 16976644 | IGJ | -2.07 | 7.53 | 0.043875221 |
| 16900162 | IGKC | -1.91 | 7.64 | 0.038095053 |
| 16965642 | RBPJ | -0.80 | 6.62 | 0.000836238 |
| 16711501 | IL2RA | -1.49 | 5.98 | 0.004954729 |
| 17111895 | IL2RG | -1.21 | 6.86 | 0.042411482 |
| 17101111 | IL3RA | -1.21 | 5.52 | 0.00768316 |
| 17115868 | IL3RA | -1.13 | 4.99 | 0.00712053 |
| 16950216 | IL5RA | -0.50 | 2.73 | 0.013591094 |
| 17044177 | IL6 | -2.46 | 5.11 | 0.003044902 |
| 16984010 | IL7R | -1.58 | 6.42 | 0.019390771 |
| 16731754 | IL10RA | -0.70 | 7.49 | 0.02889654 |
| 17084523 | IL11RA | -0.70 | 5.66 | 0.010320732 |
| 16665901 | IL12RB2 | -1.92 | 3.51 | 2.42E-06 |
| 16744415 | IL18 | 1.93 | 8.42 | 0.000197445 |
| 16693515 | ILF2 | 0.54 | 9.35 | 0.020594156 |
| 17062679 | IMPDH1 | -0.79 | 6.51 | 0.029372633 |
| 16883325 | INPP4A | -0.60 | 6.92 | 0.007785772 |
| 16892446 | INPP5D | -0.59 | 7.40 | 0.031806444 |
| 16870269 | INSL3 | -0.57 | 4.45 | 0.024509699 |
| 16686538 | IPP | 0.54 | 6.46 | 0.014082538 |
| 17115428 | IRAK1 | 0.87 | 6.88 | 0.006465241 |
| 17004167 | IRF4 | -1.65 | 5.47 | 0.004041282 |
| 16835672 | ITGA3 | 1.91 | 9.48 | 1.35E-05 |
| 16888270 | ITGA4 | -1.00 | 7.35 | 0.015998855 |
| 16765697 | ITGA7 | -1.49 | 5.36 | 0.004019872 |
| 16938989 | ITGA9 | -0.99 | 7.03 | 0.021574616 |
| 16817883 | ITGAL | -0.88 | 6.85 | 0.049019216 |
| 16713144 | ITGB1 | -0.50 | 7.78 | 0.034573378 |
| 16837938 | ITGB4 | 2.76 | 9.13 | 0.001080715 |
| 16918664 | EIF6 | 0.72 | 7.78 | 0.001436653 |
| 16991497 | ITK | -1.49 | 5.81 | 0.013521294 |
| 16910974 | ITPA | 0.53 | 6.21 | 0.01555904 |
| 16700058 | ITPKB | -0.65 | 6.66 | 0.021168723 |
| 16936947 | ITPR1 | -0.83 | 6.22 | 0.033301454 |
| 17007543 | ITPR3 | 0.69 | 8.24 | 0.04628174 |
| 16688164 | JAK1 | -0.47 | 9.80 | 0.015058806 |
| 17083319 | JAK2 | -0.58 | 7.92 | 0.019097494 |
| 16870274 | JAK3 | -1.47 | 6.08 | 0.000250224 |
| 17005042 | JARID2 | -0.69 | 6.61 | 0.012773136 |
| 16844872 | JUP | 0.91 | 7.60 | 0.02649727 |
| 16828514 | KARS | 0.42 | 8.94 | 0.026308118 |
| 16747121 | KCNA1 | -1.02 | 2.67 | 0.011077896 |
| 16690739 | KCNA2 | -0.60 | 3.17 | 0.002202594 |
| 16690754 | KCNA3 | -1.41 | 5.43 | 0.001909164 |
| 16690735 | KCNA10 | 0.44 | 3.33 | 0.019207889 |
| 16920150 | KCNB1 | 1.25 | 4.95 | 0.03519136 |
| 16925328 | KCNE1 | -0.73 | 3.97 | 0.010525225 |
| 16966855 | KIT | -1.37 | 4.57 | 0.013895473 |
| 16707468 | KIF11 | 1.31 | 6.55 | 0.033528421 |
| 16817647 | KIF22 | 0.98 | 6.61 | 0.004115128 |
| 17011992 | KPNA5 | -0.49 | 6.56 | 0.028169656 |
| 16764941 | KRT5 | 4.21 | 6.92 | 1.55E-05 |
| 16751491 | KRT7 | 2.47 | 4.58 | 0.005118245 |

| | | | | |
|---|---|---|---|---|
| 16844752 | KRT15 | 1.17 | 4.48 | 0.011712035 |
| 16751554 | KRT18 | 2.94 | 6.07 | 2.05E-07 |
| 16844775 | KRT19 | 3.73 | 8.88 | 1.95E-05 |
| 16875478 | LAIR1 | -0.62 | 5.77 | 0.035992062 |
| 17012447 | LAMA2 | -1.36 | 6.73 | 0.031938783 |
| 16920939 | LAMA5 | 1.30 | 7.99 | 0.003485 |
| 16698883 | LAMB3 | 1.73 | 5.84 | 0.042907557 |
| 16674845 | LAMC2 | 2.69 | 6.90 | 0.005232106 |
| 16683723 | STMN1 | 0.73 | 4.68 | 0.015136425 |
| 16662052 | LCK | -0.87 | 4.89 | 0.016614321 |
| 16778849 | LCP1 | -0.93 | 8.81 | 0.009309447 |
| 17051152 | LEP | -1.64 | 3.19 | 0.001850621 |
| 17042997 | LFNG | -0.83 | 5.24 | 0.004349187 |
| 16849576 | LGALS3BP | 1.01 | 9.91 | 0.000463886 |
| 16872029 | LGALS4 | -0.31 | 3.66 | 0.033703724 |
| 16933760 | LIF | 1.05 | 5.15 | 0.04155983 |
| 16929163 | LIMK2 | -1.02 | 6.29 | 0.003052261 |
| 16837820 | LLGL2 | 1.50 | 6.17 | 0.002331189 |
| 16987565 | LNPEP | -0.40 | 8.62 | 0.035352582 |
| 17066278 | LPL | -1.44 | 4.16 | 0.042550011 |
| 16949467 | LPP | -0.65 | 7.10 | 0.007097178 |
| 16904827 | LRP2 | 4.93 | 7.24 | 0.001847311 |
| 16720771 | LSP1 | -0.52 | 4.26 | 0.041605579 |
| 17026762 | LTB | -0.85 | 4.63 | 0.033528421 |
| 17029082 | LTB | -0.85 | 4.63 | 0.033528421 |
| 17031867 | LTB | -0.85 | 4.63 | 0.033528421 |
| 17034339 | LTB | -0.85 | 4.63 | 0.033528421 |
| 17036587 | LTB | -0.85 | 4.63 | 0.033528421 |
| 17039380 | LTB | -0.85 | 4.63 | 0.033528421 |
| 17041863 | LTB | -0.85 | 4.63 | 0.033528421 |
| 17017224 | LTB | -0.72 | 2.83 | 0.012161058 |
| 16863074 | BCAM | 1.58 | 7.77 | 0.019247001 |
| 17073259 | LY6E | 1.14 | 5.12 | 0.007017806 |
| 16672669 | LY9 | -1.48 | 4.81 | 0.001587867 |
| 16996813 | CD180 | -0.83 | 7.46 | 0.024493485 |
| 16869391 | LYL1 | -0.69 | 5.93 | 0.001040497 |
| 17069063 | LYN | -0.85 | 8.12 | 0.002826228 |
| 17106795 | SH2D1A | -1.35 | 4.05 | 0.000995688 |
| 16753914 | LYZ | -1.02 | 9.07 | 0.011077896 |
| 16960355 | TM4SF1 | 1.45 | 10.40 | 0.01108929 |
| 16881138 | MXD1 | -0.95 | 6.68 | 0.003989474 |
| 16979389 | MAD2L1 | 1.23 | 4.65 | 0.009225792 |
| 16971167 | SMAD1 | -0.70 | 4.63 | 0.014596176 |
| 16882834 | MAL | -1.08 | 4.53 | 0.00165586 |
| 17023150 | MAN1A1 | -0.85 | 8.70 | 0.017847035 |
| 16978444 | MANBA | -0.62 | 7.21 | 0.046767865 |
| 16677655 | MARK1 | -1.13 | 3.91 | 0.013871085 |
| 16817666 | MAZ | 0.60 | 7.34 | 0.007197952 |
| 16947061 | MBNL1 | -0.50 | 10.37 | 0.002409036 |
| 16855617 | MC4R | -0.65 | 2.73 | 0.04209629 |
| 16745281 | MCAM | -0.89 | 5.82 | 0.024427075 |
| 16692775 | MCL1 | -0.60 | 9.65 | 0.020126598 |
| 16945101 | MCM2 | 1.17 | 6.15 | 0.004108398 |
| 17020019 | MCM3 | 0.64 | 7.92 | 0.033383735 |
| 17068782 | MCM4 | 1.18 | 7.51 | 0.009296335 |
| 17060412 | MCM7 | 0.90 | 7.23 | 0.008922121 |
| 16880596 | MDH1 | 0.66 | 6.75 | 0.00299001 |
| 17047461 | MDH2 | 0.77 | 7.21 | 0.000946504 |

| | | | | |
|---|---|---|---|---|
| 16676314 | MDM4 | -0.53 | 7.71 | 0.007978753 |
| 16997953 | MEF2C | -0.94 | 5.92 | 0.000176441 |
| 16880814 | MEIS1 | -1.10 | 5.51 | 0.009251812 |
| 16807139 | MEIS2 | 1.24 | 7.06 | 0.006202121 |
| 16984945 | MAP3K1 | -0.59 | 8.48 | 0.047912995 |
| 17014501 | MAP3K4 | -0.65 | 7.00 | 0.026407004 |
| 16740074 | MEN1 | 0.57 | 6.97 | 0.006495873 |
| 16845427 | MEOX1 | -0.77 | 4.87 | 0.007619384 |
| 17051626 | MEST | 1.30 | 6.32 | 0.015375785 |
| 17050591 | MET | 2.37 | 9.41 | 0.003158441 |
| 16963428 | MFI2 | 1.30 | 7.77 | 0.021084877 |
| 16934786 | MFNG | -0.89 | 5.87 | 0.001636024 |
| 16783675 | CTAGE5 | -0.67 | 3.94 | 0.0311196 |
| 16815828 | CIITA | -1.07 | 7.89 | 0.000848478 |
| 17101193 | CD99 | -1.21 | 5.64 | 0.00330802 |
| 16928098 | MIF | 0.65 | 9.66 | 0.037184243 |
| 16942576 | MITF | -0.72 | 4.32 | 0.035352582 |
| 17014714 | MLLT4 | 0.79 | 8.28 | 0.026032596 |
| 16819064 | MMP2 | -1.30 | 10.17 | 0.017996341 |
| 16743751 | MMP12 | -2.24 | 3.26 | 0.00437143 |
| 16819653 | MMP15 | 1.46 | 7.11 | 0.017345479 |
| 16765809 | MMP19 | -1.55 | 5.13 | 0.002145853 |
| 16943944 | CD200 | 1.07 | 9.21 | 0.042051728 |
| 16803103 | MPI | 0.57 | 8.14 | 0.016435119 |
| 17115692 | MPP1 | -0.74 | 7.69 | 0.017173716 |
| 16702836 | MRC1 | -1.53 | 8.14 | 0.022837699 |
| 16702881 | MRC1 | -1.54 | 8.20 | 0.020662433 |
| 16888912 | MYO1B | -1.23 | 8.08 | 0.01256299 |
| 16879883 | MSH2 | 0.72 | 6.88 | 0.008543208 |
| 16986748 | MSH3 | 0.51 | 8.09 | 0.048021706 |
| 16954295 | MST1R | 2.83 | 5.90 | 0.000239688 |
| 17107697 | MTM1 | -0.46 | 6.23 | 0.02824918 |
| 17019831 | MUT | 0.50 | 7.44 | 0.019276798 |
| 16756804 | MVK | 0.77 | 4.91 | 0.04025301 |
| 16934491 | MYH9 | -0.61 | 9.62 | 0.036154902 |
| 16824258 | MYH11 | -2.89 | 6.25 | 0.001303698 |
| 16809971 | MYO1E | -0.56 | 7.78 | 0.025836586 |
| 16809457 | MYO5A | -0.83 | 7.87 | 0.011830864 |
| 16855196 | MYO5B | 2.24 | 7.14 | 0.004950418 |
| 16767932 | PPP1R12A | -0.36 | 8.64 | 0.04628174 |
| 16996983 | NAIP | -0.91 | 8.73 | 0.001823563 |
| 16929662 | NCF4 | -0.78 | 6.72 | 0.012753894 |
| 17000800 | NDUFA2 | 0.66 | 7.61 | 0.006187928 |
| 16865175 | NDUFA3 | 0.39 | 6.02 | 0.043458411 |
| 16868138 | NDUFA7 | 0.84 | 6.40 | 0.006823205 |
| 17098071 | NDUFA8 | 0.62 | 6.46 | 0.008452289 |
| 16825097 | NDUFAB1 | 0.54 | 6.88 | 0.028437442 |
| 16889399 | NDUFB3 | 0.58 | 5.53 | 0.036526044 |
| 16944502 | NDUFB4 | 0.58 | 5.83 | 0.002912399 |
| 17093122 | NDUFB6 | 0.65 | 6.50 | 0.047497843 |
| 16869660 | NDUFB7 | 0.72 | 6.56 | 0.03010687 |
| 17072506 | NDUFB9 | 0.58 | 5.97 | 0.031806444 |
| 16814854 | NDUFB10 | 0.58 | 5.19 | 0.007214542 |
| 16724607 | NDUFS3 | 0.58 | 6.38 | 0.018831684 |
| 16727936 | NDUFV1 | 0.69 | 6.76 | 0.002108584 |
| 16662744 | NDUFS5 | 0.48 | 8.19 | 0.035352582 |
| 17007837 | RPL10A | 0.48 | 7.97 | 0.016052877 |
| 16698984 | NEK2 | 1.04 | 4.14 | 0.036461914 |

| | | | | |
|---|---|---|---|---|
| 16779369 | NEK3 | -0.57 | 6.32 | 0.041567289 |
| 16802795 | NEO1 | 1.40 | 8.78 | 0.023863252 |
| 16920315 | NFATC2 | -0.81 | 7.01 | 0.000557252 |
| 17092490 | NFIB | -0.85 | 8.94 | 0.00309707 |
| 16856946 | NFIC | 0.49 | 9.15 | 0.040390831 |
| 17006636 | NFKBIL1 | 0.42 | 5.01 | 0.013225766 |
| 17040689 | NFKBIL1 | 0.44 | 5.15 | 0.01256299 |
| 17027771 | NFKBIL1 | 0.46 | 4.94 | 0.010685173 |
| 17030597 | NFKBIL1 | 0.46 | 4.94 | 0.010685173 |
| 17033314 | NFKBIL1 | 0.46 | 4.94 | 0.010685173 |
| 17038094 | NFKBIL1 | 0.46 | 4.94 | 0.010685173 |
| 17035395 | NFKBIL1 | 0.48 | 4.92 | 0.010007902 |
| 16835592 | NGFR | -1.38 | 4.49 | 0.002818703 |
| 16939668 | NKTR | -0.57 | 7.64 | 0.021492339 |
| 17075536 | NKX3-1 | 1.21 | 5.23 | 0.000108848 |
| 16822801 | NME3 | 0.59 | 6.63 | 0.038014865 |
| 16814211 | NME4 | 0.39 | 4.77 | 0.023863252 |
| 16834883 | NMT1 | 0.37 | 8.64 | 0.046718866 |
| 16865214 | CNOT3 | 0.36 | 7.35 | 0.043476839 |
| 16869769 | NOTCH3 | -1.14 | 7.99 | 0.029828826 |
| 17027038 | NOTCH4 | -0.78 | 4.93 | 0.009047056 |
| 17042335 | NOTCH4 | -1.07 | 5.65 | 0.005096594 |
| 17039839 | NOTCH4 | -1.03 | 5.40 | 0.004796972 |
| 17029639 | NOTCH4 | -1.05 | 5.62 | 0.004665936 |
| 17034630 | NOTCH4 | -1.09 | 5.60 | 0.004265429 |
| 17037128 | NOTCH4 | -1.08 | 5.82 | 0.004109664 |
| 16781536 | PNP | -0.67 | 6.48 | 0.015868743 |
| 16671187 | NPR1 | 1.81 | 7.25 | 0.010829092 |
| 17048742 | NPTX2 | -1.40 | 4.55 | 0.013305094 |
| 17086386 | NTRK2 | -2.18 | 4.22 | 0.000165075 |
| 17109020 | GPR143 | 1.67 | 6.41 | 0.010366891 |
| 16894402 | ODC1 | 0.68 | 9.22 | 0.048888147 |
| 16761293 | OLR1 | 1.95 | 7.09 | 0.003104576 |
| 16687188 | ORC1 | 0.80 | 4.53 | 0.038481195 |
| 16903427 | ORC4 | 0.52 | 6.59 | 0.027478999 |
| 16839872 | P2RX1 | -0.97 | 4.64 | 0.004759764 |
| 16757710 | PEBP1 | 0.72 | 9.07 | 0.013196259 |
| 16805776 | PCSK6 | 0.59 | 4.50 | 0.015274977 |
| 16872767 | PAFAH1B3 | 1.43 | 6.61 | 0.000823584 |
| 16686472 | PRDX1 | 0.46 | 10.15 | 0.019678128 |
| 16987673 | PAM | -0.88 | 7.85 | 0.011453436 |
| 16767911 | PAWR | 0.98 | 6.76 | 0.0263308 |
| 17093973 | PAX5 | -1.83 | 5.07 | 0.001726932 |
| 16779667 | PCDH9 | -0.94 | 4.06 | 0.002498679 |
| 16768857 | CDK17 | -0.49 | 7.99 | 0.042122558 |
| 16676461 | CDK18 | 0.65 | 5.14 | 0.029303762 |
| 17056426 | PDE1C | -1.15 | 3.91 | 0.00913581 |
| 16722321 | PDE3B | -1.43 | 4.00 | 0.003991338 |
| 16665757 | PDE4B | -0.79 | 4.63 | 0.00236158 |
| 17077774 | PDE7A | -0.98 | 6.60 | 0.007335327 |
| 16804294 | PDE8A | -0.67 | 6.78 | 0.005959278 |
| 16752103 | PDE1B | -0.49 | 5.11 | 0.04926514 |
| 17001578 | PDGFRB | -1.27 | 8.92 | 0.007562595 |
| 17102210 | PDK3 | -1.09 | 6.76 | 0.00521885 |
| 17080516 | ENPP2 | -1.96 | 8.11 | 0.00174497 |
| 17080554 | ENPP2 | -1.67 | 4.13 | 0.001737231 |
| 17012598 | ENPP3 | -0.82 | 3.53 | 0.001080715 |
| 17019260 | PEX6 | 0.66 | 6.63 | 0.032246839 |

| | | | | |
|---|---|---|---|---|
| 16843462 | PEX12 | 0.78 | 6.35 | 0.017592941 |
| 17110463 | CFP | -0.59 | 3.66 | 0.042386257 |
| 16914961 | PFDN4 | 0.70 | 4.82 | 0.003669752 |
| 16855510 | ATP8B1 | -1.15 | 6.95 | 0.007594687 |
| 16750523 | PFKM | 0.63 | 5.45 | 0.037844332 |
| 16960442 | PFN2 | 1.06 | 7.62 | 0.000494327 |
| 16665566 | PGM1 | 1.05 | 8.60 | 0.03424377 |
| 17085610 | PGM5 | -0.81 | 3.16 | 0.03160773 |
| 17059451 | ABCB4 | -0.79 | 4.32 | 0.00102608 |
| 16846416 | PHB | 0.72 | 5.15 | 0.000838223 |
| 17102058 | PHEX | -0.80 | 2.96 | 0.005478009 |
| 16818017 | PHKG2 | 0.77 | 6.57 | 0.004796972 |
| 16909021 | SERPINE2 | -1.40 | 5.87 | 0.032307131 |
| 17050134 | PIK3CG | -0.96 | 7.76 | 0.012947456 |
| 16712482 | PIP4K2A | -0.86 | 7.48 | 0.002553629 |
| 17000104 | PITX1 | 0.96 | 3.80 | 0.000563567 |
| 16763032 | PKP2 | 2.09 | 7.52 | 0.004486863 |
| 16771279 | PLA2G1B | 1.03 | 4.76 | 0.025292216 |
| 16660282 | PLA2G5 | -1.14 | 4.58 | 0.003271895 |
| 17024394 | PLAGL1 | -1.11 | 7.58 | 0.03201727 |
| 16821326 | PLCG2 | -0.53 | 2.77 | 0.027615981 |
| 16821330 | PLCG2 | -1.17 | 7.34 | 0.000716011 |
| 16961551 | PLD1 | -0.88 | 5.87 | 0.031303776 |
| 16880942 | PLEK | -1.15 | 7.78 | 0.003104576 |
| 16829557 | SERPINF2 | -1.02 | 4.55 | 0.014549322 |
| 16817017 | PLK1 | 1.25 | 6.59 | 0.035188462 |
| 16946485 | PLS1 | 1.35 | 4.37 | 0.017998952 |
| 16919703 | PLTP | -0.86 | 9.77 | 0.022514505 |
| 16953329 | PLXNB1 | 1.58 | 6.74 | 0.000686385 |
| 17067393 | PNOC | -0.59 | 3.32 | 0.04926514 |
| 16841561 | PMP22 | -0.71 | 7.10 | 0.023388426 |
| 17060545 | PMS2P1 | 0.82 | 4.80 | 0.002746274 |
| 17047247 | PMS2P5 | 0.72 | 4.17 | 0.00495321 |
| 16673636 | PRRX1 | -1.24 | 7.47 | 0.012778755 |
| 16847137 | 38231 | -0.93 | 5.09 | 0.001177318 |
| 17057174 | POLD2 | 0.67 | 5.87 | 0.031978027 |
| 16819509 | POLR2C | 0.54 | 8.14 | 0.009933077 |
| 16866565 | POLR2E | 0.67 | 8.28 | 0.011077896 |
| 16871613 | POLR2I | 1.14 | 7.08 | 0.000443686 |
| 16734154 | POLR2L | 0.52 | 7.02 | 0.037515824 |
| 17059932 | PON2 | 0.50 | 8.59 | 0.026095642 |
| 16744247 | POU2AF1 | -0.56 | 2.83 | 0.008973363 |
| 16872705 | POU2F2 | -0.81 | 4.80 | 0.003552569 |
| 16931339 | PPARA | -0.45 | 6.09 | 0.019097494 |
| 16937741 | PPARG | -1.61 | 5.03 | 0.000739652 |
| 17045738 | PPIA | 0.51 | 6.34 | 0.024368191 |
| 16823666 | PPL | 3.11 | 7.53 | 0.000197445 |
| 16672779 | PPOX | 0.55 | 4.67 | 0.042115558 |
| 16740977 | PPP1CA | 0.53 | 6.57 | 0.016925456 |
| 16963099 | PPP1R2 | -0.71 | 5.20 | 0.003033218 |
| 16974049 | PPP2R2C | 1.29 | 4.34 | 0.010414507 |
| 16677228 | PPP2R5A | -0.48 | 7.03 | 0.004768442 |
| 16788833 | PPP2R5C | -0.75 | 5.33 | 0.000292977 |
| 16817811 | PPP4C | 0.50 | 8.54 | 0.020401607 |
| 16715505 | PPP3CB | -0.44 | 7.70 | 0.03465356 |
| 17066627 | PPP3CC | -0.55 | 6.53 | 0.036030551 |
| 16704464 | NPY4R | 0.96 | 3.92 | 0.015074582 |
| 16761549 | PRB1 | -0.60 | 5.04 | 0.016667474 |

| | | | | |
|---|---|---|---|---|
| 16742787 | PRCP | -0.83 | 5.15 | 0.002932545 |
| 16705507 | SRGN | -0.64 | 10.80 | 0.032682761 |
| 17009862 | PRIM2 | 0.51 | 6.28 | 0.049019216 |
| 16995685 | PRKAA1 | -0.58 | 7.25 | 0.00243619 |
| 16666616 | PRKACB | -0.96 | 7.49 | 0.000942856 |
| 17054254 | PRKAR1B | 0.60 | 4.92 | 0.039218109 |
| 16817044 | PRKCB | -1.02 | 4.49 | 0.004762177 |
| 16879679 | PRKCE | -0.69 | 4.45 | 0.005553029 |
| 16785003 | PRKCH | -1.34 | 4.93 | 0.000804953 |
| 16947875 | PRKCI | 1.07 | 8.99 | 0.001754644 |
| 16711533 | PRKCQ | -1.18 | 4.86 | 0.012427259 |
| 16858468 | PRKCSH | 0.47 | 10.41 | 0.030033578 |
| 16704977 | PRKG1 | -1.59 | 5.45 | 0.007077087 |
| 16704660 | MAPK8 | -0.49 | 5.34 | 0.014924133 |
| 16677391 | PROX1 | -1.39 | 4.36 | 0.002378446 |
| 17106031 | PRPS1 | 0.86 | 7.42 | 0.002145853 |
| 17061298 | RELN | -1.97 | 4.51 | 0.001448824 |
| 16874731 | KLK10 | 1.47 | 6.44 | 0.02259675 |
| 17057035 | PSMA2 | 0.54 | 9.52 | 0.008987831 |
| 16803540 | PSMA4 | 0.62 | 7.81 | 0.013715892 |
| 16685144 | PSMB2 | 0.59 | 9.17 | 0.002565523 |
| 16833698 | PSMB3 | 0.51 | 9.22 | 0.022819564 |
| 17049965 | PSMC2 | 0.48 | 8.67 | 0.005899177 |
| 16862145 | PSMC4 | 0.63 | 8.75 | 0.011345175 |
| 16948871 | PSMD2 | 0.55 | 8.63 | 0.001837551 |
| 16861704 | PSMD8 | 0.43 | 10.64 | 0.041059079 |
| 16833139 | PSMD11 | 0.44 | 7.87 | 0.031901828 |
| 17057946 | PSPH | 0.81 | 5.96 | 0.00798639 |
| 16856257 | PTBP1 | 0.37 | 10.05 | 0.023563726 |
| 16707030 | PTEN | -0.67 | 6.87 | 0.011744728 |
| 16984287 | PTGER4 | -0.77 | 6.92 | 0.011924989 |
| 16666471 | PTGFR | -1.69 | 4.42 | 0.001218332 |
| 16873562 | PTGIR | -0.87 | 5.76 | 0.022276315 |
| 16921268 | PTK6 | 0.62 | 3.81 | 0.041591961 |
| 17097000 | PTPN3 | 1.66 | 6.02 | 0.013317113 |
| 16747623 | PTPN6 | -0.71 | 7.21 | 0.02138633 |
| 16811816 | PTPN9 | 0.66 | 7.49 | 0.011077896 |
| 16699174 | PTPN14 | 0.90 | 8.85 | 0.031140551 |
| 16767422 | PTPRB | -1.23 | 6.33 | 0.004935448 |
| 16675578 | PTPRC | -1.19 | 8.48 | 0.003485 |
| 17092331 | PTPRD | -1.43 | 5.29 | 0.020083682 |
| 16740997 | PTPRCAP | -1.43 | 7.15 | 0.01631073 |
| 16663621 | PTPRF | 2.41 | 8.96 | 1.58E-05 |
| 16875656 | PTPRH | 1.45 | 4.29 | 0.034807093 |
| 16850759 | PTPRM | -1.14 | 8.79 | 0.000769357 |
| 16863091 | PVRL2 | 0.82 | 6.94 | 0.005841687 |
| 16759592 | PXMP2 | 0.87 | 6.86 | 0.003437283 |
| 16747770 | PEX5 | 0.50 | 5.57 | 0.022002025 |
| 16739979 | PYGM | 1.71 | 5.98 | 0.027473959 |
| 16752322 | RAB5B | 0.43 | 5.98 | 0.018019088 |
| 16852463 | RAB27B | 2.13 | 6.40 | 0.041307561 |
| 16791244 | RABGGTA | 0.71 | 5.90 | 0.022575571 |
| 16934749 | RAC2 | -0.57 | 5.15 | 0.040039322 |
| 16838977 | RAC3 | 1.56 | 6.15 | 0.002929216 |
| 17087933 | RAD23B | 0.49 | 9.29 | 0.049029427 |
| 16759202 | RAN | 0.64 | 7.66 | 0.01072311 |
| 16668712 | RAP1A | -0.56 | 7.06 | 0.00643613 |
| 16753779 | RAP1B | -0.86 | 6.46 | 0.012178643 |

| | | | | |
|---|---|---|---|---|
| 16683022 | RAP1GAP | 0.99 | 3.88 | 0.01223952 |
| 16946393 | RASA2 | -0.89 | 6.93 | 0.003866024 |
| 16784664 | ARID4A | -0.44 | 6.67 | 0.048093219 |
| 16662134 | RBBP4 | 0.47 | 9.60 | 0.003132044 |
| 17109396 | RBBP7 | 0.62 | 7.99 | 0.002360681 |
| 16880414 | REL | -0.79 | 8.33 | 0.006367131 |
| 16740495 | RELA | 0.41 | 6.92 | 0.004810414 |
| 16726832 | DPF2 | 0.36 | 6.59 | 0.039984612 |
| 17022623 | REV3L | -0.77 | 7.64 | 0.000557252 |
| 17058617 | RFC2 | 0.78 | 6.52 | 0.004665936 |
| 16773946 | RFC3 | 0.59 | 6.96 | 0.047574394 |
| 16962493 | RFC4 | 0.91 | 6.01 | 0.002538591 |
| 16757687 | RFC5 | 0.86 | 6.49 | 0.004567792 |
| 16869519 | RFX1 | 0.41 | 5.48 | 0.034147773 |
| 17088230 | RGS3 | -0.55 | 4.93 | 0.042473943 |
| 16675312 | RGS13 | -1.05 | 3.38 | 0.015516112 |
| 17064544 | RHEB | 0.50 | 5.63 | 0.047708696 |
| 16790115 | RNASE1 | -0.59 | 6.41 | 0.047497843 |
| 17041209 | RNF5 | 0.46 | 7.01 | 0.033584759 |
| 16733920 | RNH1 | 0.48 | 6.62 | 0.035110005 |
| 16675903 | RNPEP | 0.37 | 8.40 | 0.038464821 |
| 16810133 | RORA | -0.82 | 5.79 | 0.039532232 |
| 17085951 | RORB | -1.12 | 3.79 | 0.005048834 |
| 17110086 | RPGR | -1.04 | 5.80 | 0.000239688 |
| 17055191 | RPA3 | 0.70 | 6.21 | 0.013011825 |
| 16859648 | RPL18A | 0.42 | 11.10 | 0.032874172 |
| 16956952 | RPL24 | 0.40 | 6.19 | 0.035188462 |
| 16865675 | RPL28 | 0.62 | 4.85 | 0.010221593 |
| 16950133 | RPL35A | 0.43 | 5.97 | 0.01541723 |
| 16837482 | RPL38 | 0.40 | 5.76 | 0.022549607 |
| 16861907 | MRPS12 | 0.81 | 4.86 | 0.016643305 |
| 16729103 | RPS3 | 0.42 | 6.58 | 0.033386639 |
| 16866282 | RPS5 | 0.58 | 11.53 | 0.016333651 |
| 16856581 | RPS15 | 0.45 | 10.87 | 0.010861211 |
| 17036038 | RPS18 | 0.35 | 6.84 | 0.04297597 |
| 16862596 | RPS19 | 0.39 | 10.97 | 0.03234765 |
| 16915676 | RPS21 | 0.69 | 6.09 | 0.041059079 |
| 16706412 | RPS24 | 0.47 | 5.77 | 0.040623853 |
| 17004551 | RREB1 | -0.36 | 7.87 | 0.038014865 |
| 16721126 | RRM1 | 0.76 | 6.91 | 0.004019872 |
| 17038750 | VPS52 | 0.35 | 5.88 | 0.049019216 |
| 17028466 | VPS52 | 0.41 | 5.85 | 0.025491785 |
| 17031280 | VPS52 | 0.41 | 5.85 | 0.025491785 |
| 17033765 | VPS52 | 0.41 | 5.85 | 0.025491785 |
| 17036029 | VPS52 | 0.41 | 5.85 | 0.025491785 |
| 17041336 | VPS52 | 0.41 | 5.85 | 0.025491785 |
| 17034947 | VPS52 | 0.42 | 8.40 | 0.021336701 |
| 16790413 | SALL2 | 0.79 | 4.87 | 0.042489049 |
| 16951409 | SATB1 | -0.95 | 6.15 | 0.000907558 |
| 16972155 | MSMO1 | 0.73 | 8.33 | 0.035188462 |
| 17015862 | ATXN1 | -0.52 | 7.54 | 0.034233212 |
| 16904514 | SCN3A | -1.14 | 3.02 | 0.010665065 |
| 17117567 | SCN8A | 0.84 | 3.96 | 0.024635244 |
| 16751319 | SCN8A | 1.38 | 5.20 | 0.019484538 |
| 16760350 | SCNN1A | 2.98 | 5.84 | 0.011426997 |
| 16833231 | CCL13 | -1.71 | 4.00 | 0.012161058 |
| 16843541 | CCL16 | -0.63 | 3.00 | 0.02159481 |
| 16833411 | CCL18 | -1.14 | 4.66 | 0.012398429 |

| | | | | |
|---|---|---|---|---|
| 17093543 | CCL21 | -3.02 | 8.62 | 0.010685173 |
| 16843567 | CCL23 | -0.68 | 3.08 | 0.017054569 |
| 17058870 | CCL24 | -1.23 | 3.12 | 0.040273669 |
| 16819484 | CX3CL1 | -0.62 | 5.64 | 0.011077896 |
| 16919567 | SDC4 | 1.83 | 8.70 | 0.000546493 |
| 16842766 | SDF2 | 0.37 | 6.90 | 0.04926514 |
| 16696251 | SELE | -2.33 | 4.85 | 0.002483481 |
| 16696237 | SELL | -1.96 | 6.73 | 0.002963593 |
| 16696217 | SELP | -1.50 | 5.33 | 0.044175368 |
| 16866993 | SGTA | 0.57 | 8.54 | 0.008999768 |
| 17094064 | SHB | 1.05 | 8.53 | 0.011819549 |
| 16842103 | SHMT1 | 0.98 | 5.49 | 0.005934022 |
| 16827793 | ST3GAL2 | -0.54 | 6.94 | 0.027548904 |
| 16762202 | ST8SIA1 | -1.10 | 3.61 | 0.000351234 |
| 16686796 | STIL | 1.10 | 6.16 | 0.018889578 |
| 16727017 | SIPA1 | -0.51 | 6.06 | 0.011077896 |
| 16984032 | SKP2 | 1.28 | 8.94 | 0.000443686 |
| 16695422 | SLAMF1 | -1.58 | 4.74 | 0.001280256 |
| 16725984 | SLC3A2 | 0.68 | 8.04 | 0.001636024 |
| 17053553 | SLC4A2 | 0.88 | 6.00 | 0.009473381 |
| 16934198 | SLC5A4 | -1.47 | 3.31 | 2.51E-05 |
| 16937645 | SLC6A1 | -1.19 | 4.51 | 0.01634837 |
| 16932706 | SLC7A4 | 1.79 | 6.15 | 0.004432742 |
| 16944588 | SLC15A2 | -0.81 | 5.71 | 0.033811243 |
| 16691023 | SLC16A1 | 1.52 | 6.48 | 0.000456269 |
| 16709713 | SLC18A2 | -0.74 | 3.51 | 0.01068741 |
| 17014442 | SLC22A3 | -2.26 | 4.80 | 0.011781352 |
| 16989018 | SLC22A5 | 1.97 | 7.68 | 0.000679899 |
| 16919547 | SLPI | 4.42 | 10.21 | 0.000456269 |
| 17077004 | SNAI2 | -1.22 | 9.57 | 0.033663804 |
| 16926433 | SUMO3 | 0.56 | 5.77 | 0.004872828 |
| 16848755 | SUMO2 | 0.65 | 8.24 | 0.013099441 |
| 16862333 | SNRPA | 0.54 | 8.85 | 0.018803979 |
| 16916546 | SNRPB | 0.73 | 8.56 | 0.007072458 |
| 17007661 | SNRPC | 0.79 | 5.48 | 0.001521727 |
| 16873391 | SNRPD2 | 0.56 | 7.20 | 0.018958351 |
| 16965519 | SOD3 | -1.72 | 6.22 | 0.001248774 |
| 16896710 | SOS1 | -0.32 | 8.53 | 0.034250461 |
| 17005276 | SOX4 | 1.37 | 9.40 | 0.003485 |
| 16840696 | SOX15 | 1.17 | 4.23 | 0.049558299 |
| 16864518 | SPIB | -0.98 | 4.65 | 0.006646723 |
| 16799690 | SPINT1 | 2.04 | 7.19 | 0.008738402 |
| 16881434 | SPR | 1.68 | 7.26 | 0.000572613 |
| 16740867 | SPTBN2 | 1.41 | 4.79 | 0.012126133 |
| 16738429 | SSRP1 | 0.75 | 7.99 | 0.008537511 |
| 16837426 | SSTR2 | -0.93 | 3.73 | 0.000217555 |
| 16906571 | STAT4 | -1.10 | 5.45 | 0.040335382 |
| 16845096 | STAT5B | -0.51 | 6.94 | 0.002567779 |
| 16920100 | STAU1 | 0.33 | 8.74 | 0.029810598 |
| 16914147 | STK4 | -0.73 | 7.80 | 0.006495873 |
| 16825377 | SULT1A2 | 1.01 | 5.09 | 0.001325644 |
| 16857703 | STXBP2 | 0.60 | 7.26 | 0.034323795 |
| 16847087 | SUPT4H1 | 0.48 | 9.71 | 0.022309677 |
| 16705531 | SUPV3L1 | 0.42 | 7.49 | 0.029382558 |
| 17086708 | SYK | -0.88 | 6.37 | 0.004665936 |
| 17068093 | TACC1 | -0.64 | 7.70 | 0.016667474 |
| 16899401 | TACR1 | -1.88 | 3.64 | 1.41E-05 |
| 17000854 | TAF7 | 0.76 | 7.51 | 0.016535009 |

| | | | | |
|---|---|---|---|---|
| 16996917 | TAF9 | 0.42 | 5.47 | 0.041012517 |
| 16686784 | TAL1 | -0.58 | 3.10 | 0.021821543 |
| 16751857 | TARBP2 | 0.48 | 5.70 | 0.041117157 |
| 16983800 | TARS | 0.67 | 7.92 | 0.021084877 |
| 17078342 | TCEB1 | 0.47 | 5.93 | 0.038221159 |
| 16823193 | TCEB2 | 0.39 | 8.78 | 0.023233376 |
| 16855382 | TCF4 | -0.94 | 8.36 | 0.007594659 |
| 16989202 | TCF7 | -1.18 | 4.76 | 0.003652987 |
| 16928988 | TCN2 | -0.89 | 5.52 | 0.004937041 |
| 16869324 | PRDX2 | 0.69 | 7.13 | 0.01758657 |
| 16722189 | TEAD1 | 0.95 | 9.30 | 0.000224628 |
| 16746906 | TEAD4 | 0.92 | 6.69 | 0.002849275 |
| 16789960 | TEP1 | -0.64 | 7.18 | 0.002929216 |
| 16961372 | TERC | 2.11 | 9.55 | 6.47E-05 |
| 17015540 | TFAP2A | 1.55 | 5.00 | 0.001049806 |
| 16915091 | TFAP2C | 1.80 | 4.88 | 0.001407849 |
| 16823512 | TFAP4 | 0.72 | 5.56 | 0.014510297 |
| 16805422 | NR2F2 | -1.02 | 4.59 | 0.00746182 |
| 16906308 | TFPI | -1.67 | 6.37 | 0.007628544 |
| 16677556 | TGFB2 | 1.78 | 7.65 | 0.049797276 |
| 16938562 | TGFBR2 | -0.75 | 9.79 | 0.033584759 |
| 16689546 | TGFBR3 | -1.14 | 6.19 | 0.010039892 |
| 16791219 | TGM1 | 3.67 | 7.80 | 0.00046013 |
| 16799315 | THBS1 | -1.67 | 10.09 | 0.031512587 |
| 16951567 | THRB | -0.93 | 4.80 | 0.019713579 |
| 16663457 | TIE1 | -1.42 | 4.88 | 0.003082722 |
| 16849379 | TK1 | 1.29 | 5.97 | 0.022323152 |
| 16867018 | TLE2 | 1.13 | 5.99 | 0.044453176 |
| 17086208 | TLE4 | -1.05 | 5.89 | 0.002954329 |
| 16972198 | TLL1 | -1.61 | 6.30 | 0.012675849 |
| 16720416 | TSPAN4 | 0.55 | 6.01 | 0.02138633 |
| 16726680 | TM7SF2 | 0.86 | 4.14 | 0.019028688 |
| 16832438 | TNFAIP1 | 0.62 | 9.03 | 0.019786978 |
| 16875599 | TNNT1 | 2.44 | 5.28 | 0.025292216 |
| 16908251 | TNS1 | -1.07 | 6.86 | 0.002145853 |
| 16844312 | TOP2A | 1.71 | 8.05 | 0.00955707 |
| 16840732 | TP53 | 0.55 | 8.39 | 0.047708696 |
| 17012281 | TPD52L1 | 1.74 | 5.54 | 0.009049385 |
| 17097941 | TRAF1 | -0.73 | 5.38 | 0.011105871 |
| 16789080 | TRAF3 | -0.51 | 6.68 | 0.026161652 |
| 16694529 | CCT3 | 0.71 | 8.82 | 0.017352007 |
| 17049557 | TRIP6 | 0.69 | 8.40 | 0.021751719 |
| 16743593 | TRPC6 | -1.09 | 3.51 | 0.00122328 |
| 17080342 | TRPS1 | -0.97 | 6.80 | 0.003898923 |
| 16736508 | TSG101 | 0.43 | 7.27 | 0.043034204 |
| 16787068 | TSHR | -0.55 | 3.03 | 0.017198424 |
| 16934671 | TST | 1.13 | 7.63 | 0.024951715 |
| 17010552 | TTK | 1.17 | 5.01 | 0.044172882 |
| 16670894 | TUFT1 | 1.74 | 6.55 | 0.00019927 |
| 16756163 | TXNRD1 | 0.90 | 6.77 | 0.009975704 |
| 16850477 | TYMS | 1.31 | 6.86 | 0.008236083 |
| 16831434 | UBB | 1.01 | 5.32 | 0.004848101 |
| 16944325 | UPK1B | 6.01 | 8.98 | 6.16E-05 |
| 16976524 | UGT2B17 | -0.90 | 1.90 | 0.000462616 |
| 16970001 | UGT8 | -1.29 | 3.81 | 0.005962736 |
| 16756627 | UNG | 0.93 | 6.59 | 0.001531279 |
| 16816739 | UQCRC2 | 0.50 | 9.53 | 0.010366891 |
| 16664048 | UROD | 0.73 | 6.91 | 0.005253203 |

| | | | | |
|---|---|---|---|---|
| 16665447 | USP1 | 0.58 | 7.72 | 0.045269698 |
| 17013283 | UTRN | -0.58 | 8.95 | 0.015983939 |
| 16857490 | VAV1 | -0.98 | 6.99 | 0.006570848 |
| 16667702 | VCAM1 | -1.36 | 7.89 | 0.04025301 |
| 16706298 | VDAC2 | 0.53 | 6.11 | 0.009910072 |
| 17025191 | EZR | 1.52 | 10.68 | 0.000356926 |
| 16939637 | VIPR1 | -0.52 | 3.75 | 0.038287583 |
| 17083197 | VLDLR | 2.26 | 8.07 | 0.008599003 |
| 16760257 | VWF | -1.66 | 8.14 | 0.002385386 |
| 16905238 | WIPF1 | -1.06 | 7.28 | 0.000180119 |
| 16846022 | WNT3 | 1.57 | 5.03 | 0.002351716 |
| 16936044 | WNT7B | 0.83 | 4.22 | 0.015700481 |
| 16668785 | WNT2B | 1.90 | 7.37 | 0.004236839 |
| 16700147 | WNT9A | 1.80 | 5.94 | 0.000241896 |
| 16737105 | WT1 | 0.98 | 8.30 | 0.043476839 |
| 16933535 | XBP1 | -0.97 | 9.01 | 0.001507011 |
| 17106852 | XPNPEP2 | -0.98 | 3.79 | 0.022708138 |
| 16914103 | YWHAB | -0.31 | 8.39 | 0.044495749 |
| 16839331 | YWHAE | 0.39 | 7.44 | 0.020583412 |
| 16883232 | ZAP70 | -1.11 | 5.24 | 0.011383908 |
| 17060394 | ZNF3 | 0.47 | 5.88 | 0.049702356 |
| 17073961 | ZNF7 | 0.41 | 4.90 | 0.035302047 |
| 16866031 | ZNF17 | 0.60 | 5.54 | 0.007777057 |
| 16713498 | ZNF32 | 0.53 | 5.48 | 0.048137916 |
| 17049090 | ZSCAN21 | 0.52 | 6.04 | 0.015886272 |
| 16933044 | ZNF70 | -0.48 | 6.72 | 0.047314746 |
| 16868410 | ZNF121 | 0.54 | 8.92 | 0.010681072 |
| 16843987 | PCGF2 | 0.51 | 7.57 | 0.03720646 |
| 17033956 | TRIM26 | 0.49 | 6.72 | 0.049788184 |
| 17041583 | TRIM26 | 0.51 | 6.74 | 0.038039243 |
| 17016832 | TRIM26 | 0.51 | 6.74 | 0.036557098 |
| 17031500 | TRIM26 | 0.51 | 6.74 | 0.036557098 |
| 17036239 | TRIM26 | 0.52 | 6.77 | 0.035669357 |
| 17026623 | TRIM26 | 0.53 | 6.72 | 0.031400664 |
| 17107919 | ZNF185 | 1.46 | 6.58 | 0.001657106 |
| 16735231 | ZNF214 | 0.55 | 4.07 | 0.045222289 |
| 16721535 | ZNF215 | -1.64 | 3.50 | 0.001657106 |
| 16873174 | ZNF229 | 1.35 | 4.89 | 0.017796154 |
| 16683250 | LUZP1 | -0.54 | 5.73 | 0.035352582 |
| 16659478 | PRDM2 | -0.46 | 6.14 | 0.024870637 |
| 16901624 | MALL | -0.74 | 4.03 | 0.01758657 |
| 16903140 | CXCR4 | -1.20 | 9.35 | 0.039290159 |
| 16941024 | SEMA3B | 2.05 | 7.47 | 0.011329237 |
| 16998532 | ST8SIA4 | -1.11 | 6.98 | 0.003801595 |
| 17017244 | BAG6 | 0.42 | 7.16 | 0.016813999 |
| 17031933 | GPANK1 | 0.46 | 4.70 | 0.012217639 |
| 17036651 | GPANK1 | 0.44 | 4.65 | 0.008999768 |
| 17017290 | GPANK1 | 0.45 | 4.62 | 0.006249259 |
| 17034403 | GPANK1 | 0.45 | 4.62 | 0.006249259 |
| 17029148 | GPANK1 | 0.45 | 4.55 | 0.005270531 |
| 17039446 | GPANK1 | 0.45 | 4.07 | 0.004759764 |
| 17041929 | GPANK1 | 0.45 | 4.07 | 0.004759764 |
| 17007393 | HSD17B8 | 0.94 | 5.90 | 0.035352582 |
| 17028442 | HSD17B8 | 0.94 | 5.90 | 0.035352582 |
| 17031254 | HSD17B8 | 0.94 | 5.90 | 0.035352582 |
| 17033739 | HSD17B8 | 0.94 | 5.90 | 0.035352582 |
| 17036003 | HSD17B8 | 0.94 | 5.90 | 0.035352582 |
| 17038722 | HSD17B8 | 0.94 | 5.90 | 0.035352582 |

| | | | | |
|---|---|---|---|---|
| 17019728 | PLA2G7 | -1.65 | 6.05 | 0.025836586 |
| 17043355 | AIMP2 | 0.98 | 7.29 | 0.00041147 |
| 17052939 | ARHGEF5 | 1.04 | 5.26 | 0.024614831 |
| 16712168 | CUBN | -1.36 | 4.15 | 1.58E-05 |
| 16719417 | ADAM12 | -1.99 | 7.59 | 0.019402743 |
| 16720219 | RASSF7 | 0.87 | 4.69 | 0.009127161 |
| 16747501 | USP5 | 0.66 | 7.46 | 0.018780741 |
| 16753923 | YEATS4 | 0.69 | 7.48 | 0.049710075 |
| 16796451 | TCL1A | -0.90 | 3.64 | 0.005113143 |
| 16857429 | CLPP | 0.58 | 8.33 | 0.047832757 |
| 16918722 | GDF5 | 1.37 | 4.23 | 0.027490456 |
| 16922584 | CHAF1B | 1.00 | 4.91 | 0.037915247 |
| 17108943 | PNPLA4 | 0.98 | 6.89 | 0.01555904 |
| 17103104 | USP11 | 0.47 | 7.78 | 0.030939687 |
| 17115597 | UBL4A | 0.75 | 6.61 | 0.006011845 |
| 17108264 | TKTL1 | -0.38 | 2.89 | 0.041841038 |
| 16881353 | DYSF | -1.26 | 6.42 | 0.03312773 |
| 16743017 | PICALM | -0.43 | 8.95 | 0.016606769 |
| 16822408 | AXIN1 | 0.58 | 6.05 | 0.049074575 |
| 17071625 | FZD6 | 0.73 | 8.03 | 0.029083363 |
| 16840145 | SLC25A11 | 0.56 | 8.51 | 0.020386669 |
| 16977833 | SPARCL1 | -1.26 | 9.43 | 0.002145853 |
| 17110071 | SRPX | -1.80 | 7.57 | 0.000494327 |
| 16670681 | ANXA9 | 2.64 | 5.78 | 0.024746435 |
| 17023677 | STX7 | -0.68 | 8.37 | 0.002826228 |
| 16825602 | DOC2A | 1.34 | 4.73 | 0.008085068 |
| 16933378 | TPST2 | -1.04 | 4.00 | 0.00102608 |
| 17046640 | TPST1 | -0.86 | 5.96 | 0.040623853 |
| 16825592 | HIRIP3 | 0.88 | 4.99 | 0.002521056 |
| 16768014 | PPFIA2 | -0.78 | 3.10 | 0.014510297 |
| 16686557 | PIK3R3 | -0.83 | 5.88 | 0.00461557 |
| 16933667 | NIPSNAP1 | 0.57 | 6.12 | 0.031697406 |
| 16836315 | DGKE | -0.93 | 5.76 | 0.008787723 |
| 16912130 | CST7 | -1.10 | 7.52 | 0.040366916 |
| 16667662 | CDC14A | -0.96 | 6.04 | 0.000837802 |
| 16679349 | KMO | -1.01 | 5.35 | 0.042809558 |
| 16923365 | PDXK | 0.68 | 5.61 | 0.002105466 |
| 16923397 | RRP1 | 0.53 | 5.75 | 0.034311793 |
| 16682691 | AKR7A2 | 0.53 | 5.35 | 0.01387128 |
| 16891208 | STK16 | 0.56 | 5.13 | 0.005350587 |
| 16905076 | SLC25A12 | -0.49 | 6.23 | 0.032309437 |
| 16873826 | PLA2G4C | -0.80 | 4.62 | 0.010610622 |
| 16958812 | RUVBL1 | 0.72 | 6.31 | 0.010778949 |
| 16866394 | PPAP2C | 2.03 | 7.14 | 0.002958086 |
| 16925674 | PSMG1 | 0.62 | 6.23 | 0.012981672 |
| 16859952 | RFXANK | 0.58 | 6.18 | 0.049131964 |
| 16752682 | HSD17B6 | 1.99 | 5.11 | 0.047708696 |
| 16846195 | SKAP1 | -1.48 | 5.15 | 0.005959278 |
| 16834516 | AOC3 | -1.63 | 6.80 | 0.004097602 |
| 17018841 | KCNK5 | 1.61 | 5.47 | 0.011077896 |
| 16904793 | ABCB11 | -0.73 | 2.70 | 0.005864399 |
| 16780917 | IRS2 | 1.02 | 7.26 | 0.047063771 |
| 17042946 | EIF3B | 0.64 | 7.33 | 0.00864139 |
| 16662031 | EIF3I | 0.51 | 8.41 | 0.035994321 |
| 16967631 | SLC4A4 | 2.30 | 8.26 | 0.034233212 |
| 16856906 | S1PR4 | -0.93 | 4.42 | 0.030146833 |
| 16957738 | B4GALT4 | 1.19 | 6.19 | 0.001384232 |
| 16681142 | TNFRSF25 | -0.48 | 4.81 | 0.027420464 |

| | | | | |
|---|---|---|---|---|
| 17002194 | ADAM19 | -1.57 | 6.94 | 0.01631073 |
| 16794321 | ADAM20 | -0.88 | 4.37 | 0.01508554 |
| 16728331 | FADD | 0.83 | 6.64 | 0.00077203 |
| 17092421 | MPDZ | -1.06 | 7.09 | 0.0148032 |
| 16899580 | SUCLG1 | 0.43 | 6.90 | 0.017337887 |
| 16727224 | BANF1 | 0.77 | 7.07 | 0.002093973 |
| 16794220 | DCAF5 | -0.46 | 7.46 | 0.035472697 |
| 16992347 | FGF18 | 2.17 | 7.24 | 0.007930215 |
| 16980160 | INPP4B | -1.35 | 5.12 | 0.000210675 |
| 16713187 | NRP1 | -1.05 | 8.77 | 0.000909279 |
| 17041393 | SYNGAP1 | -0.46 | 6.62 | 0.015976368 |
| 17007499 | SYNGAP1 | -0.51 | 6.65 | 0.010973189 |
| 16695406 | CD84 | -0.69 | 6.04 | 0.024133658 |
| 16947235 | GMPS | 0.58 | 8.20 | 0.003765835 |
| 16755131 | SOCS2 | -0.57 | 4.03 | 0.040476987 |
| 17077659 | GGH | 0.73 | 4.77 | 0.018006229 |
| 17000900 | HDAC3 | 0.48 | 6.32 | 0.025992935 |
| 16809827 | ALDH1A2 | 2.63 | 5.84 | 0.000456269 |
| 16925057 | SYNJ1 | -0.41 | 5.95 | 0.034741738 |
| 16776537 | ARHGEF7 | -0.44 | 6.40 | 0.036215521 |
| 17023736 | VNN2 | -1.70 | 4.29 | 0.000605575 |
| 16993458 | SQSTM1 | 0.52 | 6.90 | 0.017941275 |
| 16827170 | NAE1 | 0.51 | 8.14 | 0.019028688 |
| 16786548 | EIF2B2 | 0.45 | 6.98 | 0.048211231 |
| 16918485 | EIF2S2 | 0.36 | 9.22 | 0.044982261 |
| 17048908 | BUD31 | 0.64 | 6.45 | 0.002651133 |
| 17109342 | AP1S2 | -0.54 | 6.20 | 0.018616123 |
| 16810376 | HERC1 | -0.60 | 8.09 | 0.001961033 |
| 16886174 | KYNU | -1.16 | 5.65 | 0.00179239 |
| 16958963 | H1FX | 0.58 | 7.39 | 0.036437576 |
| 16726489 | RPS6KA4 | 0.55 | 5.59 | 0.031509868 |
| 16693082 | SELENBP1 | 1.30 | 7.11 | 0.0421346 |
| 16944798 | KALRN | -1.43 | 4.60 | 0.003324144 |
| 17100201 | CLIC3 | 2.19 | 5.72 | 0.000307563 |
| 16758463 | HIP1R | -0.46 | 5.04 | 0.026161652 |
| 16748529 | GPRC5A | 2.81 | 7.57 | 0.001585662 |
| 17024053 | MAP7 | 0.77 | 5.04 | 0.035188462 |
| 16918832 | NFS1 | 0.70 | 7.00 | 0.001977587 |
| 16813342 | PRC1 | 1.16 | 6.35 | 0.024418781 |
| 16790493 | SLC7A7 | 0.65 | 4.75 | 0.044982261 |
| 16696811 | ANGPTL1 | -1.47 | 6.61 | 0.03759471 |
| 17067970 | ASH2L | 0.83 | 8.60 | 0.033336533 |
| 16974626 | LDB2 | -1.47 | 5.81 | 0.000520867 |
| 16814310 | PIGQ | 0.56 | 5.58 | 0.012231536 |
| 16815513 | DNAJA3 | 0.99 | 6.71 | 0.000318147 |
| 17021323 | TBX18 | 0.89 | 8.16 | 0.004044647 |
| 16745343 | USP2 | 2.00 | 5.39 | 0.00279959 |
| 16837709 | SLC16A5 | 0.84 | 4.61 | 0.036030551 |
| 17088185 | PRPF4 | 0.57 | 7.22 | 0.032813136 |
| 16801557 | CCNB2 | 1.82 | 6.66 | 0.001303698 |
| 16860531 | PDCD5 | 0.46 | 7.70 | 0.02317122 |
| 16838855 | HGS | 0.52 | 7.76 | 0.030724616 |
| 16679411 | EXO1 | 1.03 | 4.40 | 0.036908249 |
| 17049120 | AP4M1 | 0.87 | 6.37 | 0.001080715 |
| 16753270 | SLC16A7 | -0.86 | 6.00 | 0.000968081 |
| 16778067 | DCLK1 | -1.08 | 6.37 | 0.006148242 |
| 17111918 | ZMYM3 | 0.52 | 7.39 | 0.042473943 |
| 16892918 | LRRFIP1 | -0.70 | 7.18 | 0.007197952 |

| | | | | |
|---|---|---|---|---|
| 16698697 | FAIM3 | -1.84 | 5.91 | 0.007273879 |
| 16715849 | DLG5 | 0.79 | 7.56 | 0.030804916 |
| 16681827 | DHRS3 | 0.86 | 8.53 | 0.043822882 |
| 16795794 | RPS6KA5 | -0.71 | 5.33 | 0.009917418 |
| 17074474 | MFHAS1 | -0.49 | 5.87 | 0.042255035 |
| 16676643 | MAPKAPK2 | -0.50 | 8.05 | 0.033295891 |
| 16906733 | STK17B | -1.23 | 7.98 | 0.000554518 |
| 16849501 | CYTH1 | -0.73 | 6.24 | 0.004696863 |
| 16674080 | GPR52 | -1.10 | 5.97 | 0.001029348 |
| 17051336 | ATP6V1F | 0.61 | 8.50 | 0.009786926 |
| 16982635 | TRIP13 | 1.04 | 5.25 | 0.037132095 |
| 16833441 | ZNHIT3 | 0.73 | 7.71 | 0.002719692 |
| 16760792 | CD163 | -1.20 | 8.16 | 0.016877145 |
| 16920169 | B4GALT5 | 0.76 | 9.37 | 0.003669752 |
| 16773919 | KL | -1.08 | 4.31 | 0.000446262 |
| 16811739 | COX5A | 0.71 | 8.41 | 0.01135105 |
| 16848845 | RECQL5 | 0.53 | 5.54 | 0.024413743 |
| 16930348 | GRAP2 | -1.20 | 4.26 | 0.006193453 |
| 17077723 | CYP7B1 | -0.95 | 6.91 | 0.020424774 |
| 16695121 | AIM2 | -1.23 | 5.10 | 0.027222301 |
| 16900053 | EIF2AK3 | -0.50 | 7.64 | 0.010722608 |
| 16812685 | HOMER2 | 1.11 | 5.39 | 0.007351206 |
| 17011121 | FHL5 | -2.15 | 5.16 | 0.000352982 |
| 17114520 | ARHGEF6 | -1.00 | 7.51 | 0.001217017 |
| 16858941 | IL27RA | -0.89 | 4.86 | 0.033386639 |
| 16951150 | SH3BP5 | -0.91 | 5.81 | 0.001431864 |
| 16661497 | THEMIS2 | -0.82 | 7.35 | 0.025925514 |
| 16910655 | PSMF1 | 0.39 | 8.67 | 0.01065877 |
| 16802519 | KIF23 | 1.47 | 6.31 | 0.013388643 |
| 16951756 | SLC4A7 | -0.78 | 7.43 | 0.013370922 |
| 16751269 | SLC4A8 | -0.35 | 3.30 | 0.04846312 |
| 16695627 | ADAMTS4 | -1.79 | 5.84 | 0.005999718 |
| 16976706 | ADAMTS3 | 2.04 | 6.97 | 0.03972789 |
| 16924602 | ADAMTS1 | -1.58 | 6.51 | 0.030688059 |
| 17049939 | PMPCB | 0.47 | 8.72 | 0.027924641 |
| 16872194 | GMFG | -1.08 | 9.06 | 0.003426839 |
| 16733045 | EI24 | 0.47 | 7.72 | 0.031350721 |
| 16878406 | MRPL33 | 0.61 | 5.68 | 0.016545435 |
| 16797103 | C14orf2 | 0.73 | 4.77 | 0.001688896 |
| 17047138 | GTF2IRD1 | 1.62 | 6.72 | 1.60E-05 |
| 17075529 | ENTPD4 | -1.71 | 5.34 | 0.009510468 |
| 17014295 | WTAP | -0.37 | 8.13 | 0.04995222 |
| 16903931 | CYTIP | -1.58 | 6.04 | 0.002492816 |
| 16832588 | TRAF4 | 0.65 | 5.68 | 0.026095642 |
| 16995409 | NUP155 | 0.69 | 8.09 | 0.003723708 |
| 17065173 | ARHGEF10 | 0.91 | 7.65 | 0.000114562 |
| 16696614 | KIAA0040 | -0.72 | 6.98 | 0.004123709 |
| 16929283 | DEPDC5 | -0.50 | 5.60 | 0.01286048 |
| 16663665 | KDM4A | 0.72 | 8.05 | 0.02193634 |
| 17020044 | TRAM2 | -0.95 | 9.45 | 0.02249075 |
| 16842350 | ULK2 | 1.39 | 7.50 | 0.00129038 |
| 16673012 | NOS1AP | 1.32 | 4.74 | 0.008265301 |
| 16699932 | TMEM63A | -0.58 | 7.16 | 0.008189262 |
| 16814250 | RAB11FIP3 | 0.65 | 5.82 | 0.027088074 |
| 17043882 | HDAC9 | -0.73 | 4.49 | 0.033736362 |
| 16818090 | SETD1A | 0.50 | 6.38 | 0.009510468 |
| 16822762 | IFT140 | 0.71 | 5.64 | 0.013827493 |
| 16830374 | ACAP1 | -1.45 | 6.30 | 0.010038939 |

| | | | | |
|---|---|---|---|---|
| 17013223 | PHACTR2 | -0.75 | 6.99 | 0.033075537 |
| 17104344 | STARD8 | -0.83 | 5.42 | 0.027490456 |
| 17077502 | TOX | -1.01 | 5.88 | 0.049319963 |
| 16757969 | MLEC | 0.44 | 9.21 | 0.017801063 |
| 16986700 | ZFYVE16 | -0.62 | 7.50 | 0.015569485 |
| 16810543 | KIAA0101 | 1.15 | 5.22 | 0.010683734 |
| 16916901 | RASSF2 | -1.23 | 8.43 | 0.001227082 |
| 16849667 | EIF4A3 | 0.58 | 8.12 | 0.018889578 |
| 16912492 | TM9SF4 | 0.34 | 9.16 | 0.037428899 |
| 16784710 | KIAA0586 | -0.59 | 7.46 | 0.003465238 |
| 17080897 | MTSS1 | -0.93 | 7.12 | 0.038484879 |
| 16715269 | SPOCK2 | 1.47 | 6.99 | 0.040623853 |
| 16929222 | SFI1 | -0.66 | 5.52 | 0.007438592 |
| 16868743 | KEAP1 | 0.61 | 7.70 | 0.013925031 |
| 17019287 | CUL7 | 0.56 | 6.94 | 0.017793929 |
| 16920180 | SPATA2 | 0.68 | 4.65 | 0.00995933 |
| 16665687 | DNAJC6 | 1.69 | 5.78 | 0.01677511 |
| 16789790 | KIAA0125 | -2.09 | 4.63 | 0.002692499 |
| 16808094 | LCMT2 | 0.77 | 6.43 | 0.009565363 |
| 16912192 | GINS1 | 1.41 | 5.97 | 0.004053283 |
| 16903356 | ZEB2 | -1.15 | 7.24 | 0.000494327 |
| 16765657 | TESPA1 | -1.18 | 4.90 | 0.001690497 |
| 17104283 | HEPH | -1.07 | 5.61 | 0.047497843 |
| 17056740 | ELMO1 | -1.22 | 6.89 | 0.000103096 |
| 16707884 | ZNF518A | -0.62 | 5.93 | 0.031965487 |
| 17091090 | PPP1R26 | 0.76 | 5.47 | 0.016667474 |
| 16956773 | TOMM70A | 0.46 | 7.46 | 0.039715058 |
| 16979256 | SEC24D | -0.64 | 8.54 | 0.039929076 |
| 16741864 | FCHSD2 | -0.83 | 7.83 | 0.001398413 |
| 16779792 | TBC1D4 | -0.73 | 6.82 | 0.008267155 |
| 16667516 | LPPR4 | -1.49 | 5.72 | 0.022312862 |
| 17011593 | FIG4 | -0.56 | 6.67 | 0.003068299 |
| 16805124 | SV2B | -1.08 | 4.57 | 0.020391125 |
| 16693559 | DENND4B | -0.41 | 6.69 | 0.048211231 |
| 16674025 | RABGAP1L | -0.70 | 5.70 | 0.006761023 |
| 16831247 | ARHGAP44 | 2.13 | 6.13 | 0.015855612 |
| 16803710 | ARNT2 | 1.32 | 5.81 | 0.007880507 |
| 16674319 | FAM20B | 0.68 | 7.65 | 0.014342333 |
| 16950912 | IQSEC1 | -0.66 | 7.85 | 0.00165586 |
| 16659171 | MFN2 | 0.64 | 7.38 | 0.026601496 |
| 16697695 | KIF14 | 1.39 | 5.27 | 0.036461914 |
| 16880982 | ARHGAP25 | -1.08 | 5.49 | 0.003322562 |
| 17003924 | GFPT2 | 1.63 | 8.61 | 0.002631483 |
| 17113320 | AMMECR1 | 0.83 | 6.85 | 0.015855612 |
| 16782710 | REC8 | 2.30 | 6.98 | 0.000545429 |
| 17047881 | DMTF1 | -0.46 | 8.41 | 0.047085512 |
| 17001040 | GNPDA1 | 0.55 | 4.78 | 0.033431058 |
| 16757098 | SH2B3 | -0.59 | 6.46 | 0.049456502 |
| 17093920 | GNE | -0.43 | 6.36 | 0.024664444 |
| 16836214 | TOM1L1 | 2.38 | 8.39 | 2.74E-06 |
| 17098567 | SH2D3C | -0.97 | 5.67 | 0.007880507 |
| 16947556 | SMC4 | 0.70 | 7.85 | 0.009225792 |
| 16762154 | ABCC9 | -1.77 | 7.85 | 0.000482426 |
| 17064459 | ABCF2 | 0.65 | 6.96 | 0.025590639 |
| 16694117 | SCAMP3 | 0.72 | 6.26 | 0.010631929 |
| 16727427 | DPP3 | 0.68 | 6.90 | 0.012778755 |
| 16811832 | SNUPN | 0.67 | 6.75 | 0.038187727 |
| 16920338 | ATP9A | 0.87 | 6.81 | 0.024862959 |

| | | | | |
|---|---|---|---|---|
| 17103509 | PQBP1 | 0.68 | 6.41 | 0.01349409 |
| 16811975 | TSPAN3 | 1.32 | 9.14 | 0.001754644 |
| 16691314 | TSPAN2 | -1.40 | 5.34 | 0.042865525 |
| 16814837 | NUBP2 | 0.70 | 6.54 | 0.012778755 |
| 16753202 | TSFM | 0.54 | 5.62 | 0.002708088 |
| 16706499 | PPIF | 0.65 | 7.09 | 0.036557098 |
| 16989054 | RAD50 | 0.48 | 8.93 | 0.045878888 |
| 16989636 | KIF20A | 1.82 | 5.90 | 0.01541723 |
| 16900783 | ACTR1B | 0.39 | 7.32 | 0.048675912 |
| 16897056 | LRPPRC | 0.56 | 8.30 | 0.013069553 |
| 16823413 | TRAP1 | 1.18 | 8.12 | 0.000307563 |
| 17115207 | BCAP31 | 0.90 | 7.37 | 0.000996424 |
| 16846734 | TOB1 | 1.08 | 7.89 | 0.025292216 |
| 16977925 | FAM13A | -0.59 | 6.39 | 0.024493485 |
| 16889779 | ABI2 | 0.78 | 7.52 | 0.001769304 |
| 16866337 | TRIM28 | 0.51 | 9.33 | 0.044495749 |
| 16686774 | PDZK1IP1 | 2.31 | 7.11 | 0.002643438 |
| 17059974 | SLC25A13 | 0.48 | 7.62 | 0.012947456 |
| 16940839 | RBM6 | -0.56 | 6.74 | 0.002383003 |
| 16778355 | LHFP | -1.30 | 7.70 | 0.000259924 |
| 16765945 | RNF41 | 0.53 | 7.24 | 0.046648229 |
| 16853120 | TSHZ1 | -0.52 | 5.15 | 0.013070795 |
| 16962185 | ALG3 | 0.54 | 6.39 | 0.029648298 |
| 16906285 | CALCRL | -1.64 | 7.45 | 0.008085068 |
| 16745002 | MPZL2 | -1.10 | 5.25 | 0.002351716 |
| 16665373 | INADL | 1.40 | 7.79 | 0.020271225 |
| 16773650 | USPL1 | -0.48 | 6.37 | 0.020271225 |
| 16748095 | KLRG1 | -1.43 | 4.05 | 0.000104373 |
| 16816408 | COQ7 | 0.68 | 6.70 | 0.004097602 |
| 16814366 | MSLN | 2.86 | 8.83 | 0.002360681 |
| 17049904 | LRRC17 | -0.90 | 4.00 | 0.048213306 |
| 16739942 | RASGRP2 | -0.85 | 4.73 | 0.027983291 |
| 16785540 | GPHN | -0.70 | 4.85 | 0.028312719 |
| 17049461 | POP7 | 0.52 | 5.90 | 0.034229659 |
| 16970435 | SPRY1 | -0.79 | 7.02 | 0.041594608 |
| 16810847 | DENND4A | -0.46 | 8.55 | 0.029403396 |
| 16741075 | CDK2AP2 | 0.74 | 5.53 | 0.02649727 |
| 17045787 | RAMP3 | -0.92 | 5.11 | 0.037290637 |
| 16663014 | ZMPSTE24 | 0.40 | 9.22 | 0.038484879 |
| 16856232 | FSTL3 | 1.24 | 8.34 | 0.001052997 |
| 16790823 | EFS | -0.93 | 5.06 | 0.038039243 |
| 17005799 | PRSS16 | 0.79 | 4.31 | 0.014924133 |
| 16875414 | LILRB2 | -0.93 | 5.48 | 0.019213072 |
| 16891273 | SPEG | 1.25 | 5.32 | 0.00234422 |
| 16826218 | DNAJA2 | 0.39 | 8.36 | 0.0196481 |
| 16861930 | PAK4 | 1.18 | 5.57 | 0.004665936 |
| 16810945 | SNAPC5 | 0.59 | 5.64 | 0.043440666 |
| 16996194 | CCNO | 0.70 | 3.92 | 0.040827531 |
| 16726096 | RTN3 | 0.59 | 8.52 | 0.004787777 |
| 17046041 | IKZF1 | -1.44 | 6.57 | 0.001448824 |
| 16859643 | B3GNT3 | -0.40 | 3.06 | 0.030939687 |
| 16735764 | MRVI1 | -1.15 | 5.77 | 0.003485 |
| 17091695 | TUBB4B | 0.52 | 8.32 | 0.010535139 |
| 17074848 | DLC1 | -1.24 | 5.51 | 0.005879129 |
| 17071162 | CPQ | -0.68 | 6.31 | 0.004067726 |
| 16763666 | RAPGEF3 | -0.68 | 5.01 | 0.047498576 |
| 16730503 | YAP1 | 0.42 | 8.16 | 0.026786124 |
| 16722278 | SPON1 | -1.35 | 8.94 | 0.033104806 |

| | | | | |
|---|---|---|---|---|
| 16790556 | PRMT5 | 0.79 | 6.85 | 0.013011825 |
| 16861047 | TMEM147 | 0.64 | 8.79 | 0.002687511 |
| 16726825 | CDC42EP2 | 0.51 | 4.81 | 0.040351348 |
| 16690343 | VAV3 | -1.30 | 4.80 | 0.000107648 |
| 16671381 | HAX1 | 0.71 | 5.98 | 0.007431953 |
| 16838750 | BAIAP2 | 1.69 | 6.37 | 0.000255998 |
| 16840473 | CLEC10A | -1.27 | 5.78 | 0.029648298 |
| 16984730 | FST | -1.79 | 5.20 | 0.032915321 |
| 16868038 | TIMM44 | 0.72 | 6.99 | 0.010147804 |
| 17007446 | PFDN6 | 0.49 | 5.99 | 0.013305094 |
| 17028495 | PFDN6 | 0.51 | 6.01 | 0.009527594 |
| 17031309 | PFDN6 | 0.51 | 6.01 | 0.009527594 |
| 17036058 | PFDN6 | 0.51 | 6.01 | 0.009527594 |
| 17038779 | PFDN6 | 0.51 | 6.01 | 0.009527594 |
| 16723294 | EIF3M | 0.60 | 9.49 | 0.015265839 |
| 17005138 | CAP2 | 0.92 | 7.50 | 0.035930768 |
| 16867349 | SEMA6B | -0.98 | 5.26 | 0.021140737 |
| 17059119 | SEMA3C | 1.83 | 10.20 | 0.005319332 |
| 16840018 | MYBBP1A | 0.68 | 6.57 | 0.024987511 |
| 16935042 | DDX17 | -0.53 | 9.20 | 0.00061078 |
| 16712373 | NEBL | 1.44 | 5.40 | 0.035280185 |
| 16726925 | SSSCA1 | 0.53 | 7.21 | 0.037148447 |
| 16858714 | RNASEH2A | 0.83 | 5.85 | 0.04995222 |
| 16786616 | BATF | -0.73 | 4.12 | 0.007755504 |
| 16913065 | PROCR | 2.25 | 9.10 | 0.002687511 |
| 17048859 | ARPC1A | 0.72 | 8.49 | 0.004445565 |
| 16965606 | SLC34A2 | 2.68 | 5.36 | 0.037870862 |
| 16881485 | CCT7 | 0.41 | 8.03 | 0.022048344 |
| 16898175 | CCT4 | 0.67 | 8.28 | 0.006244544 |
| 16753964 | CCT2 | 0.71 | 7.87 | 0.006889201 |
| 16716795 | SORBS1 | -1.62 | 4.74 | 0.001066574 |
| 16720077 | IFITM2 | 0.56 | 8.62 | 0.034913704 |
| 16727168 | DRAP1 | 0.50 | 5.01 | 0.033141686 |
| 16839473 | PRPF8 | 0.38 | 9.87 | 0.043268088 |
| 16786941 | AHSA1 | 0.52 | 5.54 | 0.017064738 |
| 16995957 | PAIP1 | 0.77 | 7.41 | 0.000460838 |
| 16814872 | TBL3 | 0.53 | 6.08 | 0.043292532 |
| 16887993 | MTX2 | 0.52 | 7.36 | 0.01223952 |
| 16861630 | SPINT2 | 1.27 | 7.99 | 0.046028879 |
| 16855810 | CD226 | -0.92 | 5.48 | 0.03729073 |
| 16847921 | GNA13 | -0.48 | 8.70 | 0.024291321 |
| 17075650 | PNMA2 | 0.83 | 5.74 | 0.010488802 |
| 16694094 | FAM189B | 0.80 | 5.75 | 0.000776261 |
| 16728994 | POLD3 | 0.50 | 6.05 | 0.021563285 |
| 16661323 | NUDC | 0.33 | 6.08 | 0.044561067 |
| 16766283 | PTGES3 | 0.63 | 9.10 | 0.006349684 |
| 16831621 | RAI1 | 0.61 | 6.58 | 0.015247659 |
| 16869643 | GIPC1 | 0.98 | 6.54 | 0.003283805 |
| 16906184 | NCKAP1 | 0.45 | 10.06 | 0.016666479 |
| 17112349 | CYSLTR1 | -1.12 | 5.64 | 0.004102027 |
| 16810686 | CLPX | 0.50 | 6.75 | 0.017337887 |
| 16873296 | PPP1R13L | 0.95 | 7.48 | 0.000431202 |
| 16863946 | RUVBL2 | 0.84 | 7.75 | 0.017789967 |
| 17066921 | ADAM28 | -1.23 | 6.90 | 0.014251566 |
| 16882999 | ARID5A | -0.52 | 6.15 | 0.045963111 |
| 16976117 | NMU | 3.47 | 6.76 | 0.001080715 |
| 16845812 | C1QL1 | 0.99 | 5.30 | 0.008568736 |
| 16984542 | MRPS30 | 0.69 | 7.21 | 0.005368851 |

| | | | | |
|---|---|---|---|---|
| 16669288 | WDR3 | 0.69 | 6.59 | 0.030341415 |
| 16877836 | RAB10 | 0.27 | 9.67 | 0.039003889 |
| 16913077 | MMP24 | 4.22 | 7.87 | 5.68E-05 |
| 16735751 | LYVE1 | -1.82 | 8.89 | 0.019097494 |
| 17000358 | BRD8 | 0.39 | 5.57 | 0.02134502 |
| 17032175 | EHMT2 | 0.42 | 6.85 | 0.0369283 |
| 17042143 | EHMT2 | 0.57 | 7.30 | 0.012566269 |
| 16823097 | RNPS1 | 0.38 | 8.64 | 0.018745508 |
| 16853996 | AFG3L2 | 0.79 | 7.68 | 0.003980048 |
| 17101465 | MSL3 | -0.63 | 5.38 | 0.006381972 |
| 16924305 | BTG3 | 0.75 | 5.70 | 0.028840337 |
| 16846181 | CBX1 | 0.74 | 6.16 | 0.008099407 |
| 16919508 | TOMM34 | 0.80 | 6.35 | 0.011551228 |
| 17010929 | PNRC1 | -0.53 | 9.16 | 0.044547833 |
| 16726224 | STIP1 | 0.58 | 6.51 | 0.041083214 |
| 16686088 | EBNA1BP2 | 0.61 | 6.78 | 0.0190991 |
| 16875387 | LILRB5 | -0.98 | 3.63 | 0.017463229 |
| 16865424 | LILRB4 | -0.79 | 4.61 | 0.010665065 |
| 16754373 | GLIPR1 | -0.95 | 9.07 | 0.028949304 |
| 16874740 | KLK11 | 2.55 | 7.14 | 0.000218948 |
| 16875432 | LILRA3 | -0.71 | 3.65 | 0.000716615 |
| 16996956 | SMA4 | -0.82 | 7.36 | 0.02212934 |
| 17110670 | PIM2 | -1.56 | 6.21 | 0.012043754 |
| 16740770 | B3GNT1 | 0.66 | 6.07 | 0.0217199 |
| 16915656 | ADRM1 | 0.70 | 6.96 | 0.010515102 |
| 17070514 | WWP1 | -0.55 | 8.30 | 0.012333777 |
| 17088589 | CNTRL | -0.82 | 6.09 | 0.001958832 |
| 16914315 | UBE2C | 1.31 | 4.79 | 0.028201334 |
| 16713562 | C10orf10 | -1.32 | 5.54 | 0.023369511 |
| 17090827 | CACFD1 | 0.53 | 4.31 | 0.049973013 |
| 16719066 | ATE1 | -0.48 | 6.69 | 0.006889201 |
| 16878069 | EMILIN1 | -1.46 | 6.99 | 0.029770839 |
| 16756475 | PWP1 | 0.44 | 8.45 | 0.028218895 |
| 16817824 | CORO1A | -0.80 | 8.76 | 0.042473943 |
| 17067902 | ERLIN2 | 0.61 | 6.52 | 0.0190991 |
| 16996684 | ADAMTS6 | -1.77 | 5.06 | 0.028963716 |
| 16959187 | MRPL3 | 0.43 | 8.58 | 0.026295083 |
| 17098322 | RPL35 | 0.46 | 5.93 | 0.024547543 |
| 16886717 | GALNT5 | -1.94 | 5.91 | 0.017710657 |
| 16956749 | FILIP1L | -0.88 | 4.30 | 0.020424774 |
| 16891843 | SP140 | -1.18 | 4.70 | 0.015906168 |
| 16918455 | PXMP4 | 0.61 | 5.84 | 0.043561541 |
| 16843795 | SYNRG | -0.36 | 8.19 | 0.028880252 |
| 16779766 | KLF12 | -1.19 | 7.65 | 0.00514969 |
| 17104159 | KLF8 | -0.89 | 4.66 | 0.022688153 |
| 16952349 | SCN11A | -0.46 | 2.94 | 0.029219679 |
| 17003748 | MGAT4B | 0.70 | 7.67 | 0.004620619 |
| 16849355 | TMC6 | -0.67 | 5.96 | 0.021336701 |
| 16760649 | PHB2 | 0.60 | 8.80 | 0.003570315 |
| 16807605 | OIP5 | 1.11 | 4.35 | 0.010148425 |
| 16981523 | SCRG1 | -0.68 | 2.76 | 0.006394524 |
| 16792954 | NID2 | -1.12 | 7.88 | 0.043846677 |
| 17062049 | TFEC | -0.71 | 5.61 | 0.043148562 |
| 16735994 | RRAS2 | 0.86 | 6.49 | 0.044547833 |
| 16844207 | IKZF3 | -1.60 | 6.13 | 0.00565905 |
| 16907912 | IKZF2 | -0.84 | 4.58 | 0.002145853 |
| 16970536 | HSPA4L | 1.16 | 6.08 | 0.019439063 |
| 17082309 | PUF60 | 0.66 | 4.33 | 0.012774275 |

| | | | | |
|---|---|---|---|---|
| 16898617 | AAK1 | -0.50 | 6.88 | 0.026758922 |
| 17048706 | LMTK2 | 0.49 | 7.01 | 0.043890331 |
| 16813871 | CHSY1 | -0.77 | 7.03 | 0.007562595 |
| 16840321 | NLRP1 | -1.16 | 7.14 | 0.000370855 |
| 16990862 | ABLIM3 | -0.90 | 5.56 | 0.043476839 |
| 16830957 | ARHGEF15 | -0.86 | 5.30 | 0.017595598 |
| 16873880 | CARD8 | -0.72 | 5.81 | 0.000566528 |
| 16967563 | RUFY3 | -0.87 | 7.28 | 0.003485 |
| 16939592 | TRAK1 | -0.52 | 6.57 | 0.010728175 |
| 16940110 | SACM1L | -0.42 | 8.32 | 0.02604879 |
| 16968878 | MMRN1 | -2.94 | 4.46 | 0.000107648 |
| 16917859 | CD93 | -1.18 | 7.90 | 0.002746274 |
| 16983172 | CCT5 | 0.53 | 7.36 | 0.035352582 |
| 16912379 | TPX2 | 1.70 | 7.09 | 0.012000329 |
| 16877795 | EFR3B | 0.88 | 5.66 | 0.022575571 |
| 16918102 | NINL | 1.38 | 6.03 | 0.00129038 |
| 16746348 | IGSF9B | 1.08 | 5.28 | 0.038093304 |
| 16749398 | STK38L | -0.76 | 6.63 | 0.017801063 |
| 16770828 | FBXO21 | 0.54 | 7.27 | 0.011376867 |
| 16900474 | SNRNP200 | 0.33 | 8.82 | 0.036136556 |
| 16956285 | PDZRN3 | -1.12 | 5.99 | 0.02298019 |
| 16660624 | KDM1A | 0.46 | 7.91 | 0.040623853 |
| 17010639 | DOPEY1 | -0.65 | 6.72 | 0.03559341 |
| 16784333 | SAMD4A | -0.75 | 6.29 | 0.01541723 |
| 16828046 | PHLPP2 | 1.38 | 7.18 | 0.015058806 |
| 17010789 | ZNF292 | -0.57 | 6.89 | 0.034807093 |
| 16983692 | PDZD2 | 2.73 | 6.63 | 0.001794995 |
| 16961501 | TNIK | -1.20 | 5.64 | 0.004097602 |
| 16815461 | CLUAP1 | 0.60 | 6.46 | 0.024505304 |
| 16825057 | GGA2 | -0.39 | 7.61 | 0.026095642 |
| 17099263 | SETX | -0.45 | 9.04 | 0.027880792 |
| 16682631 | EMC1 | 0.53 | 7.21 | 0.032885701 |
| 16721861 | SWAP70 | -0.63 | 7.47 | 0.014549322 |
| 16779855 | MYCBP2 | -1.07 | 8.15 | 9.89E-06 |
| 17083492 | KDM4C | -0.54 | 6.47 | 0.011809069 |
| 16990483 | ARHGAP26 | -0.97 | 6.07 | 0.002903599 |
| 16997068 | MRPS27 | 0.61 | 6.27 | 0.020945503 |
| 16829690 | RAP1GAP2 | 1.06 | 5.44 | 0.035818627 |
| 16930383 | TNRC6B | -0.54 | 7.80 | 0.005232106 |
| 16952031 | CLASP2 | -0.61 | 6.66 | 0.002113366 |
| 16959007 | PLXND1 | -0.84 | 8.23 | 0.011474569 |
| 16740161 | ATG2A | 0.56 | 5.69 | 0.019713579 |
| 16941184 | RAD54L2 | -0.41 | 6.18 | 0.049710075 |
| 16853631 | EPB41L3 | -0.91 | 7.90 | 0.011819549 |
| 16839913 | ZZEF1 | -0.29 | 7.65 | 0.042473943 |
| 16772704 | ANKLE2 | 0.44 | 6.58 | 0.029422391 |
| 16774623 | LRCH1 | -0.85 | 7.05 | 0.0009769 |
| 17082088 | ZC3H3 | 0.57 | 5.77 | 0.015333828 |
| 17113606 | 38961 | -0.77 | 6.83 | 0.009212268 |
| 16848761 | GGA3 | 0.56 | 7.48 | 0.030029639 |
| 16941560 | STAB1 | -0.87 | 8.85 | 0.026095642 |
| 16877225 | LPIN1 | -0.36 | 5.83 | 0.042615055 |
| 16739396 | GANAB | 0.42 | 9.46 | 0.018042933 |
| 16725065 | DTX4 | 1.44 | 6.87 | 0.005523101 |
| 17111611 | ARHGEF9 | -0.47 | 6.38 | 0.022811696 |
| 17057813 | COBL | 2.79 | 6.20 | 0.000882223 |
| 16850865 | ANKRD12 | -0.69 | 8.74 | 0.002496637 |
| 16776709 | MCF2L | -0.46 | 4.24 | 0.043890331 |

| | | | | |
|---|---|---|---|---|
| 16675673 | CAMSAP2 | 0.60 | 8.86 | 0.012178643 |
| 16839642 | CLUH | 0.96 | 6.82 | 0.002085347 |
| 16991991 | WWC1 | 3.54 | 7.48 | 7.26E-06 |
| 17043015 | IQCE | 0.57 | 5.57 | 0.04572034 |
| 16766403 | TMEM194A | 0.86 | 7.43 | 0.004767564 |
| 16926302 | ICOSLG | 0.68 | 5.95 | 0.029462278 |
| 16852573 | NEDD4L | 1.36 | 6.62 | 0.000942253 |
| 17013520 | SASH1 | -0.90 | 6.93 | 0.048219895 |
| 16852497 | WDR7 | -0.40 | 8.28 | 0.034568907 |
| 16850541 | SMCHD1 | -0.46 | 8.84 | 0.034030944 |
| 17084549 | KIAA1045 | -0.43 | 3.41 | 0.005350358 |
| 16861068 | HAUS5 | 0.57 | 5.09 | 0.041932468 |
| 16687638 | USP24 | -0.40 | 7.71 | 0.027615981 |
| 16908834 | OBSL1 | 1.17 | 5.71 | 0.002826228 |
| 17056680 | KIAA0895 | 1.16 | 3.94 | 0.014549322 |
| 16735121 | RRP8 | 0.45 | 5.55 | 0.031904308 |
| 16694472 | SMG5 | 0.50 | 7.10 | 0.041567289 |
| 17090357 | EXOSC2 | 0.53 | 6.93 | 0.008967779 |
| 16796325 | DICER1 | -0.60 | 8.47 | 0.006229481 |
| 17004958 | SIRT5 | 0.61 | 5.80 | 0.032819637 |
| 16767170 | GRIP1 | 1.70 | 5.43 | 0.001637265 |
| 17098477 | ANGPTL2 | -1.15 | 7.60 | 0.014745112 |
| 17078102 | TRAM1 | 0.60 | 9.67 | 0.016714625 |
| 16772486 | RIMBP2 | -0.99 | 3.00 | 0.024534533 |
| 16666965 | LRRC8B | -0.89 | 5.24 | 0.007126085 |
| 16912520 | POFUT1 | 0.63 | 6.64 | 0.013631888 |
| 16837699 | KCTD2 | 0.82 | 7.85 | 0.035256746 |
| 17082263 | SCRIB | 0.64 | 5.70 | 0.039718909 |
| 16928127 | CABIN1 | -0.43 | 6.52 | 0.011781352 |
| 16856421 | HMHA1 | -0.68 | 7.36 | 0.049487214 |
| 16963055 | ACAP2 | -0.78 | 7.04 | 0.000676748 |
| 16931788 | MAPK8IP2 | 0.95 | 4.82 | 0.040942781 |
| 17062230 | TSPAN12 | -0.48 | 3.37 | 0.012588067 |
| 16671178 | SNAPIN | 0.62 | 7.52 | 0.022323152 |
| 16819469 | ARL2BP | 0.64 | 9.64 | 0.029382558 |
| 16848489 | CDC42EP4 | 0.86 | 6.85 | 0.0492371 |
| 16765491 | SMUG1 | 0.46 | 5.05 | 0.012200196 |
| 16823750 | CARHSP1 | 1.32 | 8.51 | 0.000661477 |
| 16818600 | ORC6 | 0.94 | 4.72 | 0.009926585 |
| 16875710 | HSPBP1 | 0.70 | 5.68 | 0.019725297 |
| 16745414 | TRIM29 | 1.30 | 3.79 | 0.036347499 |
| 17056461 | LSM5 | 0.52 | 5.26 | 0.037077613 |
| 17048967 | ZKSCAN5 | 0.45 | 4.93 | 0.0263308 |
| 16661459 | STX12 | -0.42 | 8.07 | 0.027615981 |
| 16891603 | KCNE4 | -1.27 | 5.21 | 0.011031043 |
| 16986552 | BHMT2 | -0.76 | 3.26 | 0.024360334 |
| 16933445 | PITPNB | -0.48 | 6.62 | 0.025386404 |
| 16917373 | FLRT3 | 4.55 | 6.52 | 0.000103096 |
| 16936230 | BRD1 | -0.40 | 5.77 | 0.042524459 |
| 16738119 | MTCH2 | 0.54 | 8.70 | 0.037428899 |
| 17060894 | CLDN15 | 2.26 | 8.07 | 0.004187214 |
| 17019365 | ZNF318 | -0.40 | 7.21 | 0.041564991 |
| 16878994 | RASGRP3 | -1.18 | 5.61 | 0.000429178 |
| 16879174 | QPCT | -0.73 | 4.78 | 0.004432742 |
| 16697971 | LMOD1 | -2.00 | 4.24 | 0.000882223 |
| 16870387 | LSM4 | 0.69 | 8.73 | 0.009833083 |
| 16703563 | BAMBI | 1.41 | 6.71 | 0.019856998 |
| 16726439 | PRDX5 | 1.32 | 8.68 | 5.60E-05 |

| | | | | |
|---|---|---|---|---|
| 16737260 | ABTB2 | 1.57 | 5.59 | 0.004759764 |
| 16967875 | PARM1 | -1.73 | 7.11 | 0.001944711 |
| 16857353 | RPL36 | 0.62 | 9.52 | 0.000869046 |
| 16823746 | TMEM186 | 0.62 | 4.61 | 0.023880365 |
| 16956792 | ABI3BP | -1.87 | 8.25 | 0.005048834 |
| 16708489 | DPCD | 0.54 | 5.57 | 0.023959933 |
| 16693762 | C1orf43 | 0.49 | 10.29 | 0.035297293 |
| 16937181 | THUMPD3 | 0.59 | 6.50 | 0.007519822 |
| 16724901 | ZDHHC5 | 0.35 | 8.27 | 0.038009976 |
| 16939439 | MYRIP | -0.78 | 4.28 | 0.01965373 |
| 16854360 | ZNF521 | -1.11 | 6.27 | 0.01864703 |
| 16837205 | NOL11 | 0.54 | 8.67 | 0.035073833 |
| 16898533 | CNRIP1 | -0.92 | 5.25 | 0.028346472 |
| 17002078 | GEMIN5 | 0.65 | 7.27 | 0.005048834 |
| 16919022 | SAMHD1 | -0.67 | 9.27 | 0.008516971 |
| 16916712 | C20orf194 | -0.57 | 7.36 | 0.029435864 |
| 16890794 | PNKD | 0.40 | 6.10 | 0.04997158 |
| 17021922 | PNISR | -0.57 | 8.39 | 0.018559034 |
| 16687598 | PARS2 | 0.84 | 5.27 | 0.01256299 |
| 16664091 | MMACHC | 0.72 | 5.35 | 0.00931027 |
| 16947287 | TIPARP | -0.82 | 7.16 | 0.032307131 |
| 16913305 | AAR2 | 0.44 | 6.77 | 0.013650974 |
| 16941405 | DNAH1 | -0.80 | 6.44 | 0.006549575 |
| 16893349 | SNED1 | -1.07 | 6.29 | 0.038156908 |
| 16829972 | RNF167 | 0.55 | 7.29 | 0.0232947 |
| 16725556 | DAK | 0.64 | 5.69 | 0.017033223 |
| 16859294 | FAM32A | 0.50 | 9.11 | 0.043034204 |
| 16833171 | TMEM98 | 1.48 | 8.64 | 0.003800106 |
| 16785410 | PLEKHG3 | 1.09 | 6.18 | 0.012947456 |
| 16852132 | SETBP1 | -1.22 | 6.45 | 0.010414232 |
| 16913666 | PPP1R16B | -1.50 | 5.68 | 0.00086785 |
| 16842587 | POLDIP2 | 0.72 | 9.65 | 0.001485978 |
| 17001846 | CCDC69 | -1.35 | 5.74 | 5.29E-06 |
| 16823991 | RSL1D1 | 0.88 | 8.78 | 0.002932971 |
| 16915609 | MTG2 | 0.65 | 5.79 | 0.012428724 |
| 16691090 | PTPN22 | -1.19 | 6.43 | 0.00329089 |
| 16669389 | PHGDH | 1.90 | 6.05 | 0.001587867 |
| 16967286 | STAP1 | -1.90 | 5.07 | 0.043148562 |
| 16681735 | FBXO2 | 1.46 | 6.10 | 0.030199753 |
| 16679777 | OR2L2 | -0.64 | 2.90 | 0.023391738 |
| 16679769 | OR2L1P | -0.65 | 6.07 | 0.020016721 |
| 17000256 | KLHL3 | -1.51 | 5.20 | 0.000440433 |
| 17094009 | FBXO10 | -0.45 | 5.76 | 0.043369986 |
| 16682785 | PLA2G2D | -2.49 | 4.75 | 0.002261678 |
| 16832610 | ERAL1 | 0.63 | 6.44 | 0.012379122 |
| 16935703 | ARFGAP3 | -0.79 | 7.47 | 0.001636024 |
| 17098079 | LHX6 | -0.86 | 4.45 | 0.00173818 |
| 16793999 | PLEK2 | 1.24 | 6.40 | 0.018745508 |
| 16708122 | CNNM1 | 1.13 | 3.66 | 0.041840468 |
| 16738536 | TIMM10 | 0.52 | 6.12 | 0.042079131 |
| 16793460 | TIMM9 | 0.64 | 6.29 | 0.01631073 |
| 16744408 | TIMM8B | 0.83 | 6.90 | 0.000997071 |
| 17085975 | OSTF1 | -0.90 | 7.70 | 0.000838223 |
| 17058499 | TBL2 | 0.58 | 6.23 | 0.026107361 |
| 16823046 | SNORD60 | 1.39 | 6.93 | 0.044452617 |
| 16869291 | SNORD41 | 0.69 | 11.28 | 0.010677187 |
| 17064054 | TPK1 | -0.65 | 4.72 | 0.005871795 |
| 17105712 | NGFRAP1 | 0.77 | 3.80 | 0.00150143 |

| | | | | |
|---|---|---|---|---|
| 16969229 | DAPP1 | -1.26 | 5.37 | 0.001016216 |
| 16842242 | B9D1 | 0.73 | 4.75 | 0.002714294 |
| 16837172 | CACNG4 | 4.34 | 7.09 | 0.000310311 |
| 16674089 | CACYBP | 0.43 | 5.60 | 0.045169965 |
| 16822014 | CPNE7 | 1.08 | 4.68 | 0.037223575 |
| 17020942 | FILIP1 | -1.56 | 5.83 | 0.00077321 |
| 16890998 | STK36 | 0.65 | 6.44 | 0.011796115 |
| 16976994 | NAAA | -0.74 | 7.58 | 0.035900295 |
| 16993027 | PRELID1 | 0.52 | 5.27 | 0.017591588 |
| 16693626 | SLC39A1 | 0.52 | 5.23 | 0.01432291 |
| 17102801 | GPR82 | 1.22 | 4.10 | 0.028625366 |
| 16863593 | C5AR2 | -1.30 | 4.65 | 0.001525473 |
| 16884050 | SULT1C4 | -1.08 | 4.33 | 0.011072258 |
| 17093713 | SIT1 | -1.08 | 4.56 | 0.015439351 |
| 16876182 | CHMP2A | 0.57 | 9.64 | 0.006957854 |
| 16903461 | MMADHC | 0.57 | 7.57 | 0.003460416 |
| 16775136 | PCDH17 | -1.23 | 6.40 | 0.031977413 |
| 16937930 | LSM3 | 0.75 | 6.84 | 0.012428734 |
| 16661508 | SMPDL3B | 1.22 | 5.29 | 0.030880448 |
| 16982161 | PDLIM3 | -1.88 | 6.97 | 0.008839991 |
| 17066961 | ADAMDEC1 | -2.33 | 5.35 | 0.004022384 |
| 16914888 | MOCS3 | 0.95 | 5.08 | 0.014510297 |
| 16742814 | RAB30 | -0.67 | 5.05 | 0.001398413 |
| 16721055 | PGAP2 | 0.59 | 5.34 | 0.029821026 |
| 17105076 | P2RY10 | -1.70 | 5.71 | 0.001831526 |
| 17107293 | HTATSF1 | 0.44 | 6.41 | 0.033613941 |
| 16875763 | UBE2S | 0.89 | 5.16 | 0.047497843 |
| 16738869 | PRPF19 | 0.67 | 8.15 | 0.012588067 |
| 17090109 | TOR1B | 0.47 | 6.92 | 0.037129821 |
| 16935767 | MCAT | 0.60 | 4.74 | 0.027628988 |
| 16930446 | SGSM3 | -0.48 | 5.24 | 0.02490063 |
| 16881786 | HTRA2 | 0.47 | 6.81 | 0.048976319 |
| 17059249 | PCLO | 1.48 | 4.08 | 0.02389242 |
| 16782026 | TRAV20 | -1.62 | 5.23 | 0.005554394 |
| 16782090 | TRAJ17 | -2.28 | 3.66 | 0.000318238 |
| 16782116 | TRAC | -1.06 | 2.84 | 0.013925031 |
| 16912309 | REM1 | -1.18 | 3.96 | 0.000519244 |
| 16671889 | LAMTOR2 | 0.63 | 5.11 | 0.016643305 |
| 16845259 | COA3 | 0.80 | 6.96 | 0.001080715 |
| 16842999 | GIT1 | 0.74 | 7.65 | 0.029648298 |
| 16988539 | SNX24 | 0.53 | 6.03 | 0.019555184 |
| 16729444 | AAMDC | 0.92 | 5.19 | 0.025040481 |
| 17006324 | MRPS18B | 0.75 | 7.03 | 0.006495873 |
| 17027506 | MRPS18B | 0.75 | 7.03 | 0.006495873 |
| 17030351 | MRPS18B | 0.75 | 7.03 | 0.006495873 |
| 17033056 | MRPS18B | 0.75 | 7.03 | 0.006495873 |
| 17035176 | MRPS18B | 0.75 | 7.03 | 0.006495873 |
| 17037835 | MRPS18B | 0.75 | 7.03 | 0.006495873 |
| 17040549 | MRPS18B | 0.75 | 7.03 | 0.006495873 |
| 16827687 | NOB1 | 0.61 | 8.77 | 0.033319597 |
| 17080614 | MRPL13 | 0.65 | 5.54 | 0.013658915 |
| 17080749 | ATAD2 | 0.93 | 7.33 | 0.00821564 |
| 16904956 | METTL5 | 0.45 | 6.04 | 0.024505304 |
| 17068956 | MRPL15 | 0.97 | 8.05 | 0.002108584 |
| 16698023 | UBE2T | 1.27 | 6.29 | 0.003879445 |
| 16853042 | TIMM21 | 0.67 | 6.93 | 0.011353392 |
| 16991447 | MRPL22 | 0.52 | 4.33 | 0.047497843 |
| 16752223 | ORMDL2 | 0.53 | 7.99 | 0.032946177 |

| | | | | |
|---|---|---|---|---|
| 16677933 | CNIH4 | 0.89 | 6.87 | 0.000739652 |
| 16826871 | C16orf80 | 0.52 | 7.70 | 0.043289987 |
| 16748205 | CLEC2D | -1.15 | 6.97 | 0.035404894 |
| 16716918 | BLNK | -0.77 | 6.08 | 0.03949699 |
| 16801122 | TMOD2 | -0.72 | 6.86 | 0.038484879 |
| 16905175 | OLA1 | 0.51 | 8.10 | 0.033104806 |
| 16933049 | VPREB3 | -0.70 | 2.86 | 0.004830661 |
| 16889829 | ICOS | -1.19 | 4.26 | 0.033839976 |
| 17054540 | SNX8 | 0.48 | 6.07 | 0.034147773 |
| 16865730 | CCDC106 | 0.57 | 5.25 | 0.007315962 |
| 16960554 | GPR171 | -0.97 | 4.26 | 0.04496503 |
| 16829508 | TIMM22 | 0.56 | 7.27 | 0.04926514 |
| 16937152 | LINC00312 | -2.18 | 4.50 | 0.001977587 |
| 16797224 | GPR132 | -0.83 | 4.86 | 0.00982264 |
| 17105315 | RPA4 | -0.65 | 3.48 | 0.002942907 |
| 16692892 | CERS2 | 0.63 | 6.47 | 0.02028869 |
| 17054532 | FTSJ2 | 0.53 | 5.48 | 0.030777154 |
| 16727650 | RHOD | 1.18 | 8.06 | 0.018177667 |
| 16937137 | LMCD1 | -1.32 | 7.57 | 0.024427075 |
| 17098642 | ST6GALNAC6 | -0.70 | 8.07 | 0.001501303 |
| 16993335 | ZNF354C | 0.58 | 5.54 | 0.04212478 |
| 16848731 | NT5C | 0.80 | 6.87 | 0.007767765 |
| 16868000 | CD209 | -1.89 | 4.98 | 0.000244467 |
| 16833616 | SOCS7 | 0.61 | 5.92 | 0.007097819 |
| 16807763 | EHD4 | -0.82 | 7.22 | 0.023557189 |
| 16878731 | EHD3 | -1.31 | 6.01 | 0.01993518 |
| 16756212 | CHST11 | -0.62 | 6.45 | 0.036136556 |
| 16772588 | GALNT9 | 2.24 | 6.08 | 0.001847311 |
| 16817271 | IL21R | -1.05 | 5.37 | 0.009363653 |
| 16895208 | ITSN2 | -0.39 | 7.76 | 0.043645591 |
| 17007795 | DEF6 | -0.92 | 5.72 | 0.010039892 |
| 16839254 | GEMIN4 | 0.80 | 6.28 | 0.011691773 |
| 16885638 | ARHGEF4 | 0.94 | 4.54 | 0.022966771 |
| 17107907 | NSDHL | 0.85 | 7.15 | 0.00287891 |
| 16761502 | TAS2R14 | -0.94 | 6.15 | 0.007580112 |
| 16695490 | F11R | 1.15 | 8.52 | 0.001518036 |
| 16943719 | TRAT1 | -1.96 | 5.45 | 0.002963593 |
| 16820249 | PARD6A | 0.68 | 5.30 | 0.007464485 |
| 16921331 | STMN3 | 0.79 | 7.30 | 0.012502456 |
| 16745870 | CDON | 1.57 | 8.24 | 0.009837228 |
| 16899050 | TPRKB | 0.50 | 5.26 | 0.03697616 |
| 16791044 | EMC9 | 0.60 | 5.04 | 0.018309158 |
| 17023308 | HDDC2 | 0.67 | 8.83 | 0.003033218 |
| 16715426 | MRPS16 | 0.52 | 7.76 | 0.02649727 |
| 17060909 | FIS1 | 0.64 | 5.86 | 0.042007207 |
| 16670391 | BOLA1 | 0.63 | 5.41 | 0.015247659 |
| 16779444 | VPS36 | -0.46 | 7.43 | 0.048968767 |
| 16661063 | ZNF593 | 0.65 | 5.90 | 0.020059911 |
| 17005396 | GMNN | 1.23 | 5.72 | 0.002454214 |
| 16718047 | CALHM2 | -0.53 | 6.53 | 0.036944981 |
| 17019319 | MRPL2 | 0.51 | 7.16 | 0.02743648 |
| 16858122 | MRPL4 | 0.83 | 7.24 | 0.003888986 |
| 16786475 | FCF1 | 0.43 | 7.55 | 0.047708696 |
| 16910485 | THAP4 | 0.62 | 6.64 | 0.005086295 |
| 16837754 | MRPS7 | 0.72 | 9.09 | 0.006214756 |
| 16826760 | PLLP | 5.13 | 8.88 | 2.45E-05 |
| 16731605 | SIDT2 | -0.59 | 6.34 | 0.016574588 |
| 16679650 | SCCPDH | 1.25 | 8.56 | 0.000440433 |

| | | | | |
|---|---|---|---|---|
| 16913936 | IFT52 | 0.61 | 6.10 | 0.01270852 |
| 16684241 | MECR | 0.49 | 5.13 | 0.032399453 |
| 16692741 | APH1A | 0.61 | 6.87 | 0.001070637 |
| 17078121 | LACTB2 | 1.44 | 7.14 | 0.006465241 |
| 17091097 | MRPS2 | 0.44 | 4.38 | 0.042011774 |
| 16992446 | RPL26L1 | 0.67 | 4.62 | 0.000995688 |
| 16774808 | PHF11 | -0.77 | 5.91 | 0.003485 |
| 16750277 | IRAK4 | -0.58 | 6.59 | 0.001978684 |
| 17057983 | CHCHD2 | 0.88 | 6.56 | 0.000496545 |
| 16760546 | ING4 | 0.41 | 6.57 | 0.0303931 |
| 16660199 | MRTO4 | 0.78 | 6.36 | 0.008922121 |
| 16848739 | HN1 | 0.85 | 6.01 | 0.042914577 |
| 17091281 | EGFL7 | -1.21 | 5.47 | 0.001263485 |
| 16978834 | LEF1 | -0.99 | 5.56 | 0.040845786 |
| 16834015 | RAPGEFL1 | 0.64 | 4.42 | 0.019555184 |
| 16792810 | NIN | -0.68 | 7.82 | 0.008112069 |
| 17051553 | CPA4 | 3.80 | 7.50 | 0.000182085 |
| 17066018 | ZDHHC2 | 1.00 | 7.52 | 0.020424774 |
| 16799793 | NUSAP1 | 1.62 | 7.64 | 0.002287834 |
| 16836977 | TACO1 | 0.68 | 6.26 | 0.024631948 |
| 16787951 | GLRX5 | 0.64 | 3.94 | 0.012193296 |
| 16790202 | ZNF219 | 0.84 | 4.85 | 0.006678351 |
| 16846163 | COPZ2 | -1.06 | 7.34 | 0.040783602 |
| 16925495 | PIGP | 0.63 | 5.53 | 0.004872828 |
| 16874467 | VRK3 | 0.62 | 6.31 | 0.005187186 |
| 16879067 | CRIM1 | 1.31 | 10.29 | 0.000799328 |
| 16989867 | PAIP2 | 0.30 | 7.14 | 0.034568907 |
| 17111808 | PDZD11 | 0.83 | 7.34 | 0.002226908 |
| 16664150 | TMEM69 | 0.65 | 7.25 | 0.022323152 |
| 17056515 | NT5C3A | 0.79 | 5.55 | 0.030622512 |
| 16664947 | MRPL37 | 0.61 | 8.57 | 0.019439063 |
| 16760406 | MRPL51 | 0.51 | 5.33 | 0.011383858 |
| 16725608 | TMEM216 | 0.43 | 4.71 | 0.047447463 |
| 16761259 | CLEC1A | -1.00 | 4.85 | 0.010414507 |
| 16868130 | CD320 | 0.92 | 6.90 | 0.010228669 |
| 17001024 | PCDH12 | -0.92 | 3.60 | 0.01303921 |
| 17015324 | NRN1 | -1.68 | 6.02 | 0.009527594 |
| 17101537 | TLR8 | -1.03 | 5.93 | 0.002849275 |
| 16980974 | FAM198B | -1.33 | 5.24 | 0.000588116 |
| 16882416 | MRPL35 | 0.70 | 7.96 | 0.003521128 |
| 16837298 | AMZ2 | 0.56 | 9.03 | 0.018889578 |
| 16804778 | NGRN | 0.70 | 7.11 | 0.022031904 |
| 16725184 | MS4A4A | -0.95 | 6.25 | 0.033731714 |
| 16784760 | DACT1 | -1.52 | 5.29 | 0.015132334 |
| 16770961 | TAOK3 | -0.49 | 6.96 | 0.035352582 |
| 16723283 | WT1-AS | 0.97 | 5.29 | 0.019614135 |
| 17102017 | MBTPS2 | 0.55 | 7.96 | 0.003883275 |
| 16665302 | HOOK1 | 1.39 | 5.27 | 0.048263673 |
| 17046249 | MRPS17 | 0.59 | 6.17 | 0.032925202 |
| 16820584 | NIP7 | 0.50 | 8.09 | 0.030242791 |
| 16831442 | TRPV2 | -0.82 | 5.53 | 0.022026034 |
| 16869221 | WDR83OS | 0.45 | 7.05 | 0.04750453 |
| 16728949 | PPME1 | 0.52 | 7.53 | 0.020617927 |
| 16764732 | BIN2 | -0.79 | 6.60 | 0.023247247 |
| 16959441 | AMOTL2 | 0.85 | 6.79 | 0.004969977 |
| 17014091 | SNX9 | -0.58 | 9.20 | 0.039065942 |
| 17067314 | SCARA3 | 1.69 | 8.64 | 0.021334442 |
| 16661663 | YTHDF2 | 0.37 | 6.42 | 0.046598957 |

| | | | | |
|---|---|---|---|---|
| 16788339 | EVL | -0.83 | 6.11 | 0.005286964 |
| 16870401 | ISYNA1 | 2.06 | 8.37 | 0.000416005 |
| 16739887 | TRMT112 | 0.39 | 5.65 | 0.015003145 |
| 16677201 | DTL | 1.06 | 6.45 | 0.038949092 |
| 16953679 | NCKIPSD | 0.50 | 5.57 | 0.042473943 |
| 17004760 | TMEM14C | 0.57 | 9.00 | 0.002202594 |
| 16919408 | OSER1 | 0.56 | 6.76 | 0.012502456 |
| 16865726 | ZNF581 | 0.90 | 6.27 | 0.008922121 |
| 17018256 | CUTA | 0.54 | 5.69 | 0.009991301 |
| 17042650 | CUTA | 0.55 | 5.80 | 0.007983133 |
| 16860946 | LSR | 1.92 | 6.77 | 0.000239688 |
| 16673822 | METTL13 | 0.44 | 6.99 | 0.04882767 |
| 16895172 | SF3B14 | 0.43 | 8.35 | 0.010414232 |
| 17018685 | PPIL1 | 0.77 | 7.42 | 0.007759919 |
| 16878662 | YPEL5 | -0.62 | 5.65 | 0.016561255 |
| 16827234 | FAM96B | 0.43 | 7.68 | 0.049276937 |
| 16846954 | MRPS23 | 1.21 | 6.65 | 0.000300887 |
| 17063656 | MRPS33 | 0.72 | 4.96 | 0.028551639 |
| 16847260 | PTRH2 | 0.69 | 5.67 | 0.00995933 |
| 17058891 | STYXL1 | 0.85 | 6.66 | 0.00608227 |
| 16828886 | GINS2 | 1.53 | 4.95 | 0.005871795 |
| 16876881 | CPSF3 | 0.36 | 7.75 | 0.040273669 |
| 16821882 | TRAPPC2L | 0.87 | 7.76 | 0.013750102 |
| 17013072 | HECA | -0.65 | 6.73 | 0.013011825 |
| 16978354 | EMCN | -1.43 | 6.01 | 0.006296201 |
| 16816424 | SYT17 | 2.32 | 6.90 | 0.000279195 |
| 16762597 | TM7SF3 | 0.80 | 9.14 | 0.029999113 |
| 17021911 | COQ3 | 0.56 | 3.92 | 0.048490926 |
| 16897946 | BCL11A | -1.76 | 4.26 | 0.001512304 |
| 16923179 | UBASH3A | -0.90 | 4.92 | 0.045521155 |
| 16703340 | MYO3A | 1.55 | 4.00 | 0.020126598 |
| 16749010 | SLCO1C1 | -1.03 | 3.12 | 3.06E-05 |
| 16924966 | MIS18A | 0.68 | 5.65 | 0.011455321 |
| 17117918 | LRRC3DN | 0.59 | 3.50 | 0.037187959 |
| 16925911 | RIPK4 | 2.49 | 5.55 | 0.00457055 |
| 17019029 | TREM2 | 1.32 | 7.14 | 0.006826972 |
| 16784157 | GNG2 | -1.36 | 5.11 | 1.58E-05 |
| 17070082 | GDAP1 | 0.75 | 5.07 | 0.032508512 |
| 16921428 | SOX18 | -1.06 | 5.27 | 0.006473873 |
| 16973934 | CYTL1 | -1.06 | 6.66 | 0.024291321 |
| 16683221 | WNT4 | 1.65 | 4.74 | 0.047708696 |
| 17106877 | SASH3 | -0.85 | 6.41 | 0.021751719 |
| 17045198 | ANLN | 1.66 | 7.26 | 0.024133658 |
| 16895118 | ATAD2B | -0.51 | 6.66 | 0.010665065 |
| 16706779 | CCSER2 | -0.59 | 7.79 | 0.012656127 |
| 16820414 | PRMT7 | 0.59 | 6.27 | 0.032878371 |
| 16695907 | TMCO1 | 0.50 | 9.33 | 0.017455477 |
| 16979875 | PCDH18 | -1.35 | 7.32 | 0.005406762 |
| 17073527 | EXOSC4 | 0.64 | 6.09 | 0.032843247 |
| 16888708 | ASNSD1 | 0.46 | 7.04 | 0.03626571 |
| 16707503 | EXOC6 | -0.71 | 6.65 | 0.006109041 |
| 16994969 | MTMR12 | 0.44 | 7.80 | 0.04146164 |
| 16958096 | WDR5B | 0.84 | 5.61 | 0.013786789 |
| 16996771 | SGTB | -0.73 | 7.23 | 0.033386639 |
| 16680258 | MXRA8 | -0.96 | 8.15 | 0.032622497 |
| 16775643 | NDFIP2 | 1.21 | 8.51 | 0.007435833 |
| 17057329 | DDX56 | 0.52 | 7.53 | 0.012367099 |
| 16996119 | ARL15 | -0.72 | 6.10 | 0.008103354 |

| | | | | |
|---|---|---|---|---|
| 16872203 | PAF1 | 0.46 | 6.96 | 0.031799831 |
| 16691078 | RSBN1 | -0.51 | 7.01 | 0.002026515 |
| 16911238 | CRLS1 | 0.63 | 8.02 | 0.01444663 |
| 16940593 | P4HTM | 0.59 | 6.14 | 0.03500606 |
| 16683875 | GPN2 | 0.51 | 6.61 | 0.011077896 |
| 16815670 | RBFOX1 | 1.48 | 4.45 | 0.007077087 |
| 16866667 | PCSK4 | 0.52 | 4.63 | 0.037230334 |
| 16827874 | HYDIN | 0.79 | 4.17 | 0.02083209 |
| 16969414 | TET2 | -0.61 | 7.06 | 0.004464778 |
| 16666448 | GIPC2 | -1.37 | 4.27 | 0.017996341 |
| 16810177 | VPS13C | -0.43 | 8.72 | 0.041992918 |
| 16742963 | SYTL2 | -1.51 | 5.43 | 0.002498679 |
| 16944055 | SIDT1 | -1.25 | 4.53 | 0.005028618 |
| 16669278 | FAM46C | -1.52 | 7.27 | 0.003955122 |
| 16939796 | SNRK | -0.75 | 6.71 | 0.000996424 |
| 16865590 | EPS8L1 | 1.55 | 4.74 | 0.02957219 |
| 16667530 | PALMD | -1.47 | 6.89 | 0.033848844 |
| 17007673 | UHRF1BP1 | 0.88 | 7.11 | 0.010853229 |
| 16907526 | INO80D | -0.41 | 7.85 | 0.030199753 |
| 16806564 | MTMR10 | -0.40 | 8.14 | 0.036621116 |
| 16660212 | PQLC2 | 0.73 | 5.68 | 0.009786926 |
| 16676217 | LAX1 | -1.42 | 5.36 | 0.013094763 |
| 16847007 | MKS1 | 0.45 | 5.74 | 0.046389438 |
| 17042735 | HEATR2 | 0.87 | 6.65 | 0.002185771 |
| 16874047 | RASIP1 | -1.44 | 4.98 | 0.009309447 |
| 16870543 | TMEM161A | 0.85 | 6.83 | 0.036337183 |
| 16943404 | TRMT10C | 0.52 | 6.55 | 0.048683111 |
| 16662525 | ADPRHL2 | 0.94 | 6.41 | 0.001238619 |
| 16685427 | C1orf109 | 0.54 | 4.47 | 0.014304573 |
| 16810725 | PARP16 | 0.49 | 7.18 | 0.04025301 |
| 16873654 | TMEM160 | 0.86 | 8.22 | 0.028755503 |
| 16727770 | SSH3 | 1.27 | 6.08 | 0.000821889 |
| 16725405 | TMEM132A | 1.15 | 5.90 | 0.011735645 |
| 16991604 | THG1L | 0.67 | 6.35 | 0.010563409 |
| 16823255 | HCFC1R1 | 0.64 | 6.30 | 0.023703726 |
| 16915804 | GID8 | 0.44 | 7.70 | 0.034720834 |
| 16938429 | OXSM | 0.73 | 5.41 | 0.003040233 |
| 16680274 | AURKAIP1 | 0.57 | 6.10 | 0.044926034 |
| 16929056 | TUG1 | -0.51 | 9.55 | 0.00760586 |
| 16741643 | LAMTOR1 | 0.38 | 6.46 | 0.028880252 |
| 16931197 | FAM118A | -1.12 | 4.79 | 0.007595006 |
| 16874313 | PIH1D1 | 0.54 | 6.13 | 0.013925031 |
| 16909303 | PID1 | -0.87 | 3.96 | 0.021086941 |
| 16969267 | BANK1 | -2.06 | 4.25 | 0.001263485 |
| 17113710 | TMEM255A | 2.15 | 6.63 | 0.015592393 |
| 16852008 | MOCOS | 0.81 | 5.86 | 0.041059079 |
| 16848079 | WIPI1 | -0.91 | 8.56 | 0.040273669 |
| 16820676 | PDPR | 0.70 | 7.35 | 0.040039322 |
| 17011378 | SOBP | -1.06 | 5.11 | 0.014335286 |
| 17105914 | CXorf57 | -0.63 | 3.09 | 0.019306979 |
| 16861969 | SAMD4B | 0.49 | 7.85 | 0.04545095 |
| 16872594 | ATP5SL | -1.60 | 4.80 | 0.000661483 |
| 16674292 | RALGPS2 | -1.24 | 7.10 | 0.018180207 |
| 16986450 | AGGF1 | 0.39 | 8.19 | 0.046240214 |
| 16866912 | PLEKHJ1 | 0.80 | 7.49 | 0.021222619 |
| 16734779 | TRIM68 | 0.71 | 6.13 | 0.001833969 |
| 16662648 | CDCA8 | 1.45 | 5.27 | 0.017160609 |
| 17076821 | THAP1 | 0.41 | 6.57 | 0.020357132 |

| | | | | |
|---|---|---|---|---|
| 17043418 | ZDHHC4 | 0.65 | 5.88 | 0.003082046 |
| 17077760 | ARMC1 | 0.55 | 7.15 | 0.042182779 |
| 16673983 | DARS2 | 0.53 | 6.55 | 0.026999666 |
| 16835346 | PNPO | 0.86 | 7.56 | 0.007813504 |
| 17009482 | CENPQ | 0.94 | 5.43 | 0.012156683 |
| 17019208 | MRPS10 | 0.44 | 7.47 | 0.02650514 |
| 16836504 | SMG8 | 0.57 | 5.22 | 0.01647169 |
| 16749747 | KIAA1551 | -0.61 | 7.26 | 0.00671532 |
| 16769514 | APPL2 | -0.42 | 6.95 | 0.029435864 |
| 16974925 | LGI2 | -1.12 | 6.28 | 0.044058872 |
| 16692805 | GOLPH3L | 0.72 | 7.88 | 0.036610869 |
| 16804559 | FANCI | 1.37 | 6.90 | 0.000644597 |
| 16715155 | LRRC20 | 1.00 | 4.89 | 0.001374972 |
| 17009676 | LRRC1 | 2.70 | 8.34 | 0.001049806 |
| 16873541 | PNMAL1 | 1.53 | 4.97 | 0.004588824 |
| 16884956 | STEAP3 | 1.37 | 7.29 | 0.030609357 |
| 16972616 | NEIL3 | 1.36 | 4.56 | 0.01976673 |
| 16774669 | NUDT15 | 0.53 | 5.03 | 0.044982261 |
| 16717498 | CWF19L1 | 0.69 | 6.69 | 0.04028811 |
| 17051943 | TMEM140 | -0.69 | 6.28 | 0.014395131 |
| 16689020 | MCOLN3 | 1.37 | 4.53 | 0.011077896 |
| 16980693 | FBXW7 | -0.75 | 6.28 | 0.001978684 |
| 16749537 | CCDC91 | -0.51 | 5.44 | 0.018661333 |
| 16983907 | BRIX1 | 0.67 | 6.38 | 0.006254419 |
| 17053384 | GIMAP4 | -0.66 | 7.34 | 0.044173415 |
| 16820737 | DDX19A | 0.54 | 7.04 | 0.00982264 |
| 17095043 | RFK | 0.76 | 5.07 | 0.04997158 |
| 16911070 | AP5S1 | 0.52 | 5.35 | 0.034540826 |
| 16916396 | TMEM74B | -0.54 | 3.62 | 0.013096869 |
| 16843179 | COPRS | 0.55 | 5.96 | 0.014173779 |
| 17071208 | LAPTM4B | 0.90 | 9.58 | 0.043723507 |
| 17009132 | TMEM63B | 0.64 | 6.66 | 0.010973189 |
| 16920699 | PPP4R1L | -0.84 | 3.88 | 0.048943191 |
| 16889503 | STRADB | 0.87 | 5.46 | 0.006294787 |
| 16704182 | CSGALNACT2 | -0.69 | 7.87 | 0.009910072 |
| 16827606 | SMPD3 | 2.50 | 6.60 | 0.008999768 |
| 17079005 | TMEM55A | -0.60 | 6.38 | 0.038633276 |
| 16736120 | SOX6 | 2.52 | 5.32 | 0.014818595 |
| 16883552 | CNOT11 | 0.32 | 7.13 | 0.029999113 |
| 16755988 | STAB2 | -2.03 | 3.97 | 0.004041282 |
| 16693789 | UBE2Q1 | 0.60 | 7.13 | 0.007777057 |
| 16861987 | MED29 | 0.72 | 8.08 | 0.004621635 |
| 16695463 | ITLN1 | 6.45 | 8.13 | 0.000466702 |
| 17048576 | PPP1R9A | 1.55 | 4.96 | 0.006504942 |
| 16917061 | FERMT1 | 1.01 | 5.66 | 0.041564991 |
| 16917400 | KIF16B | -0.79 | 6.24 | 0.014395164 |
| 16909081 | DOCK10 | -1.02 | 8.34 | 0.002003568 |
| 16867278 | STAP2 | 1.63 | 4.90 | 0.001363353 |
| 16688386 | DEPDC1 | 1.37 | 4.39 | 0.01805536 |
| 17069272 | CHD7 | -0.61 | 6.11 | 0.012310204 |
| 17003479 | NHP2 | 0.82 | 7.08 | 0.006826972 |
| 16875979 | ZNF416 | 0.88 | 5.18 | 0.01631073 |
| 16786780 | GPATCH2L | -0.55 | 6.32 | 0.019655181 |
| 16730296 | KDM4D | 0.61 | 4.63 | 0.019555184 |
| 16677616 | IARS2 | 0.54 | 7.79 | 0.033810453 |
| 16897719 | CCDC88A | -0.64 | 7.56 | 0.035825301 |
| 16687418 | NDC1 | 1.09 | 7.50 | 0.000466755 |
| 16919864 | ZNF334 | 1.29 | 5.57 | 0.001212101 |

| | | | | |
|---|---|---|---|---|
| 16826779 | DOK4 | 0.69 | 7.44 | 0.024493485 |
| 16839582 | TSR1 | 0.75 | 6.96 | 0.008799118 |
| 16662009 | IQCC | 0.85 | 4.53 | 0.006109041 |
| 16869588 | ASF1B | 0.95 | 6.03 | 0.02412805 |
| 16762573 | ASUN | 0.73 | 7.77 | 0.004960091 |
| 16918633 | EDEM2 | 0.53 | 6.61 | 0.028094589 |
| 16968051 | 40787 | -1.03 | 7.47 | 0.046212555 |
| 16907458 | WDR12 | 0.43 | 5.57 | 0.029382558 |
| 16768675 | FGD6 | 1.47 | 8.66 | 0.000587344 |
| 17075168 | CSGALNACT1 | -0.71 | 3.98 | 0.045963111 |
| 16827566 | DDX28 | 0.56 | 5.08 | 0.026981053 |
| 16941885 | CACNA2D3 | 1.40 | 4.92 | 0.04962496 |
| 17078558 | PAG1 | -0.87 | 6.89 | 0.03559341 |
| 16798652 | DCAF6 | 1.07 | 5.12 | 0.006244544 |
| 16950632 | EMC3 | 0.59 | 8.07 | 0.009225792 |
| 16944574 | EAF2 | -1.23 | 7.47 | 0.001175595 |
| 16886200 | ARHGAP15 | -1.51 | 5.24 | 0.000141059 |
| 16886232 | ARHGAP15 | -1.76 | 4.37 | 6.22E-06 |
| 17075776 | PBK | 1.77 | 5.64 | 0.002567779 |
| 16947796 | MYNN | 0.49 | 6.62 | 0.00760586 |
| 16749162 | CMAS | 0.52 | 7.60 | 0.023657938 |
| 17046181 | LANCL2 | 0.87 | 5.87 | 0.000858371 |
| 16930811 | 37865 | 0.97 | 5.44 | 0.04086658 |
| 16768628 | NDUFA12 | 0.27 | 3.92 | 0.047315765 |
| 17060143 | BAIAP2L1 | 1.30 | 6.93 | 0.006294787 |
| 16671653 | SLC50A1 | 0.88 | 8.11 | 0.002316293 |
| 16816996 | UBFD1 | 0.50 | 8.49 | 0.024950681 |
| 16990312 | PCDHB13 | 1.22 | 6.85 | 0.015965317 |
| 16990304 | PCDHB12 | 1.55 | 7.01 | 0.020046072 |
| 16990292 | PCDHB9 | 1.37 | 5.04 | 0.041965303 |
| 17081106 | GSDMC | -1.14 | 2.91 | 0.000149647 |
| 16660992 | MTFR1L | 0.46 | 5.74 | 0.04249774 |
| 16917004 | GPCPD1 | -0.85 | 8.21 | 0.004665936 |
| 16903863 | RPRM | 1.43 | 5.07 | 0.010665065 |
| 16771632 | DIABLO | 0.42 | 6.12 | 0.014793498 |
| 16708370 | C10orf2 | 0.66 | 5.18 | 0.047832543 |
| 16721746 | AKIP1 | 0.55 | 6.81 | 0.038485765 |
| 17078355 | JPH1 | 1.97 | 5.43 | 0.002177593 |
| 16916104 | SLC2A4RG | 0.59 | 6.62 | 0.042217762 |
| 16726372 | GPR137 | 0.52 | 5.28 | 0.006272434 |
| 16880924 | PNO1 | 0.61 | 6.24 | 0.037830553 |
| 16811299 | THAP10 | 0.88 | 4.97 | 0.024678151 |
| 16854016 | SPIRE1 | 0.57 | 7.67 | 0.040039322 |
| 16872567 | EXOSC5 | 1.02 | 6.67 | 0.041591961 |
| 16867541 | DUS3L | 0.68 | 6.45 | 0.019678128 |
| 16743285 | SMCO4 | -0.61 | 4.99 | 0.024277737 |
| 16945357 | C3orf37 | 1.02 | 8.62 | 0.007017806 |
| 16946228 | MRPS22 | 0.43 | 6.14 | 0.029648298 |
| 16999974 | C5orf15 | 0.48 | 9.36 | 0.017345479 |
| 16831598 | NT5M | 0.66 | 3.65 | 0.03424377 |
| 16943313 | NIT2 | 0.98 | 7.70 | 0.000696933 |
| 16988931 | CDC42SE2 | -0.66 | 5.39 | 0.005934022 |
| 16955822 | ADAMTS9 | -1.78 | 7.33 | 0.000639199 |
| 17045354 | YAE1D1 | 0.77 | 8.45 | 0.004294068 |
| 16847605 | CCDC47 | 0.43 | 9.25 | 0.027945513 |
| 16727891 | CABP4 | -0.46 | 4.63 | 0.039731905 |
| 16819497 | COQ9 | 1.13 | 7.98 | 0.001049806 |
| 16826767 | CIAPIN1 | 0.90 | 7.87 | 0.003264143 |

| | | | | |
|---|---|---|---|---|
| 17024414 | HYMAI | -0.99 | 4.47 | 0.002975858 |
| 16659054 | AGTRAP | 0.57 | 5.91 | 0.035847469 |
| 16760116 | PARP11 | -0.58 | 5.34 | 0.011913718 |
| 16760216 | ANO2 | -0.87 | 4.76 | 0.000808862 |
| 16865693 | NAT14 | 0.53 | 4.78 | 0.017757647 |
| 16753800 | NUP107 | 0.59 | 6.87 | 0.035847469 |
| 16740725 | CD248 | -1.25 | 6.77 | 0.045815477 |
| 16898326 | PELI1 | -0.94 | 7.08 | 0.011910205 |
| 16920370 | SALL4 | 1.08 | 4.39 | 0.023388426 |
| 16928533 | ASPHD2 | -0.68 | 4.53 | 0.026524724 |
| 17003034 | KIAA1191 | 0.64 | 7.61 | 0.001591953 |
| 16875952 | VN1R1 | 0.91 | 3.48 | 0.002957169 |
| 17081829 | SLC45A4 | 1.17 | 6.63 | 0.013350291 |
| 17013126 | GPR126 | 2.83 | 8.61 | 0.000127126 |
| 16672635 | VANGL2 | 1.09 | 5.97 | 0.04926514 |
| 17012963 | KIAA1244 | 2.28 | 5.94 | 0.010320732 |
| 17024198 | NHSL1 | 0.67 | 5.75 | 0.046224516 |
| 16831338 | ZNF286A | 0.72 | 6.55 | 0.049767345 |
| 16956897 | SENP7 | -0.63 | 6.77 | 0.009447187 |
| 17005348 | MRS2 | 0.73 | 7.35 | 0.009830557 |
| 16785127 | RHOJ | -2.03 | 5.85 | 0.000514187 |
| 16823561 | NMRAL1 | 0.60 | 6.96 | 0.011734289 |
| 16848784 | MIF4GD | 0.83 | 6.28 | 0.007211899 |
| 16878800 | BIRC6 | -0.40 | 8.80 | 0.014432391 |
| 16681159 | PLEKHG5 | -0.48 | 4.77 | 0.047359928 |
| 16766923 | PPM1H | 1.23 | 5.07 | 0.018617743 |
| 16903919 | ERMN | -0.90 | 3.30 | 0.023829296 |
| 16921402 | ZNF512B | 0.59 | 7.00 | 0.037218869 |
| 17110977 | SHROOM4 | -1.29 | 5.08 | 0.0009769 |
| 17013694 | PLEKHG1 | -1.09 | 6.36 | 0.010005726 |
| 16815985 | MKL2 | -0.95 | 8.64 | 0.000912967 |
| 16879441 | MTA3 | 0.58 | 5.22 | 0.01629462 |
| 16911077 | MAVS | 0.59 | 6.64 | 0.009758006 |
| 16999321 | ZNF608 | -0.94 | 5.43 | 0.019678128 |
| 16774188 | COG6 | -0.69 | 7.02 | 0.027431694 |
| 16944344 | ARHGAP31 | -1.02 | 6.79 | 0.002383003 |
| 16800117 | STARD9 | -1.33 | 6.33 | 0.000134884 |
| 16906749 | HECW2 | -1.38 | 5.11 | 0.007595006 |
| 16782862 | NYNRIN | -0.99 | 6.32 | 0.017880257 |
| 16670866 | CGN | 2.35 | 6.14 | 0.00376529 |
| 16964764 | TBC1D14 | -0.47 | 7.49 | 0.006275479 |
| 16965190 | CC2D2A | -0.69 | 5.40 | 0.016061466 |
| 16695216 | IGSF9 | 2.15 | 6.02 | 0.001196221 |
| 16730471 | KIAA1377 | -0.90 | 5.50 | 0.012778755 |
| 16854602 | KLHL14 | -1.11 | 3.40 | 0.000127126 |
| 16793632 | TRMT5 | 0.43 | 6.56 | 0.042050127 |
| 16727843 | CARNS1 | 2.33 | 6.77 | 0.002105113 |
| 16920047 | PREX1 | -0.75 | 7.47 | 0.015698334 |
| 16712944 | KIAA1462 | -1.71 | 6.45 | 0.007110118 |
| 16860266 | ZNF492 | 1.12 | 3.42 | 0.033528421 |
| 16884827 | DPP10 | 1.88 | 5.10 | 0.019721473 |
| 16833629 | ARHGAP23 | 0.81 | 7.40 | 0.005966995 |
| 16772197 | DHX37 | 0.59 | 5.65 | 0.016484012 |
| 16662159 | KIAA1522 | 1.80 | 6.18 | 3.57E-05 |
| 16671723 | HCN3 | 1.04 | 3.97 | 0.001844689 |
| 16857676 | CAMSAP3 | 1.22 | 4.71 | 0.006570848 |
| 16885080 | EPB41L5 | 1.10 | 6.87 | 0.003837347 |
| 17063394 | KIAA1549 | 0.91 | 5.62 | 0.024368191 |

| | | | | |
|---|---|---|---|---|
| 17018654 | CPNE5 | -0.67 | 4.98 | 0.046240214 |
| 16704690 | WDFY4 | -1.14 | 5.96 | 0.002351716 |
| 16711562 | SFMBT2 | -0.67 | 8.26 | 0.048517249 |
| 16708340 | SEMA4G | 0.73 | 4.75 | 0.041013206 |
| 16990288 | PCDHB16 | 1.66 | 5.81 | 0.020483503 |
| 16870174 | ANO8 | 0.68 | 6.51 | 0.049710075 |
| 16919769 | NCOA5 | 0.42 | 7.36 | 0.030339395 |
| 16973753 | ZFYVE28 | -0.49 | 3.70 | 0.049824339 |
| 16667456 | PTBP2 | -0.64 | 7.32 | 0.011913718 |
| 16821467 | WFDC1 | -1.95 | 5.06 | 0.017942017 |
| 16921832 | JAM2 | -1.21 | 5.59 | 0.014326211 |
| 17082935 | ZNF250 | -0.70 | 6.33 | 0.012401471 |
| 16864220 | SCAF1 | 0.58 | 6.62 | 0.035352582 |
| 16683541 | IL22RA1 | 0.73 | 3.79 | 0.031230388 |
| 16961806 | GNB4 | -0.56 | 7.24 | 0.041965303 |
| 16751769 | C12orf10 | 0.66 | 6.51 | 0.006229481 |
| 17115617 | FAM3A | 0.47 | 5.43 | 0.018617743 |
| 16848793 | SLC25A19 | 0.89 | 6.14 | 0.029372633 |
| 16749511 | MRPS35 | 0.67 | 7.29 | 0.016367995 |
| 16889375 | NIF3L1 | 0.68 | 7.52 | 0.005937876 |
| 16730742 | AASDHPPT | 0.74 | 6.71 | 0.004796972 |
| 16878036 | AGBL5 | 0.59 | 4.59 | 0.022937911 |
| 16696504 | GAS5 | 0.58 | 7.45 | 0.04025301 |
| 16972773 | TRAPPC11 | -0.34 | 7.65 | 0.036619298 |
| 16735205 | MRPL17 | 0.44 | 6.44 | 0.040366916 |
| 16847321 | HEATR6 | 0.47 | 8.18 | 0.046598957 |
| 17066224 | SH2D4A | 1.22 | 6.33 | 0.001992479 |
| 16913403 | MANBAL | 0.82 | 7.29 | 0.006011845 |
| 17002396 | C5orf54 | 1.02 | 5.10 | 0.033848844 |
| 16911394 | ANKEF1 | 0.83 | 5.16 | 0.031386654 |
| 16915448 | FAM217B | 0.62 | 6.72 | 0.009296335 |
| 17017805 | GPSM3 | -0.70 | 5.14 | 0.015377204 |
| 17057381 | MYO1G | -1.12 | 6.73 | 0.025298818 |
| 16861641 | C19orf33 | 4.09 | 8.79 | 1.41E-05 |
| 17095345 | SLC28A3 | 2.69 | 6.55 | 0.039993467 |
| 16985911 | MCCC2 | 0.83 | 6.39 | 0.006570848 |
| 16893634 | GAL3ST2 | 3.24 | 7.14 | 0.000393759 |
| 16931068 | PARVG | -0.56 | 5.73 | 0.049710075 |
| 17108694 | CRLF2 | -0.53 | 2.63 | 0.01133074 |
| 16839116 | FN3K | 0.92 | 5.00 | 0.00078335 |
| 16688799 | ELTD1 | -1.79 | 8.72 | 0.002958086 |
| 16843221 | C17orf75 | 0.65 | 5.95 | 0.036591224 |
| 16965346 | NCAPG | 1.38 | 6.19 | 0.0274033 |
| 16906440 | OSGEPL1 | 0.58 | 4.51 | 0.028581919 |
| 16701407 | TFB2M | 0.70 | 8.57 | 0.038712086 |
| 16815023 | MLST8 | 0.52 | 7.37 | 0.030724616 |
| 16909891 | RAB17 | 0.95 | 4.39 | 0.032354151 |
| 16822296 | RHBDF1 | 0.80 | 5.76 | 0.002974203 |
| 16908433 | RNF25 | 0.46 | 7.15 | 0.038494747 |
| 17068972 | SOX17 | -0.98 | 4.85 | 0.006181299 |
| 16766539 | ARHGAP9 | -0.81 | 4.90 | 0.013923264 |
| 16785606 | MPP5 | 0.87 | 7.40 | 0.00597007 |
| 17000928 | ARAP3 | -0.82 | 4.77 | 0.019555184 |
| 17084990 | POLR1E | 0.58 | 6.93 | 0.049710075 |
| 16822548 | NARFL | 0.51 | 5.53 | 0.008464073 |
| 17049426 | MOSPD3 | 0.58 | 6.07 | 0.014155577 |
| 17075628 | EBF2 | -2.28 | 5.40 | 0.000255998 |
| 16882544 | ANAPC1 | 0.65 | 6.56 | 0.024961361 |

| | | | | |
|---|---|---|---|---|
| 16925508 | TMPRSS3 | 3.10 | 5.64 | 0.000456269 |
| 16663033 | SMAP2 | -1.14 | 7.83 | 0.003033218 |
| 16862646 | ZNF574 | 0.53 | 5.80 | 0.01758657 |
| 16731105 | C11orf1 | 0.76 | 5.26 | 0.031989369 |
| 16819678 | GINS3 | 0.65 | 5.24 | 0.021641874 |
| 16720268 | EPS8L2 | 1.01 | 5.79 | 0.001637265 |
| 17060923 | RABL5 | 0.93 | 5.72 | 0.000873526 |
| 17099309 | DDX31 | 0.49 | 5.56 | 0.039993467 |
| 16895941 | FNDC4 | -1.26 | 5.02 | 0.015377204 |
| 16771397 | C12orf43 | 0.35 | 5.79 | 0.042642625 |
| 16913811 | LPIN3 | 0.95 | 6.33 | 0.000941995 |
| 16796590 | BCL11B | -1.00 | 5.23 | 0.046767865 |
| 16869891 | RASAL3 | -0.93 | 6.43 | 0.03351212 |
| 17019549 | MRPL14 | 0.59 | 5.47 | 0.010414232 |
| 17046740 | STAG3L4 | 0.68 | 6.46 | 0.009758006 |
| 16985614 | CENPH | 0.76 | 3.76 | 0.026323983 |
| 16685281 | MRPS15 | 0.46 | 8.79 | 0.015998855 |
| 16804458 | MRPS11 | 0.47 | 8.03 | 0.038253759 |
| 16900245 | MRPS5 | 0.51 | 7.16 | 0.014049167 |
| 16994045 | MRPL36 | 0.47 | 4.54 | 0.003485 |
| 16740797 | MRPL11 | 0.79 | 7.19 | 0.004320025 |
| 16827394 | ACD | 0.54 | 5.39 | 0.013222891 |
| 16884200 | SOWAHC | 0.76 | 4.77 | 0.011986686 |
| 16995339 | C5orf42 | 0.79 | 7.30 | 0.015503452 |
| 16687264 | SELRC1 | 0.66 | 4.81 | 0.0108719 |
| 17082192 | PYCRL | 0.74 | 5.80 | 0.023113528 |
| 16835497 | UBE2Z | 0.54 | 7.97 | 0.013011825 |
| 17073994 | C8orf33 | 0.82 | 7.46 | 0.00995933 |
| 16758885 | AACS | 0.69 | 6.72 | 0.013973413 |
| 16825819 | ZNF747 | 0.39 | 5.48 | 0.041638363 |
| 16916667 | DDRGK1 | 0.49 | 7.51 | 0.026785346 |
| 16822809 | MRPS34 | 0.89 | 7.47 | 0.001997816 |
| 17053316 | LRRC61 | 1.13 | 5.93 | 0.005316307 |
| 16834711 | C17orf53 | 0.96 | 4.87 | 0.00935104 |
| 17082081 | RHPN1-AS1 | 0.73 | 3.50 | 0.032673404 |
| 16683712 | AUNIP | 0.72 | 3.44 | 0.02649727 |
| 16829426 | DBNDD1 | 0.78 | 4.69 | 0.036145279 |
| 16859486 | DDA1 | 0.56 | 8.43 | 0.030724616 |
| 17056358 | GGCT | 0.74 | 5.35 | 0.005096594 |
| 16750488 | TMEM106C | 0.91 | 4.77 | 0.006778957 |
| 17043437 | C7orf26 | 0.40 | 6.05 | 0.030676619 |
| 16752586 | NABP2 | 0.64 | 7.54 | 0.007705785 |
| 16742610 | ALG8 | 0.47 | 7.95 | 0.047708696 |
| 16994244 | FASTKD3 | 0.56 | 5.24 | 0.018394064 |
| 16825794 | DCTPP1 | 0.75 | 7.79 | 0.010862113 |
| 16739435 | C11orf48 | 0.60 | 5.55 | 0.012429258 |
| 16867715 | SLC25A23 | 1.16 | 6.41 | 0.011744728 |
| 16875323 | MBOAT7 | 0.85 | 5.59 | 0.004670637 |
| 16833476 | DHRS11 | 0.88 | 5.68 | 0.031938783 |
| 16755902 | GNPTAB | -0.75 | 2.13 | 0.032925202 |
| 17059427 | TMEM243 | -0.52 | 6.59 | 0.026751385 |
| 16846157 | PRR15L | 3.00 | 5.87 | 0.010973066 |
| 16937909 | TMEM43 | 0.56 | 9.68 | 0.017064738 |
| 16826586 | IRX3 | 1.30 | 5.67 | 0.011910205 |
| 16815316 | THOC6 | 0.59 | 8.17 | 0.006257496 |
| 16694960 | FCRL2 | -2.27 | 3.54 | 0.001727434 |
| 16758321 | B3GNT4 | 0.71 | 3.53 | 0.017982198 |
| 16850246 | C17orf62 | -0.46 | 8.34 | 0.032246839 |

| | | | | |
|---|---|---|---|---|
| 16889209 | C2orf47 | 0.69 | 6.19 | 0.010039892 |
| 16694728 | MRPL24 | 0.73 | 6.86 | 0.009385376 |
| 16682835 | MUL1 | 0.74 | 5.87 | 0.013408734 |
| 16774917 | RNASEH2B | -0.65 | 6.68 | 0.004282625 |
| 16970465 | FAT4 | -1.13 | 7.66 | 0.027873442 |
| 16823636 | ROGDI | 0.94 | 6.57 | 0.031596331 |
| 17114489 | MAP7D3 | -0.89 | 7.04 | 0.002221865 |
| 16814738 | TMEM204 | -1.01 | 7.60 | 0.044926034 |
| 16971308 | ARHGAP10 | -0.72 | 5.56 | 0.017172103 |
| 16836538 | DHX40 | 0.64 | 7.54 | 0.01890385 |
| 17071086 | PLEKHF2 | -0.68 | 6.84 | 0.013989156 |
| 16839106 | FN3KRP | 0.60 | 6.77 | 0.029647339 |
| 16982024 | MLF1IP | 1.06 | 5.26 | 0.022208653 |
| 16796412 | LINC00341 | -1.60 | 5.30 | 0.000628104 |
| 17118421 | ZNF322 | 0.57 | 6.62 | 0.040623853 |
| 17113079 | MORC4 | 0.62 | 7.35 | 0.016877145 |
| 16791086 | IPO4 | 0.69 | 6.65 | 0.031509868 |
| 16903327 | GTDC1 | -0.78 | 6.03 | 0.009837228 |
| 16663231 | PPCS | 0.48 | 6.56 | 0.02250299 |
| 16702685 | SUV39H2 | 0.79 | 5.44 | 0.020770795 |
| 16825813 | ZNF768 | 0.51 | 6.43 | 0.022377746 |
| 16736638 | E2F8 | 1.34 | 5.79 | 0.022514505 |
| 16767788 | BBS10 | 0.62 | 6.53 | 0.035226588 |
| 16688864 | TTLL7 | -1.12 | 5.73 | 0.025836586 |
| 17110352 | CXorf36 | -1.57 | 5.56 | 0.001263485 |
| 16875776 | ISOC2 | 1.23 | 7.82 | 0.000297388 |
| 16820053 | ELMO3 | 1.19 | 4.84 | 0.032160898 |
| 16998162 | MCTP1 | -1.66 | 6.38 | 0.000393343 |
| 17093038 | MOB3B | -0.68 | 3.19 | 0.004785635 |
| 16688235 | WDR78 | 0.73 | 5.29 | 0.028176721 |
| 16795908 | CATSPERB | -0.63 | 2.85 | 0.023938113 |
| 16945289 | EFCC1 | -0.40 | 4.20 | 0.033386639 |
| 16852966 | CCDC102B | -1.65 | 6.55 | 0.001934668 |
| 16738137 | AGBL2 | 1.35 | 4.24 | 0.035604525 |
| 16909042 | FAM124B | -0.80 | 4.29 | 0.008505961 |
| 16732716 | C11orf63 | -0.89 | 5.33 | 0.016484012 |
| 17019040 | TREML2 | -0.58 | 3.09 | 0.020009556 |
| 16758671 | TCTN2 | 0.99 | 7.52 | 0.005287219 |
| 17106246 | ALG13 | -0.53 | 7.22 | 0.032715823 |
| 16869506 | PODNL1 | -1.63 | 6.28 | 0.045169965 |
| 16887589 | CYBRD1 | 0.60 | 10.17 | 0.030557939 |
| 16816386 | TMC7 | -0.76 | 4.14 | 0.030724616 |
| 16833488 | MRM1 | 0.83 | 5.49 | 0.011460725 |
| 16661058 | FAM110D | -0.78 | 3.75 | 0.002689483 |
| 16792688 | L2HGDH | 0.58 | 4.15 | 0.046164473 |
| 17092208 | ERMP1 | 0.98 | 6.84 | 0.015182653 |
| 16867733 | DENND1C | -1.03 | 5.96 | 0.016550099 |
| 16854046 | CEP76 | 0.55 | 5.57 | 0.044373565 |
| 16750792 | DNAJC22 | 1.98 | 5.29 | 0.001035194 |
| 17027518 | ATAT1 | 0.42 | 5.61 | 0.049710075 |
| 17006336 | ATAT1 | 0.45 | 5.58 | 0.043107468 |
| 17030363 | ATAT1 | 0.45 | 5.58 | 0.043107468 |
| 17033068 | ATAT1 | 0.45 | 5.58 | 0.043107468 |
| 17035188 | ATAT1 | 0.45 | 5.58 | 0.043107468 |
| 17037847 | ATAT1 | 0.45 | 5.58 | 0.043107468 |
| 17040561 | ATAT1 | 0.45 | 5.58 | 0.043107468 |
| 16978310 | DNAJB14 | -0.51 | 6.13 | 0.019201137 |
| 16851309 | GREB1L | 1.25 | 4.86 | 0.02522701 |

| | | | | |
|---|---|---|---|---|
| 16827574 | ESRP2 | 2.43 | 5.65 | 0.002116254 |
| 17067031 | DOCK5 | 0.75 | 8.06 | 0.022446726 |
| 16975234 | TMEM156 | -1.28 | 4.36 | 0.003329614 |
| 16837849 | MYO15B | -0.65 | 6.02 | 0.00879171 |
| 16910601 | NRSN2 | 0.74 | 5.64 | 0.008632924 |
| 16887097 | CSRNP3 | -0.85 | 4.48 | 0.032254679 |
| 16857794 | LRRC8E | 0.82 | 5.02 | 0.014748667 |
| 17098745 | PTGES2 | 0.48 | 5.89 | 0.031350721 |
| 16968122 | FRAS1 | 2.30 | 7.70 | 0.00108891 |
| 16720049 | ATHL1 | -0.89 | 5.60 | 0.00234422 |
| 17013851 | MYCT1 | -2.11 | 6.23 | 0.00234422 |
| 16815108 | C16orf59 | 0.71 | 4.95 | 0.034233212 |
| 16843680 | MYO19 | 0.61 | 6.70 | 0.002652296 |
| 16778887 | KIAA0226L | -1.16 | 5.85 | 0.001545581 |
| 16925398 | RUNX1-IT1 | -1.79 | 6.25 | 0.002390586 |
| 16670547 | TARS2 | 0.56 | 5.80 | 0.033541237 |
| 17076285 | RAB11FIP1 | 0.94 | 6.25 | 0.02716733 |
| 17109893 | CXorf21 | -0.79 | 5.60 | 0.012588067 |
| 17069728 | PREX2 | -1.81 | 5.92 | 0.004002822 |
| 16818114 | HSD3B7 | 0.90 | 7.55 | 0.00431596 |
| 16671516 | FLAD1 | 0.58 | 5.11 | 0.029921031 |
| 16713113 | EPC1 | -0.40 | 7.22 | 0.043423949 |
| 16992557 | CPEB4 | -0.98 | 6.66 | 0.008999768 |
| 16891107 | WNT10A | 1.29 | 4.14 | 0.013450106 |
| 16676999 | TRAF3IP3 | -1.31 | 5.97 | 0.002633541 |
| 16834351 | COASY | 0.56 | 6.74 | 0.02522701 |
| 17097560 | AKNA | -1.05 | 6.40 | 0.002885546 |
| 17006276 | PRR3 | 0.41 | 5.71 | 0.043846966 |
| 17033009 | PRR3 | 0.41 | 5.71 | 0.043846966 |
| 17035129 | PRR3 | 0.41 | 5.71 | 0.043846966 |
| 17027459 | PRR3 | 0.42 | 5.70 | 0.040076207 |
| 17030304 | PRR3 | 0.42 | 5.70 | 0.040076207 |
| 17037788 | PRR3 | 0.42 | 5.70 | 0.040076207 |
| 17040502 | PRR3 | 0.42 | 5.70 | 0.040076207 |
| 16711598 | ITIH5 | -1.43 | 4.36 | 0.010822287 |
| 17047560 | UPK3B | 5.57 | 8.48 | 1.39E-05 |
| 16657730 | GLTPD1 | 0.60 | 5.68 | 0.025812227 |
| 16885028 | TMEM177 | 0.72 | 6.23 | 0.008787723 |
| 16793096 | DDHD1 | -0.74 | 7.26 | 0.006123056 |
| 17105655 | BHLHB9 | 0.57 | 4.29 | 0.035788812 |
| 16934434 | APOL3 | -0.75 | 4.98 | 0.02939432 |
| 17063507 | JHDM1D | -0.84 | 6.65 | 0.000929601 |
| 16980005 | SETD7 | -0.83 | 5.72 | 0.003537095 |
| 16674742 | NPL | -0.80 | 7.13 | 0.020512308 |
| 16920651 | ZBP1 | -0.78 | 3.88 | 0.024368191 |
| 16720165 | PTDSS2 | 0.50 | 6.12 | 0.049233283 |
| 16923625 | LRRC3 | 1.02 | 4.73 | 0.03137603 |
| 16742244 | GDPD5 | 1.04 | 5.98 | 0.010655184 |
| 17057897 | VOPP1 | -0.61 | 4.46 | 0.003177931 |
| 16894710 | FAM49A | -1.08 | 6.91 | 0.004191867 |
| 16810828 | VWA9 | 0.52 | 7.61 | 0.031794929 |
| 16900591 | LMAN2L | 0.85 | 6.30 | 0.000837761 |
| 16674973 | C1orf21 | -0.80 | 5.35 | 0.014793498 |
| 16830988 | NDEL1 | -0.68 | 8.08 | 0.014626078 |
| 16918280 | PDRG1 | 0.70 | 5.53 | 0.01065877 |
| 16748490 | APOLD1 | -0.61 | 6.16 | 0.024260471 |
| 17020268 | COL21A1 | -1.01 | 4.18 | 0.010156453 |
| 16978969 | PLA2G12A | 1.45 | 7.70 | 0.017591588 |

| | | | | |
|---|---|---|---|---|
| 16821869 | CDT1 | 0.83 | 5.12 | 0.019390771 |
| 16779546 | DIAPH3 | 1.30 | 6.15 | 0.021931658 |
| 17060599 | TSC22D4 | 0.53 | 4.99 | 0.020571399 |
| 16816627 | LOC81691 | 0.61 | 4.56 | 0.0263308 |
| 16812009 | LINC00597 | -0.98 | 5.36 | 0.031509868 |
| 17082982 | DOCK8 | -0.83 | 7.64 | 0.027569071 |
| 16975203 | TLR10 | -1.47 | 4.62 | 0.004162135 |
| 17004769 | TMEM14B | 0.64 | 6.08 | 0.018036573 |
| 16864331 | MED25 | 0.70 | 5.13 | 0.006589098 |
| 16686158 | HYI | 1.39 | 7.06 | 0.001049806 |
| 16814847 | FAHD1 | 0.97 | 5.26 | 0.000138799 |
| 16736891 | KIF18A | 1.83 | 6.25 | 0.000519244 |
| 16860103 | ZNF93 | 0.76 | 6.06 | 0.034834596 |
| 16840362 | PITPNM3 | 0.89 | 4.79 | 0.041873851 |
| 16694886 | FCRL5 | -2.07 | 4.38 | 0.004665936 |
| 17058582 | ABHD11 | 0.75 | 5.69 | 0.017686424 |
| 16760621 | CDCA3 | 0.79 | 4.49 | 0.022781737 |
| 16968497 | ARHGAP24 | -1.24 | 6.24 | 0.000393499 |
| 17082362 | EPPK1 | 3.05 | 5.77 | 0.000494242 |
| 16870193 | PLVAP | -1.14 | 8.02 | 0.016484012 |
| 17074567 | SOX7 | -0.95 | 4.61 | 0.013898337 |
| 16940208 | LRRC2-AS1 | -0.38 | 2.91 | 0.031413638 |
| 17110040 | TMEM47 | -1.21 | 8.50 | 0.030029639 |
| 17045761 | CCM2 | -0.52 | 5.33 | 0.017854783 |
| 16902611 | AMMECR1L | 0.32 | 7.07 | 0.027628988 |
| 16804051 | FAM103A1 | 0.59 | 8.27 | 0.013604132 |
| 16711826 | CCDC3 | -0.84 | 3.79 | 0.003130407 |
| 17074641 | FAM167A | 0.81 | 4.26 | 0.019499404 |
| 16912941 | DYNLRB1 | 0.39 | 5.38 | 0.013533716 |
| 16746867 | RHNO1 | 0.60 | 5.11 | 0.043499696 |
| 16726255 | FERMT3 | -0.67 | 6.88 | 0.032418879 |
| 16760031 | NRIP2 | -0.66 | 4.58 | 0.001958832 |
| 16863783 | GRWD1 | 0.60 | 6.19 | 0.043458411 |
| 17095948 | ZNF484 | -0.55 | 6.13 | 0.03312773 |
| 16657737 | TAS1R3 | -0.33 | 4.18 | 0.0338111 |
| 17049924 | ARMC10 | 0.51 | 6.99 | 0.024771781 |
| 16946173 | ESYT3 | 1.26 | 3.86 | 0.014670645 |
| 16774789 | SETDB2 | -0.49 | 5.40 | 0.042489049 |
| 16702330 | TAF3 | -0.48 | 6.34 | 0.016136191 |
| 17058878 | TMEM120A | 0.53 | 7.34 | 0.005937876 |
| 16731225 | BCO2 | 2.89 | 7.03 | 0.00234422 |
| 16870150 | USHBP1 | -0.62 | 3.17 | 0.010037299 |
| 16829764 | GSG2 | 1.03 | 4.34 | 0.042485814 |
| 16730467 | TMEM133 | -1.21 | 5.85 | 0.035604525 |
| 16916682 | SLC4A11 | 1.09 | 5.32 | 0.046063999 |
| 16796229 | IFI27L2 | -0.59 | 4.08 | 0.009539495 |
| 16814143 | ITFG3 | 0.46 | 6.28 | 0.043995971 |
| 17079774 | NCALD | -1.06 | 3.12 | 0.000864133 |
| 16847432 | BRIP1 | 1.23 | 5.80 | 0.014510297 |
| 16928716 | KREMEN1 | -0.84 | 5.91 | 0.005312114 |
| 16980405 | SLC10A7 | -0.66 | 6.11 | 0.002543286 |
| 16903028 | ZRANB3 | 0.48 | 5.25 | 0.012588067 |
| 16928699 | ZNRF3 | 0.91 | 6.17 | 0.040039322 |
| 16689042 | SYDE2 | 1.49 | 4.69 | 0.002844935 |
| 16705199 | ARID5B | -1.02 | 7.66 | 0.020099003 |
| 16859319 | C19orf44 | 0.74 | 4.93 | 0.04926514 |
| 17084936 | ZCCHC7 | -0.46 | 7.13 | 0.024677029 |
| 16750300 | TMEM117 | -0.80 | 4.65 | 0.016606769 |

| | | | | |
|---|---|---|---|---|
| 16666982 | LRRC8C | -1.02 | 3.38 | 6.65E-05 |
| 16729684 | TMEM126A | 0.54 | 6.20 | 0.037835537 |
| 16891637 | RHBDD1 | -0.44 | 5.12 | 0.018112692 |
| 16743779 | DCUN1D5 | 0.40 | 6.24 | 0.041691579 |
| 16869242 | FBXW9 | 0.57 | 4.27 | 0.041064833 |
| 17054460 | PSMG3 | 0.97 | 7.25 | 0.000351234 |
| 16857438 | ALKBH7 | 0.82 | 7.30 | 0.038931085 |
| 17095307 | C9orf64 | 0.59 | 5.52 | 0.035073833 |
| 16884505 | CHCHD5 | 0.40 | 4.67 | 0.040623853 |
| 17058551 | DNAJC30 | 0.55 | 5.25 | 0.0421346 |
| 16678838 | NTPCR | 0.55 | 4.58 | 0.020126598 |
| 16740645 | EIF1AD | 0.47 | 7.13 | 0.016435119 |
| 16858668 | WDR83 | 0.50 | 4.85 | 0.027983291 |
| 16833605 | MRPL45 | 0.68 | 9.29 | 0.016667474 |
| 16834441 | VPS25 | 0.59 | 9.06 | 0.026919424 |
| 16822466 | C16orf13 | 0.62 | 6.85 | 0.020046072 |
| 16845518 | TMEM101 | 0.58 | 5.40 | 0.035547006 |
| 16869017 | ELOF1 | 0.55 | 7.36 | 0.043034204 |
| 16902357 | MKI67IP | 0.63 | 9.22 | 0.018347115 |
| 16989977 | CYSTM1 | 0.83 | 6.98 | 0.04086658 |
| 16678851 | KIAA1804 | 1.01 | 4.45 | 0.004665936 |
| 16822109 | SPIRE2 | 1.01 | 5.06 | 0.006340971 |
| 16937405 | JAGN1 | 0.63 | 6.56 | 0.003264143 |
| 16912954 | MAP1LC3A | 0.60 | 5.07 | 0.013011825 |
| 16978896 | COL25A1 | -0.66 | 4.43 | 0.02004605 |
| 16914867 | PARD6B | 3.11 | 7.25 | 0.002498679 |
| 17105082 | GPR174 | -1.78 | 7.04 | 0.015203053 |
| 16896279 | DPY30 | 0.62 | 9.20 | 0.002870355 |
| 16815498 | GLIS2 | 0.87 | 7.34 | 0.011924989 |
| 17055804 | FAM126A | -1.25 | 7.40 | 0.005048834 |
| 16984294 | CARD6 | -0.71 | 5.21 | 0.038523268 |
| 16899298 | PCGF1 | 0.34 | 5.89 | 0.044678725 |
| 16865647 | SUV420H2 | 0.44 | 4.85 | 0.041488155 |
| 16874633 | C19orf48 | 1.49 | 6.47 | 0.000246254 |
| 16831313 | MGC12916 | -1.04 | 4.48 | 0.012524658 |
| 17022216 | RTN4IP1 | -0.53 | 5.02 | 0.020794253 |
| 16830182 | TXNDC17 | 0.77 | 6.02 | 0.010610622 |
| 16937440 | IL17RC | 0.45 | 6.34 | 0.016295421 |
| 16672946 | FCRLA | -1.01 | 3.25 | 0.007716466 |
| 16885421 | SFT2D3 | 0.44 | 5.04 | 0.019678128 |
| 17117934 | MGC15705 | -0.74 | 3.01 | 0.035378999 |
| 17012392 | RSPO3 | -1.22 | 4.56 | 0.042921768 |
| 16662945 | MFSD2A | 1.71 | 5.67 | 0.00461557 |
| 16715088 | AIFM2 | 1.03 | 5.26 | 0.001431864 |
| 17098900 | ZDHHC12 | 0.58 | 6.86 | 0.040801922 |
| 16871180 | CEP89 | 0.53 | 6.61 | 0.006597901 |
| 17093724 | ARHGEF39 | 0.72 | 4.46 | 0.015375785 |
| 16884403 | TMEM87B | 0.35 | 7.68 | 0.02889654 |
| 16820537 | CIRH1A | 0.68 | 7.73 | 0.005001538 |
| 17024653 | LRP11 | 0.98 | 6.61 | 0.037172643 |
| 16875799 | FIZ1 | 0.93 | 4.97 | 0.003723708 |
| 16944724 | DIRC2 | 0.44 | 8.99 | 0.027628988 |
| 17062853 | TMEM209 | 0.65 | 7.22 | 0.027490456 |
| 16812803 | WDR73 | 0.56 | 6.13 | 0.024493485 |
| 17073405 | TIGD5 | 0.68 | 5.75 | 0.022531696 |
| 17080171 | NUDCD1 | 0.75 | 7.48 | 0.007852844 |
| 16661398 | SYTL1 | -0.50 | 4.16 | 0.019390771 |
| 16790614 | AJUBA | 1.28 | 5.63 | 1.86E-05 |

| | | | | |
|---|---|---|---|---|
| 17072351 | FAM83A | 0.97 | 3.11 | 0.048093219 |
| 17073865 | PPP1R16A | 0.57 | 5.66 | 0.022531696 |
| 16811656 | UBL7 | 0.49 | 7.87 | 0.038093304 |
| 17091312 | TMEM141 | 0.60 | 6.59 | 0.036764716 |
| 17021946 | USP45 | -0.58 | 5.96 | 0.039276829 |
| 17016457 | HIST1H2BK | 1.14 | 7.72 | 0.015377204 |
| 16931815 | SHANK3 | -1.60 | 5.82 | 0.001448824 |
| 16936325 | TUBGCP6 | -0.53 | 6.32 | 0.009155343 |
| 16982672 | NKD2 | 0.80 | 4.87 | 0.027924641 |
| 16871202 | RHPN2 | 3.39 | 7.14 | 1.62E-06 |
| 16710852 | KNDC1 | 1.13 | 4.54 | 0.007938986 |
| 16738409 | TNKS1BP1 | 0.87 | 7.46 | 0.006504942 |
| 16897797 | PNPT1 | 0.48 | 7.54 | 0.017303401 |
| 16756865 | ANKRD13A | -0.56 | 8.43 | 0.021398717 |
| 16933314 | HPS4 | -0.41 | 6.11 | 0.025466682 |
| 16675794 | NAV1 | -1.09 | 8.02 | 0.033023532 |
| 17086818 | FGD3 | -0.69 | 5.35 | 0.048938728 |
| 16728731 | ATG16L2 | -0.54 | 5.18 | 0.030939687 |
| 16962085 | KLHL6 | -1.21 | 6.03 | 0.002202594 |
| 17063922 | OR6W1P | -0.43 | 2.78 | 0.047394383 |
| 17098880 | WDR34 | 0.70 | 4.90 | 0.034118755 |
| 16816186 | C16orf45 | -0.66 | 5.46 | 0.048147783 |
| 16733719 | GLB1L2 | 1.45 | 5.13 | 0.013621346 |
| 16819450 | RSPRY1 | 0.79 | 8.18 | 0.017303401 |
| 17021167 | UBE3D | -0.71 | 3.80 | 0.048996153 |
| 17103525 | CCDC120 | 1.22 | 5.38 | 0.003200808 |
| 16914345 | ZSWIM1 | 0.39 | 5.42 | 0.04146164 |
| 16862529 | CEACAM21 | -0.76 | 4.46 | 0.002757052 |
| 16875026 | ZNF616 | 0.74 | 4.33 | 0.013827493 |
| 16804631 | TICRR | 1.53 | 5.31 | 0.027862114 |
| 16869387 | GADD45GIP1 | 0.58 | 6.23 | 0.027171438 |
| 16683574 | STPG1 | 0.60 | 5.20 | 0.037184243 |
| 16834523 | AOC4P | -0.98 | 3.26 | 0.000191736 |
| 16778005 | STARD13 | -0.97 | 5.37 | 0.00236158 |
| 16860123 | ZNF486 | 1.26 | 5.19 | 0.011105871 |
| 16936253 | LOC90834 | -0.76 | 5.27 | 0.005021773 |
| 16822939 | ZNF598 | 0.48 | 5.78 | 0.026455239 |
| 16814779 | HN1L | 1.32 | 7.69 | 0.000146244 |
| 17083433 | IL33 | -1.90 | 5.59 | 0.004486863 |
| 16691621 | ZNF697 | 0.83 | 5.55 | 0.031378105 |
| 16745693 | ESAM | -1.20 | 6.40 | 0.009486909 |
| 17052306 | ADCK2 | 0.46 | 5.31 | 0.047540957 |
| 16974900 | CCDC149 | -0.62 | 5.60 | 0.004487209 |
| 16853674 | L3MBTL4 | 1.35 | 6.20 | 0.0108719 |
| 17002912 | BOD1 | 0.64 | 5.19 | 0.009571117 |
| 16933030 | GUSBP11 | -0.54 | 6.38 | 0.008300012 |
| 16933062 | DERL3 | -1.01 | 5.45 | 0.044787174 |
| 16928411 | IGLL3P | -0.82 | 4.22 | 0.012287873 |
| 17000066 | CDKN2AIPNL | 0.75 | 5.42 | 0.023845531 |
| 16906000 | SESTD1 | -1.01 | 7.02 | 0.01225416 |
| 16860580 | C19orf40 | 0.87 | 4.82 | 0.026981053 |
| 16750416 | PCED1B | -0.77 | 4.98 | 0.014793498 |
| 16906872 | ANKRD44 | -0.89 | 7.73 | 0.003650135 |
| 16758569 | C12orf65 | 0.56 | 5.50 | 0.027959341 |
| 16982426 | YTHDC1 | -0.37 | 8.29 | 0.045774129 |
| 16976502 | YTHDC1 | -0.67 | 5.18 | 0.040039322 |
| 16794555 | ELMSAN1 | -0.44 | 5.22 | 0.049487214 |
| 16788973 | WDR20 | -0.38 | 5.09 | 0.036591224 |

| | | | | |
|---|---|---|---|---|
| 16811061 | CALML4 | 0.96 | 6.21 | 0.020083682 |
| 17002115 | TIMD4 | -2.26 | 3.52 | 0.000936814 |
| 16815925 | SNX29 | -0.71 | 7.90 | 0.001231555 |
| 16905521 | TTC30A | 1.02 | 5.15 | 0.024264728 |
| 16673393 | RCSD1 | -0.88 | 5.60 | 0.003394282 |
| 16985629 | MRPS36 | 0.83 | 5.28 | 0.001266727 |
| 16757831 | CCDC64 | 2.23 | 7.12 | 0.013362278 |
| 16834700 | G6PC3 | 0.70 | 8.57 | 0.004796972 |
| 16862066 | TIMM50 | 0.64 | 7.76 | 0.017060413 |
| 16838931 | MAFG-AS1 | 0.76 | 4.33 | 0.013222891 |
| 16911675 | MGME1 | 0.53 | 6.95 | 0.021212202 |
| 16829422 | CENPBD1 | 0.71 | 5.28 | 0.013869973 |
| 16885526 | IMP4 | 0.44 | 6.07 | 0.047590624 |
| 16889154 | MARS2 | 0.56 | 5.55 | 0.038935768 |
| 16892122 | B3GNT7 | 1.36 | 5.74 | 0.01202954 |
| 17071871 | PKHD1L1 | 3.62 | 6.78 | 0.012552128 |
| 16871359 | DMKN | 2.51 | 6.20 | 0.000242765 |
| 16868418 | ZNF561 | 0.49 | 5.43 | 0.017198424 |
| 16988565 | PRDM6 | 1.21 | 5.01 | 0.047359928 |
| 16870131 | HAUS8 | 0.71 | 5.05 | 0.024260471 |
| 16659021 | FBXO44 | 0.75 | 5.11 | 0.0168028 |
| 16868265 | MUC16 | 4.12 | 7.58 | 0.001016216 |
| 16860087 | ZNF101 | -0.73 | 5.51 | 0.029656021 |
| 17112623 | SYTL4 | -0.89 | 4.56 | 0.020277577 |
| 16824690 | ERI2 | 0.81 | 5.70 | 0.007832502 |
| 16875559 | RDH13 | 0.90 | 5.52 | 0.013989156 |
| 16817337 | CCDC101 | 0.56 | 7.62 | 0.004663101 |
| 16845826 | PLCD3 | 1.33 | 8.03 | 0.005220318 |
| 16747612 | C12orf57 | 0.54 | 6.32 | 0.031596331 |
| 17043588 | GLCCI1 | -1.01 | 4.72 | 0.005927861 |
| 16781235 | ADPRHL1 | 0.67 | 4.82 | 0.029882468 |
| 16934045 | PIK3IP1 | -0.78 | 5.33 | 0.042302863 |
| 16990083 | SLC35A4 | 0.51 | 8.26 | 0.037800534 |
| 16923929 | MCM3AP-AS1 | 0.65 | 4.49 | 0.009627203 |
| 16763195 | SLC2A13 | -0.73 | 5.47 | 0.010678024 |
| 17072125 | MAL2 | 3.96 | 6.80 | 0.000295474 |
| 16684902 | CSMD2 | -1.23 | 4.75 | 0.018958874 |
| 16695392 | SLAMF6 | -1.82 | 6.59 | 0.006448951 |
| 16767794 | OSBPL8 | -0.65 | 8.34 | 0.015983939 |
| 16951883 | OSBPL10 | -1.14 | 5.35 | 0.001637265 |
| 16987986 | EPB41L4A-AS1 | 0.76 | 4.81 | 0.012008193 |
| 17068560 | SMIM19 | 0.75 | 5.98 | 0.006571101 |
| 16999421 | 37681 | -1.16 | 5.61 | 0.025832762 |
| 16779839 | KCTD12 | -0.62 | 9.13 | 0.005086295 |
| 17042844 | GPR146 | -0.67 | 5.04 | 0.004796972 |
| 16694980 | FCRL1 | -2.64 | 4.04 | 0.000588116 |
| 16694928 | FCRL3 | -1.99 | 5.28 | 0.003119909 |
| 16664912 | LRRC42 | 1.06 | 6.84 | 0.000456269 |
| 17044285 | MALSU1 | 0.77 | 5.78 | 0.00071212 |
| 17083452 | UHRF2 | -0.66 | 7.41 | 0.001755664 |
| 16935512 | TNFRSF13C | -1.50 | 4.13 | 0.013895473 |
| 16887194 | NOSTRIN | -1.74 | 4.31 | 7.10E-05 |
| 16855545 | ALPK2 | -1.43 | 4.72 | 0.033104806 |
| 16774976 | WDFY2 | -1.13 | 6.38 | 0.000318147 |
| 16985043 | RAB3C | -0.45 | 2.83 | 0.007460396 |
| 16924592 | CYYR1 | -1.39 | 5.49 | 0.0011262 |
| 16960344 | TM4SF18 | -1.06 | 4.43 | 0.016637188 |
| 17115777 | RAB39B | -0.52 | 3.41 | 0.037048064 |

| | | | | |
|---|---|---|---|---|
| 16697196 | FAM129A | -1.29 | 6.98 | 0.000446262 |
| 16744708 | APOA5 | -0.35 | 4.55 | 0.042473943 |
| 16911026 | HSPA12B | -0.81 | 5.28 | 0.030880448 |
| 16766658 | AGAP2 | -0.89 | 5.20 | 0.022837699 |
| 16688961 | SSX2IP | 1.06 | 5.16 | 0.007813504 |
| 16847621 | FTSJ3 | 0.56 | 6.88 | 0.01135105 |
| 16938133 | GALNT15 | -1.38 | 4.80 | 0.006396074 |
| 17025230 | TAGAP | -1.01 | 6.80 | 0.017847035 |
| 17085868 | TMC1 | -0.37 | 2.84 | 0.02004605 |
| 16748453 | LOH12CR1 | -0.54 | 5.90 | 0.013305094 |
| 16977251 | ANTXR2 | -1.15 | 7.93 | 0.001017272 |
| 16715494 | MSS51 | -0.64 | 5.17 | 0.006706077 |
| 16717005 | PIK3AP1 | -0.98 | 7.76 | 0.001049806 |
| 16719171 | CPXM2 | -1.91 | 6.16 | 0.001841098 |
| 16743262 | SLC36A4 | 0.51 | 6.81 | 0.012044671 |
| 16731515 | NXPE2 | -0.51 | 2.58 | 0.0196481 |
| 16744967 | AMICA1 | -0.91 | 5.68 | 0.033528421 |
| 16735223 | OR2D2 | -0.83 | 2.80 | 0.002351716 |
| 16749939 | LRRK2 | -0.89 | 5.78 | 0.006495873 |
| 16763911 | ZNF641 | 0.90 | 6.03 | 0.010610622 |
| 16761830 | ERP27 | -1.37 | 5.23 | 0.002351716 |
| 16769868 | ALKBH2 | 0.61 | 4.13 | 0.025292216 |
| 16796919 | ANKRD9 | 0.92 | 5.50 | 0.016208242 |
| 16789589 | C14orf79 | 0.86 | 5.54 | 0.002745485 |
| 16795943 | TC2N | -1.23 | 7.34 | 0.01864703 |
| 16796667 | SLC25A29 | 0.77 | 6.20 | 0.028063824 |
| 16824301 | FOPNL | 0.65 | 8.84 | 0.007880507 |
| 16822050 | SPATA33 | 0.96 | 5.04 | 0.01287137 |
| 16816542 | IQCK | 0.75 | 7.01 | 0.03238455 |
| 16828608 | CDYL2 | -0.97 | 6.15 | 0.012566269 |
| 16823588 | ANKS3 | 0.33 | 5.44 | 0.047825453 |
| 16823579 | UBALD1 | 0.59 | 6.63 | 0.023307375 |
| 16825081 | EARS2 | 0.47 | 5.97 | 0.034451766 |
| 16836375 | MSI2 | 1.08 | 8.50 | 0.013772958 |
| 16830782 | CYB5D1 | 0.80 | 6.46 | 0.018678568 |
| 16831046 | USP43 | 1.51 | 4.33 | 0.005368851 |
| 16845727 | CCDC43 | 0.50 | 6.63 | 0.0238318 |
| 16832695 | ANKRD13B | 1.32 | 6.31 | 0.004767564 |
| 16830041 | ZFP3 | 0.59 | 6.47 | 0.033584759 |
| 16840054 | GGT6 | 0.35 | 3.44 | 0.048761811 |
| 16829801 | SPNS2 | -1.27 | 6.28 | 0.00955707 |
| 16846121 | MRPL10 | 0.53 | 5.39 | 0.014793498 |
| 16854088 | FAM210A | 0.75 | 6.54 | 0.027767488 |
| 16854954 | LOXHD1 | -0.53 | 3.19 | 0.009049385 |
| 16874568 | JOSD2 | 0.59 | 5.77 | 0.025906647 |
| 16872239 | EID2B | 0.47 | 3.23 | 0.024885713 |
| 16856998 | GIPC3 | -1.10 | 5.07 | 0.022575571 |
| 16856249 | MISP | 2.55 | 5.64 | 0.000310311 |
| 16860766 | WTIP | 0.74 | 7.19 | 0.000700211 |
| 16871305 | ZNF792 | -0.48 | 5.37 | 0.045510264 |
| 16870581 | NR2C2AP | 1.05 | 5.75 | 0.014312739 |
| 16664828 | PODN | -1.05 | 9.06 | 0.02770472 |
| 16685255 | OSCP1 | 0.64 | 5.10 | 0.038527446 |
| 16673043 | UHMK1 | 0.51 | 7.99 | 0.01303921 |
| 16694617 | IQGAP3 | 1.37 | 5.38 | 0.023440167 |
| 16672097 | APOA1BP | 1.21 | 9.03 | 0.000505614 |
| 16678496 | HIST3H2BB | 1.67 | 5.52 | 0.000393343 |
| 16914925 | TSHZ2 | -1.71 | 6.75 | 0.003366453 |

| | | | | |
|---|---|---|---|---|
| 16915405 | ZNF831 | -1.12 | 4.54 | 0.007419057 |
| 16928339 | SGSM1 | -0.57 | 4.00 | 0.015592393 |
| 16928735 | EMID1 | -0.68 | 4.71 | 0.017461527 |
| 16884426 | FBLN7 | -0.75 | 5.08 | 0.024155995 |
| 16902865 | FAM168B | 0.57 | 7.91 | 0.001312698 |
| 16906991 | RFTN2 | -1.45 | 4.87 | 0.00073594 |
| 16891555 | SGPP2 | 2.80 | 6.86 | 0.009861007 |
| 16886448 | LYPD6 | 0.95 | 3.92 | 0.007922723 |
| 16891392 | TMEM198 | 0.62 | 4.25 | 0.019818196 |
| 16891820 | FBXO36 | 0.81 | 5.63 | 0.032046985 |
| 16938228 | KCNH8 | -0.46 | 2.63 | 0.024885512 |
| 16961919 | DNAJC19 | 0.60 | 6.57 | 0.030724616 |
| 16957433 | CD200R1 | -1.18 | 5.07 | 0.007148503 |
| 16950999 | CHCHD4 | 0.63 | 5.08 | 0.016439345 |
| 16943107 | CRYBG3 | -0.56 | 7.48 | 0.014549322 |
| 16949792 | FAM43A | -1.07 | 6.26 | 0.006259841 |
| 16979719 | SCLT1 | -0.80 | 5.62 | 0.002226908 |
| 16969817 | C4orf32 | -0.97 | 6.05 | 0.012588067 |
| 16976110 | PDCL2 | 1.30 | 3.77 | 0.048620662 |
| 16978525 | SLC9B2 | -0.68 | 6.01 | 0.034072327 |
| 16984189 | EGFLAM | -0.94 | 4.53 | 0.001561317 |
| 16988471 | ZNF474 | -0.59 | 2.63 | 0.022417587 |
| 16990897 | AFAP1L1 | -1.01 | 4.95 | 0.010039892 |
| 17002510 | NUDCD2 | 0.72 | 5.41 | 0.01135105 |
| 17024362 | ADAT2 | -1.01 | 5.57 | 0.00131925 |
| 17013468 | STXBP5 | -0.86 | 7.46 | 0.032819637 |
| 17024669 | RAET1E | 1.98 | 4.92 | 0.038476061 |
| 17081347 | TMEM71 | -0.68 | 4.65 | 0.047027139 |
| 17069194 | UBXN2B | 0.80 | 5.93 | 0.002579982 |
| 17068064 | LETM2 | 1.10 | 5.48 | 0.017160609 |
| 17099731 | C9orf116 | 1.15 | 4.81 | 0.011228185 |
| 17110342 | FUNDC1 | 0.53 | 6.11 | 0.017527748 |
| 17115677 | GAB3 | -0.98 | 5.92 | 0.000819564 |
| 17107983 | ZFP92 | 0.83 | 4.04 | 0.029372633 |
| 16930173 | APOBEC3D | -0.73 | 7.41 | 0.047497843 |
| 16934012 | SELM | -0.82 | 5.04 | 0.030015351 |
| 16921064 | GATA5 | 1.34 | 5.12 | 0.033075537 |
| 16916289 | C20orf96 | 0.69 | 5.92 | 0.02942075 |
| 16912455 | CCM2L | -1.19 | 5.19 | 0.003946412 |
| 16884980 | TMEM37 | 0.80 | 5.58 | 0.02389048 |
| 16705754 | ADAMTS14 | -1.46 | 5.13 | 0.03047644 |
| 17094946 | TRPM6 | -0.99 | 3.59 | 0.005048834 |
| 16916352 | SRXN1 | 0.95 | 5.58 | 0.000675056 |
| 16913198 | ROMO1 | 1.05 | 6.23 | 0.000180119 |
| 16918132 | NANP | 0.54 | 5.43 | 0.029372633 |
| 16912317 | LINC00028 | -0.46 | 2.97 | 0.026095642 |
| 16695478 | ITLN2 | 2.55 | 5.57 | 0.004651327 |
| 16709537 | TRUB1 | 0.48 | 6.13 | 0.04628174 |
| 16707343 | HECTD2 | -0.76 | 6.08 | 0.025305516 |
| 16730429 | ARHGAP42 | -1.16 | 6.75 | 0.020919614 |
| 16743994 | CWF19L2 | -0.34 | 5.60 | 0.044495749 |
| 16758135 | TMEM120B | 0.54 | 5.44 | 0.017919538 |
| 16748111 | A2M-AS1 | -1.39 | 5.64 | 0.000159962 |
| 16789429 | C14orf144 | -0.39 | 4.12 | 0.043774545 |
| 16788829 | LINC00239 | -0.39 | 3.20 | 0.045035006 |
| 16786060 | LOC145474 | -0.89 | 4.32 | 0.040783602 |
| 16786304 | PTGR2 | 0.72 | 5.03 | 0.033386639 |
| 16783739 | LRFN5 | -0.61 | 3.70 | 0.033104806 |

| | | | | |
|---|---|---|---|---|
| 16805397 | LINC00924 | -1.13 | 3.52 | 0.000204333 |
| 16802316 | C15orf61 | 0.58 | 4.63 | 0.030187411 |
| 16813029 | HAPLN3 | -0.95 | 6.51 | 0.041229531 |
| 16811886 | NRG4 | 2.87 | 5.76 | 0.004665417 |
| 16820208 | RLTPR | -0.75 | 5.40 | 0.01875379 |
| 16827324 | KCTD19 | 0.90 | 3.51 | 0.018575482 |
| 16819816 | BEAN1 | 1.43 | 4.74 | 0.032508512 |
| 16823704 | C16orf89 | -0.85 | 4.02 | 0.03411456 |
| 16845794 | KIF18B | 1.18 | 5.88 | 0.044112912 |
| 16835797 | EME1 | 0.79 | 4.42 | 0.048923179 |
| 16842850 | DHRS13 | 0.96 | 5.13 | 0.016295421 |
| 16838300 | TMC8 | -1.02 | 6.39 | 0.024904242 |
| 16831908 | TRIM16L | 0.64 | 4.26 | 0.042260099 |
| 16868838 | SPC24 | 1.09 | 5.43 | 0.043290212 |
| 16866750 | ATP8B3 | 0.53 | 3.96 | 0.012366834 |
| 16671305 | CREB3L4 | 0.72 | 5.04 | 0.013273644 |
| 16696548 | RC3H1 | -0.42 | 7.62 | 0.007595006 |
| 16663413 | WDR65 | 0.56 | 2.93 | 0.048490926 |
| 16663828 | CCDC24 | 0.88 | 4.83 | 0.000907211 |
| 16678501 | RNF187 | 0.68 | 7.06 | 0.005197521 |
| 16672373 | PYHIN1 | -1.62 | 5.99 | 0.003782007 |
| 16932988 | ZDHHC8P1 | 1.19 | 4.00 | 0.019555184 |
| 16901957 | CKAP2L | 1.53 | 5.45 | 0.013096869 |
| 16876742 | LOC150622 | 3.13 | 5.09 | 0.000679804 |
| 16905516 | TTC30B | 1.10 | 4.83 | 0.004995947 |
| 16886602 | ARL6IP6 | 0.59 | 5.72 | 0.013031472 |
| 16879205 | RMDN2 | -0.51 | 4.88 | 0.027216605 |
| 16909528 | LINC00471 | 1.08 | 4.55 | 0.005638276 |
| 16881770 | LBX2-AS1 | 0.58 | 4.20 | 0.037446768 |
| 16905216 | GPR155 | -0.76 | 6.69 | 0.017033223 |
| 16951485 | SGOL1 | 1.58 | 5.72 | 0.020787539 |
| 16947613 | PPM1L | -0.49 | 3.78 | 0.01133074 |
| 16961250 | WDR49 | -0.45 | 3.19 | 0.031341948 |
| 16957363 | BTLA | -1.76 | 4.99 | 0.012178643 |
| 17084866 | GLIPR2 | -0.91 | 7.07 | 0.019503195 |
| 16938654 | CMTM8 | 2.25 | 8.50 | 4.13E-06 |
| 16945659 | NUDT16P1 | 0.95 | 5.96 | 0.027487868 |
| 16950056 | NCBP2-AS2 | 0.67 | 5.81 | 0.013482206 |
| 16938007 | FGD5 | -1.37 | 5.92 | 0.000929601 |
| 16950655 | CIDECP | 1.02 | 4.44 | 0.00214664 |
| 16966127 | KLB | -0.48 | 2.49 | 0.045576132 |
| 16973561 | FAM53A | 0.72 | 3.43 | 0.02785898 |
| 16977892 | PPM1K | -1.24 | 5.22 | 0.003420039 |
| 16977309 | RASGEF1B | -0.96 | 5.37 | 0.018146777 |
| 16985688 | MARVELD2 | 1.73 | 5.02 | 0.001850621 |
| 16994081 | IRX2 | 0.81 | 4.58 | 0.037964557 |
| 16990572 | SH3RF2 | 2.17 | 6.83 | 0.021987733 |
| 17013264 | ZC2HC1B | -0.73 | 2.85 | 0.001769304 |
| 17053371 | GIMAP8 | -1.01 | 6.40 | 0.001403221 |
| 17064160 | ZNF425 | 0.68 | 3.36 | 0.01373974 |
| 17070013 | RDH10 | 2.48 | 9.59 | 0.00061078 |
| 17081002 | FAM84B | 1.86 | 7.42 | 0.01091826 |
| 17074029 | TDRP | 1.07 | 6.69 | 0.015175122 |
| 17078254 | SBSPON | 3.61 | 7.31 | 0.014880251 |
| 17098048 | TTLL11 | -0.45 | 5.18 | 0.037022715 |
| 17092579 | TTC39B | -0.72 | 5.15 | 0.010875341 |
| 17092531 | FREM1 | -1.23 | 4.24 | 0.009461259 |
| 17092233 | KIAA2026 | -0.60 | 7.49 | 0.002309584 |

| | | | | |
|---|---|---|---|---|
| 17088139 | KIAA1958 | 0.87 | 5.45 | 0.012588067 |
| 17095056 | PRUNE2 | -1.55 | 5.38 | 0.005023525 |
| 17111883 | CXorf65 | -0.78 | 4.03 | 0.030609357 |
| 16761193 | CLECL1 | -0.65 | 3.10 | 0.047659102 |
| 16769481 | ALDH1L2 | -2.30 | 6.31 | 0.001070637 |
| 16762941 | DENND5B | -0.64 | 6.35 | 0.036742278 |
| 16751420 | GRASP | -1.44 | 5.29 | 0.0009769 |
| 16796414 | SYNE3 | -1.43 | 5.59 | 1.07E-05 |
| 16792211 | CLEC14A | -1.06 | 6.01 | 0.013211011 |
| 16793644 | TMEM30B | -0.81 | 4.41 | 0.036610869 |
| 16800191 | ADAL | 0.82 | 6.00 | 0.033546474 |
| 16854102 | ZNF519 | 0.60 | 4.11 | 0.049952116 |
| 16864829 | ZNF610 | 1.26 | 5.37 | 0.02377921 |
| 16872243 | EID2 | 0.50 | 5.29 | 0.013450106 |
| 16871321 | LGI4 | -0.51 | 4.30 | 0.026095642 |
| 16674446 | TOR1AIP2 | 0.69 | 3.26 | 0.011244089 |
| 16696870 | TOR1AIP2 | 0.93 | 8.31 | 0.000796119 |
| 16685868 | CITED4 | 0.63 | 4.04 | 0.024686756 |
| 16689490 | HFM1 | -0.53 | 2.62 | 0.013317113 |
| 16917054 | LRRN4 | 5.33 | 9.24 | 4.83E-05 |
| 16901109 | LONRF2 | 1.31 | 5.25 | 0.020617927 |
| 16884162 | CCDC138 | 1.39 | 5.84 | 2.39E-05 |
| 16877637 | UBXN2A | 0.64 | 6.42 | 0.022417587 |
| 16944673 | PARP15 | -2.09 | 5.39 | 0.000739182 |
| 16971382 | DCLK2 | -1.09 | 4.84 | 0.017956375 |
| 16974779 | GPR125 | 0.57 | 6.77 | 0.041125604 |
| 16997097 | ZNF366 | -0.72 | 4.29 | 0.015830468 |
| 17057599 | PKD1L1 | -0.58 | 3.48 | 0.006811348 |
| 17053379 | GIMAP7 | -1.12 | 6.05 | 0.0023633 |
| 17045078 | BMPER | -1.11 | 4.01 | 0.002145853 |
| 16714104 | C10orf128 | -0.73 | 4.70 | 0.021693616 |
| 16982870 | ADAMTS16 | -1.88 | 5.25 | 0.01563567 |
| 16828550 | ADAMTS18 | -0.96 | 3.54 | 0.011077896 |
| 17026687 | PPP1R18 | -0.57 | 7.63 | 0.04926514 |
| 17031616 | PPP1R18 | -0.57 | 7.63 | 0.04926514 |
| 17016946 | PPP1R18 | -0.60 | 7.99 | 0.047180396 |
| 17034070 | PPP1R18 | -0.60 | 7.99 | 0.047180396 |
| 17036337 | PPP1R18 | -0.60 | 7.99 | 0.047180396 |
| 17028837 | PPP1R18 | -0.62 | 8.03 | 0.031794929 |
| 16970118 | SYNPO2 | -1.78 | 7.38 | 0.001145514 |
| 16776100 | CLYBL | 0.43 | 3.71 | 0.044661767 |
| 16662430 | AGO4 | -0.64 | 6.89 | 0.002908654 |
| 17096205 | ZNF367 | 1.03 | 5.28 | 0.041965303 |
| 16718779 | EMX2OS | -0.62 | 3.21 | 0.006811348 |
| 16714086 | VSTM4 | -0.82 | 5.70 | 0.021123453 |
| 16791319 | ADCY4 | -1.56 | 5.64 | 0.001070637 |
| 16792644 | C14orf183 | -0.65 | 4.60 | 0.025491785 |
| 16821581 | LINC00311 | -0.63 | 2.84 | 0.011131142 |
| 16828344 | MLKL | -0.87 | 6.27 | 0.003322562 |
| 16814389 | WDR90 | 0.44 | 5.13 | 0.025694063 |
| 16815394 | CASP16 | 0.40 | 4.14 | 0.040366916 |
| 16825196 | NSMCE1 | 0.53 | 7.61 | 0.046324881 |
| 16939315 | TTC21A | -0.51 | 4.72 | 0.032748845 |
| 16873049 | CADM4 | 1.67 | 6.10 | 0.001303698 |
| 16859562 | FAM129C | -1.58 | 4.94 | 0.004872828 |
| 16880955 | APLF | -0.61 | 4.35 | 0.025210832 |
| 16890126 | PIKFYVE | -0.46 | 7.65 | 0.00690961 |
| 16878284 | KRTCAP3 | 1.25 | 4.98 | 0.029372633 |

| | | | | |
|---|---|---|---|---|
| 16949942 | SLC51A | 0.75 | 4.01 | 0.002244491 |
| 16841768 | CENPV | 1.57 | 6.16 | 0.003040233 |
| 16841852 | PLD6 | 0.61 | 5.81 | 0.03559341 |
| 16850063 | STRA13 | 1.06 | 7.51 | 0.012217639 |
| 16866292 | ZNF584 | 1.11 | 5.54 | 0.004762177 |
| 16944199 | TIGIT | -0.78 | 3.28 | 0.01384768 |
| 16974588 | TAPT1 | -0.61 | 5.88 | 0.007550063 |
| 17020499 | KHDRBS2 | -0.91 | 3.16 | 0.009776407 |
| 17027559 | TUBB | 0.65 | 11.23 | 0.000230412 |
| 17026211 | TUBB | 0.65 | 11.39 | 0.000146108 |
| 17030404 | TUBB | 0.65 | 11.39 | 0.000146108 |
| 17033109 | TUBB | 0.65 | 11.39 | 0.000146108 |
| 17035229 | TUBB | 0.65 | 11.39 | 0.000146108 |
| 17037888 | TUBB | 0.65 | 11.39 | 0.000146108 |
| 17040602 | TUBB | 0.65 | 11.39 | 0.000146108 |
| 17006378 | TUBB | 0.66 | 11.50 | 0.000141059 |
| 17088408 | C9orf91 | -0.52 | 5.85 | 0.034225578 |
| 17093042 | C9orf72 | -0.64 | 6.11 | 0.012143042 |
| 17107773 | VMA21 | 0.66 | 5.23 | 0.00320039 |
| 16722890 | ANO5 | 1.75 | 4.98 | 0.00279959 |
| 16732520 | TBCEL | -0.48 | 6.92 | 0.0148032 |
| 16732419 | TMEM136 | 1.33 | 5.76 | 0.001063044 |
| 16741314 | MRPL21 | 0.56 | 6.13 | 0.01256299 |
| 16738628 | OR5B21 | -0.59 | 2.94 | 0.021492339 |
| 16738694 | MPEG1 | -1.16 | 8.99 | 0.008189262 |
| 16738736 | PATL1 | 0.44 | 9.35 | 0.009632832 |
| 16732394 | OAF | -0.85 | 4.04 | 0.004347375 |
| 16714547 | FAM13C | -1.34 | 4.81 | 0.002760845 |
| 16714798 | JMJD1C | -0.50 | 8.54 | 0.045262457 |
| 16711839 | UCMA | 0.43 | 3.24 | 0.026873849 |
| 16739479 | LRRN4CL | -0.77 | 5.12 | 0.034568907 |
| 16777278 | SKA3 | 1.30 | 5.77 | 0.046605563 |
| 16773191 | SPATA13 | -0.74 | 4.82 | 0.048241036 |
| 16773197 | SPATA13 | -0.66 | 5.26 | 0.012043754 |
| 17022980 | FAM162B | -1.30 | 6.08 | 0.002351716 |
| 17019749 | GPR116 | -1.60 | 7.56 | 0.001021274 |
| 17019389 | LRRC73 | 0.75 | 4.47 | 0.019664797 |
| 17008428 | ADCY10P1 | -0.77 | 4.35 | 0.015779003 |
| 17041421 | ZBTB9 | 0.57 | 5.40 | 0.027033615 |
| 17007529 | ZBTB9 | 0.57 | 5.97 | 0.018745508 |
| 17039661 | ZBTB12 | 0.43 | 3.87 | 0.02389048 |
| 17006361 | C6orf136 | 0.63 | 6.07 | 0.005689827 |
| 17027543 | C6orf136 | 0.69 | 5.94 | 0.002826228 |
| 17030388 | C6orf136 | 0.69 | 5.94 | 0.002826228 |
| 17033093 | C6orf136 | 0.69 | 5.94 | 0.002826228 |
| 17035213 | C6orf136 | 0.69 | 5.94 | 0.002826228 |
| 17037872 | C6orf136 | 0.69 | 5.94 | 0.002826228 |
| 17040586 | C6orf136 | 0.69 | 5.94 | 0.002826228 |
| 17005169 | KDM1B | 0.55 | 6.70 | 0.025491785 |
| 17004836 | SMIM13 | 0.69 | 6.66 | 0.031932637 |
| 17055263 | THSD7A | -1.43 | 4.43 | 0.000170382 |
| 17057354 | TMED4 | 0.43 | 8.16 | 0.033104806 |
| 17044692 | PRR15 | 3.61 | 5.90 | 0.000197445 |
| 17061504 | ATXN7L1 | -0.43 | 5.95 | 0.049710075 |
| 16878541 | SPDYA | -1.04 | 4.73 | 0.008944992 |
| 16918235 | DEFB124 | -0.65 | 3.37 | 0.002117934 |
| 16977196 | CNOT6L | -0.71 | 7.81 | 0.001219947 |
| 16697843 | TMEM9 | 0.74 | 5.42 | 0.002360681 |

| | | | | |
|---|---|---|---|---|
| 16714536 | IPMK | -0.70 | 7.27 | 0.010635655 |
| 16946366 | ZBTB38 | -0.73 | 5.82 | 0.035930768 |
| 16719562 | EBF3 | -1.32 | 5.05 | 0.019506711 |
| 16817721 | ASPHD1 | 2.03 | 6.78 | 0.000679869 |
| 17112376 | BRWD3 | -0.80 | 7.38 | 0.002958463 |
| 16885191 | LOC254128 | 0.57 | 5.54 | 0.008916461 |
| 16729025 | RNF169 | 0.37 | 7.45 | 0.047708696 |
| 16974722 | LCORL | -0.46 | 5.90 | 0.029372633 |
| 16727363 | CNIH2 | 0.60 | 4.13 | 0.03267614 |
| 16709760 | CASC2 | 0.67 | 4.39 | 0.04997158 |
| 16982936 | LINC01018 | 1.59 | 5.02 | 0.024933926 |
| 16969495 | NPNT | 1.92 | 8.14 | 0.020277577 |
| 16830284 | BCL6B | -1.70 | 5.45 | 0.010857434 |
| 16773556 | PAN3 | -0.43 | 8.05 | 0.016370602 |
| 17090216 | HMCN2 | -1.35 | 4.07 | 0.000933017 |
| 16733963 | C11orf35 | 0.65 | 4.99 | 0.040242253 |
| 16739346 | EML3 | -0.41 | 7.52 | 0.030289959 |
| 17022276 | SCML4 | -1.11 | 3.79 | 0.003859461 |
| 16979675 | MFSD8 | -0.37 | 7.00 | 0.047315765 |
| 16727377 | TMEM151A | 2.33 | 5.73 | 0.002740044 |
| 16754348 | GLIPR1L1 | -0.45 | 3.05 | 0.033496003 |
| 16868145 | KANK3 | -0.77 | 5.05 | 0.013658915 |
| 17095217 | FRMD3 | -0.84 | 4.84 | 0.001690497 |
| 16695535 | ARHGAP30 | -0.82 | 6.23 | 0.009926585 |
| 16731670 | RNF214 | 0.43 | 6.25 | 0.009571117 |
| 16688506 | NEGR1 | -1.06 | 5.12 | 0.024677029 |
| 16697544 | ASPM | 2.85 | 7.17 | 1.15E-05 |
| 16761526 | TAS2R30 | -0.89 | 5.68 | 0.01223952 |
| 16761511 | TAS2R20 | -0.76 | 5.81 | 0.044561067 |
| 16673466 | TIPRL | 0.60 | 7.80 | 0.00565905 |
| 16927985 | RGL4 | -0.61 | 3.92 | 0.010563409 |
| 16935686 | ATP5L2 | -0.67 | 4.23 | 0.047708696 |
| 17041450 | ZNF311 | 0.91 | 4.06 | 0.003922556 |
| 17038835 | ZNF311 | 0.84 | 3.91 | 0.003283805 |
| 17016642 | ZNF311 | 0.95 | 4.02 | 0.001657106 |
| 17026490 | ZNF311 | 0.95 | 4.02 | 0.001657106 |
| 17028549 | ZNF311 | 0.95 | 4.02 | 0.001657106 |
| 17031330 | ZNF311 | 0.95 | 4.02 | 0.001657106 |
| 17033786 | ZNF311 | 0.95 | 4.02 | 0.001657106 |
| 16740378 | SLC25A45 | -0.40 | 5.18 | 0.034175166 |
| 16744648 | LINC00900 | 0.38 | 3.30 | 0.038095053 |
| 16742086 | PGM2L1 | -0.68 | 5.61 | 0.036717693 |
| 16726448 | CCDC88B | -0.61 | 4.20 | 0.026768373 |
| 16725921 | TTC9C | 0.45 | 5.97 | 0.048241036 |
| 16760760 | CD163L1 | -1.99 | 5.01 | 0.000143661 |
| 17117636 | LOC283588 | -0.54 | 3.09 | 0.018745508 |
| 16790229 | LINC00641 | -0.83 | 5.53 | 0.012719084 |
| 16789536 | CEP170B | 0.64 | 5.93 | 0.031846554 |
| 16801376 | LINC00926 | -1.75 | 5.43 | 0.000784502 |
| 16806624 | LOC283710 | -0.85 | 3.02 | 0.008922121 |
| 16825539 | C16orf54 | -0.86 | 4.86 | 0.006458814 |
| 16840769 | LOC284023 | 0.64 | 4.75 | 0.030109851 |
| 16845671 | FAM171A2 | 1.23 | 5.32 | 0.007077087 |
| 16846539 | LOC284080 | 0.48 | 3.31 | 0.037628129 |
| 16838663 | ENDOV | 0.37 | 4.76 | 0.048934623 |
| 16838787 | C17orf89 | 0.52 | 5.98 | 0.049338055 |
| 16841842 | LOC284191 | -0.41 | 4.18 | 0.028472331 |
| 16872496 | C19orf54 | 1.25 | 5.96 | 0.001207195 |

| | | | | |
|---|---|---|---|---|
| 16874032 | MAMSTR | 0.66 | 4.32 | 0.043107468 |
| 16868251 | ACTL9 | -0.52 | 3.09 | 0.03805209 |
| 16694178 | RUSC1-AS1 | 0.51 | 4.99 | 0.021212202 |
| 16685413 | RSPO1 | 2.51 | 7.89 | 0.01325826 |
| 16663223 | RIMKLA | 1.13 | 3.28 | 0.013225766 |
| 16914595 | LINC00494 | -0.75 | 2.76 | 0.010583835 |
| 16916462 | SIRPB2 | -0.66 | 5.21 | 0.024893542 |
| 16905963 | CCDC141 | -1.51 | 3.94 | 7.26E-06 |
| 17117853 | FLJ38379 | -0.73 | 3.04 | 0.002492816 |
| 16879232 | CYP1B1-AS1 | -0.92 | 3.08 | 0.007909082 |
| 16960084 | SLC9A9 | -1.18 | 6.83 | 0.000568641 |
| 16956002 | EOGT | -0.76 | 8.03 | 0.03234765 |
| 16968834 | FAM13A-AS1 | -0.69 | 4.86 | 0.031596331 |
| 16977970 | GPRIN3 | -0.98 | 6.52 | 0.024635244 |
| 17008676 | RPL7L1 | 0.42 | 5.36 | 0.019402743 |
| 17066811 | LOC286059 | -0.45 | 2.77 | 0.020424774 |
| 17082250 | FAM83H | 2.16 | 7.00 | 3.66E-05 |
| 17074075 | LOC286083 | -0.31 | 3.10 | 0.025496024 |
| 17073297 | ZFP41 | 0.50 | 5.05 | 0.033530783 |
| 17088886 | CRB2 | 2.65 | 6.64 | 0.000275103 |
| 17098364 | SCAI | 0.88 | 6.65 | 0.047261273 |
| 17100382 | TPRN | 1.12 | 4.01 | 0.003394282 |
| 17087779 | LOC286367 | -0.76 | 4.30 | 0.012656127 |
| 17116745 | P2RY8 | -0.92 | 5.41 | 0.03949699 |
| 17108740 | P2RY8 | -0.81 | 5.68 | 0.00795511 |
| 17117114 | BCORP1 | -1.07 | 3.46 | 0.000626937 |
| 16700034 | LIN9 | 0.82 | 5.28 | 0.00989778 |
| 16796626 | CCDC85C | 1.01 | 4.42 | 0.007072458 |
| 16837609 | RAB37 | -0.72 | 4.38 | 0.012455266 |
| 16769924 | MMAB | 0.88 | 6.39 | 0.001961033 |
| 16988906 | CHSY3 | -1.19 | 5.59 | 0.010016784 |
| 17073290 | GPIHBP1 | -0.85 | 4.75 | 0.010320732 |
| 16720115 | B4GALNT4 | 1.94 | 5.64 | 0.000211324 |
| 16769761 | TMEM119 | -1.27 | 4.70 | 0.003652987 |
| 16836788 | METTL2A | 0.79 | 7.37 | 0.014510297 |
| 16849913 | ARL16 | 0.53 | 6.88 | 0.013011761 |
| 16871680 | ZNF260 | 0.65 | 8.04 | 0.008632924 |
| 16867989 | CLEC4G | -1.15 | 4.01 | 0.001727434 |
| 16680342 | TMEM240 | 0.65 | 3.94 | 0.039715058 |
| 16684674 | MTMR9LP | -1.32 | 4.87 | 0.002226908 |
| 16897998 | LOC339803 | 0.93 | 6.15 | 0.000836238 |
| 16964107 | NAT8L | 1.11 | 4.55 | 0.021198014 |
| 17024559 | ZC3H12D | -0.89 | 4.58 | 0.014108262 |
| 17044315 | FAM221A | 1.39 | 6.04 | 0.01135105 |
| 17082336 | NRBP2 | 0.73 | 7.06 | 0.01384768 |
| 17092512 | ZDHHC21 | -0.63 | 7.14 | 0.006567598 |
| 17111994 | RGAG4 | -0.60 | 3.88 | 0.019330881 |
| 17104832 | NHSL2 | -0.92 | 5.55 | 0.038335962 |
| 17106067 | VSIG1 | -0.94 | 4.21 | 0.02957219 |
| 16709795 | NANOS1 | 0.79 | 5.66 | 0.017847035 |
| 16829815 | SMTNL2 | 2.08 | 5.72 | 0.003837347 |
| 16900910 | KIAA1211L | 1.62 | 5.57 | 0.002889117 |
| 16902945 | NCKAP5 | -1.03 | 4.71 | 0.01390577 |
| 16938620 | ZNF860 | -0.80 | 3.83 | 0.013986609 |
| 16995802 | PLCXD3 | -0.92 | 3.64 | 0.030086333 |
| 17011980 | RSPH4A | -0.55 | 3.23 | 0.007281523 |
| 17093397 | KIF24 | 1.16 | 4.33 | 0.004236839 |
| 16776936 | TMEM255B | -1.10 | 5.31 | 0.001233922 |

| | | | | |
|---|---|---|---|---|
| 16847238 | SKA2 | 0.71 | 6.16 | 0.024547429 |
| 16664754 | FAM159A | -1.02 | 3.81 | 0.00597007 |
| 16936191 | C22orf34 | -0.85 | 3.41 | 0.004491121 |
| 16963375 | WDR53 | 0.40 | 5.69 | 0.022514505 |
| 17045258 | GPR141 | -0.51 | 4.53 | 0.042473943 |
| 16697580 | ZBTB41 | 0.77 | 7.84 | 0.012000329 |
| 16725041 | FAM111B | 1.44 | 6.05 | 0.015787574 |
| 16725969 | TMEM179B | 0.51 | 5.80 | 0.006294787 |
| 16727820 | TBC1D10C | -0.96 | 5.62 | 0.021693616 |
| 16748196 | LOC374443 | -0.79 | 6.77 | 0.036793593 |
| 16754646 | PTPRQ | 3.28 | 6.18 | 0.000275103 |
| 16769315 | C12orf42 | -0.76 | 3.08 | 0.015935542 |
| 16672214 | PEAR1 | -1.04 | 4.72 | 0.014210405 |
| 16895193 | PFN4 | 0.50 | 3.91 | 0.028472331 |
| 16903529 | RBM43 | 0.67 | 5.69 | 0.045048058 |
| 16949991 | NRROS | -0.54 | 4.45 | 0.006258072 |
| 17020480 | GUSBP4 | -0.89 | 5.81 | 0.013211011 |
| 16657598 | AGRN | 1.79 | 8.37 | 0.000628104 |
| 17062955 | MKLN1-AS1 | -0.79 | 6.94 | 0.035930768 |
| 17015972 | NHLRC1 | 0.68 | 3.45 | 0.03720646 |
| 16996246 | RNF138P1 | -1.00 | 4.48 | 0.005046944 |
| 16975560 | KCTD8 | 2.45 | 5.27 | 0.005638276 |
| 16923653 | KRTAP10-7 | -0.45 | 2.76 | 0.036136556 |
| 17023066 | CEP85L | -1.06 | 3.82 | 0.000738173 |
| 17023405 | THEMIS | -1.40 | 4.44 | 0.004067726 |
| 16707836 | CC2D2B | -0.63 | 3.51 | 0.012704815 |
| 16721304 | OR56B1 | -0.84 | 2.43 | 0.035352582 |
| 16735214 | GVINP1 | -1.50 | 5.49 | 0.007187466 |
| 16742115 | LIPT2 | 1.00 | 5.61 | 0.000623709 |
| 16810270 | C2CD4B | -0.79 | 3.66 | 0.035930768 |
| 16817320 | SBK1 | 0.74 | 4.26 | 0.040504046 |
| 16826212 | C16orf87 | 0.65 | 7.05 | 0.042961325 |
| 16828228 | C16orf47 | -0.44 | 2.86 | 0.038878172 |
| 16859034 | CLEC17A | -1.86 | 3.92 | 0.001618285 |
| 16875760 | TMEM238 | 1.38 | 7.17 | 0.012000329 |
| 16658350 | RNF207 | 0.66 | 5.84 | 0.03972536 |
| 16661342 | TRNP1 | 1.19 | 5.66 | 0.005187186 |
| 16675533 | C1orf53 | 0.68 | 5.56 | 0.047528766 |
| 16678907 | COA6 | 0.94 | 5.03 | 0.00234422 |
| 16921627 | LINC00478 | -1.42 | 5.00 | 0.01384768 |
| 16721307 | OR52N4 | -1.09 | 3.17 | 0.002085347 |
| 16860545 | NUDT19 | 0.79 | 6.99 | 0.010172466 |
| 16679816 | OR2G6 | -0.62 | 2.94 | 0.026981053 |
| 16895268 | PTRHD1 | 0.61 | 4.52 | 0.002177593 |
| 17042925 | ELFN1 | 2.00 | 7.08 | 0.002202594 |
| 16866702 | MEX3D | 0.86 | 6.33 | 0.012065993 |
| 16813537 | LOC400456 | -1.71 | 3.86 | 2.42E-06 |
| 16824566 | KNOP1 | 0.72 | 6.60 | 0.002890948 |
| 16829476 | C17orf97 | 1.05 | 5.74 | 0.048934623 |
| 16831857 | FLJ35934 | 0.84 | 4.93 | 0.034084034 |
| 16832024 | GRAPL | -2.12 | 4.92 | 0.000224628 |
| 16875955 | ZNF772 | 0.66 | 4.80 | 0.014525825 |
| 16674273 | C1orf220 | -1.38 | 4.73 | 0.001049806 |
| 16677808 | FAM177B | -1.54 | 3.60 | 0.000837761 |
| 16935020 | LOC400927 | -0.47 | 5.62 | 0.034899663 |
| 16876753 | LOC400940 | 1.21 | 4.03 | 0.029372633 |
| 16877530 | LINC00954 | -0.82 | 3.11 | 0.006577006 |
| 16898375 | LOC400958 | -0.62 | 2.29 | 0.012022748 |

| | | | | |
|---|---|---|---|---|
| 16886257 | TEX41 | -0.62 | 2.79 | 0.03773156 |
| 16949780 | LINC00884 | 1.09 | 5.09 | 0.042473943 |
| 16949933 | LINC00885 | 1.14 | 4.07 | 0.047153863 |
| 16965880 | DTHD1 | -1.40 | 4.15 | 0.004759764 |
| 16968895 | CCSER1 | -0.85 | 3.63 | 0.009778355 |
| 16979317 | C4orf3 | -0.35 | 4.91 | 0.044982261 |
| 16985229 | RGS7BP | -1.21 | 3.94 | 0.00241872 |
| 17026469 | LOC401242 | 0.30 | 3.10 | 0.048925884 |
| 17031327 | LOC401242 | 0.30 | 3.10 | 0.048925884 |
| 17033777 | LOC401242 | 0.30 | 3.10 | 0.048925884 |
| 17038814 | LOC401242 | 0.30 | 3.10 | 0.048925884 |
| 17016621 | LOC401242 | 0.34 | 3.09 | 0.023657938 |
| 17028916 | LINC00243 | -1.13 | 4.05 | 0.033997626 |
| 17019348 | CRIP3 | -0.41 | 3.82 | 0.03485236 |
| 17020214 | KLHL31 | 2.42 | 5.65 | 0.002498679 |
| 17055777 | LOC401312 | -0.77 | 2.90 | 0.002633541 |
| 17092486 | FLJ41200 | -1.11 | 5.00 | 0.024771781 |
| 17088148 | SNX30 | -0.54 | 7.86 | 0.026912903 |
| 17101183 | CD99P1 | -0.76 | 5.26 | 0.015377204 |
| 17115913 | CD99P1 | -1.39 | 3.55 | 0.005113143 |
| 17110372 | FLJ25917 | 1.20 | 4.91 | 0.041567289 |
| 17051194 | LINC01000 | -0.54 | 7.13 | 0.006811348 |
| 16734303 | IFITM10 | -1.13 | 4.75 | 0.019402743 |
| 16868035 | CTXN1 | 1.75 | 6.11 | 0.002719692 |
| 16788534 | MIR127 | -0.75 | 3.97 | 0.017337887 |
| 16847083 | MIR142 | -1.86 | 4.76 | 0.011744728 |
| 16833017 | MIR193A | 0.71 | 3.94 | 0.043618386 |
| 17104279 | MIR223 | -0.97 | 4.56 | 0.011735645 |
| 17060442 | MIR25 | 0.74 | 3.57 | 0.011024744 |
| 17002176 | FNDC9 | -0.39 | 3.00 | 0.024746435 |
| 17007417 | HCG25 | 0.41 | 5.85 | 0.025491785 |
| 17082817 | C8orf82 | 0.62 | 5.00 | 0.022323152 |
| 16702229 | PRKCQ-AS1 | -1.66 | 3.85 | 0.000363245 |
| 16706610 | LINC00857 | 1.36 | 4.61 | 0.005959278 |
| 16755056 | PLEKHG7 | -0.47 | 2.55 | 0.043397402 |
| 16795826 | CCDC88C | -0.97 | 5.80 | 0.002145853 |
| 16798570 | HERC2P9 | -0.76 | 7.19 | 0.001587867 |
| 16817583 | SNX29P2 | -1.06 | 5.52 | 0.000310311 |
| 16851230 | ANKRD20A5P | -1.61 | 5.18 | 0.049767345 |
| 16853325 | HSBP1L1 | 1.18 | 7.14 | 0.001080715 |
| 16870925 | ZNF724P | 1.56 | 5.08 | 0.000378504 |
| 16896170 | CAPN14 | -0.47 | 2.50 | 0.020770795 |
| 16884280 | LOC440894 | 1.33 | 7.71 | 0.002529855 |
| 16977378 | TMEM150C | -0.86 | 6.29 | 0.048213306 |
| 16989038 | C5orf56 | -0.52 | 6.59 | 0.047315765 |
| 17047597 | DTX2P1-UPK3BP1-PMS2P11 | 0.91 | 7.23 | 0.018538243 |
| 17072052 | AARD | 2.94 | 5.27 | 0.008607343 |
| 16914733 | ZFAS1 | 0.68 | 8.66 | 0.00995933 |
| 17056845 | TARP | -0.57 | 3.47 | 0.048620662 |
| 17056813 | TARP | -1.81 | 5.62 | 0.005410697 |
| 17056823 | TARP | -1.81 | 5.62 | 0.005410697 |
| 16940687 | STGC3 | -0.74 | 3.42 | 0.049287931 |
| 17064269 | GIMAP6 | -0.64 | 6.31 | 0.047015132 |
| 16756202 | EID3 | 0.89 | 6.12 | 0.041638363 |
| 16664235 | LURAP1 | -0.46 | 4.19 | 0.030029639 |
| 17055786 | LOC541472 | -1.61 | 4.54 | 0.004187214 |
| 16754324 | ATXN7L3B | 0.55 | 7.06 | 0.019818196 |
| 16999754 | LOC553103 | 1.46 | 4.87 | 0.013650974 |

| | | | | |
|---|---|---|---|---|
| 17094667 | PGM5-AS1 | -0.64 | 2.90 | 0.049004829 |
| 16755035 | CLLU1 | -0.57 | 2.62 | 0.004796703 |
| 16692772 | ADAMTSL4-AS1 | -1.37 | 5.52 | 0.004462291 |
| 16702870 | MIR511-1 | -0.69 | 2.60 | 0.015878225 |
| 16702914 | MIR511-1 | -0.69 | 2.60 | 0.015878225 |
| 17000641 | ECSCR | -1.02 | 3.32 | 0.015592393 |
| 17000644 | ECSCR | -1.55 | 6.18 | 0.0023633 |
| 16893704 | FAM110C | 1.93 | 6.14 | 0.004796972 |
| 16706562 | LOC642361 | 0.57 | 4.78 | 0.047709521 |
| 16719498 | FAM196A | 0.96 | 4.15 | 0.038720439 |
| 16982083 | SLED1 | -1.52 | 4.06 | 0.011453436 |
| 16996605 | SMIM15 | 0.49 | 7.35 | 0.016535009 |
| 17091815 | EHMT1-IT1 | -0.79 | 5.49 | 0.010685173 |
| 16713754 | LINC00842 | 3.86 | 7.20 | 0.000268728 |
| 17011735 | TRAF3IP2-AS1 | -0.61 | 4.58 | 0.014314937 |
| 16826606 | CRNDE | 1.37 | 5.23 | 0.024591035 |
| 16995866 | FLJ32255 | -1.16 | 5.61 | 0.008607343 |
| 16680362 | C1orf233 | 1.08 | 6.30 | 0.013854361 |
| 16861314 | SDHAF1 | 0.62 | 3.92 | 0.022989941 |
| 16691879 | PPIAL4G | -0.64 | 2.89 | 0.012533126 |
| 16735656 | LOC644656 | 0.47 | 3.98 | 0.046856391 |
| 16842196 | FAM83G | 0.87 | 4.16 | 0.010876802 |
| 16901558 | FLJ38668 | 0.63 | 4.32 | 0.026842368 |
| 16867427 | ARRDC5 | -0.97 | 4.82 | 0.004469784 |
| 16703431 | LINC00264 | -0.58 | 2.69 | 0.034373373 |
| 16882671 | ANKRD36BP2 | -1.15 | 3.17 | 0.002929216 |
| 16666730 | LOC646626 | -0.54 | 3.82 | 0.038867549 |
| 17056285 | LOC646762 | 0.98 | 5.60 | 0.034240458 |
| 16775234 | LOC647264 | 0.45 | 4.43 | 0.04086658 |
| 16854792 | LINC00669 | 0.72 | 3.06 | 0.032512111 |
| 16776953 | GAS6-AS1 | -0.75 | 5.30 | 0.001837551 |
| 16996969 | GUSBP3 | -0.97 | 6.67 | 0.036886537 |
| 16827255 | KIAA0895L | -0.47 | 5.92 | 0.031341948 |
| 16817562 | RRN3P2 | -0.84 | 4.83 | 0.011603633 |
| 16987992 | SNORA13 | 0.93 | 4.73 | 0.013450106 |
| 16847393 | SCARNA20 | 0.90 | 4.77 | 0.014739525 |
| 16677254 | SNORA16B | -1.41 | 4.08 | 0.000380459 |
| 16874641 | SNORD88B | 0.88 | 5.83 | 0.010861211 |
| 16811884 | FBXO22-AS1 | 2.27 | 5.21 | 0.010973189 |
| 16720213 | LOC692247 | 1.15 | 4.97 | 0.030086333 |
| 16670918 | MIR554 | 1.91 | 4.97 | 0.000907211 |
| 16878888 | MIR558 | -0.56 | 2.79 | 0.038481195 |
| 16963685 | MIR571 | -0.80 | 5.35 | 0.008275304 |
| 16996133 | MIR581 | -1.42 | 4.98 | 0.000293147 |
| 16705006 | MIR605 | -1.47 | 2.23 | 0.000107648 |
| 16769838 | MIR619 | -1.17 | 5.18 | 0.00546344 |
| 16775763 | MIR622 | 1.72 | 4.44 | 0.001587867 |
| 16776050 | MIR623 | -0.94 | 4.75 | 0.01135105 |
| 16809645 | MIR628 | -0.67 | 2.95 | 0.013211011 |
| 16912939 | MIR644A | -0.79 | 7.79 | 0.019306979 |
| 17076273 | LOC728024 | 0.78 | 2.99 | 0.005089028 |
| 16893697 | LOC728323 | -0.53 | 8.31 | 0.033319597 |
| 16685359 | LOC728431 | 0.77 | 5.73 | 0.029382558 |
| 16932735 | GGT2 | -0.37 | 4.00 | 0.03238455 |
| 16769403 | C12orf73 | 0.69 | 6.00 | 0.014510297 |
| 16663291 | CCDC30 | 0.96 | 3.68 | 0.040628159 |
| 16663282 | CCDC30 | 0.81 | 4.29 | 0.036610869 |
| 16713760 | HNRNPA1P33 | 4.00 | 6.88 | 0.000152715 |

| | | | | |
|---|---|---|---|---|
| 16867326 | PLIN4 | -1.59 | 4.58 | 0.016925456 |
| 17014421 | LOC729603 | -0.50 | 4.33 | 0.040776405 |
| 16682044 | FLJ37453 | 0.59 | 4.05 | 0.017198424 |
| 16971443 | FAM160A1 | 2.05 | 5.10 | 0.001044656 |
| 16879276 | MORN2 | 0.60 | 6.71 | 0.037022715 |
| 16824915 | RRN3P1 | -0.90 | 2.65 | 0.000259924 |
| 17009615 | LOC730101 | -0.82 | 3.95 | 0.009537272 |
| 16696785 | LOC730102 | -0.68 | 6.69 | 0.045389123 |
| 16725901 | METTL12 | 0.66 | 5.13 | 0.043230543 |
| 16975157 | RELL1 | -0.67 | 6.64 | 0.019390771 |
| 16970068 | SNHG8 | 0.65 | 6.97 | 0.043323912 |
| 16858120 | SNORD105B | 0.65 | 11.98 | 0.021656568 |
| 16914743 | SNORD12B | 0.82 | 5.39 | 0.025662544 |
| 16916156 | MIR941-1 | -0.81 | 7.99 | 0.007917033 |
| 16833019 | MIR365B | 0.96 | 3.92 | 0.004969977 |
| 16707824 | C10orf131 | -0.77 | 2.72 | 0.002328909 |
| 16673652 | LOC100127910 | -1.86 | 6.61 | 0.003044902 |
| 17117631 | LOC100128075 | -1.25 | 4.97 | 0.000180119 |
| 17073477 | FAM83H-AS1 | 0.65 | 5.33 | 0.022294811 |
| 17107323 | LINC00892 | -0.80 | 3.04 | 0.018616123 |
| 17118074 | LOC100128482 | -0.98 | 4.44 | 0.009842076 |
| 16703062 | NEBL-AS1 | 0.56 | 3.72 | 0.04997158 |
| 17113038 | LOC100128594 | -0.42 | 3.22 | 0.024904242 |
| 17117414 | LOC100128751 | -0.96 | 4.93 | 0.004347375 |
| 17096145 | LINC00476 | -0.42 | 3.09 | 0.040335382 |
| 17053769 | LINC01003 | 0.66 | 5.49 | 0.042105503 |
| 17072931 | LOC100129104 | 0.43 | 3.95 | 0.033731714 |
| 17118138 | LOC100129233 | 2.28 | 5.75 | 0.00150143 |
| 16943976 | LOC100129297 | -0.69 | 3.04 | 0.008738402 |
| 16680634 | LOC100129534 | 0.79 | 4.63 | 0.035879312 |
| 16821324 | LOC100129617 | -1.06 | 4.72 | 0.000300887 |
| 16821889 | LOC100129697 | -0.60 | 4.38 | 0.007777057 |
| 17117811 | LOC100129831 | -0.94 | 4.25 | 0.010854508 |
| 16933406 | LOC100129936 | -0.56 | 3.51 | 0.024368191 |
| 16682726 | LOC100130193 | -0.96 | 5.24 | 0.002597144 |
| 17080991 | LINC00861 | -1.71 | 3.63 | 0.001997066 |
| 17004710 | TFAP2A-AS1 | 0.68 | 3.22 | 0.031525772 |
| 17077583 | LOC100130298 | -0.64 | 3.17 | 0.025023521 |
| 17117547 | LOC100130428 | -0.93 | 5.50 | 0.038303393 |
| 17118376 | LOC100130458 | -0.66 | 2.73 | 0.006803129 |
| 17024176 | LOC100130476 | -0.56 | 3.04 | 0.025025521 |
| 16853355 | PARD6G-AS1 | 0.62 | 3.83 | 0.025023521 |
| 17011185 | TSTD3 | -0.76 | 5.27 | 0.011702473 |
| 17014235 | C6orf99 | 0.51 | 3.08 | 0.033279228 |
| 16813590 | LOC100130976 | -1.44 | 3.41 | 2.74E-06 |
| 16727795 | LOC100130987 | 0.54 | 4.08 | 0.038481195 |
| 16697654 | MIR181A1HG | -0.80 | 5.06 | 0.038039179 |
| 17005847 | LOC100131289 | -0.35 | 3.25 | 0.0421346 |
| 17117545 | LOC100131541 | -1.01 | 6.57 | 0.048514946 |
| 16776048 | FKSG29 | -1.10 | 6.29 | 0.002089143 |
| 17117973 | LOC100131802 | -0.98 | 4.67 | 0.014395164 |
| 17118030 | LOC100131826 | -1.90 | 4.87 | 0.010957166 |
| 17069937 | LOC100132891 | -0.90 | 5.52 | 0.042432839 |
| 16953237 | LOC100133032 | -0.75 | 4.12 | 0.049767345 |
| 16777832 | LINC00426 | -1.07 | 3.86 | 0.006821203 |
| 16824865 | LOC100190986 | -0.70 | 9.54 | 0.022002025 |
| 16712071 | PPIAP30 | -1.09 | 5.67 | 0.001285787 |
| 16763608 | PCED1B-AS1 | -1.09 | 5.60 | 0.003296619 |

| | | | | |
|---|---|---|---|---|
| 17118102 | LOC100272216 | -0.76 | 6.28 | 0.029083363 |
| 17118111 | LOC100272216 | -0.76 | 6.28 | 0.029083363 |
| 17118115 | LOC100272216 | -0.76 | 6.28 | 0.029083363 |
| 17118062 | LOC100272216 | -0.76 | 6.49 | 0.026095642 |
| 17118070 | LOC100272216 | -0.76 | 6.49 | 0.026095642 |
| 17118125 | LOC100272216 | -0.76 | 6.49 | 0.026095642 |
| 17118132 | LOC100272216 | -0.76 | 6.49 | 0.026095642 |
| 17118136 | LOC100272216 | -0.76 | 6.49 | 0.026095642 |
| 17118121 | LOC100272216 | -0.78 | 5.85 | 0.018572209 |
| 16996941 | LOC100272216 | -1.01 | 7.43 | 0.015058806 |
| 16814353 | LOC100287175 | 0.64 | 3.87 | 0.025903868 |
| 16700507 | LINC00582 | -1.03 | 3.42 | 0.00461557 |
| 16714269 | TIMM23 | 0.49 | 9.19 | 0.035365838 |
| 16750398 | LOC100288798 | -0.63 | 4.40 | 0.032095172 |
| 17101387 | LOC100288814 | 0.62 | 3.62 | 0.042051728 |
| 16896343 | LOC100288911 | 1.82 | 6.29 | 0.006006236 |
| 16692764 | LOC100289061 | -0.75 | 5.14 | 0.016954776 |
| 17117829 | LOC100293044 | 0.87 | 6.03 | 0.012000329 |
| 17056785 | MIR1200 | -1.63 | 3.85 | 0.000282222 |
| 16831427 | MIR1288 | -0.48 | 3.45 | 0.024677029 |
| 17011165 | MIR2113 | -0.51 | 3.34 | 0.038367592 |
| 16888669 | MIR1245A | -1.53 | 3.16 | 0.045223684 |
| 16705437 | MIR1254-1 | -0.68 | 6.15 | 0.029770839 |
| 16823889 | MIR548H2 | -0.85 | 6.54 | 0.031759503 |
| 16709237 | MIR548E | -0.53 | 2.37 | 0.037383347 |
| 16828072 | SNORA70D | 0.60 | 4.05 | 0.033104806 |
| 16981500 | MIR548T | -0.58 | 3.81 | 0.0162893 |
| 17075060 | MIR548V | -1.84 | 4.81 | 0.002360681 |
| 16956053 | MIR3136 | -0.68 | 2.61 | 0.020357132 |
| 16980714 | MIR3140 | -1.17 | 3.41 | 0.027676678 |
| 16709317 | MIR4295 | -1.00 | 6.25 | 0.009910072 |
| 17095638 | MIR4290 | -0.63 | 3.33 | 0.020221958 |
| 16971046 | MIR3139 | -0.92 | 4.26 | 0.038064633 |
| 16907639 | MIR2355 | -0.86 | 3.85 | 0.049077824 |
| 16920610 | MTRNR2L3 | -0.43 | 2.76 | 0.014739525 |
| 16748119 | LINC00987 | -0.99 | 4.57 | 0.002736976 |
| 16999767 | MIR3936 | 2.21 | 5.32 | 0.002719692 |
| 16989241 | MIR3661 | 0.94 | 5.02 | 0.032953656 |
| 16852564 | LOC100505549 | -0.69 | 4.94 | 0.009663603 |
| 17008189 | LOC100505550 | -0.32 | 3.18 | 0.044342925 |
| 16815852 | LOC100505564 | -0.76 | 4.35 | 0.00052561 |
| 16833917 | LRRC3C | -0.79 | 3.69 | 0.014748667 |
| 16862651 | LOC100505622 | -0.52 | 3.85 | 0.00507933 |
| 16672489 | LOC100505633 | 2.53 | 5.91 | 0.000443686 |
| 16948555 | LINC00888 | -0.65 | 3.69 | 0.031117432 |
| 16983152 | SNHG18 | 1.11 | 6.57 | 0.00467563 |
| 16968293 | LINC00989 | -0.81 | 3.53 | 0.003130957 |
| 17044166 | LOC100506178 | -0.82 | 3.43 | 0.005903384 |
| 16748539 | LOC100506314 | 1.39 | 5.02 | 0.002226908 |
| 16700070 | ITPKB-IT1 | -0.88 | 4.37 | 0.000366196 |
| 16762642 | LOC100506578 | -0.58 | 3.36 | 0.048490926 |
| 16757863 | PXN-AS1 | 0.57 | 4.94 | 0.021838852 |
| 16771319 | DYNLL1-AS1 | 0.65 | 5.92 | 0.004314048 |
| 16843446 | SLFN12L | -0.95 | 5.55 | 0.025898916 |
| 17045320 | TRG-AS1 | -0.74 | 3.57 | 0.04803565 |
| 16660392 | LOC100506801 | -0.83 | 3.83 | 0.001108949 |
| 16766794 | LOC100506844 | 0.49 | 3.33 | 0.016782224 |
| 16888183 | TTN-AS1 | -0.57 | 5.72 | 0.048943191 |

| | | | | |
|---|---|---|---|---|
| 17105719 | LOC100506901 | 2.01 | 4.92 | 0.000244467 |
| 16942419 | PSMD6-AS2 | -0.80 | 5.78 | 0.035784036 |
| 17118039 | LOC100507209 | -1.30 | 5.30 | 0.002318907 |
| 16838094 | SNHG16 | 0.71 | 8.80 | 0.012241205 |
| 17012676 | LINC01013 | -0.64 | 2.69 | 0.001384232 |
| 16865718 | ZNF865 | 0.61 | 4.27 | 0.0338111 |
| 16949785 | TMEM44-AS1 | 0.62 | 4.17 | 0.04997158 |
| 16823043 | LOC100507303 | 1.12 | 6.44 | 0.010660757 |
| 17082032 | LOC100507316 | 0.87 | 4.21 | 0.004636978 |
| 16754118 | LOC100507330 | -0.59 | 3.05 | 0.005892147 |
| 17010273 | KCNQ5-IT1 | -1.30 | 4.23 | 0.015886272 |
| 16797326 | LOC100507437 | 0.91 | 4.41 | 0.004002822 |
| 17077191 | LOC100507516 | -1.26 | 5.21 | 0.012455266 |
| 17077376 | LINC00968 | -0.60 | 2.46 | 0.002459618 |
| 17117480 | LOC100507663 | -0.75 | 5.87 | 0.017767118 |
| 16955935 | LOC100508226 | -1.17 | 4.29 | 0.007777057 |
| 17088116 | MIR4668 | -1.06 | 2.87 | 0.031440911 |
| 16872227 | MIR4530 | 0.69 | 3.69 | 0.03805209 |
| 16957673 | MIR4796 | -0.97 | 2.96 | 0.005979006 |
| 16909154 | MIR4439 | -0.86 | 2.25 | 0.003033218 |
| 16935510 | MIR378I | -1.24 | 4.85 | 0.023743259 |
| 17093990 | MIR4540 | -0.93 | 2.45 | 0.006037426 |
| 16777209 | MIR4499 | -0.88 | 2.34 | 0.004020055 |
| 17082258 | MIR4664 | 1.35 | 3.83 | 0.0009769 |
| 16968521 | MIR4451 | -1.17 | 5.81 | 0.029382558 |
| 16817918 | MIR4518 | -1.17 | 3.68 | 0.000976305 |
| 16855161 | MIR4744 | -0.66 | 3.22 | 0.019306979 |
| 17069359 | MIR4470 | 0.52 | 3.00 | 0.024885713 |
| 16750429 | MIR4698 | -0.47 | 3.16 | 0.045327886 |
| 16992195 | MIR378E | -1.14 | 4.48 | 0.003270512 |
| 16816680 | SNX29P1 | -0.62 | 3.18 | 0.048028746 |
| 17118432 | RBSG2 | -0.45 | 4.25 | 0.027628988 |
| 16756222 | IGANRP | -1.38 | 6.16 | 0.002498679 |
| 16797535 | LOC100653084 | -1.98 | 3.44 | 0.016193023 |
| 16904775 | CERS6-AS1 | 0.51 | 2.72 | 0.040827531 |
| 16773581 | RNU6-82P | -1.10 | 3.38 | 0.00251945 |
| 16667948 | VAV3-AS1 | -0.87 | 3.08 | 0.001238051 |
| 17056734 | AOAH-IT1 | -1.09 | 4.60 | 0.007097819 |
| 17054885 | RNF216-IT1 | -0.42 | 5.49 | 0.01689906 |
| 16753767 | IFNG-AS1 | -1.75 | 4.03 | 0.005962736 |
| 16849391 | LOC100996291 | -0.40 | 3.46 | 0.04275753 |
| 16989423 | LOC100996485 | 0.72 | 4.31 | 0.025496024 |
| 16987087 | MEF2C-AS1 | -0.80 | 3.06 | 0.000514472 |

## Appendix 4.1 - Coverage Across Reference for Each Matched Tumour and Normal Pair in Discovery Cohort

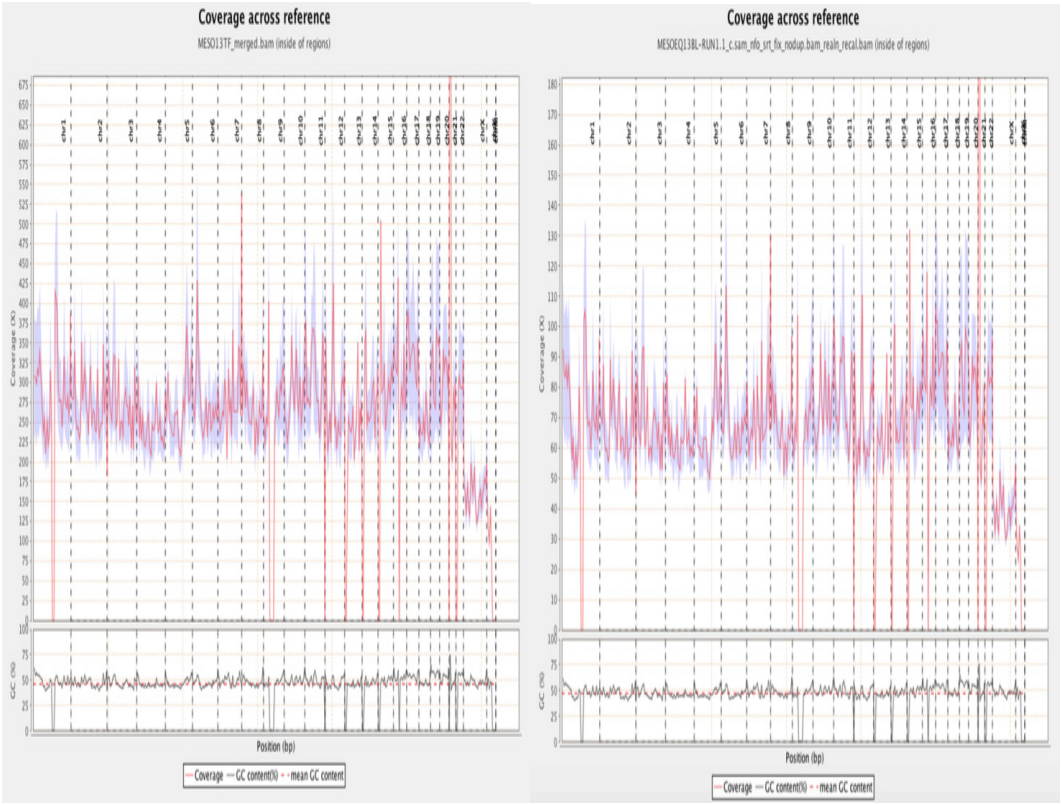

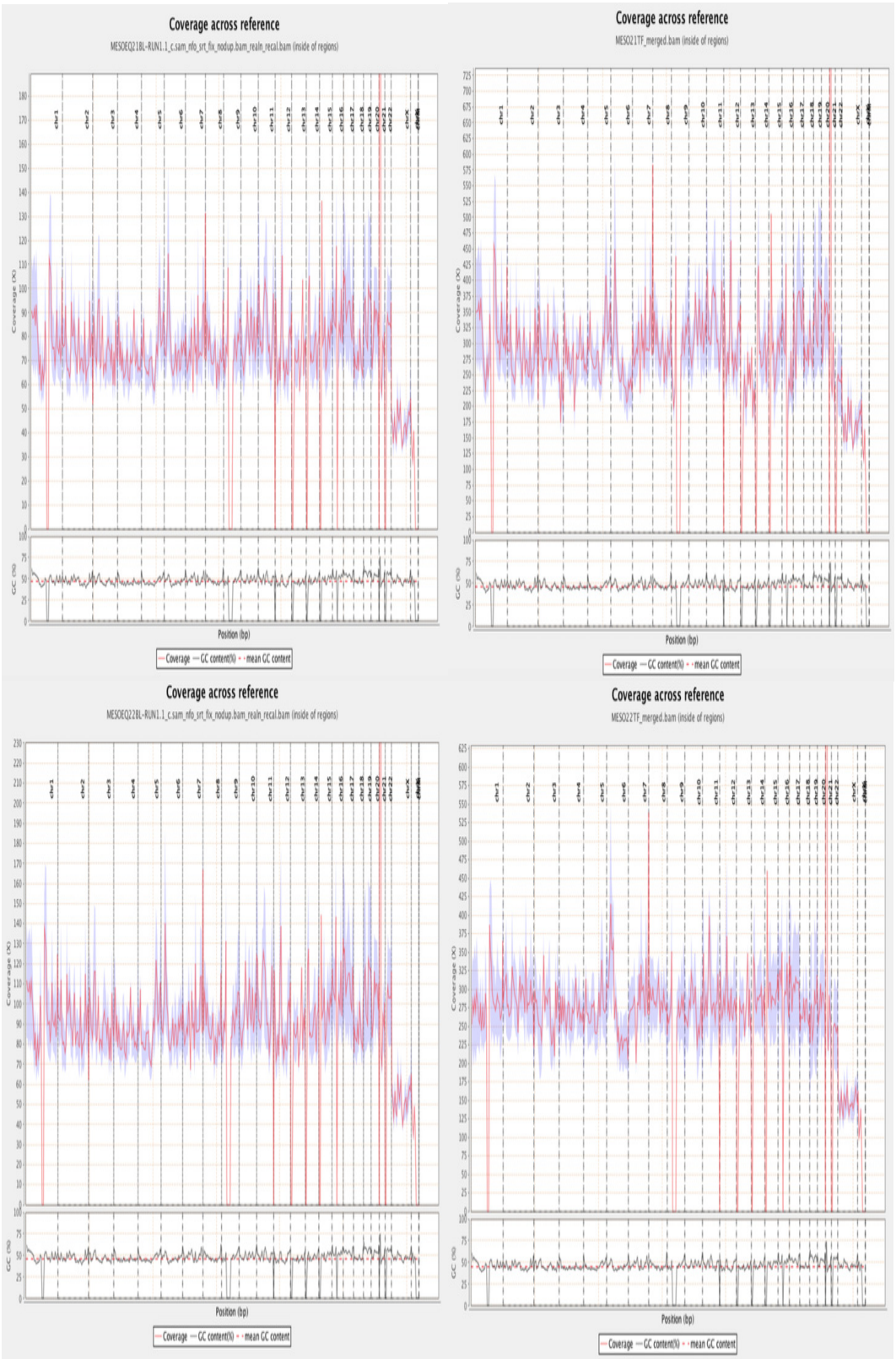
Coverage across reference
MESOEQ21BL-RUN1.1_c.sam_nfo_srt_fix_nodup.bam_realn_recal.bam (inside of regions)
Coverage (X)
GC (%)
Position (bp)
Coverage
GC content(%)
mean GC content
Coverage across reference
MESO21TF_merged.bam (inside of regions)
Coverage (X)
GC (%)
Position (bp)
Coverage
GC content(%)
mean GC content
Coverage across reference
MESOEQ22BL-RUN1.1_c.sam_nfo_srt_fix_nodup.bam_realn_recal.bam (inside of regions)
Coverage (X)
GC (%)
Position (bp)
Coverage
GC content(%)
mean GC content
Coverage across reference
MESO22TF_merged.bam (inside of regions)
Coverage (X)
GC (%)
Position (bp)
Coverage
GC content(%)
mean GC content

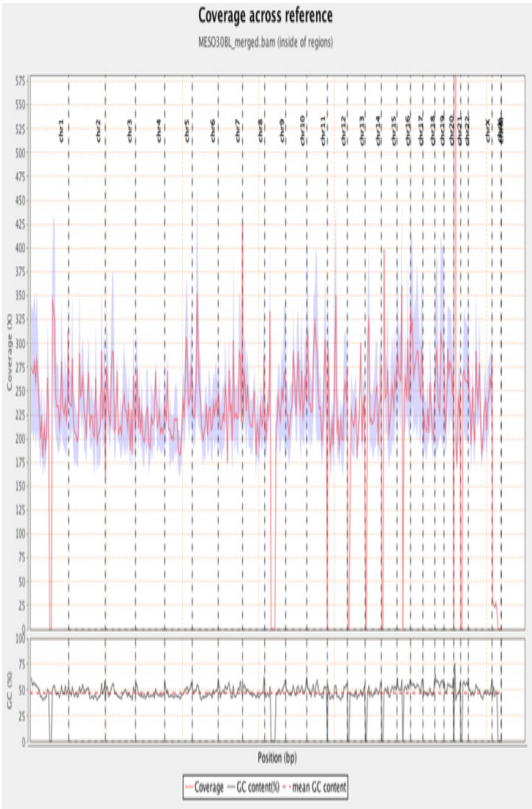
Coverage across reference
MESO30BL_merged.bam (inside of regions)
Coverage (X)
GC (%)
Position (bp)
Coverage
GC content(%)
mean GC content

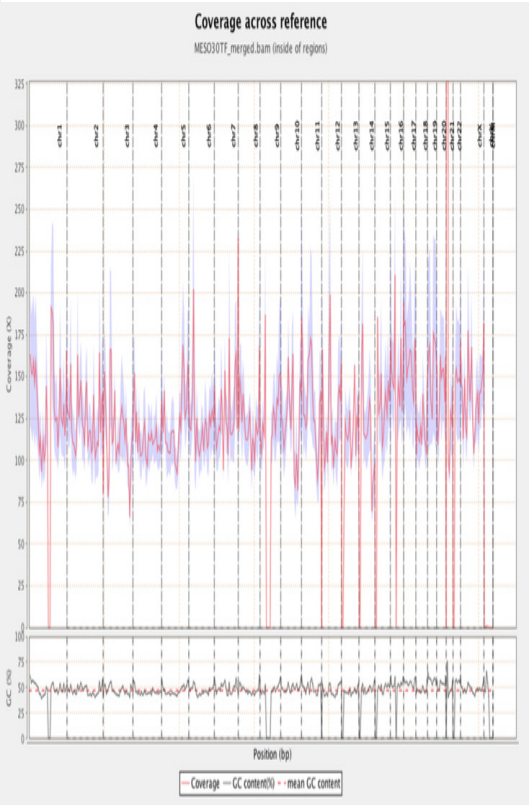
Coverage across reference
MESO30TF_merged.bam (inside of regions)
Coverage (X)
GC (%)
Position (bp)
Coverage
GC content(%)
mean GC content

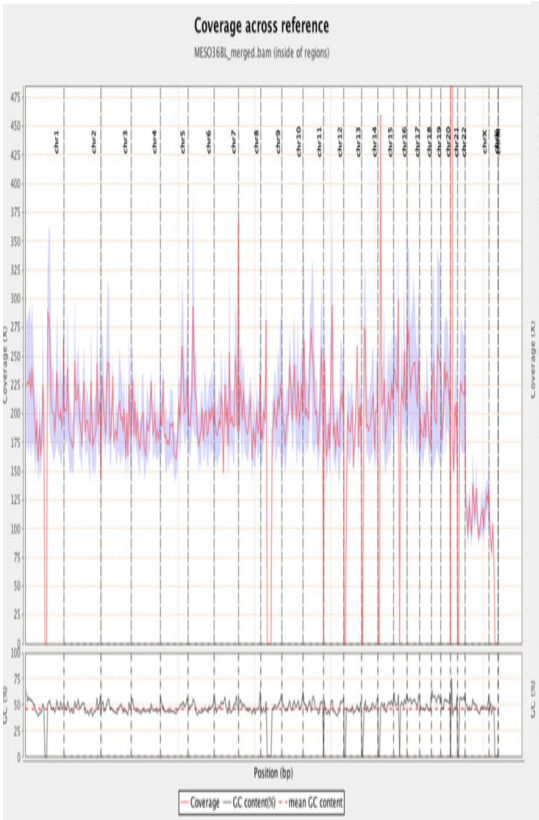
Coverage across reference
MESO36BL_merged.bam (inside of regions)
Coverage (X)
GC (%)
Position (bp)
Coverage
GC content(%)
mean GC content

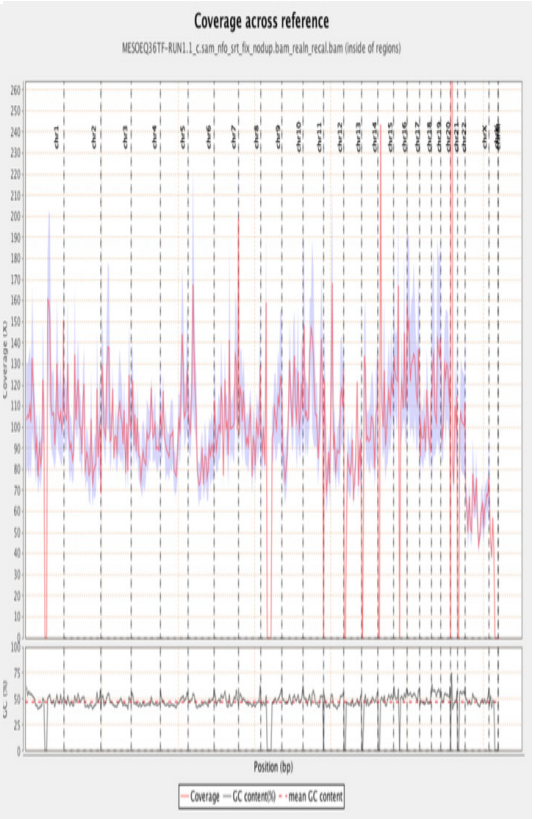
Coverage across reference
MESOEQ36TF-RUN1.1_c.sam_nfo_srt_fix_nodup.bam_realn_recal.bam (inside of regions)
Coverage (X)
GC (%)
Position (bp)
Coverage
GC content(%)
mean GC content

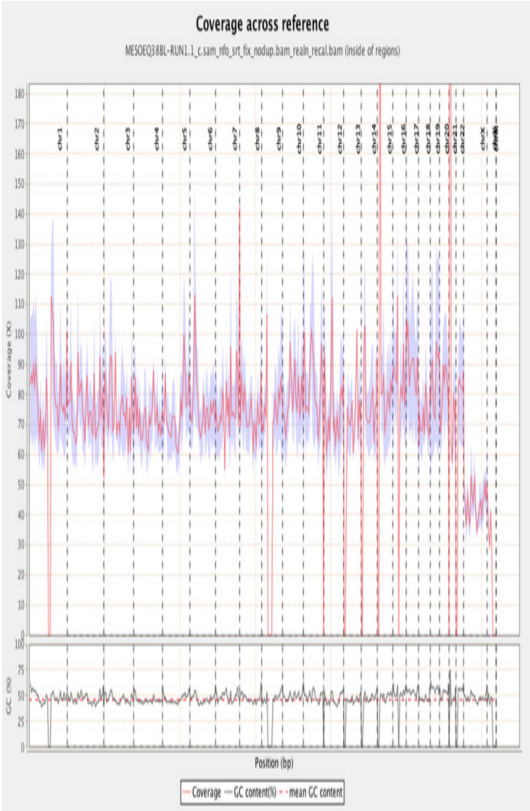
Coverage across reference
MESOEQ38BL-RUN1.1_c.sam_nfo_srt_fix_nodup.bam_realn_recal.bam (inside of regions)
Coverage (X)
GC (%)
Position (bp)
Coverage
GC content(%)
mean GC content

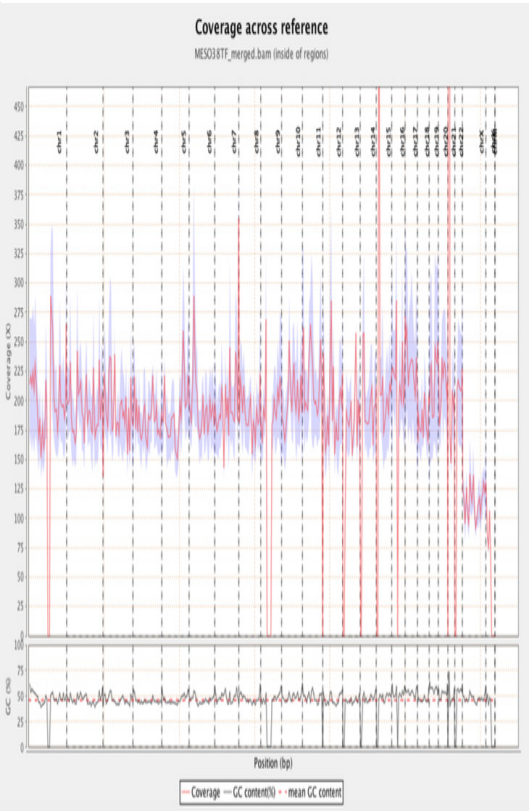
Coverage across reference
MESO38TF_merged.bam (inside of regions)
Coverage (X)
GC (%)
Position (bp)
Coverage
GC content(%)
mean GC content

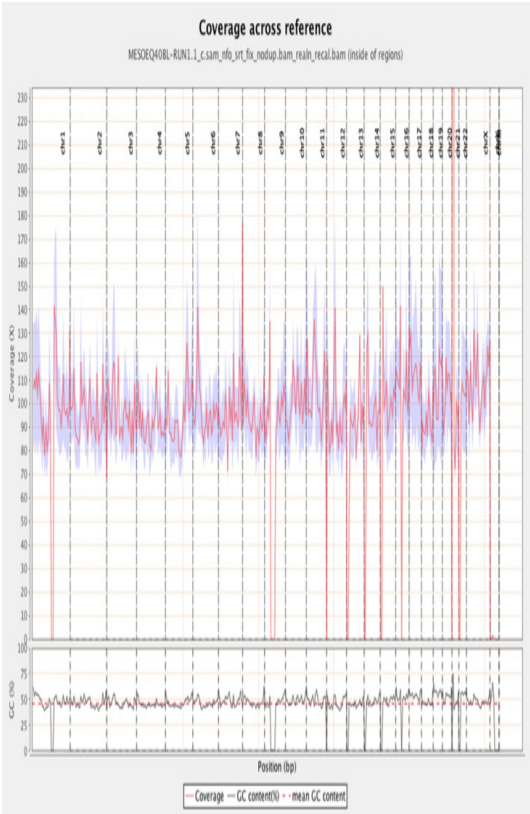
Coverage across reference
MESOEQ40BL-RUN1.1_c.sam_nfo_srt_fix_nodup.bam_realn_recal.bam (inside of regions)
Coverage (X)
GC (%)
Position (bp)
Coverage
GC content(%)
mean GC content

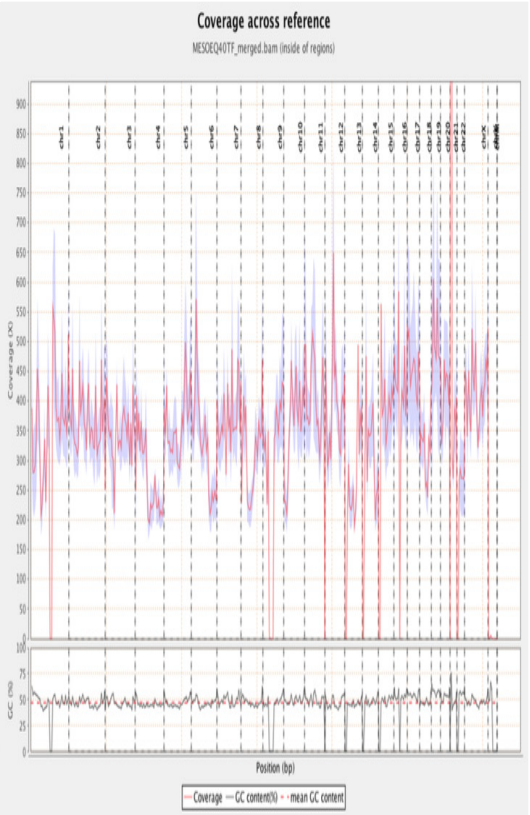
Coverage across reference
MESOEQ40TF_merged.bam (inside of regions)
Coverage (X)
GC (%)
Position (bp)
Coverage
GC content(%)
mean GC content

## Appendix 4.2 - Functional Prediction of Nonsynonymous SNV with SIFT, Polyphen2 and MutationTaster

| Gene | Exon | Codon | protein | SIFT | Polyphen2 | Mutation Taster |
|---|---|---|---|---|---|---|
| GOLGA6L4 | exon3 | c.G253C | p.E85Q | T | . | P |
| HS3ST6 | exon1 | c.G77T | p.R26L | T | . | D |
| MAB21L1 | exon1 | c.C280G | p.L94V | T | B | D |
| MPPED1 | exon2 | c.A20C | p.D7A | T | B | D |
| PLXDC1 | exon13 | c.C1303G | p.L435V | T | B | D |
| KLHL6 | exon3 | c.C733T | p.H245Y | T | B | D |
| ASH1L | exon3 | c.G2233A | p.V745I | T | B | D |
| ANO3 | exon2 | c.G121A | p.A41T | T | B | D |
| NOP9 | exon4 | c.G869A | p.R290H,NOP9 | T | B | D |
| TFAP2D | exon2 | c.C200A | p.T67N | T | B | D |
| XRN2 | exon21 | c.G1967A | p.R656Q | T | B | D |
| HNRNPU | exon7 | c.G1420A | p.E474K,HNRNPU | T | B | D |
| DNAJB12 | exon1 | c.G153C | p.K51N,DNAJB12 | T | B | D |
| KCNB1 | exon2 | c.G1882A | p.G628R | T | B | D |
| TCEA3 | exon8 | c.C782T | p.A261V | T | B | D |
| ROR1 | exon6 | c.G910A | p.A304T,ROR1 | T | B | D |
| SP6 | exon2 | c.G250A | p.D84N,SP6 | T | B | D |
| KRTAP5-1 | exon1 | c.T70C | p.C24R | T | B | D |
| ADCY3 | exon8 | c.G1653T | p.Q551H | T | B | D |
| PHF21A | exon18 | c.A1805G | p.N602S,PHF21A | T | B | D |
| PLXNA3 | exon6 | c.C1477A | p.Q493K | T | B | D |
| RTKN | exon3 | c.G359T | p.R120L,RTKN | T | B | D |
| GIGYF1 | exon11 | c.G1223T | p.G408V | T | B | D |

| | | | | | | |
|---|---|---|---|---|---|---|
| HOXC5 | exon1 | c.A209C | p.H70P | T | B | D |
| TTC7A | exon4 | c.C556A | p.R186S,TTC7A | T | B | D |
| SNRPD2 | exon3 | c.G268A | p.V90I,SNRPD2 | T | B | D |
| AMMECR1L | exon5 | c.G554T | p.R185L,AMMECR1L | T | B | D |
| MAP3K10 | exon3 | c.C1000A | p.R334S | T | B | D |
| TIMM44 | exon9 | c.G914T | p.R305L | T | B | D |
| PIK3CB | exon3 | c.G426T | p.M142I,PIK3CB | T | B | D |
| LRRC2 | exon3 | c.G162T | p.R54S | T | B | D |
| SOCS5 | exon2 | c.G1040A | p.S347N,SOCS5 | T | B | D |
| DOCK5 | exon2 | c.C67A | p.Q23K | T | B | D |
| RUNX3 | exon4 | c.G650T | p.G217V,RUNX3 | T | B | D |
| ACTN1 | exon19 | c.G2334T | p.M778I,ACTN1 | T | B | D |
| TXN | exon2 | c.G40T | p.A14S,TXN | T | B | D |
| INF2 | exon18 | c.C2704A | p.Q902K,INF2 | T | B | D |
| ACSM4 | exon3 | c.C460A | p.L154I | T | B | D |
| TPM4 | exon1 | c.C17A | p.S6Y | T | B | D |
| ACOT1 | exon1 | c.A439G | p.T147A | T | B | D |
| CYP3A5 | exon10 | c.G889T | p.A297S,CYP3A5 | T | B | D |
| RBPJL | exon6 | c.C553A | p.H185N,RBPJL | T | B | D |
| KRTAP2-1 | exon1 | c.C335A | p.P112H | T | B | D |
| EIF4G1 | exon2 | c.C31A | p.P11T,EIF4G1 | T | B | D |
| MPLKIP | exon1 | c.G83T | p.R28L | T | B | D |
| PRRX2 | exon4 | c.C637A | p.P213T | T | B | D |
| TPD52L1 | exon1 | c.C14A | p.A5E,TPD52L1 | T | B | D |
| LPIN1 | exon4 | c.G389A | p.G130D,LPIN1 | T | B | D |
| PRKAR2B | exon1 | c.G197T | p.G66V | T | B | D |
| SLC9A5 | exon5 | c.C856A | p.L286I | T | B | D |
| TRAK2 | exon14 | c.G1802T | p.G601V | T | B | D |
| CARM1 | exon1 | c.C211A | p.L71I | T | B | D |

| | | | | | | |
|---|---|---|---|---|---|---|
| CENPI | exon6 | c.C607A | p.H203N | T | B | D |
| TVP23C | exon3 | c.G152A | p.C51Y,TVP23C-CDRT4 | T | B | D |
| AGAP7P | exon7 | c.C1718A | p.A573D | T | B | D |
| ANP32A | exon4 | c.G333C | p.K111N | T | B | D |
| COL8A1 | exon4 | c.G1560T | p.E520D,COL8A1 | T | B | D |
| NSUN7 | exon9 | c.C1207A | p.Q403K | T | B | D |
| TTC28 | exon15 | c.G4278T | p.E1426D | T | B | D |
| RPL17 | exon4 | c.G119T | p.W40L,RPL17-C18orf32 | T | B | D |
| NBEAL2 | exon6 | c.G534T | p.Q178H | T | B | D |
| INTS4 | exon14 | c.G1756T | p.A586S | T | B | D |
| CCDC74A | exon1 | c.G68T | p.R23L,CCDC74A | T | B | D |
| PRKDC | | | | T | B | D |
| SHANK3 | exon21 | c.G3376A | p.G1126R | T | D | N |
| WNT6 | exon4 | c.C824T | p.T275M | T | D | N |
| KIAA1462 | exon3 | c.C1391T | p.A464V | T | D | N |
| SREBF1 | exon3 | c.G535T | p.G179W,SREBF1 | T | D | N |
| SIGLEC11 | exon3 | c.C671T | p.T224I,SIGLEC11 | T | D | N |
| HMBS | exon2 | c.C47A | p.P16Q,HMBS | T | D | N |
| ARID3A | exon3 | c.C605A | p.P202H | T | D | N |
| LRFN3 | exon2 | c.T676C | p.S226P | T | D | N |
| CASP10 | exon5 | c.C598A | p.P200T,CASP10 | T | D | N |
| C1orf167 | exon15 | c.C3275A | p.P1092Q | T | D | N |
| RGPD3 | exon17 | c.A2468C | p.K823T | T | D | N |
| ACAN | exon11 | c.C2258A | p.P753Q,ACAN | T | D | N |
| NOTCH1 | exon34 | c.G6733T | p.G2245W | T | D | N |
| SPATA31D1 | exon4 | c.C1634A | p.P545Q | T | D | N |
| FAM9A | exon4 | c.C259A | p.P87T,FAM9A | T | D | N |

| | | | | | | |
|---|---|---|---|---|---|---|
| EFCAB12 | exon5 | c.G1001A | p.G334D | T | D | N |
| AMH | exon5 | c.G1183T | p.G395C | T | D | N |
| FOXE3 | exon1 | c.G112T | p.G38W | T | D | N |
| OBSCN | exon47 | c.C12614T | p.T4205I,OBSCN | T | D | N |
| PKD1 | exon10 | c.C2027T | p.P676L,PKD1 | T | D | N |
| IVL | exon2 | c.G846C | p.Q282H | T | D | N |
| ANKRD2 | exon3 | c.C352A | p.L118M,ANKRD2 | T | D | N |
| FAM214B | exon3 | c.G39T | p.E13D | T | D | N |
| PLEKHA5 | exon8 | c.C557A | p.P186H,PLEKHA5 | T | D | N |
| TOR2A | exon1 | c.G112T | p.G38C,TOR2A | T | D | N |
| TCTN1 | exon12 | c.C1349A | p.P450Q,TCTN1 | T | D | N |
| OTUD6A | exon1 | c.C854A | p.P285Q | T | D | N |
| WISP3 | exon1 | c.C94A | p.L32M,WISP3 | T | D | N |
| CCDC9 | exon12 | c.C1426A | p.P476T | T | D | N |
| RGPD3 | exon17 | c.T2435G | p.L812R | T | D | N |
| KIF20B | exon13 | c.C1445A | p.P482Q,KIF20B | T | D | N |
| MCF2L | exon1 | c.C52A | p.L18M | T | D | N |
| KLF2 | exon2 | c.C581A | p.P194Q | T | D | N |
| FRG2C | exon4 | c.C605A | p.P202Q | T | D | N |
| COL12A1 | exon16 | c.G3305A | p.S1102N | T | D | D |
| DMAP1 | exon3 | c.G202A | p.A68T,DMAP1 | T | D | D |
| SEC23IP | exon16 | c.G2605A | p.D869N | T | D | D |
| GLTSCR1 | exon7 | c.C2248T | p.P750S | T | D | D |
| GPHN | exon7 | c.A468C | p.Q156H,GPHN | T | D | D |
| URGCP-MRPS24 | exon4 | c.G157A | p.D53N,URGCP | T | D | D |
| GAB2 | exon4 | c.G947C | p.R316P,GAB2 | T | D | D |
| POM121L2 | exon1 | c.G2677A | p.G893R | T | D | D |
| SPAG9 | exon5 | c.A662G | p.N221S,SPAG9 | T | D | D |

| | | | | | | |
|---|---|---|---|---|---|---|
| ALDH16A1 | exon15 | c.G2042A | p.C681Y,ALDH16A1 | T | D | D |
| LRP12 | exon4 | c.C841G | p.R281G,LRP12 | T | D | D |
| TBX22 | exon5 | c.A772G | p.T258A,TBX22 | T | D | D |
| KLHL6 | exon7 | c.C1696T | p.R566W | T | D | D |
| PTPN1 | exon5 | c.G415T | p.V139L,PTPN1 | T | D | D |
| GLTSCR1L | exon5 | c.A460G | p.N154D | T | D | D |
| SLC43A2 | exon5 | c.C554G | p.P185R,SLC43A2 | T | D | D |
| ITPR1 | exon20 | c.A2353C | p.T785P,ITPR1 | T | D | D |
| FES | exon14 | c.A1778G | p.E593G,FES | T | D | D |
| FLT3 | exon7 | c.C772T | p.P258S | T | D | D |
| GRID2 | exon6 | c.G745A | p.D249N,GRID2 | T | D | D |
| KLHL2 | exon13 | c.G1387A | p.D463N,KLHL2 | T | D | D |
| FAM118B | exon7 | c.C932A | p.P311Q | T | D | D |
| SETD6 | exon7 | c.T1043C | p.V348A,SETD6 | T | D | D |
| GRIA4 | exon15 | c.G2314A | p.V772I | T | D | D |
| LRIT1 | exon2 | c.G346T | p.G116W | T | D | D |
| ZNF680 | exon4 | c.G736A | p.A246T | T | D | D |
| STAB1 | exon15 | c.C1598A | p.S533Y | T | D | D |
| SOBP | exon6 | c.A1412C | p.N471T | T | D | D |
| BANP | exon2 | c.C59A | p.P20H,BANP | T | D | D |
| BRSK1 | exon14 | c.C1514A | p.P505H | T | D | D |
| DNAAF3 | exon6 | c.G725T | p.W242L,DNAAF3 | T | D | D |
| MED25 | exon7 | c.T716C | p.L239P | T | D | D |
| MYOG | exon2 | c.C512A | p.P171Q | T | D | D |
| FDFT1 | exon3 | c.C311A | p.P104Q,FDFT1 | T | D | D |
| PLLP | exon3 | c.G352A | p.A118T | T | D | D |
| STYK1 | exon4 | c.C88T | p.P30S | T | D | D |
| WDR59 | exon24 | c.G2453T | p.W818L | T | D | D |
| PKHD1 | exon5 | c.G308C | p.G103A,PKHD1 | T | D | D |

| | | | | | | |
|---|---|---|---|---|---|---|
| TMEM25 | exon5 | c.C745A | p.L249I,TMEM25 | T | D | D |
| UBTF | exon7 | c.C607A | p.Q203K,UBTF | T | D | D |
| P2RX4 | exon1 | c.G133T | p.G45W,P2RX4 | T | D | D |
| LRSAM1 | exon2 | c.C61A | p.Q21K,LRSAM1 | T | D | D |
| CLEC2L | exon1 | c.G174T | p.W58C | T | D | D |
| FAM43B | exon1 | c.C467A | p.P156Q | T | D | D |
| MMRN2 | exon6 | c.T2263G | p.F755V | T | D | D |
| SMPD4 | exon14 | c.G1591T | p.D531Y,SMPD4 | T | D | D |
| TTC7A | exon17 | c.C1001A | p.A334D,TTC7A | T | D | D |
| LAMA5 | exon44 | c.G5773T | p.A1925S | T | D | D |
| DDHD2 | exon8 | c.C868A | p.L290M,DDHD2 | T | D | D |
| CSDE1 | exon17 | c.G2238T | p.R746S,CSDE1 | T | D | D |
| FOXRED1 | exon8 | c.C838A | p.Q280K | T | D | D |
| NCL | exon8 | c.G1218T | p.Q406H | T | D | D |
| CCDC108 | exon16 | c.G2615T | p.R872L | T | D | D |
| PDCL3 | exon5 | c.C376A | p.L126I | T | D | D |
| PBX4 | exon1 | c.C100A | p.L34M | T | D | D |
| COL16A1 | exon63 | c.G3903T | p.Q1301H | T | D | D |
| ZNF511 | exon1 | c.G134T | p.R45L | T | D | D |
| AIDA | exon6 | c.G387T | p.L129F | T | D | D |
| ARHGEF10L | exon8 | c.G794T | p.G265V,ARHGEF10L | T | D | D |
| COL12A1 | exon33 | c.G4047T | p.L1349F,COL12A1 | T | D | D |
| PIGS | exon8 | c.G840T | p.L280F | T | D | D |
| CFAP43 | exon29 | c.G3663T | p.E1221D | T | D | D |
| CCDC33 | exon4 | c.C407A | p.P136H | T | D | D |
| FBN3 | exon55 | c.C7073A | p.T2358N | T | D | D |
| ARPP21 | exon2 | c.C71A | p.P24Q,ARPP21 | T | D | D |
| NEB | exon94 | c.G13954T | p.A4652S,NEB | T | D | D |

| | | | | | | |
|---|---|---|---|---|---|---|
| KIAA1549 | exon9 | c.G3832T | p.G1278C,KIAA1549 | T | D | D |
| IGF2BP2 | exon14 | c.G1437T | p.Q479H,IGF2BP2 | T | D | D |
| SOX18 | exon2 | c.C592A | p.R198S | T | D | D |
| GADL1 | exon3 | c.G221T | p.W74L | T | D | D |
| CEP250 | exon10 | c.C880A | p.Q294K | T | D | D |
| BCAM | exon14 | c.C1769A | p.P590Q | T | D | D |
| PRKDC | | | | T | D | D |
| NBPF9 | | | | T | D | D |
| C10orf82 | exon4 | c.C412G | p.L138V | T | P | N |
| RASGRP4 | exon5 | c.C409A | p.H137N,RASGRP4 | T | P | N |
| BEND2 | exon4 | c.C391G | p.Q131E,BEND2 | T | P | N |
| SPACA3 | exon2 | c.G37A | p.V13M | T | P | N |
| COL22A1 | exon37 | c.A2824G | p.R942G | T | P | N |
| SCG2 | exon2 | c.C1024A | p.P342T | T | P | N |
| DPCR1 | exon2 | c.C2204T | p.P735L | T | P | N |
| ZNF486 | exon4 | c.C917G | p.P306R | T | P | N |
| CRB2 | exon10 | c.G2791T | p.G931W | T | P | N |
| CABIN1 | exon31 | c.C5294A | p.P1765Q,CABIN1 | T | P | N |
| CUX2 | exon6 | c.C490A | p.L164I | T | P | N |
| RSPH10B2 | exon14 | c.C1589A | p.P530Q,RSPH10B | T | P | N |
| SEMA3G | exon1 | c.C31A | p.L11M | T | P | N |
| ZNF471 | exon4 | c.C227T | p.T76M | T | P | N |
| FRG2 | exon4 | c.G450T | p.R150S,FRG2 | T | P | N |
| MRPL11 | exon1 | c.G13T | p.G5C,MRPL11 | T | P | N |
| AVIL | exon16 | c.G2011T | p.A671S | T | P | N |
| MMP11 | exon1 | c.C92A | p.A31D | T | P | N |
| ALG1 | exon7 | c.C758A | p.P253Q | T | P | N |
| OR5H1 | exon1 | c.G149T | p.W50L | T | P | N |
| ELF4 | exon9 | c.C1213A | p.H405N,ELF4 | T | P | N |

| | | | | | | |
|---|---|---|---|---|---|---|
| RAET1G | exon2 | c.C134A | p.P45H | T | P | N |
| C19orf52 | exon2 | c.C212A | p.A71E | T | P | N |
| P2RX4 | exon1 | c.C26A | p.A9E,P2RX4 | T | P | N |
| CNTRL | exon17 | c.C2803A | p.L935I | T | P | N |
| SPATA31E1 | exon4 | c.G3386A | p.C1129Y | T | P | N |
| TCEB3CL | exon1 | c.C905G | p.A302G,TCEB3C | T | P | N |
| BCAR1 | exon2 | c.C386A | p.P129Q,BCAR1 | T | P | N |
| ZNF552 | exon3 | c.C248A | p.A83E | T | P | N |
| SHANK3 | exon21 | c.C2375A | p.P792Q | T | P | N |
| TBX10 | exon2 | c.G80T | p.W27L | T | P | N |
| ANKRD20A3 | exon3 | c.C382T | p.L128F,ANKRD20A 2 | T | P | N |
| MAPKBP1 | exon23 | c.G2675T | p.R892M,MAPKBP1 | T | P | N |
| CGN | exon12 | c.C2146A | p.Q716K | T | P | N |
| CCDC159 | exon5 | c.C406A | p.Q136K | T | P | N |
| MUC20 | exon2 | c.G1087T | p.A363S,MUC20 | T | P | N |
| TARBP1 | exon1 | c.C305T | p.A102V | T | P | N |
| C9orf3 | exon10 | c.C1703A | p.A568D,C9orf3 | T | P | N |
| MUC20 | exon2 | c.G1114T | p.G372C,MUC20 | T | P | N |
| TJP3 | exon5 | c.C311A | p.P104H,TJP3 | T | P | N |
| ADAMTS16 | exon1 | c.C40A | p.L14M | T | P | N |
| FBRSL1 | exon17 | c.C2612A | p.A871E | T | P | N |
| SMYD3 | exon8 | c.G732A | p.M244I,SMYD3 | T | P | D |
| KCNN1 | exon3 | c.C339A | p.F113L | T | P | D |
| FOXK1 | exon2 | c.C631A | p.P211T | T | P | D |
| MN1 | exon1 | c.C1802T | p.P601L | T | P | D |
| FAM73B | exon9 | c.A942C | p.R314S | T | P | D |
| SEMA5A | exon4 | c.C193A | p.P65T | T | P | D |
| WBSCR17 | exon10 | c.C1573A | p.R525S | T | P | D |

| | | | | | | |
|---|---|---|---|---|---|---|
| NBEAL1 | exon38 | c.C5953A | p.P1985T | T | P | D |
| FAM20C | exon1 | c.C581A | p.P194H | T | P | D |
| FANCD2 | exon34 | c.G3457A | p.E1153K,FANCD2 | T | P | D |
| HIVEP2 | exon6 | c.G5197T | p.D1733Y | T | P | D |
| CELSR2 | exon17 | c.C6271A | p.Q2091K | T | P | D |
| PIEZO1 | exon24 | c.C3436G | p.P1146A | T | P | D |
| SYN1 | exon12 | c.G1505T | p.S502I,SYN1 | T | P | D |
| POU3F1 | exon1 | c.G344T | p.R115L | T | P | D |
| EPB41 | exon13 | c.C2044A | p.Q682K,EPB41 | T | P | D |
| CDKAL1 | exon6 | c.C427A | p.Q143K | T | P | D |
| KIAA1244 | exon25 | c.C4133A | p.P1378Q | T | P | D |
| CDH22 | exon7 | c.C1234A | p.L412M | T | P | D |
| ITGA9 | exon16 | c.G1695T | p.R565S | T | P | D |
| SLC24A5 | exon8 | c.C1114A | p.L372I | T | P | D |
| SEZ6L | exon12 | c.C2572A | p.H858N,SEZ6L | T | P | D |
| USH2A | exon46 | c.G9063T | p.Q3021H | T | P | D |
| RGMA | exon1 | c.G3T | p.M1I,RGMA | T | P | D |
| C10orf54 | exon6 | c.G880C | p.V294L | T | P | D |
| NAB2 | exon2 | c.T622C | p.F208L | T | P | D |
| SMOC1 | exon1 | c.C22A | p.R8S,SMOC1 | T | P | D |
| MRPS6 | exon1 | c.C7A | p.R3S | T | P | D |
| C1orf106 | exon9 | c.C1570A | p.Q524K,C1orf106 | T | P | D |
| DNAH17 | exon70 | c.G11282T | p.G3761V | T | P | D |
| SPEG | exon4 | c.C2036A | p.P679H | T | P | D |
| ADCY10 | exon14 | c.G1526T | p.R509L,ADCY10 | T | P | D |
| ADARB2 | exon8 | c.G1812T | p.E604D | T | P | D |
| ADAMTS6 | exon20 | c.G2460T | p.L820F | T | P | D |
| DGKQ | exon4 | c.G506T | p.R169L | T | P | D |
| SLC6A7 | exon14 | c.C1734A | p.D578E | T | P | D |

| | | | | | | |
|---|---|---|---|---|---|---|
| SLC52A2 | exon3 | c.C199A | p.L67I,SLC52A2 | T | P | D |
| TUBGCP5 | exon22 | c.C2971A | p.H991N,TUBGCP5 | T | P | D |
| HK2 | exon18 | c.A2627T | p.H876L | T | P | D |
| MUC16 | exon66 | c.T41639G | p.L13880W | T | P | . |
| NOS1AP | exon6 | c.C578A | p.P193Q,NOS1AP | T | P | . |
| MUC16 | exon55 | c.A40562G | p.N13521S | T | P | . |
| MUC16 | exon55 | c.G40547A | p.R13516K | T | P | . |
| C1orf167 | exon2 | c.C44A | p.P15Q | D | . | N |
| POTEJ | exon13 | c.C1547A | p.P516Q | D | . | N |
| CFAP46 | exon29 | c.G3968T | p.C1323F | D | . | N |
| TTC34 | exon4 | c.G628T | p.G210W | D | . | N |
| SEC14L6 | exon9 | c.C743A | p.P248H | D | . | D |
| MUC3A | exon2 | c.C956T | p.T319I | D | . | . |
| IL19 | exon1 | c.G10A | p.E4K | D | B | N |
| MAPK13 | exon3 | c.G293A | p.R98H | D | B | N |
| PLEKHA4 | exon20 | c.G2263A | p.G755R | D | B | N |
| PRR29 | exon5 | c.G604A | p.V202I | D | B | N |
| OR4C12 | exon1 | c.T806C | p.V269A | D | B | N |
| RASIP1 | exon5 | c.C1493T | p.A498V | D | B | N |
| PRR25 | exon1 | c.T235G | p.W79G | D | B | N |
| TMEM173 | exon5 | c.C694T | p.H232Y,TMEM173 | D | B | N |
| COL27A1 | exon2 | c.C77A | p.S26Y | D | B | N |
| MUC5B | exon31 | c.A5779T | p.T1927S | D | B | N |
| PHKB | exon25 | c.G2353A | p.G785R | D | B | N |
| PODN | exon1 | c.C19A | p.R7S,PODN | D | B | N |
| DUSP13 | exon2 | c.G3T | p.M1I | D | B | N |
| ATP13A2 | exon27 | c.G3389T | p.W1130L | D | B | N |

| | | | | | | |
|---|---|---|---|---|---|---|
| MAMLD1 | exon5 | c.C2977A | p.Q993K | D | B | N |
| OLFML2A | exon1 | c.C71A | p.P24H | D | B | N |
| NOC2L | exon16 | c.G1826T | p.R609L | D | B | N |
| KRTAP4-8 | exon1 | c.G470T | p.R157L | D | B | N |
| S1PR5 | exon2 | c.G775T | p.A259S,S1PR5 | D | B | N |
| ZNF140 | exon4 | c.C1000A | p.L334I,ZNF140 | D | B | N |
| NTN3 | exon6 | c.C1562A | p.P521H | D | B | N |
| PNCK | exon10 | c.G1115T | p.R372L,PNCK | D | B | N |
| ZNF75D | exon3 | c.C533A | p.S178Y,ZNF75D | D | B | N |
| FOXD4L1 | exon1 | c.C1132A | p.Q378K | D | B | N |
| PRSS58 | exon4 | c.G330T | p.E110D | D | B | N |
| ATAD3A | exon3 | c.G363T | p.Q121H | D | B | N |
| IGSF9B | exon18 | c.G3821T | p.G1274V | D | B | D |
| RPL10 | exon2 | c.C19T | p.R7C,RPL10 | D | B | D |
| ATG2B | exon2 | c.G264T | p.Q88H | D | B | D |
| TRIB1 | exon1 | c.C49A | p.R17S | D | B | D |
| SNRPD2 | exon3 | c.C273G | p.N91K,SNRPD2 | D | B | D |
| CLK1 | exon9 | c.A1124G | p.D375G,CLK1 | D | B | D |
| PRPH | exon1 | c.C433A | p.Q145K | D | B | D |
| GNA11 | exon1 | c.G21T | p.M7I | D | B | D |
| RPL4 | exon7 | c.G773T | p.R258L | D | B | D |
| CNN2 | exon1 | c.G37T | p.G13W,CNN2 | D | B | D |
| AIDA | exon1 | c.G32T | p.R11L | D | B | D |
| CYP4F3 | exon13 | c.C1495T | p.R499C,CYP4F3 | D | B | D |
| USP17L2 | exon1 | c.C337A | p.H113N | D | B | D |
| MUC16 | exon14 | c.G36759T | p.R12253S | D | B | . |
| FAM179B | exon1 | c.C1807T | p.H603Y | D | D | N |
| ARHGEF11 | exon26 | c.T2374A | p.W792R,ARHGEF11 | D | D | N |
| ZNF646 | exon2 | c.C2615A | p.P872H | D | D | N |

| | | | | | | |
|---|---|---|---|---|---|---|
| PCDHGA5 | exon1 | c.G2086A | p.A696T,PCDHGA5 | D | D | N |
| KIR3DL1 | exon3 | c.C90G | p.F30L | D | D | N |
| PITPNM1 | exon4 | c.C382G | p.L128V,PITPNM1 | D | D | N |
| PPP1R1A | exon1 | c.C38G | p.T13R | D | D | N |
| ZNF845 | exon4 | c.C1276A | p.L426I | D | D | N |
| COQ9 | exon1 | c.C5A | p.A2E | D | D | N |
| SLC38A9 | exon8 | c.G586T | p.G196W,SLC38A9 | D | D | N |
| GNB1L | exon3 | c.G106T | p.G36W | D | D | N |
| PCDHA6 | exon1 | c.C1406A | p.P469Q,PCDHA6 | D | D | N |
| SATL1 | exon3 | c.C1726A | p.L576I | D | D | N |
| SPIDR | exon4 | c.A190T | p.R64W,SPIDR | D | D | N |
| ENSA | exon2 | c.G189T | p.W63C | D | D | N |
| MUC1 | exon2 | c.G282T | p.W94C,MUC1 | D | D | N |
| ACAD10 | exon12 | c.C1628A | p.P543H,ACAD10 | D | D | N |
| ARHGEF35 | exon2 | c.C1352A | p.P451H | D | D | N |
| AKNA | exon22 | c.G4213T | p.A1405S | D | D | N |
| CTC1 | exon10 | c.C1733A | p.A578D | D | D | N |
| CR1 | exon34 | c.C5552A | p.P1851Q,CR1 | D | D | N |
| RHBDF2 | exon2 | c.G25T | p.G9W,RHBDF2 | D | D | N |
| LCE1D | exon2 | c.C131A | p.S44Y | D | D | N |
| LAT2 | exon12 | c.C671A | p.P224Q,LAT2 | D | D | N |
| PPP1R3F | exon4 | c.G261T | p.Q87H,PPP1R3F | D | D | N |
| MIER2 | exon8 | c.G731T | p.R244M | D | D | N |
| LILRB1 | exon14 | c.A1789T | p.T597S,LILRB1 | D | D | N |
| ZNF624 | exon2 | c.G34T | p.G12W | D | D | N |
| CNTNAP3 | exon22 | c.G3616T | p.G1206W | D | D | N |
| IFNA10 | exon1 | c.G202T | p.G68C | D | D | N |
| GZMH | exon1 | c.G49T | p.G17W,GZMH | D | D | N |
| AKR7A2 | exon1 | c.G274T | p.G92W | D | D | N |

| | | | | | | |
|---|---|---|---|---|---|---|
| CCL8 | exon3 | c.C233A | p.P78H | D | D | N |
| CDC25A | exon1 | c.C14A | p.P5Q,CDC25A | D | D | N |
| SHANK3 | exon11 | c.G1375T | p.G459C | D | D | N |
| TNXB | exon23 | c.G8038T | p.G2680W | D | D | N |
| KIR3DL2 | exon2 | c.C62A | p.P21Q,KIR3DL2 | D | D | N |
| DNAH12 | | | | D | D | N |
| PPM1F | exon8 | c.G1076T | p.C359F | D | D | D |
| GPX8 | exon1 | c.G3A | p.M1I | D | D | D |
| DENND5A | exon12 | c.G2312A | p.G771D,DENND5A | D | D | D |
| FCN2 | exon7 | c.T710A | p.L237Q,FCN2 | D | D | D |
| PPRC1 | exon8 | c.C3754T | p.R1252W,PPRC1 | D | D | D |
| MAP1A | exon4 | c.A2714C | p.K905T | D | D | D |
| STK4 | exon6 | c.G659A | p.G220E | D | D | D |
| CACNA1B | exon28 | c.A4196G | p.Y1399C,CACNA1B | D | D | D |
| INADL | exon33 | c.C4334T | p.S1445L | D | D | D |
| MORN3 | exon4 | c.G541A | p.G181S | D | D | D |
| ARHGAP44 | exon16 | c.A1490G | p.D497G | D | D | D |
| LIG4 | exon2 | c.C2241G | p.C747W,LIG4 | D | D | D |
| MYH11 | exon8 | c.C817T | p.R273C,MYH11 | D | D | D |
| FZD2 | exon1 | c.G1399A | p.V467M | D | D | D |
| KSR1 | exon15 | c.G1462A | p.G488S | D | D | D |
| RAPGEF3 | exon23 | c.G2248A | p.D750N,RAPGEF3 | D | D | D |
| MYH7B | exon34 | c.C4054T | p.R1352C | D | D | D |
| KCNH6 | exon5 | c.A998C | p.H333P,KCNH6 | D | D | D |
| GGT7 | exon2 | c.G308A | p.R103H | D | D | D |
| PRDM16 | exon7 | c.C919T | p.R307C,PRDM16 | D | D | D |
| COPS4 | exon6 | c.G574T | p.A192S,COPS4 | D | D | D |
| WDR13 | exon7 | c.G980A | p.R327H,WDR13 | D | D | D |
| SALL4 | exon2 | c.G194A | p.R65Q | D | D | D |

| | | | | | | |
|---|---|---|---|---|---|---|
| PCDH8 | exon1 | c.C1456T | p.R486C,PCDH8 | D | D | D |
| AICDA | exon3 | c.G374T | p.G125V | D | D | D |
| NPTXR | exon1 | c.C460T | p.L154F | D | D | D |
| MPPE1 | exon8 | c.G873C | p.E291D,MPPE1 | D | D | D |
| KMT2A | exon3 | c.G1259A | p.R420Q,KMT2A | D | D | D |
| ADD3 | exon10 | c.T1315C | p.W439R,ADD3 | D | D | D |
| KIF26B | exon12 | c.G4535A | p.G1512E | D | D | D |
| SLC25A23 | exon6 | c.G679T | p.G227W | D | D | D |
| MBOAT7 | exon4 | c.G362A | p.R121H,MBOAT7 | D | D | D |
| KCTD11 | exon1 | c.T569G | p.V190G | D | D | D |
| AK2 | exon6 | c.T644C | p.I215T,AK2 | D | D | D |
| CNBD2 | exon11 | c.T1274G | p.F425C | D | D | D |
| MYO18A | exon22 | c.G3518T | p.R1173L,MYO18A | D | D | D |
| PYGB | exon12 | c.A1462C | p.T488P | D | D | D |
| IL17RE | exon14 | c.C1597T | p.R533C,IL17RE | D | D | D |
| HK3 | exon12 | c.G1675A | p.V559M | D | D | D |
| DNAJC11 | exon8 | c.C778T | p.R260W | D | D | D |
| YME1L1 | exon14 | c.G1601T | p.R534L,YME1L1 | D | D | D |
| PKN1 | exon8 | c.G1244T | p.W415L,PKN1 | D | D | D |
| ADCY2 | exon25 | c.C3218T | p.T1073M | D | D | D |
| RUNX1 | exon6 | c.C1330A | p.R444S,RUNX1 | D | D | D |
| KBTBD11 | exon2 | c.C1012T | p.R338C | D | D | D |
| LAMA5 | exon16 | c.G2080T | p.G694W | D | D | D |
| SNPH | exon6 | c.T793C | p.S265P | D | D | D |
| NFKBIB | exon3 | c.C190A | p.R64S,NFKBIB | D | D | D |
| ZCCHC2 | exon1 | c.C473A | p.P158Q | D | D | D |
| SYNE1 | exon126 | c.G22811T | p.W7604L,SYNE1 | D | D | D |
| MFRP | exon8 | c.G904T | p.G302W | D | D | D |

| | | | | | | |
|---|---|---|---|---|---|---|
| COL18A1 | exon7 | c.G1735A | p.G579S,COL18A1 | D | D | D |
| MLPH | exon8 | c.C1001T | p.S334L,MLPH | D | D | D |
| AIFM1 | exon4 | c.G296T | p.R99L,AIFM1 | D | D | D |
| NCF1 | exon2 | c.G95T | p.W32L | D | D | D |
| SERPINB12 | exon4 | c.G482T | p.W161L | D | D | D |
| TTC39B | exon14 | c.G1312T | p.G438W,TTC39B | D | D | D |
| CMA1 | exon5 | c.G631T | p.G211W | D | D | D |
| MYL6 | exon3 | c.C128A | p.P43H,MYL6 | D | D | D |
| DNAH7 | exon53 | c.G10061T | p.W3354L | D | D | D |
| SLC6A13 | exon4 | c.G450T | p.W150C | D | D | D |
| JMJD1C | exon5 | c.A188T | p.D63V,JMJD1C | D | D | D |
| SLC34A1 | exon6 | c.C557A | p.P186H,SLC34A1 | D | D | D |
| POLR1A | exon13 | c.G1727T | p.R576L | D | D | D |
| ETV4 | exon8 | c.G703T | p.G235W,ETV4 | D | D | D |
| AR | exon1 | c.C110A | p.P37Q | D | D | D |
| SENP8 | exon2 | c.C469A | p.Q157K,SENP8 | D | D | D |
| TRIM39-RPP21 | exon3 | c.A647G | p.E216G,TRIM39 | D | D | D |
| HERC2 | exon77 | c.C11716T | p.R3906C | D | D | D |
| LRP8 | exon5 | c.G514T | p.G172W,LRP8 | D | D | D |
| YAF2 | exon2 | c.G138T | p.K46N,YAF2 | D | D | D |
| NDUFV1 | exon5 | c.C662A | p.P221H,NDUFV1 | D | D | D |
| LACTB2 | exon4 | c.G503T | p.G168V | D | D | D |
| MLXIPL | exon16 | c.G2350T | p.G784W,MLXIPL | D | D | D |
| HSPA8 | exon2 | c.G99T | p.Q33H,HSPA8 | D | D | D |
| USP6 | exon6 | c.C371A | p.P124H | D | D | D |
| FYTTD1 | exon7 | c.C728A | p.P243Q,FYTTD1 | D | D | D |
| EPB41 | exon6 | c.C965A | p.P322Q,EPB41 | D | D | D |
| FAM205A | exon4 | c.G923T | p.W308L | D | D | D |
| ARHGEF11 | exon3 | c.G187T | p.G63W,ARHGEF11 | D | D | D |

| | | | | | | |
|---|---|---|---|---|---|---|
| CLASP1 | exon20 | c.G1942T | p.G648W,CLASP1 | D | D | D |
| SRCAP | exon19 | c.C2842A | p.L948I | D | D | D |
| DOCK1 | exon49 | c.C5068A | p.L1690M,DOCK1 | D | D | D |
| MMP3 | exon3 | c.A364G | p.T122A | D | D | D |
| SEMA4D | exon13 | c.G1079T | p.G360V,SEMA4D | D | D | D |
| FAM129B | exon10 | c.G1274T | p.R425L,FAM129B | D | D | D |
| TARBP2 | exon2 | c.C29A | p.P10Q,TARBP2 | D | D | D |
| TECR | exon13 | c.C829A | p.Q277K | D | D | D |
| NOS3 | exon12 | c.C1577A | p.S526Y,NOS3 | D | D | D |
| KIF1A | exon46 | c.G5066T | p.R1689L,KIF1A | D | D | D |
| ZNF600 | exon3 | c.G1061T | p.G354V | D | D | D |
| TNKS1BP1 | exon4 | c.G757T | p.G253W | D | D | D |
| FILIP1L | exon2 | c.G240T | p.E80D,FILIP1L | D | D | D |
| KNDC1 | exon10 | c.C1688A | p.A563D | D | D | D |
| TMLHE | exon5 | c.G757T | p.G253C,TMLHE | D | D | D |
| SKP1 | exon4 | c.G264T | p.W88C,SKP1 | D | D | D |
| SAFB2 | exon15 | c.G2169T | p.Q723H | D | D | D |
| ETHE1 | exon7 | c.G743T | p.G248V | D | D | D |
| EBI3 | exon5 | c.C604A | p.Q202K | D | D | D |
| EP400 | exon37 | c.A6646C | p.T2216P | D | D | D |
| NRK | exon9 | c.C725A | p.S242Y | D | D | D |
| BZRAP1 | exon12 | c.G1319T | p.R440L,BZRAP1 | D | D | D |
| SEC14L4 | exon9 | c.C701A | p.P234H,SEC14L4 | D | D | D |
| ISG20 | exon3 | c.C406T | p.R136C | D | D | D |
| CACNA1A | exon44 | c.G6328T | p.G2110W,CACNA1A | D | D | D |
| SCFD2 | exon2 | c.G905T | p.G302V | D | D | D |
| PCDH19 | exon2 | c.G2458T | p.G820C,PCDH19 | D | D | D |
| DDX17 | exon6 | c.G873T | p.L291F,DDX17 | D | D | D |
| HECTD4 | exon57 | c.G8442T | p.Q2814H | D | D | D |

| | | | | | | |
|---|---|---|---|---|---|---|
| AGAP1 | exon16 | c.C2012A | p.P671Q,AGAP1 | D | D | D |
| NKIRAS2 | exon3 | c.C113T | p.T38M,NKIRAS2 | D | D | D |
| STRN4 | exon13 | c.G1651T | p.G551W,STRN4 | D | D | D |
| CTDSP2 | exon4 | c.C322A | p.L108I | D | D | D |
| PROS1 | exon4 | c.G283T | p.G95W | D | D | D |
| HERC2 | exon28 | c.G4309T | p.G1437C | D | D | D |
| CDC14A | exon4 | c.G298T | p.G100C,CDC14A | D | D | D |
| ABHD5 | exon5 | c.C769A | p.P257T | D | D | D |
| CAPN5 | exon2 | c.A86C | p.D29A | D | D | D |
| YY1AP1 | exon2 | c.G263T | p.R88M,YY1AP1 | D | D | D |
| HELZ2 | exon2 | c.G11T | p.W4L | D | D | D |
| TBPL1 | exon7 | c.C527A | p.P176Q,TBPL1 | D | D | D |
| TRIM72 | exon7 | c.C1007A | p.A336E | D | D | D |
| TSSC1 | exon9 | c.C1078A | p.P360T | D | D | D |
| HMGA1 | exon2 | c.G36T | p.L12F,HMGA1 | D | D | D |
| WAS | exon7 | c.G641T | p.G214V | D | D | D |
| TRPV1 | exon6 | c.C1222A | p.P408T,TRPV1 | D | D | D |
| PALLD | exon9 | c.G1459T | p.V487F,PALLD | D | D | D |
| DBF4 | exon12 | c.C1841A | p.P614Q | D | D | D |
| PRDM4 | exon11 | c.G2009T | p.G670V | D | D | D |
| SLC4A5 | exon16 | c.G2185T | p.G729C,SLC4A5 | D | D | D |
| UTP20 | exon49 | c.C6532A | p.H2178N | D | D | D |
| CHRNA1 | exon6 | c.G547T | p.D183Y,CHRNA1 | D | D | D |
| OR2T8 | exon1 | c.C842A | p.P281H | D | D | D |
| APBA2 | exon13 | c.C2175A | p.F725L,APBA2 | D | D | D |
| UBB | exon2 | c.C337A | p.P113T,UBB | D | D | D |
| KCNH6 | exon7 | c.G1525T | p.G509W,KCNH6 | D | D | D |
| FDFT1 | exon3 | c.C374A | p.P125Q,FDFT1 | D | D | D |
| PATL2 | exon12 | c.G1208T | p.R403M | D | D | D |

| | | | | | | |
|---|---|---|---|---|---|---|
| CDC25A | exon1 | c.G166T | p.G56C,CDC25A | D | D | D |
| FYCO1 | exon5 | c.G311T | p.G104V | D | D | D |
| XPC | exon8 | c.G920T | p.R307L | D | D | D |
| IL17RD | exon11 | c.G1147T | p.D383Y | D | D | D |
| OTOG | exon29 | c.A3703C | p.T1235P,OTOG | D | D | D |
| TXN | exon2 | c.G56T | p.G19V,TXN | D | D | D |
| HUWE1 | exon26 | c.G2545T | p.D849Y | D | D | D |
| CTDSP2 | exon1 | c.G35T | p.R12M | D | D | D |
| SEC24A | exon6 | c.C1148A | p.P383Q,SEC24A | D | D | D |
| TFR2 | exon15 | c.G1796T | p.S599I,TFR2 | D | D | D |
| DHX40 | exon13 | c.G1525T | p.A509S,DHX40 | D | D | D |
| CD6 | exon12 | c.G1877T | p.G626V | D | D | D |
| GRIN2C | exon13 | c.C2645A | p.P882Q | D | D | D |
| GABPA | exon9 | c.G1069A | p.A357T,GABPA | D | D | D |
| GLE1 | exon15 | c.C2000A | p.S667Y | D | D | D |
| UBE2S | exon3 | c.G200T | p.G67V | D | D | D |
| COL13A1 | exon21 | c.G1134T | p.K378N,COL13A1 | D | D | D |
| AIM1L | exon14 | c.G4166T | p.C1389F | D | D | D |
| PROSER2 | exon4 | c.C1105T | p.R369C | D | D | D |
| RPS3 | exon4 | c.C110A | p.P37H,RPS3 | D | D | D |
| TUBGCP6 | exon13 | c.G2223T | p.R741S | D | D | D |
| HS6ST2 | exon4 | c.G1004T | p.W335L,HS6ST2 | D | D | D |
| WIPF3 | exon3 | c.C212A | p.P71Q | D | D | D |
| SEC16A | exon16 | c.C5407G | p.Q1803E,SEC16A | D | D | D |
| TCEB2 | exon3 | c.G181A | p.G61S,TCEB2 | D | D | D |
| FLNB | exon34 | c.C5759A | p.A1920D,FLNB | D | D | D |
| GOLGA3 | exon4 | c.G518T | p.R173M,GOLGA3 | D | D | D |
| PCDH15 | exon7 | c.G652T | p.V218F,PCDH15 | D | D | D |
| SEMA4C | exon4 | c.G266T | p.W89L | D | D | D |

| | | | | | | |
|---|---|---|---|---|---|---|
| EXOC3L1 | exon3 | c.G71T | p.R24L | D | D | D |
| GGT5 | exon3 | c.G422T | p.G141V,GGT5 | D | D | D |
| MYRF | exon3 | c.G184T | p.G62W,MYRF | D | D | D |
| PRELID1 | exon5 | c.C578A | p.A193D,PRELID1 | D | D | D |
| NDST3 | exon5 | c.C1286A | p.P429H | D | D | D |
| SYNE2 | exon105 | c.C19046A | p.S6349Y,SYNE2 | D | D | D |
| LTBP1 | exon1 | c.C220T | p.R74C | D | D | D |
| NPHS1 | exon19 | c.G2635T | p.G879W | D | D | D |
| RABEP2 | exon5 | c.G875T | p.W292L | D | D | D |
| L3MBTL4 | exon14 | c.G1147T | p.G383W | D | D | D |
| UNC80 | exon23 | c.C3641A | p.P1214H,UNC80 | D | D | D |
| CDIPT | exon4 | c.G304T | p.G102W,CDIPT | D | D | D |
| GABRA3 | exon3 | c.G253T | p.G85W | D | D | D |
| COL2A1 | exon29 | c.G1762T | p.G588C,COL2A1 | D | D | D |
| CALR3 | exon1 | c.G89T | p.G30V | D | D | D |
| MMADHC | exon4 | c.G226T | p.G76W | D | D | D |
| NPHP3 | exon24 | c.C3512A | p.P1171H | D | D | D |
| ACTL6A | exon1 | c.G23T | p.G8V | D | D | D |
| VWA5A | exon14 | c.C1636T | p.H546Y,VWA5A | D | D | D |
| SYNM | | | | D | D | D |
| PRSS48 | exon2 | c.T86C | p.V29A | D | P | N |
| CAMSAP1 | exon11 | c.C2702T | p.A901V | D | P | N |
| ENDOV | exon2 | c.C79T | p.H27Y,ENDOV | D | P | N |
| C12orf40 | exon6 | c.C530T | p.T177I | D | P | N |
| GPR25 | exon1 | c.G424T | p.V142L | D | P | N |
| KIR2DL4 | exon3 | c.C182G | p.T61R,KIR2DL4 | D | P | N |
| WDR87 | exon6 | c.G3410A | p.R1137Q,WDR87 | D | P | N |
| L1TD1 | exon4 | c.C1792G | p.H598D,L1TD1 | D | P | N |

| | | | | | | |
|---|---|---|---|---|---|---|
| KIR2DL1 | exon6 | c.G801C | p.W267C | D | P | N |
| MYO1A | exon24 | c.G2534T | p.R845M,MYO1A | D | P | N |
| ZNF93 | exon4 | c.T556C | p.S186P | D | P | N |
| OPN1MW | exon5 | c.C893A | p.P298H,OPN1MW2 | D | P | N |
| NBPF12 | exon9 | c.G426T | p.Q142H | D | P | N |
| VEGFB | exon6 | c.A458C | p.D153A,VEGFB | D | P | N |
| SHC2 | exon1 | c.C113T | p.A38V | D | P | N |
| MUC5B | exon8 | c.C884A | p.P295H | D | P | N |
| SAFB2 | exon21 | c.A2848C | p.T950P | D | P | N |
| SLC20A2 | exon7 | c.G910T | p.G304C,SLC20A2 | D | P | N |
| GGT1 | exon5 | c.C43A | p.L15M,GGT1 | D | P | N |
| FAM153A | exon10 | c.G365T | p.G122V | D | P | N |
| CNTN5 | exon14 | c.C1856T | p.P619L,CNTN5 | D | P | D |
| RYR2 | exon37 | c.T5186C | p.M1729T | D | P | D |
| XIRP2 | exon7 | c.G8170C | p.E2724Q,XIRP2 | D | P | D |
| SLC25A5 | exon2 | c.T244A | p.F82I | D | P | D |
| ASH2L | exon1 | c.C143A | p.S48Y | D | P | D |
| FAM86B1 | exon6 | c.C751T | p.R251C | D | P | D |
| ATN1 | exon5 | c.C2227A | p.P743T,ATN1 | D | P | D |
| ANTXR2 | exon11 | c.G896T | p.G299V,ANTXR2 | D | P | D |
| XPC | exon9 | c.T1271G | p.V424G | D | P | D |
| ARHGAP6 | exon9 | c.G1269T | p.M423I,ARHGAP6 | D | P | D |
| BAI2 | exon4 | c.G124T | p.A42S,BAI2 | D | P | D |
| RPL7A | exon3 | c.C157A | p.R53S | D | P | D |
| AIFM1 | exon4 | c.G366T | p.K122N,AIFM1 | D | P | D |
| PELP1 | exon7 | c.G929T | p.W310L,PELP1 | D | P | D |
| SEMA6B | exon17 | c.G1883T | p.R628L | D | P | D |
| PDLIM7 | exon5 | c.C352A | p.P118T,PDLIM7 | D | P | D |
| TMEM129 | exon3 | c.G701T | p.G234V | D | P | D |

| | | | | | | |
|---|---|---|---|---|---|---|
| ATP1A1 | exon14 | c.G1845T | p.M615I,ATP1A1 | D | P | D |
| TLK2 | exon17 | c.G1732C | p.E578Q,TLK2 | D | P | D |
| AGAP4 | exon7 | c.G1040T | p.G347V,AGAP4 | D | P | D |
| MYH14 | exon25 | c.G3236T | p.G1079V,MYH14 | D | P | D |
| RAB34 | exon1 | c.G32T | p.R11M,RAB34 | D | P | . |
| DOCK9 | exon1 | c.C23A | p.P8H | . | B | D |
| RFFL | exon6 | c.G910T | p.G304W | . | B | D |
| RGAG1 | exon3 | c.G1057A | p.A353T | . | D | N |
| TEX11 | exon8 | c.G538T | p.G180W,TEX11 | . | D | N |
| WDR86 | exon3 | c.G487T | p.G163W,WDR86 | . | D | N |
| MUC4 | exon2 | c.G11554T | p.G3852C | . | D | N |
| DLG5 | exon23 | c.G4463T | p.R1488M | . | D | N |
| OTUD7B | exon4 | c.A466C | p.I156L | . | D | D |
| ANK2 | exon30 | c.C3443A | p.P1148Q,ANK2 | . | D | D |
| KIAA0100 | exon14 | c.G1771T | p.G591C | . | D | D |
| NAV2 | exon17 | c.G2711T | p.S904I,NAV2 | . | D | D |
| ADARB2 | exon8 | c.G1864T | p.G622C | . | D | D |
| MXD4 | exon2 | c.G164T | p.R55M | . | D | D |
| UGT2B7 | exon6 | c.G1455T | p.W485C | . | D | D |
| HSD3B2 | exon3 | c.G244T | p.A82S,HSD3B2 | . | D | D |
| LRP2 | exon8 | c.C803A | p.P268Q | . | D | D |
| NRXN3 | exon3 | c.G13T | p.D5Y | . | D | D |
| GATA3 | exon2 | c.C182A | p.P61Q,GATA3 | . | D | D |
| TENM4 | exon13 | c.G1735T | p.G579W | . | D | D |
| SIK1 | exon7 | c.G748T | p.D250Y | . | D | D |
| MUC4 | exon2 | c.C10976G | p.T3659R | . | P | N |
| TELO2 | exon13 | c.C1562A | p.A521D | . | P | N |
| C16orf62 | exon22 | c.C2077G | p.L693V,C16orf62 | . | P | D |

| | | | | | | |
|---|---|---|---|---|---|---|
| PCBD1 | exon2 | c.G8A | p.G3D | . | P | D |
| SPICE1 | exon8 | c.G751T | p.A251S | . | P | D |
| MOCS1 | exon1 | c.G98T | p.G33V | . | P | D |
| TAGLN2 | exon3 | c.C346A | p.L116I,TAGLN2 | . | P | D |
| CTAGE5 | exon20 | c.C1639A | p.L547I,CTAGE5 | . | P | D |

## Appendix 4.3 - Variants Chosen for Sanger Sequencing and the Corresponding Primers

| Gene | Chromosome | Protein change | Mutation type | Forward primer | Reverse primer | Tumour ID |
|---|---|---|---|---|---|---|
| INADL | chr1:62550277 | p.1216_1216del, | nonframeshift deletion | GAACTGCTCCACCGCCAA | GGAAATGACGCCACAAAAGC | MESOD5 |
| INADL | chr1:62393477 | p.S1445L | nonsynonymous | TCCTGTCACACACACACGTA | AGCCTAGCAACTCACCTTGA | MESOEQ40 |
| JMJD1C | chr10:64928295 | p.T2241I | nonsynonymous | GAACAGGACCTAGAACACCCA | TGGCTTTTCTTTGCTCCACC | MESOD15 |
| JMJD1C | chr10:64975401 | p.D63V | nonsynonymous | GCGTCGTGATGTAATGCCAA | GGATCCCAAGCTGATTTCTAAAC | MESOEQ36 |
| SETD2 | chr3:47161908 | p.1380_1406del, | frameshift deletion | TGTCCTGAAGCTCACCATCA | AAGGGGTCAGTGCAAGCA | MESOD26 |
| SETD2 | chr3:47059172 | p.G2497fs | frameshift insertion | AGGTACACAGTTTGCCCAGA | ACAACTCCTTGCCCTCTCTG | MESOEQ40 |
| CACNA1B | chr9:140952590 | p.Y613C, | nonsynonymous | TTAGGGCTGTCTCCTTTGGG | TCCACTGCAAGACTCCACAG | MESOEQ21 |
| CACNA1B | chr9:140938328 | p.M1130T | nonsynonymous | CAAGCAGAGGGGAAGAAGGA | CTGGCTACTGAGATCCCACG | MESOD15 |
| RASGRP4 | chr19:38910871 | p.H137N, | nonsynonymous | CAGGGAAGAGGGGAGCAC | CCCCTAGCTCAGCACCTAG | MESOEQ21 |
| STK4 | chr20:43623864 | p.G165E | nonsynonymous | ATACCATGGCCAAGCGGAAT | GTGCTGGGATTACACGTGTG | MESOEQ40 |
| FZD2 | chr17:42636455 | p.V467M | nonsynonymous | CACCATCATGAAGCACGACG | TGAGCGTCATGAGGTATTTGA | MESOEQ30 |
| ASH1L | chr1:1554 | p.V745I | nonsyno | GCAAGAGATGG | GCCTAAGTACTA | MESOEQ21 |

| | | | | | | |
|---|---|---|---|---|---|---|
| | 50428 | | nymous | AGCTGTGGA | GTTTGCAGTCC | |
| SETD6 | chr16:58552374 | p.V348A, | nonsynonymous | TTGTAGACTGGGTGGCAGAC | TCAGCTCCTCTTCAGTCAGC | MESOEQ36 |
| SMYD3 | chr1:246078913 | p.M55I, | nonsynonymous | GGCAACGGAAACAGTCACAT | ACGTGTGATCATTTGGGTAGAG | MESOEQ30 |
| DMAP1 | chr1:44680379 | p.A68T | nonsynonymous | ACCTGAAGTCTTTTGCTCCAG | GGAAGAACATTGCTCCGTCC | MESOEQ40 |
| PHF21A | chr11:45955757 | p.N556S | nonsynonymous | ACAGGTTTGGAGAGGTCGAT | TGTTCCTTAGGTGGTAGCCG | MESOEQ30 |
| SETD1B | chr12:122242657 | p.H5fs | frameshift deletion | TTTCGCGTGTGTGTAGAAGC | CGGTACAGTTTATGATGCCCC | MESOEQ30 |
| CDH8 | chr14:21873555 | p.N1040fs | frameshift deletion | TTGCGCAACTCCATCATTGT | TGAGAATGTTCGCCCTCATCT | MESOEQ30 |
| TBL1XR1 | chr3:176769332 | p.N129fs | frameshift deletion | CTGCACATGTACCCCGAATT | GATGCCGTAATGCCTGATGT | MESOEQ30 |
| NF2 | chr22:30035190 | p.76_76del, | nonframeshift deletion | GTGTGTTTGTCTTTTGCTCTGC | ACTCCTGGGCAAGTTCTCTC | MESOEQ40 |
| NF2 | chr22:30057302 | p.R221X, | stopgain SNV | GCTGTTCTTATTGGATCCACAGA | AGGGAAAGATCTGCTGGACC | MESOD14 |
| BAP1 | chr3:52440373 | p.R227C | nonsynonymous | GCAGAGGCCAGGAAGAAAGG | GGGGCCTATACCTACAGCTG | MESOEQ22 |
| BAP1 | chr3:52436624 | p.Q684X, | stopgain SNV | CTCTCATGGCCCTCCCTG | GACCAGAGAAGGACCCACAA | MESOD13 |
| BAP1 | chr3:52441430 | p.H141P, | nonsynonymous | AACAGAGTCAGGGCCCAAAA | CTGCTCTCTGAAGCTTTGCC | MESOD18 |
| FLT3 | chr13:28623882 | p.P258S | nonsynonymous | ACCTCCTCGAGTGCTTTGTT | AGGATATCTTTTGTGATGAGGCA | MESOEQ30 |
| GPHN | chr14:67389394 | p.76_76del | nonsynonymous | CGAAACAGTTTGATTGCCACC | CTGGTAGTAGGAGGAGGGGA | MESOEQ30 |

| | | | | | | |
|---|---|---|---|---|---|---|
| PRDM16 | chr16_1:3321337 | p.R307C | nonsynonymous | AGCTGTATGGTTGGGGTCC | GCAGTTTTCACATTCGAAGCG | MESOEQ30 |
| RPL10 | chrx:153626879 | p.R7C | nonsynonymous | GGTGAGTAAGCGCAGTTGTC | CGGGAGGTGTAAAACATAGGG | MESOEQ30 |
| MN1 | chr22:28194730 | p.P601L | nonsynonymous | TACGGGGCAGCAGGTCTC | CGGCCCTCATGATTAAGCAG | MESOEQ30 |

## Appendix 4.4 - Genes Implicated in Cancer Identified in Discovery Cohort

| Gene | Mutation types | Protein | Tumour ID (D) |
|---|---|---|---|
| AR | nonsynonymous SNV | p.P37Q | MESOEQ22 |
| ATP1A1 | nonsynonymous SNV | p.M615I,ATP1A1 | MESOEQ22 |
| BAP1 | stopgain | p.E373X | MESOEQ22 |
| CCDC6 | stopgain | p.L265X | MESOEQ30 |
| CHD8 | frameshift deletion | p.N1040fs,CHD8 | MESOEQ30 |
| CLASP1 | nonsynonymous SNV | p.G648W,CLASP1 | MESOEQ22 |
| CNTRL | nonsynonymous SNV | p.L935I | MESOEQ30 |
| COL2A1 | nonsynonymous SNV | p.G588C,COL2A1 | MESOEQ22 |
| CSF3R | stopgain | p.E24X,CSF3R | MESOEQ22 |
| ELF4 | nonsynonymous SNV | p.H405N,ELF4 | MESOEQ22 |
| ETV4 | nonsynonymous SNV | p.G235W,ETV4 | MESOEQ22 |
| FAM118B | nonsynonymous SNV | p.P311Q | MESOEQ22 |
| FANCD2 | nonsynonymous SNV | p.E1153K,FANCD2 | MESOEQ40 |
| FLT3 | nonsynonymous SNV | p.P258S | MESOEQ30 |
| FOXK1 | nonsynonymous SNV | p.P211T | MESOEQ30 |
| GATA3 | nonsynonymous SNV | p.P61Q,GATA3 | MESOEQ22 |
| GNA11 | nonsynonymous SNV | p.M7I | MESOEQ22 |
| GPHN | nonsynonymous SNV | p.Q156H,GPHN | MESOEQ30 |
| HMGA1 | nonsynonymous SNV | p.L12F,HMGA1 | MESOEQ22 |
| HSP90AA1 | stopgain | p.G168X,HSP90AA1 | MESOEQ22 |
| KDR | stopgain | p.G794X | MESOEQ22 |
| KIAA1549 | nonsynonymous SNV | p.G1278C,KIAA1549 | MESOEQ22 |
| KMT2A | nonsynonymous SNV | p.R420Q,KMT2A | MESOEQ30 |
| MN1 | nonsynonymous SNV | p.P601L | MESOEQ30 |
| MUC1 | nonsynonymous SNV | p.W94C,MUC1 | MESOEQ22 |

| | | | |
|---|---|---|---|
| MYH11 | nonsynonymous SNV | p.R273C,MYH11 | MESOEQ22 |
| NAB2 | nonsynonymous SNV | p.F208L | MESOEQ36 |
| NF2 | nonframeshift deletion | p.76_76del,NF2 | MESOEQ40 |
| NF2 | splicing | | MESOEQ13 |
| NOTCH1 | nonsynonymous SNV | p.G2245W | MESOEQ22 |
| PRDM16 | nonsynonymous SNV | p.R307C,PRDM16 | MESOEQ30 |
| RNF213 | nonsynonymous SNV | p.K1552T | MESOEQ30 |

# Appendix 4.5 - Genes Implicated in Cancer Identified in Both Discovery and Validation cohorts

| Gene | Mutation type | protein change | MESO D10 | MESO D12 | MESO D13 | MESO D14 | MESO D15 | MESO D16 | MESO D17 | MESO D18 | MESO D19 | MESO D1 | MESO D21 | MESO D22 | MESO D24 | MESO D25 | MESO D26 | MESO D27 | MESO D28 | MESO D29 | MESO D2 | MESO D30 | MESO D31 | MESO D32 | MESO D33 | MESO D34 | MESO D35 | MESO D3 | MESO D5 | MESO D6 | MESO D8 |
|---|---|---|---|---|---|---|---|---|---|---|---|---|---|---|---|---|---|---|---|---|---|---|---|---|---|---|---|---|---|---|---|
| AR | frameshift deletion | p.Q60fs, | 0/0 | 0/1 | 0/0 | 0/0 | 0/0 | 0/0 | 0/0 | 0/0 | 0/0 | 0/0 | 0/0 | 0/0 | 0/0 | 0/0 | 0/0 | 0/0 | 0/0 | 0/0 | 0/0 | 0/0 | 0/0 | 0/0 | 0/0 | 0/0 | 0/0 | 0/0 | 0/0 | 0/0 | 0/0 |
| AR | frameshift deletion | p.60_63del, | 0/0 | 0/1 | 0/0 | 0/0 | 0/0 | 0/0 | 0/0 | 0/0 | 0/0 | 0/0 | 0/0 | 0/0 | 0/0 | 0/0 | 0/0 | 0/0 | 0/0 | 0/0 | 0/0 | 0/0 | 0/0 | 0/0 | 0/0 | 0/0 | 0/0 | 0/0 | 0/0 | 0/0 | 0/0 |
| AR | nonframeshift deletion | p.57_65del, | 0/0 | 0/5 | 0/4 | 0/0 | 2/3 | 0/4 | 0/6 | 0/5 | 0/0 | 0/0 | 0/0 | 4/5 | 0/0 | 3/3 | 3/3 | 6/6 | 6/6 | 0/0 | 4/5 | 2/3 | 0/0 | 2/4 | 1/6 | 0/3 | 0/0 | 0/0 | 2/3 | 2/2 | 2/2 |
| AR | nonframeshift deletion | p.457_460del, | 0/0 | 0/3 | 0/0 | 0/3 | 2/2 | 0/0 | 0/0 | 0/3 | 0/0 | 0/0 | 0/0 | 0/0 | 0/0 | 3/3 | 0/0 | 3/3 | 0/0 | 0/0 | 0/0 | 3/3 | 3/3 | 0/0 | 0/0 | 1/1 | 0/0 | 0/0 | 0/0 | 0/0 | 0/2 |
| BAP1 | frameshift deletion | p.56_62del, | 0/0 | 0/0 | 0/0 | 0/0 | 0/0 | 0/0 | 0/0 | 0/0 | 0/0 | 0/0 | 0/0 | 0/0 | 0/0 | 0/0 | 0/0 | 0/1 | 0/0 | 0/0 | 0/0 | 0/0 | 0/0 | 0/0 | 0/0 | 0/0 | 0/0 | 0/0 | 0/0 | 0/0 | 0/0 |
| BAP1 | frameshift deletion | p.R114fs, | 0/0 | 0/0 | 0/0 | 0/0 | 0/0 | 0/0 | 0/0 | 0/0 | 0/0 | 0/0 | 0/0 | 0/1 | 0/0 | 0/0 | 0/0 | 0/0 | 0/0 | 0/0 | 0/0 | 0/0 | 0/0 | 0/0 | 0/0 | 0/0 | 0/0 | 0/0 | 0/0 | 0/0 | 0/0 |
| BAP1 | frameshift deletion | p.558_560del, | 0/0 | 0/0 | 0/0 | 0/0 | 0/0 | 0/0 | 0/1 | 0/0 | 0/0 | 0/0 | 0/0 | 0/0 | 0/0 | 0/0 | 0/0 | 0/0 | 0/0 | 0/0 | 0/0 | 0/0 | 0/0 | 0/0 | 0/0 | 0/0 | 0/0 | 0/0 | 0/0 | 0/0 | 0/0 |
| BAP1 | frameshift deletion | p.162_162del, | 0/0 | 0/0 | 0/0 | 0/1 | 0/0 | 0/0 | 0/0 | 0/0 | 0/0 | 0/0 | 0/0 | 0/0 | 0/0 | 0/0 | 0/0 | 0/0 | 0/0 | 0/0 | 0/0 | 0/0 | 0/0 | 0/0 | 0/0 | 0/0 | 0/0 | 0/0 | 0/0 | 0/0 | 0/0 |
| BAP1 | frameshift deletion | p.146_147del, | 0/1 | 0/0 | 0/0 | 0/0 | 0/0 | 0/0 | 0/0 | 0/0 | 0/0 | 0/0 | 0/0 | 0/0 | 0/0 | 0/0 | 0/0 | 0/0 | 0/0 | 0/0 | 0/0 | 0/0 | 0/0 | 0/0 | 0/0 | 0/0 | 0/0 | 0/0 | 0/0 | 0/0 | 0/0 |
| BAP1 | frameshift insertion | p.K658fs, | 0/0 | 0/0 | 0/0 | 0/0 | 0/0 | 0/0 | 0/0 | 0/0 | 0/0 | 0/0 | 0/0 | 0/0 | 0/0 | 0/1 | 0/0 | 0/0 | 0/0 | 0/0 | 0/0 | 0/0 | 0/0 | 0/0 | 0/0 | 0/0 | 0/0 | 0/0 | 0/0 | 0/0 | 0/0 |
| BAP1 | nonframeshift deletion | p.659_659del, | 0/0 | 0/0 | 0/0 | 0/0 | 0/0 | 0/0 | 0/0 | 0/0 | 0/0 | 0/0 | 0/0 | 0/0 | 0/0 | 0/1 | 0/0 | 0/0 | 0/0 | 0/0 | 0/0 | 0/0 | 0/0 | 0/0 | 0/0 | 0/0 | 0/0 | 0/0 | 0/0 | 0/0 | 0/0 |
| BAP1 | nonsynonymous SNV | p.H141P, | 0/0 | 0/0 | 0/1 | 0/0 | 0/0 | 0/0 | 0/0 | 0/0 | 0/0 | 0/0 | 0/0 | 0/0 | 0/0 | 0/0 | 0/0 | 0/0 | 0/0 | 0/0 | 0/0 | 0/0 | 0/0 | 0/0 | 0/0 | 0/0 | 0/0 | 0/0 | 0/0 | 0/0 | 0/0 |
| BAP1 | stopgain SNV | p.Q684X, | 0/0 | 0/0 | 0/0 | 0/0 | 0/0 | 0/0 | 0/0 | 0/1 | 0/0 | 0/0 | 0/0 | 0/0 | 0/0 | 0/0 | 0/0 | 0/0 | 0/0 | 0/0 | 0/0 | 0/0 | 0/0 | 0/0 | 0/0 | 0/0 | 0/0 | 0/0 | 0/0 | 0/0 | 0/0 |
| FOXK1 | nonsynonymous SNV | p.T683P, | 0/0 | 0/1 | 0/1 | 0/1 | 0/0 | 0/1 | 0/0 | 0/0 | 0/0 | 0/1 | 0/1 | 0/0 | 0/0 | 0/0 | 0/1 | 0/1 | 0/1 | 0/1 | 0/0 | 0/0 | 0/1 | 0/1 | 0/1 | 0/0 | 0/0 | 0/0 | 0/1 | 0/0 | 0/0 |
| GATA3 | nonsynonymous SNV | p.S407L,GATA3 | 0/0 | 0/0 | 0/0 | 0/0 | 0/0 | 0/0 | 0/0 | 0/0 | 0/0 | 0/0 | 0/0 | 0/0 | 0/0 | 0/0 | 0/0 | 0/0 | 0/0 | 0/0 | 0/0 | 0/0 | 0/0 | 0/0 | 0/0 | 0/0 | 0/0 | 0/1 | 0/0 | 0/0 | 0/0 |
| GNA11 | nonsynonymous SNV | p.S50R, | 0/0 | 0/0 | 0/0 | 0/0 | 0/0 | 0/0 | 0/0 | 0/0 | 0/0 | 0/0 | 0/0 | 0/0 | 0/0 | 0/0 | 0/0 | 0/0 | 0/0 | 0/0 | 0/0 | 0/0 | 0/0 | 0/0 | 0/0 | 0/0 | 0/0 | 0/0 | 0/0 | 0/0 | 0/1 |
| NAB2 | nonsynonymous SNV | p.P504S, | 0/0 | 0/0 | 0/0 | 0/0 | 0/0 | 0/0 | 0/0 | 0/0 | 0/0 | 0/0 | 0/0 | 0/0 | 0/0 | 0/0 | 0/0 | 0/0 | 0/0 | 0/0 | 0/0 | 0/0 | 0/1 | 0/0 | 0/0 | 0/0 | 0/0 | 0/0 | 0/0 | 0/0 | 0/0 |
| NF2 | frameshift deletion | p.A354fs,NF2 | 0/0 | 0/0 | 0/0 | 0/0 | 0/0 | 0/1 | 0/0 | 0/0 | 0/0 | 0/0 | 0/0 | 0/0 | 0/0 | 0/0 | 0/0 | 0/0 | 0/0 | 0/0 | 0/0 | 0/0 | 0/0 | 0/0 | 0/0 | 0/0 | 0/0 | 0/0 | 0/0 | 0/0 | 0/0 |
| NF2 | frameshift deletion | p.F35fs,NF2 | 0/0 | 0/1 | 0/0 | 0/0 | 0/0 | 0/0 | 0/0 | 0/0 | 0/0 | 0/0 | 0/0 | 0/0 | 0/0 | 0/0 | 0/0 | 0/0 | 0/0 | 0/0 | 0/0 | 0/0 | 0/0 | 0/0 | 0/0 | 0/0 | 0/0 | 0/0 | 0/0 | 0/0 | 0/0 |
| NF2 | frameshift insertion | p.P129fs,NF2 | 0/0 | 0/0 | 0/0 | 0/0 | 0/0 | 0/0 | 0/0 | 0/0 | 0/0 | 0/0 | 0/0 | 0/0 | 0/0 | 0/0 | 0/0 | 0/0 | 0/0 | 0/0 | 0/0 | 0/1 | 0/0 | 0/0 | 0/0 | 0/0 | 0/0 | 0/0 | 0/0 | 0/0 | 0/0 |
| NF2 | stopgain SNV | p.R221X,NF2 | 0/0 | 0/0 | 0/0 | 0/1 | 0/0 | 0/0 | 0/0 | 0/0 | 0/0 | 0/0 | 0/0 | 0/0 | 0/0 | 0/0 | 0/0 | 0/0 | 0/0 | 0/0 | 0/0 | 0/0 | 0/0 | 0/0 | 0/0 | 0/0 | 0/0 | 0/0 | 0/0 | 0/0 | 0/0 |
| NOTCH1 | nonsynonymous SNV | p.T349P, | 0/1 | 0/1 | 0/0 | 0/0 | 0/0 | 0/0 | 0/1 | 0/1 | 0/0 | 0/0 | 0/1 | 0/1 | 0/1 | 0/1 | 0/1 | 0/1 | 0/1 | 0/1 | 0/1 | 0/1 | 0/1 | 0/1 | 0/1 | 0/0 | 0/1 | 0/1 | 0/1 | 0/1 | 0/0 |
| NOTCH1 | nonsynonymous SNV | p.T194P, | 0/1 | 0/1 | 0/0 | 0/0 | 0/0 | 0/0 | 0/0 | 0/1 | 0/0 | 0/0 | 0/0 | 0/0 | 0/1 | 0/0 | 0/1 | 0/0 | 0/0 | 0/0 | 0/0 | 0/0 | 0/1 | 0/0 | 0/1 | 0/0 | 0/1 | 0/0 | 0/0 | 0/1 | 0/0 |
| RNF213 | nonsynonymous SNV | p.L4696P, | 0/0 | 0/0 | 0/0 | 0/0 | 0/0 | 0/0 | 0/0 | 0/0 | 0/0 | 0/0 | 0/0 | 0/0 | 0/0 | 0/0 | 0/0 | 0/0 | 0/0 | 0/0 | 0/0 | 0/0 | 0/0 | 0/0 | 0/0 | 0/0 | 0/0 | 0/1 | 0/0 | 0/0 | 0/0 |
| RNF213 | nonsynonymous SNV | p.D578N,RNF2 | 0/0 | 0/1 | 0/0 | 0/0 | 0/0 | 0/0 | 0/0 | 0/0 | 0/0 | 0/0 | 0/0 | 0/0 | 0/0 | 0/0 | 0/0 | 0/0 | 0/0 | 0/0 | 0/0 | 0/0 | 0/0 | 0/0 | 0/0 | 0/0 | 0/0 | 0/0 | 0/0 | 0/0 | 0/0 |
| SETD2 | frameshift deletion | p.1380_1406del | 0/0 | 0/0 | 0/0 | 0/0 | 0/0 | 0/0 | 0/0 | 0/0 | 0/0 | 0/0 | 0/0 | 0/0 | 0/0 | 0/0 | 0/1 | 0/0 | 0/0 | 0/0 | 0/0 | 0/0 | 0/0 | 0/0 | 0/0 | 0/0 | 0/0 | 0/0 | 0/0 | 0/0 | 0/0 |
| USP6 | nonsynonymous SNV | p.I67M, | 0/1 | 0/1 | 0/1 | 0/1 | 0/1 | 0/1 | 0/1 | 0/1 | 0/1 | 0/0 | 0/1 | 0/1 | 0/1 | 0/1 | 0/1 | 0/0 | 0/1 | 0/1 | 0/1 | 0/1 | 0/1 | 0/1 | 0/1 | 0/1 | 0/1 | 0/1 | 0/1 | 0/1 | 0/1 |
| USP6 | nonsynonymous SNV | p.R68W, | 0/1 | 0/1 | 0/1 | 0/1 | 0/1 | 0/1 | 0/1 | 0/1 | 0/1 | 0/0 | 0/1 | 0/1 | 0/1 | 0/1 | 0/1 | 0/0 | 0/1 | 0/1 | 0/1 | 0/1 | 0/1 | 0/1 | 0/1 | 0/1 | 0/1 | 0/1 | 0/1 | 0/1 | 0/1 |